MODELLING INTERACTIONS BETWEEN CLIMATE AND GLOBAL VEGETATION IN RESPONSE TO CLIMATE CHANGE

by

Susan Elizabeth Lee

Department of Animal and Plant Sciences

University of Sheffield

A thesis submitted for the degree of Doctor of Philosophy

December 1997

ACKNOWLEDGEMENTS

I would like to thank Professor Ian Woodward, my supervisor, for all his help and advice, and for providing me with the opportunity to do this Ph.D.

I am also extremely grateful to Dr. Peter Mitchell for his constructive comments and useful advice and for proof-reading this thesis. Thanks also to Dr. Andrew Terry and my parents for their proof-reading. Thanks too, to Dr. Mark Lomas for invaluable discussions concerning the DOLY model.

Special thanks to Dr. Peter Cox and Mr. Richard Betts from the Hadley Centre for the provision of the UKMO GCM data, for collaborative work on coupling the DOLY model with the GCM, and for their helpful comments. Thanks also to all my other colleagues in the TIGER IV 3b) consortium.

I would also like to thank Professor Wolfgang Cramer of the Potsdam Institute for Climate Impact Research in Germany, Dr. Rik Leemans of the Department of Terrestrial Ecology and Global Change, Bilthoven, The Netherlands for the provision of climate data, along with Dr. Tom Smith, Department of Environmental Science, University of Virginia for his equation for absolute minimum temperature.

The N.E.R.C. provided funding for the TIGER Project which enabled me to undertake this Ph.D.

Finally, I would like to thank Richard, and my family and friends for all their encouragement and support.

Dedicated to my sister, Jane.

MODELLING INTERACTIONS BETWEEN CLIMATE AND GLOBAL VEGETATION IN RESPONSE TO CLIMATE CHANGE

SUMMARY

Climate change associated with increasing concentrations of the greenhouse gas, carbon dioxide (CO_2), is expected to lead to an increase in global mean temperature of between 1 and 3.5°C by the end of the 21st century, with regional changes in rainfall and humidity.

This thesis is concerned with modelling the effects of a changing climate and atmospheric CO_2 on global vegetation. The process-based model, DOLY (Dynamic glObaL phytogeographY), is used. It is able to operate using three climate variables, two soil variables and an atmospheric CO_2 concentration. Its outputs are leaf area index (LAI), and net primary productivity (NPP).

The LAI and NPP values predicted by DOLY were used to run a life-form model with a climate change scenario. It was found that warming lead to the spread of trees into tundra regions. The DOLY model was also coupled with the Hadley Centre general circulation model to determine the feedbacks of vegetation on climate. With global warming of 2°C, the global feedback of vegetation on temperature was a decrease of 1°C. However at the regional scale the feedback was ± 2°C, of similar magnitude to the driving temperature change. Finally, the DOLY model was run with transient climate data from the Hadley Centre. The boreal forest moved north, and the Gobi desert and the southern steppes in the former Soviet Union shrank in area.

The sensitivity of the model to its soil and climate inputs have also been analysed over a range of environments and the model has been validated with reference to satellite data and experimental data. It was found to perform well.

This thesis has shown that it is possible to predict current and possible future distributions of vegetation with climate change using a vegetation model.

ACRONYMS AND ABBREVIATIONS

APAR	Absorbed Photosynthetically Active Radiation.
AVHRR	Advanced Very High Resolution Radiometer.
DOLY	**D**ynamic Gl**O**ba**L** Phytogeograph**Y** model.
FT	Functional Type
GCM	General Circulation Model.
GCTE	Global Change and Terrestrial Ecosystems.
HadCM2	Second Hadley Centre coupled ocean-atmosphere GCM.
IIASA	International Institute for Applied Systems Analysis.
IGBP	International Geosphere–Biosphere Programme.
IPCC	Intergovernmental Panel on Climate Change.
ISLSCP	International Satellite Land Surface Climatology Project.
LAI	Leaf Area Index.
NDVI	Normalised Difference Vegetation Index.
NPP	Net Primary Productivity.
PAR	Photosynthetically Active Radiation.
PILPS	Project for Intercomparison of Land Surface Parameterization Schemes.
SDGVM	Sheffield Dynamic Global Vegetation Model.
TIGER	Terrestrial Initiative in Global Environmental Research.
UKMO	United Kingdom Meteorological Office.
VPD	Vapour Pressure Deficit.
WHS	Wilson and Henderson-Sellers.

CONTENTS

LIST OF TABLES

LIST OF FIGURES

CHAPTER 1

1 Introduction

1.1 The history of the study of climate and vegetation

A number of authors have attempted to link vegetation and climate and these have met with varying degrees of success. The earliest attempts were by plant geographers, von Humboldt and Bonpland (1805) and later, Köppen (1936). Köppen used an empirical classification in which climates are grouped according to specific temperature and aridity criteria. These criteria had been deduced in part from work done by de Candolle (1855). He was also concerned with the distribution of various plant species related to climate.

Most of the earlier schemes relied on two basic criteria—the degree of aridity and of warmth. These criteria also formed the basis for work undertaken by Holdridge (1947). Temperature and precipitation interact through potential evapotranspiration (the amount of evapotranspiration that would occur given an unlimited water supply) to define humidity provinces and so define a functional relationship between vegetation and climate. Box (1981) adopted a similar approach. He introduced a dominance hierarchy of plant growth forms or functional types (e.g. tree, shrub, etc.) and provided more detail on the climate variables used. Both Box and Holdridge predicted vegetation types by correlation. This approach is of limited use in understanding the processes that are occurring between climate and vegetation, although it does provide an indication as to possible mechanisms that might be operating. Their work has also been useful as it demonstrates that important links do exist between vegetation physiognomy (general structure and size) and the climate, where temperature and the water budget represent the climate.

To predict the current distribution of today's vegetation from current

global climate data, one is in effect assuming that global vegetation is in equilibrium with the current climate. In other words, present-day vegetation is a result of present-day climate This is not entirely true because, as Prentice (1986) states: "Vegetation is a dynamical system that is continuously responding to variations in its parameters caused directly or indirectly by the changing climate." He goes on to discuss the various ways in which dynamical systems respond to parameter variation and concludes that there is no single answer to whether vegetation is in equilibrium with climate. It depends on the system under consideration and the response time of the vegetation to the rate of climate change. Each species has its own "fundamental niche" which includes all the environmental conditions it requires to survive assuming no competition or other influences from other species (IPCC, 1996). In reality, in most ecosystems, a species occupies a "realized niche" whereby it competes and interacts with other species. At any given time, an ecosystem consists of a number of species that are within their fundamental niche. If, however, the temperature rises, say, then they may be no longer in this niche and some will begin to die. Alternatively, some species may still be within their fundamental niche but outside their realized niche. The original species' continued survival is then dependent on the other species present in an area. It is not valid to say simply that a specific climate characterizes a specific biome. These systems are in flux and a given vegetation type in a given area is due not only to its climate but also its underlying soils, as well as human activities.

To summarize, an ecosystem is never in true equilibrium with climate but in a state of flux. Evidence for this can be found in the way that species behave in plant communities. These species compete and interact with each other but these processes can change if some kind of disturbance occurs. The process of succession whereby species recolonize an area after disturbance, or a change in soil or climatic conditions, can be described as the outcome of species losses and invasions (Whittaker, 1975). It is known that plant communities will not move together with a changing environment. It is more likely that with this

sequence of invasions and losses completely new communities will be formed as appears to have occurred over the previous 10,000 years since the last Ice Age (Davis *et al.*, 1986; Webb and Bartlein, 1992).

There is also always some lag in the system whereby species take some time to respond to a change in climate. Over the past 10,000 years climate has remained fairly stable (global temperature changes of less than 1 °C over a hundred-year period (IPCC, 1996)). This has given vegetation time to respond and adapt to its new environment. However, now that the human race has begun to influence the amount of pollutants going into the atmosphere, changes are likely to be more rapid. The greenhouse gas, carbon dioxide (CO_2) has increased by nearly a third since the time of the Industrial Revolution. The amount of other greenhouse gases such as methane (CH_4) has doubled and nitrous oxide (N_2O) has increased by 15% (IPCC, 1996) over the same time. These gases are now at their greatest concentrations than at any time over the last 160,000 years (this is as far back as atmospheric compositions can be detected from the analysis of ice-core data (IPCC, 1996)). CO_2 has contributed about 65% of the combined radiative (heating) effects of long-lived gases over the last 100 years. Methane has contributed 20% and nitrous oxide, 5% (IPCC, 1996).

Most climate models predicted a rise in global annual mean temperature of 1 °C over the same period, but there is some debate concerning how much actual warming has really occurred to date (Schneider, 1992). Wigley and Rapier (1990) used a simple one-dimensional climate model of atmosphere and oceans to show that the predicted 0.5 to 1°C warming over the last 100 years or so, broadly agrees with, although is slightly greater than, the observed values. A global mean temperature rise of between 1 and 3.5 °C is predicted for the year 2100 (IPCC, 1996). In order for the distribution of the world's vegetation to respond to this increase in temperature and CO_2, it would need to move at rates never before observed in the natural world. Aber (1992) states that in the central portion of North America, a 3°C increase in mean temperature could lead to a

northward shift of 300–375 km in the biome-climate equilibrium boundaries. This could take place within a hundred years (IPCC, 1990). However, studies on the rate of species re-invasion following the last de-glaciation suggest that species move much more slowly. Davis (1981) gives a rate of 25 to 40 km per century and a maximum distance moved of 200 km.

1.2 Historical evidence of climatic change

Over the last hundred years or so, human disturbances have become increasingly influential on the Earth's climate. The increase in the amount of atmospheric CO_2 has been attributed to increases in fossil fuel use (IPCC, 1990, 1996) and has led to the so-called "greenhouse-effect." This effect is so-called because incoming short-wave radiation from the Sun is transmitted through the Earth's atmosphere which contains the greenhouse gases of methane, water vapour, carbon dioxide and ozone. However, the Earth's surface absorbs just under half of the incoming radiation. The rest is absorbed by clouds, particles and gases (25%) or reflected to space (30%) (Schneider, 1992). The atmosphere with its greenhouse gases traps most of the outgoing terrestrial long-wave radiation (88%). This is also due to absorption and re-emission of this infra-red radiation by clouds and particles in the atmosphere. This keeps the surface and the troposphere (the lowest part of the atmosphere from the surface to around 10–15 km) about 33°C warmer than they would be otherwise (IPCC, 1995). The rest of the terrestrial long-wave radiation "escapes" to space (12%). The clouds and the atmosphere act like the glass in a greenhouse: they allow sunlight in, but prevent heat from escaping.

To consider the climate changes that may occur in the future from current human influences it is important to first consider the past. This should provide some indicators as to the possible impact of high concentrations of CO_2 that have previously arisen naturally, on global climate.

Fluctuations in the Earth's climate occur for a number of reasons. One of these is due to shifts in continental earth masses leading to the creation of mountain chains such as the Alps, Andes, Rockies and the Himalayas. Such mountain chains have a profound influence on the physical properties of air masses, as well as atmospheric circulation patterns. Movements in the position of continents also alter ocean circulation patterns. The ascent or descent of air causes adiabatic (involving no addition or subtraction of heat) changes of temperature caused by changes in pressure. Dynamic processes in the middle and upper troposphere are a major cause of air mass modification (Barry and Chorley, 1976). In addition, mountain climates tend to be windier, wetter, snowier, cloudier and cooler with greater extremes of temperature than at lower levels (Barry and Chorley, 1976; Beniston & Fox, 1996).

Volcanic eruptions cause other fluctuations in climate. They lead either to the creation or destruction of land. They also contribute to the amount of dust in the atmosphere and sulphuric acid aerosols in the stratosphere. The stratosphere is the middle atmosphere, (i.e. the layer above the troposphere that extends upwards to about 50 km (30 miles)). This can cause cooling globally by affecting the global surface energy balance (Turco, 1992). This occurred with the Mount Pinatubo explosion in the Philippines in 1991 which led to a slight decrease in the rate of climate warming. In fact, a cooling of the global surface temperature observed following this eruption reached a maximum of 0.3 to 0.5 °C during 1992 (IPCC, 1995). Volcanic aerosols may also "speed up" certain reactions that lead to substantial ozone depletion in the stratosphere. This should also cause some cooling as ozone is a greenhouse gas. This effect may be enhanced in the future if concentrations of atmospheric concentrations of chlorine continue to increase (Turco, 1992). Other reasons for modification of the Earth's climate are changes in the orbital parameters of the Earth. There are three main variations in these parameters that Milankovitch (Milankovitch (1920, 1930, 1941) cited in Woodward, 1987) describes. These include (Kutzbach, 1992) the following:

i) Changes in orbital eccentricity (range: 0 to 0.06) every 100,000 years. This involves fluctuations in the Earth's orbit from almost circular (which it is at the present) to elliptical.

ii) Changes in the axial tilt (range: 22° to 24.5°) every 41,000 years. The value for the present is 23.4° (Tennent, 1976). An increase in the angle of tilt leads to an increase in the contrast between summer and winter climate.

iii) Changes in the season of perihelion (range: all times of the year) every 22,000 years. At the moment the perihelion (the shortest distance from the Earth to the Sun) is in December. This means that the value of the solar constant (the irradiance of an area at right angles to the solar beam and outside the Earth's atmosphere (Woodward, 1987)) is at its greatest. This situation will reverse in 10,000 years time due to wobble in the Earth's axis. This will lead to the northern hemisphere summer being warmer than the summer hemisphere summer, and to greater differences between summer and winter climates.

New techniques are being used to determine past climates from ice core analysis, soils, lake and ocean sediments (Kutzbach, 1992). Polar ice and deep sea sediment records contain information about leads and lags between climate variables and changes in radiatively active trace gas concentrations (Raynaud and Siegenthaler, 1993). In addition, tree rings (Briffa *et al.,* 1990) and pollen grains (Webb, 1986) can be analysed. More plant samples are also being taken worldwide and dated radiometrically. This radiometric process involves the analysis of the ratio of radioactive carbon isotope, ^{14}C, to the carbon isotope, ^{12}C, in plant material. The carbon isotope, ^{14}C, is one of three naturally occurring carbon isotopes in the Earth's atmosphere, seas and biosphere. However, unlike ^{12}C and ^{13}C, it is unstable. Cosmic rays entering the atmosphere maintain its atmospheric concentration by reacting with nitrogen molecules turning them into ^{14}C (Schneider, 1996). The process of photosynthesis uses all three forms of atmospheric carbon and converts them into organic carbon compounds. Whilst a plant is alive the amount of ^{14}C it contains is in relative equilibrium with that in the atmosphere. However, when the plant dies there is a decrease in

the amount of ^{14}C as it is no longer being replenished. The present-day ratio between carbon isotope, ^{12}C and ^{14}C is assumed to be the same as that at the time when the plant died. Any deviation from this ratio, therefore, gives an estimate as to the possible age of the plant sample.

Clear correlations between CO_2 and global mean temperature are evident in much of the glacial-interglacial palaeo-record (Genthon *et al.* 1987, Jouzel *et al.* 1987, 1993). Temperature increases tend to occur when atmospheric CO_2 concentration increases. Dansgaard *et al.* (1993) measured the amount of oxygen isotope O^{18} in an ice core from the Greenland Ice-core Project Summit. From this they were able to calculate the relative deviation of the oxygen isotope O^{18} to oxygen isotope O^{16} ratio from that in standard mean ocean water. In polar glacier snow and ice, the temperature of the formation of the precipitation mainly determines this deviation (Dansgaard *et al.*, 1993; Johnsen *et al.*, 1992). They present a stable-isotope record from this ice core that shows that marked climate instability appears to have occurred during the last interglacial. This is in contrast to the extremely stable climate of the Holocene (i.e. the last 10,000 years). They suggest that instability has dominated the North Atlantic climate over the last 230,000 years and question how long the Holocene will remain stable given the increase in atmospheric pollution. Genthon *et al.*, (1987) have carried out other work in this field. From the Vostock ice core in eastern Antarctica they derived time series of the central East Antarctic atmospheric temperature and of atmospheric CO_2 content over the last 160,000 years. A signal of around 100,000 years dominates these time series. They also show a concentration of variance near orbital frequencies and suggest that there is an interaction between CO_2, orbital forcing and climate on the time-scale of glacial-interglacial episodes. They performed a multivariate statistical analysis between the Vostock isotope temperature record and multiple climatic inputs. These inputs were:

i) a Northern Hemisphere input of July insolation at 65°N;

ii) a Southern Hemisphere input of either local insolation received during the whole year or mean daily November insolation at 60°S; and

iii) the radiative forcing associated with variations in atmospheric CO_2 concentration. An empirical formula calculated this forcing in terms of its direct temperature effect.

They conclude from their analysis that CO_2 changes play a more important climatic role than orbital variations, though they do stress that orbital forcing is also implicitly present in the CO_2 forcing.

Barnola *et al.* (1987) have also carried out work on the Vostock ice core. They analysed the amount of CO_2 contained in air trapped as bubbles inside the ice and were able to extend the ice core record of atmospheric CO_2 back 160,000 years through the last interglacial-glacial cycle. The very low temperatures at Vostock (present-day mean annual temperature is –55.5 °C) and the high quality of the ice core, which has a length of 2,083 m, enabled them to do this. Over this period they found two very large changes in the CO_2 record. One change occurred in the more recent part of the record (about 400 m depth or 15,000 years ago) when the CO_2 level fell to 190 ppmv. The other change occurred near the earliest part of the record (about 1950 m depth or 140,000 years ago) when the CO_2 level rose to 280 ppmv. This high level is comparable with the "pre-industrial" atmospheric CO_2 level of around 280 ppmv. Of the known geological history of carbon dioxide over the last 100 million years the low level is among the lowest values (Barnola *et al.*, 1987). They suggest that depending on whether the climate shifts from a glacial to an interglacial or vice versa the interactions between climate and atmospheric CO_2 could be different. In the case where conditions are shifting from interglacial to glacial, (i.e. a cooling event), orbital and orbitally derived forcing could have influenced the noticeable cooling trend in the Antarctic. Before the likely climatic effect of the change in CO_2 concentrations this forcing would have been a major contribution to the temperature decrease (Barnola *et* al., 1987).

They suggest also that radiative effect of CO_2 coupled with associated feedback processes appear likely to be one of the stimuli behind the paleo-temperature changes recorded in the Vostock core. This is consistent with the findings of Dansgaard *et al.*(1993) on the same core.

Studies concerned with the links between climate and vegetation, and the climate changes that have occurred in the past have been considered. We can now turn our attention to the problem of trying to recreate such past climates using models. The prediction of possible future climates with an increase in atmospheric CO_2 would be aided by such work.

1.3 Modelling past climates

There needs to be an assessment of the ability and accuracy of the current suite of GCMs (general circulation models) to model past climates before any predictions can be made with regard to likely future climates. The present-day climate can be compared with similar climates in the past and the results of climate change analysed.

Comparison of climates predicted by GCMs with those deduced from the geological record has two main aims:

i) to aid in the analysis of the causes and processes of climatic change, and

ii) to determine how well the models predict palaeoclimates (Guetter and Kutzbach, 1990).

Climatologists now have the opportunity to investigate and determine the processes and feedbacks that are operating to change the climate. This is due to the possibility that relatively small changes in the Earth's orbital parameters essentially drive large climatic changes (see section 1.2).

Various studies have addressed some of the issues of relating climate to vegetation (Guetter and Kutzbach, 1990). The Cooperative Holocene Mapping Project (COHMAP, 1988) used geological data and a GCM to study climatic change in the last 18,000 years. The project assembled near-global data sets of

pollen and land vegetation for this period. The geologic data included pollen analysis from lake sediments, records of water levels in closed-basin lakes, of plankton in ocean sediment cores, and of the amount and orientation of fossil sand dunes. There was a simulation of climates from 18,000 years ago to the present at 3000 year intervals. Webb *et al.* (1987) determined previous vegetation from past climate simulations, and then compared this inferred vegetation with the observed vegetation as estimated from pollen records. Solomon (1986) described attempts to link forest-stand models to climatic variables from GCMs. The comparison of palaeoclimate simulation results from different models should help to isolate model bias errors (Schneider, 1986).

It is also possible to simulate glacial climates with GCMs which is of interest as such climates were very different to those of today. The CLIMAP project (CLIMAP Project Members, 1981) has provided estimates of ice-age conditions such as the extent of ice sheets, vegetation and sea surface temperatures. Large areas of high pressure tend to develop over the ice sheets, temperatures are lower and there is a reduction in precipitation. The levels of atmospheric CO_2 are also reduced. There is still some uncertainty as to changes in the ocean circulation, as well as in the biogeochemical cycles. Recent work by Sutton and Allen (1997) has, however, demonstrated that North Atlantic sea surface temperatures and associated sea-level pressure anomalies are involved in a whole-ocean oscillation. In addition, they show a link between the subtropical and tropical North Atlantic sea surface temperatures which is of specific importance to climate prediction. Further work on modelling the various mechanisms involved is still required.

Other work (Kutzbach, 1992) has used a GCM to model the climate of 9000 years ago when it is known that the orbital parameters were noticeably different from those of the present day. The perihelion (the shortest distance from the Earth to the Sun) was in July and the axial tilt was greater than at present. The solar radiation averaged over the northern hemisphere in July was about 7% (30 W m^{-2}) greater than at present. This period provides information

about what would happen to the climate given an enhanced seasonal cycle in the northern hemisphere caused by greater insolation, and a reduced seasonal cycle in the southern hemisphere. The model showed enhanced summer temperatures over land (temperature increases of between 2 and 4°C) and cooler winter temperatures. There was not much temperature change over the ocean due to its high heat capacity. Northern hemisphere monsoons intensify caused by the differential heating of land and sea. Pressure is lower over the land than over the sea which leads to a larger and deeper area of low pressure over southern Asia and north Africa. This creates strong summer monsoon winds and increases in precipitation in these regions. These effects have been noted from palaeobotanical evidence. For instance, Gallimore and Kutzbach (1989) observed that, 9000 years ago, northern continental summers were warmer inland and drier than at present. Also, between 12000 and 6000 years ago, lakes and savanna vegetation were about 1000 km north of their present location in tropical North Africa (Kutzbach, 1992).

Once a model of a past or present climate is created, one needs to consider the influence of vegetation on such a climate. This is explained in the next section.

1.4 The importance of vegetation to climate

Climate can be defined as the average conditions representative of the long term state of the atmosphere and variability (Barry and Chorley, 1976). In other words it is the average weather over a given period. Large-scale circulation processes mainly influence the climate of a region, but regional and micro-scale processes, which are influenced by the ground surface, also have effects. The magnitude of this influence depends on whether the ground surface is covered by water, ice or snow, urban areas, vegetation or nothing at all. Aspect (i.e. the direction in which a slope faces) and topography are also

important. Only the effect of vegetation on climate is of interest to this thesis, so this is the only land cover type considered here.

The effect of vegetation on climate can be divided into four main categories. These are: energy transfers, momentum flux and airflow, the latent heat flux and the humidity environment, and the sensible heat flux and the thermal environment (Barry and Chorley, 1976; Oke, 1978). Sensible heat is the heat that is released when energy is supplied, or removed from, a body. Latent heat is the heat released when a substance such as water, undergoes a phase change from a vapour (a high energy state) to a liquid (a lower energy state). To enable a substance to change from a liquid at a given temperature to a vapour at the same temperature, heat is required This heat is not sensed as a temperature change but is held within the vapour so that if it reverts to its former state of water it is released (Oke, 1978).
These categories will be considered in turn.

i) Energy transfers.

An important effect of a vegetated canopy such as a forest is to absorb and reflect both incoming and outgoing radiation. The albedo (shortwave reflectivity) of vegetation is dependent on its character (e.g. height, moisture content) and its density. Values range from 18–25% for a short grass crop (Monteith, 1973) to 10% for a fir in a temperate forest (Barry and Chorley, 1976). Higher albedos of 30% to 38% (Barry and Chorley, 1976) occur in desert shrubland. The amount of incoming solar radiation absorbed is higher over a vegetated area and there is less radiation reflected back into the atmosphere than there would be over dry and light-coloured bare ground (Oke, 1978). Vegetation also shades the ground from incoming solar radiation (Dickinson *et al.,* 1986).

The plant canopy absorbs solar radiation. The vertical attenuation of solar radiation affects not only the radiation intensity but also its wavelength, or spectral composition. Plant pigments (e.g. carotenoids and chlorophyll) are particularly good absorbers in the blue (0.4 to 0.51 μm) and red (0.61 to 0.7 μm)

bands of the visible portion of the electromagnetic spectrum and are at the centre of the photosynthetic process. The waveband between 0.4 and 0.7 μm is therefore specified as photosynthetically active radiation or PAR (Oke, 1978). Leaves absorb PAR more strongly than the longer wavelengths of short-wave radiation (i.e. in the near infra-red). This selective absorption reduces the photosynthetic value of the radiation as it penetrates (Oke, 1978). The level of absorption is dependent on crown density, the age and height of the vegetation, as well as the type of vegetation and the time of year. For instance, consider a birch–beech forest. In winter such a forest will have no leaves and between 60–80% of incoming radiation would be able to penetrate to the woodland floor. In summer, this value would be of the order of 5% if the canopy was dense (Barry and Chorley, 1976). If the leaves wilt or are dead then this would decrease the albedo but if they were covered with dew in the early morning this would increase the albedo (Oke, 1978).

ii) Momentum flux and airflow.

Vegetation such as forests obstruct the lateral and vertical flow of air. An area that is forested increases the turbulence of the air above and reduces the wind speed within its interior. If a profile of wind speed against height is drawn for a vegetated canopy it would display a characteristic logarithmic form above the canopy (Monteith, 1973). That is, as the distance from the canopy increases then so does the wind speed. The closer one gets to the top of the vegetation canopy, the lower the wind speed. This is the result of drag exerted on the atmospheric airflow by the top of the canopy. Within the canopy the profile would be dependent on the structure of the vegetation. In most cases the wind speed would be lowest in the areas where the foliage density was greatest (i.e. near the crown in a tree canopy). It would be slightly higher in the more open stem area and then decrease to zero at the ground (Oke, 1978).

iii) Latent heat flux and the humidity environment

The humidity within a forest differs markedly from that outside. Evaporation from the forest floor is usually much less due to lower wind speeds, lower maximum temperatures, lower incoming solar radiation and generally lower forest air humidities (Barry and Chorley, 1976). During the hours of daylight leaves transpire water through their stomata. This process is controlled by wind speed around the leaf, leaf temperature, vapour pressure deficits, available radiant energy, the length of day and the leaf surface area, the tree species and its age.

The vegetated canopy can intercept precipitation. This amount of interception varies with the time of year, the crown density and rainfall intensity. Throughfall is the amount of incoming rainfall that reaches the ground surface after allowing for interception by the vegetation. Some of the intercepted water evaporates whilst the remainder is added to throughfall, as leaf drip and as stemflow (water flow down the stems and branches). Throughfall decreases as the amount of leaves in the canopy increases (Rutter *et al.*, 1975).

iv) Sensible heat flux and the thermal environment

The air temperature is reduced within a forest, but extremes of temperature are not encountered (i.e. there is a smaller amplitude of diurnal temperature compared with outside the forest). This is due to the limited temperature range caused by protection from the insulation effect and shelter provided by the trees (Barry and Chorley, 1976). During the day the crown of a forest is warmer than the floor due to evapotranspiration and radiative heating. Beneath this canopy there is a temperature inversion where the temperature decreases with depth. This situation reverses at night. Below the canopy there is little long-wave radiation loss and hence milder conditions prevail to those outside the forest. The greatest frost and dewfall occur therefore just beneath the canopy crown (Oke, 1978).

All these processes need to be taken into account when constructing models of the soil-Earth-atmosphere system. Such models are now considered.

1.5 Models

Vegetation models can be divided into three main groups (Foley *et al.*, 1996). These groups are: biogeographical, biogeochemical and biophysical (or land surface climatology) models. Each of these groups will be considered.

1.5.1 Biogeographical models

Ecologists such as Woodward (1987), Emanuel *et al.*, (1985a, b), and Smith *et al.*, (1992) have produced ecologically–based biogeography models. These predict the current distribution of the world's vegetation to determine the future distribution. Other biogeographical models include those from Prentice (1990) and Haxeltine *et al.* (1996) who developed and used the BIOME model and Nielson (1995) who created the MAPPS model. These particular models, however, are of limited use as they are constrained by their specific use of parameters set for present-day biomes though they do indicate the sensitivity of vegetation to climate change. Biogeographical models predict the potential natural vegetation for a given climate and soils input, but no account is taken of human interference and influence. They are also static so that a given climate will produce a given vegetation but there is no account of transient dynamics. This means that ecological responses to climate change such as migration cannot yet be modelled. Such models simulate current vegetation patterns and predict likely vegetation changes with a change in climate. However, they do not account for changes that may arise from the vegetation influencing climate.

1.5.2 Biogeochemical models

There are a variety of biogeochemical vegetation models that have been designed to predict vegetation at different scales of study. Ryan *et al.*, (1996, I and II) reviewed seven models of ecosystem function for temperate conifer forest and divided the models into four classes based on their resolution. These models included BIOMASS (McMurtrie *et al.*, 1990b, 1992; McMurtrie and Landsberg, 1992), BIOME-BGC (Running and Hunt, 1993) and HYBRID (Friend *et al.*, 1993) at the plant physiological level. CENTURY (Parton *et al.*, 1987) is classified as an ecosystem model, as are the following: MBL-GEM, which is a process-based biogeochemical model (Rastetter *et al.*, 1991), PnET-CN (Aber and Federer, 1992), a simple, lumped-parameter monthly-time-step model of carbon and water balances of forests, and Q, a forest growth model developed by Rolff and Ågren (in preparation). Other models that were not compared by Ryan *et al.* (1996, I and II) include, at the regional to global scale, the models developed by Raich *et al.* (1991) and McGuire *et al.* (1992) and, at the patch scale, the population models (JABOWA /FORET) of Botkin *et al.* (1972), and Shugart (1984). In the JABOWA /FORET models, individual trees are allowed to grow and compete for light against each other, and use population dynamics. Some of these models were concerned with specific vegetation types or regions, initially, but have gradually developed and expanded to the global level (Running and Hunt, 1993; Parton *et al.*, 1993; Melillo *et al.*, 1993; Raich *et al.*, 1991; McGuire *et al.*, 1992). It should be noted that all of these models have constrained behaviour because of set-up values. In effect, they need to be "told" something about the vegetation types they are modelling.

Ryan *et al.* (1996) stress that when selecting a vegetation model one needs to consider both the time-scale and spatial scale of the processes being considered. In addition to this, population and ecosystem models require details from physiologically-based models to ensure that calculations of growth processes are realistic and that climate change can be dealt with adequately.

Urban and Shugart (1992) reviewed several gap models, which have been developed from a forestry background. When a tree dies and falls to the ground, it creates a gap in a forest. This gap allows other trees to become established and grow within this space. At any one time a forest can contain a selection of gaps, each of which is at various stages of the growth cycle. Ågren *et al.*, (1991) also studied and compared a variety of different models used to determine ecosystem response to climate change. The ecosystems considered were grasslands and coniferous forests.

To determine the combined effects of both climate and atmospheric chemistry on terrestrial carbon balances, models, based more on the physiology of ecosystem function, can be used (Aber, 1992). Such models include LINKAGES (Pastor and Post, 1986), which is specifically concerned with plants in the eastern U.S. It operates using plant responses to light, nitrogen, growing season heat sum, and water stress. FORENA (Solomon, 1986) is a similar model which is based on the plot, individual stem, and species level. The CENTURY model can also be classified as a physiologically-based model of ecosystem function, particularly regarding grasslands.

1.5.3 Biophysical models

At the same time as these ecological models have been developing, climatologists have been examining ways of incorporating vegetation into GCMs. Shukla and Mintz (1982) were the first to use a simple model to demonstrate the significant impact that vegetation could have on climate by affecting the hydrological cycle, the carbon cycle and energy transfers between the Earth's surface and the atmosphere.

Until about 10 years ago, the land surface properties regulating the momentum, latent and sensible heat fluxes between the land surface and the atmosphere were regarded as parameters that could be prescribed within a general circulation model (GCM) (Sellers, 1992). This led to a number of errors with such models. Surface albedos were deemed to be too low, surface

roughness parameters were inadequate (there was often one value used globally), and the amount of moisture in the soil also often had one global value held in a "bucket." In addition, surface resistance in the Penman–Monteith equation was not adequately accounted for, which led to an overestimation of surface evaporation in humid regions (Sellers, 1992).

Since the mid-1980's this situation has improved. Dickinson (1984) and Sellers *et al.,* (1986) made some of the first attempts to model the land surface parameters from a biophysical (land surface climatology) standpoint. Dickinson *et al.* (1986) developed the BATS model, Sellers *et al.* (1986, 1992), the SiB model, and more recently, the SiB2 model (Sellers *et al.,* 1996a, b, c). Such models operate globally with vegetation and soil characteristics geographically predefined.

The climate from GCMs can be used in a number of ways by ecological modellers. For instance, climate has been used in a number of ecological models to determine the current distribution of biomes, (Emanuel *et al.*, 1985a, b; Prentice *et al.,* 1992; Woodward and Lee, 1994) net primary productivity, (NPP) (Raich *et al.* 1991; Lieth, 1975) and leaf area index (LAI) (Neilson and Marks, 1995). Global ecosystem sensitivity to climate can be determined and be incorporated into global carbon cycle models such as those by Dai and Fung (1993). Quantitative tests of vegetation model simulations of NPP and LAI against water and carbon flux simulations could be carried out applying the methodology used in intercomparison projects such as the Project for Intercomparison of Land Surface Parameterization Schemes (PILPS) (Henderson-Sellers *et al.*, 1995).

Vegetation in most GCMs is prescribed with set values for parameters such as roughness length or rooting depth. There are no changes with time. This is an unsatisfactory situation, as a number of authors (Rowntree, 1988; Sellers *et al.*, 1996a, b, c; Randall *et al.,* 1996; Henderson-Sellers and McGuffie, 1995; Bonan *et al.*, 1992; Foley *et al.*, 1994) have shown that land surface cover in

GCM simulations affects the climate. To simulate climate change effects accurately, there needs to be inclusion of an interactive global vegetation. This would also enable the prediction of future vegetation given a future climate.

To summarize, the main problem with the biophysical models is that they ignore changes in vegetation cover, as their vegetation characteristics and soil are prescribed. The overall problem with biosphere models is that they do not model the dynamic behaviour of ecosystems. There is a requirement for the incorporation of such dynamics to deal with changing land use, increasing CO_2 and climate.

The global productivity and phytogeography model introduced by Woodward *et al.* (1995) addressed some of these problems. It was able to predict LAI and NPP from simple climate inputs. Representations of basic plant processes were combined to successfully model vegetation responses to environmental change that enabled vegetation response mechanisms to be identified.

This thesis is concerned with the model, DOLY. This has been developed from the model described by Woodward *et al.* (1995). This model has been improved so that it is able to incorporate soil feedbacks using the CENTURY model (Parton *et al.,* 1993), has a better hydrological sub-model incorporating the water dynamics used by the CENTURY model, and is able to run with transient climate data. The model's sensitivity to its soils and climate inputs is examined and discussed. In addition, DOLY has been coupled with the UKMO GCM to model feedback effects between climate and vegetation both for the present day and for a $2 \times CO_2$ climate. There is a simulation of the effects of climate change on global vegetation using DOLY and a life-form (functional type) model. Also, the latest transient climate data from the UKMO are used to demonstrate likely changes in LAI and NPP between now and the end of the 21st century.

1.6 Form of thesis

This thesis is divided into two sections. The first section concerns model development, and the second section concerns the applications of the model output.

Chapter 2 introduces the World and DOLY models. There is a description of the development from the prototype presented by Woodward (1987) to the present model, DOLY. The following two chapters examine the sensitivity of the DOLY model to changes in soils and climate inputs. The remaining chapters consider the applications of the model output. Chapter 5 examines the impact of climate change simulations on NPP and LAI, and shows maps of functional types derived from a life-form model. An example of the change in tree cover at the boreal forest and tundra boundary provides a case study. In Chapter 6, DOLY and the United Kingdom meteorological office (UKMO) general circulation model are coupled to determine the impact of vegetation and the effects of feedbacks on the GCM. Chapter 7 considers the effect of using of different climate datasets on the DOLY model outputs. A chapter then follows on the effect of climate change, as simulated by the transient data from the GCM, on LAI and NPP values. There is an attempt to validate the outputs of LAI and NPP from DOLY against field and satellite data in Chapter 9. The thesis concludes with a discussion of the results obtained.

1.7 Aims of thesis

i) To determine the distribution of global vegetation and the effects of climate change on that vegetation using a simple **Dynamic Global** Phytogeography model, (DOLY) and a life–form (functional type) model.

ii) To use the output from the DOLY model in a general circulation model (GCM) to determine the feedback effects of vegetation on climate.

iii) To use the output from the DOLY model to determine the changes in LAI and NPP with a transient change in climate.

CHAPTER 2

2 Model development

2.1 Introduction

Most of the results presented in this Ph.D. have been obtained from runs of the Dynamic Global Phytogeography Model (DOLY), described in Woodward *et al.* (1995). This model was developed from an earlier and simpler water-based model called World, which in turn was derived from a model described by Woodward (1987). Other models have since been developed to create the more recent DOLY model which can operate with soil feedbacks.

This chapter will describe each of these models in turn and their contribution to the development and creation of the water and soil feedback version of DOLY. Examples of output from the World model will be shown and limitations of this model discussed. DOLY will also be described together with details of modifications made to the water initialisation and the soil feedbacks. A life-form model was developed to determine the distribution of functional types calculated from net primary productivity (NPP) and leaf area index (LAI). This is described in detail in Chapter 5.

2.2 World

In the introduction to this thesis the need was stressed for a global vegetation model that is able to interact with the global climate to give the current distribution of the world's vegetation. Such a model would enable the ecological community to look forward and predict what will happen to the world's vegetation in the future with a change in climate. A global vegetation

model is also required by the United Kingdom Meteorological Office (UKMO) to be used in conjunction with their general circulation model (GCM) to enable a more representative vegetated surface to be incorporated into the world's climate.

The aim of this section is to introduce and describe a simple biogeography model called World and to discuss its development. Global maps of LAI and NPP will be presented. NPP is the rate of production of biomass by green plants in a year (gC m^{-2} yr^{-1}or tC ha $^{-1}$ yr^{-1}). Problems involved with World will be discussed and the following section (2.3) will introduce the more advanced successor to this model, DOLY.

World is a simple mechanistic model. A prototype was described in Woodward (1987), and later in Woodward (1993). World relies on a water balance approach to predict leaf area index, which is defined as the amount of leaf per unit area of ground (m^2 leaf /m^2 ground). Woodward (1987) made three assumptions:

i) as LAI increases then so does transpiration,

ii) throughfall (the amount of precipitation reaching the ground (including stemflow) after interception by the vegetation and evaporation off the vegetated surface) decreases as LAI increases and is the only source of water for transpiration, and finally,

iii) vegetation will have the maximum LAI that can be supported in terms of transpiration.

The model is run with several values of LAI to determine the equilibrium value of LAI for hydrological balance. In other words, the LAI for a given site is assumed to correspond to the value for which evapotranspiration matches precipitation. The model is driven by climate data inputs recorded at a standard meteorological site: monthly totals or means of precipitation, solar radiation, air temperature, relative humidity and wind speed close to the land surface. Evapotranspiration is calculated using the Penman–Monteith equation (Monteith, 1973) and general formulae are used to determine boundary layer

and stomatal conductances (Monteith, 1973; Grace, Fasehun and Dixon, 1980; Jones, 1983).

A number of alterations have been made to this prototype to enable the model to operate with other climate datasets. In addition, the model has been extended to predict net primary productivity. Water use efficiency and evapotranspiration are used to determine the gross yield and a respiration term is subtracted to give NPP. Furthermore, improvements have been made to calculations used within the model, such as boundary layer conductance and stomatal conductance.

The original use of this model was to predict the distribution of global vegetation from the water balance alone, and to determine the impact of climate change on this distribution. This was not an easy task as a number of other variables, for instance soils, also influence global vegetation distribution through the carbon and nitrogen cycles. A number of problems were encountered in achieving these aims and they are discussed in section 2.2.8.

Figure 2.1 shows how climate inputs, solar radiation and atmospheric CO_2 are used in the various processes within the World model. The links between these processes are also displayed. Humidity is used to calculate vapour pressure deficit but is not shown. Additional inputs of canopy details, which influence soil water and evapotranspiration, and site details, which influence solar radiation, are also not shown but they are described in section 2.2.1.

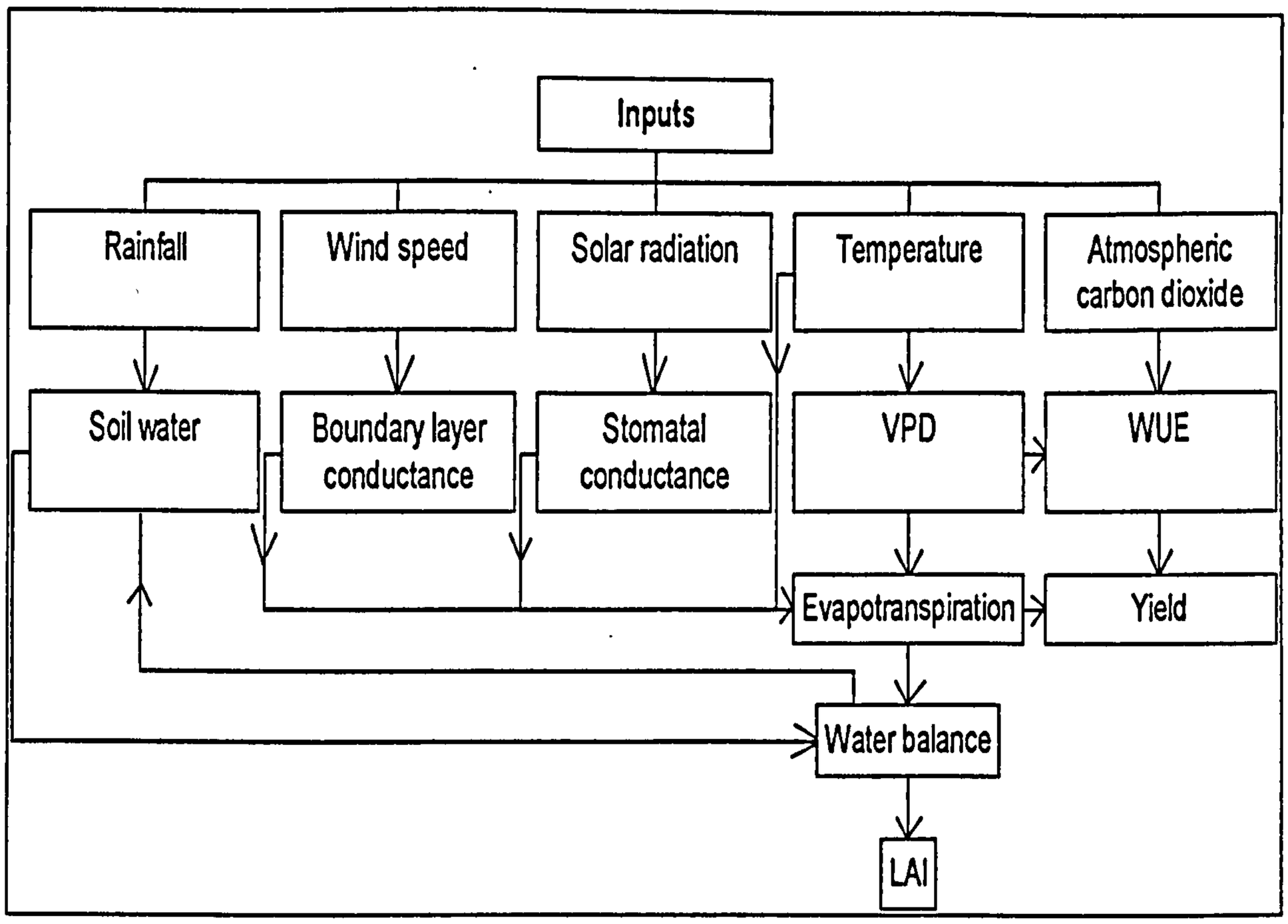

Figure 2.1 The main inputs, processes and outputs of the model World.

The following sections provide additional details on the World model and the response of its variables to environmental inputs. Sections 2.2.1 to 2.2.3 describe all the inputs to World, and the calculation of stomatal conductance and boundary layer conductance. Section 2.2.4 is concerned with evapotranspiration, and its sensitivity to changing temperature and vapour pressure deficit. The water balance calculation used by the World model is described in section 2.2.5 and section 2.2.6 describes how water use efficiency is calculated and used with evapotranspiration to determine yield and NPP. Finally, in sections 2.2.7 and 2.2.8 the LAI and NPP results are presented and discussed.

2.2.1 Inputs to World

There are three main inputs into the World model: climate, canopy details and site details. The site details consist of the latitude and longitude of the site. The latitude is used together with the solar declination to calculate the solar radiation at the Earth's surface. The values of the solar declination vary through the year. The value for the 15th day of each month was used within the program in order to speed computation. The canopy details are the leaf dimension (cm), throughfall (%), canopy reflectivity (%), and the amount of LAI, at each of six canopy levels (strata). The total leaf area is divided into these six strata. Stratum one is the herbaceous layer, at ground level. Strata two and three form the boundary beneath the main canopy crown, which has the greatest leaf area density in stratum five. All these parameters are set for LAI values ranging between 1 and 9 at the start of the program and were derived by Woodward (1987) from a variety of publications. The leaf dimension is the characteristic dimension which is related to the mean width of the leaf, and increases as the leaf area index increases. Throughfall is the percentage of incoming rainfall that reaches the ground surface after allowing for interception by the vegetation (remaining as a thin layer of surface water on leaves, branches and trunks). Some of the intercepted water evaporates whilst the remainder is added to throughfall as leaf drip. No allowance is made for stemflow. Throughfall decreases as the leaf area index increases (Rutter *et al.*, 1975). Canopy reflectivity (albedo) also varies with leaf area index, ranging in value from 15 to 19 % with a mean value of 16 % (Woodward, 1987). These parameters are shown in Tables 2.1 and 2.2.

Table 2.1 Values of throughfall, canopy reflectivity and leaf size for values of LAI from 1 to 9

Parameter	LAI ($m^2 m^{-2}$)								
	1	2	3	4	5	6	7	8	9
Throughfall (%)	95.0	93.5	92.0	90.5	89.0	87.5	86.0	84.5	83.0
Canopy reflectivity (%)	19	18	17	16	15	15	15	15	15
Leaf size (cm)	0.50	0.75	1.00	1.75	2.50	3.75	5.00	6.75	7.50

Table 2.2 The distribution of LAI through the six strata of the canopy for values of LAI from 1 to 9.

LAI	LAI for each stratum (1 to 6)					
	1	2	3	4	5	6
1	0.10	0.50	0.20	0.05	0.05	0.10
2	0.20	0.90	0.56	0.07	0.07	0.20
3	0.30	1.30	0.90	0.10	0.10	0.30
4	0.40	1.55	1.00	0.55	0.15	0.35
5	0.50	1.80	1.10	1.00	0.20	0.40
6	0.50	2.15	1.50	0.95	0.30	0.60
7	0.50	2.50	1.90	0.90	0.40	0.80
8	0.50	2.50	2.20	1.55	0.45	0.80
9	0.50	2.50	2.50	2.20	0.50	0.80

The climate data were obtained from Müller (1982) which contains climate data for around 2000 stations, world-wide, and includes the following variables for each month:

i) mean daily temperature (°C),

ii) temperature range (°C), i.e. mean daily maximum temperature minus mean daily minimum temperature,

iii) absolute minimum temperature (°C),

iv) mean relative humidity (%),

v) mean monthly precipitation (mm),

vi) solar radiation (ly day^{-1}),

vii) mean wind speed (m s^{-1}) for each month.

Due to its better spatial coverage, the IIASA climate dataset (Leemans and Cramer, 1991) was used in later versions of the World model. This is on a 0.5° latitude by 0.5° longitude grid, but has fewer variables than Müller. Precipitation and temperature data from IIASA were used in the model, together with humidity data supplied by Rik Leemans (pers. comm. 1993). The wind speed had to be set to a global value of 2 m s^{-1}, as these data were not available globally on this grid. Solar radiation was calculated from the latitude of the site, solar declination (Jones, 1983), the solar constant and attenuation in the atmosphere. Further details are given in the next section. Absolute minimum temperature was calculated from the mean temperature using the following formula supplied by Dr. Tom Smith, Department of Environmental Sciences University of Virginia.

$$t_{abmin} = 1.3t - 20 \qquad \textbf{(2.1)}$$

where t_{abmin} is the absolute minimum temperature (°C) and t is the monthly mean temperature (°C).

This absolute minimum temperature formula gives similar results to the formula used by Prentice *et al.* (1992), which is also based on the mean temperature at a site. It is used as a threshold value for different functional types of vegetation (see Chapter 5). Further details will be given later in this chapter. Wind speed is used in the calculation of boundary layer conductance, which in turn is used within the Penman–Monteith equation for evapotranspiration.

2.2.2 Solar radiation and stomatal conductance

Incoming solar irradiance (W m^{-2}) at the Earth's surface, for an average day of a given month is calculated from the latitude and solar declination. Solar declination, δ, is calculated using the formula from Jones (1983):

$$\delta = -23.4 \times \cos\left(\frac{360(T_d + 10)}{365}\right) \quad \textbf{(2.2)}$$

where T_d is the number of the day in the year. T_d = 1 on January 1st. Note that solar declination is zero at the equinoxes, –23.4 at the winter solstice and 23.4 at the summer solstice. The values used in the model are shown in Table 2.3

Table 2.3 Solar declination for the middle day of each month through the year.

Month	1	2	3	4	5	6
Solar Declination	–21.3	–13.7	–2.9	9.3	18.7	23.3
Month	7	8	9	10	11	12
Solar Declination	21.5	13.8	2.3	–9.5	–16.4	–23.3

The solar irradiance, S, at each hour of the day has been predicted from daily published integrals by the following:

$$S = S_m(\sin\ \phi \sin\ \delta) + (\cos\ \phi \cos\ \delta \cos\ h) \quad \textbf{(2.3a)}$$

The maximum daily solar irradiance S_m (W m^{-2}) received at the Earth's surface is calculated from the incoming solar radiation, both direct and diffuse, with allowance for the depth of the atmosphere, absorption by the atmosphere and cloud cover (Woodward, 1987; Jones, 1983):

$$S_m = \frac{\Sigma S\pi \times 0.55 \times 1360 \times 0.7^{1.32}}{2N \times 3600} \quad \textbf{(2.3b)}$$

where ΣS is the published daily integral of irradiance, the solar constant (incoming solar radiation on an area at right angles to the solar beam and

outside the Earth's atmosphere) has a value of 1360 W m^{-2}, and mean atmospheric transmittance is set as 0.7 which is close to a value for a clear dry atmosphere (Woodward, 1987, derived from Gates, 1980).

The daylength, N (hrs) is estimated from:

$$N = \frac{2 \sec h}{15} \tag{2.4}$$

where

$$\cos h = \frac{-(\sin\phi \sin\delta)}{(\cos\phi \cos\delta)} \tag{2.5}$$

and h is the time measured as an hour angle, sec h is the secant of the hour angle, ϕ is the latitude and δ is the solar declination (Gates, 1980; Woodward and Sheehy, 1983). The hour angle of the sun is the measure of time from solar noon and one hour is equivalent to 15°. At solar noon cos h = 1. The daylength is converted to seconds by multiplying by 3600 (seconds in an hour). The depth, or air mass, m, of the atmosphere, is related to the solar zenith angle and increases with latitude. It is set as a mean value of 1.32 in World (z = 41°) from Jones (1983). There is also an adjustment for cloud cover, and a global mean value of 55% was chosen (the global range is of the order of 40 to 70% (Woodward, 1987)).

Leaf area is divided into six strata (see Table 2.2). The average irradiance on a horizontal surface below a leaf area index, L_a, is derived from Beer's law (Woodward, 1987):

$$I = I_0 e^{-kL_a} \tag{2.6}$$

where

I_0 is the irradiance at the top of the canopy (W m^{-2}). The parameter, k, is an extinction coefficient; a typical value is 0.5, which was used in the program.

Leaf stomatal conductance, s_c is calculated from (Jones 1983; Woodward, 1987):

$$s_c = \frac{1}{\left(r_{min} + \frac{b}{I_L} \right)} \qquad (2.7)$$

where r_{min} is the minimum stomatal resistance and b is a measure of the sensitivity of stomatal resistance, r (=$1/s_c$), to the radiant flux on a unit area of leaf surface, I_L. A fixed value of 400 s m^{-1} was selected for r_{min} on the basis of a review by Körner, Scheel and Bauer (1979) who found that this was a typical mean value for a variety of floras. This is itself no doubt dependent on vapour pressure deficit. The sensitivity of stomatal resistance to irradiance, b, has a value of 29500 s m^{-1} W m^{-2}, which predicts significant increases in stomatal resistance at irradiances below about 200 W m^{-2}.

In order to calculate canopy stomatal conductance, g_c , the leaf stomatal conductance, s_c is integrated through all the layers of the canopy:

$$g_c = \int_0^L s_c dL \qquad (2.8)$$

where L is the leaf area index of the canopy.

This equation may be integrated analytically for simple light response curves such as equation 2.7 providing that Beer's law can be assumed to hold with a vertically uniform extinction coefficient. The data from Table 2.2 are therefore not used here. Substituting equations 2.6 and 2.7 into 2.8 gives the following integral:

$$g_c = \int_0^L \frac{I_0 e^{-kL}}{a I_0 e^{-kL} + b} dL \qquad (2.9)$$

where a is r_{min} and b is 29500 s m^{-1} W m^{-2}.

Integrating equation 2.9 gives:

$$g_c = \frac{1}{ka} \ln \left\{ \frac{aI_0 + b}{aI_0 e^{-kL} + b} \right\} \qquad \textbf{(2.10)}$$

The integration for equations 2.8 to 2.10 was calculated by Dr. Peter Cox of the Hadley Centre.

Prior to this calculation, and in earlier versions of World, canopy stomatal conductance was calculated using LAI, the leaf stomatal conductance values and the LAI for each stratum. The LAI for each stratum of the canopy was multiplied by the leaf stomatal conductance for that stratum and this product was added to that for the stratum above.

For example, the canopy stomatal conductance down to stratum 3 in the canopy would be:

$$g_{c3} = g_{c4} + (s_{c3} \times L_3) \qquad \textbf{(2.11)}$$

where

g_{c3} is the canopy stomatal conductance from stratum 6 (top) to 3 for a given LAI.

g_{c4} is the canopy stomatal conductance from stratum 6 (top) to 4 for a given LAI.

s_{c3} is the leaf stomatal conductance for stratum 3 for a given LAI

L_3 is the LAI for stratum 3

The new equation (2.10) for stomatal conductance avoids the need to divide up the values of LAI according to depth within the canopy, and is a much simpler equation to use. Figure 2.2 shows how canopy stomatal conductance varies with incoming solar radiation and LAI. As the LAI increases then canopy stomatal conductance increases for the same solar radiation value. There is also a greater range of canopy stomatal conductance values with higher LAI values than with the lower values.

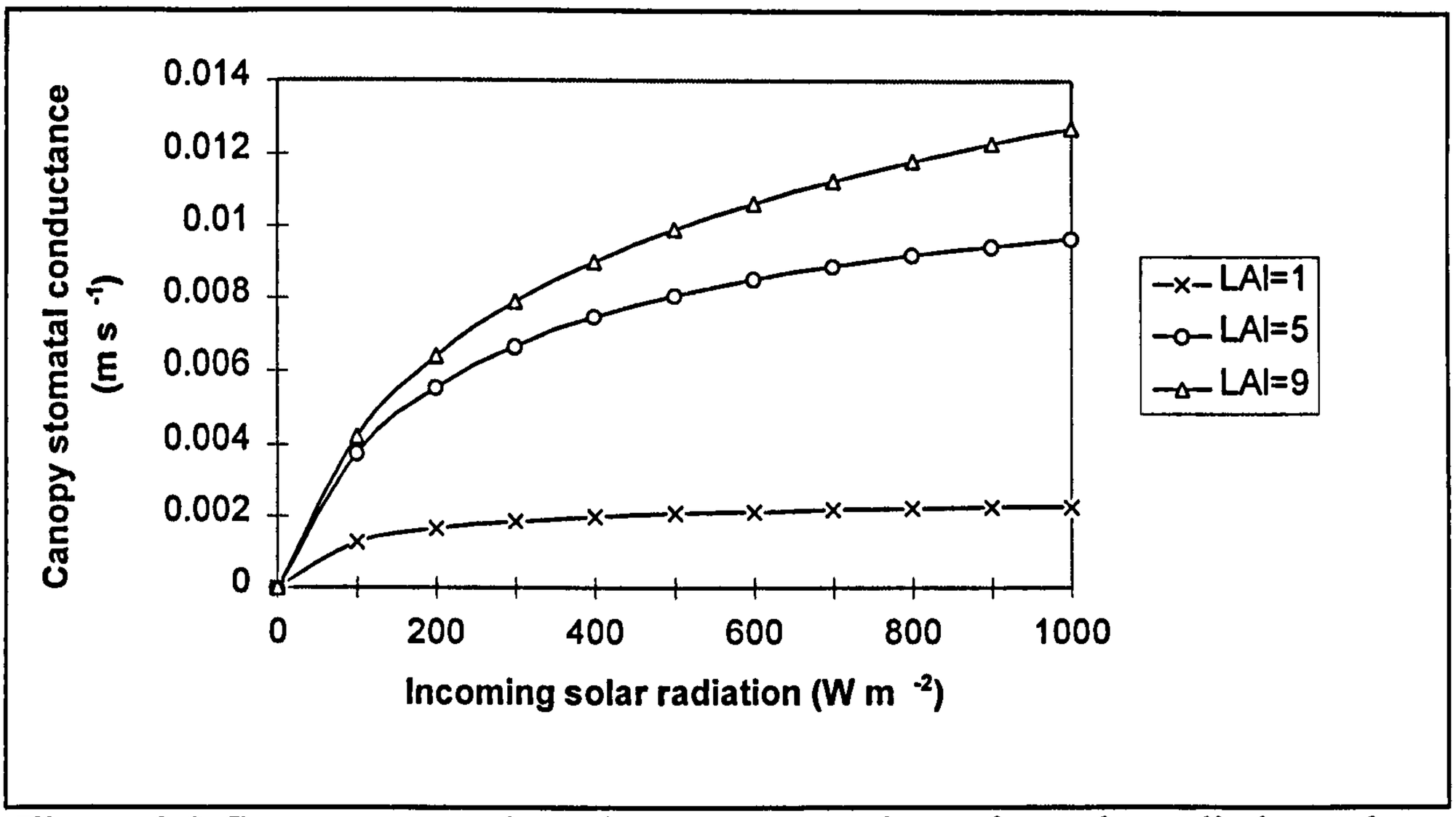

Figure 2.2 Canopy stomatal conductance versus incoming solar radiation values for three values of leaf area index (LAI), 1, 5 and 9.

To further improve the calculation of canopy stomatal conductance within World and to replace the single global value of r_{min}, which is clearly unsatisfactory given the variety of vegetation types and climates across the world, a look-up table was incorporated into the model. In fact, from Körner *et al.* (1979), the range of maximum stomatal conductance values for woody plants was 0.1 to 0.5 cm s^{-1} (1000 to 200 sm^{-1} minimum stomatal resistance) and, for herbaceous plants, 0.2 to 1.4 cm s^{-1} (500 to 71 sm^{-1} minimum stomatal resistance) with a value of 0.6 cm s^{-1} (167 sm^{-1} minimum stomatal resistance) occurring most often. The look-up table was produced using data from Woodward and Smith (1994b). They showed how both stomatal conductance and photosynthesis varied globally in response to temperature, irradiance, vapour pressure deficit (VPD) and soil types. They used the Holdridge life-zone classification to divide up the major biomes of the world on the basis of annual precipitation, potential evapotranspiration and annual biotemperature. Biotemperature is defined as the average of the temperatures (daily, weekly or monthly) through the year that exceed 0 °C. If temperatures equal or are below 0°C then they are set to 0 °C. Woodward and Smith

(1994b) then extracted maximum stomatal conductance values from experimental data, obtained by Körner (1994), and Woodward and Smith (1994a), for each of these biomes. Using the Leemans and Cramer (1991) climate dataset to obtain the monthly mean temperature and annual precipitation of each 0.5 by 0.5 degree grid cell it is possible to derive an annual average climate. This climate is used to define the expected biome from the Holdridge classification and the associated maximum stomatal conductance for each cell. The following table (Table 2.4) was produced for the 36 biomes. The asterisk (*) denotes biomes for which the model predicted value of G_{max} (mmol H_2O m^{-2} s^{-1}) from Woodward and Smith (1994b) has been used due to the lack of an observed value.

Table 2.4 Biome number, description, and maximum stomatal conductance (G_{max}) predicted on the basis of mean monthly temperature and annual precipitation limitations by Woodward and Smith (1994b).

Biome Number	Description	Maximum stomatal conductance (mmol m^{-2} s^{-1})
1	Polar dry tundra	150
2	Polar moist tundra	260
3	Polar wet tundra	290
4	Polar rain tundra	160
5	Boreal desert	180
6*	Boreal dry bush	249
7	Boreal moist forest	240
8	Boreal wet forest	240
9	Boreal rain forest	170
10	Cool temperate desert	202
11	Cool temperate desert bush	240
12	Cool temperate steppe	287
13	Cool temperate moist forest	300
14	Cool temperate wet forest	196
15	Cool temperate rain forest	190
16	Warm temperate desert	100
17	Warm temperate desert bush	262
18	Warm temperate thorn steppe	281
19	Warm temperate dry forest	285
20	Warm temperate moist forest	390
21	Warm temperate wet forest	290
22	Warm temperate rain forest	180
23	Subtropical desert	100
24	Subtropical desert bush	205
25	Subtropical thorn steppe	273
26	Subtropical dry forest	330
27	Subtropical moist forest	407
28*	Subtropical wet forest	392
29	Subtropical rain forest	320
30	Tropical desert	120
31*	Tropical desert bush	41
32*	Tropical thorn steppe	82
33	Tropical very dry forest	400
34	Tropical dry forest	354
35	Tropical moist forest	482
36	Tropical wet forest	320

Mean monthly temperature and annual precipitation values were calculated from the Leemans and Cramer (1991) dataset and, by using Table 2.4 as a look-up table within World, the appropriate maximum stomatal conductance value was extracted. The evapotranspiration calculation (equation 2.17) includes conductances in non-molar units (m s^{-1}). This stomatal conductance value was therefore converted using equation 2.12 and the reciprocal taken to obtain the minimum stomatal resistance (r_{min}).

Non-molar canopy stomatal conductance (g_c) is calculated as follows:

$$g_c = \frac{RT_k g_{cmol}}{1000P_a} \qquad \textbf{(2.12)}$$

g_c is in units of m s^{-1},

g_{cmol} is in units of mmol m^{-2} s^{-1},

P_a is atmospheric pressure at sea level, Pa; set as a constant for sea-level pressure, 101325 Pa,

T_k is absolute temperature (kelvin) derived by adding 273 to the mean monthly temperature value.

R is the gas constant =8.3144 J mol^{-1} K^{-1}.

The minimum stomatal resistance value was then used as variable, a, in equation 2.10. Figure 2.3 shows the values of canopy stomatal conductance for a range of G_{max} values.

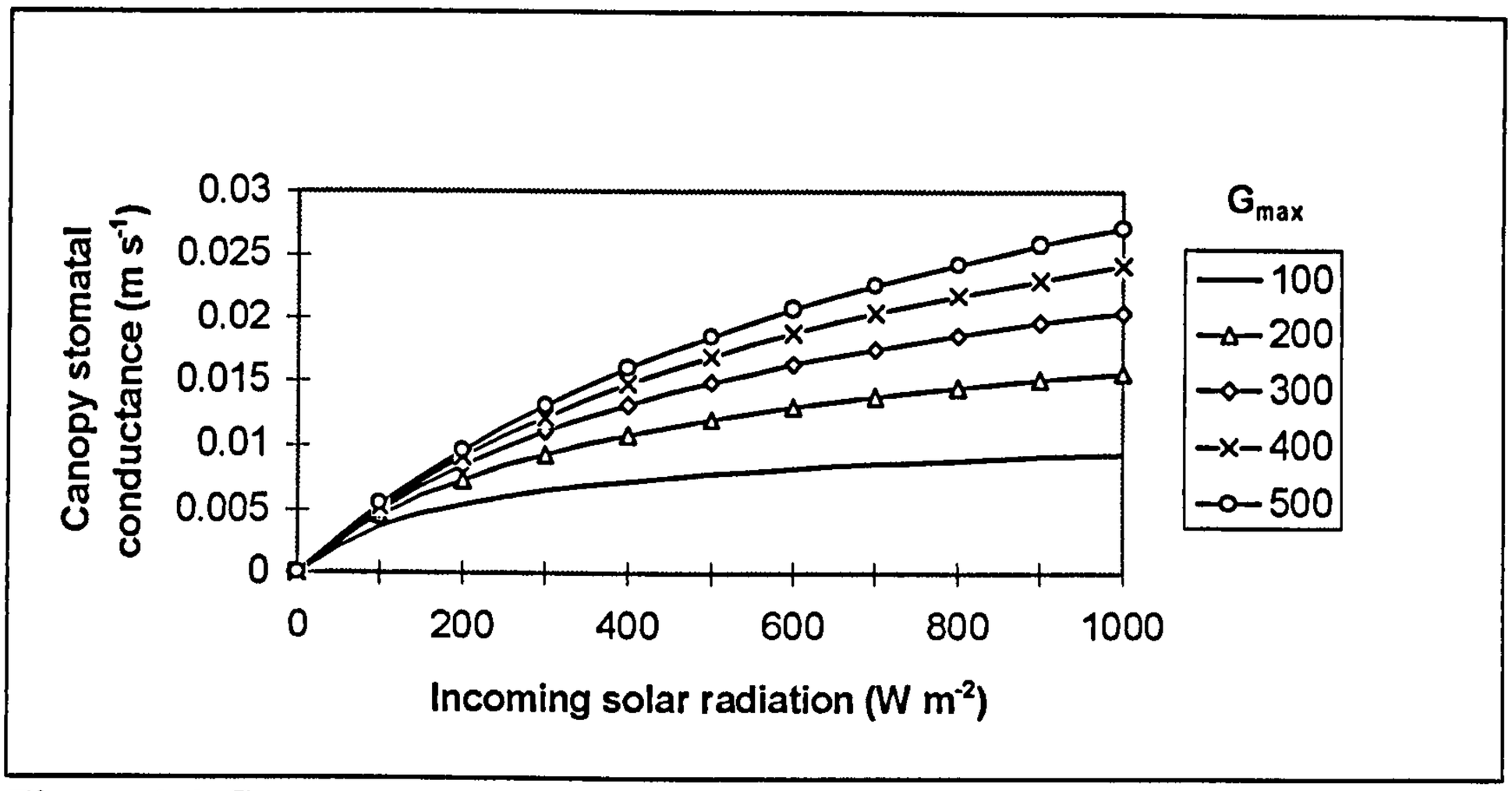

Figure 2.3 Canopy stomatal conductance for a range of incoming solar radiation values and for different G_{max} values (mmol m^{-2} s^{-1}). The LAI is 5 and the temperature is 15°C.

Comparing Figure 2.3 with Figure 2.2 it can be seen that the canopy stomatal conductance values for an LAI of 5 in Figure 2.2 are close to those for the G_{max} value of 100 mmol m^{-2} s^{-1} in Figure 2.3. This is due to the fact that the r_{min} value of 400 s m^{-1} is close to the G_{max} value of 100 mmol m^{-2} s^{-1} at a temperature of 15°C. It can also be seen that by using higher values of G_{max} the canopy stomatal conductance increases for a given solar radiation. This comparison highlights the limitation of using just one global value for stomatal resistance. The G_{max} value of 100 mmol m^{-2} s^{-1} occurs in many arid areas, as shown in Table 2.4 and caused the World model to predict lower values of canopy stomatal conductance than would have occurred in reality. From Table 2.4 and Figure 2.3 it can be seen that in climates where there was no shortage of water, for instance, in the tropics, temperate latitudes, boreal and arctic regions, the stomatal conductance would be greater.

2.2.3 Boundary layer conductance

Boundary layer conductance (g_a) was initially derived using wind speed, LAI and leaf dimension. For a given LAI, the boundary layer conductance is calculated by cumulating the individual boundary layer conductance values for each layer of the canopy and is obtained from the following formulae. These formulae were derived from relationships established by Monteith (1973), and Grace, Fasehun, and Dixon (1980), and are for conditions of forced convection i.e. when there is a flow of air (as opposed to free convection which occurs when there is a difference between the leaf and air temperatures):

$$g_{a3} = g_{a4} + (s_{a3} \times L_3) \qquad \textbf{(2.13)}$$

where

g_{a3} is the canopy boundary layer conductance from stratum 6 (top) to 3 for a given LAI,

g_{c4} is the canopy boundary layer conductance from stratum 6 (top) to 4 for a given LAI,

s_{a3} is the leaf boundary layer conductance for stratum 3 for a given LAI, L_3 is the LAI for stratum 3 and,

s_{as} the boundary layer conductance for leaf stratum, s, is calculated as follows,

$$s_{as} = \frac{0.015\exp(0.56\log(\mu))}{\exp(0.46\log(D_L/100))} \qquad \textbf{(2.14)}$$

where

D_L is the leaf dimension (cm) for LAI, L.

μ is wind speed (m s^{-1}) recorded at a meteorological station. This is set to 2 m s^{-1} for the top layer of the canopy and 0.2 m s^{-1} within the canopy when wind speed data are not available for a site. Landsberg and James (1971) suggested a value of 0.4 m s^{-1} within woody canopies, but within grasses and near to the ground the wind speed would be close to zero, so a mean of 0.2 m s^{-1} was selected.

Once the IIASA dataset was used, and wind speed was no longer available, an alternative equation to equation 2.14 had to be employed. This new equation is also used by the DOLY model (Woodward *et al.*, 1995) which is described in detail in section 2.3. Boundary layer conductance is calculated from a standard logarithmic height function of vegetation height, h (Friend and Woodward, 1990; Jones 1992):

$$g_a = \frac{3.36}{\ln\left(\frac{2000-7h}{h}\right)^2} \qquad \textbf{(2.15)}$$

where canopy height, h (m) is derived from a simple function of leaf area index (Shugart, 1984):

$$h = 0.807\, L_a^{2.137} \qquad \textbf{(2.16)}$$

Wind speed is assumed to be 20 m s^{-1} at 200m, a height well above the highest predicted canopy surface.

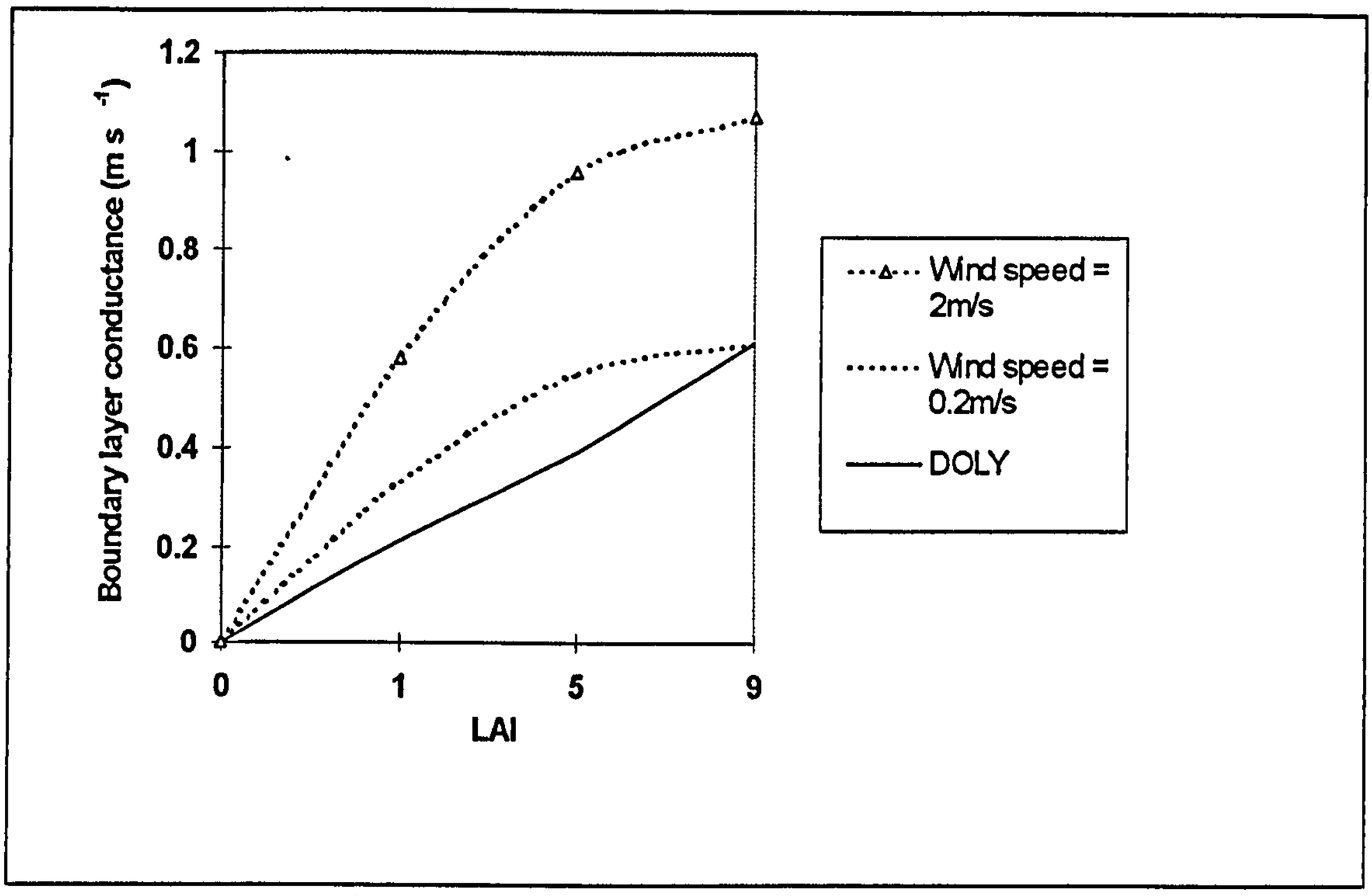

Figure 2.4 Canopy boundary layer conductance for a range of LAIs using two values of wind speed for World (equation 2.14), and the height equation (equation 2.15) as used in DOLY (wind speed assumed to be 20 m s^{-1} at a height of 200m).

It can be seen from Figure 2.4 that the boundary layer conductance as used in World has similar values to those used in DOLY when a wind speed of 0.2 m s^{-1} is used, particularly at high and low values of LAI. If the wind speed increases then there is a greater differential between the boundary layer conductance calculated by World and the DOLY value derived from LAI alone. Boundary layer conductance is used in the Penman–Monteith equation (see section 2.2.4) in both models. The World calculation gives more accurate values of boundary layer conductance but, as evapotranspiration is relatively insensitive to this conductance compared with other variables, the equation used within DOLY is adequate for most circumstances.

2.2.4 Evapotranspiration

Evapotranspiration is calculated from the Penman–Monteith equation (Monteith, 1973). This equation is a modification of the original equation presented by Penman (1948) which estimated the potential evaporation for a site using standard meteorological measurements such as wind speed, solar radiation and temperature. This calculation of potential evaporation assumes that there is an unlimited supply of water available to be evaporated to the atmosphere. This is inappropriate for plant canopies where the water supply is dependent on the characteristics of the plant canopy itself. Monteith (1965) modified Penman's equation to take account of different vegetation surfaces with differing stomatal conductances and LAI values. This equation for evapotranspiration is used to provide hourly values for an average day for each month of the year.

$$E_T = \frac{sA + c_p \rho g_a D}{\lambda \left(s + \gamma \left(1 + \frac{g_a}{g_n} \right) \right)} \qquad \textbf{(2.17)}$$

where

E_T is the evapotranspiration flux, g m^{-2} s^{-1},

s is the vapour pressure parameter, Pa $°C^{-1}$,

A is the available energy of the canopy, W m^{-2},

c_p is the specific heat capacity of air, J $g^{-1}°C^{-1}$, and is set at a constant value of 1.01 J $g^{-1}°C^{-1}$ in World, although it does vary slightly with temperature,

ρ is the density of air, g m^{-3} ,

D is vapour pressure deficit, (VPD) Pa,

λ is the latent heat of vaporization, J g^{-1},

g_a is boundary layer conductance, m s^{-1},

g_n is non-molar stomatal conductance, m s^{-1}, and

γ is the psychrometric constant, Pa $°C^{-1}$.

The net radiant balance of the canopy, R_n, (W m^{-2}), is calculated from incoming solar radiation, I_o. This is an empirical relationship used by Monteith (1973) and Rosenberg (1974).

$$R_n = 0.84I_o - 94.1 \quad \textbf{(2.18)}$$

The soil heat flux, G, is approximately constant for a range of different vegetation types as shown in Monteith (1976):

$$G = 0.033\, R_n. \quad \textbf{(2.19)}$$

As the available energy, A, is:

$$A = R_n - G \quad \textbf{(2.20)}$$

then

$$A = 0.967(0.84I_o - 94.1) \quad \textbf{(2.21)}$$

The vapour pressure parameter (s), the latent heat of vaporization (λ), and the density of air (ρ) are all dependent on hourly temperature. λ and ρ decrease with increasing temperature but the vapour pressure parameter increases.

The rate of change of saturation pressure, s (Pa $°C^{-1}$) with temperature, t (°C), is non-linear.

$$s = 48.7 \exp(0.0532t) \quad \textbf{(2.22)}$$

The density of air, ρ (g m^{-3}) is calculated as follows:

$$\rho = 1288.4 - 4.103t \quad \textbf{(2.23)}$$

The latent heat of vaporization of water, λ (J g^{-1}) which is also dependent on temperature is:

$$\lambda = 2500.9 - 2.37t \quad \textbf{(2.24)}$$

The psychrometric constant, γ (Pa $°C^{-1}$) is derived as follows:

$$\gamma = P_a c_p / 0.622\lambda \quad \textbf{(2.25)}$$

Atmospheric pressure, P_a, is set at 101325 Pa.

The vapour pressure deficit, D is defined as the difference between the actual vapour pressure (e) and the saturation vapour pressure at the temperature of the sample (e_s (t)). It is obtained in the following manner. The saturation vapour pressure, e_s (t), at the wet-bulb temperature (Pa), is the maximum amount of water the air can hold in the vapour stage. It is related to temperature and is derived from the following equation, (Jones, 1983):

$$e_s(t) = 610.8\exp((17.269t)/(237.3 + t)) \qquad \textbf{(2.26)}$$

The vapour pressure, e (Pa) is the pressure exerted by the amount of water vapour content in the air. It is derived from mean relative humidity. Relative humidity is easy to measure using hygrometers or wet and dry-bulb thermometers but it is difficult to find a single value to represent relative humidity for the whole day. The commonly recorded daily value at nine o'clock in the morning may not be suitable for modelling. When World was written, such data were the only indication available as to the humidity at a site. The use of weather generators in the future may be of some help and show the variation of relative humidity values throughout the day. At the moment, though, it is not a valid exercise to extrapolate values for the rest of the day. Therefore, hourly values of relative humidity were not calculated within the program, so the value of e is obtained from the daily mean temperature, t, and the daily mean relative humidity, R_h. It should be noted though that it is possible to predict a daily trend in the vapour pressure deficit if it is assumed that the dew point temperature is constant through the day and the dry-bulb temperature has the same diurnal trend. Humidity data were either extracted for individual sites from the Müller dataset (1982), or on a global grid from data supplied by Rik Leemans (pers. comm. 1993).

$$e = (R_h/100)\,610.8\exp((17.269t)/(237.3 + t)) \qquad \textbf{(2.27)}$$

t is the daily mean temperature (°C).

The terms g_a and g_s in the Penman–Monteith equation are boundary layer resistance and stomatal conductance and have been discussed above.

The equation for evapotranspiration in terms of W m^{-2} can be converted to the more convenient units of kg m^{-2} hr^{-1} (which happens to be numerically equivalent to mm hr^{-1}) by the following equation:

$$E_{Tmm} = 3600\ E_T/1000 \qquad \textbf{(2.28)}$$

E_{Tmm} is evapotranspiration for the whole canopy in units of kg H_2O m^{-2} hr^{-1}.

Vapour pressure deficit (VPD) is calculated from humidity and temperature. Figure 2.5 shows how VPD varies with temperature for a range of humidities. VPD increases with increasing temperature, but the amount and rate of increase decreases, as the relative humidity increases. If VPD is kept constant with a constant incoming solar radiation value of 500 W m^{-2} and LAI of 5 the evapotranspiration decreases slightly (of the order of 100 W m^{-2} over a 45 °C temperature range) as temperatures rise (see Figure 2.6).

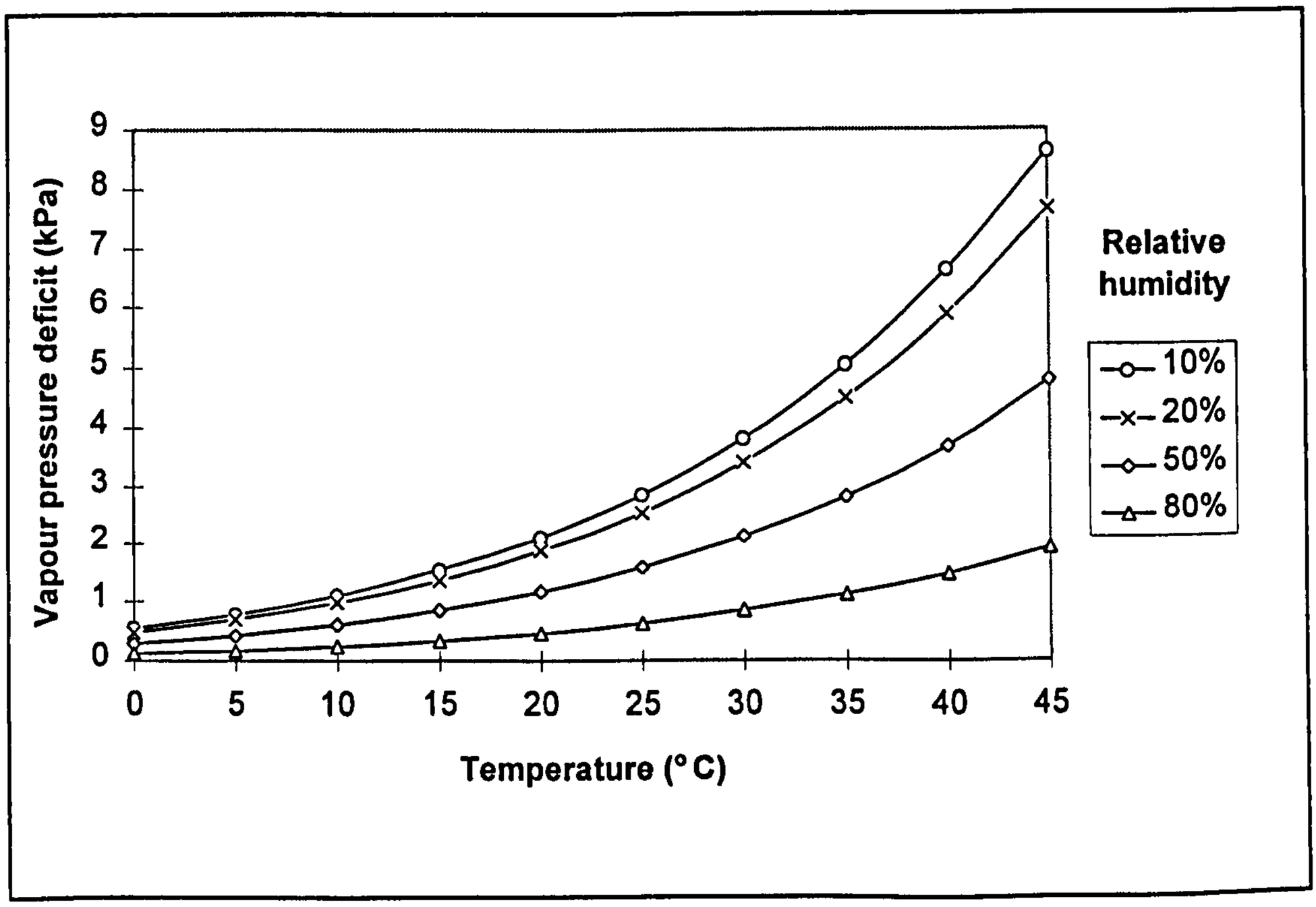

Figure 2.5 The response of vapour pressure deficit (VPD) to increasing temperature for four different relative humidity (RH) values.

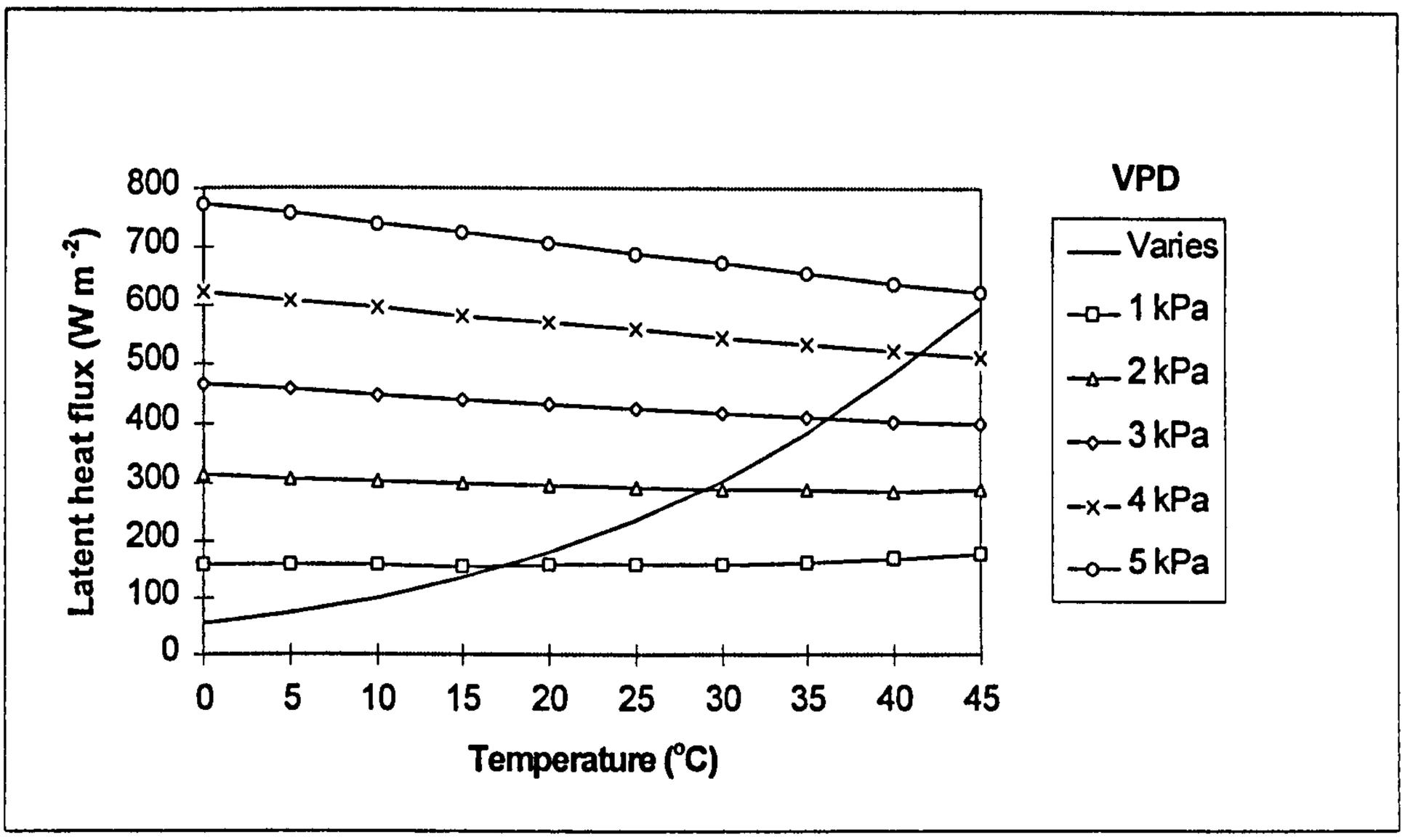

Figure 2.6 The response of latent heat flux to increasing temperature for five different VPD values. The LAI is 5 and the incoming solar radiation, I_o, is set at 500 W m^{-2}. Stomatal conductance is held as a constant. Varies means that the VPD is allowed to vary with temperature (i.e.the equations 2.26 and 2.27 have been used with the relative humidity set to 50%). Latent heat flux increases rapidly if both the temperature and the VPD increase. The other VPD values are set as constants ranging between 1 kPa and 5 kPa in the evapotranspiration equation.

From Figure 2.6 it can also be seen how latent heat flux increases with VPD for a given temperature. The highest latent heat flux values occur with the highest VPD.

Latent heat flux also increases with increases in net radiation, stomatal conductance and temperature alone. In Figure 2.2 as the incoming solar radiation increases so does the stomatal conductance. The increase with temperature and incoming solar radiation is shown in the following figure (Figure 2.7) which demonstrates how latent heat flux varies over a range of temperatures for an LAI of 5 for two different scenarios. One includes an increase in incoming solar radiation with temperature, the other keeps the incoming solar radiation constant but increases the temperature.

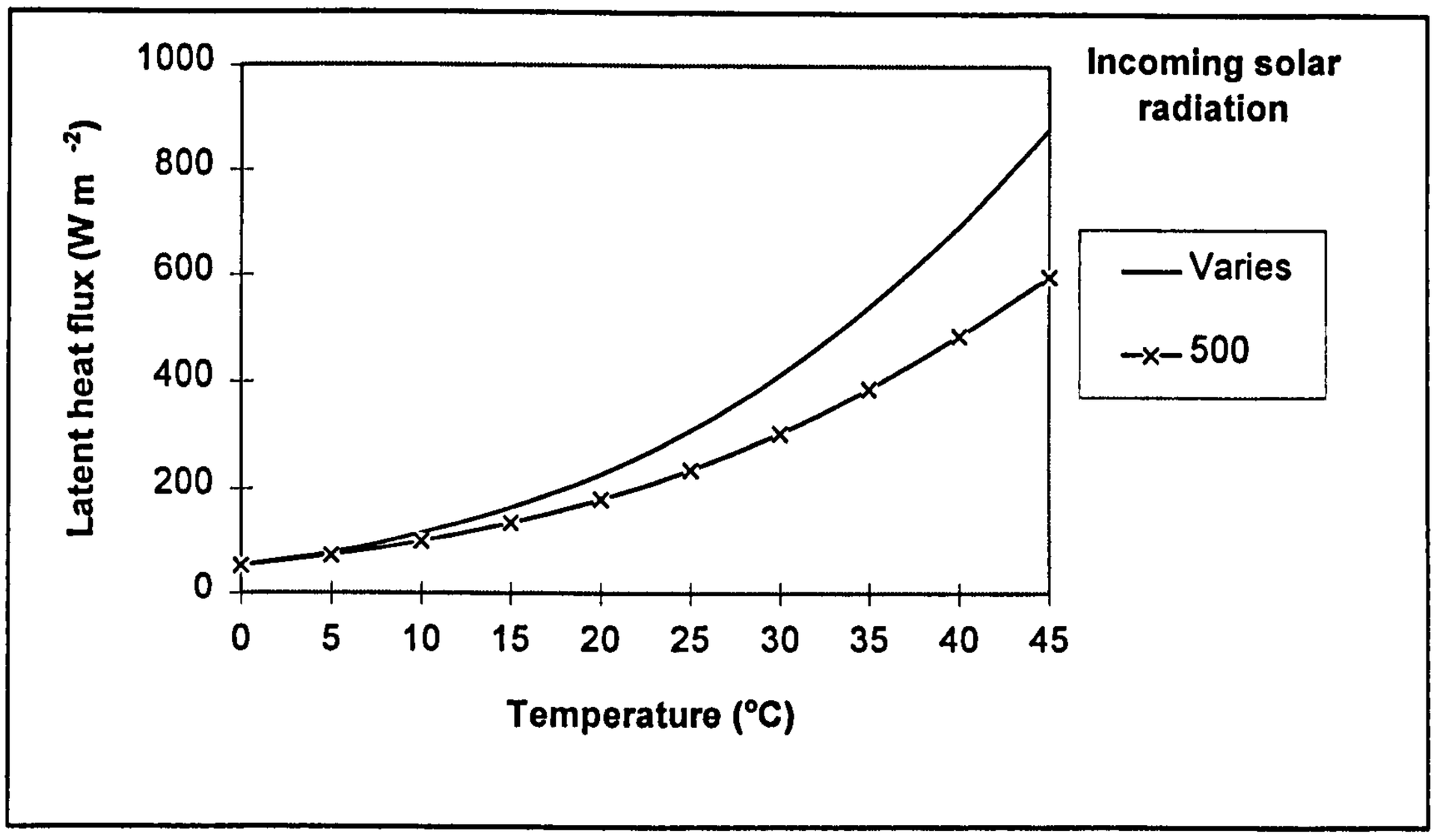

Figure 2.7 Latent heat flux calculated using the World model for an LAI of 5 and a relative humidity of 50% over a range of temperatures. The incoming solar radiation increases with temperature as in Figure 2.6. Two scenarios are shown:

i) the incoming solar radiation has been increased from 500 W m^{-2} to 1400 W m^{-2} in increments of 100 W m^{-2} for each 5°C temperature rise, and

ii) the incoming solar radiation has been set at a constant value of 500 W m^{-2} .

An increase in incoming solar radiation causes an increase in latent heat flux, both directly, through an increase in net radiation, as well as indirectly through an increase in stomatal conductance. At higher incoming solar radiation values, though, the rate of change in stomatal conductance with increasing radiation is small. Evapotranspiration is very closely related to stomatal conductance and would almost double (factor of 1.97 at temperatures below 20°C for an LAI of 5), if the stomatal conductance is doubled. However, as temperatures rise and exceed 20 °C the influence of stomatal conductance diminishes slightly and the evapotranspiration would increase by a factor of 1.8 for a temperature of 45 °C and an LAI of 5 for a doubling of stomatal conductance from 0.003 to 0.006 m s^{-1} .

It has been shown how net radiation and temperature influence a number of variables used within the Penman–Monteith equation for evapotranspiration. These influences need to be considered when analysing the response of the model to changes in climate. In Chapter 4, a sensitivity analysis considers these responses using the water version of the DOLY model (see section 2.4 for a description) in relation to the effect of changing climate input variables.

2.2.5 Water Balance

The amount of soil water at a vegetated site is determined by rainfall, LAI and evapotranspiration. Precipitation that falls at a given site has two paths to the ground surface. It is either intercepted, with allowance made for some evaporation off the leaf surface, and then drips to the ground, or reaches the ground via stemflow, or it falls directly to the ground as throughfall. Throughfall varies with LAI and the values used in the model are shown in Table 2.1. Some of this water goes to the soil (and is then accumulated through the year) and the rest is evaporated, so at the end of the year we have a situation where all the water that has fallen at a site has been accounted for. The soil is assumed to be a bucket and to be at field capacity at the start of the year. No allowance is made for snow accumulation or melting.

The amount of water available to vegetation at a site is calculated through the year. Water is added according to the amount of precipitation, and evaporated according to temperature, LAI and humidity, with the amount in the soil fluctuating accordingly. If the cumulative water balance falls below minus 80 mm then a drought is assumed to have occurred, causing leaves to drop off the vegetation. This rounded value was chosen from work done by Priestley and Taylor, (1972) and Lockwood (1979) who determined that 75 mm of water (rainfall equivalent measurement of volume) was available for transpiration from the soil at field capacity. Providing the water balance is

greater than minus 80 mm there is enough water for any vegetation at the site to survive.

2.2.6 Water use efficiency

Water use efficiency was not calculated in the original program described by Woodward (1987) but is used in World to derive net primary productivity (see section 2.2.7). A general definition of water use efficiency (WUE) is the ratio of net assimilation to water loss, although there are a variety of other definitions (Jones, 1992). These are dependent on factors such as whether the water use is defined as total transpiration alone or evapotranspiration, which includes soil evaporation and rainfall interception losses. Also, net assimilation can be in terms of net CO_2 exchange, or in terms of total dry matter, or above ground dry matter. In addition, molar or mass units may be used.

WUE is required along with evapotranspiration data, to calculate yield in the absence of any nutrient and photosynthetic input in the World model. It can be calculated as an instantaneous rate, or as a rate occurring over a longer time period of at least a day. In World, values of vapour pressure deficit and evapotranspiration are calculated for the hours of daylight only, which means, in effect, that only daytime assimilation is available, instead of the net CO_2 exchange for the whole plant community for the full 24 hours. In view of this, the proportion of assimilation that is lost in respiration needs to be calculated. It is convenient to divide this respiration into growth respiration (that is the respiration produced in connection with growth) and maintenance respiration (that is the respiration produced by maintaining the current plant parts). In reality, there is no biochemical separation in these respiration terms in the plant. To calculate the amount of dry weight produced for a given growth respiration, a conversion efficiency of 0.53 g dry weight per g CO_2 is given by Jones (1992). Also, maintenance respiration is given as 15 to 30% of net assimilation,

which means that between 0.37 and 0.45 g dry weight are produced per g CO_2 overall. A mean value of 0.4 g dry weight produced per g CO_2 of respiration (growth and maintenance) is used in the model.

The long-term water use efficiency is calculated from atmospheric CO_2 and vapour pressure deficit using a simplified version of the equation presented by Farquhar *et al.* (1982):

$$WUE = \frac{(1-\phi)(P_a - P_i)}{1.6D} \qquad (2.29)$$

where the units of WUE are mmol CO_2 (mol H_2O) $^{-1}$,

ϕ is the proportion of net daytime fixation of carbon in the shoots which is lost by respiration and is set as 0.3, for an average crop plant growing under good conditions.

P_a is atmospheric CO_2 partial pressure, Pa,

P_i is the partial pressure of CO_2 in intercellular spaces, P_a, and is set to $0.7P_a$

D is vapour pressure deficit, Pa.

The factor 1.6 arises because water vapour diffuses through air more rapidly than does CO_2 .

Figure 2.8 shows how WUE varies with vapour pressure deficit. It can be seen that at low values of vapour pressure deficit (high values of relative humidity) the WUE is very high. In fact if the vapour pressure is less than 100 Pa, WUE approaches infinity. Most of the global sites have vapour pressure deficit values between 0.5 and 2 kPa which give WUEs of between 9 and 2 mmol CO_2 mol H_2O^{-1}. However, in high latitudes where temperatures are low and the humidity values are 80% or higher, the VPD is 100 Pa or lower. This leads to high values of NPP as shown in Figure 2.10 and is discussed in the next section (2.2.7).

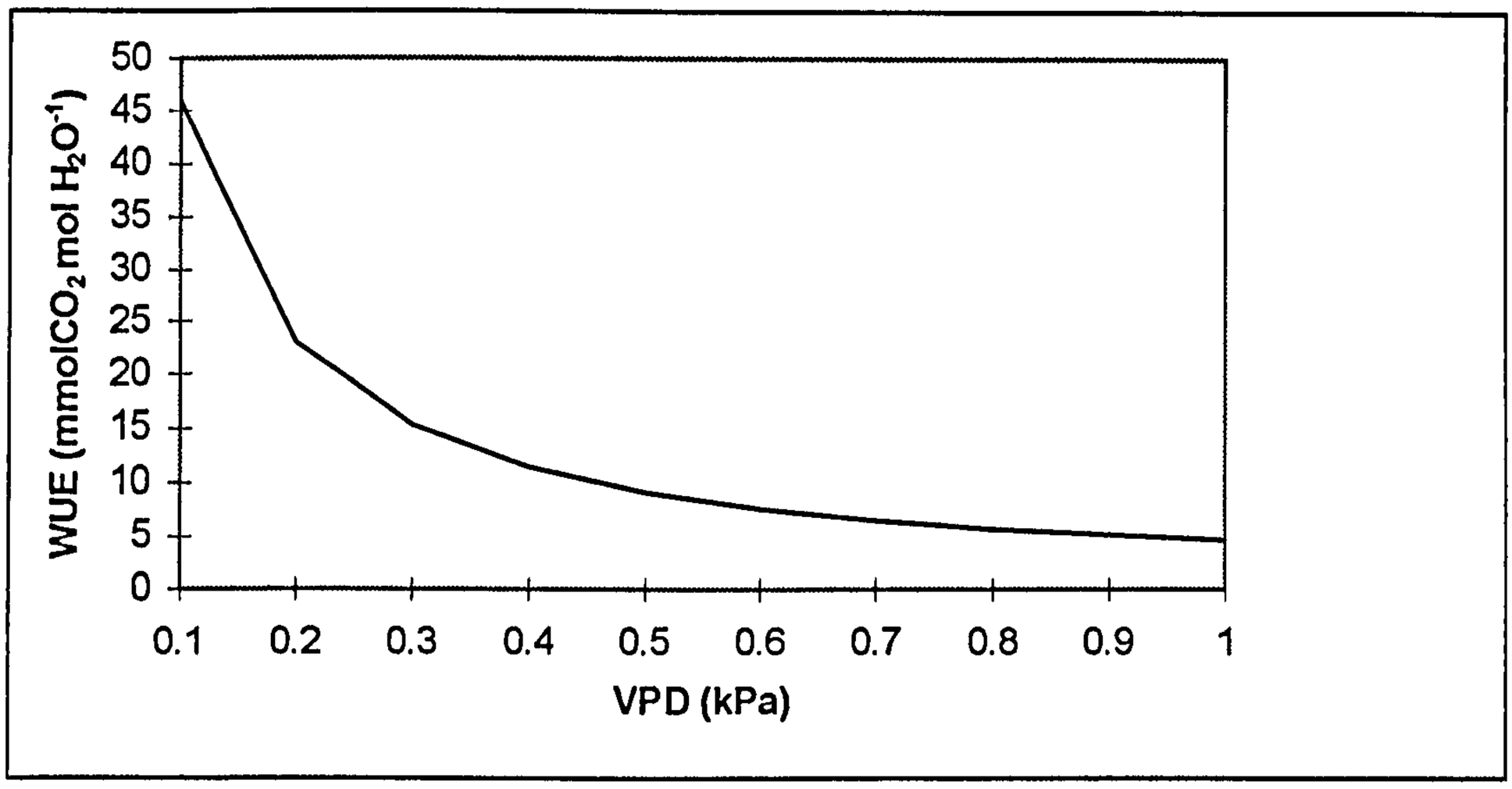

a) VPD range 0.1 to 1 kPa

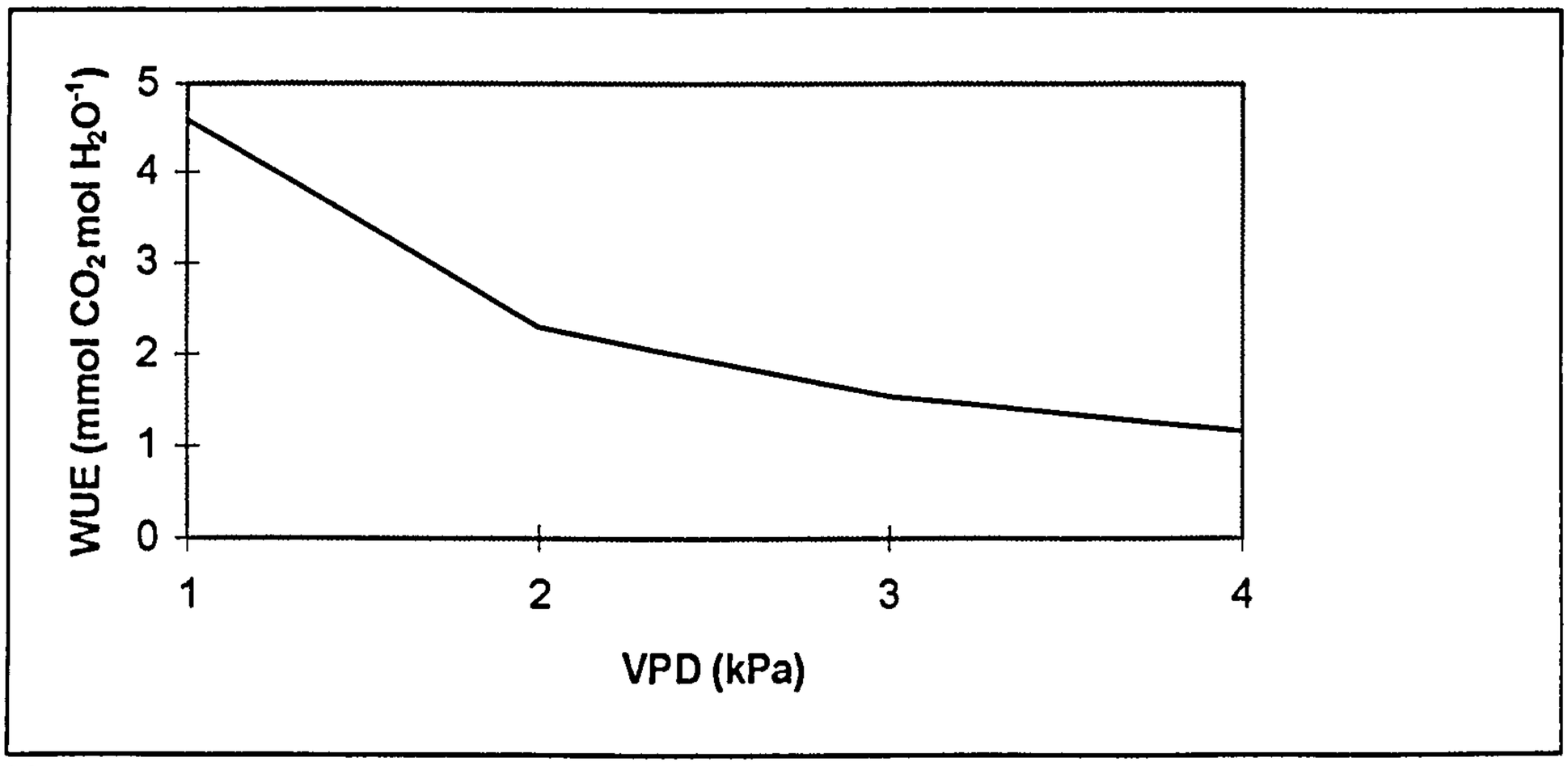

b) VPD range 1 to 4 kPa

Figure 2.8 Relationship between water use efficiency (WUE) and vapour pressure deficit (VPD) for a range of VPD values from a) 0.1 to 1 kPa and b) 1 to 4 kPa.

The WUE values for a VPD less than 0.1 kPa have not been shown because WUE approaches infinity as VPD approaches zero.

2.2.7 LAI and NPP from World

LAI was the only output from the model described in Woodward (1987). World, however, has the additional output of NPP. LAI is determined from the water balance and is set to the maximum value that satisfies the annual moisture requirements. The hourly yield of vegetation can be derived from water use efficiency and evaporation or transpiration. In the following equation (Jones, 1992), evapotranspiration has been used instead of transpiration alone, so that water evaporated from the ground surface is also included:

$$\text{Yield} = (\text{WUE} \times 2.44 \times \text{Evapotranspiration}) \qquad \textbf{(2.30)}$$

where yield is in units of g CO_2 m^{-2} hr^{-1}

The figure of 2.44 converts the units of WUE mmol CO_2 (mol H_2O)$^{-1}$ to g CO_2 (kg H_2O) $^{-1}$ as follows:

$$WUE_g = WUE \times \frac{44}{18} \qquad \textbf{(2.31)}$$

where

WUE_g is WUE in units of g CO_2/kg H_2O,

The molecular weight of carbon dioxide is 44g mol $^{-1}$ and the molecular weight of water is 18g mol $^{-1}$ (44/18=2.44).

Equation 2.30 is multiplied by 0.4 to allow for both growth and maintenance respiration (see section 2.2.6) and, as net primary productivity (NPP) is usually expressed in terms of carbon, the dry matter value is converted accordingly. The molecular weight of carbon is 12 g mol^{-1} and the molecular weight of CO_2 is 44 g mol $^{-1}$ (12/44=0.27).

Daily NPP is calculated using yield and the daylength which is calculated within the model:

$$\text{NPP} = \frac{0.4 \times 0.27 \times \text{YIELD}_{CO2} \times \text{hrs}}{100} \qquad \textbf{(2.32)}$$

where NPP is net primary productivity in units of tC ha $^{-1}$ day^{-1} (= gC m^{-2} day $^{-1}$/100) and hrs is daylength (hours).

This daily NPP is cumulated through the growing season to obtain an annual NPP value for each LAI. The NPP output by the model is that for the maximum LAI.

2.2.8 Results and discussion

The following maps show the results from the methods described in the previous sections for determining LAI and NPP. Figure 2.9 shows the global distribution of LAI values and Figure 2.10 the global distribution of NPP as predicted by World. A number of errors are immediately evident. In Figure 2.9, the LAI values of 9 for Siberia, Southern Greenland, northern Scandinavia are obviously incorrect as these are areas with tundra vegetation or boreal forest with relatively low LAI values of 5 or below (Tieszen, 1978; Cannell, 1982). The rest of the world shows a reasonable distribution of LAI with high values of 7 to 9 in the equatorial rain forests of South America and central Africa, intermediate values of 4 to 6 in the temperate forests of Europe and eastern America, values of 1 to 3 in grassland and savannah areas of Africa, America and Asia, and zero values in desert areas such as central Australia, the Gobi and the Sahara (see Archibold, 1995 for maps of the global distribution of these vegetation types). Any errors that arise in LAI impact on the NPP map because the NPP selected by the model is dependent on the LAI value. This can be seen in Figure 2.10. In high latitudes, values of NPP exceed 10 tC ha^{-1} yr^{-1} in the same areas where high LAI values arise; in addition, in the temperate latitudes, where lower LAI values are predicted the NPP is still high. High values of NPP also occur in the equatorial rain forest regions where they exceed 13 tC ha^{-1} yr^{-1}. These values are higher than measured NPP values which are around 10 tC ha^{-1} yr^{-1} (McGuire *et al.*, 1992; Cannell, 1982). There are also errors in the Himalayas where high NPP values of greater than 13 tC ha^{-1} yr^{-1} have occurred. In reality there would be very low yield in this region due to the

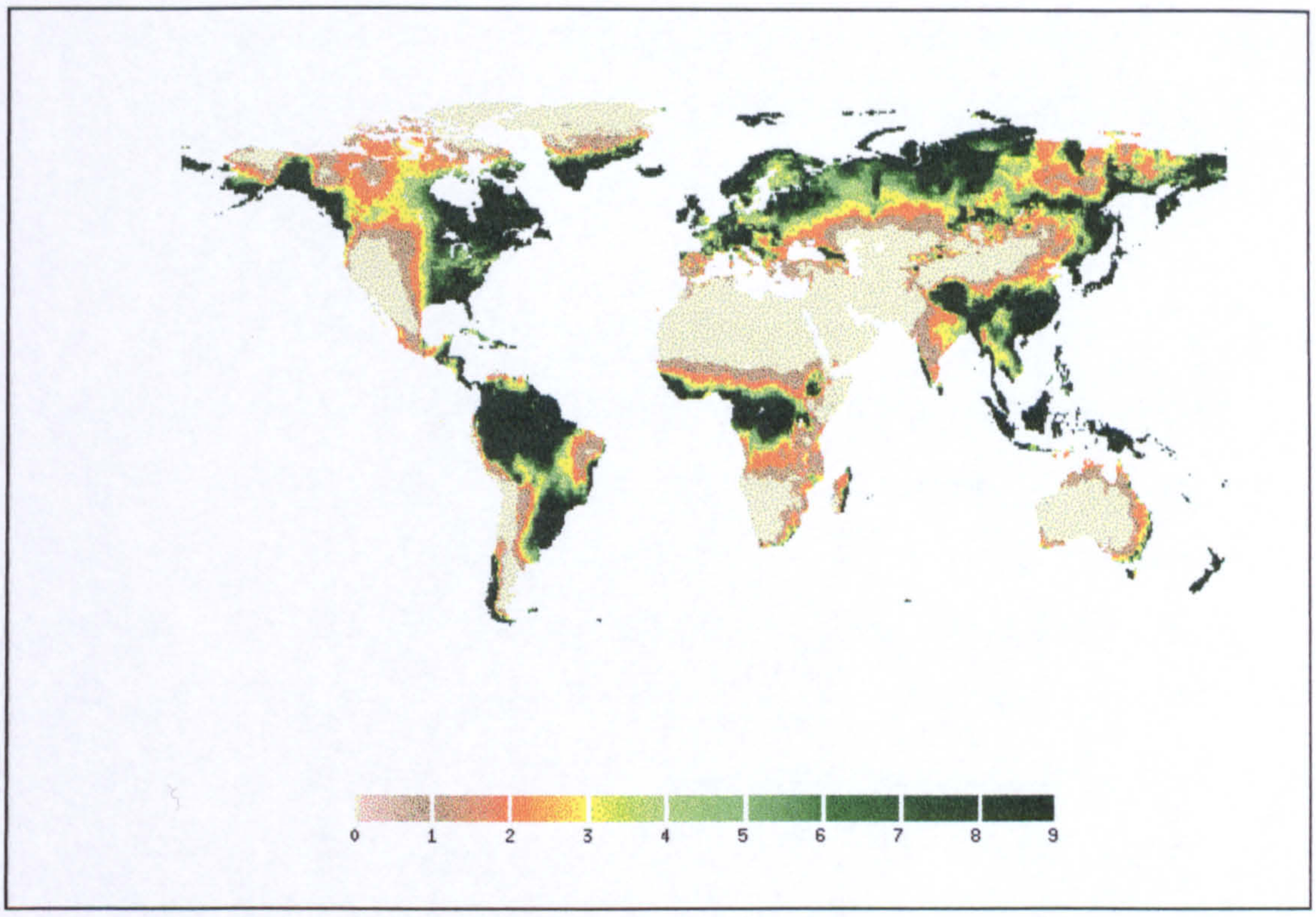

Figure 2.9 Global distribution of leaf area index derived from the World model using the IIASA dataset (1° × 1° grid).

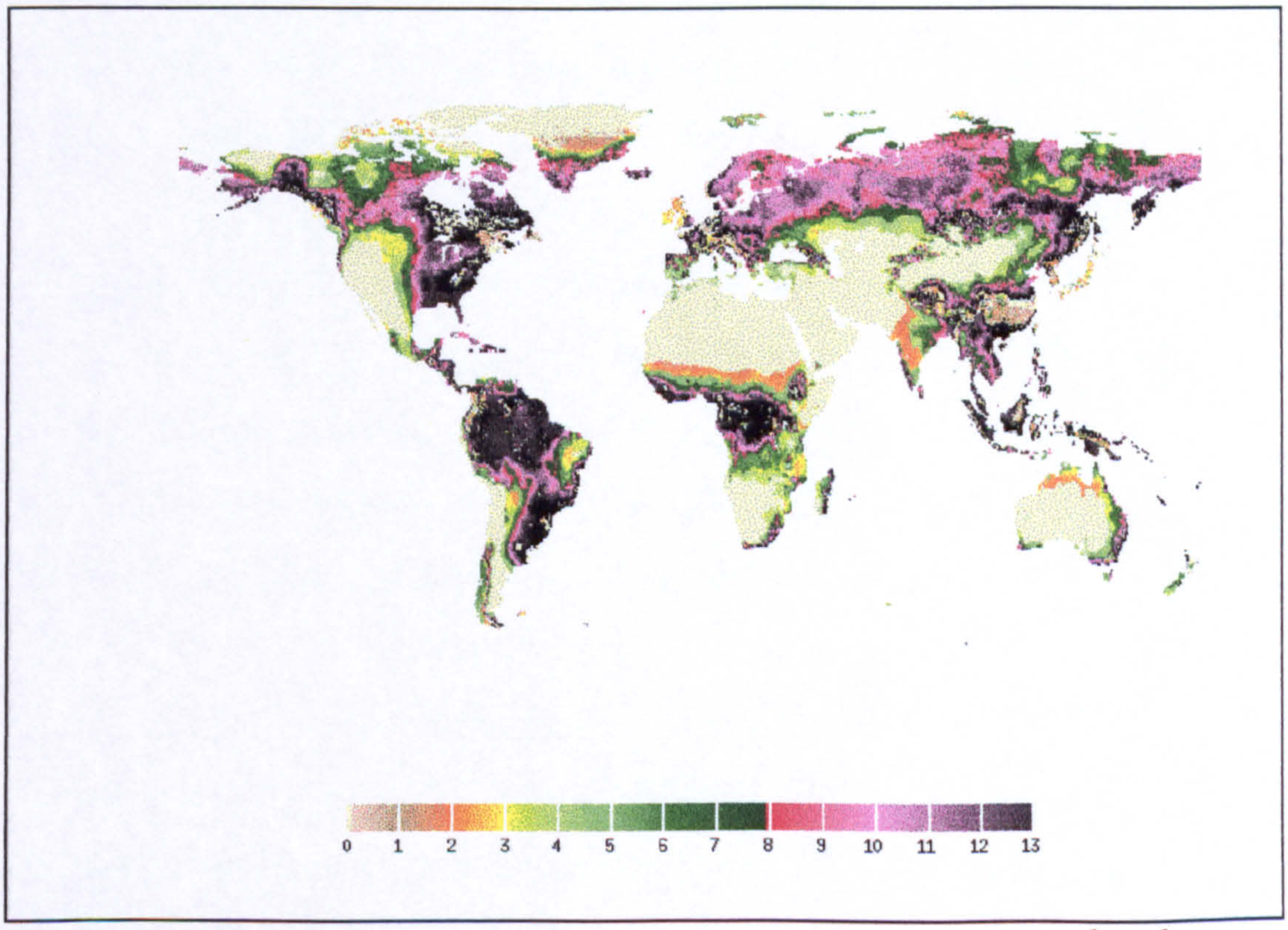

Figure 2.10 Global distribution of net primary productivity (tC ha $^{-1}$ yr^{-1}). derived from the World model using the IIASA dataset (1° × 1° grid).

short growing season and low temperatures leading to sparse vegetation on the mountains. Overall the map is poor and demonstrates that the direct use of water use efficiency and evapotranspiration for calculating NPP were not successful at a global scale.

Figure 2.8 demonstrated how WUE increases rapidly with low values of vapour pressure deficit. In high latitude areas, which have high humidities and low rates of evapotranspiration (which seldom exceed precipitation) the model predicts high values of LAI and, in turn, NPP. In addition, the lack of carbon limitation at such latitudes, and the lack of consideration of the turnover of plant parts in the derivation of yield, generally, also contributed to these unrealistically high values of LAI and NPP. This indicates that the limited growing season and lack of nutrients has more influence on LAI and NPP values than does the amount of water availability in such regions. The fact that there is no water limitation on LAI leads to highest possible values of NPP being selected. Further south, in the more temperate regions, where humidity and water use efficiency are lower, NPP is still high despite the lower values of LAI. Evapotranspiration, however, is still high due to the moderate LAI and a plentiful supply of water, so the NPP remains high.

In spite of these problems, the model World has been shown to be particularly suited to predicting LAI and NPP in water-limited regions of the world, such as Africa, where it performs well, and the LAI predictions are broadly applicable to much of the temperate and tropical regions of the globe. It is, however, deficient in areas where other factors such as nutrient availability play a major role in the growth and development of vegetation. This causes NPP values to be excessively high.

Due to the problems caused by the omission of carbon and plant turnover, and because a new model was being developed that could incorporate nitrogen uptake and model photosynthesis, attention was switched from World to the new model, DOLY. This model is described in the next section.

2.3 DOLY

The DOLY (Dynamic glObaL phytogeographY) model is a global vegetation model that has been developed by Woodward *et al.* (1995). The equations used within the model are described here. Additional information on improvements made to the DOLY model since its publication is provided in section 2.3.12. The DOLY model was designed to be a mechanistic model and to be modular. This modularity means that DOLY can be relatively easily incorporated into other models and that additional processes can be added without too many problems. Output from the DOLY model has been used in the United Kingdom Meteorological Office (UKMO) general circulation model (GCM) in order to determine the GCM's sensitivity to vegetation inputs, and to identify any feedbacks occurring between the climate and vegetation when the GCM is run off-line. Further details of this work are in Chapter 6.

2.3.1 Inputs to DOLY

The main inputs to DOLY are the climate variables: mean monthly precipitation (mm), mean monthly relative humidity (%) and mean monthly temperature (°C) and the soils data. The climate data have been obtained from the IIASA dataset (Leemans and Cramer, 1991) which has a global resolution of 0.5° longitude by 0.5° latitude. Soil carbon and nitrogen values have been obtained, for each 0.5 by 0.5 degree IIASA cell, from the literature (Woodward and Smith, 1994b; Post *et al.*, 1985) and are in terms of gC m^{-2} and gN m^{-2}, respectively. For a given climate, anywhere in the world, DOLY is able to predict the vegetation properties of leaf area index (LAI) and net primary productivity (NPP), as well as canopy stomatal conductance. Additional climate datasets have been used with DOLY. The results obtained from these datasets are presented and discussed in Chapter 7.

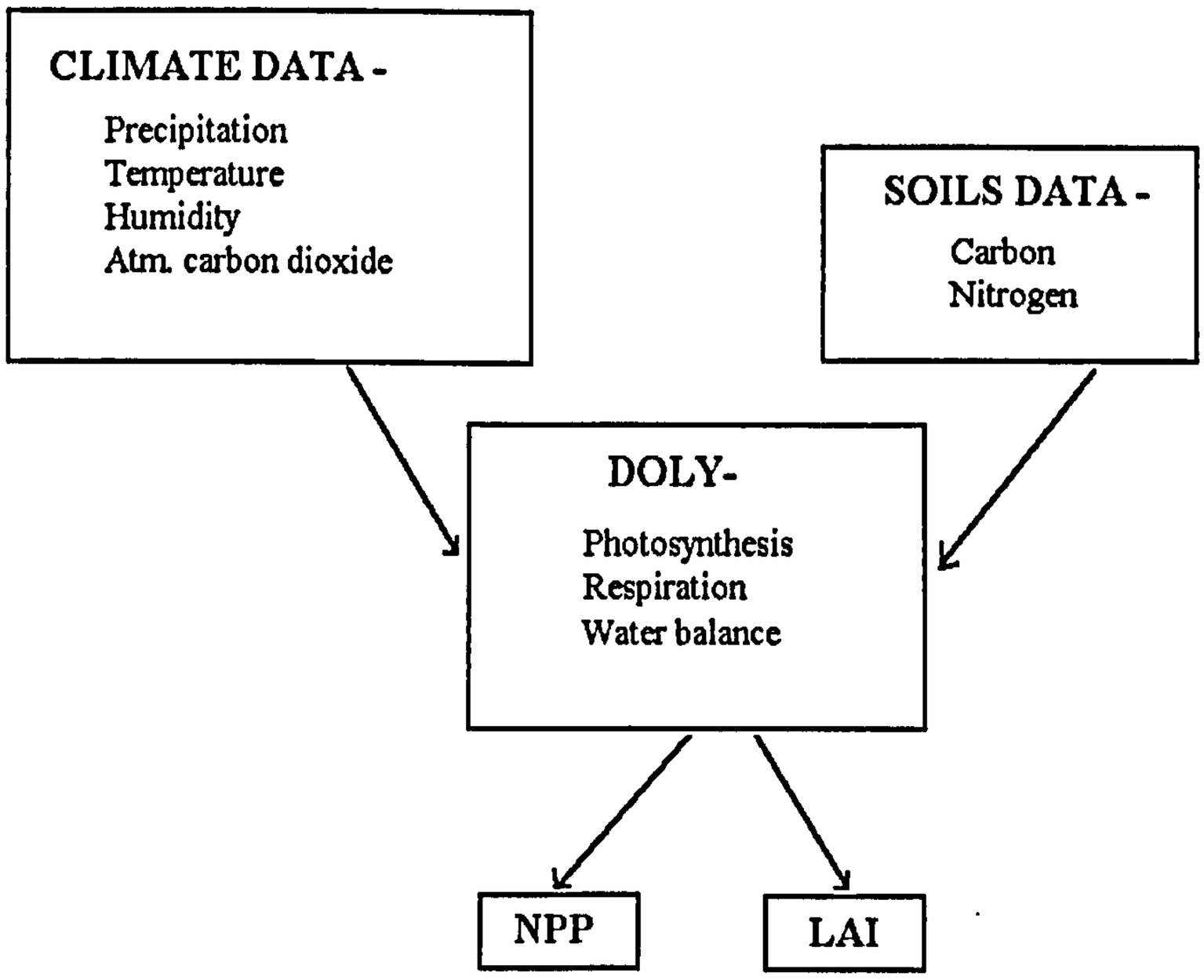

Figure 2.11 Block diagram of the inputs to, and outputs from the DOLY model. This shows the basic structure of the DOLY model. The model is usually run from climate data presented on a 0.5 by 0.5 degree global grid with 62,483 land cells (Leemans and Cramer, 1991). Both the climate and soils data are used in the calculations of nitrogen and water uptake.

2.3.2 DOLY model parameters

Parameters in the model include specific leaf area, which is the amount of leaf area per gram of leaf, and ranges from 0.007 $m^2\ g^{-1}$ in a boreal evergreen forest to 0.018 $m^2\ g^{-1}$ in a temperate deciduous forest (derived from values in Cannell, 1982). The value set in DOLY is 0.01 $m^2\ g^{-1}$ for simplicity, although it is recognised that this value is not globally applicable. Other set parameters include the initial soil water content, set at field capacity with a value of 0.15 g water $(g\ soil)^{-1}$ (Russell, 1988), and atmospheric CO_2 partial pressure which is 35 Pa for the present day. The amount of respiration in light per unit area of leaf due to processes other than photorespiration is set at 0.82 $\mu mol\ CO_2\ m^{-2}\ s^{-1}$ (Harley *et al.*, 1992), and the partial internal oxygen pressure at 21000 Pa

(Farquhar *et al.*, 1980). These are values which have been used in the calculation of the net rate of CO_2 assimilation.

2.3.3 DOLY model overview

The model has been developed in modules which can be used independently. The model first predicts the uptake of nitrogen and water from the soil. The rate of nitrogen uptake determines the rates of leaf photosynthesis, dark respiration and stomatal conductance (Woodward and Smith, 1994 a,b). These rates are then integrated to provide predictions of canopy evapotranspiration and net assimilation (photosynthesis minus respiration). Leaf area index is set to the maximum value that satisfies annual moisture and carbon balances. This is shown in Figure 2.12. Figure 2.13 shows the inputs, processes and feedbacks in the calculation of assimilation and stomatal conductance. The processes are described in sections 2.3.5 to 2.3.11 of this chapter.

2.3.4 Water and nitrogen uptake from the soil

Woodward and Smith (1994 a,b) examined work done by Read (1990) on mycorrhizas, and discussed the influence of the soil nutrient status on photosynthesis. They also described water uptake from the soil. Soil water content controls leaf stomatal conductance and this is described in section 2.3.7. Details concerning soil nutrients and nitrogen uptake are provided in sections 3.1 and 3.2 of Chapter 3.

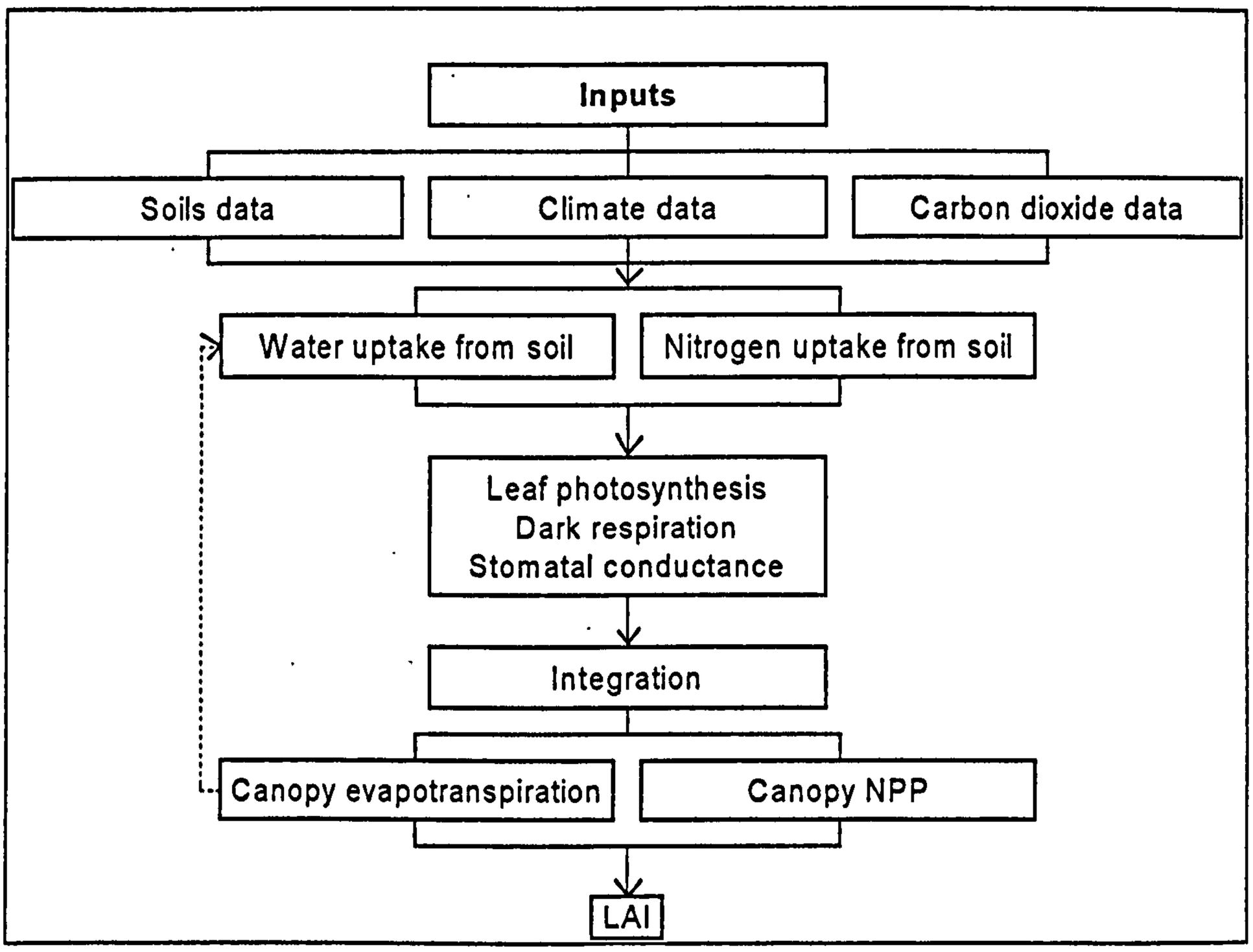

Figure 2.12 Block diagram of DOLY processes. Soil nutrient status, water holding capacity, climate and CO_2 concentration are used for the first stage in predicting leaf and canopy gas exchange. The second stage predicts leaf photosynthesis, dark respiration and stomatal conductance. Finally, these responses are run through a year to determine canopy evapotranspiration, net primary productivity (NPP) and leaf area index (LAI). There is also a feedback from canopy processes to plant uptake of water and leaf gas exchange depicted by the dashed arrow.

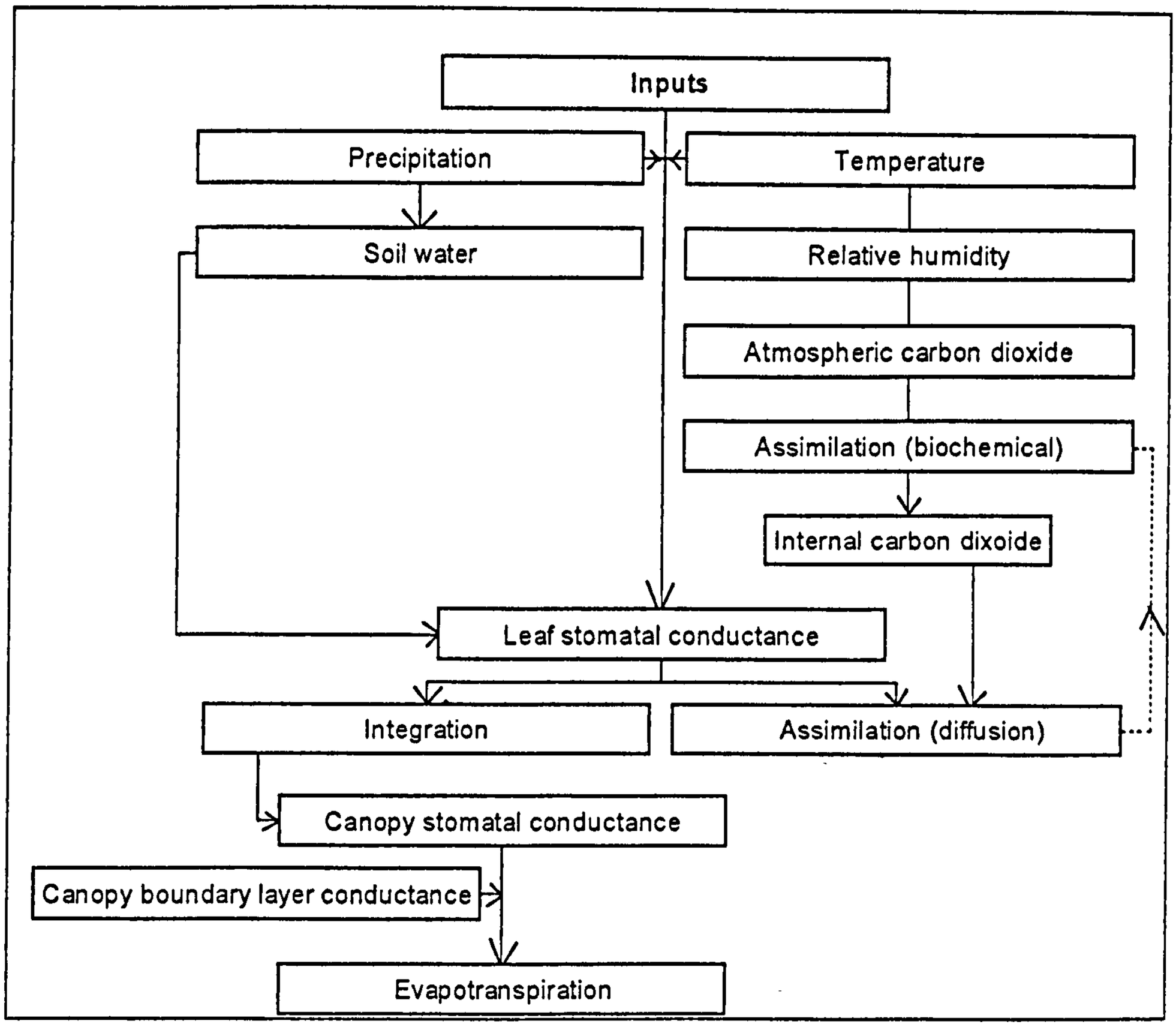

Figure 2.13 Block diagram showing the inputs, processes and feedbacks in the calculation of assimilation, and canopy stomatal conductance together with the link to the evapotranspiration calculation. Canopy boundary layer conductance is also used in this calculation. Temperature, precipitation, relative humidity, atmospheric CO_2 and assimilation (biochemical) are the inputs. The dotted arrow depicts the iteration that arises by setting the assimilation rate implied by the diffusion gradient (2.58) equal to the assimilation rate derived from the Farquhar model (2.33) with the carboxylation rate, V_c, equal to the minimum of W_c, W_j, and W_p. This is used to determine the internal CO_2 partial pressure.

2.3.5 Leaf photosynthesis

In order to determine leaf photosynthesis, the Farquhar model is used (Farquhar *et al.*, 1980). According to this model, the photosynthetic rate of a leaf is determined by the minimum rate of at least two carboxylation processes, one, W_c, involving ribulose bisphosphate carboxylase-oxygenase (rubisco) and the other, W_j, ribulose bisphosphate (RuBP). An additional rate, W_p, discussed by Sharkey (1985) involves triose phosphate utilization, and this is also used in DOLY. The net rate of CO_2 assimilation, A_b, implied by biochemical processes is as follows:

$$A_b = V_c\left(1 - \left(0.5P_o / \Gamma P_c\right)\right) - R_d \qquad \textbf{(2.33)}$$

where

V_c is the rate of carboxylation and equals min $\{W_c, W_j, W_p\}$,

P_o is the internal partial pressure of oxygen = 21,000 Pa,

P_c is the internal partial pressure of carbon dioxide,

Γ is the specificity factor of rubisco for CO_2 relative to O_2 (Jordan and Ogren, 1984) and is dependent on temperature,

R_d is the rate of respiration in light per unit area of leaf due to processes other than photorespiration (Harley *et al.*, 1992) and is set as a constant 0.82 μmol CO_2 m^{-2} s^{-1}.

The specificity factor, Γ, depends on temperature (Harley *et al.*, 1992):

$$\Gamma\left(T_k\right) = e^{-\left(3.949 - \frac{28.99}{0.00831 T_k}\right)} \qquad \textbf{(2.34)}$$

where T_k is absolute temperature (kelvin).

If rubisco activity controls photosynthesis, then the carboxylation rate is

$$W_c = \frac{V_c^{\max} P_c}{P_c + K_c\left(1 + P_o / K_o\right)} \qquad \textbf{(2.35)}$$

where V_c^{max} is the maximum rate of carboxylation by rubisco. The parameters K_c and K_o are Michaelis coefficients for carboxylation and the competing process of oxygenation by rubisco (Farquhar *et al.*, 1980; Harley *et al.*, 1992). These coefficients depend on temperature, T_k, (kelvin).

$$K_c(T_k) = e^{35.8 - \frac{80.5}{0.00831 T_k}} \quad \textbf{(2.36)}$$

$$K_o(T_k) = 1000e^{9.6 - \frac{14.51}{0.0831 T_k}} \quad \textbf{(2.37)}$$

Substituting W_c from equation 2.35 for Vc in equation 2.33 and solving for V_c^{max} gives:

$$V_c^{max} = \frac{(A_b + R_d)[P_c + K_c(1 + P_o/K_o)]}{P_c - 0.5P_o/\Gamma} \quad \textbf{(2.38)}$$

The maximum rate of carboxylation V_c^{max} is calculated from equation 2.38 with the internal partial pressure, P_c set to 70% of its atmospheric partial pressure, P_a= 35 Pa (Friend, 1991; Reynolds *et al.*, 1992) and with $A_b = A_{max}$, the maximum light-saturated rate of photosynthesis. The effects of temperature on this maximum carboxylation rate can be incorporated by the use of a response function k_v (T) derived from a general function by McMurtrie and Wang (1993).

$$V_c^{max}(T) = V_c' k_v(T) \quad \textbf{(2.39)}$$

where V_c' is the carboxylation rate derived from equation 2.38.

The temperature response function is:

$$k_v(T) = 1 + 0.051(T - 25) - 2.48 \times 10^{-4}(T-25)^2 - 8.09 \times 10^{-5}(T-25)^3 \quad \textbf{(2.40)}$$

where T is temperature (°C).

This response function was found to increase at temperatures below 9.5°C, so an adjustment was made within the DOLY model to prevent this occurring. See section 2.4.5 for further details.

If the rate of RuBP regeneration is limiting photosynthesis then the carboxylation rate W_j depends on the rate of electron transport, J (Farquhar and Von Caemmerer, 1982):

$$W_j = \frac{JP_c}{4(P_c + P_o/\Gamma)} \qquad \textbf{(2.41)}$$

The photosynthetically active quantum flux density, I_q, (μmol m^{-2} s^{-1}) drives electron transport, J (Farquhar *et al.*, 1980; Harley *et al.*, 1992):

$$J = \frac{\alpha I_q}{\left(1 + \frac{\alpha^2 I_q^2}{J^2_{max}}\right)^{0.5}} \qquad \textbf{(2.42)}$$

where J_{max} is the light saturated rate of electron transport. The parameter $\alpha = 0.24$ mol electrons (mol photons)$^{-1}$ is the efficiency of light conversion (Harley *et al.*, 1992). I_q (also called photon flux density) is obtained from the incoming solar irradiance, I, as follows:

$$I_q = 0.5I \times 4.255 \times 10^{-6} \qquad \textbf{(2.43)}$$

The ratio of photosynthetically active radiation to incoming solar irradiance is 0.5 (Jones, 1992), and the conversion from W m^{-2} to mol m^{-2} s^{-1} is 4.255×10^{-6} (Woodward and Sheehy, 1983). This conversion factor is a conservative figure and varies somewhat between authors. Monteith and Unsworth (1990) suggest using a figure for total radiation close to 4.6×10^{-6} mol J^{-1} (PAR). They also refer to work by Howell *et al.* (1983) who give values ranging from 2.1 μmol J^{-1} total radiation for California to 2.9 μmol J^{-1} in Texas. This compares with the average energy content in the PAR for solar radiation of 220 kJ mol^{-1} (4.54×10^{-6} mol J^{-1} conversion factor) assumed by Jones (1992). In view of these figures the conversion factor in the model may

be slightly on the low side, however this does not appear to have a major impact on the output of the model.

Wullschleger (1993) and Reynolds *et al.* (1992) show that the maximum rate of carboxylation V_c^{max} and the light-saturated rate of electron transport J_{max} are closely correlated. Light-saturated electron transport is linearly dependent on maximum carboxylation rate with parameters derived by Wullschleger (1993) from data on a 106 plant species:

$$J_{max} = 29.1 + 1.64\, V_c^{max} \qquad \textbf{(2.44)}$$

Again a response function describes the effect of leaf temperature on light-saturated electron transport. It is assumed that $V_c^{max} = V_c'$ evaluated by 2.38 is for a temperature of 25 °C, and

$$J_{max} = \left(29.1 + 1.64 V_c'\right) k_J(T) \qquad \textbf{(2.45)}$$

where the temperature response is

$$k_J(T) = 1 + 0.041(T-25) - 1.54\times10^{-3}(T-25)^2 - 9.42\times10^{-5}(T-25)^3. \qquad \textbf{(2.46)}$$

This response function was also found to increase at low temperatures (6.3°C in this case), so as with $k_v(T)$, an adjustment was made within the model. See section 2.4.5 for further details.

If triose phosphate utilization, U, limits photosynthesis, the rate of carboxylation is

$$W_p = 3U + \frac{0.5 W_{min} P_o}{\Gamma P_c} \qquad \textbf{(2.47)}$$

where W_{min} is the minimum of W_c and W_j.

Just as V_c^{max} and J_{max} are closely correlated, so also are U and J_{max} (Wullschleger, 1993) and a linear function describes this relationship:

$$U = 5.79\times10^{-7} + 0.0569 J_{max} \qquad \textbf{(2.48)}$$

The (Farquhar *et al.*, 1980) model of photosynthesis has a number of plant variables which need to be automatically derived for every biome and climate. Accordingly, the approach by Woodward and Smith (1994a, b) has

been used in which the maximum light-saturated rate of photosynthesis, A_{max} is determined from the rate of nitrogen uptake, which is also temperature and soil dependent. It is an empirical function, which relates the maximum rate of photosynthesis in any leaf layer to nitrogen uptake, N (see equation 2.50):

$$A_{max} = \frac{190N}{360 + N} \tag{2.49}$$

Finally V_c^{max} is determined from A_{max} (equation 2.38), followed by J_{max}, W_p and U.

Nitrogen is allocated to leaf layers of the canopy in response to the mean irradiance of the leaves:

$$N = N_T \frac{I_q}{I_{oq}} \tag{2.50}$$

where N is the rate of leaf nitrogen uptake (mol g^{-1} day^{-1}), I_{oq} is the photon flux density at the top of the canopy (umol m^{-2} s^{-1}) and N_T is the total nitrogen uptake (mol $g^{-1} \cdot day^{-1}$). This is described in detail in sections 3.1 and 3.2 of Chapter 3.

2.3.6 Dark respiration

The dark respiration rate (μmol CO_2 m^{-2} s^{-1}) of a leaf layer is determined from the rate of nitrogen uptake into the leaves and depends on temperature (Harley *et al.*, 1992).

$$R = \frac{N}{50} e^{r_1(T) - \frac{r_2(T)}{8.3144 T_k}} \tag{2.51}$$

The temperature response functions are:

$$r_1(T) = 20 + 36 \exp(-0.14T) \tag{2.52}$$

and

$$r_2(T) = 50{,}000 + 81000 \exp(-0.14T) \tag{2.53}$$

2.3.7 Canopy stomatal conductance

Stomatal conductance for CO_2 from the atmosphere into the intercellular air spaces, is estimated for each leaf layer, derived from LAI, and then accumulated for the canopy. It varies across a range of environmental conditions, including the atmospheric CO_2 concentration (Jones, 1992). Ball *et al.* (1987) presented an empirical relationship for representing stomatal conductance responses to a range of environmental conditions. These conditions have been modified by Woodward *et al.*, (1995) in order to include the effects of soil moisture.

$$g_s = \left(g_0(T) + g_1(T) A R_h / P_a\right) k_g(w_s) \qquad \textbf{(2.54)}$$

where

g_o (T) is the stomatal conductance when assimilation is zero at the light compensation point mmol m^{-2} s^{-1},

g_1(T) is an empirical sensitivity coefficient,

A is the assimilation rate, μmol CO_2 m^{-2} s^{-1},

R_h is relative humidity of the air surrounding the leaf, %,

P_a is atmospheric CO_2 partial pressure, usually set as 35 Pa,

k_g (w_s) is a function which describes the response of stomatal conductance to soil water content,

T is temperature, °C.

There are some problems, noted by Aphalo and Jarvis (1991,1993), in connection with the appropriateness of some of the response variables such as the relative humidity variable, but due to the lack of a mechanistic model of stomatal conductance to parallel the photosynthetic model this equation was deemed to be adequate to use with some modification.

Stomatal conductance measurements from different climates were analysed by Woodward and Smith (1994b) who showed that g_o and g_1 were approximately linearly dependent on temperature:

$$g_o(T) = 142.4 - 4.8T \quad (2.55)$$

$$g_1(T) = 12.7 - 0.207T \quad (2.56)$$

T is the mean monthly temperature (°C).

The values of these parameters, however, are restricted.

g_o ranges between 8 and 80 μmol m^{-2} s^{-1} and

g_1 ranges between 6.9 and 10 μmol m^{-2} s^{-1} .

Water potential of the soil and leaf are important factors controlling stomatal conductance (Jones, 1980) and it seems reasonable to conclude that stomata close when the leaf water potential falls below a certain threshold value (Jones, 1980, 1992). Gollan *et al.*, (1986, 1992) from their work with sunflowers demonstrate that reductions in stomatal conductance occur as the soil water content declines, even though the leaf water potential remains unchanged. This response is attributed to non-hydraulic communication between the root and shoot probably by abscisic acid (ABA) with a response of decreasing stomatal conductance to increasing rate of ABA supply to the leaves (Gollan *et al.*, 1992). In DOLY, the stomatal conductance is assumed to respond to ABA and soil water content alone.

The response of soil water content, w_s, on stomatal conductance, g_s is defined by a hyperbolic response function based on data in Gollan *et al.*, (1992):

$$k_g(w_s) = \frac{s_1(w_s - s_0)}{w_s - 2s_0 + s_2} \quad (2.57)$$

where the s coefficients define the water holding capacity of the soil and the shape of the response curve of stomatal conductance to soil water content. The parameter, s_0 is the value of the soil water content at which the stomatal conductance is zero, s_1 defines the slope of the response of stomatal conductance to increases of soil water content above s_0, and s_2 is the rate at which the conductance response flattens as soil water reaches its maximum value.

2.3.8 Canopy assimilation

The diffusion of CO_2 from the atmosphere into the intercellular air spaces is controlled by stomatal conductance. It therefore affects the supply of CO_2 in the three rates of carboxylation, W_c, W_j, W_p (equations 2.35, 2.41 and 2.47). Demand from photosynthetic processes is balanced with supply by diffusion through the adjustment of intercellular CO_2. Stomatal conductance varies with a range of environmental conditions including CO_2 concentration (Jones, 1992). This means that as the stomatal conductance varies so does the photosynthetic rate and vice versa (Harley *et al.*, 1982). The assimilation rate, A_d (μmol CO_2 m^{-2} s^{-1}) implied by the diffusion gradient in CO_2 concentration from the atmosphere into the intercellular air spaces is:

$$A_d = \frac{1000 g_s}{1.6} \frac{(P_a - P_c)}{P_{atm}} \qquad \textbf{(2.58)}$$

g_s is stomatal conductance to water vapour (mmol m^{-2} s^{-1}). The factor 1.6 arises because water vapour diffuses through air more rapidly than does CO_2.

P_a and P_c are partial pressures (Pa) of atmospheric CO_2 and internal CO_2, repectively. The atmospheric pressure, P_{atm} is equal to 101,325 Pa.

P_c is derived by setting A_d equal to A_b. A cubic equation is formed from the equations defining assimilation rate (A_b), stomatal conductance (2.54), CO_2 partial pressure (2.58) and the carboxylation rate (W_c, W_j, W_p). The cubic equation is solved and the largest real root is assumed to be the assimilation rate.

2.3.9 Boundary layer conductance

Boundary layer conductance of water, g_a, (m s^{-1}) is derived simply from a logarithmic function of vegetation height, h, (see equations 2.15 and 2.16) which in turn is derived from a function of leaf area index. It is a general descriptor of the role of atmospheric turbulence in the evaporative process and is dependent on wind speed, surface roughness and atmospheric stability. Wind speed in the DOLY model is assumed to be uniformly 20 m s^{-1} at a height well above the highest predicted canopy (200 m).

2.3.10 Water Balance

Changes in soil moisture affect stomatal conductance and in turn assimilation (see equations 2.54 and 2.58). Soil moisture is derived from the amount of precipitation falling at a given site added to the soil water already in the soil and available to the plant, less interception and evapotranspiration as derived from the Penman–Monteith equation (Monteith, 1965). See section 2.2.4 for further information about this equation.

The amount of soil water is adjusted on a daily basis according to the amount of precipitation falling through the vegetation canopy, after allowing for interception, and evapotranspiration. The rate of change in the mass of soil water per unit area, w'_s is:

$$\frac{d}{dt} w'_s = F_p - E_T \qquad (2.59)$$

where

F_p is precipitation throughfall to the soil (g m^{-2} s^{-1}), and

E_T is the evapotranspiration flux (g m^{-2} s^{-1}).

2.3.11 LAI and NPP from DOLY

The two main outputs of DOLY are LAI and NPP.

NPP is calculated from net CO_2 assimilation, A, (i.e. net of leaf respiration in light) accumulated through the year, or growing season, less dark respiration, R, both for the leaves and non-leaf tissue.

Over a growing season or a given time period of, say a year, ($t_1 < t < t_2$), the amount of photosynthate that is available for tissue synthesis and to meet maintenance respiration requirements is:

$$\int_{t_1}^{t_2} (A - R)\,dt \qquad \textbf{(2.60)}$$

where A is net canopy CO_2 assimilation (μmol m^{-2} s^{-1}) and
R is dark respiration of the whole canopy (μmol CO_2 m^{-2} s^{-1}).

If m'_L is the mass of leaves in CO_2 equivalents synthesized during this period and if the synthesis respiration is assumed to be one third of the mass synthesized (Hay and Walker, 1989) then the amount of photosynthate available to synthesize tissue other than leaves and for maintenance is:

$$\int_{t_1}^{t_2} (A - R)dt - \left(1 + \frac{1}{3}\right) m'_L \qquad \textbf{(2.61)}$$

Respiration to maintain tissue other than leaves, R_m (μmol CO_2 m^{-2} s^{-1}) depends on the mass of living tissue (i.e. stems and roots), m'_w, and on absolute temperature (T_k):

$$R_m = k_m m'_w R_R(T_k) \qquad \textbf{(2.62)}$$

where m'_w is the mass of tissue other than leaves per unit area of ground (μmol m^{-2}), and k_m is the constant of proportionality for the dependence of maintenance respiration on the mass of tissue. Woodward *et al.* (1995) set this

value to 0.35 s^{-1}. $R_R(T_k)$ is the temperature response function for maintenance respiration and is calculated as follows:

$$R_R(T_k) = e^{21.6 - \frac{5.367 \times 10^4}{8.3144\, T_k}} \qquad \textbf{(2.63)}$$

Over the period, t_1 to t_2, the maintenance respiration required for non-leaf tissue is:

$$R'_m = k_m \int_{t_1}^{t_2} m'_w(t) R_R(T_k)\, dt \qquad \textbf{(2.64)}$$

If m'_W is the mass of tissue other than leaves (i.e. stems and roots) synthesized during the period, t_1 to t_2, per unit ground area, and synthesis respiration for that tissue is again assumed to be one third of the mass synthesized, then

$$\left(1+\frac{1}{3}\right)m'_w + k_m \int_{t_1}^{t_2} m'_w(t) R_R(T_k)\, dt = \int_{t_1}^{t_2} (A-R)\, dt - \left(1+\frac{1}{3}\right)m'_L \qquad \textbf{(2.65)}$$

A part of the photosynthetic product (equation 2.61) is used to maintain tissue that is present at the beginning of the year or time interval, t_1. However, as it dies, the maintenance requirements of that tissue decrease during the period t_1 to t_2. Likewise, synthesis of new tissue during the period t_1 to t_2 increases maintenance demands. If the mass of tissue other than leaves is assumed constant and equal to the total mass of non-leaf tissue synthesized, then an appropriate allocation of photosynthetic products can be derived:

$$\left(1+\frac{1}{3}\right)m'_w + k_m m'_w \int_{t_1}^{t_2} R_R(T_k)\, dt = \int_{t_1}^{t_2} (A-R)\, dt - \left(1+\frac{1}{3}\right)m'_L \qquad \textbf{(2.66)}$$

and the mass of non-leaf tissue synthesized is:

$$m'_w = \frac{\int_{t_1}^{t_2}(A-R)\,dt - \left(1+\frac{1}{3}\right)m'_L}{\left(1+\frac{1}{3}\right) + k_m \int_{t_1}^{t_2} R_R(T_k)\,dt} \qquad \textbf{(2.67)}$$

Using this approximation NPP, P_N, (μmol m^{-2} s^{-1}) over the time interval, t_1 to t_2 is

$$P_N = \frac{m'_w + m'_L}{t_2 - t_1} \tag{2.68}$$

where the mass of leaves synthesized per unit ground area, m'_L, (μmol CO_2 m^{-2}) is:

$$m'_L = \frac{1}{k_L} L_a \tag{2.69}$$

and, k_L is specific leaf area set as 0.01 m^2 g^{-1}, (100 cm^2 g^{-1}), a typical value from Cannell (1982), which is converted to molar units. L_a is leaf area index.

LAI is essentially derived from the water balance budget. The highest LAI that can be supported by the water balance is predicted. Further tests are then carried out within the model to ensure that this LAI can be supported by the NPP predicted, along with assimilation. If this is not the case, further runs have to be carried out and a lower LAI selected. This is shown by the following equations.

For a particular LAI the model first tests whether net assimilation is sufficient to synthesize the implied mass of leaf tissue:

$$\int_{t_1}^{t_2} (A - R)dt \geq \left(1 + \frac{1}{3}\right) m'_L \tag{2.70}$$

If the implied mass of leaf tissue can be synthesized, the model tests that NPP can be maintained:

$$P_N > 0 \tag{2.71}$$

and that net assimilation occurs in the leaf layer at the bottom of the canopy:

$$\int_{t_1}^{t_2} (A_n - R_n)dt \geq 0 \tag{2.72}$$

where the subscript n denotes the bottom layer.

If net assimilation in the lowest leaf layer is less than, or equals zero, the LAI is too high, so the program loops back and selects the previous LAI. Finally, if the carbon constraints are satisfied, the model tests that precipitation meets or exceeds precipitation loss:

$$\int_{t_1}^{t_2} F_p \, dt \geq \int_{t_1}^{t_2} E_T \, dt \qquad \textbf{(2.73)}$$

where

F_p is the precipitation throughfall to the soil, and

E_T is the evapotranspiration water flux, g m^{-2} s^{-1}.

2.3.12 Changes made to the DOLY model

The model described in Woodward *et al.* (1995) operated with whole number values of LAI. In order to introduce better resolution into the model the LAI loop was altered by Dr. Mark Lomas, University of Sheffield, so that LAI was calculated at fractional values. An iterative procedure is adopted whereby a limited number of LAI values are checked to see whether they fulfill the criteria specified in section 2.3.11. To do this, a tolerance level (0.1) is set within the program along with a step size for the LAI (1.0). These values can be altered if the program needs to be run more quickly or a different level of precision is required. The program is initialized with an LAI = 1. If the criteria are not fulfilled with the current LAI then the previous LAI value is checked. When the difference between the largest LAI that is sustainable and the smallest LAI value that is not sustainable is less than the tolerance level then the largest LAI is the one selected by the program. This process speeds up the program as it enables a quicker selection of LAI and avoids having to check each individual LAI value.

In addition to this the assimilation calculations were simplified into sub-routines and calculated every few days, previously the daily assimilation had been calculated from monthly values.

This version of the DOLY model is referred to as the "standard" version. Two more versions of the model have also been created: DOLY (water version) and DOLY (water and soils version). Maps of LAI and NPP from the DOLY (water and soils) version are shown in Figure 2.21. In addition, difference maps show areas where LAI and NPP differ from the DOLY (water version) (Figure 2.22) and from the World model (Figure 2.23). These two new versions of the model will be briefly described in the next two sections.

2.4 DOLY (water version)

This version of the DOLY model is derived from the standard version described in section 2.3. In the standard version, the initial soil water content was set to field capacity. This section describes how the DOLY model has been altered so that soil water is modelled more realistically and to ensure that the initial soil water conditions vary between sites (see section 2.4.1). This has been accomplished by incorporating the water dynamics used by the CENTURY model (Parton *et al.,* 1993) into the DOLY model. Dr. Mark Lomas (University of Sheffield) altered the model to incorporate these changes. In addition, the LAI iteration performed by the model has also been altered and the amount of evapotranspiration restricted by the amount of water in the soil (see section 2.4.3). Other changes include:

i) dividing the soil into four layers, the top layer of which is only 3 cm deep (see section 2.4.2),

ii) using soil texture data from the ISLSCP (International Satellite Land Surface Climatology Project) dataset produced by Meeson *et al.*(1995), and Sellers *et al.* (1995) (see section 2.4.2),

iii) developing an LAI iteration which uses fractional numbers as opposed to integer values (see section 2.4.3),

iv) enabling the model to run with either C_3 or C_4 photosynthesis (see section 2.4.4),

v) capping the temperature response functions for V_{max} and J_{max} at their respective minimum values (see section 2.4.5),

vi) including the effect of soil water content on the composite nitrogen uptake rate (see section 2.4.6),

vii) calculating the amount of root and stem carbon to be used in the calculation of annual NPP (see section 2.4.7).

This new version is called the DOLY (water version) model. All the inputs and outputs are the same as those described previously. This section will describe these changes in more detail. The sensitivity of this model to the

climate inputs is examined in Chapter 4. Further changes to the DOLY model incorporated soil feedbacks. The soil in each cell is able to interact with the overlying vegetation as represented by LAI and NPP. Section 2.5 describes this water and soils version of DOLY.

In order to show how these processes interact within the DOLY (water version) model, two block diagrams have been produced. Figure 2.14 shows the inputs and outputs in the soil water calculation. Figure 2.15 shows the other processes of LAI iteration, assimilation, nitrogen uptake and the calculation of NPP. These processes are described in sections 2.4.4 to 2.4.7.

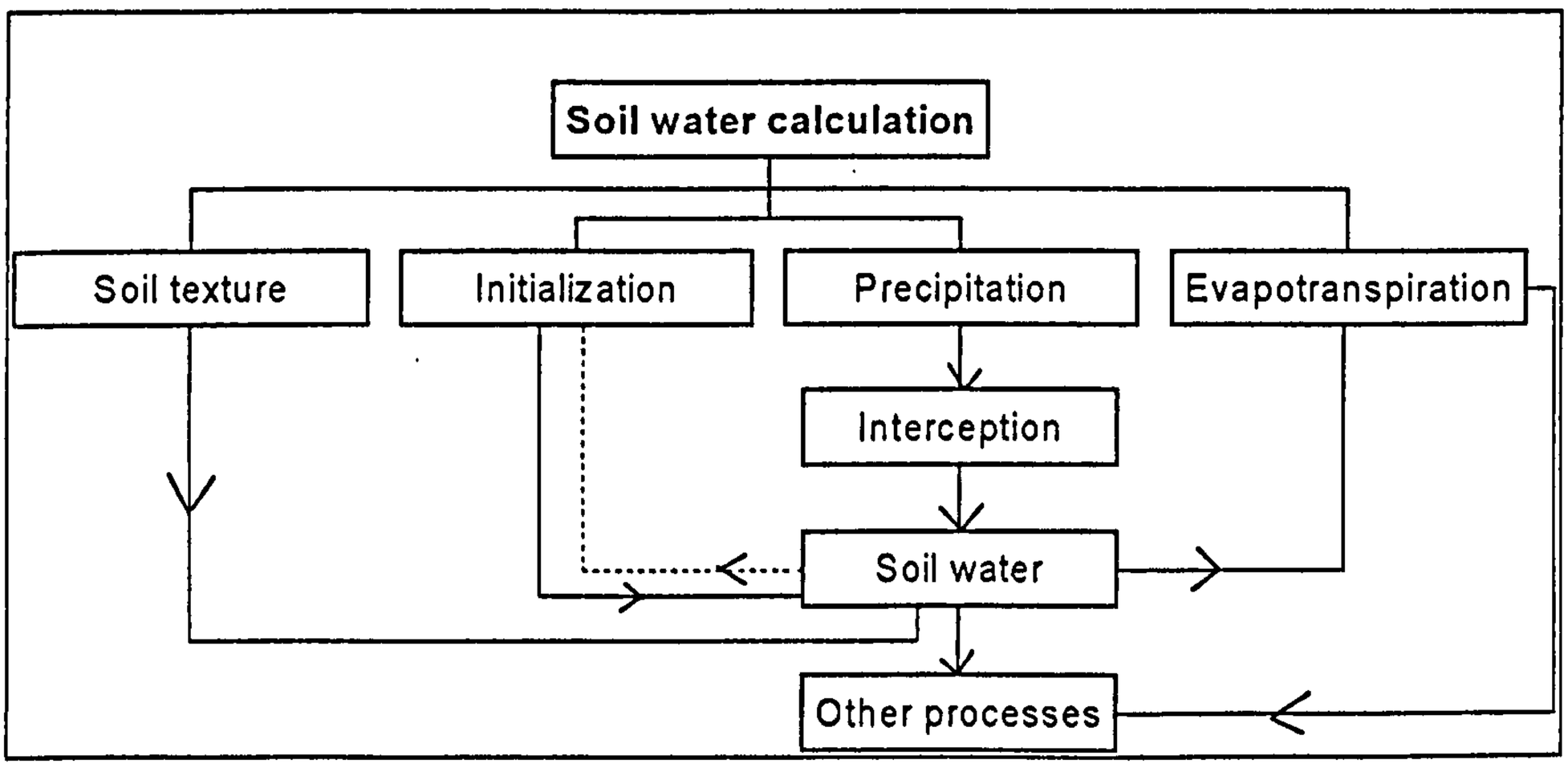

Figure 2.14 A simplified block diagram showing the variables and processes used to calculate soil water. It should be noted that, in this diagram, precipitation includes snow, and evapotranspiration includes bare soil evaporation, as well as evaporation from the snow. The dotted line represents the initialisation process required to obtain the soil water at the start of the year. See sections 2.4.1 and 2.4.2 for further details. The other processes are shown in Figure 2.15.

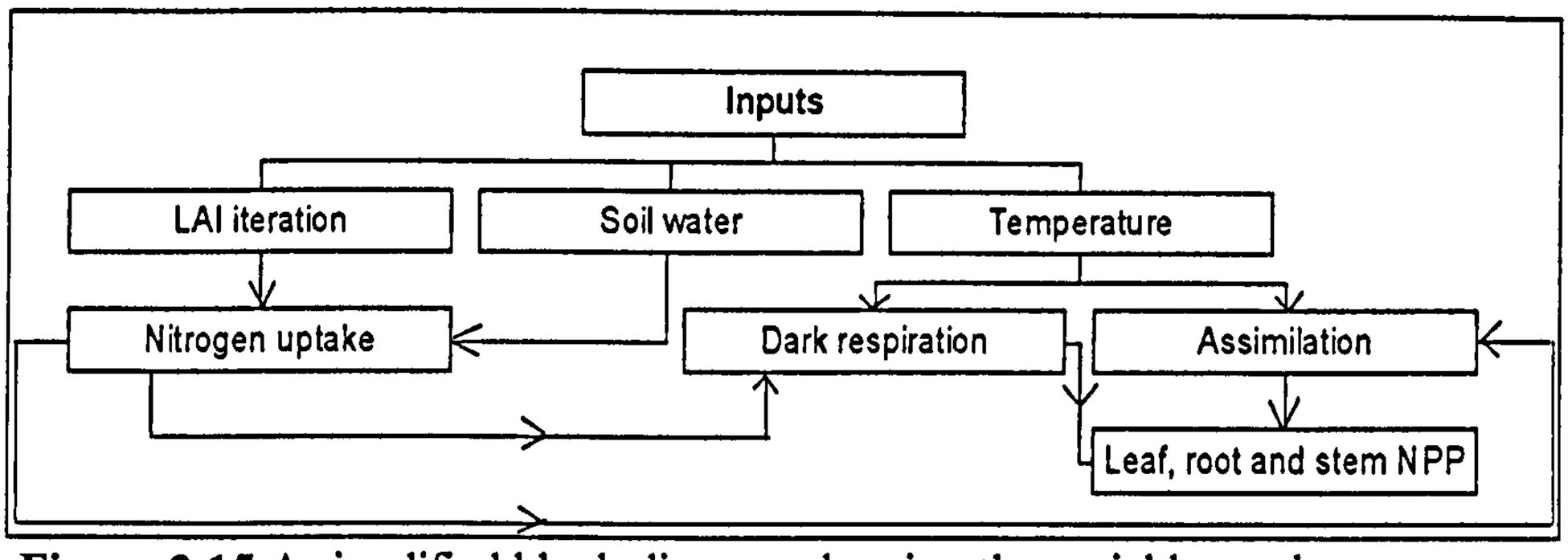

Figure 2.15 A simplified block diagram showing the variables and processes used to calculate leaf, root and stem NPP. It should be noted that nitrogen uptake is influenced by temperature, but to retain clarity in the diagram this link is not shown here. See sections 2.4.3 and 2.4.7 for further details.

2.4.1 Initialization

Soil water content in the original version of the DOLY model (Woodward *et al.*, 1995) was initialized using a parameter, which assumed that the soil was at field capacity at the start of the year. This assumption however is not valid at sites where there is an arid period at the start of the year. The water in the soil would be well below field capacity at such sites. Also, assuming that the soil was at field capacity meant that the assimilation calculations within the program were not made with the correct water profile. These assimilation calculations are dependent on both the initial condition of the soil water profile and the day of the year the simulation is started. This also changes the water profile. The soil is assumed to be analogous to a bucket which is filled and emptied according to inputs of precipitation and leaf drip and the output of evapotranspiration. In order to obtain a better representation of the water in the soil at the beginning of a given year the model is run for a number of years. This enables the amount of water that is in the soil to be compared with that of the previous year. If there is a large difference in these values, further runs are carried out until the values converge or are within a given range. This allows for the possibility that the period of the water bucket

cycle is longer than one year. In order to identify the cycle at a site, the values of the water buckets on the last day of each year are checked against the values of previous years. If the value has occurred previously, within a set tolerance level (0.01 mm in the case of the present version), then a cycle is assumed to have occurred. The average of the NPP values over the cycle is then calculated. This method can however be computationally burdensome due to the fact that at some sites the period of the water cycles is very large (e.g. 20 years). As this does not happen in reality, because the system is not driven by the same input data year after year, it seems reasonable to simply average the NPP values if the system has not converged after some pre-set number of years. In the DOLY (water version) model, if the model has not converged after 7 years then the average of the previous 5 years of NPP values is used.

2.4.2 Soil water

The CENTURY model calculates monthly evaporation and transpiration water loss, water content of the soil layers, snow water content and saturated flow of water between soil layers. If the mean monthly air temperature falls below 0°C the monthly precipitation falls as snow. Actual evapotranspiration is calculated within DOLY using the Penman–Monteith equation (Monteith, 1965) (see section 2.2.4), but in addition the potential evapotranspiration rate is also calculated using the same equations as Parton *et al.* (1993). This potential evapotranspiration rate is used to determine the sublimation (the change in state from a solid to a vapour, without going through the liquid state) of water from the snow pack which occurs at the same rate. Snow melt occurs if the temperature exceeds 0°C and is a linear function of the air temperature. Allowance is also made for bare soil evaporation and interception water loss. These are calculated as fractions of the monthly precipitation and are subtracted from the total monthly precipitation, with the remainder of the water added to the soil. These calculations were incorporated

into the DOLY model. Water is spread through the different soil layers by adding the water to the top layer and then allowing excess water (water above field capacity) to flow into the next layer. The number of soil layers was kept to four but instead of these being sub-divided into 15 cm increments down to 60 cm, as in CENTURY, three of the lower layers were sub-divided equally down to 1 m depth. This was done so that a shallow top layer could be incorporated into the model. This top layer was set to a depth of 3 cm. The moisture content of this layer could then be used to determine the flammability of the leaf litter on the surface of the soil. These data are used in a later model (the Sheffield Dynamic Global Vegetation Model, (SDGVM)) to determine the likelihood of fire.

In CENTURY the field capacity and wilting point for the different soil layers is calculated as a function of the bulk density, soil texture and organic matter content using an equation developed by Gupta and Larson (1979). In the DOLY model (water version), due to the limited availability of data on the physical properties of soils, such as the particle size and structure, an alternative approach is used. Cosby *et al.* (1984) proposed a method whereby it is possible to determine the moisture characteristics of a soil from its texture alone by the use of regression analysis. The following equation is used:

$$\Psi = \Psi_s \left(\Theta / \Theta_s \right)^{-b} \qquad \textbf{(2.74)}$$

where

ψ is matric potential (cm),

ψ_s is the "saturation" matric potential (cm),

b is the slope of the moisture retention curve,

Θ is the moisture content (vol. vol.$^{-1}$),

Θ_s is the saturated moisture content (vol. vol.$^{-1}$).

It should be noted that the various "potential" terms, referred to in this section, are suction potentials in the soil scientists' sense (therefore they are positive) as opposed to water potentials which would be negative.

By analysing 1448 soil samples from across the USA and using analysis of variance and multiple regression techniques, Cosby *et al.* (1984) were able to obtain the variables, ψ_s and b, for each soil textural class, as well as the saturated hydraulic conductivity and the saturated water content. The percentage sand, silt and clay for each class was based on the mid-point values of each of these textural classes on the US Department of Agriculture textural triangle. The corners of the triangle represent 100% of each of the three categories, sand, silt and clay. Any point within the diagram defines the percentage proportions of the three categories. Figure 2.16 shows the principles used. For the point marked there is 15% silt, 65% sand and 20% clay. This would be defined as a sandy clay loam.

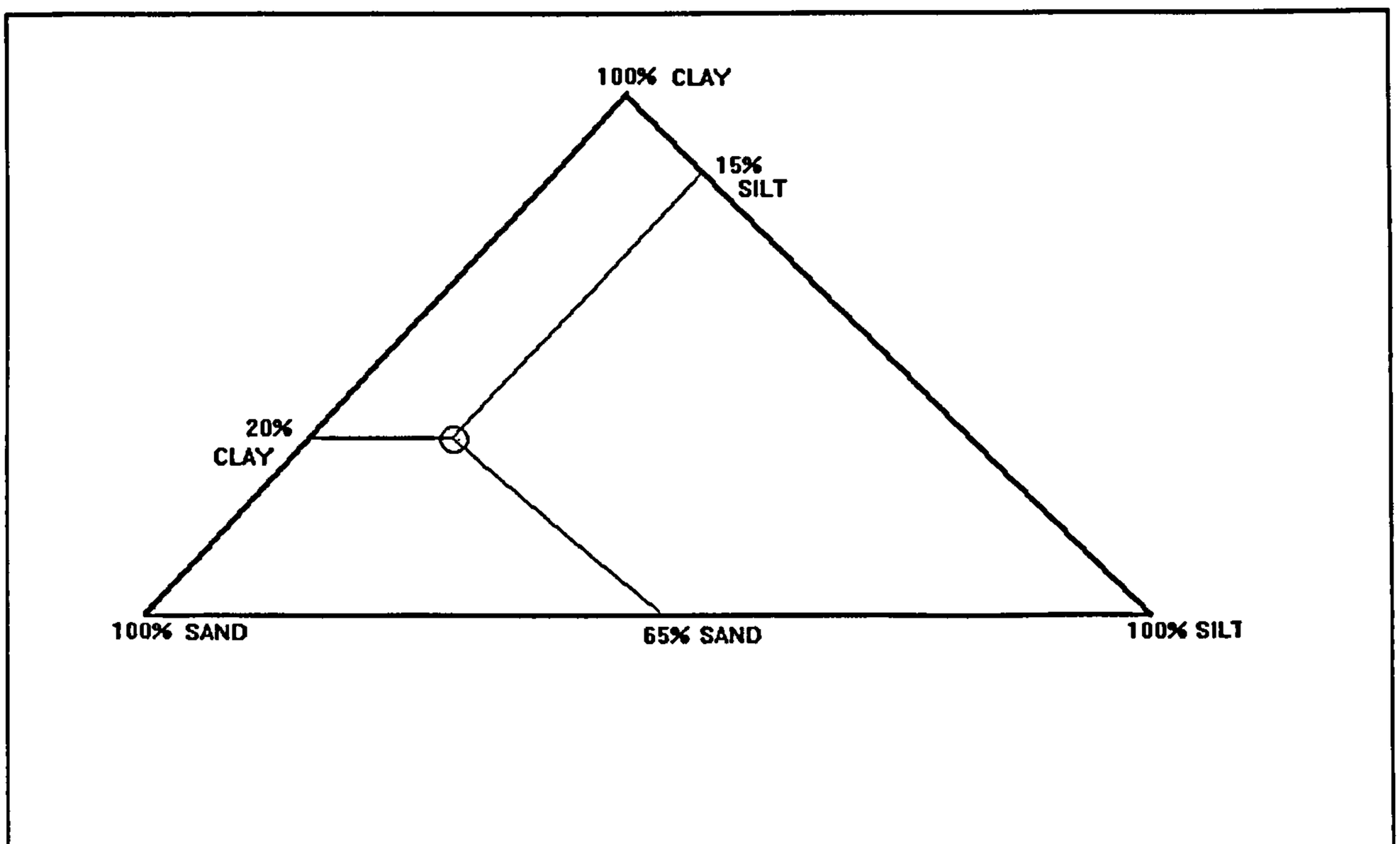

Figure 2.16 An example of a soil textural class on a soil textural triangle. This soil would be defined as a sandy clay loam.

Multiple linear regression analysis was performed on the means and standard deviations of each parameter using the percentage sand, silt and clay for each textural class as the independent variables. This analysis was designed to pick the most important variable (in the sense of the most parameter variance explained by the regression) from sand, silt or clay, and having corrected for the linear relationship in that variable, select the second most important variable from the two remaining. The following equations have been produced from the results of this analysis on the means and standard deviations of b, saturation matric potential (ψ_s) and saturated moisture content (Θ_s) :

$$b = 3.1 + 0.157c - 0.003s \quad (2.75)$$

$$\Theta_s = 50.5 - 0.142s - 0.037c \quad (2.76)$$

$$\log \Psi_s = 1.54 - 0.0095s + 0.0063z \quad (2.77)$$

where s is % sand, c is % clay and z is % silt.

The data for the soil texture values were extracted from the ISLSCP dataset (Meeson *et al.*, 1995; and Sellers *et al.*, 1995). The percentages of soil clay, sand, and silt were estimated from the soil classification on the ISLSCP soil texture file. This results in the classifications shown in the following table (Table 2.5):

Table 2.5 The percentages of sand, silt and clay for different soil types together with the index number allocated by ISLSCP.

ISLSCP Index	Clay (%)	Sand(%)	Silt(%)	Soil type
1	7	80	13	loamy sand
2	12	62	26	sandy loam
3	18	42	40	loam
4	27	63	10	sandy clay loam
5	30	35	35	clay loam
6	0	0	0	ice
7	18	42	40	loam
8	0	0	0	ocean

Field capacity is defined as the amount of water held in the soil after the excess has drained away and after the rate of downward movement has materially decreased. As Russell (1988) points out, deciding when the flow of water has "materially decreased" is difficult, and open to discussion. This time period can range from a few days to several weeks. In order to get around this problem, the moisture content at field capacity has been defined in terms of matric suction. Colman (1947) found 33 kPa (0.33 bar) to be an acceptable value for the soils he studied, and the value selected for use in the DOLY model (water version) is 306 cm of water (30 kPa). Rearranging equation 2.74 in order to obtain the moisture content of the soil at field capacity (θ_{fc}) gives equation 2.78:

$$\Theta_{fc} = \left(\frac{\Psi_{fc}}{\Psi_s} \right)^{(-1/b)} \Theta_s \qquad (2.78)$$

where

ψ_s is the "saturation" matric potential (cm),

ψ_{fc} is the field capacity matric potential (cm)

Θ_{fc} is the moisture content at field capacity (vol. vol. $^{-1}$)

For a soil at field capacity, as in this case, the mass of soil water per unit area, (Θ_{fc}') is related to the soil water content (Θ_{fc}) and soil bulk density, k_W for a known soil depth as follows:

$$\Theta_{fc}' = k_w \times \Theta_{fc} \qquad (2.79)$$

where

Θ_{fc} is the soil water content (vol. vol.$^{-1}$) and,

k_w is a form of soil bulk density (g m^{-3}) assuming a known soil depth.

The moisture content at the wilting point is calculated in a similar manner:

$$\Theta_{wp} = \left(\frac{\Psi_{wp}}{\Psi_s}\right)^{(-1/b)} \Theta_s \qquad (2.80)$$

where

ψ_{wp} is the wilting point matric potential (cm) and is usually set to 15300 cm of water (1.5 MPa), the standard value used (Russell, 1988).

2.4.3 LAI iteration

In the version of DOLY described by Woodward *et al.* (1995), LAI is determined from hydrological and primary productivity constraints. For a given LAI, the model tests whether there is sufficient net assimilation to synthesize the implied mass of leaf tissue. If this tissue can be synthesized, the model then tests that NPP can be maintained and that net assimilation occurs in the leaf layer at the bottom of the canopy. Finally, if these carbon constraints are satisfied the model tests that precipitation meets or exceeds moisture loss.

There is however a problem with this final test. The moisture loss, as represented by evapotranspiration, from the model is not limited by the amount of water available in the soil. It is in fact set equal to the maximum amount of evapotranspiration, calculated from the Penman–Monteith equation, (Monteith and Unsworth, 1990) that the vegetation can support. This means that the LAI loop may be left too early due to too high a value of evapotranspiration. If the

water that was actually available in the soil was transpired a higher LAI value would be supported and, providing the other criteria were fulfilled, a higher NPP. To remedy this problem, the amount of transpiration was restricted by the soil water content, on a daily basis. The water balance exit condition is no longer used in the model.

In addition to this change, the LAI iteration itself was also altered. An initial step size of 0.3 and tolerance of 0.1 were set for the non-integer LAI calculation. Values of the maximum and minimum LAI sustainable were set, together with three switches which were altered according to whether specific conditions were met. They are set to zero, if a condition is not met, and one, if the condition is met. These switches are as follows:

i) checks whether an LAI of less than one has been tried,

ii) resets the step size after LAI has been less than one and subsequently greater than one,

iii) records a sustainable LAI.

Another variable is set equal to the maximum minus minimum LAI sustainable, and the LAI loop is exited when this is less than the tolerance value. Finally, the variable, rem, is calculated as follows:

$$\text{rem} = \text{rlai} - \text{int}(\text{rlai}) \tag{2.81}$$

where

rlai is the fractional number value of LAI, and

int(rlai) is the integer value of LAI.

This adjusts a number of equations in the model that previously operated with integer LAI values. In order to demonstrate the approach adopted using the fractional LAI values, the following example shows the procedure to compute an LAI between 2 and 3, say, lai = 2 + rem.

Consider the Beer's law calculation:

$$I_q = I_{0q} e^{-kL_a} \tag{2.82}$$

where

I_{0q} is the irradiance on the canopy

(μmol photons m^{-2} s^{-1}),

I_q is the irradiance at L_a depth from the top of the canopy

(μmol photons m^{-2} s^{-1}),

L_a is the fractional LAI, and

k is the extinction coefficient.

The irradiance within the canopy, I, is determined by calculating the irradiance for each layer and cumulating this through all the layers of the canopy. These irradiance values are then used to determine the rate of nitrogen uptake. Nitrogen is allocated to leaf layers of the canopy in proportion to the mean irradiance of the leaves:

$$N = N_T \frac{I_q}{I_{0q}} \qquad \textbf{(2.83)}$$

where

N is the rate of leaf nitrogen uptake (mol g^{-1} day^{-1}),

N_T is the rate of total nitrogen uptake (mol g^{-1} day^{-1}).

This equation is altered in the following manner. The irradiances for the first three LAI layers are denoted by r_1, r_2 , r_3. In order to keep the nitrogen distribution consistent with that of the integer LAI calculations, it is distributed in the following irradiances r_1, r_2 , and $r_3 \times$ rem, so that where

$$sum = (r_1 + r_2) + r_3 \times rem, \qquad \textbf{(2.84)}$$

the nitrogen given to each layer is,

$$N_T \times \frac{r_1}{sum}, \; N_T \times \frac{r_2}{sum}, \; N_T \times \frac{r_3 \times rem}{sum}, \text{ respectively.} \qquad \textbf{(2.85)}$$

It is assumed that the assimilation rate for a fraction of leaf area with the same fraction of nitrogen available to it, produces the same assimilation rate as the full unit leaf layer with all of the nitrogen available to it. Using this assumption the fractional leaf area can be treated as a full unit leaf area and its assimilation rate computed. This assimilation rate will then be equal to the assimilation rate of the fractional leaf area on the basis that the assumption is correct.

In order to calculate the third LAI layer assimilation rate, the nitrogen which is allocated to that layer is scaled up so as to represent a full unit leaf area, i.e. the nitrogen uptake is scaled by a factor of 1/rem. The assimilation rate is then calculated in the usual manner, as described in the previous section. The nitrogen uptake for the three unit layers is:

$$N_1 = \frac{N_T \times r_1}{sum}, \quad N_2 = \frac{N_T \times r_2}{sum}, \quad N_3 = \frac{N_T \times r_3}{sum}. \qquad \textbf{(2.86)}$$

Now, say these values give rise to assimilation rates of A(1), A(2) and A(3), then the assimilation rate of the fractional leaf area is equal to A(3). So that the net assimilation rate (assim) for this system would be:

$$assim = A(1) - dresp(1) + A(2) - dresp(2) + ((A(3) - dresp(3)) \times rem) \qquad \textbf{(2.87)}$$

where

assim is the amount of photosynthate that is available for tissue synthesis and to meet maintenance respiration requirements,

A(1) to A(3) are the assimilation rates for each leaf layer (1 to 3),

dresp(1) to dresp(3) are the dark respiration rates for each leaf layer (1 to 3).

To test whether or not this method was correct, plots of NPP vs. LAI were made. If the method was correct these curves should be continuous and pass through the points that the normal integer LAI calculation would yield and also be smooth. In the plots examined these criteria were satisfied.

2.4.4 Assimilation and photosynthesis

The original DOLY model as described in Woodward *et al.* (1995) calculated C_3 photosynthesis from the model developed by Farquhar *et al.* (1980) and the empirical stomatal conductance model of Ball *et al.* (1987). These equations are simple to use and are able to model important responses. However, the C_4 pathway of photosynthesis was not modelled, although it was mentioned that the DOLY model could be extended to include this pathway. Many tropical and sub-tropical grasses use this pathway together with crops such as maize, sorghum and pasture grasses. More recent work has used the DOLY model (water and soils version) in conjunction with another model to determine global vegetation in terms of functional types. For this work a distinction needed to be made between grass types, as to whether there were C_3 or C_4 grasses present. The C_4 model of Collatz *et al.* (1992) was used to do this. The DOLY (water version) model can be run using either the C_3 or C_4 pathway. The pathway to be used is selected at the start of the program. This C_4 model predicts photosynthesis and stomatal conductance as a function of leaf temperature, photosynthetically active quantum flux density, CO_2 partial pressure and relative humidity at the leaf surface. The important adjustable variables are the capacities of rubisco and PEP carboxylase to fix CO_2 which can be estimated from leaf photosynthetic responses to light and CO_2. A number of variables were set as constant by Collatz *et al.* (1992) and tabulated. The ones used within the DOLY (water version) are shown in Table 2.6.

Table 2.6 Variables used within the DOLY (water version) that were obtained from Collatz *et al.* (1992).

Name	Symbol	Value
PEP carboxylase rate constant for CO_2	k_p	0.7 mol m^{-2} s^{-1}
Proportional increase in a parameter value for a 10°C increase in leaf temperature	Q_{10}	2
Atmospheric pressure at sea level	P	101325 Pa
Leaf quantum absorptance	a	0.8
RuBP quantum requirement	α_r	0.11 mol mol^{-1}
Fractional RuBP quantum requirement	f	0.6

Note that Collatz *et al.* (1992) used a value of 10^5 Pa for atmospheric pressure.

According to Collatz *et al.* (1992) there are three limiting processes that determine net photosynthesis for C_4 plants (A_{c4}) and the relationships between these processes and A_{c4} may be expressed as:

$$A_{c4} = \min\left\{ \begin{array}{c} J_i, f\left(\alpha, Q_p\right) \\ J_c, g\left(p_i, k, T_L\right) \\ J_e, h\left(V_{\max}, T_L\right) \end{array} \right\} - R_{d,} i\left(T_L\right) \qquad \textbf{(2.88)}$$

where

J_i is the light-dependent rate of assimilation,

J_c is the CO_2–limited flux,

J_e is the assimilation rate limited by the capacity for CO_2 fixation by rubisco,

f, g, h, and i denotes separate functions of α and Q_p, p_i, k, and T_L, V_{max} and T_L, and $T_{L,}$ respectively.

α is the product of leaf absorptance and the intrinsic quantum utilization efficiency,

R_d is the rate of CO_2 release or respiration in light due to processes other than photorespiration, a typical value is 0.82 μmol m^{-2} s^{-1},

T_L is leaf temperature,

k is the initial slope of the photosynthetic CO_2 response,

V_{max} is maximum rubisco capacity, and

Q_p is the incident photosynthetically active quantum flux density.

This equation is the same general form as that used by Farquhar *et al.* (1980) for C_3 photosynthesis and the one used within DOLY (see section 2.3.5). These three processes are modelled within the DOLY (water version) using sub-routines. The sub-routine for C_4 assimilation computes the assimilation rate by forming a cubic equation from the three equations defining stomatal conductance, CO_2 partial pressure and the carboxylation rate. The cubic equation is solved and the largest real root is assumed to be the assimilation rate (J_c). This is then compared with the light dependent assimilation (J_i) and V_{max} dependent assimilation (J_e) and the minimum value is selected.

To determine the CO_2–limited flux, J_c , the following equation from Collatz *et al.* (1992) was used:

$$J_c = p_i\left(k_p - \frac{L}{p_i}\right)\Big/P \qquad \textbf{(2.89)}$$

where

p_i is the CO_2 concentration in the intercellular spaces of the mesophyll,

k_p is a pseudo-first-order rate constant for PEP carboxylase with respect to P_i, and set to 0.7 mol m^{-2} s^{-1} by Collatz *et al.*, (1992),

P is atmospheric pressure,

L is the leak of CO_2 between the bundle sheaf and the mesophyll and is derived from $L = (p_{bs} - p_i)/P\,r_c$, where p_{bs} is the bundle sheath CO_2 partial pressure, and r_c is the resistance to CO_2 diffusion through the bundle sheath walls and membranes.

To determine the assimilation rate limited by the capacity for CO_2 fixation by rubisco, J_e , the following equation from Collatz *et al.* (1992) was employed:

$$J_e = V_{max} \tag{2.90}$$

The temperature dependence of the substrate saturated rubisco capacity, V_{max}, is calculated from A_{max} (the maximum light-saturated rate of photosynthesis) derived from the rate of leaf nitrogen uptake and adjusted for temperature using Q_{10}. V_{max} is given as a Q_{10} function and is further restricted by upper and lower temperature limits on net assimilation. The temperature dependence of the substrate saturated rubisco capacity is calculated within the model using a slightly modified version of equation 5B from Collatz *et al.* (1992). This is equation 2.91. V_{max} is reduced at low temperatures and temperatures above 35°C but increased at temperatures between 25°C and 35°C values. These limits were derived by Collatz *et al.* (1992) from approximate responses of C_4 plants to extreme temperatures. Using equation 2.91 means that the V_{max} values in the DOLY (water version model) would be slightly higher than the values derived from the Collatz *et al.* (1992) equation up to 25°C, about the same for temperatures between 25°C and 35°C and higher for temperatures above 35°C.

$$V_T = \frac{V_{max} Q_{10}^{\frac{T_l - 25}{10}}}{\left(1 + e^{0.3(10 - T_l)}\right)\left(0.8 + e^{0.14(T_l - 36)}\right)} \tag{2.91}$$

where

V_T is the temperature-dependent V_{max},

Q_{10} is the proportional increase in a parameter value for a 10°C increase in leaf temperature, and

T_L is leaf temperature (°C).

Finally the light-dependent flux, J_i , was derived using the following equation:

$$J_i = a\alpha_r f Q_p \tag{2.92}$$

where

a is leaf quantum absorptance,

α_r is the ribulose bisphosphate (RuBP) quantum requirement (the intrinsic quantum yield of C_3 photosynthesis), set at 0.11 mol mol^{-1} by Collatz *et al.* (1992).

f is the fractional RuBP quantum requirement (the fraction of absorbed photons used by the C_3 reactions), set at 0.6 by Collatz *et al.* (1992), and

Q_p is the incident photosynthetically active quantum flux density.

The assimilation rate, calculated for a given LAI, using C_4 photosynthesis is compared to the rates calculated using V_{max} and J_{max} for C_3 photosynthesis. These values of V_{max} and J_{max} are calculated from the maximum light saturated rate of photosynthesis which is related to nitrogen uptake (see equation 2.49). If the C_3 photosynthesis value derived from V_{max} is less than the value derived using J_{max} then this is the assimilation rate selected for that LAI. However, should the assimilation rate from the C_4 photosynthesis calculation exceed this value then this is the rate selected . The model calculates assimilation rates for all layers of the canopy. The canopy assimilation rate, for the LAI selected by the program, is used to calculate annual NPP. The annual assimilation rate for the lowest layer of the canopy is also recorded so that the model can test that net assimilation does actually occur in this lowest layer.

2.4.5 Temperature response functions for V_{max} and J_{max}

The response of V_{max} to temperature takes the form of a cubic curve so that once a minimum value is reached it starts to increase and once a maximum value is reached it starts to decrease. Providing the temperature exceeds 9.5°C then, as in Woodward *et al.* (1995), the temperature response function, $k_v(T)$ is:

$$k_v(T) = 1 + 0.051(T-25) - 2.48\times10^{-4}(T-25)^2 - 8.09\times10^{-5}(T-25)^3 \qquad \textbf{(2.93)}$$

where T is temperature (°C)

However, for temperatures lower than 9.5°C , the minimum value, the temperature response function starts to increase and give spurious results. In order to prevent this occurring, $k_v(T)$ is set at 0.459 which is the value obtained by substituting for T=9.5 in equation 2.93. Similarly, for the temperature response function for J_{max}. At temperatures above 6.3°C the temperature response function, ($k_J(T)$ is:

$$k_J(T) = 1 + 0.041(T-25) - 1.54\times10^{-3}(T-25)^2 - 9.42\times10^{-5}(T-25)^3 \qquad \textbf{(2.94)}$$

For temperatures lower than 6.3°C the minimum value, the temperature response function, $k_J(T)$ is set at 0.313, which is the value obtained by substituting for T=6.3 in equation 2.94.

2.4.6 Plant nitrogen uptake and soil water

In the original DOLY model, plant nitrogen uptake was dependent solely on the amount of soil carbon and soil nitrogen, but no allowance was made for the amount of water in the soil. The ability of a plant to extract nitrogen will be reduced as the soil becomes drier. In order to remedy the deficiency in the original equation, the plant nitrogen uptake calculation was altered to respond to the soil water content. This is now:

$$N_p = 120\min\{s_n/600,1\}e^{-8\times10^{-5}s_c}\times\frac{\Theta_s}{\Theta_{fc}} \qquad \textbf{(2.95)}$$

where

Θ_s is soil moisture content (g water g soil^{-1}),

Θ_{fc} is the moisture content at field capacity(g water g soil^{-1}), and

s_c and s_n are soil carbon and soil nitrogen per unit land area, respectively.

2.4.7 Annual net primary productivity

The amount of photosynthate that is available for tissue synthesis and to meet maintenance respiration requirements over a time period, t_1 to t_2 (typically one year or growing season) is:

$$\int_{t_1}^{t_2} (A - R) dt \qquad \textbf{(2.96)}$$

where

A is net canopy CO_2 assimilation (μmol m^{-2} s^{-1}) , and

R is dark respiration of the whole canopy (μmol m^{-2} s^{-1}) which depends on nitrogen uptake and temperature.

If m'_L is the mass of leaves in CO_2 equivalents synthesized during the interval, t_1 to t_2, and if the growth respiration of the leaves is assumed to be one quarter of the mass synthesized then the amount of photosynthate available to synthesize tissue other than leaves and for maintenance is:

$$\int_{t_1}^{t_2} (A - R) dt - \left(1 + \frac{1}{4}\right) m'_L \qquad \textbf{(2.97)}$$

This growth respiration is slightly lower than the previous value of one third as used in Woodward *et al.* (1995), but the same as used by McGuire *et al.* (1992) in the terrestrial ecosystem model (TEM). It should also be noted the current year's photosynthate is dependent in part on the leaf growth that has occurred in previous years. This is considered later in this section (see equations 2.105 and 2.69).

The model records the length of the growing season by ascertaining whether there is sufficient water available to support leaves, and whether the temperature is high enough. The temperature limit for the growing season is 5°C, which is the minimum temperature for growth for trees of cold environments (Prentice, 1992). Hence, no leaves are grown below this temperature in the model. Also, if the wilting point is reached in the soil then there are no leaves.

Respiration to maintain tissue other than leaves depends on the mass of living tissue (i.e. stems and roots) and on temperature:

$$R_m = k_m m'_w R_R(T_k) \qquad \textbf{(2.98)}$$

where

m'_w is the mass of stems and roots,

k_m is the constant of proportionality for the dependence of maintenance respiration on the mass of tissue and is set by Woodward *et al.* (1995) to $0.35\ s^{-1}$.

$R_R(T_k)$ is the temperature response function for maintenance respiration and is calculated as follows, where T_k is the temperature in terms of kelvin.

$$R_R(T_k) = e^{21.6 - \frac{5.367 \times 10^4}{8.3144\, T_k}} \qquad \textbf{(2.99)}$$

Over the period, t_1 to t_2, the maintenance respiration required for non-leaf (or woody) tissue is:

$$R'_m = k_m \int_{t1}^{t2} m'_w(t) R_R(T_k) dt \qquad \textbf{(2.100)}$$

If m'_w is the mass of tissue other than leaves (i.e. stems and roots) synthesized during the period, t_1 to t_2, and synthesis respiration for that tissue is again assumed to be one quarter of the mass synthesized, then

$$\left(1+\frac{1}{4}\right) m'_w + k_m \int_1^2 m'_w(t) R_R(T_k) dt = \int_1^2 (A-R) dt - \left(1+\frac{1}{4}\right) m'_L \qquad \textbf{(2.101)}$$

This woody tissue consists of roots and stems and can be divided between the two, m'_r and m'_s, respectively.

$$\left(1+\frac{1}{4}\right)m'_r+\left(1+\frac{1}{4}\right)m'_s+k_m\int_{t_1}^{t_2}m'_r(t)R_R(T_k)dt$$
$$+k_m\int_{t_1}^{t_2}m'_s(t)R_R(T_k)dt=\int_{t_1}^{t_2}(A-R)dt-\left(1+\frac{1}{4}\right)m'_L \quad \textbf{(2.102)}$$

Assuming that NPP is the total of the three masses for leaf, root and stems then the following equation holds true:

$$P_N - m'_s = m'_L + m'_r \quad \textbf{(2.103)}$$

where P_N is the annual net primary productivity (μmol m^{-2} s^{-1})

It is assumed that 30% of the carbohydrates stored in roots and stems from the previous year goes into the present year's leaf production. This is a somewhat arbitrary figure but due to the lack of data on root production and biomass, a "best-guess" had to be made from data in the literature such as Cannell (1982). The root carbohydrate carried over from the previous year is calculated as follows:

$$0.3\,t_{gr}\left(\frac{1}{4}\right)m'_L \quad \textbf{(2.104)}$$

and the mass of leaves produced for the current year is in fact:

$$(1-0.3)t_{gr}\left(1+\frac{1}{4}\right)m'_L \quad \textbf{(2.105)}$$

where

t_{gr} is the length of the growing season (months), and

m'_L is the mass of leaf (in molar units) calculated from equation 2.69

Re-arranging equation 2.102 and including equations 2.104 and 2.105 yields:

$$\left(1+\frac{1}{4}\right)m'_s+k_m\int_{t_1}^{t_2}m'_s(t)R_R(T_k)dt=\int_{t_1}^{t_2}(A-R)dt-(1-0.3)t_{gr}\left(1+\frac{1}{4}\right)m'_L$$
$$-0.3t_{gr}\left(\frac{1}{4}\right)m'_L-\left(1+\frac{1}{4}\right)m'_r-k_m\int_{t_1}^{t_2}m'_r(t)R_R(T_k)dt$$

(2.106)

and the mass of stem (m'_s) synthesized during the period t_1 to t_2 as:

$$\frac{\int_{t_1}^{t_2}(A-R)dt-(1-0.3)t_{gr}\left(1+\frac{1}{4}\right)m'_L-0.3t_{gr}\left(\frac{1}{4}\right)m'_L-\left(1+\frac{1}{4}\right)m'_r-k_m\int_{t_1}^{t_2}m'_r(t)R_R(T_k)dt}{\left(1+\frac{1}{4}\right)+k_m\int_{t_1}^{t_2}R_R(T_k)dt} \quad \textbf{(2.107)}$$

Root carbon production (P_r) was determined for a number of temperate and tropical sites across the world from data produced by Cannell (1982) for forests (including drought deciduous forest). Dry matter values were converted into carbon values, and evapotranspiration data were calculated by the DOLY model for the same site co-ordinates. Regressing root carbon production against annual evapotranspiration (E_{Tann}) for 5 sites yielded the following relationship ($r^2 = 0.97$):

$$P_r = E_{Tann} / 13.4 \quad \textbf{(2.108)}$$

where

P_r is annual root productivity (gC m^{-2} yr^{-1})

E_{Tann} is annual evapotranspiration (mm yr^{-1})

The root carbon productivity values were checked by substituting them in equation 2.110 and examining the resulting NPP values to see whether they differed greatly from the NPP values determined previously by using assimilation, respiration and leaf mass alone. The mass of root, m'_r, produced in a year can be determined from the root carbon productivity by converting into molar units as follows, (12 gC mol^{-1}):

$$m'_r = P_r / 12 \quad \textbf{(2.109)}$$

Knowing the mass of leaf carbon and root carbon together with the respiration and assimilation values enables the stem carbon to be derived from equation 2.106 and subsequently, NPP from equation 2.110.

NPP, P_t, (units of tC ha^{-1} yr^{-1}) for the time period t_1 to t_2 is calculated from m'_L, m'_s and m'_r derived from equations 2.96 to 2.110 and a conversion factor of 12/100 is used to convert from molar units to tC ha^{-1} yr^{-1}:

$$P_t = \left(m'_s + 0.7m'_L \times t_{gr} + m'_r\right) \times \frac{12}{100} \qquad \textbf{(2.110)}$$

2.5 DOLY (water and soils version)

This version of the DOLY model is derived from the water version described in section 2.4. All the calculations used in the DOLY (water version) are used in this model with the addition of the calculation of soil carbon and nitrogen. The equations used to perform these calculations have been extracted from the CENTURY model (Parton *et al.*, 1993) and Dr. Mark Lomas has incorporated them into the DOLY (water version) in order to create the DOLY (water and soils version). This section describes this particular version of DOLY. It incorporates the soil dynamics used by the CENTURY model and is able to model interactions between vegetation and the soil, in relation to given soil texture and climatic inputs.

The CENTURY model can simulate the dynamics of carbon, nitrogen, phosphorus and sulphur for different plant-soil systems. It was originally designed for grasslands but has been modified to include forests and croplands using sub-models. All these sub-models are linked to a common soil organic matter (SOM) sub-model. This particular sub-model simulates the flow of selected elements through the different organic and inorganic pools in the soil, running on a monthly time-step.

2.5.1 Soil feedbacks

The decomposition and soil organic matter sub-model from CENTURY has been incorporated into the DOLY model (water and soils version) with a few modifications. In CENTURY, soil carbon is divided into three main components which include active, passive and slow soil carbon. These components are further sub-divided into eight different carbon pools. These pools consist of surface and soil structural material, active soil organic matter (SOM), surface microbes, surface and soil metabolic material, slow and passive SOM fractions. The flows of carbon are controlled by the maximum decomposition rate of each of the pools and the water and temperature-controlled decomposition factor. The DOLY model (water and soils version) simulates the dynamics of these eight carbon pools. The nitrogen pools are then calculated from these pools. Soil carbon and nitrogen are given by the sum of their respective pools. The dynamics of the carbon pools are governed by linear differential equations over any monthly period. The dynamic parameters are computed from average monthly values of temperature, precipitation, humidity, water flow, potential evapotranspiration and litter. If the system is driven with these values from some arbitrary initial condition then, after a period of 1000 years or so, the model will converge on a limit cycle with a period of one year. In order to avoid such a long initialisation process, the average values of the limit cycle can be estimated, by averaging the linear systems over a one year period, and the equilibrium solution of this system found. This technique works well and the exact solutions of each of the carbon pools oscillate around the averaged solutions.

The variables which couple DOLY and the soils model for a given value of LAI, are NPP, soil carbon and nitrogen (soilc and soiln).

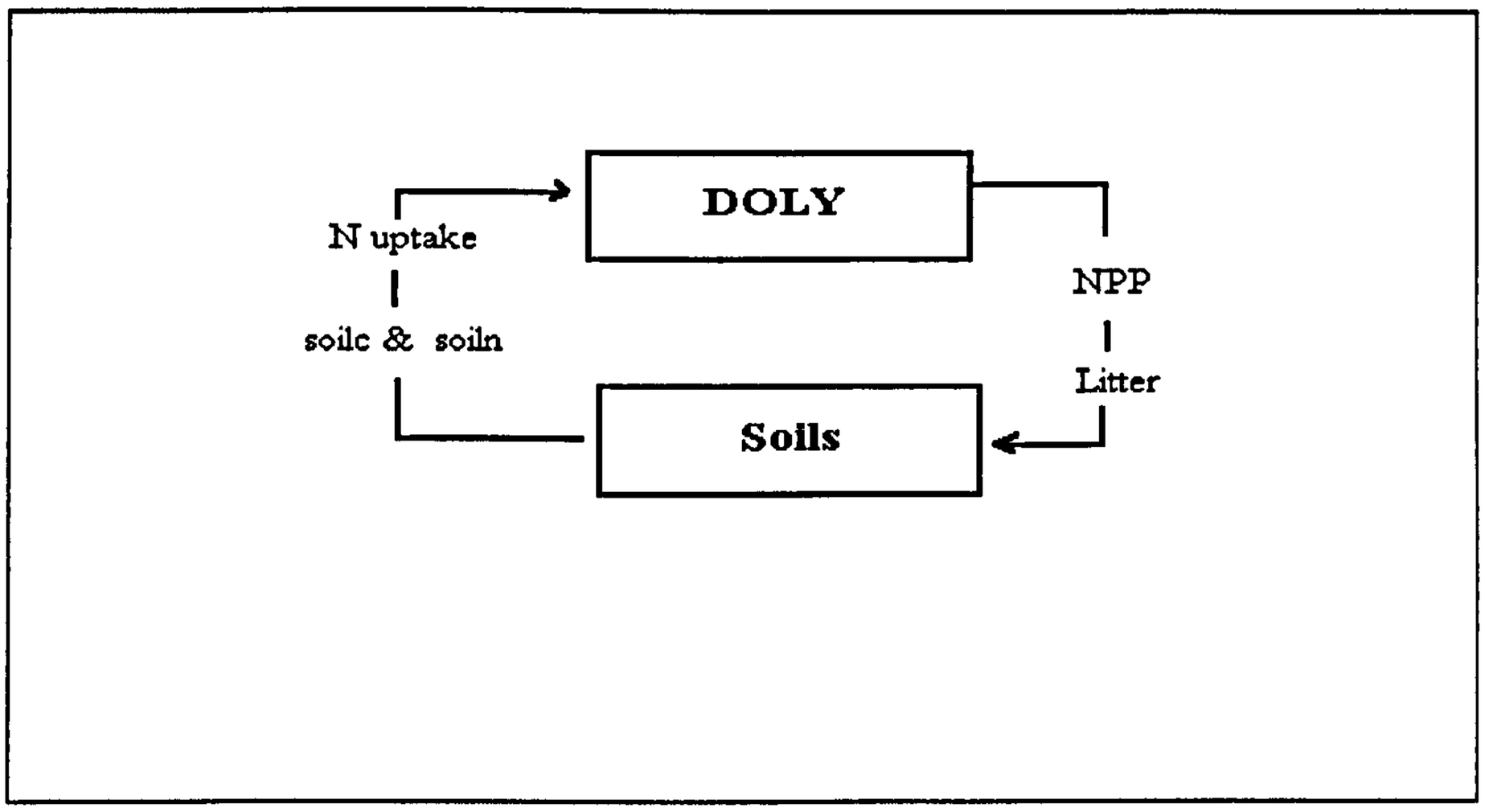

Figure 2.17 Inputs and outputs between the DOLY model and the soils model.

Figure 2.17 shows how the NPP output from the DOLY model is used to calculate litter which is an input into the soils model. The soils model predicts soil carbon and nitrogen, which are required by the DOLY model to calculate nitrogen uptake. The dynamics of the soils model $\left(\dot{S}\right)$ can be represented by the following equation:

$$\dot{S} = C(NPP, S) \tag{2.111}$$

where

C represents the function of NPP and S derived using the CENTURY model

S represents soilc and soiln. Note that although S represents two variables, there is only one degree of freedom between them. This is because the nitrogen flows in CENTURY follow the carbon flows between pools. Any change in a carbon flow will impact on a nitrogen flow.

For a given value of LAI, DOLY has no dynamics (i.e. there is no change) and can be represented by an algebraic equation:

$$0 = D(NPP, S) \tag{2.112}$$

where

D represents the function of NPP and S derived using the DOLY (water and soils) model

The solution needs to be found to this differential/algebraic system in order to determine the soil carbon and nitrogen value for a given NPP. To do this consider the differential part of the system for varying NPP (litter). As the litter input increases the equilibrium value of the soil model increases. When no litter is input into the system then the equilibrium value of S is zero as shown in the phase portrait Figure 2.18. Any point on the line C (NPP, S) is zero. This means that if NPP increases in CENTURY which causes the amount of litter to increase, the amount of soil carbon and nitrogen will increase but there will always be a unique solution which falls on the line C(NPP, S). If soil C and soil N decrease they will still have a unique solution for each NPP value. Convergence on the line is represented by the arrows.

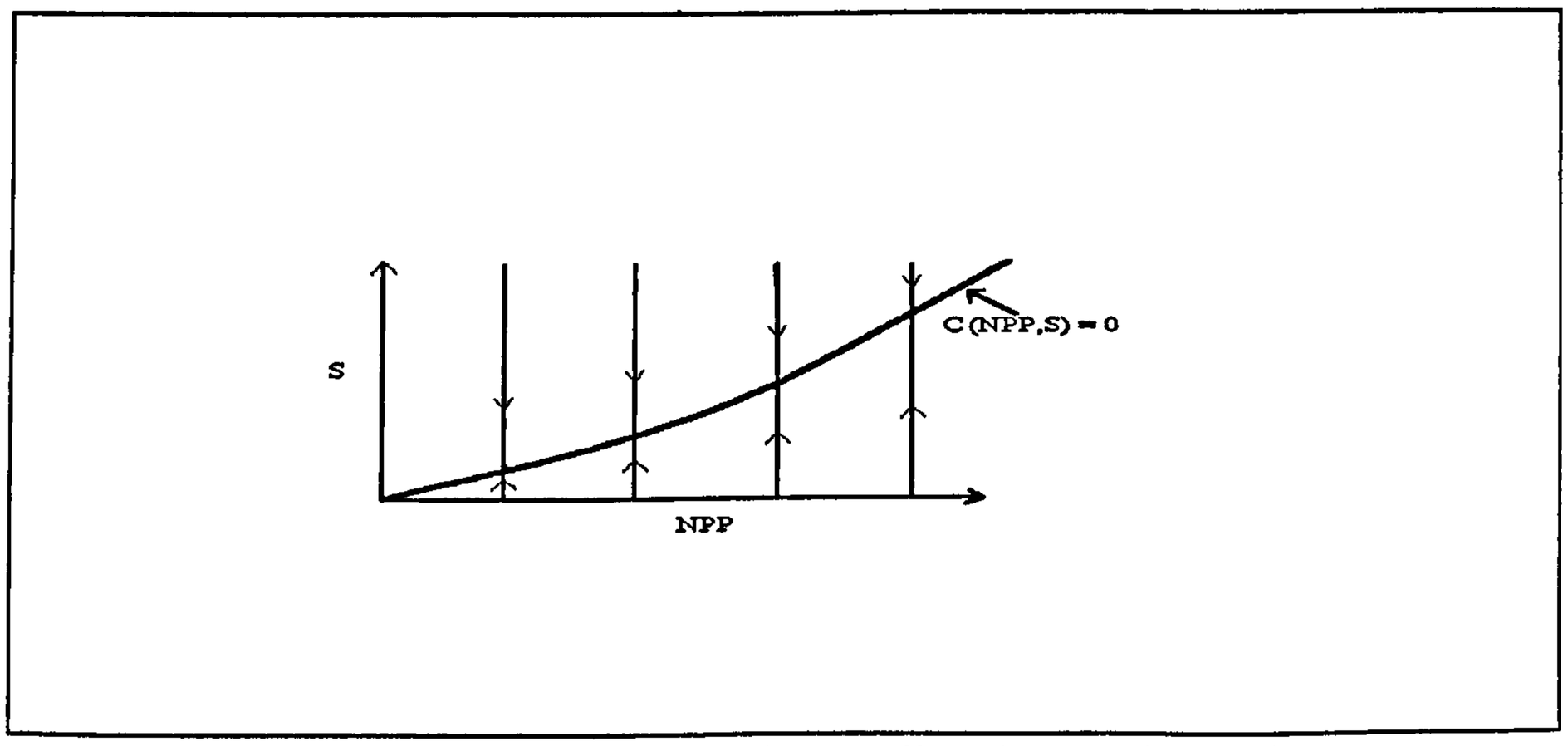

Figure 2.18 A phase portrait showing how soil carbon and soil nitrogen, as represented by S, in CENTURY, vary over a range of NPP values. For each soil carbon and nitrogen value there is a unique solution of NPP.

If a similar process is carried out with the DOLY model then a typical solution curve to the algebraic part of the system (DOLY for some value of LAI) is displayed in Figure 2.19. Here it can be seen that as the soil carbon and nitrogen levels increase from zero, the resulting NPP increases until it becomes carbon saturated, at which point the NPP starts to decrease. This differs from the situation with the CENTURY model in Figure 2.18 whereby the soil carbon and nitrogen continued to increase as NPP increased.

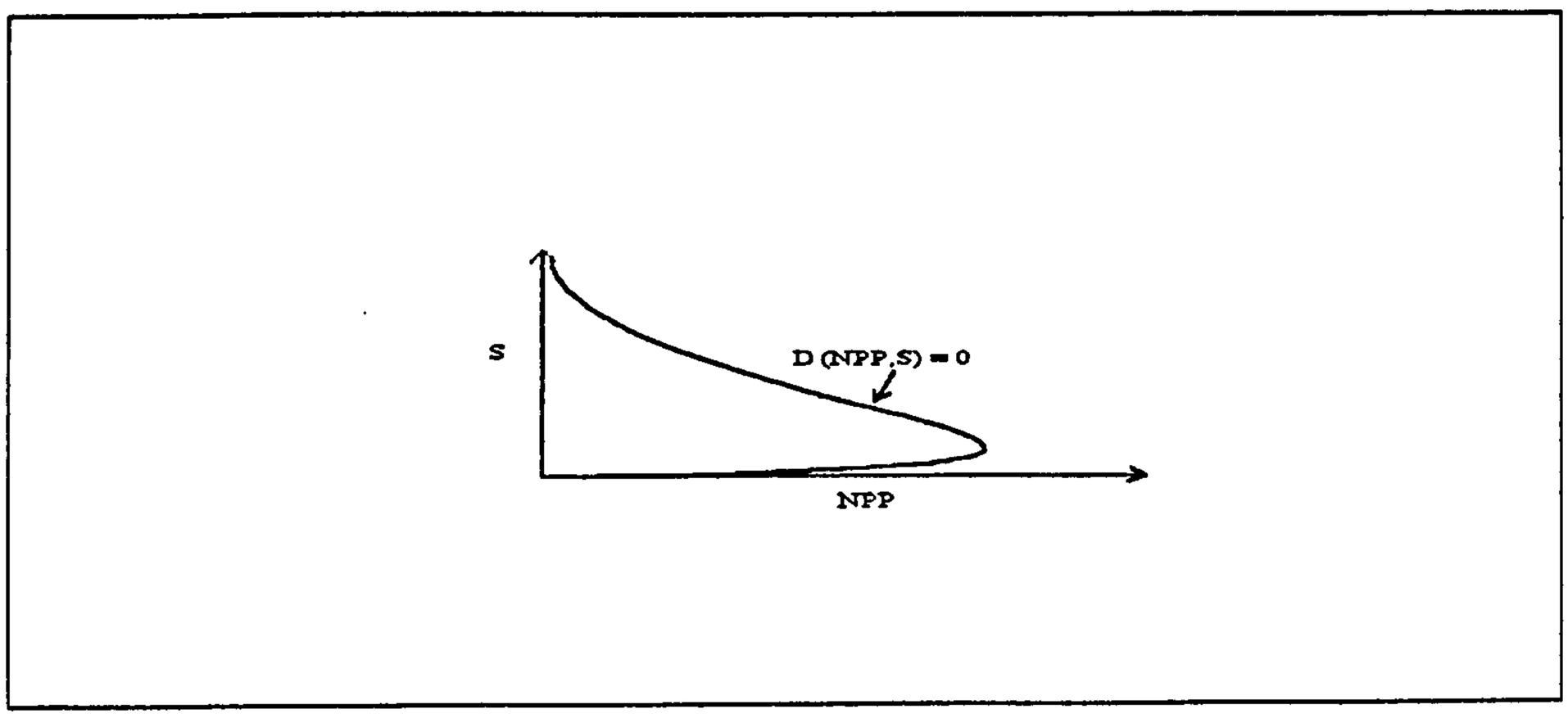

Figure 2.19 The response of NPP to increasing soil nitrogen and soil carbon. Once NPP becomes carbon saturated the NPP values decrease with increasing soil carbon and nitrogen.

In the differential/algebraic system the dynamics described by the differential part of the system as represented by CENTURY are constrained to lie on the surface defined by the algebraic part of the system as represented by DOLY. Combining figures 2.18 and 2.19 gives Figure 2.20. Due to the inherent characteristics of CENTURY, such as the decay of its nutrient pools, there will exist only one solution to both these functions as shown in Figure 2.20. This one solution will always be stable.

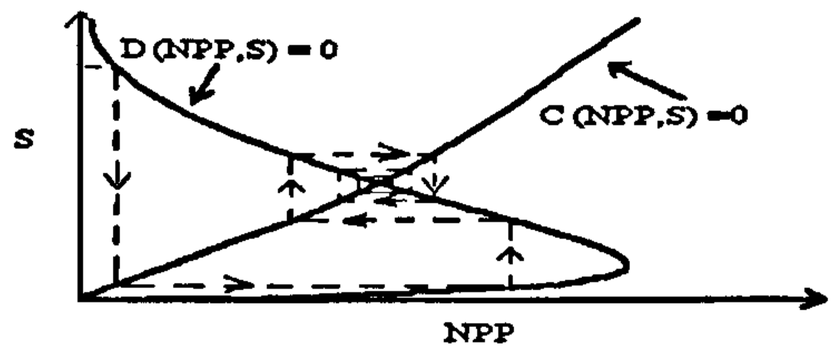

Figure 2.20 The iterative scheme showing how a soil carbon and nitrogen value are selected for a given NPP. It should be noted that this technique will not always converge on the solution but will at least converge on a cycle that contains the solution. If this does occur then the cycle can be used to estimate the solution.

Equations 2.113 and 2.114 are solved to determine the value of the solution.

$$D\,(NPP,\ S) = 0 \qquad \textbf{(2.113)}$$

$$C\,(NPP,\ S) = 0 \qquad \textbf{(2.114)}$$

The following iteration scheme is employed:

- Initialize S, at present $S = S_1$ is used, where S_1 represents soilc = 8000 gC m^{-2} and soiln = 800 gN m^{-2}.
- Solve D (NPP, S_1) = 0 to give NPP_1 (run DOLY(water and soils version)).
- Solve C (NPP_1, S) = 0 to give S_2 (compute soils equilibrium value).
- Solve D (NPP, S_2) = 0 to give NPP_2 (run DOLY(water and soils version)).
- Solve C (NPP_2, S) = 0 to give S_3 (compute soils equilibrium value), etc.

2.5.2 A comparison between LAI and NPP from DOLY (water and soils version) and previous versions of the model

In order to highlight the differences in LAI and NPP values arising from the use of different versions of the DOLY model and to compare these with the prototype model, World, the following maps were produced:

i) LAI and NPP from DOLY (water and soils version), (Figure 2.21).

ii) Difference maps of LAI and NPP between DOLY (water and soils version) and DOLY (water version), (Figure 2.22).

iii) Differences maps of LAI and NPP between DOLY (water and soils version) and World, (Figure 2.23).

All versions of the model were run with IIASA data on a 0.5 by 0.5 degree grid (62483 terrestrial cells).

By examining the LAI map in Figure 2.21 it can be seen how the general pattern of high LAI in the Tropics and low LAI in the high latitudes is evident. This is also reflected in the NPP map. These figures compare well with the measured NPP and LAI values discussed in section 2.2.8. In order to highlight areas where the LAI and NPP values from DOLY (water version) differed from the later DOLY (water and soils version), difference maps were produced (Figure 2.22). In the tundra regions the inclusion of soil feedbacks in the later model lead to an increase in LAI of 1. Hot and arid areas such as the northern savannah of Africa, eastern Australia, the steppe of the former Soviet Union and the Namib desert show a similar increase with the more recent version of the model. The increases in LAI predicted by the newer version of the model are most probably due to increased soil water availability in the arid areas and to a decrease in the amount of soil carbon generated by the model in cooler, wetter areas, which would also increase NPP. Decreases in LAI of 1 and 2 occur on the northern fringes of the tropical rain forest in central Africa, eastern China, parts of Siberia, southern Brazil and northern Argentina. Similar patterns emerge with NPP, but with additional decreases in NPP in eastern U.S.A., Peru and northern Brazil. In these regions, soil feedbacks have

led to a reduction in NPP and consequently, LAI. This suggests that nitrogen uptake in DOLY (water and soils version) has been reduced due to an increase in soil carbon generated by the model.

Turning now to consider the differences that arise between DOLY (water and soils version) and World (Figure 2.23). Figure 2.21 may also be compared with Figure 2.9 (p.52). It is clear that major changes are evident between the two models. In the newer version of the model LAI values are much higher (LAI difference = 3) than those from World over much of Australia, the savannah regions of Africa, eastern Brazil, India and the central U.S.A. They are much lower (LAI difference = –3) in much of Europe, northern parts of the Former Soviet Union, eastern North America and much of Alaska. In northern Brazil, Peru, Colombia and the tropical rain forests of central Africa the LAI difference is smaller (–1 or – 2). Extremely large negative differences in NPP ($\leq$ -4 tC ha^{-1} yr^{-1}) can be seen between the models (Figure 2.23) over much of northern Asia and northern parts of North America, as well as Chile.

These difference maps show how the inclusion of carbon flows in vegetation as used within DOLY (water and soils version) has markedly reduced the NPP values over much of the northern hemisphere and led to the prediction of more realistic values (see Tieszen, 1978; Cannell, 1982). In addition, the NPP values in the tropical regions have also been reduced. Some positive differences in NPP of mostly 1 tC ha^{-1} yr^{-1} arising from the use of DOLY (water and soils version) have occurred on the fringes of drier areas such as the northern savannah of Africa and central Australia. Increases in soil water availability within the model have led to increased LAI values but reductions in NPP in areas such as India, the savannah regions of Africa and eastern Brazil.

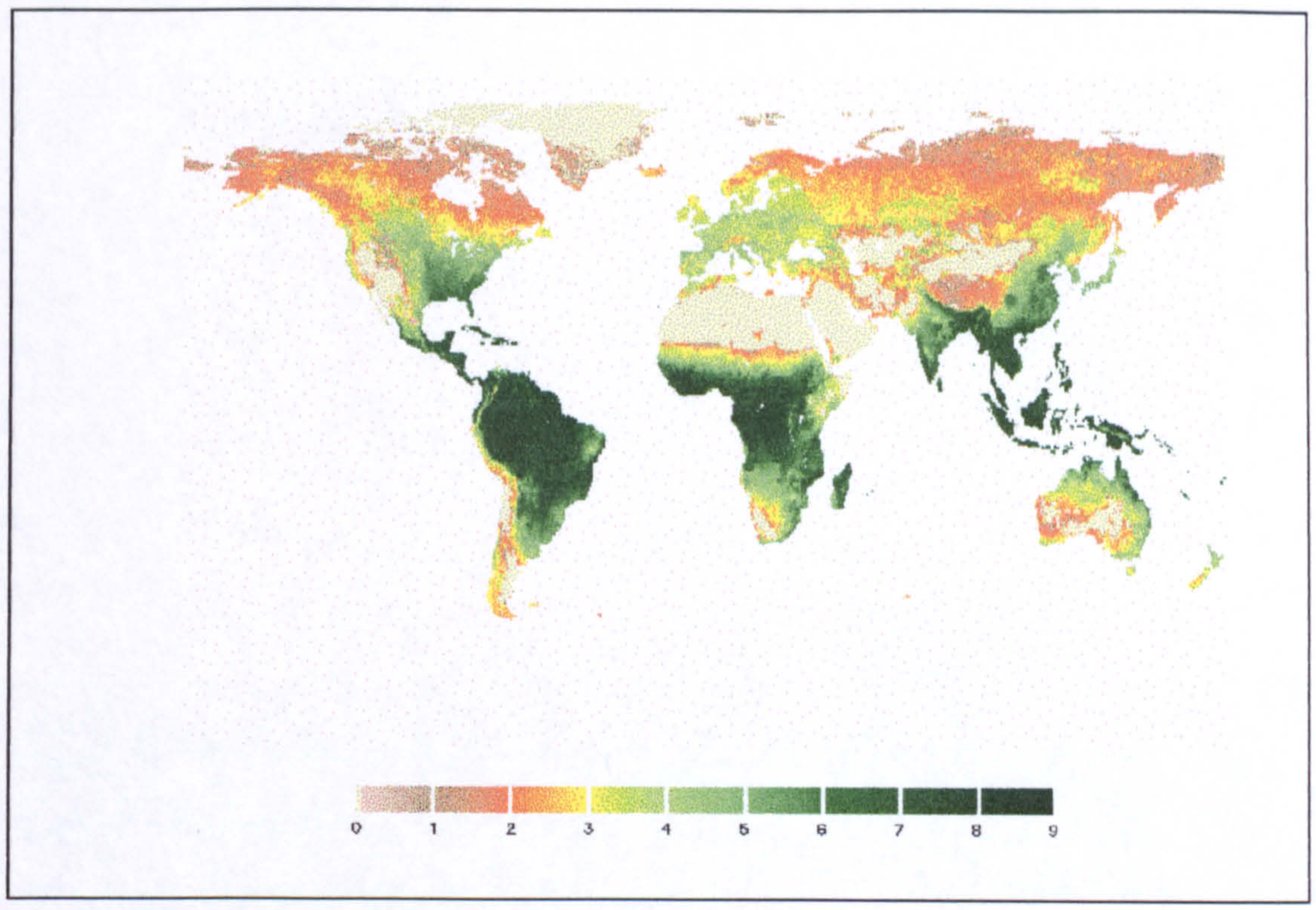

Figure 2.21 a) Global distribution of LAI derived from DOLY (water and soils version) run with the IIASA dataset (0.5 ° × 0.5° grid).

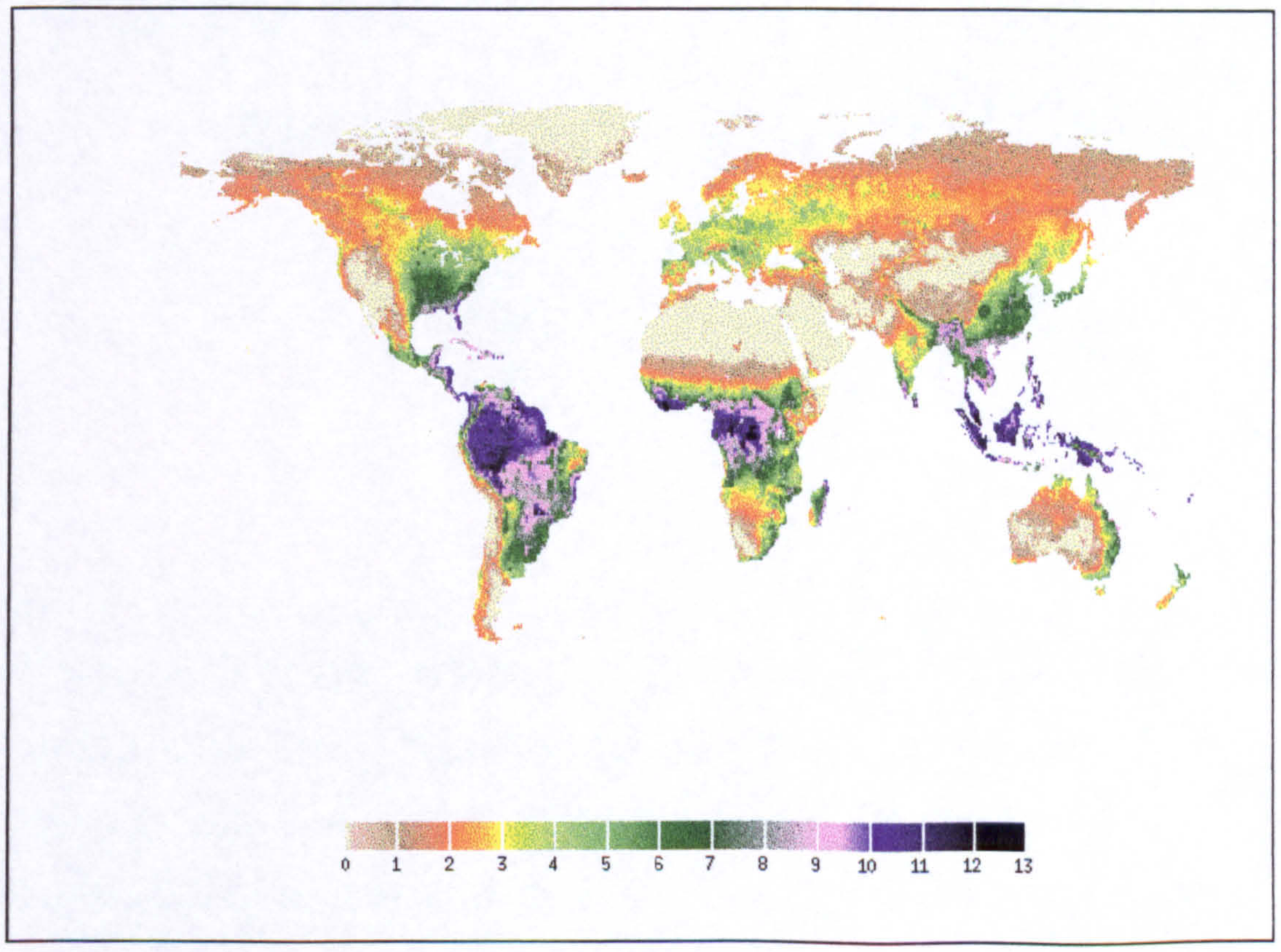

Figure 2.21 b) Global distribution of NPP derived from DOLY (water and soils version) run with the IIASA dataset (0.5 ° × 0.5° grid).

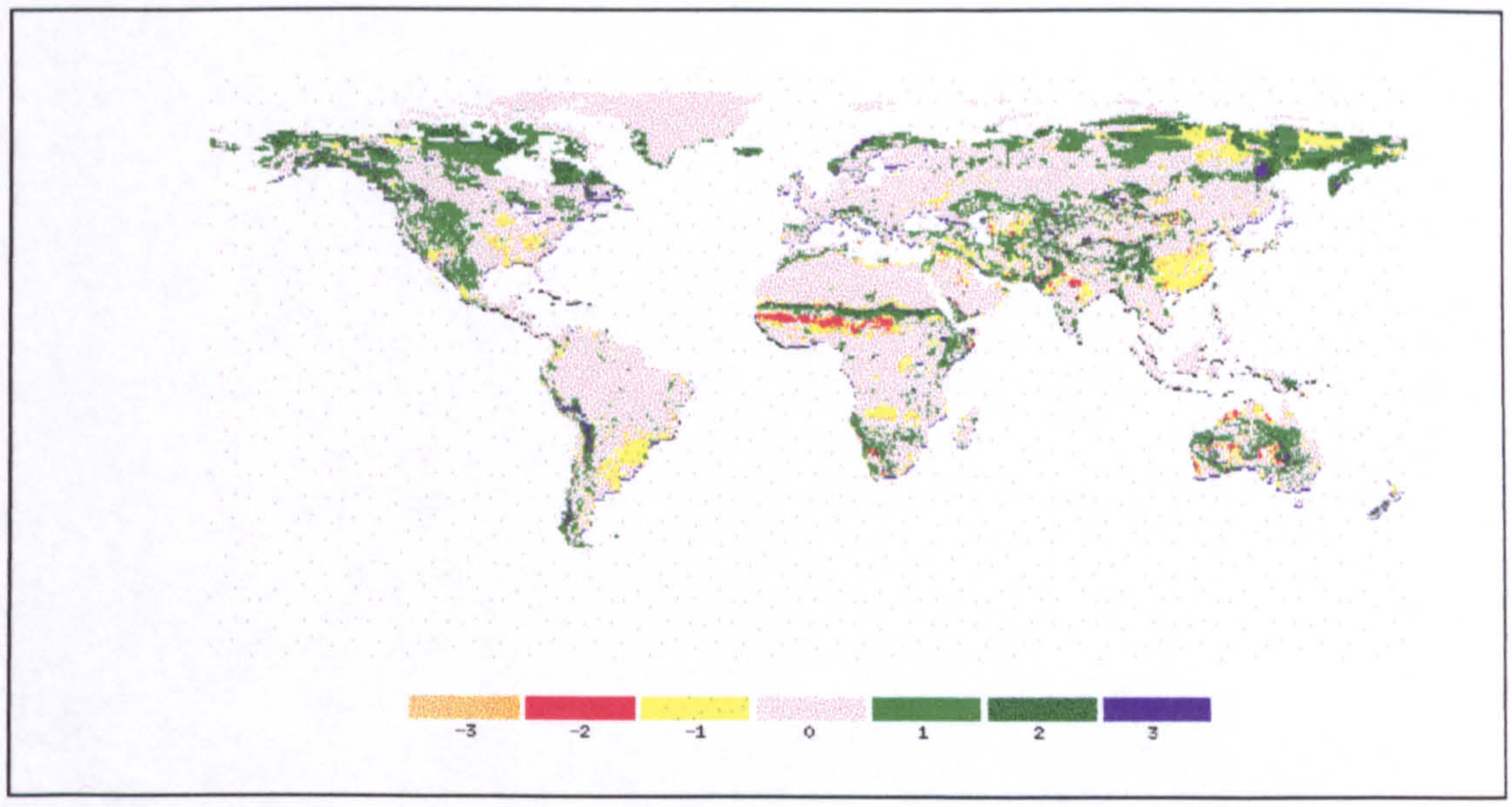

Figure 2.22 a) Change in LAI values derived from DOLY (water and soils version) and the DOLY (water version) run with the IIASA dataset (0.5° × 0.5° grid). The absolute values of LAI range between 0 and 12. Positive deviations occur when the LAI values from DOLY (water and soils version) exceed those from DOLY (water version) and negative values are for the reverse situation.

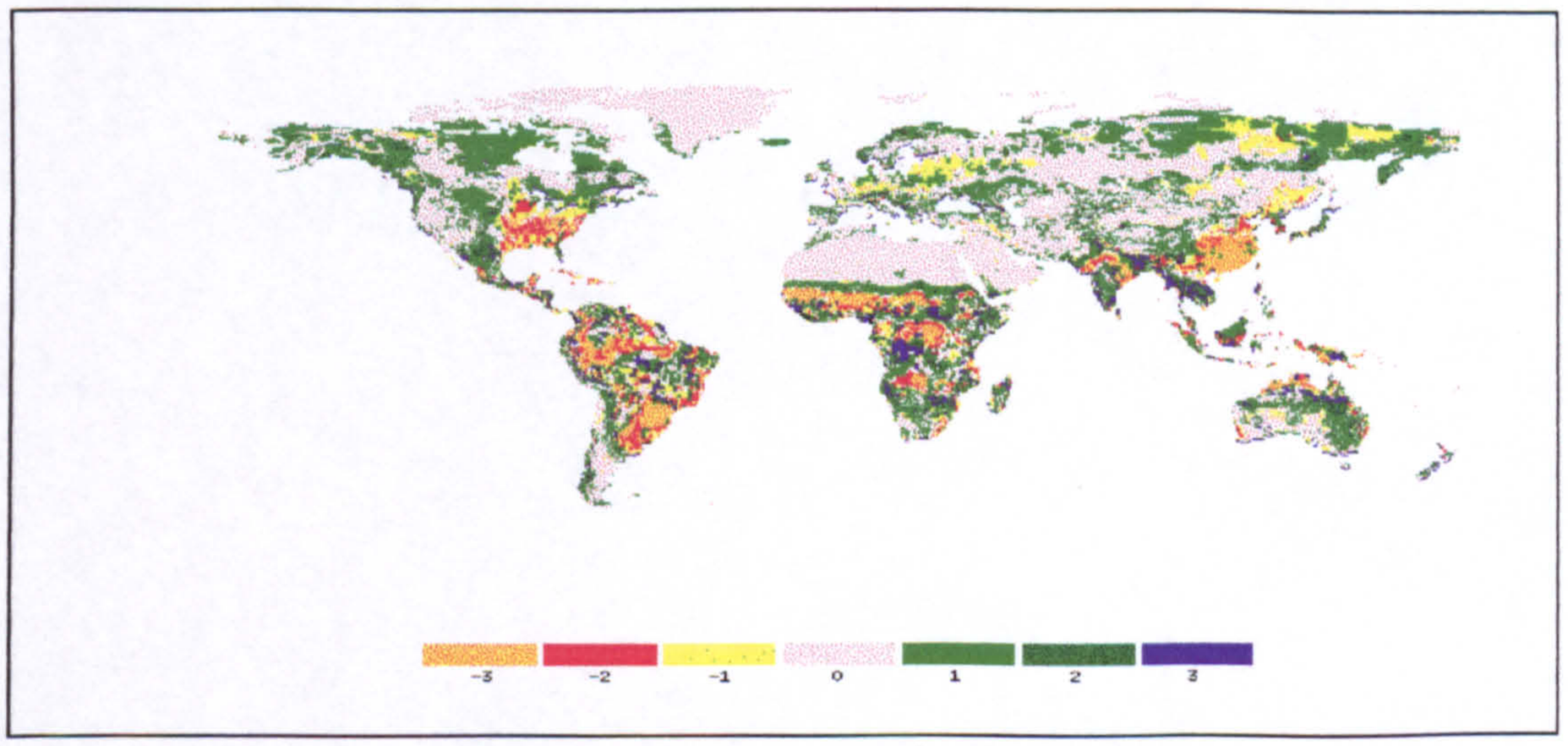

Figure 2.22 b) Change in NPP values derived from DOLY (water and soils version) and the DOLY (water version) run with the IIASA dataset (0.5° by 0.5° grid). The absolute values of NPP range between 0 and 13 tC ha^{-1} yr^{-1}. Positive deviations occur when the LAI values from DOLY (water and soils version) exceed those from DOLY (water version) and negative values are for the reverse situation.

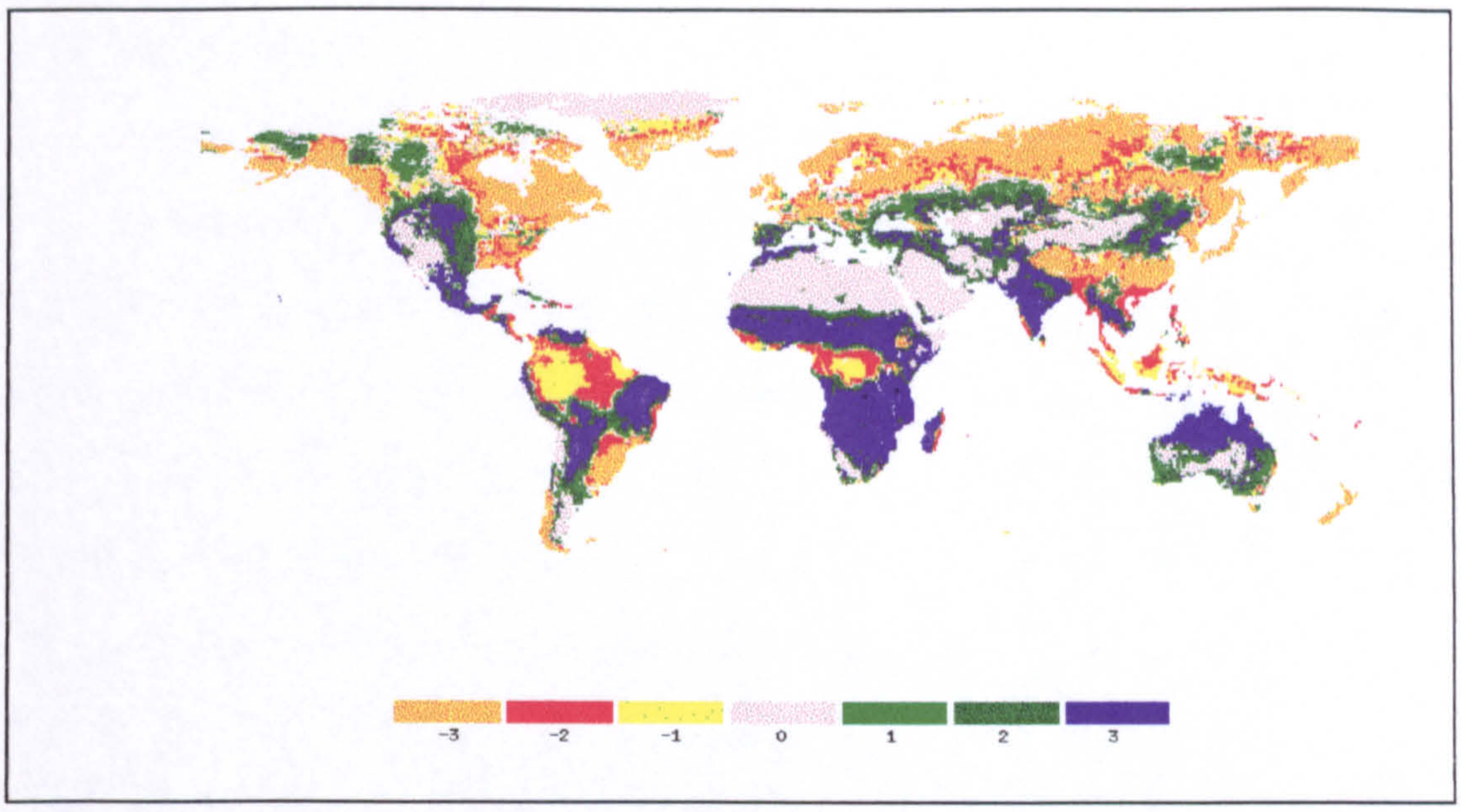

Figure 2.23 a) Change in LAI values derived from DOLY (water and soils version) and World run with the IIASA dataset (0.5° by 0.5° grid). The absolute values of LAI range between 0 and 12. Positive deviations occur when the LAI values from DOLY (water and soils version) exceed those from World and negative values are for the reverse situation.

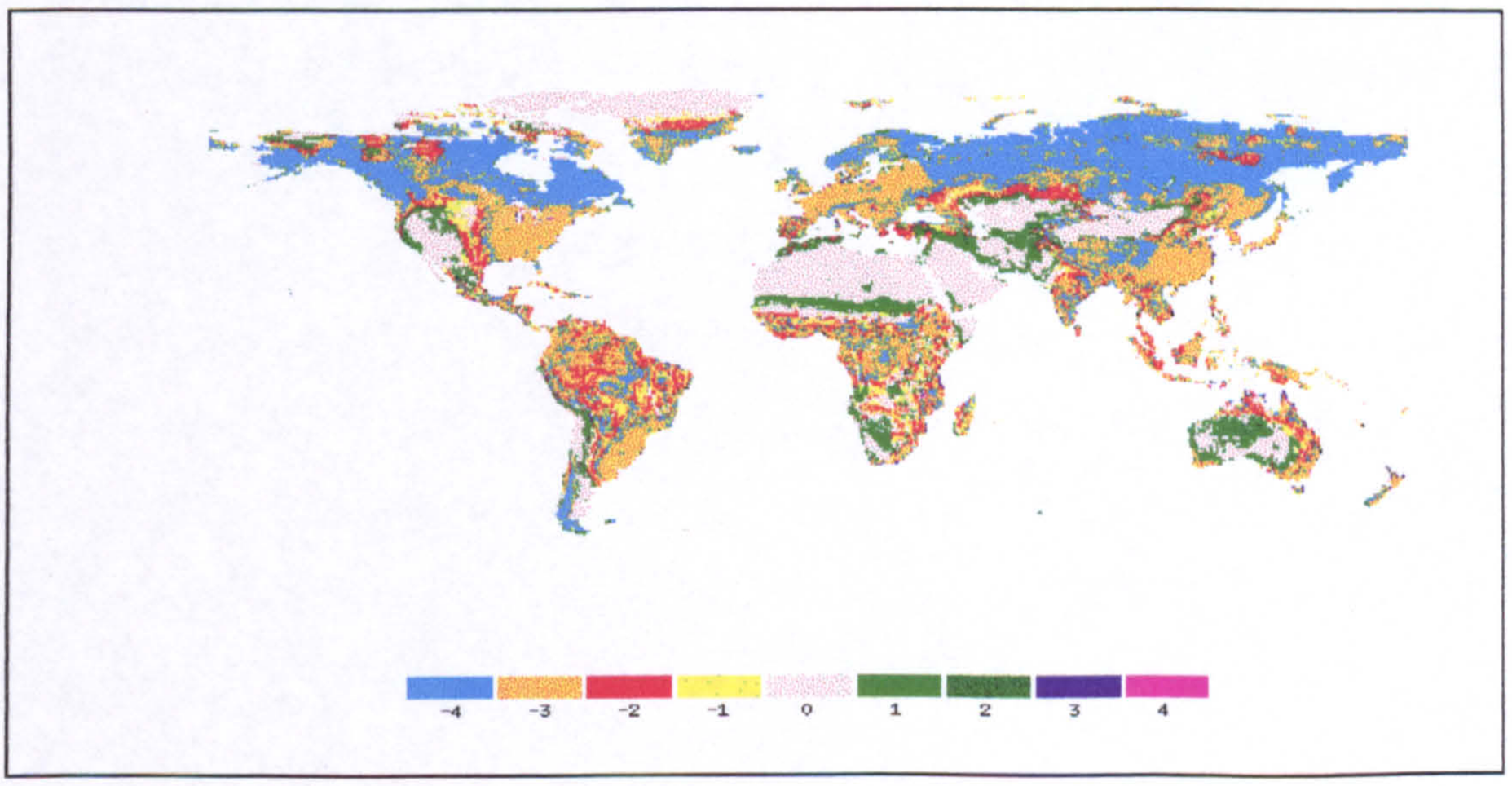

Figure 2.23 b) Change in NPP values derived from DOLY (water and soils version) and World run with the IIASA dataset (0.5° by 0.5° grid). The absolute values of LAI range between 0 and 12. Positive deviations occur when the LAI values from DOLY (water and soils version) exceed those from World and negative values are for the reverse situation.

2.6 Discussion

In this chapter it has been shown how the simple World model has been expanded and developed to the more complex and detailed DOLY (water and soils version) model. The comparison between the LAI and NPP values from the different model versions has illustrated how the output from the DOLY (water and soils version) differs from its predecessors. Although much additional computational effort has been required to include the carbon flows in vegetation, to initialise soil water conditions, and to incorporate soil feedbacks, these maps have shown the importance of modelling such processes in order to obtain the most realistic (relative to the limited number of observational data) representation of global LAI and NPP values. This additional effort has been shown to be especially important for determining NPP values in the northern hemisphere.

The following chapters will use all the different versions of the DOLY model described in this chapter. Chapter 3 is concerned with the sensitivity of the DOLY (standard version) model to changes in the soil input variables, and Chapter 4 looks at the sensitivity of DOLY (water version) model to changes in climate inputs. The standard version is used with a life-form model in Chapter 5 and a general circulation model (GCM) in Chapter 6 for some climate change scenarios. The effect of different datasets on the DOLY (standard version) model is examined in Chapter 7. The output from DOLY (water and soils version) run with transient climate data for the period 1861 to 2100, supplied by the United Kingdom Meteorological Office is analysed and discussed in Chapter 8. Validation issues are addressed in Chapter 9.

CHAPTER 3

3.0 A sensitivity analysis of the DOLY model to soils

3.1 Introduction

An important process in the development of any model is the analysis of the model's sensitivity to its input data. This aids in the analysis of the results and provides useful information as to a likely response for a given change in input data. It also enables one to focus on the variables which are the most influential on the output data, and any spurious results or errors in the program can be highlighted and identified. In addition to the sensitivity analysis, some kind of validation needs to be carried out in order to check on the model's performance. This is not an easy task when dealing with global data and the lack of suitable global datasets for comparison. However, a few datasets have been obtained for Chapter 7. These provide a yardstick against which the DOLY model's results can be compared.

Chapter 3 is concerned with the sensitivity of the DOLY model to its inputs of soils, and Chapter 4 considers the climate inputs. These two chapters show results of how these variables affect the leaf area index (LAI) and net primary productivity (NPP) values predicted by the model. In addition, the issue of validation is discussed in Chapter 9.

Soils vary greatly across the world in texture, structure and nutrient content. They exert a strong influence on their overlying vegetation through drainage and nutrient availability.

In tropical forests, the oxisol, predominates. This deeply weathered soil

with a high clay content, and low organic content is deficient in plant nutrients (Archibold, 1995). Soil nitrogen reserves are often greater than those of the litter and plants, although many of the nutrients stored in the forest biomass are resistant to leaching. Soil phosphorous levels are also high, although only a small fraction is available to plants. Plant roots are near to the surface in tropical forests and can effectively absorb nutrients as they become available (Stark and Jordan, 1978). The presence of mycorrhizal infection of the roots (Bagyaraj, 1989) also enhances nutrient uptake. The stem tissue of a plant retains potassium but the nitrogen is rapidly removed when this tissue decomposes. Nitrogen levels tend to decline steadily in plant tissue until replenished by bacterial fixation or rainfall. Additions from rainfall, however, account for less than 7% of total available nitrogen found in tropical forests (Edmisten, 1970; Nye and Greenland, 1960).

Soil nutrient levels particularly of nitrogen and phosphorous (Risser, 1988) frequently limit production, particularly in grassland areas, where climatic conditions mainly control plant composition and growth. The natural addition of nitrogen is mainly by precipitation and dry deposition (Woodmansee, 1978). However, leaching causes little nitrogen loss because the soils under grasslands are low in nitrates and actively growing plants quickly remove any soluble nitrate. The plant canopy rapidly absorbs ammonia released during decomposition of plant litter (Clark *et al.*, 1980).

In savannah regions, the plant cover stores phosphorous, an important nutrient in these regions (Sarmiento, 1984). The low soil reserves in such regions and fast recycling rates suggest that the availability of phosphorous potentially impedes productivity. Reserves of nitrogen and other elements are much greater in the soil than in the vegetation it supports. The live aerial biomass contains about 60 kg ha^{-1} nitrogen; 65% of this eventually transfers to the roots. Root decomposition releases approximately 10 kg ha^{-1} of nitrogen annually. Nitrogen uptake during the growing season is around 30 kg ha^{-1}, and losses in drainage amount to only 2 kg ha^{-1} each year (Archibold, 1995).

Nitrogen is the nutrient most limiting to production in both northern hardwoods (Nadelhoffer, Aber and Melillo, 1983; Pastor *et al* , 1984) and boreal forests (Van Cleve and Oliver, 1982; Pastor *et al.*, 1987). The type of species in these forests has a major influence on the nitrogen cycle, which is coupled to the carbon cycle. The nitrogen cycle also influences several other processes such as successional dynamics and herbivory (Flanagan and Van Cleve, 1983; Chapin, Vitousek and Van Cleve, 1986). The availability of soil nitrogen is a limiting factor to net carbon fixation in these forests. However, the type of carbon compounds found produced in leaf litter in turn affects nitrogen availability by limiting soil microbial activity (Chapin, Vitousek and Van Cleve, 1986; Pastor *et al.*, 1987). This means that there is a reciprocal link between the carbon and nitrogen cycles. Decay rates and chemistry of their litters vary between temperate deciduous and boreal forests. The leaf litters of deciduous trees such as sugar maple and yellow birch have high nitrogen and low lignin contents, allowing them to be easily decomposed by soil microbes (McClaugherty *et al.*, 1985). In contrast the leaf litters of evergreen conifers such as spruce and balsam fir have lower nitrogen and higher lignin contents (Hayes, 1965; Moore, 1984). The high nitrogen availability supports the high productivity of the temperate deciduous forests, which ranges from 7 to 12 tC ha^{-1} yr^{-1} (Cannell, 1982). In boreal conifer stands there is a reduction of net nitrogen availability compared with that in northern hardwoods (Gordon and Van Cleve, 1983). Immobilization of nitrogen by microbes decomposing these leaf litters continues for three or more years (Moore, 1984). Nitrogen availability beneath boreal conifers is usually below 40 kg ha^{-1} yr^{-1}, about half that in northern hardwoods (Gordon, 1983). The greater efficiency in the use of this element by conifers (Chapin, Vitousek and Van Cleve, 1986) partly compensates for the low nitrogen availability. There are several ways of achieving this efficiency. For example, there is a reduced requirement for nitrogen to produce a given amount of tissue. Also, these trees can possess substantial photosynthetic rates at low leaf nitrogen concentrations (Mooney

and Gulmon, 1982) and there is a low leaf turnover rate (Sprugel, 1989). However, these adaptations also contribute to the low rates of nitrogen cycling. A high nutrient use efficiency means high C:N (carbon to nitrogen) ratios and hence low decomposability of leaf litters. Low leaf turnover rates mean slower rates of nitrogen return to the soil. There is partial production of lignin and other recalcitrant carbon compounds to physically protect leaves during their retention of three or more years and delay their decomposition in the soil (Pastor and Mladenoff, 1992).

There is a high correlation between soil and vegetation types, with boreal forest communities most frequency associated with podsol soils. The levels of nitrogen and nutrients are low (Elliott-Fisk, 1988).

In tundra regions, there is a reduction in primary production because of the short growing season, although the long days of summer at high latitudes partly offset this. Further limits to the production in tundra communities occur because leaf expansion takes up a significant part of the growing season and because of the low nutrient status of most tundra soils. Low soil temperatures slow the rate of decomposition of organic matter, and mineral weathering is minimal where permafrost underlies the soil (Archibold, 1995). Nitrogen is particularly deficient. The result of fertiliser trials also suggests that low soil nitrogen levels limit plant growth (McCown, 1978). Free–living blue–green algae associated with wet mossy sites fix most of the nitrogen in tundra ecosystems. Species such as lichen have a symbiotic relationship with these algae. This means that the lichen and the algae are able to extract more nitrogen between them than they would be able to do so individually, which provides additional supplies.

Woodward and Smith (1994 a, b) have shown that the soil nutrient status strongly controls the relationship between leaf nitrogen and photosynthesis. The increasing dependence on nitrogen supply from mycorrhizas as soil organic carbon increases leads to decreasing rates of nitrogen uptake (Read, 1990). Decreasing rates of photosynthesis

parallel these decreasing rates of nitrogen uptake (Reid *et al.* 1983; Woodward and Smith, 1994 a, b). The results from other terrestrial ecosystem models also suggest similar negative correlations between increasing soil organic carbon content and photosynthetic rates (Raich *et al.*, 1991; Hunt *et al.*, 1991; McGuire *et al.*, 1992).

Nitrogen uptake is used within the DOLY model to determine assimilation, and dark respiration. These variables determine the NPP output by the model, and, in conjunction with water availability, the LAI (see Chapter 2 for more details).

This section will provide some background information on the equations used to calculate nitrogen uptake within the DOLY model, and show how soil carbon and nitrogen inputs influence this uptake. A description of the methods adopted to determine the sensitivity of the DOLY model to the soils data will follow along with the results. There is then a discussion of these results.

3.2 Nitrogen uptake

Woodward and Smith (1994 a, b) derived an empirical relationship for the dependence of plant nitrogen uptake on soil carbon and nitrogen contents, and the original equation, derived from observations around 20°C was:

$$N_p = 120 \min\{s_n/600, 1\} e^{-8\times10^{-5} S_c} \qquad \textbf{(3.1)}$$

N_p is the composite nitrogen uptake rate (mol N g^{-1} plant d^{-1}) and s_n and s_c are soil nitrogen and carbon (g m^{-2}), respectively. For soil nitrogen values between 1 and 600 gN m^{-2}, a fraction of 1/600th is calculated as a multiplier. Above this value of soil nitrogen the multiplier is set to 1.

Further modification included temperature dependence based on uptake kinetics, which gave the temperature-dependent nitrogen uptake, N_T, (mol N g^{-1} plant d^{-1}) through the following equations, 3.2 to 3.8. The activation

energy for a process (Jones, 1992) has also been considered in the calculation of this temperature response.

$$u_1 = 40.8 + 0.01T - 0.002T^2 \quad \textbf{(3.2)}$$

$$u_2 = 0.738 - 0.002T \quad \textbf{(3.3)}$$

$$u_3 = 97.412 - 2.504 \ln N_P \quad \textbf{(3.4)}$$

$$num = \exp\left(u_1 - \frac{u_3}{0.00831 T_k} \right) \quad \textbf{(3.5)}$$

$$denom = 1.0 + \exp\left(\frac{u_2 T_k - 205.9}{0.00831 T_k} \right) \quad \textbf{(3.6)}$$

where T is temperature (°C) and T_k is temperature (kelvin).

The uptake kinetics were derived from experimental systems applied at a range of temperatures. Woodward *et al.* (1995) refer to the work done by Clarkson and Warner (1979), Bravo and Uribe (1981) and Clarkson (1985) as the experimental basis for these equations. An empirical response function, κ_T (T) accounts for soil carbon that does not influence nitrogen uptake because of freezing (Bonan, 1992). Where soil carbon, s_c, is greater than 13000 gC m^{-2} and temperature is less than 15°C,

$$\kappa_T(T) = (1 + (15 - T)/30)\left(1 + s_c - \frac{13000}{10000}\right) \quad \textbf{(3.7)}$$

Otherwise, the value of the response function κ_T (T) is 1.

$$N_T = \left(\frac{num}{denom} \right) \kappa_T(T) \quad \textbf{(3.8)}$$

The following tests demonstrate the sensitivity of the nitrogen uptake calculated within the DOLY model to changing temperature, and to soil carbon and nitrogen values. The values for these tests were chosen to demonstrate the difference in nitrogen uptake values that occur with and without the response function set to one (equation 3.7).

Test 3.1: to demonstrate the effect of soil carbon on nitrogen uptake for a given temperature and soil nitrogen value.
Set soil nitrogen to a value of 800 gN m^{-2} and temperature to 17°C. Run with soil carbon values of 12000 gC m^{-2} and 14000 gC m^{-2}. The value of the response function is one.

Test 3.2: to demonstrate the effect of temperature on nitrogen uptake for a given soil carbon and soil nitrogen value.
Set soil nitrogen to a value of 800 gN m^{-2} and temperature to 12°C. Run with a value of soil carbon value of 14000 gC m^{-2}. Repeat with the temperature set to 17°C. The value of the response function is equal to 1.21 at 12°C.

The nitrogen uptake values from Tests 3.1 and 3.2 are shown in Table 3.1

Table 3.1 Composite nitrogen uptake rate, N_p, the response function, $\kappa_T(T)$, and nitrogen uptake, N_T, for soil carbon (s_c) values of 12000 gC m^{-2} and 14000 gC m^{-2} at 17°C, and for a soil carbon value of 14000 gC m^{-2} at 12°C. Soil nitrogen is a constant value of 800 gN m^{-2}.

Variable	T_k = 290 K, T = 17°C		T_k = 285 K, T = 12°C
	s_c = 12000 gC m^{-2}	s_c = 14000 gC m^{-2}	s_c = 14000 gC m^{-2}
N_p	45.95	39.15	39.15
$\kappa_T(T)$	1	1	1.21
N_T	34.66	29.49	26.11

Table 3.1 shows how the nitrogen uptake (N_T) is reduced at lower temperatures for a soil carbon value of 14000 gC m^{-2}. At 17°C the uptake value is 29.49 µmol m^{-2} g^{-1} d^{-1} compared to 26.11 µmol m^{-2} g^{-1} d^{-1} at 12°C, for a soil carbon value of 14000 gC m^{-2}. This table also shows how, as the amount of soil carbon increases from 12000 gC m^{-2} to 14000 gC m^{-2}, nitrogen uptake decreases from 34.66 to 29.49 µmol m^{-2} g^{-1} d^{-1}.

Test 3.3: to demonstrate the effect of soil nitrogen on nitrogen uptake for a given temperature and soil carbon value. Set soil carbon to a value of 12000 gC m^{-2} and temperature to 17°C. Run with soil nitrogen values of 800 and 1000 gN m^{-2}. The value of the response function is one.

Test 3.4: to demonstrate the effect of temperature on nitrogen uptake for a given soil carbon and soil nitrogen value. Set soil carbon to a value of 12000 gC m^{-2} and temperature to 12°C. Run with a value of soil nitrogen value of 1000 gC m^{-2}. Repeat with the temperature set to 17°C. The value of the response function is one.

If soil carbon is kept constant at a value of 12000 gC m^{-2} and the soil nitrogen values are varied then there is no change in nitrogen uptake for a given temperature of 17°C as in Table 3.2. There is, however, a decrease in nitrogen uptake with a decrease in temperature.

Table 3.2 Composite nitrogen uptake rate, N_p, the response function, $\kappa_T(T)$, and nitrogen uptake, N_T, for soil nitrogen (s_n) values of 800 gN m^{-2} and 1000 gN m^{-2} at 17°C, and for a soil nitrogen value of 1000 gN m^{-2} at 12°C. Soil carbon is a constant value of 12000 gC m^{-2} .

Variable	T_k = 290 K, T = 17°C		T_k = 285 K, T = 12°C
	s_n = 800 gN m^{-2}	s_n = 1000 gN m^{-2}	s_n = 1000 gN m^{-2}
N_P	45.95	45.95	45.95
$\kappa_T(T)$	1	1	1
N_T	34.66	34.66	25.44

It should be noted that soil nitrogen does not have an impact on nitrogen uptake above a value of 600 gN m^{-2}. If soil nitrogen values of less than 600 gN m^{-2} occur, then nitrogen uptake decreases proportionally as the amount of nitrogen decreases. This is shown in Figure 3.1. Nitrogen uptake is also influenced by the amount of soil water available to plants. This has been

incorporated into more recent versions of the DOLY model so that as the amount of available water increases up to soil water saturation, nitrogen uptake increases. Figure 3.1 shows the temperature responses of nitrogen uptake for soils with soil carbon values of 10000 gC m^{-2} and 20000 gC m^{-2} and with two soil nitrogen values of 300 gN m^{-2} and 600 gN m^{-2} over a range of temperatures from 0 to 40°C. This figure shows that nitrogen uptake increases with decreasing soil carbon. Nitrogen uptake also increases with increasing temperatures up to 28°C before declining for both values of soil nitrogen. At a soil carbon value of 20000 gC m^{-2}, and at temperatures of 15°C and below, it can be seen how the response function comes into play and raises the nitrogen uptake at these lower temperatures. Above 15°C the uptake declines slightly to 20°C before increasing again to 28°C and then declining. The nitrogen uptake increases as soil nitrogen increases, and also the rate of uptake is greater at temperatures of 15°C and below.

Tests 3.1 to 3.4 have shown how temperature, and soil carbon and nitrogen values influence nitrogen uptake. NPP and LAI both tend to increase as nitrogen uptake increases, providing there is sufficient water available and mean monthly temperatures do not exceed 28°C. In the next section (3.3) a sensitivity analysis determines the impact of global values of soil carbon and nitrogen on NPP and LAI predicted by the DOLY model. There are no changes made to other input variables. The results of the sensitivity analysis are presented in section 3.4

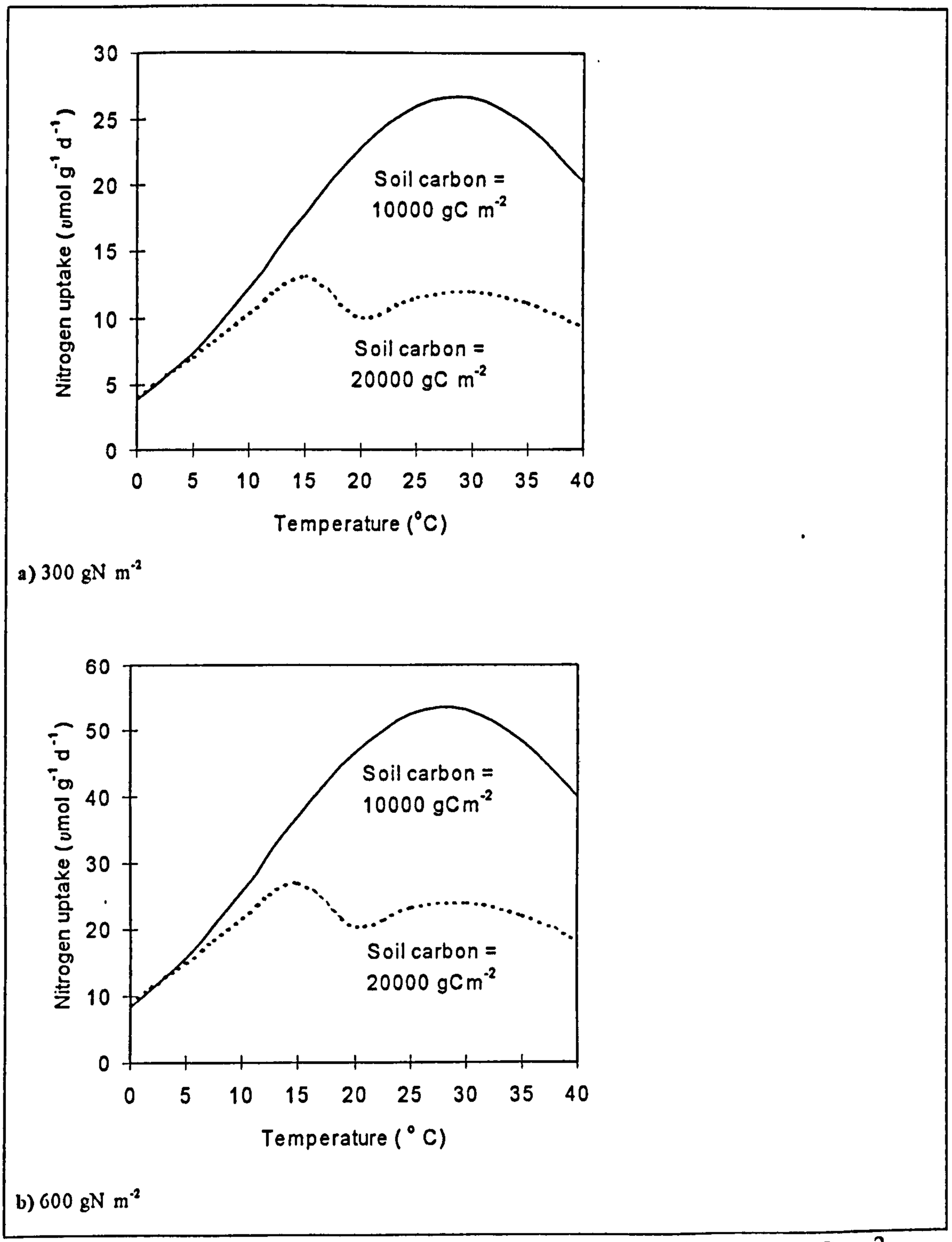

Figure 3.1 Nitrogen uptake as a function of temperature for 10000 gC m^{-2} and 20000 gC m^{-2} of soil carbon.

a) 300 gN m^{-2} of soil nitrogen

b) 600 gN m^{-2} of soil nitrogen.

The dip in the curve for the soil carbon value of 20,000 gC m^{-2} is due to the effect of the response function κ_T (T). This increases the nitrogen uptake at temperatures below 15°C for soil carbon values exceeding 13000 gC m^{-2}.

3.3 Methods

Soils data are input into the DOLY (standard version) model with reference to latitude and longitude. Each cell has two values, one for soil carbon and nitrogen with units of gC m^{-2} and gN m^{-2} respectively. Post *et al.* (1982,1985) and Zinke *et al.* (1984) related estimates of soil carbon and soil nitrogen to global patterns of climate and vegetation by classifying each soil profile by the Holdridge Life-Zone in which it was found. The Holdridge classification (Holdridge, 1947), which was mentioned in section 2.2.2, is a bioclimatic classification scheme, which relates the distribution of the major biomes of the world to the climatic variables of the ratio of potential evapotranspiration to precipitation, mean annual precipitation and biotemperature. The three variables are represented by three points of an equilateral triangle. Each biome is represented by a climate zone, which in effect are hexagons with a unique combination of precipitation, potential evapotranspiration and biotemperature. In addition there is a line representing the occurrence of potentially killing frosts which separates the temperate biomes from the tropical biomes. There are obvious errors in using a scheme of this type such as its lack of seasonality, and it is correlative, as opposed to mechanistic, but it has been found to produce a reasonably accurate way of relating climate and the distribution of biomes at the global scale (Smith *et al.*,1992). Woodward and Smith (1994a) also used this classification to estimate soil carbon and soil nitrogen values based on values from Post *et al.* (1982, 1985). The global distribution of these values is shown in Figure 3.2, which also shows that soil carbon and soil nitrogen are strongly correlated. Dr. Tom Smith (University of Virginia, U.S.A) provided these data.

To determine the sensitivity of leaf area index (LAI) and net primary productivity (NPP) to soil carbon and soil nitrogen, the following approach was adopted. First, the mean global soil carbon value and nitrogen value were calculated for the 62,483 terrestrial cells. These values are shown in Table 3.3. Each cell was set to the mean values. The model was then run twice. One run

used the usual soils dataset with spatially variable soil carbon and nitrogen values, and the other, using only the calculated mean values of soil carbon and nitrogen. The LAI and NPP values derived from the two approaches were then examined. In order to aid interpretation of the changes that occurred using the two different soil inputs, two difference maps were produced. One of these maps is for changes in NPP and the other for changes in LAI. The GIS (Geographic Information System) package, IDL (Interactive Data Language supplied by Research Systems, Inc., Boulder, Colorado), was used to create these maps. Positive differences occur when the NPP calculated from the variable soils dataset is greater than that calculated using a mean global value of soil carbon and soil nitrogen, and negative values occur when the reverse is true (Figure 3.3). The same convention is also used with the LAI difference map (Figure 3.4).

The aim of this exercise was to highlight areas that are especially sensitive to the soils data input. For instance, if the mean soil carbon and nitrogen values for a cell were lower than the variable values, would this cause the NPP and LAI value to decrease or increase? In an area where there was a deficiency of soil carbon, the mean soil carbon value would be expected to be higher than the variable value. This would lead to a reduction in the nitrogen uptake and one would therefore expect the NPP to decrease.

3.4 Results

Figure 3.2 shows the global distribution of soil carbon and soil nitrogen as used in the DOLY model (Post *et al.*, 1982, 1985; Zinke *et al.*, 1984). The patterns are broadly consistent with those stated in the literature. Moderate to high soil carbon values (i.e. in the range 12000 to 42000 gC m^{-2}) occur in the mid- to high-latitudes, and high soil nitrogen values (2400 to 3000 gN $m^{-2)}$ in tropical areas. There are a few exceptions to this. For instance, in Labrador,

Canada where the soils have a relatively high soil nitrogen content of between 1800 and 2400 gN m^{-2} and, in eastern Papua New Guinea where the soils have a high soil carbon content of the order of 30000 gC m^{-2}. Despite these exceptions the general patterns hold true. Table 3.3 shows the average soil carbon and soil nitrogen values used in the sensitivity analysis.

Table 3.3 The average global soil carbon and nitrogen values used in the sensitivity analysis. The soil carbon values range from 0 to 36600 gC m^{-2} and the soil nitrogen values from 0 to 2853 gN m^{-2}.

Average global soil carbon value (gC m^{-2})	Average global soil nitrogen value (gN m^{-2})
12011	793

From section 3.2 it was stated that soil nitrogen does not have an impact on nitrogen uptake above a value of 600 gN m^{-2} in the model. This means that the soil nitrogen only affects nitrogen uptake, and hence LAI and NPP, in regions where the soil nitrogen values are below 600 gN m^{-2}. The use of a single global mean value of 793 gN m^{-2} of soil nitrogen in such regions will therefore increase nitrogen uptake. In areas which have current soil nitrogen values greater than 600 gN m^{-2} then the use of the single global mean value of 793 gN m^{-2} will have no affect on the nitrogen uptake. This uptake will however still be affected by changes in soil carbon. These factors need to be considered when analyzing the following results.

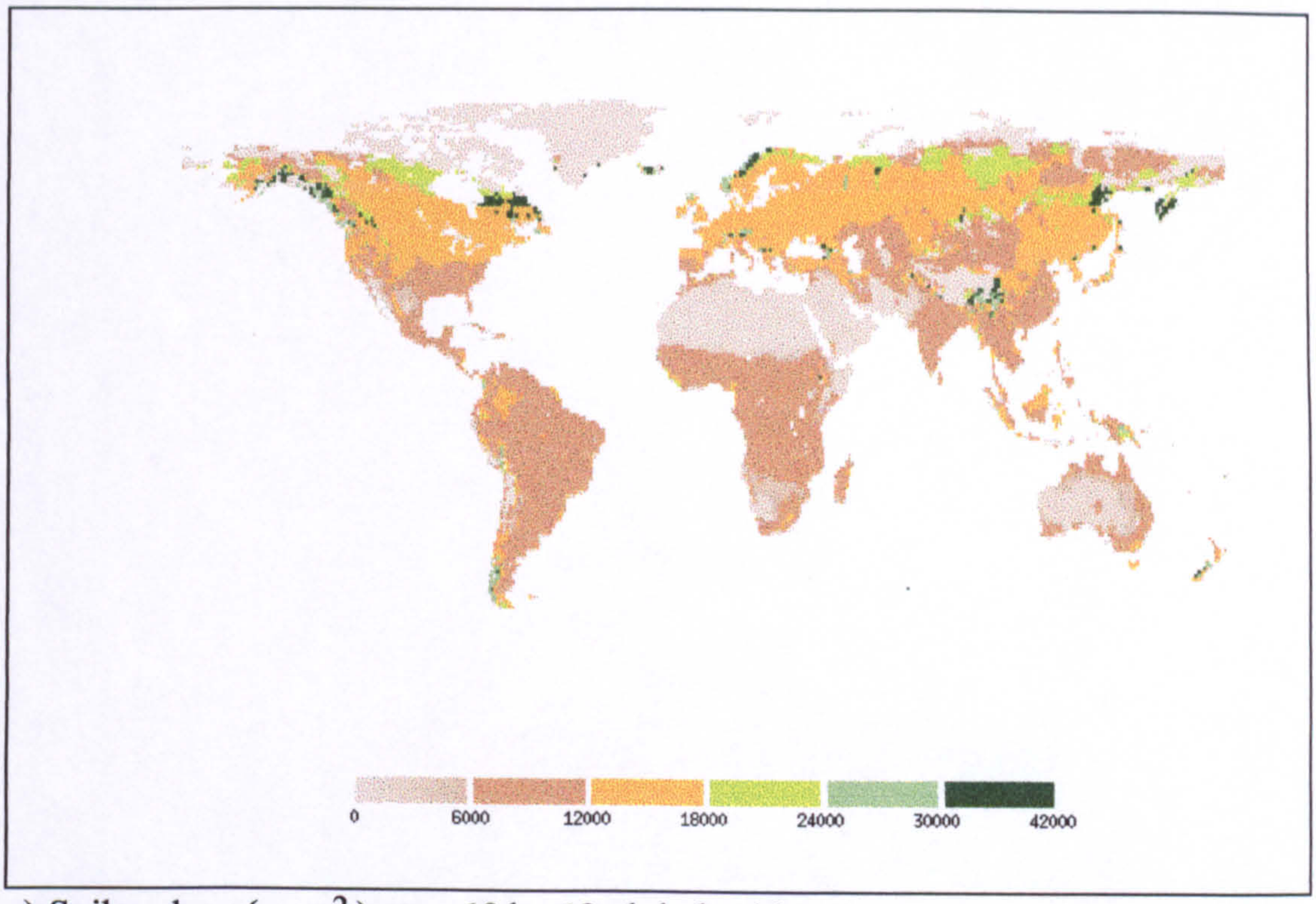

a) Soil carbon (g m^{-2}) on a 1° by 1° global grid.

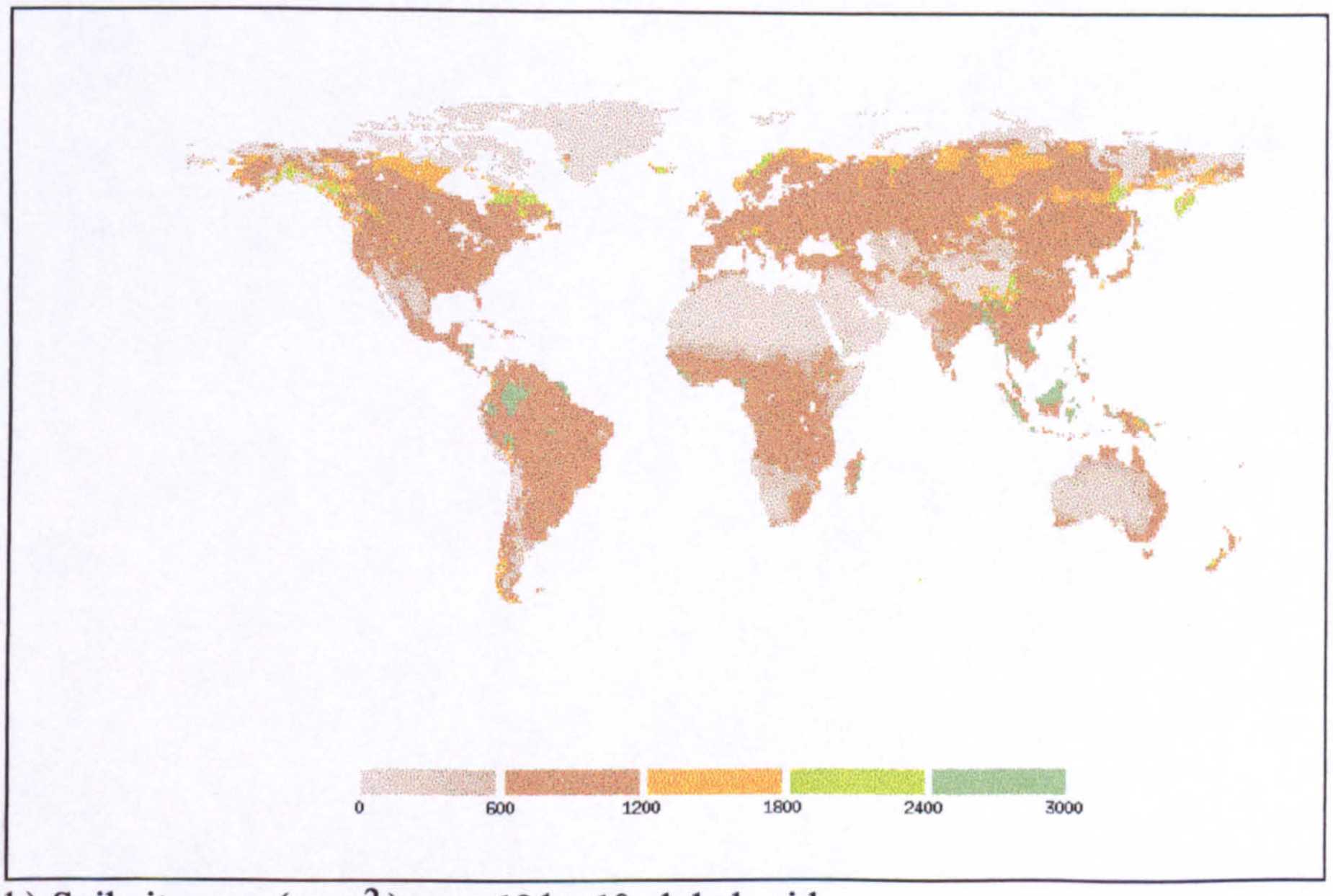

b) Soil nitrogen (g m^{-2}) on a 1° by 1° global grid.

Figure 3.2 Global soil carbon and soil nitrogen (g m^{-2}) on a 1° by 1° global grid. These data were assembled by Woodward and Smith (1994a) from data obtained by Zinke and co–workers (Zinke *et al.*, 1984; Post *et al.*, 1982, 1985) from site observations across the world.

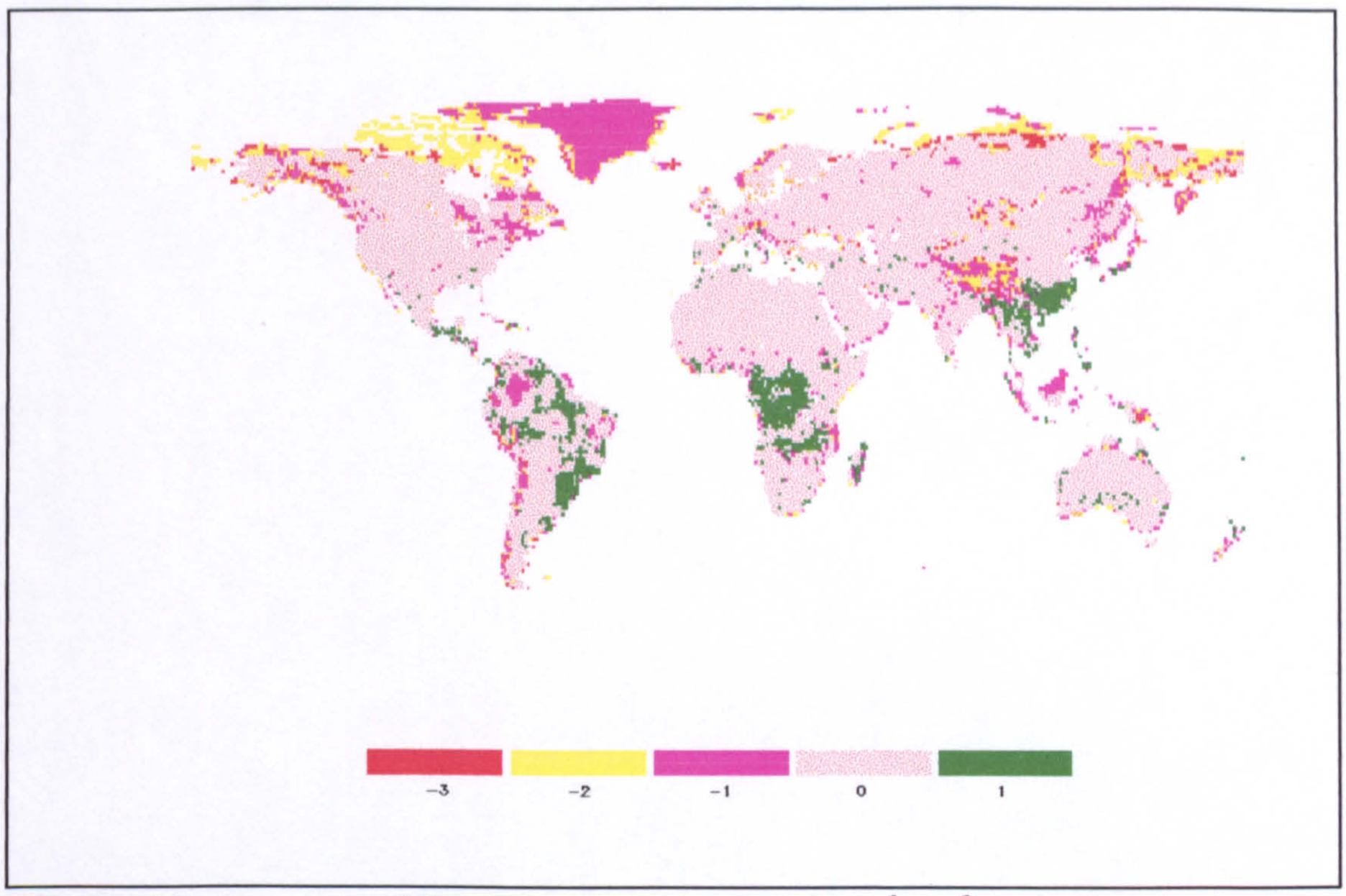

Figure 3.3 shows the difference map of NPP (tC ha^{-1} yr^{-1}) calculated using variable soil values and a mean single global value of soil carbon and soil nitrogen. The global range of NPP is between 0 and 13 tC ha^{-1} yr^{-1}. Areas where the NPP calculated from variable soils data is greater than the values obtained using the mean single global value are shown as positive values and the reverse situation as negative values.

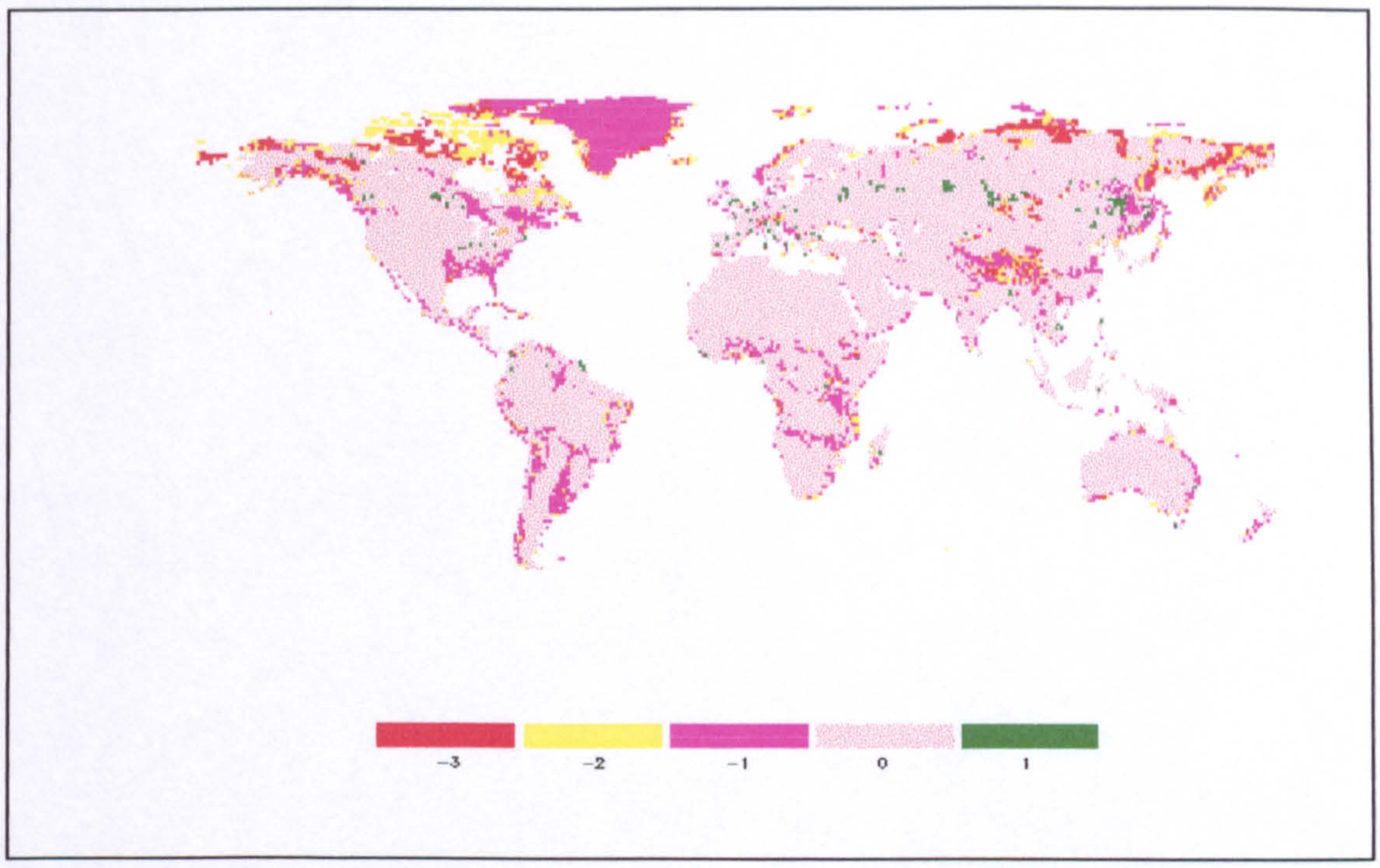

Figure 3.4 shows the difference map of LAI calculated using variable soil values and a mean single global value of soil carbon and soil nitrogen. The global range of LAI is between 0 and 9. Areas where the LAI calculated from variable soils data is greater than the values obtained using the mean single global value are shown as positive values and the reverse situation as negative values.

If the variable soil carbon and nitrogen values are used instead of the single mean global value (Figure 3.3) then the NPP values are greater than those calculated with the mean soil values by 1 tC ha^{-1} yr^{-1} in Uruguay, southern Brazil, the Amazon and Tocantins river basins of Brazil, and the other equatorial rain forest regions of the world—Zaire, and Indonesia. Also, the southern savannah regions of Africa, southern Mexico, Panama and eastern China have NPP values that are greater with the variable soil carbon and nitrogen values. In eastern China, the actual soil carbon values are lower than the mean by about 3000 gC m^{-2} and the soil nitrogen is above 600 gN m^{-2}. This means that by using the mean soil carbon value, instead of the variable soil carbon value, nitrogen uptake decreases. Thus the uptake is higher with the variable soil carbon and the NPP is higher. At the global level, the total global

NPP value calculated from the model run with the mean soil carbon value is 53.4 GtC km^2 yr^{-1} but with the variable soil carbon value it is lower with a value of 48.9 GtC km^2 yr^{-1}. This shows that the use of the mean value decreases the total amount of soil carbon globally, increasing nitrogen uptake and NPP.

The negative values that occur in Greenland and the far northern coastline of both Canada, Alaska and Siberia are caused by the fact that the program allocates values of –1 for snow and ice, and –2 for bare ground, the soil carbon and nitrogen for these regions is zero and also the NPP. These areas can be more easily identified from Figure 3.2. Actual decreases in NPP of mostly 1 tC ha^{-1} yr^{-1} occur on the Kamchatka peninsular and along the coast of the Sea of Okhotsk in eastern Siberia, also along the Yukon coast in western Canada going north into Alaska, and in Labrador. Here the carbon values of the soils are high so the use of the mean value causes an increase in nitrogen uptake which gives a greater NPP value than occurs with the variable soils, and hence a negative difference value. This situation also arises in Colombia, the eastern part of the Tibetan plateau, the Alps, the coast of Norway, Sarawak in Indonesia and southern Chile, the far north of Scotland and Iceland. All these areas have soil carbon values which exceed the average. The greatest negative difference of 3 tC ha^{-1} yr^{-1} occurs in Papua New Guinea, again because of the large amount of soil carbon here.

We can conclude from this that soils do have an impact on NPP in areas where soil carbon is high (i.e. greater than 24000 gC m^{-2}).

Figure 3.4 shows that similar patterns occur with the negative difference values of LAI as with NPP but there are some subtle differences and some additional areas of negative difference. For instance there are the same patterns in the far North due to snow, ice and bare ground. Also Ontario, Quebec and Maine show similar decreases in LAI with a single global value used instead of a variable soil carbon and nitrogen value. In these areas the carbon values of the soils are higher than the average value so there is an

increase in nitrogen uptake which gives a greater LAI value than occurs with the variable soils, and hence a negative difference value. The low nitrogen concentration in the soil appears to be influential in both the northern and southern savannah regions of Africa as well as southern Argentina. The average soil nitrogen value is greater than the variable value and causes an increase in nitrogen uptake. This increases LAI and causes a negative difference value. However this increased nitrogen uptake has not been sufficient to increase the annual NPP value although it has led to improved water use efficiency which means that a larger LAI can be supported by the same NPP. In the equatorial regions where the NPP is greater with the variable soil carbon value than with the average value which has a lower nitrogen uptake, there is no change in LAI. There is sufficient water in these regions for no extra benefit to be gained from increased LAI even though there is greater NPP. Soil carbon has a greater impact on NPP where water is plentiful and soil nitrogen affects LAI in arid areas when it is low. The mean global LAI value for the variable soil carbon value is 3.6 and for the mean soil carbon value it is 3.7. Although there is little change in the LAI value between the two soil treatments the amount of vegetated area is greater with a value of 113.9×10^6 km^2 for the mean soil carbon value compared with 102.7×10^6 km^2 for the variable soil carbon value. This shows that the use of the mean soil carbon value increases the vegetated area and causes a slight increase in the global LAI.

3.5 Discussion

The aim of this sensitivity analysis was to examine the influence of soil carbon and nitrogen on the DOLY model. This simple technique has demonstrated quite clearly the importance of soil carbon and nitrogen in certain regions of the world such as the tropics and the tundra regions. This analysis has shown that there are large areas where the model outputs of LAI and NPP are insensitive to the soils data. It has also highlighted areas where the

difference between the cell soil value and the average global value is small. In this study soil carbon and soil nitrogen have been the only nutrients examined. Phosphorous is also important and has an impact on vegetation, particularly in areas such as the tropics but this has not yet been included in DOLY. More detailed soils information on the texture, and depth of soils is now available on CD-ROM in the ISLSCP database (Meeson *et al.*, 1995; Sellers *et al.*, 1995). The DOLY (water and soils version) model uses these soil texture data. The model creates its own soil which interacts with the vegetation component of the model. The soil texture influences the amount of water in the soil available to the vegetation, and, in turn, nitrogen uptake.

In conclusion, soil nitrogen and soil carbon do have an effect on the output of the DOLY model. This effect is regional, and soil nitrogen only influences NPP and LAI at low nitrogen values. Soil carbon can have a significant impact on the final NPP value produced by DOLY, through its influence on nitrogen uptake. It is most influential in the tropics where there are small amounts, and the uptake of nitrogen is high; this in turn increases NPP. LAI output is less sensitive to soil carbon and nitrogen globally although there are some regional effects.

CHAPTER 4

4.0 The sensitivity of the DOLY model to climate, atmospheric carbon dioxide and climate change

4.1 Introduction

Climate has an important influence on global vegetation and there have been numerous studies that link the distribution of global vegetation with the current climate (Holdridge, 1947; Box, 1981; Woodward, 1987; Prentice *et al.*, 1992). Individual climate variables influence vegetation in many different ways and can affect both the physiological processes operating within plants as well as their structural characteristics. For instance, temperature and relative humidity influence transpiration, stomatal conductance and photosynthesis, and the wind speed influences the growth and structure of vegetation. Precipitation is of vital importance without which no plant growth would be possible.

In Chapter 3, there was an examination of the sensitivity of leaf area index (LAI), and net primary productivity (NPP) to soil inputs. This section aims to examine the sensitivity of these variables, together with stomatal conductance, to the climate variables of temperature, relative humidity and precipitation. Stomatal conductance is an important input variable to general circulation models (GCMs) (see Chapter 6). There is also an analysis of the sensitivity of the model to atmospheric carbon dioxide, together with a climate change scenario. In this scenario, all the climate variables alter together. It should be stressed that this scenario is a model sensitivity test and is not intended to predict what will happen with an actual change in climate. The following section describes the methods adopted to determine the sensitivity of the DOLY model to the climate data, along with the results. There is then a discussion of these results.

4.2 Methods

The water version of the DOLY model is used in this sensitivity analysis. This means that the soil inputs are the same as with the standard version of the model. For more details of different versions of the model see Chapter 2.

There are three stages to this sensitivity analysis.

Stage 1: This stage determines how each climate variable would influence each output variable over a given range of climate values. This provides information about the range of climate values that cause the greatest response in the output variable.

Stage 2: This stage calculates the sensitivity of each output variable to a given percentage change in the climate value. This is aided by the results from Stage 1.

Stage 3: The final stage examines the effect of a set change in a combination of climate variables to see the effect they would have on the output variables. This stage aims to determine the dominant climate variable in a climate change scenario.

Stage 1: To determine the influence of each climate variable on the output variables, LAI, NPP and stomatal conductance over a given range of input values.

Eight test sites were chosen to represent seven of the world's major biomes. Details of these sites are in Table 4.1. The availability of suitable climate data (Müller, 1982; Leemans and Cramer, 1991) together with the fact that the vegetation at these sites was readily identifiable as a discrete biome (Archibold, 1995; Barbour and Billings, 1988) influenced the choice of these sites. Sites 5, 6 and 8 are close to sites used by McGuire and co-workers (1992) to calibrate their terrestrial ecosystem model (TEM). Some authors have stated that the greatest temperature increases with climate change are likely to occur in the higher latitudes (Greco *et al.*, 1994) due to sea-ice

interactions with the atmosphere and changes in albedo. The boreal forest–tundra boundary is identified as an area with the greatest sensitivity to climate change (Bonan *et al.* 1990, 1992; Kauppi & Posch, 1985). The selection of three sites, one tundra site and two boreal sites, provided additional details as to the actual sensitivity of these regions. A small LAI (0.18) is predicted by the DOLY model for the tundra site. The northern boreal site is close to the boundary with the tundra and the more southerly site to that with temperate deciduous forest (Barbour and Billings, 1988). Both these sites are in North America.

Table 4.1 Location and the biome represented for each of the 8 test sites used in the climate sensitivity analysis.

Site	Latitude	Longitude	Location details	Biome
1	67.5°N	115.0°W	Coppermine, Northwest Territories, Canada	Tundra
2	61.0°N	113.5°W	Fort Resolution, Northwest Territories, Canada	Northern boreal forest
3	49.0°N	82.0°W	Cochrane, Ontario, Canada	Southern boreal forest
4	48.5°N	7.5°E	Strasbourg, France	Temperate deciduous forest
5	37.5°N	100.0°W	Dodge City, Kansas, USA	Grassland
6	21.0°N	72.5°E	Surat, India	Drought deciduous forest
7	0.5°N	25.5°E	Kisangani, Zaire	Tropical rain forest
8	15.0°S	28.5°E	Lusaka, Zambia	Savannah

The DOLY model was run with the usual mean monthly climate values, (see Table 4.2 for the mean monthly and annual values), but with one variable fixed so that it did not alter throughout the year. Further runs of the program used the three monthly climate variables but over a range of fixed values for one of these variables. Most of these combinations are physically realistic, although some are unlikely to occur in reality. For instance, low temperatures at a tropical site, low rainfall at a rain forest site, or low humidities (less than 20%) at a high latitude site. These combinations have been included in the analysis for completeness. To determine the sensitivity of the model to temperature, the model was run with mean monthly values of relative humidity and precipitation, over a range of temperatures from 0 to 40°C. In January the monthly precipitation and relative humidity was input as usual, but the monthly temperature was set at 0°C. This process was repeated for February through to December to derive an annual value of LAI, NPP and stomatal conductance at 0°C. This process was also repeated with the temperature set at 10°C and so on, until all values had been calculated up to 40°C. The precipitation and humidity data are not linked to each other within the model. However, temperature and humidity both influence the vapour pressure deficit, (see Chapter 2, equations 2.26 and 2.27). It can be seen from equation 2.26 and Figure 2.5 that, for a given vapour pressure, if the air temperature increases the saturation vapour pressure, e_s (t), and hence the vapour pressure deficit (VPD) increase. Thus, relative humidity decreases as VPD increases. If the temperature is raised but relative humidity remains the same, then the vapour pressure deficit increases. This affects the calculation of evapotranspiration. The rate of evapotranspiration increases as both vapour pressure deficit and temperature increase (Figure 2.6).

An additional run of the program was carried out whereby the temperature was set at a range of fixed values but the vapour pressure deficit was kept at the monthly values as shown in Table 4.2e. In effect, VPD was not

allowed to increase with increasing temperature. All the other monthly variables were retained as with previous runs.

The aim of this exercise is to demonstrate how different biomes, represented by these test sites, would respond to changes over the full range of global temperatures, precipitation and humidities. It is also important to test that the DOLY model is able to operate outside its usual climate ranges. This would check whether the model produced spurious results or "crashed" in certain circumstances such as runs with low values of atmospheric carbon dioxide.

Table 4.2 shows that the tundra and boreal sites (sites 1, 2, and 3) have an annual mean temperature below 5°C. This value usually represents the minimum temperature (base temperature) for growth (Prentice et al. 1992). At these three sites, the mean monthly temperature is above 5°C for only 2, 5 and 6 months of the year, respectively. There is, therefore, a restriction on the potential for growth.

Table 4.2 Climatic details for each of the 8 test sites used in the climate sensitivity analysis. The location and details of these sites are in Table 4.1

Table 4.2a Annual mean temperature, relative humidity, and precipitation and total precipitation for the 8 test sites

Site	Annual mean temperature (°C)	Annual mean relative humidity (%)	Monthly mean precipitation (mm)	Annual total precipitation (mm)
1	-11	79	16	191
2	-4	77	28	331
3	1	80	71	846
4	10	78	64	763
5	13	65	50	598
6	27	59	84	1010
7	24	86	151	1813
8	21	62	73	874

Table 4.2b Mean monthly temperatures (°C) for each of the 8 test sites

Mean monthly temperature (°C)												
	Month Number											
Site	1	2	3	4	5	6	7	8	9	10	11	12
1	-29	-31	-25	-16	-5	3	9	8	2	-7	-19	-26
2	-27	-24	-16	-5	5	11	15	14	7	-1	-12	-22
3	-17	-15	-9	1	8	14	17	16	11	5	-4	-13
4	1	2	6	10	14	17	19	18	15	10	6	2
5	0	2	7	13	18	24	27	26	22	15	7	2
6	22	24	28	31	32	31	28	28	28	29	26	23
7	25	25	25	25	25	24	24	24	24	24	24	24
8	22	22	22	21	18	16	16	19	22	25	23	22

Table 4.2c Mean monthly precipitation (mm) for each of the 8 test sites

Mean monthly precipitation (mm)												
	Month Number											
Site	1	2	3	4	5	6	7	8	9	10	11	12
1	9	8	9	7	13	15	32	30	24	19	14	11
2	14	14	16	16	26	36	55	44	43	25	21	21
3	58	47	53	54	74	89	82	84	90	72	80	63
4	61	52	44	54	63	87	83	82	71	56	59	51
5	12	17	28	55	91	87	75	80	57	53	25	18
6	3	2	2	4	6	198	407	188	149	41	8	2
7	83	95	150	176	168	117	137	156	184	221	201	125
8	228	181	103	20	4	0	0	0	0	16	94	228

Table 4.2d Mean monthly humidity (%) for each of the 8 test sites

Mean monthly humidity (%)												
	Month Number											
Site	1	2	3	4	5	6	7	8	9	10	11	12
1	89	83	82	81	74	62	65	77	82	91	87	80
2	86	79	69	71	68	65	67	73	77	83	92	96
3	91	89	84	71	69	70	71	76	81	83	88	89
4	84	81	75	70	71	72	71	75	79	83	86	87
5	68	66	61	64	67	65	67	63	64	64	65	69
6	47	48	44	49	60	71	81	79	74	55	47	47
7	84	81	84	86	86	87	88	88	87	87	86	88
8	83	87	80	72	64	60	35	46	41	40	61	80

Table 4.2e Mean monthly vapour pressure deficit (Pa) for each of the 8 test sites

Mean monthly vapour pressure deficit (x 10^2 Pa)												
	Month Number											
Site	1	2	3	4	5	6	7	8	9	10	11	12
1	0.1	0.1	0.1	0.3	1.1	3.0	4.0	2.5	1.3	0.3	0.2	0.1
2	0.1	0.2	0.5	1.2	2.9	4.6	5.6	4.2	2.4	1.0	0.2	0.1
3	0.1	0.2	0.5	1.8	3.4	4.9	5.7	4.3	2.4	1.5	0.6	0.3
4	1.1	1.4	2.4	3.7	4.7	5.6	6.4	5.3	3.7	2.1	1.3	0.9
5	1.9	2.4	3.8	5.4	7.0	10.4	11.6	12.5	9.2	6.1	3.4	2.1
6	14.4	15.4	20.7	22.3	18.7	12.9	7.4	7.9	9.9	17.7	17.9	15.1
7	4.9	5.9	5.0	4.4	4.3	3.9	3.5	3.5	3.8	3.9	4.2	3.6
8	4.4	3.4	5.1	6.8	7.6	7.3	11.9	11.5	15.6	18.7	11.2	5.4

The following tests were performed.

1. a) The mean monthly temperature values were varied between 0 and 40°C for each site but there was no alteration to the other site details.

1. b) The mean monthly temperature values were varied between 0 and 40°C for each site, and monthly vapour pressure deficit values from Table 4.2e were used. There was no alteration to the other site details.

2. The mean monthly precipitation values were varied between 0 and 200 mm for each site, but the other site input details were not altered.

3. The mean monthly relative humidity values were varied between 0 and 100% for each site, but the other site input details were not altered.

4. The atmospheric CO_2 partial pressure was varied between 0 Pa to 70 Pa for each site, but the other site input details were not altered.

Additional tests were performed using a sensitivity index, β (after Gates, 1985).

Stage 2: To calculate the sensitivity of each output variable to a given percentage change in the input variable.

The DOLY model was run as normal for a full year using the data from the test sites to obtain initial values of NPP, LAI and stomatal conductance (see Table 4.3). The model was run again but this time, one of the climatic variables was increased by 10%, whilst the other variables remained unchanged. This test was repeated with further increases of 20 and 30% for temperature, precipitation, relative humidity and atmospheric CO_2 as well as decreases of 10, 20 and 30% for precipitation and relative humidity. Atmospheric CO_2 was also increased by 60 and 100% in order to simulate increases of atmospheric CO_2 partial pressure to 56 Pa and 70 Pa respectively (based on a present day atmospheric CO_2 partial pressure of 35 Pa). Percentage values were used so that the sensitivity of the model to such changes could be more easily calculated. An index of sensitivity was then calculated for each variable. It was decided to examine only increases of temperature and atmospheric CO_2 as they are not expected to decrease in climate change scenarios. There is, however, considerable uncertainty as to whether precipitation and relative humidity will increase or decrease (IPCC, 1990,1992) so the index of sensitivity was calculated for both situations with these variables. It has also been stated that there will be considerable regional variations in the magnitude of temperature increases (IPCC, 1990,1992) so a range of increases from 10 to 30% were selected for all the sites to give a reasonable indication of the likely impact of rising temperatures. This was also done with the other variables to provide comparisons.

Table 4.3 LAI, NPP and stomatal conductance predicted by the DOLY model for each of the 8 test sites for the current climate.

Site	Mean LAI for the year	Annual NPP ($tC\ ha^{-1}\ yr^{-1}$)	Mean annual canopy stomatal conductance ($m\ s^{-1}$)
1	0.18	0.57	0.23
2	0.94	2.12	0.82
3	1.29	3.18	1.25
4	2.94	5.50	2.65
5	1.87	6.86	1.85
6	2.21	6.89	1.97
7	7.53	14.98	6.72
8	2.38	7.33	2.61

Stage 3:

Finally, all the variables were altered together as a climate change simulation (Test 9). According to the IPCC (1990) report the global mean temperature is expected to rise by 3°C, annual precipitation to increase by 10% and atmospheric CO_2 partial pressure to double to 70 Pa by the late 21st century. These changes were made to the climate inputs and the results analyzed. Relative humidity was also increased by 10% in order to ascertain its impact. In addition to this, a further analysis was performed to determine the percentage changes in LAI, NPP and stomatal conductance in response to the climatic changes (Test 10).

4.3 Results

The following results were obtained from each test performed. Table 4.4 shows the site number and biome for each of the eight test sites.

Table 4.4 Site number and the corresponding biome description for the eight test sites.

Site no.	Biome description
1	Tundra
2	Boreal (N) forest
3	Boreal (S) forest
4	Temperate deciduous forest
5	Grass
6	Drought deciduous forest
7	Tropical rain forest
8	Savannah

Stage 1

Test 1a: The climate inputs were kept constant except for monthly temperature which was increased between 0 and 40°C.

Figure 4.1 shows the effect of increasing temperature on LAI, NPP and stomatal conductance for each of the 8 sites. The northern boreal forest and grassland sites (sites 2 and 5) behaved in a similar manner with LAI values increasing sharply between 0 and 10°C and then gradually decreasing to an LAI value of zero by 40°C. The tundra site (site 1) has a very low LAI, close to 1, which increases slightly between 5 and 10°C and 20 and 25°C before declining again as temperatures continue to rise. The southern boreal forest, temperate deciduous forest and rain forest sites (sites 3, 4 and 7) had similar patterns with their peak LAI values occurring around 25°C. The dry deciduous and savannah sites (sites 6 and 8) also behaved similarly with a peak LAI value

of 2 occurring at 15°C with little change as temperatures rise. A more symmetrical pattern emerges with NPP. Sites 3, 4, 6, 7 and 8 attain their maximum NPP values at 25°C before declining. Sites 1, 2 and 5 show a rise in values between 5 and 10°C but little change at higher temperatures, and decline above 30°C. Stomatal conductance exhibits similar characteristics to LAI with increasing temperature for five of the sites. However, sites 3, 4 and 7 show a decrease in stomatal conductance after 15 or 20°C instead of around 25°C as with the LAI values. It is interesting to note that the NPP values for sites 3 and 8, which have similar precipitation totals, (Table 4.2a) have a similar response to increasing temperature, although site 3 is much colder. This suggests that the NPP value for a site is more dependent on its precipitation, than its temperature. This will be examined in Test 2.

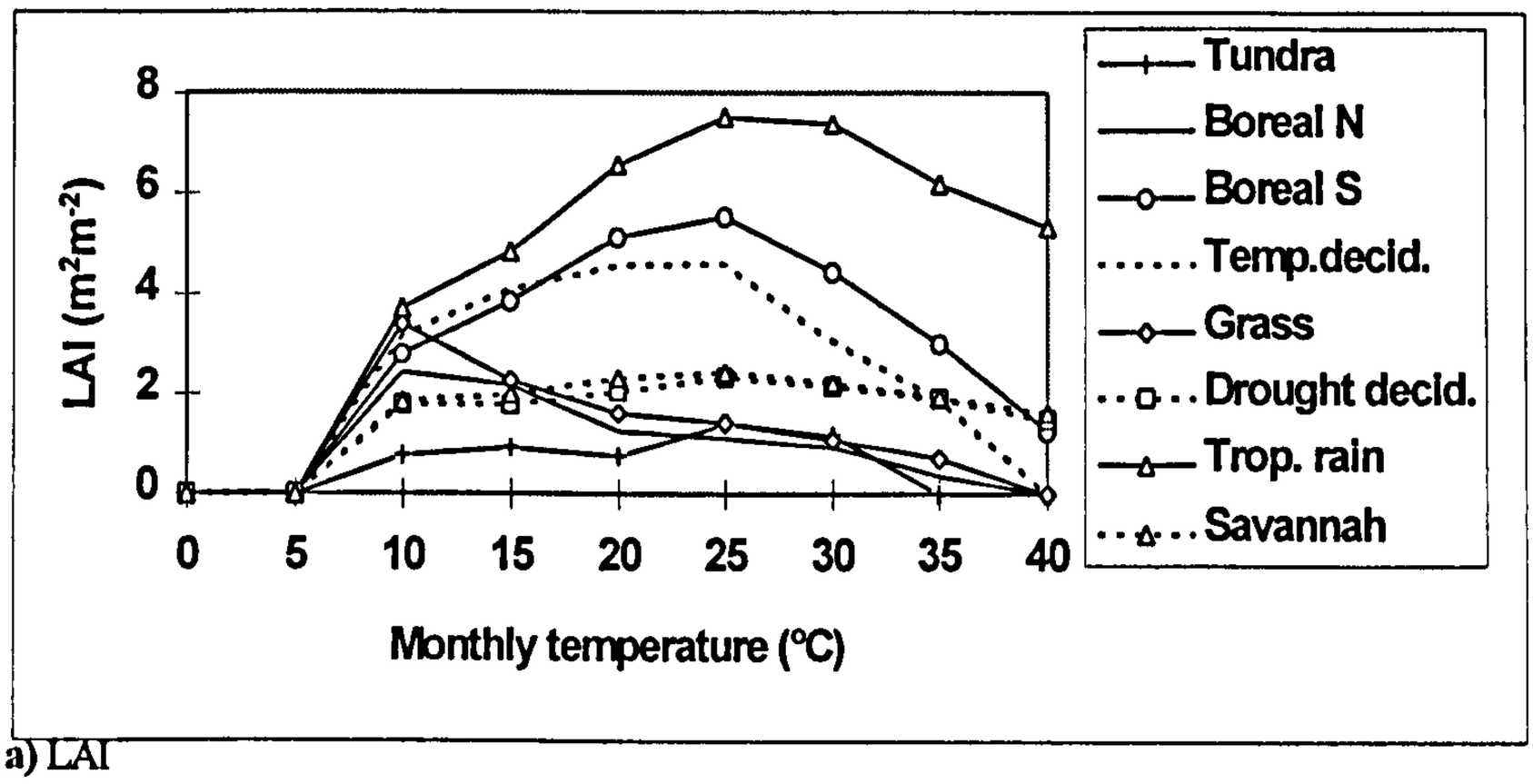

a) LAI

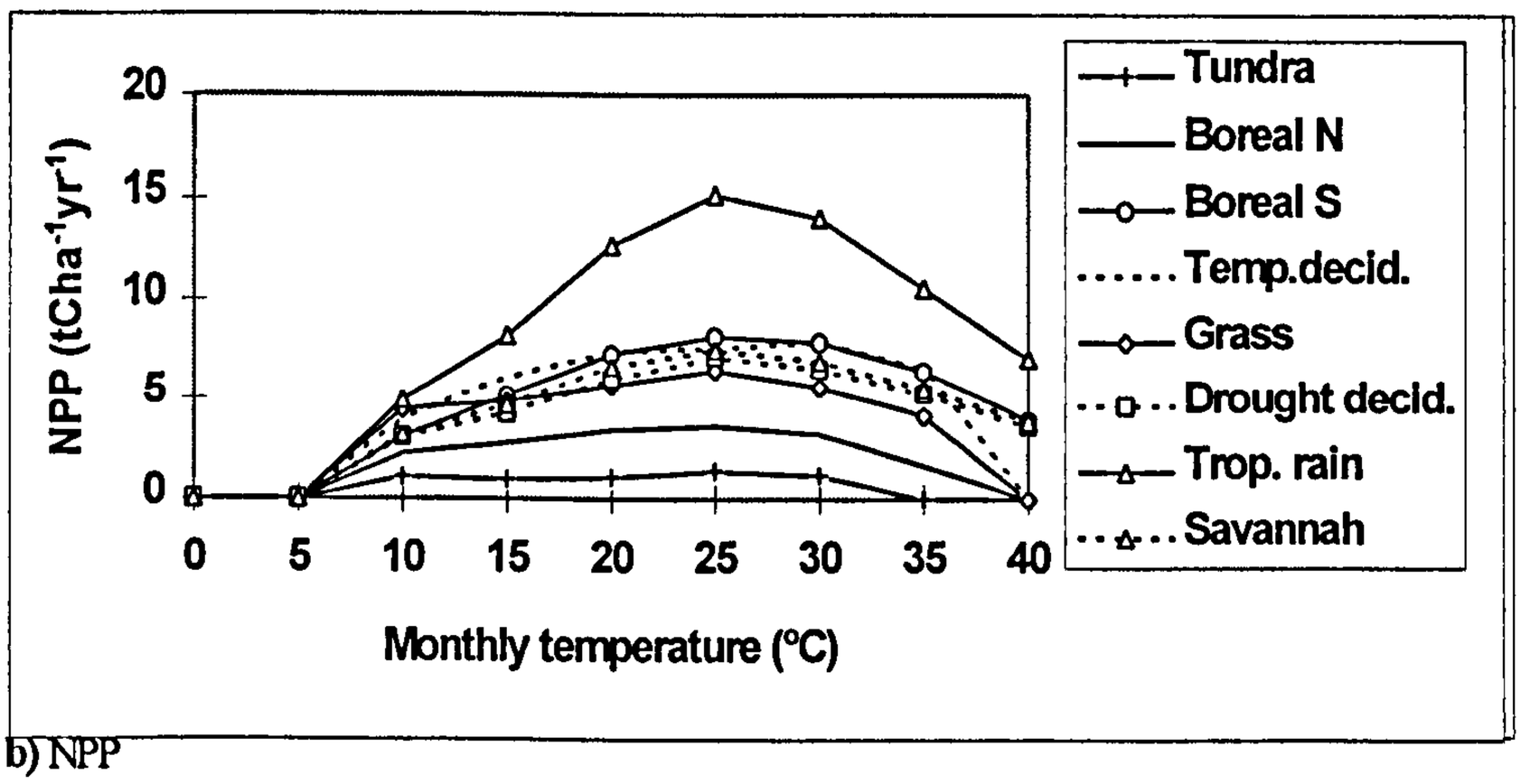

b) NPP

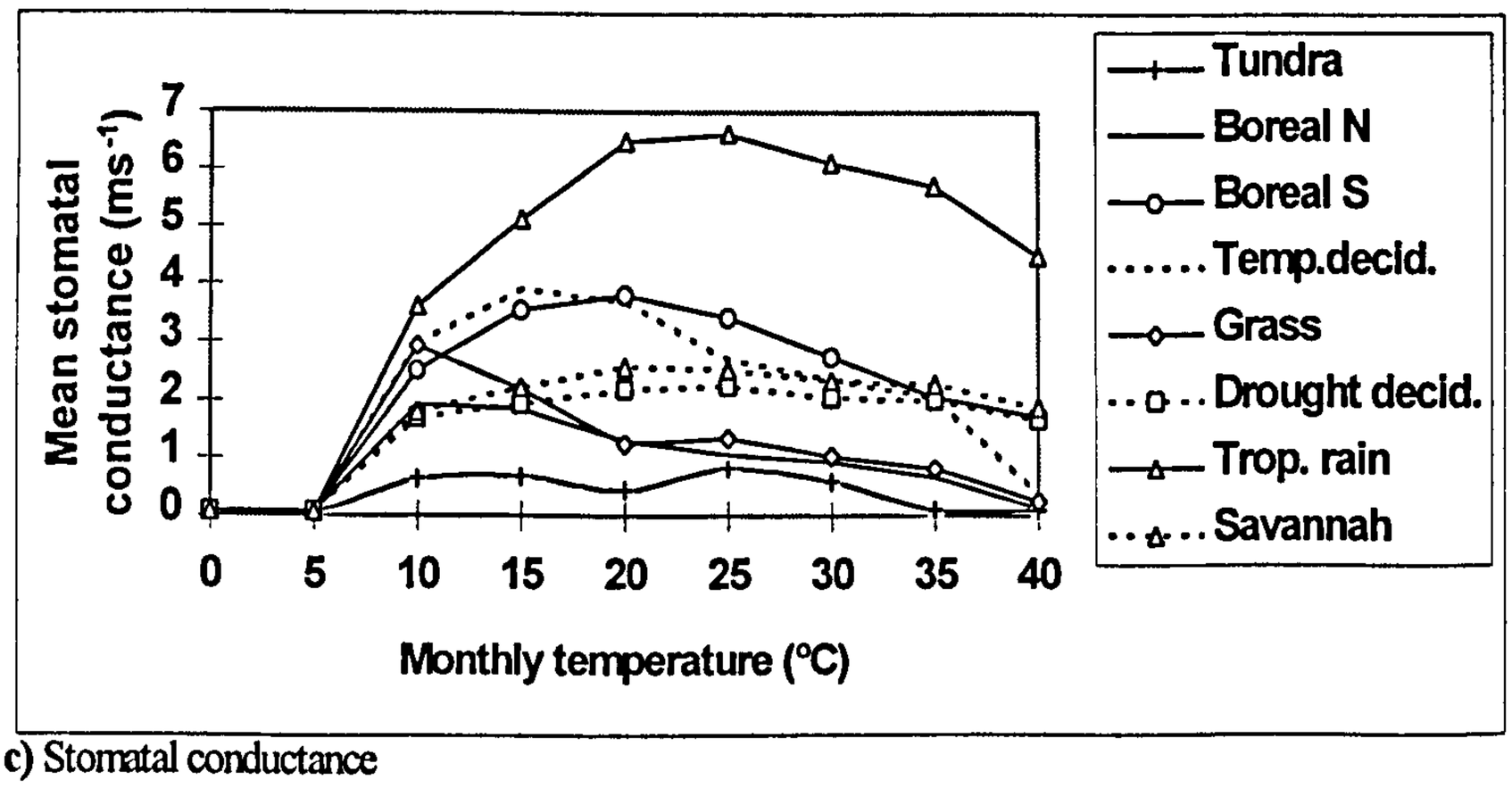

c) Stomatal conductance

Figure 4.1 a) to **c).** Values of a) LAI, b) NPP and c) stomatal conductance for a range of temperatures between 0 and 40°C for each of the 8 test sites.

Test 1b: The climate inputs were kept constant except for monthly temperature which was increased between 0 and 40°C and monthly vapour pressure deficit values from Table 4.2e were used.

It can be seen from Figure 4.2a the impact on LAI of retaining the monthly vapour pressure deficits for each site whilst allowing temperature to increase. At sites 3, 4, and 7 the LAI values remain high (around 6 or 7) and do not decrease as markedly when the temperature exceeds 25°C as they do in Figure 4.1a. This is due to the fact that the rising temperature is not having any effect on the vapour pressure deficit values. In Figure 4.1a, the LAI values were reduced above 25°C by the high vapour pressure deficit values which increased the evapotranspiration, and reduced the amount of water in the soil. The boreal north site benefits from the raised temperatures and is able to maintain an LAI of around 4 up to 30°C. The tundra and grassland sites also benefit from raised temperatures and no changes in VPD. The LAI at the tundra site reaches 2 at 25°C, and LAI at the grassland site, which is also around 2, decreases beyond 25°C. The savannah, and drought deciduous sites show little change between the two methods. From Table 4.2e, it can be seen that these sites have high VPD values relative to the other sites, as well as being hot, with low humidities (Table 4.2a, b and d). An increase in temperature would not, therefore, have a major impact on LAI as the VPDs are high already (Table 4.2e).

All sites, except 6 and 8, show an increase in NPP values over the previous test (1a) which is particularly noticeable between 20 and 30°C (Figure 4.2b) and is greatest for the temperate deciduous and the southern boreal sites (about 2 tC ha^{-1} yr^{-1} increase). The stomatal conductance (Figure 4.2c) tends to remain higher for longer (compared to Test 1a) at all sites with Test 1b with the exception of sites 6 and 8. The curves of the boreal south and temperate deciduous sites have similar behaviour which can be attributable to their similar climate (Tables 4.2a to 4.2e). The curves of the boreal north and grassland sites

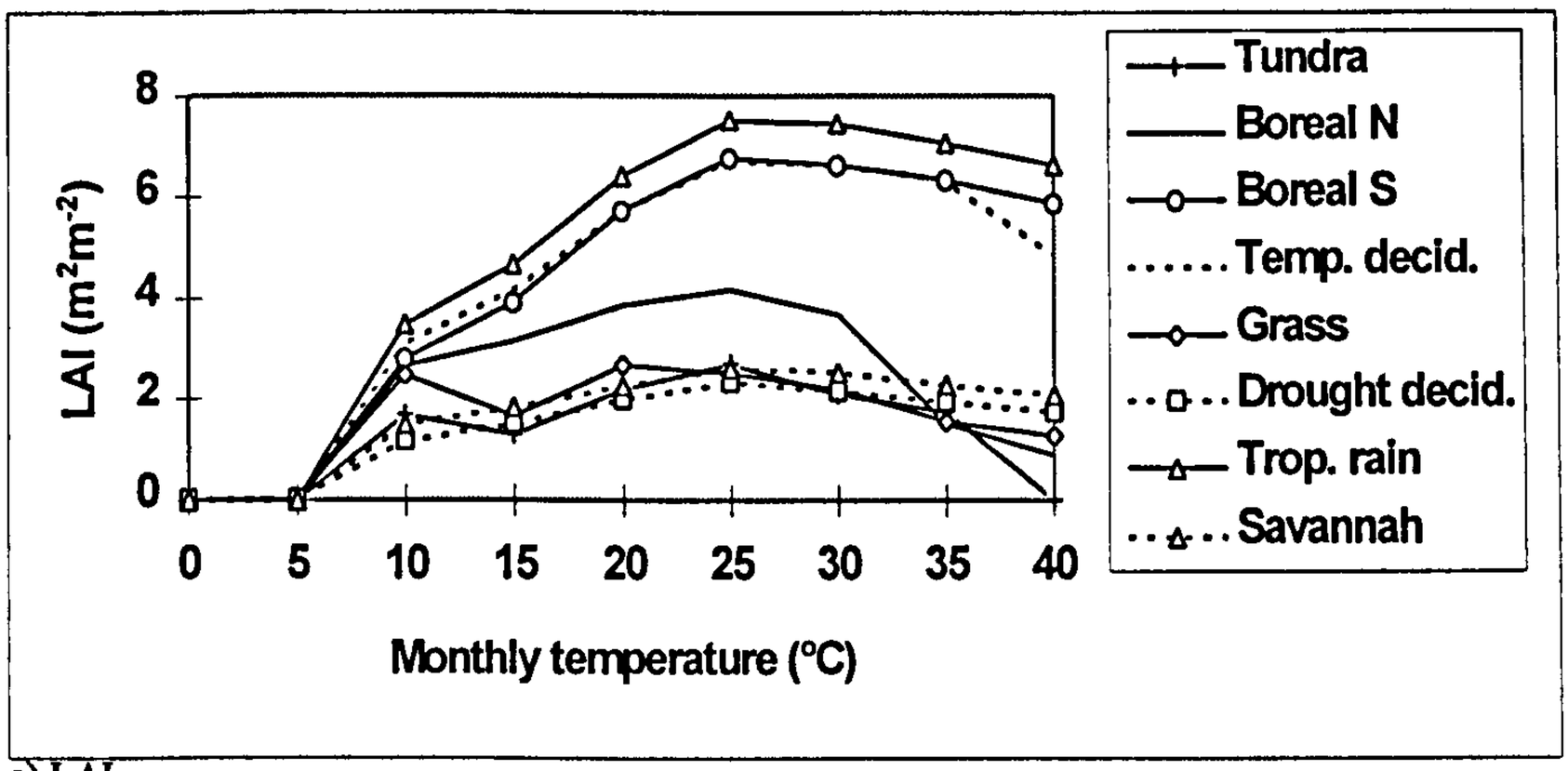

a) LAI

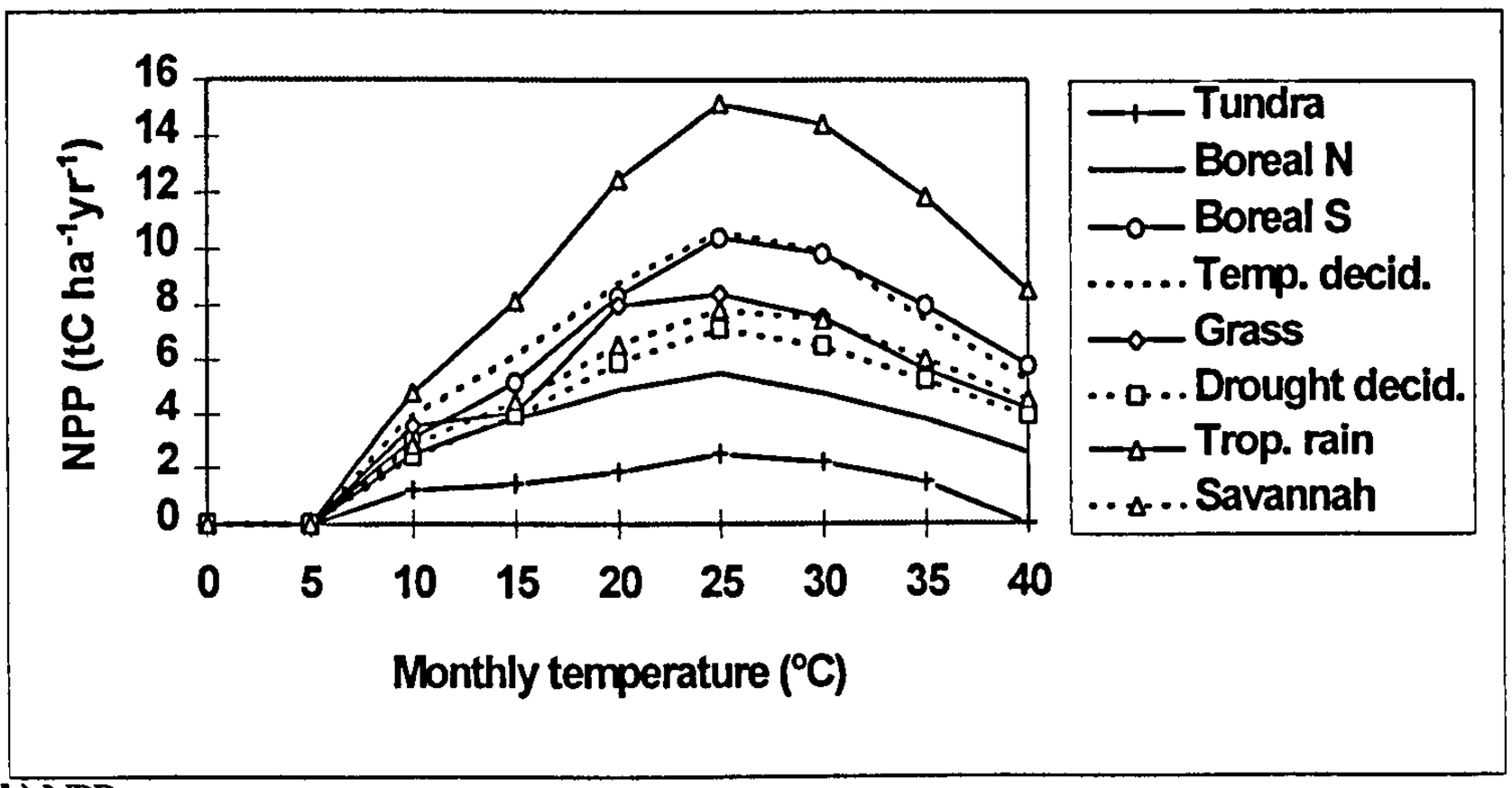

b) NPP

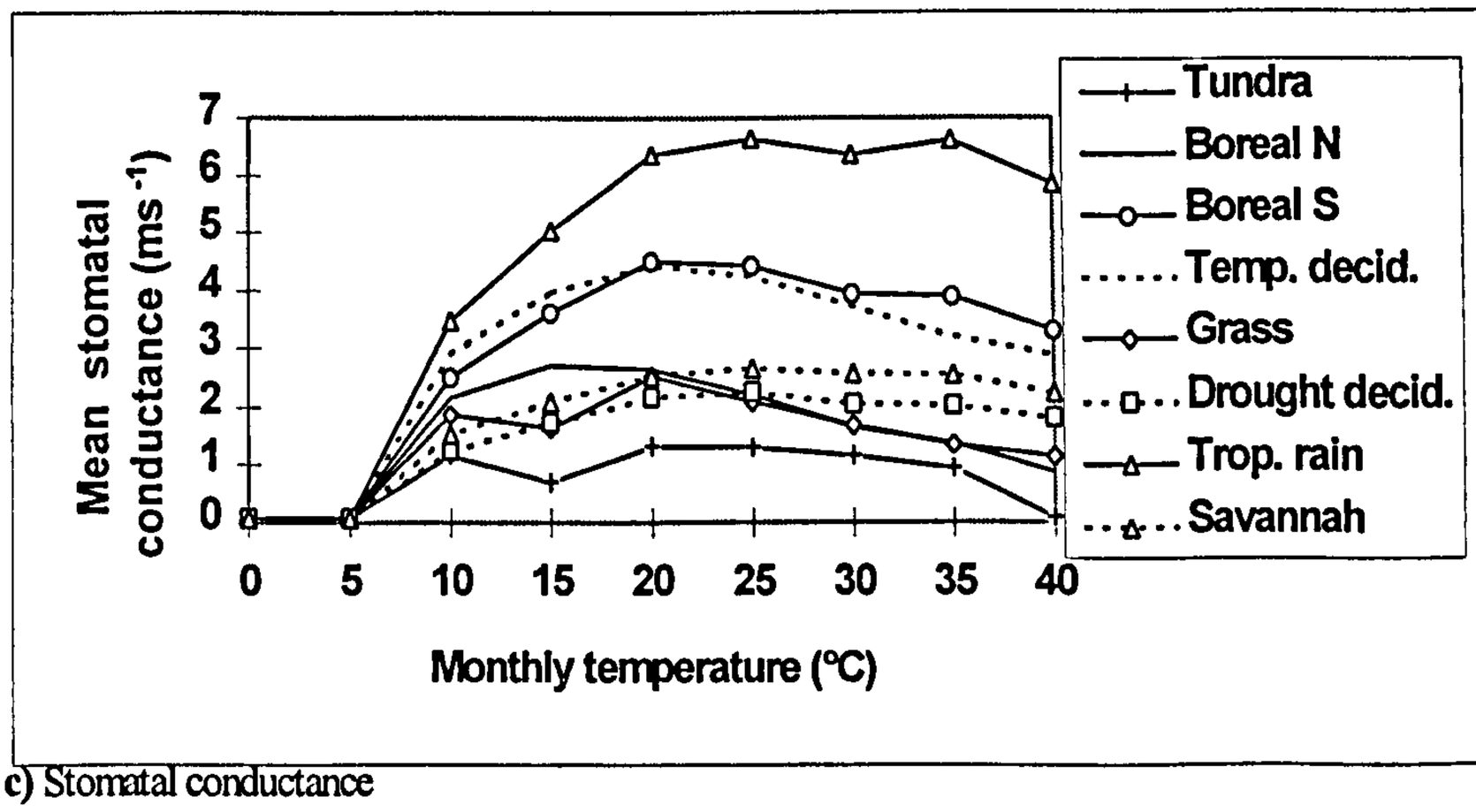

c) Stomatal conductance

Figure 4.2 a) to **c)** Values of a) LAI, b) NPP and c) stomatal conductance for a range of temperatures between 0 and 40° C for each of the 8 test sites. The monthly vapour pressure deficit for each site is taken from Table 4.2e.

are also similar. These sites have similar precipitation totals (Table 4.2a) although other aspects of their climate are different.

Test 2: The site details were kept constant except for monthly precipitation which was increased between 0 and 200 mm.

At sites 1, 2, 3 and 4, LAI increased with monthly precipitation up to 50 mm, and then no further increase occurred (Figure 4.3). At site 5, a maximum LAI of around 5 was reached at 150 mm. Sites 6 and 8 also reached a maximum LAI at 150 mm and site 7 around 100 mm. The same pattern emerged for NPP with sites 1 to 4 being unresponsive to precipitation above 50 mm and sites 5 to 8 being very responsive up to 150 mm, particularly site 6, the drought deciduous site. This highlights the importance of precipitation on NPP values in arid areas. The effect of precipitation on stomatal conductance shows the same patterns as for LAI, but there is more divergence between the values of stomatal conductance for sites 6 and 8.

Test 3: The site details were kept constant except for monthly relative humidity which was increased between 0 and 100% (Figure 4.4).

Most sites showed little change in LAI between relative humidity values of 0 and 60%. Above 80% relative humidity, the LAI value for site 5 (the grassland site) increased from 2 to 4, and the value for site 7 from 7 to 8. The LAI value for sites 6 and 8 rose from 2 to 3 above this relative humidity. Most sites also had little change in their NPP values between 0 and 70% humidity but showed a slight rise above 70%, particularly sites 5, 6, 7, and 8. Stomatal conductance rises gradually with relative humidity at most sites except for sites 1 and 3 (the tundra and southern boreal sites) which change very little as the relative humidity increases.

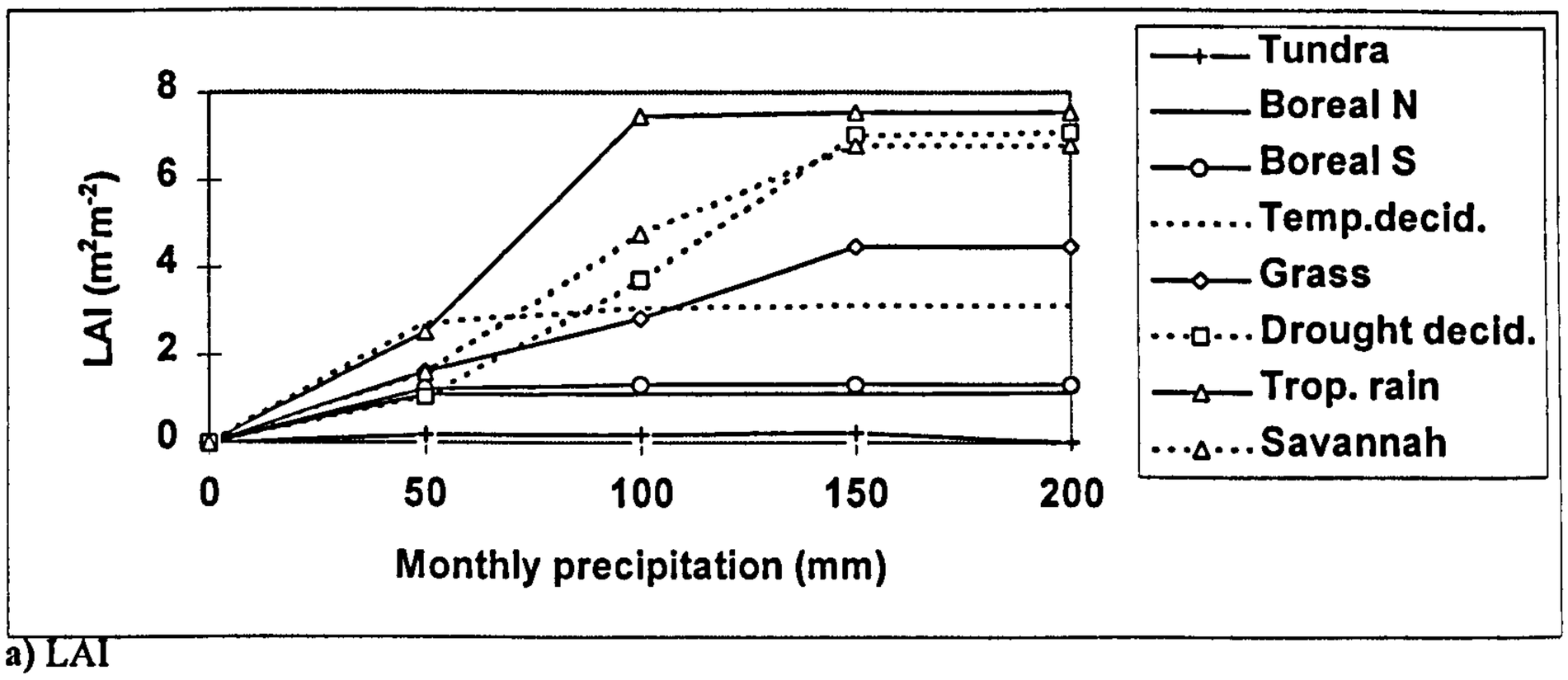

a) LAI

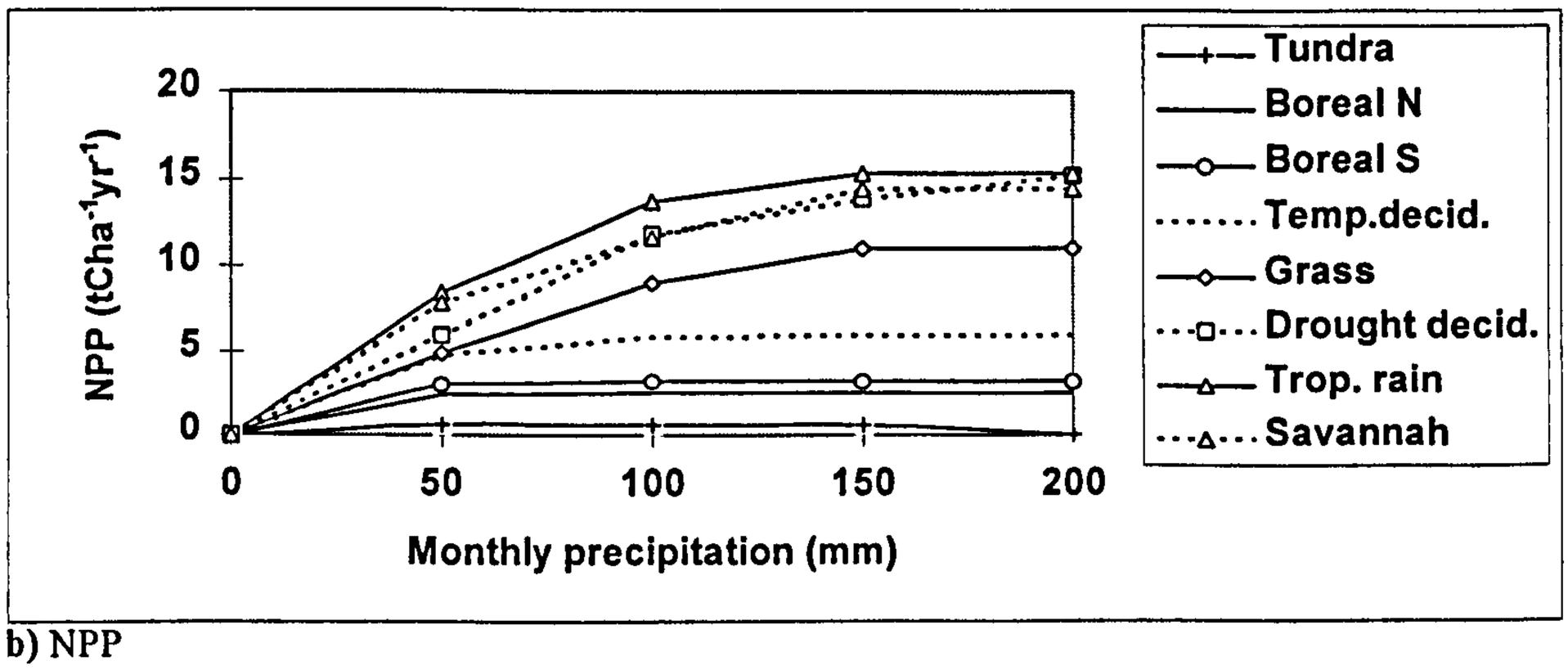

b) NPP

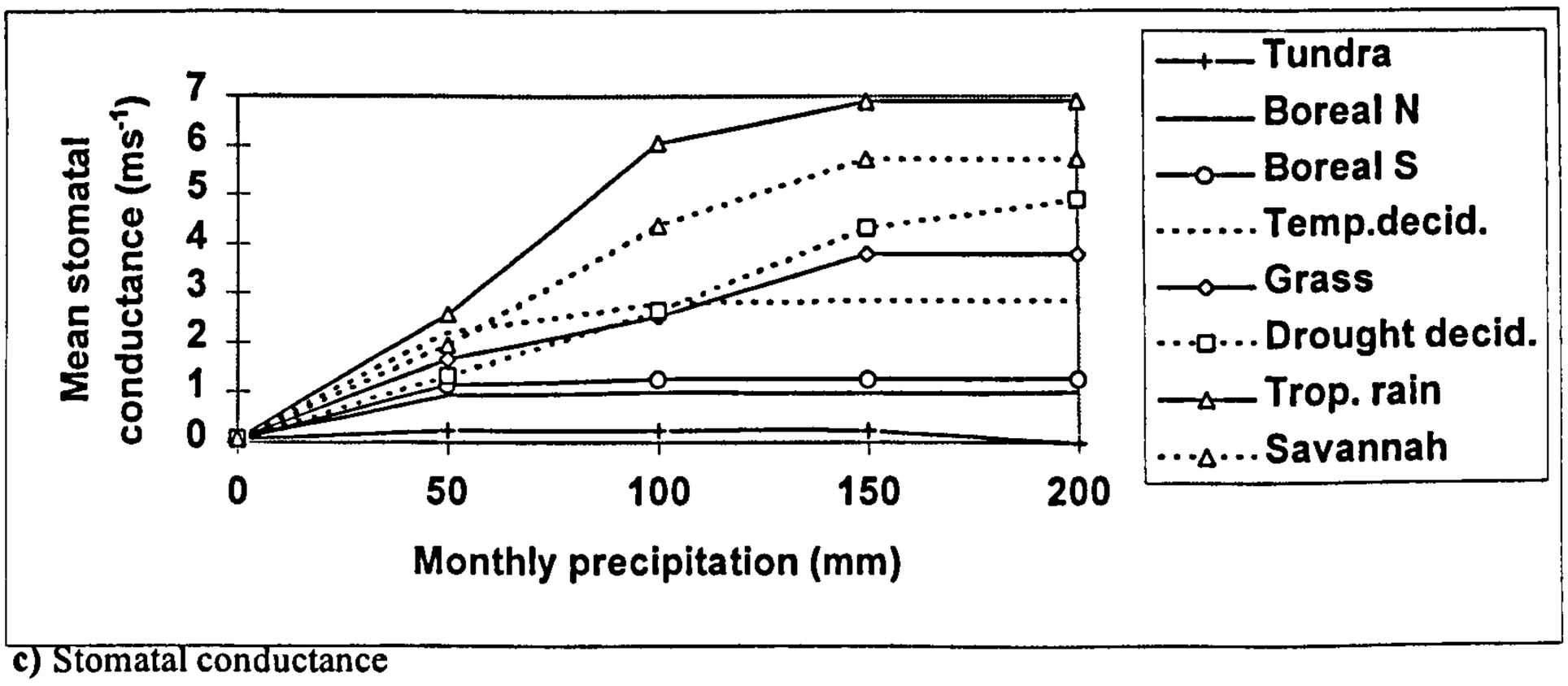

c) Stomatal conductance

Figure 4.3 a) to **c)** Values of a) LAI, b) NPP and c) stomatal conductance for a range of precipitation between 0 and 200 mm for each of the 8 test sites.
N.B. The apparent decline in the tundra above 150 mm is due to the inadequate reproduction of this graph within this document. It is not a real effect.

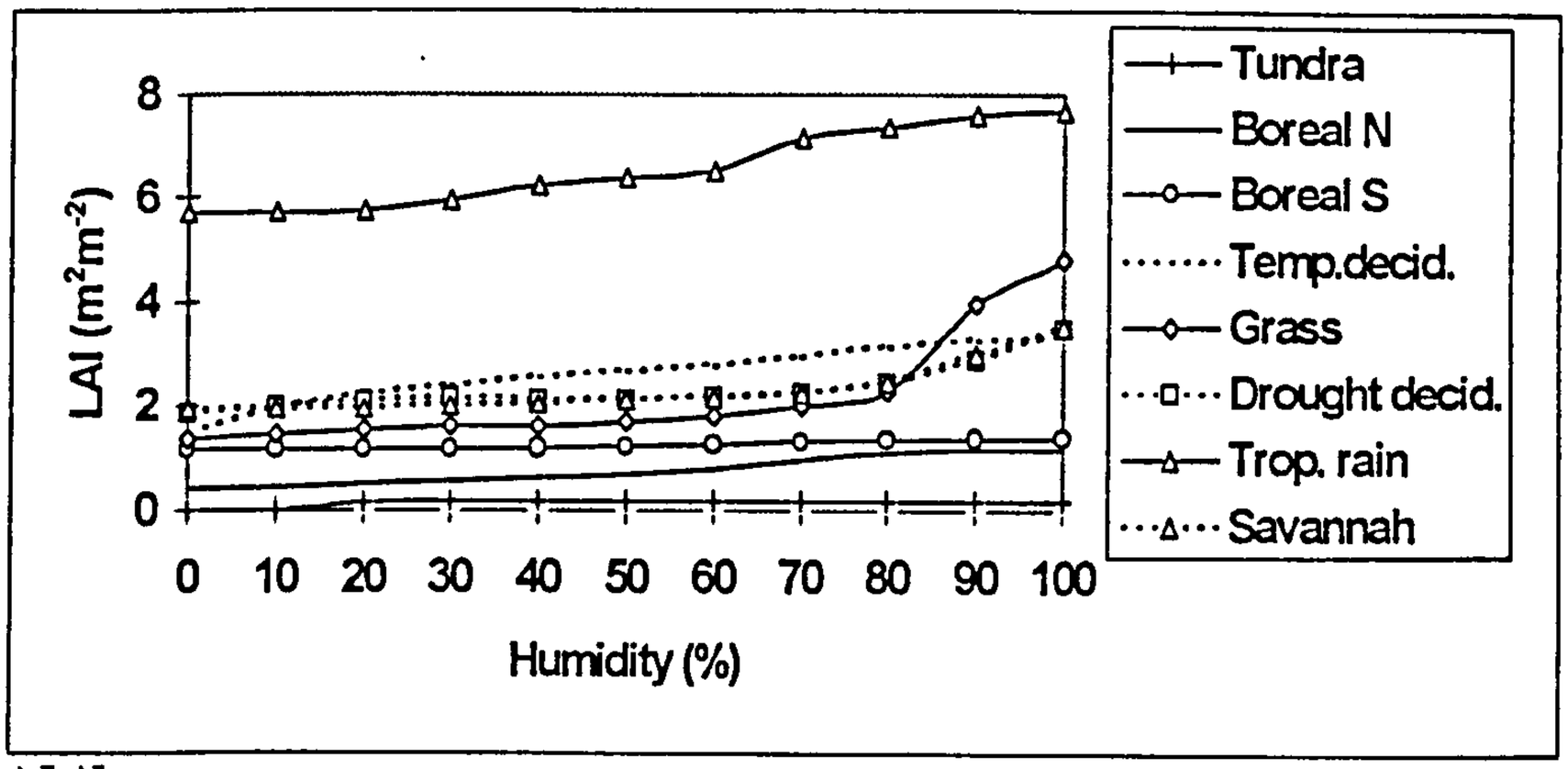

a) LAI

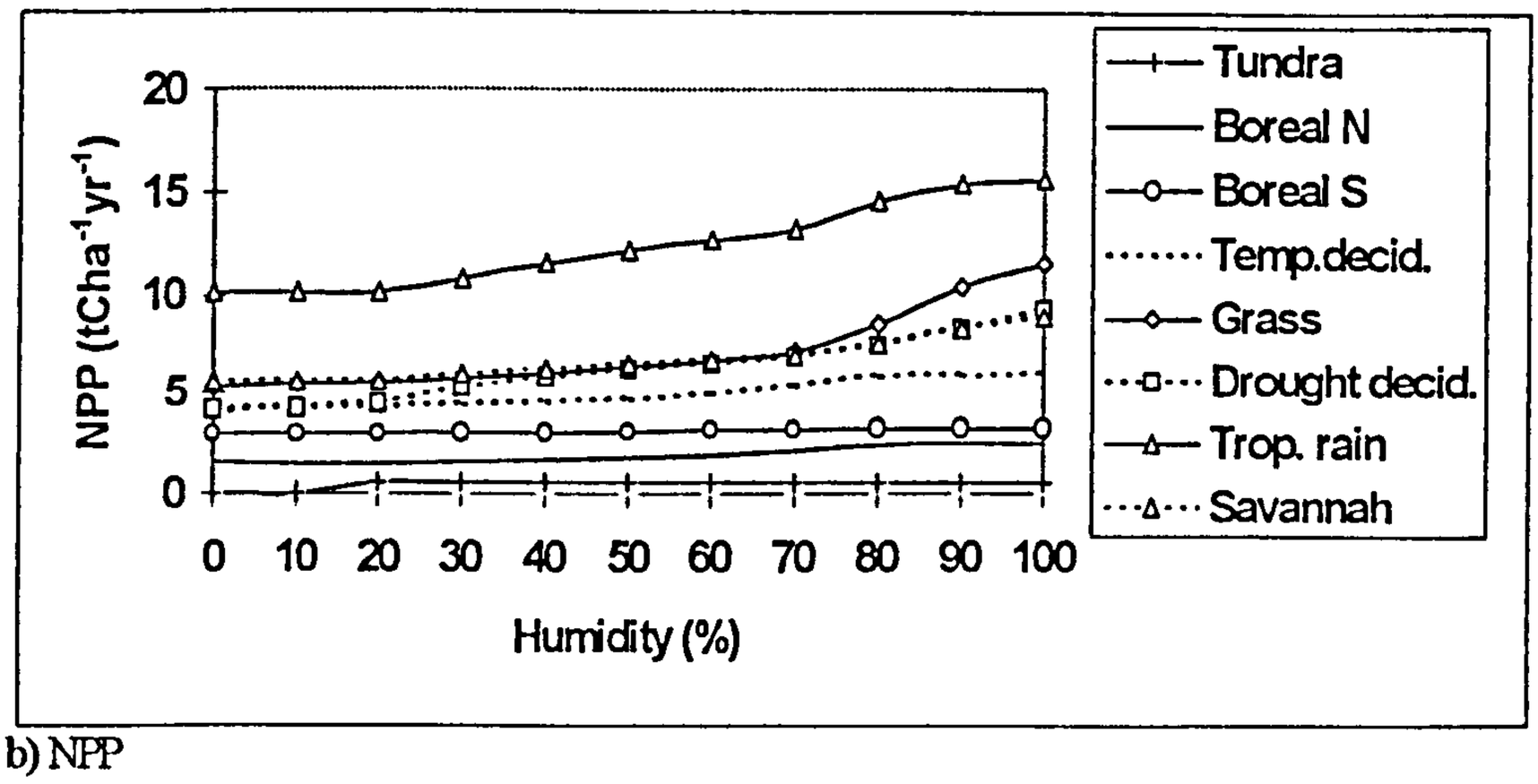

b) NPP

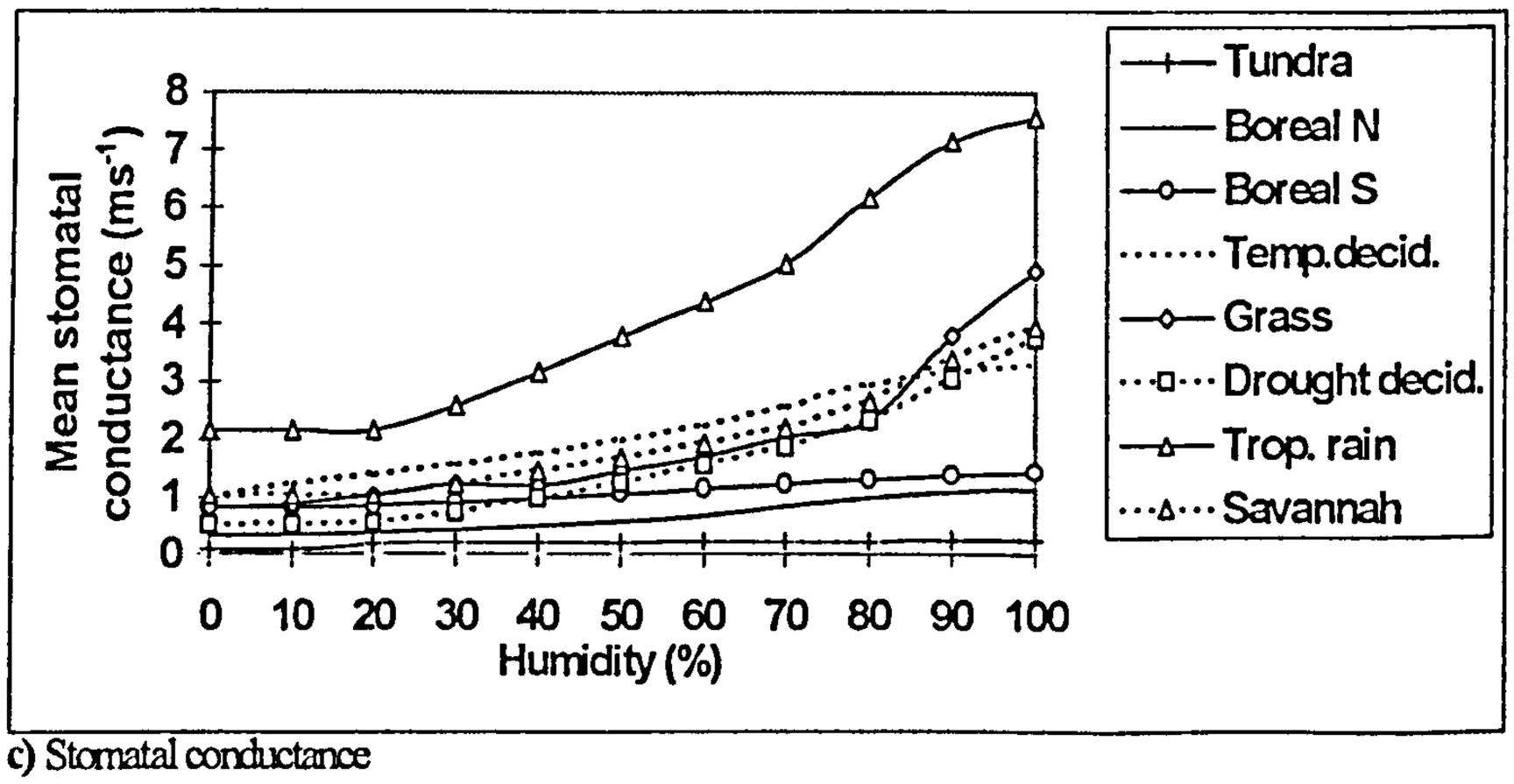

c) Stomatal conductance

Figure 4.4 a) to **c)** Values of a) LAI, b) NPP and c) stomatal conductance for a range of humidities between 0 and 100% for each of the 8 test sites.

Test 4: The site details are kept constant except for the atmospheric carbon dioxide value which is increased between 0 and 70 Pa (Figure 4.5).

LAI increases with an increase in CO_2 partial pressure from 0 to 30 Pa at all sites before the rate of increase becomes very small. The LAI at site 7 shows the greatest change, rising from 0 to 7 between 0 and 30 Pa. The NPP varies little with increasing CO_2 at sites 1 to 3. The other sites show a gradual increase with site 7 again being the most responsive. Figure 4.5c shows that there is very little change in stomatal conductance with increasing CO_2 at all the sites. Site 7 shows the greatest change in stomatal conductance which decreases from 6.5 m s^{-1} at 20 Pa to 6 m s^{-1} at 70 Pa. The fall in stomatal conductance that is shown between 0 and 10 Pa for all the sites is a result of the use of the Ball and Berry (1982) equation (see equation 2.54) in which stomatal conductance is dependent on photosynthesis. Empirical studies show that, at low CO_2 concentrations, photosynthesis increases linearly from the compensation point (near 0 Pa for C_4 plants, and 5 Pa for C_3 plants (Jones, 1992)) to saturation which occurs at an intercellular CO_2 partial pressure of around 10 Pa (Collatz *et al.*, 1992) for C_4 plants, and 20 to 23 Pa for C_3 plants (Jones, 1992). This is a "real" artifact as stomatal conductance should be very high at such low concentrations of CO_2. It should be noted that the DOLY model has been designed to operate at atmospheric carbon dioxide values above 30 Pa. Any values below 30 Pa would not normally be calculated however, it is important to be aware of such artifactual effects within the model. This has been highlighted by this test.

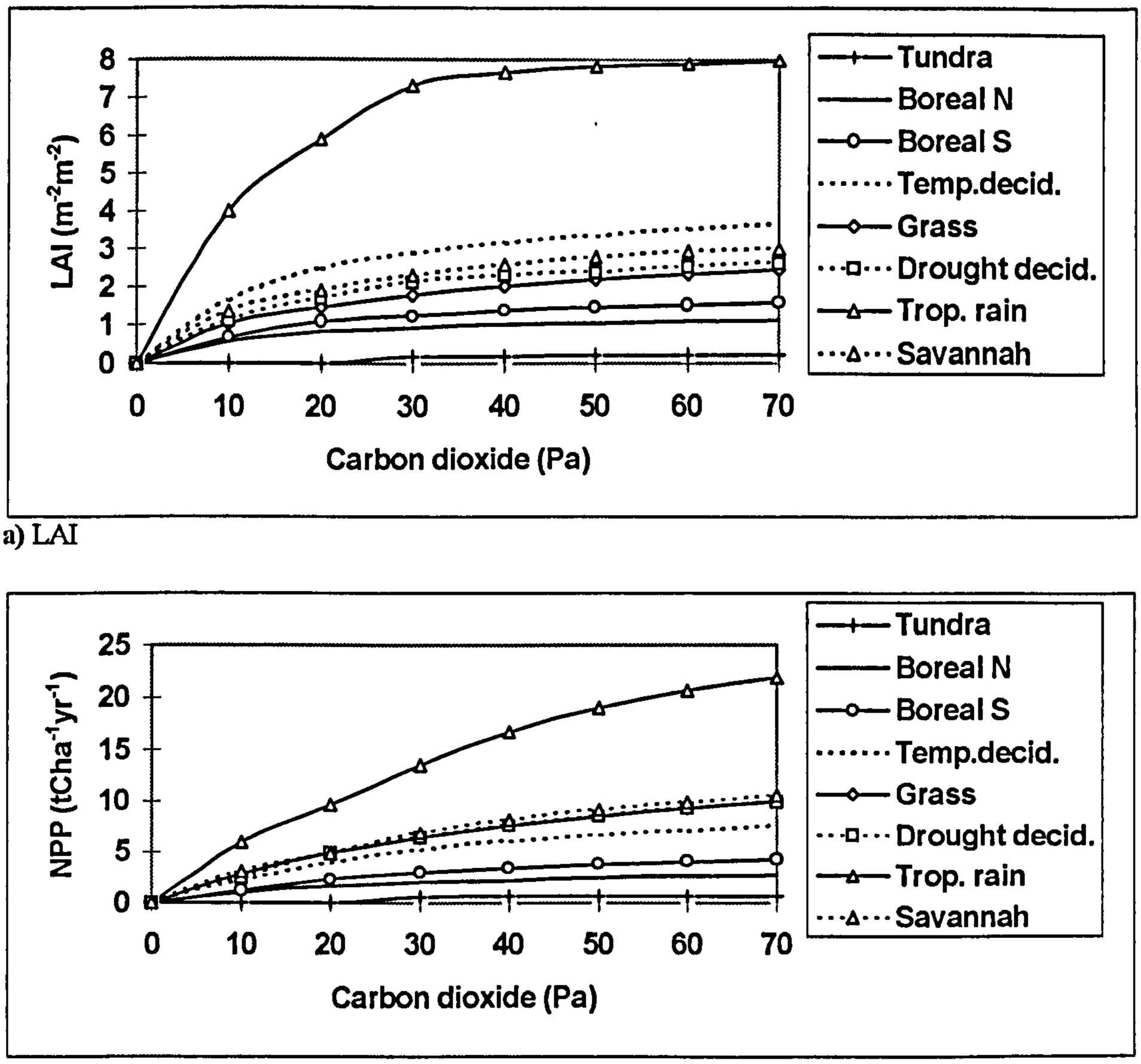

a) LAI

b) NPP

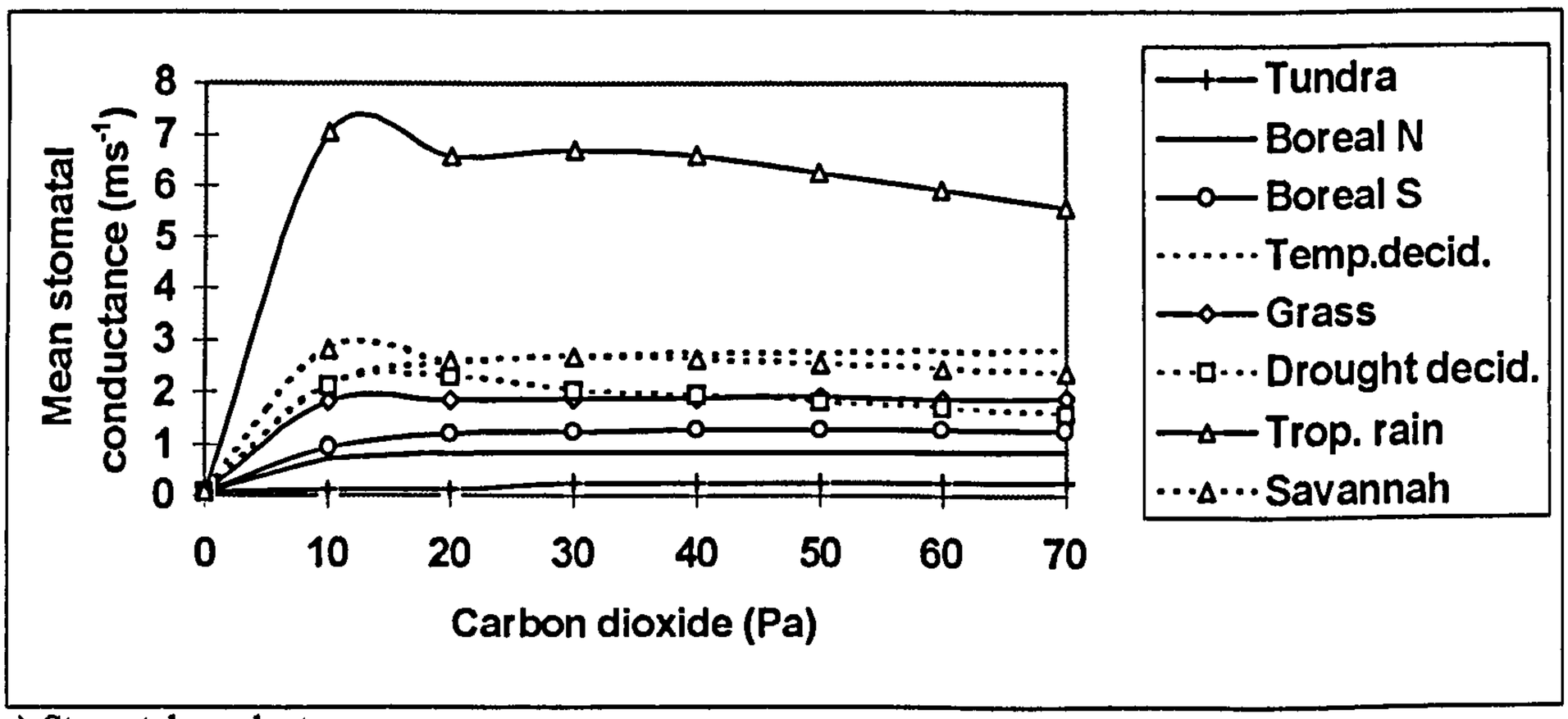

c) Stomatal conductance

Figure 4.5 a) to **c)** Values of a) LAI, b) NPP and c) stomatal conductance for a range of atmospheric carbon dioxide values between 0 and 70 Pa for each of the 8 test sites.

These tests have shown how LAI, NPP and stomatal conductance respond to the main climate inputs. It can be seen that there is very little sensitivity of NPP and LAI to changes in relative humidity across the range of normally observed values, but some increases do occur with high humidities. Also, stomatal conductance rises gradually with increasing relative humidity. LAI and NPP increase as the atmospheric CO_2 increases above 30 Pa and stomatal conductance decreases only slightly or, not at all, at some sites (sites 1, 2 and 3). The responses for the values of the CO_2 partial pressure below 10 Pa are clearly incorrect due to the use of the Ball and Berry (1982) equation and the stomatal conductances should be greater than those shown.

Increases in rainfall cause increases in NPP, LAI and stomatal conductance and these increases are greatest at dry sites such as 6 and 8. The responses of the output variables to temperature is more complex. Nitrogen uptake is dependent on temperature and increases with increasing temperature up to 25°C. Above this temperature, the influence of the uptake kinetics means that this uptake then decreases as temperature continues to rise (see section 3.2). The temperature dependence of nitrogen uptake directly affects LAI and NPP, through its use in the calculation of assimilation and dark respiration (see equations 2.49 and 2.51, respectively). Dark respiration increases with increasing temperature. The combination of these effects means that NPP also decreases as temperatures rise above 25°C, as does LAI (see section 2.3.11), and this is highlighted in Figures 4.1a, 4.1b, 4.2a and 4.2b for most sites, except the northern boreal and the grassland site. These two sites were affected by increasing VPD (Figure 4.1a). Temperature, humidity, assimilation and soil water content all directly affect stomatal conductance (see equation 2.54). When assimilation decreases with increasing temperature this is also reflected in a decrease of the mean annual stomatal conductance.

Stage 2

The following four tests change the input variables of temperature, relative humidity, precipitation and atmospheric CO_2, by given percentages. The DOLY model was run as normal for a full year using the data from the test sites to obtain initial values of NPP, LAI and stomatal conductance (Table 4.3). The model was then run again but this time one of the monthly climatic variables was increased or decreased by 10, 20 or 30% whilst the other variables remained unchanged. Obviously, a 10% increase in, say, temperature at 10°C, will give a different output variable compared with a 10% increase at 30 °C. Also, if units of kelvin are used instead of degrees Celsius this too would give different results. Alternatively, if a set increase of 3°C was applied, this would have a greater impact on a cold site and would be a greater fraction of the annual temperature figure than at a tropical site.

The aim of this particular exercise was to ensure that the changes made to each site were standardised in percentage terms, so that a fractional change in an output variable could be determined from a given fractional change in an input variable. For example, consider monthly temperatures in which each of the 12 monthly values is increased by 10% using the following equation:

$$t_{m10} = t_m + 0.1 \times t_m \qquad (4.1)$$

where

t_{m10} is the monthly temperature with a 10% increase, and

t_m is the monthly temperature prior to the increase.

The model was run with t_{m10} but with no change to the other monthly climatic variables. The output values of NPP, LAI and stomatal conductance were recorded, and the percentage change from the values in Table 4.3 calculated. This process was repeated for a 20 and 30% increase. It should be noted that the vapour pressure deficit was allowed to respond to increasing temperatures in Test 5a. It was shown in Stage 1 (Figures 4.1 and 4.2) how this approach affects the output variables over a range of temperatures. Below a

temperature of 10°C this did not cause much difference. It did, however, have a noticeable effect on outputs for the northern boreal site and the grassland site above a temperature of 10 °C so a further test (Test 5b) was carried out. Test 5b is the same as Test 5a except that the VPD is not permitted to vary with temperature and the data from Table 4.2e are used as input.

An index of sensitivity (β) was then calculated for each variable. β is defined as the fractional change in the output variable with a fractional change in the input variable value (after Gates, 1985).

$$\beta = \left(\frac{V_2 - V_1}{V_1}\right) \Big/ \left(\frac{P_2 - P_1}{P_1}\right) \qquad (4.1)$$

where

V_1 is the output variable when the input variable is P_1,

and V_2 is the output variable when the input variable is P_2.

For a 10% increase this simplifies to:

$$\beta = \left(\frac{V_2 - V_1}{V_1}\right) \Big/ 0.1 \qquad (4.2)$$

In the case of temperature, if say the LAI value 0.18 for site 1 (see Table 4.3) had risen to 0.25 with a 10% increase in temperature, this would be recorded as a 39% increase in LAI. The index of sensitivity would then be 3.9 (0.39/0.1). To interpret the index of sensitivity, consider the situation where the input variable has been increased by 10% and the index of sensitivity is greater than 1. This means that the input variable has caused an increase in the output variable of greater than 10%. The reverse is true if the values are less than 1. A value of 1 means that the output variable has responded in exactly the same way as the input variable; i.e. increased by 10% in this case. A value of zero means that there has been no response of the output variable to the increase or decrease in the input variable. If the input variable has decreased by a given

percentage, and the output variable has also decreased, then the index of sensitivity is positive. If the input variable has decreased by a given percentage, and the output variable has increased, then the index of sensitivity is negative. The site numbers and their associated biomes are shown in Table 4.1.

Test 5a: Mean monthly temperatures were increased by 10, 20 and 30% to ascertain the sensitivity indices of LAI, NPP and stomatal conductance (for each of the 8 sites). The vapour pressure deficit is allowed to vary with temperature. The original temperature data are presented in Table 4.2b and the sensitivity results are shown in Figure 4.6. This figure shows how the index of sensitivity varies for LAI, NPP and stomatal conductance with 10, 20 and 30% increases in mean monthly temperature.

The least sensitive sites with respect to LAI are the rain forest and savannah sites (sites 7 and 8) with little or no change with an increase in temperature. Sites 1, 2, 4, 5, and 6 show a little more sensitivity. The northern boreal forest, grassland and dry deciduous sites (sites 2, 5 and 6) have negative values, i.e. their LAI values decrease slightly as temperature increases, and the tundra and temperate deciduous forest sites (sites 1 and 4) have a small positive value. At all these sites, the sensitivity is less than unity which means that the increase or decrease is less than the temperature change of 10, 20 or 30%. Site 3 (southern boreal) is the most sensitive site with a β value of 3.3, i.e. there has been a 33% increase in LAI for a 10% increase in temperature. This sensitivity however, decreases with increasing temperature. This means that as the mean monthly temperatures increase the response of the LAI is reduced. This can be seen in Figure 4.1 for the temperature range 5 to 25°C (this is the range which is covered by the monthly temperatures between May and October, including the percentage increases, for site 3) as shown in Table 4.2b.

Site 3 is also sensitive with regards to NPP with an increase of almost 20% for all the temperature increases. Site 1 has a β value equal to 1 for a 30%

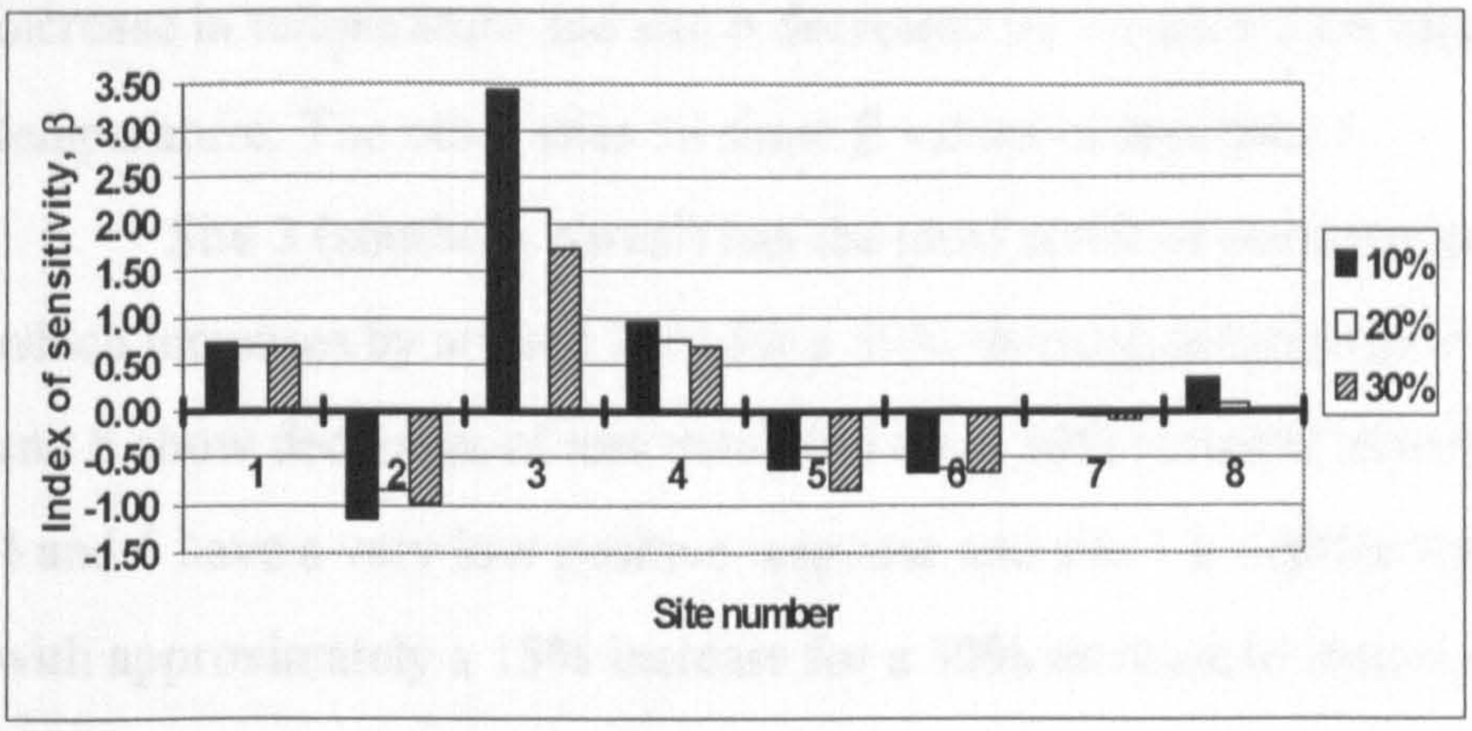

a) LAI

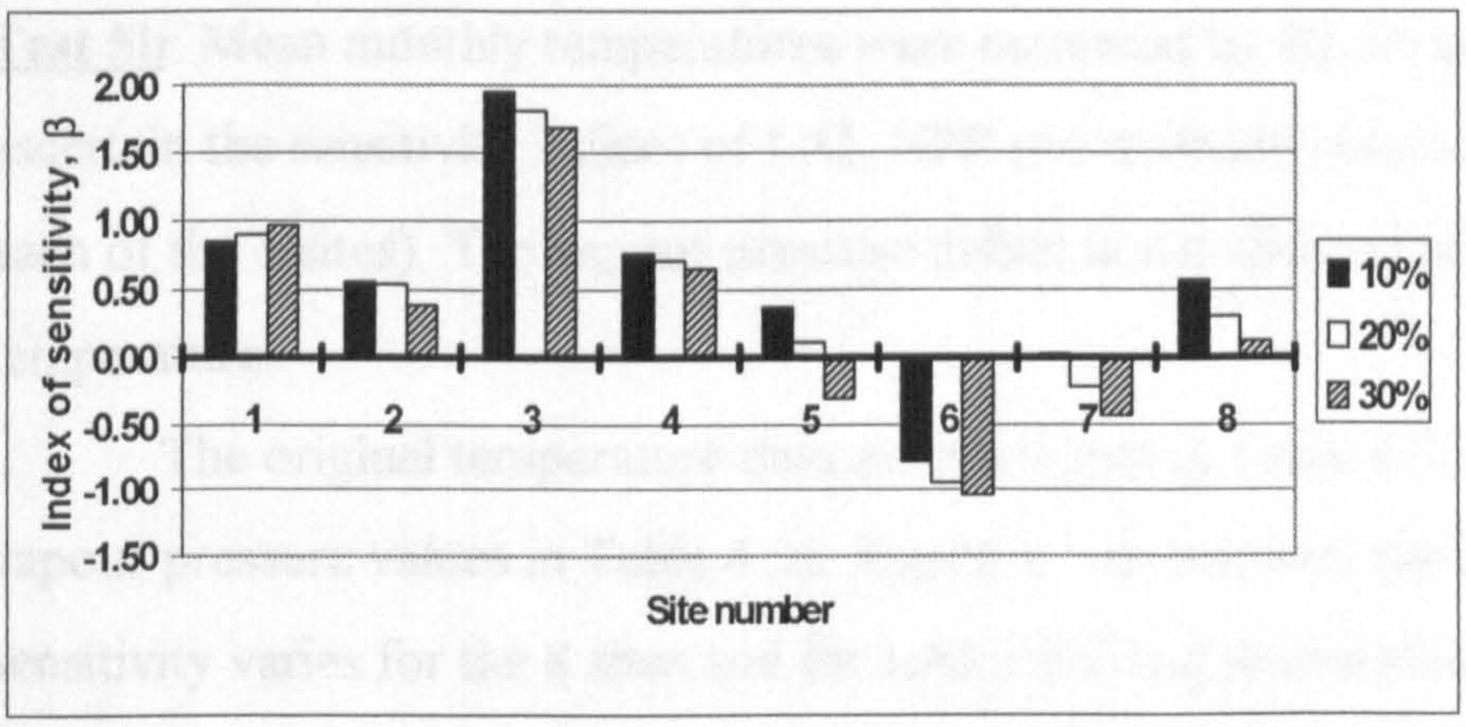

b) NPP

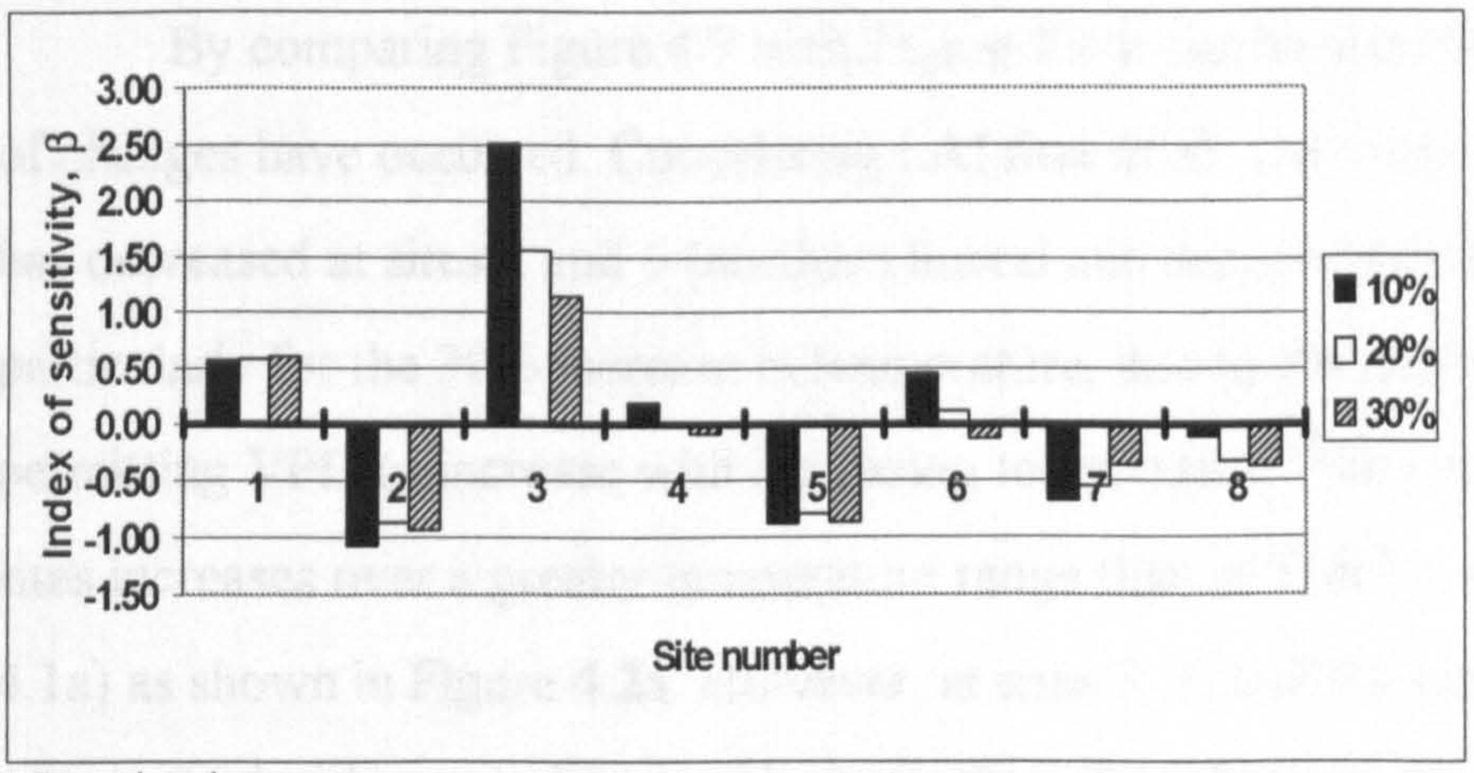

c) Stomatal conductance

Figure 4.6 a) to **c)**. The index of sensitivity for a) LAI, b) NPP and c) stomatal conductance to 10, 20 and 30% increases in temperature for 8 test sites.

increase in temperature and site 6 decreases by 1 with a 30% increase in temperature. The other sites all show β values of less than 1.

Site 3 (southern boreal) has the most sensitive stomatal conductance which increases by around 25% for a 10% increase in temperature. Sites 2, 5, 7 and 8 show decreases of less than 30% for a 30% increase in temperature. Sites 4 and 6 have a very low positive response and site 1 a slightly higher response with approximately a 15% increase for a 30% increase in temperature.

Test 5b: Mean monthly temperatures were increased by 10, 20 and 30% to ascertain the sensitivity indices of LAI, NPP and stomatal conductance (for each of the 8 sites). The vapour pressure deficit is not allowed to vary with temperature.

The original temperature data are presented in Table 4.2b, and the vapour pressure values in Table 4.2e. Figure 4.7 shows how the index of sensitivity varies for the 8 sites and for LAI, NPP and stomatal conductance with 10, 20 and 30% increases in mean monthly temperature.

By comparing Figure 4.7 with Figure 4.6 it can be seen that a number of changes have occurred. Considering LAI first of all, the index of sensitivity has decreased at sites 2 and 6 (northern boreal and drought deciduous sites), particularly for the 30% increase in temperature, due to the effect of not permitting VPD to increase with increasing temperature. The LAI for these sites increases over a greater temperature range than in Test 1a (see Figure 4.1a) as shown in Figure 4.2a. However, at sites 3, 4, and 8 (southern boreal, temperate deciduous and savannah sites), the index of sensitivity has increased, and, in the case of site 5 (grass), risen from a negative to a positive value (although the positive sensitivity is not as great as the negative sensitivity from Test 5a). In the case of sites 3 and 4 this is due to a greater increase in LAI with temperature over the range 15 to 25 °C (Figure 4.2a) than occurred when VPD increased with temperature (Figure 4.1a). At site 5 (grass), LAI decreases with increasing temperature above a temperature of 10°C (Figure 4.1a)

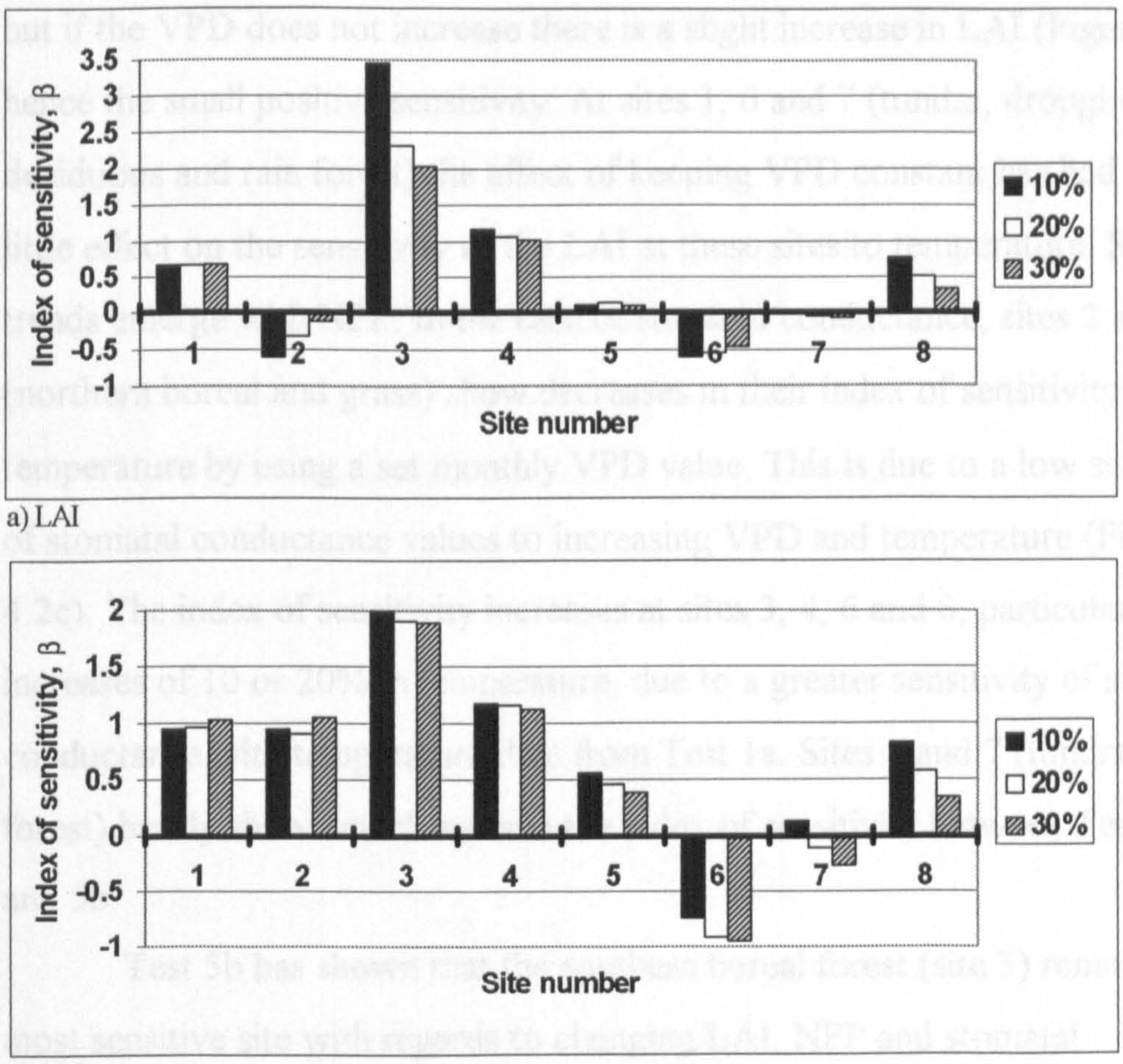

a) LAI

b) NPP

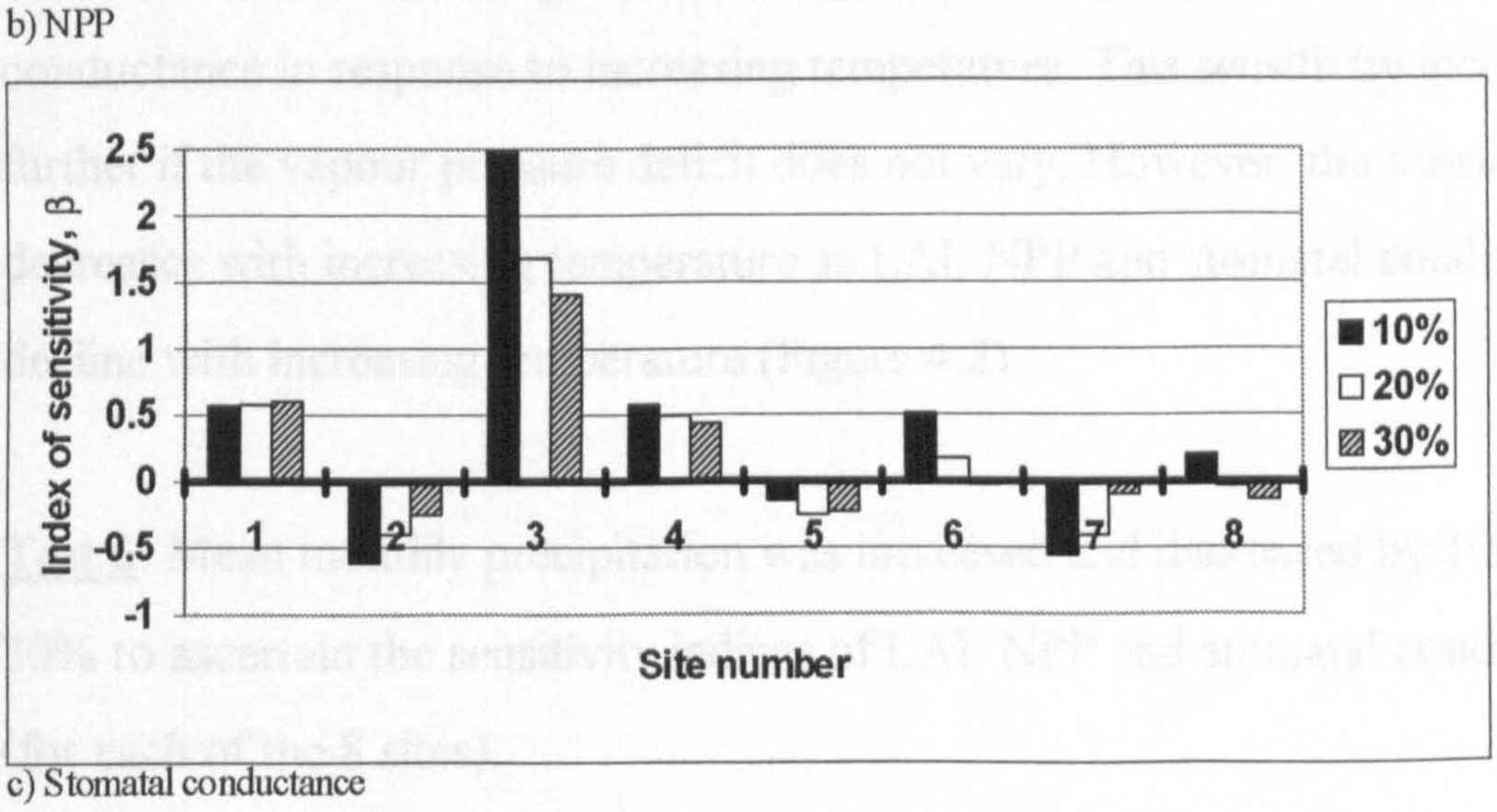

c) Stomatal conductance

Figure 4.7 a) to **c)**. The index of sensitivity for a) LAI, b) NPP and c) stomatal conductance to 10, 20 and 30% increases in temperature for 8 test sites. Vapour pressure deficit does not vary with temperature.

but if the VPD does not increase there is a slight increase in LAI (Figure 4.2a), hence the small positive sensitivity. At sites 1, 6 and 7 (tundra, drought deciduous and rain forest) the effect of keeping VPD constant has had very little effect on the sensitivity of the LAI at these sites to temperature. Similar trends emerge with NPP. In the case of stomatal conductance, sites 2 and 5 (northern boreal and grass) show decreases in their index of sensitivity to temperature by using a set monthly VPD value. This is due to a low sensitivity of stomatal conductance values to increasing VPD and temperature (Figure 4.2c). The index of sensitivity increases at sites 3, 4, 6 and 8, particularly for increases of 10 or 20% in temperature, due to a greater sensitivity of stomatal conductance with temperature than from Test 1a. Sites 1 and 7 (tundra and rain forest) hardly show any changes in the index of sensitivity between Tests 5a and 5b.

Test 5b has shown that the southern boreal forest (site 3) remains the most sensitive site with regards to changing LAI, NPP and stomatal conductance in response to increasing temperature. This sensitivity increases further if the vapour pressure deficit does not vary. However, the sensitivity decreases with increasing temperature as LAI, NPP and stomatal conductance decline with increasing temperature (Figure 4.2).

Test 6: Mean monthly precipitation was increased and decreased by 10, 20 and 30% to ascertain the sensitivity indices of LAI, NPP and stomatal conductance (for each of the 8 sites).

The original precipitation data are presented in Table 4.2c. Figure 4.8 shows how the index of sensitivity varies for the 8 sites and for LAI, NPP and stomatal conductance with 10, 20 and 30% increases and decreases in mean monthly precipitation. It should be noted that the index of sensitivity is positive in all cases. At all sites the LAI responds in the same manner as the precipitation. For instance, as precipitation increases, LAI increases, and as precipitation decreases, LAI decreases. The LAI values at sites 2 (northern

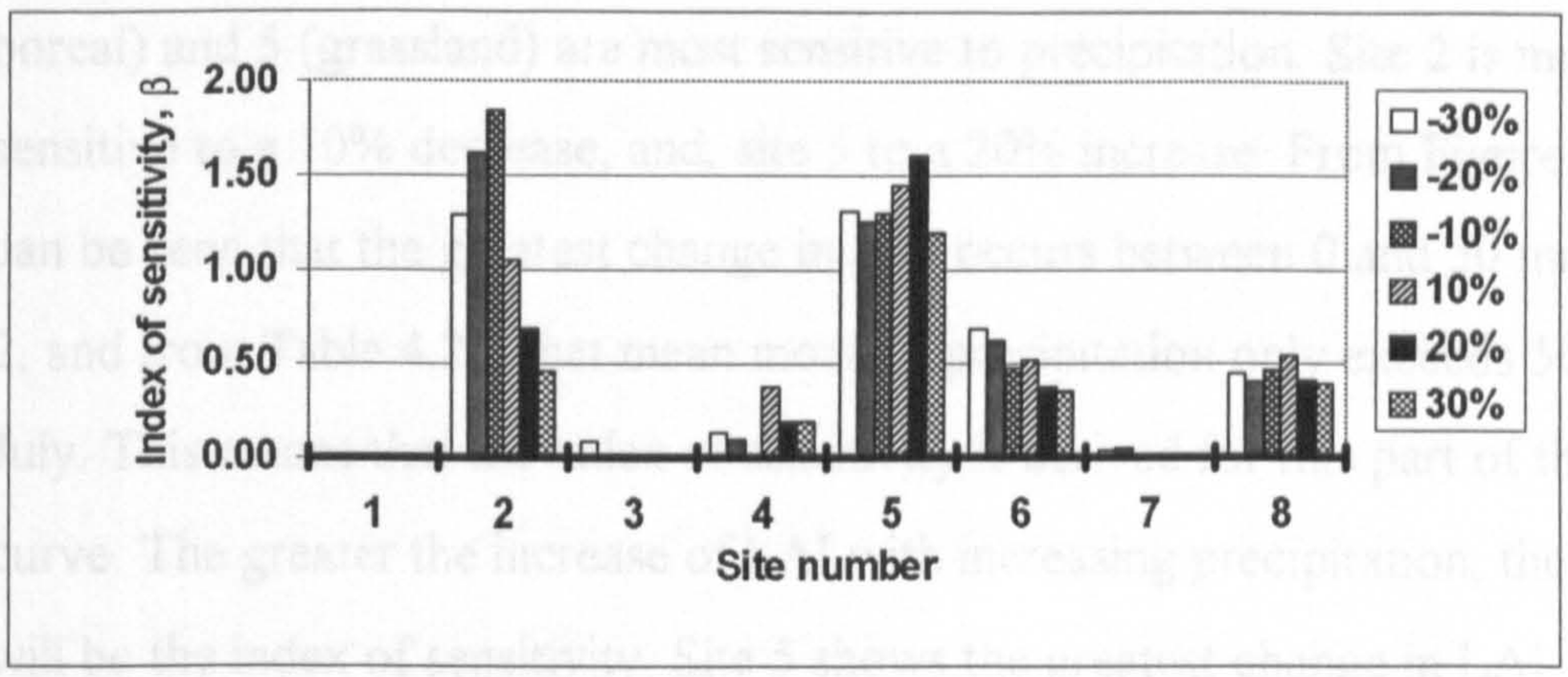

a) LAI

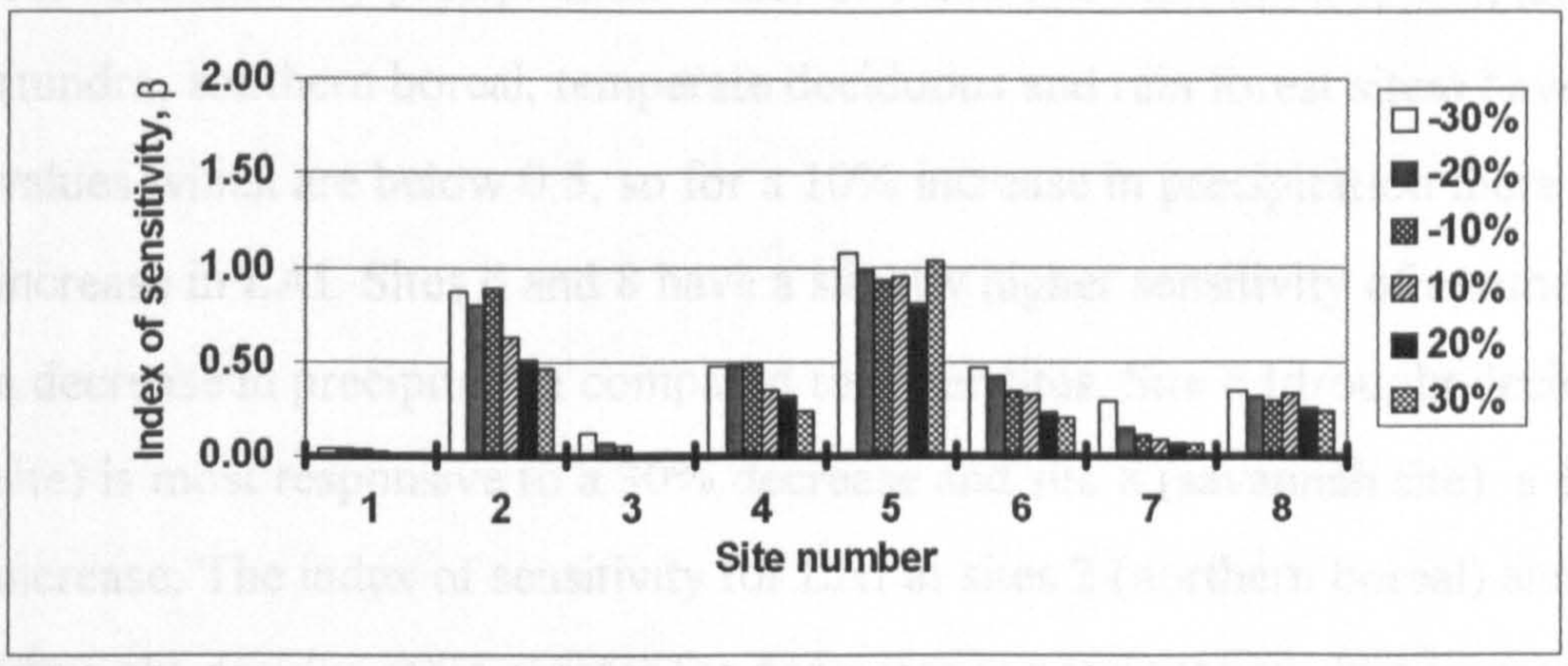

b) NPP

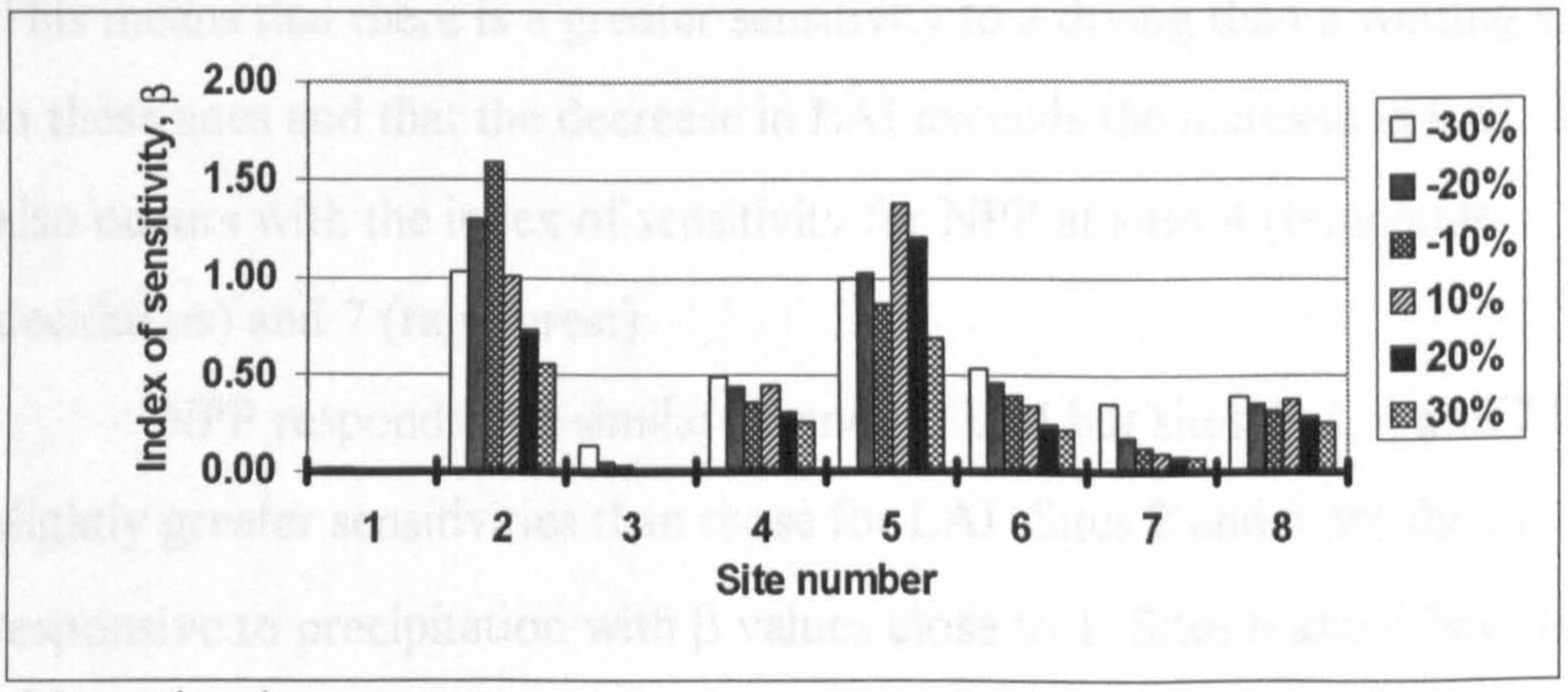

c) Stomatal conductance

Figure 4.8 a) to **c)** The index of sensitivity of LAI, NPP and stomatal conductance to 10, 20 and 30% decreases and increases in precipitation for 8 test sites

boreal) and 5 (grassland) are most sensitive to precipitation. Site 2 is most sensitive to a 10% decrease, and, site 5 to a 20% increase. From Figure 4.3a it can be seen that the greatest change in LAI occurs between 0 and 50 mm at site 2, and from Table 4.2c, that mean monthly precipitation only exceeds 50 mm in July. This means that the index of sensitivity is derived for this part of the curve. The greater the increase of LAI with increasing precipitation, the greater will be the index of sensitivity. Site 5 shows the greatest change in LAI between monthly precipitation values of 0 and 150 mm. Sites 1, 3, 4, and 7 (tundra, southern boreal, temperate deciduous and rain forest sites) have β values which are below 0.5, so for a 10% increase in precipitation there is a 5% increase in LAI. Sites 6 and 8 have a slightly higher sensitivity of around 0.5 to a decrease in precipitation compared to other sites. Site 6 (drought deciduous site) is most responsive to a 30% decrease and site 8 (savannah site), a 10% increase. The index of sensitivity for LAI at sites 2 (northern boreal) and 6 (drought deciduous) is greater for decreases in precipitation than increases. This means that there is a greater sensitivity to a drying than a wetting situation at these sites and that the decrease in LAI exceeds the increase in LAI. This also occurs with the index of sensitivity for NPP at sites 4 (temperate deciduous) and 7 (rain forest).

NPP responds in a similar manner to LAI but sites 1, 3, 4 and 7 have slightly greater sensitivities than those for LAI. Sites 2 and 5 are the most responsive to precipitation with β values close to 1. Sites 6 and 8 have lower β values than with LAI, which decrease with increasing precipitation. Stomatal conductance responses show the same sort of patterns as NPP for sites 6, 7, and 8, and as LAI for sites 2 and 5.

The index of sensitivity tends to decrease with increasing precipitation for most of the sites. This reflects the saturating response that is evident in Figure 4.3.

Test 7: Mean monthly humidity was increased and decreased by 10, 20 and 30% to ascertain the sensitivity indices of LAI, NPP and stomatal conductance (for each of the 8 sites).

The original humidity data are presented in Table 4.2d. The sensitivity results are shown in Figure 4.9. This figure shows how the index of sensitivity varies for the 8 sites and for LAI, NPP and stomatal conductance with 10, 20 and 30% increases and decreases in mean monthly relative humidity.

The LAI at most sites has a low sensitivity to relative humidity, with the value of β for the tundra, southern boreal forest, temperate deciduous and rain forest sites (sites 1, 3, 4, 6, and 7) either close to or below 0.5. Site 8 (savannah) has a β value around 1 for 10, 20 and 30% increases and site 2 (northern boreal) for decreases of 10, 20 and 30%. The site displaying the greatest sensitivity is the grassland site (site 5) with a 60% increase in LAI for a 30% increase in relative humidity. Figure 4.4 shows how the LAI increases sharply at humidities greater than 80% for the grassland site. NPP also has low sensitivity values to relative humidity with all but site 5 having a β value below 1. Stomatal conductance is more sensitive to relative humidity than NPP with a highest β value of 1.8 which occurs at site 5 with a 10% increase in relative humidity. Most sites are close to a β value of 1, and sites 1 and 3 have values of less than 0.5. Site 5 is a site with high temperatures and fairly low humidity. It has a moderate NPP, together with a moderate to low stomatal conductance and LAI (see Table 4.3). If humidity increases and there is no change in temperature then there is a decrease in VPD. As temperatures are high this decrease is greater (Figure 2.5) than would occur at lower temperatures. Although stomatal conductance increases with the increase in humidity this is offset by the large fall in VPD. The decrease in VPD therefore reduces evaporation and contributes to the increase in both LAI and NPP.

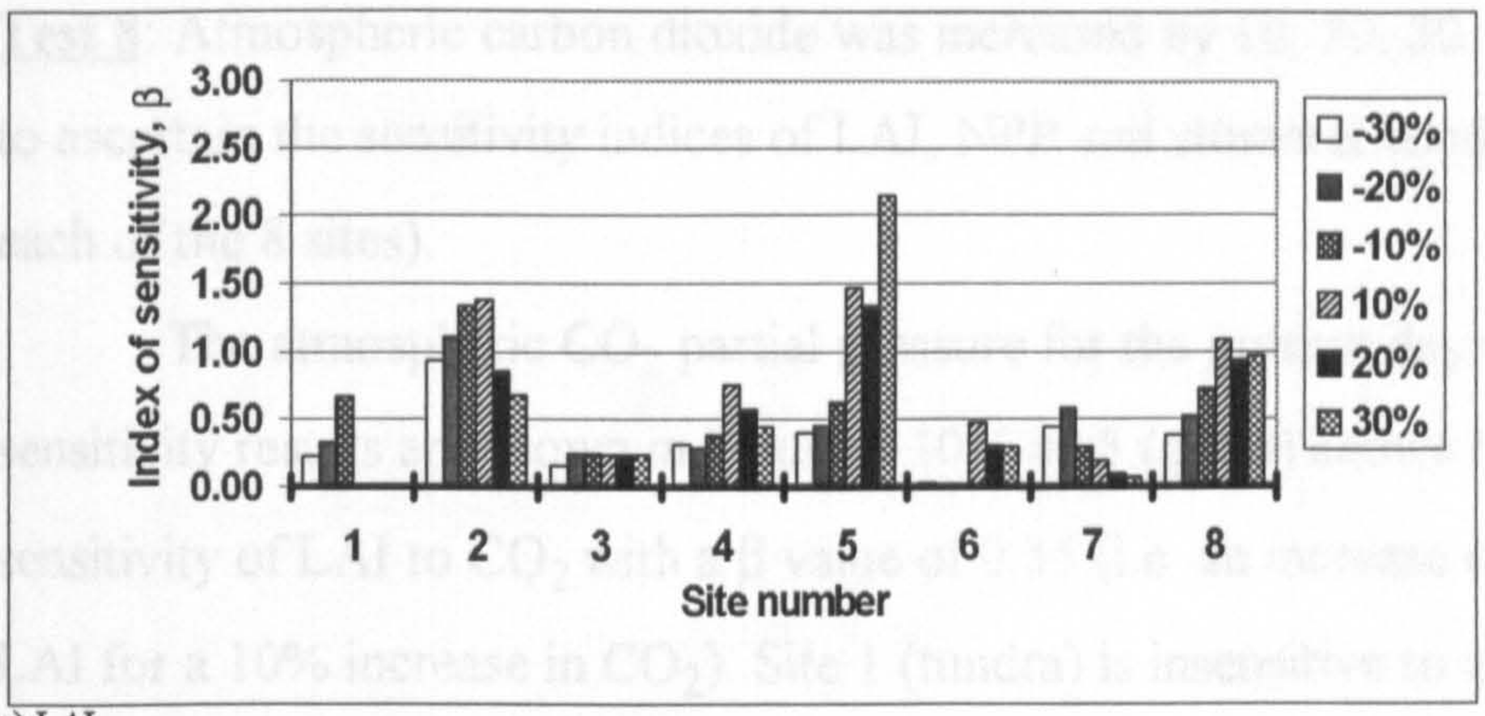

a) LAI

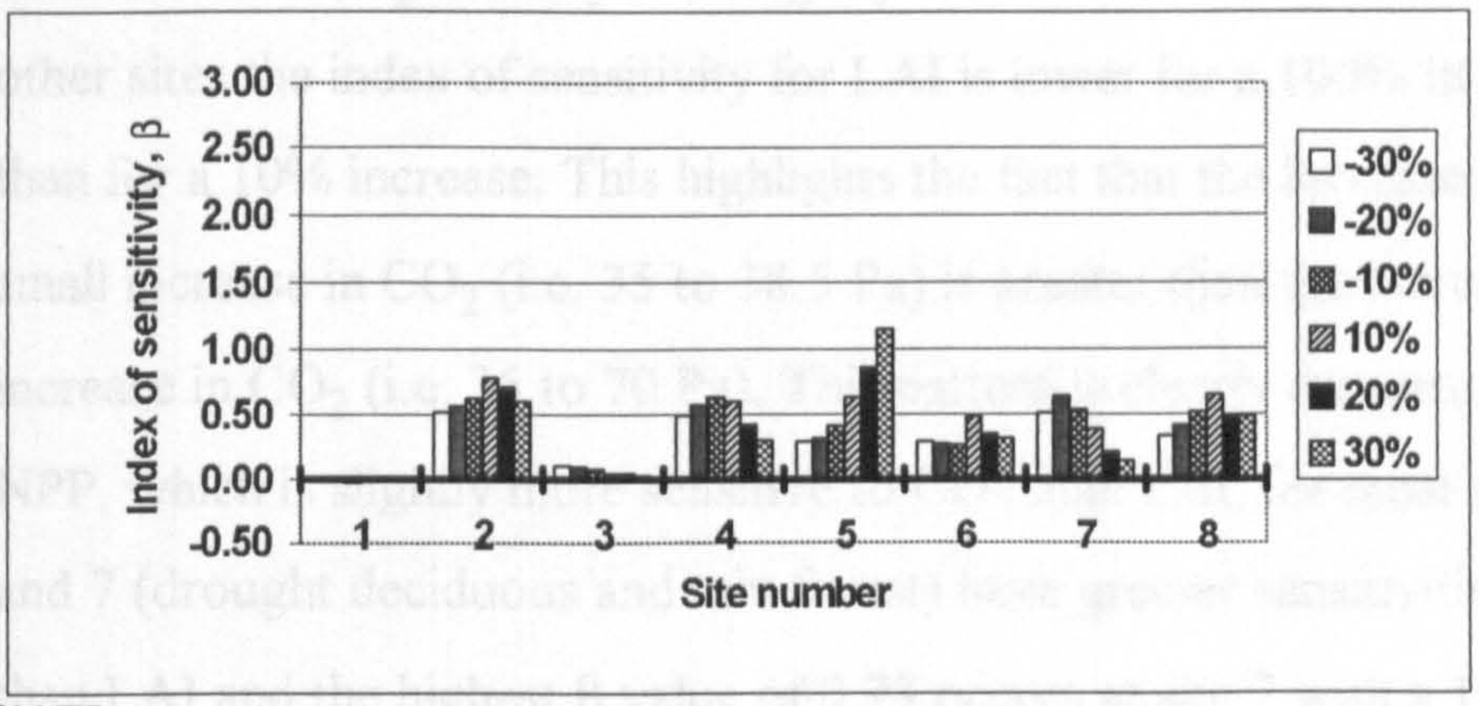

b) NPP

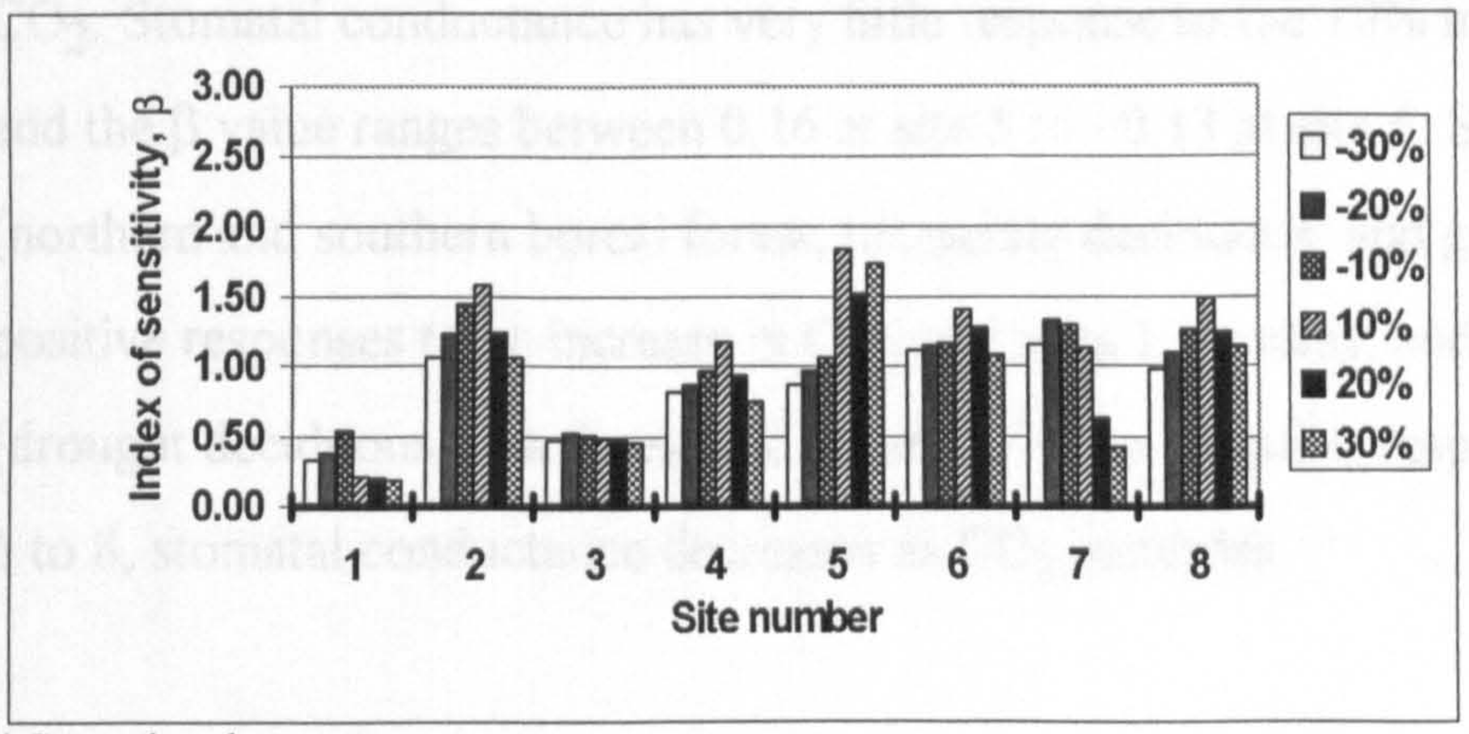

c) Stomatal conductance

Figure 4.9 a) to **c)** Index of sensitivity of LAI, NPP and stomatal conductance to 10, 20 and 30% increases and decreases in humidity for 8 test sites.

Test 8: Atmospheric carbon dioxide was increased by 10, 20, 30, 60 and 100% to ascertain the sensitivity indices of LAI, NPP and stomatal conductance (for each of the 8 sites).

The atmospheric CO_2 partial pressure for the present day is 35 Pa. The sensitivity results are shown in Figure 4.10. Site 5 (grass) shows the greatest sensitivity of LAI to CO_2 with a β value of 0.55 (i.e. an increase of 5.5 % in LAI for a 10% increase in CO_2). Site 1 (tundra) is insensitive to an increase of 10 or 20% of CO_2 but responds slightly when it increases to 30%. At all the other sites the index of sensitivity for LAI is lower for a 100% increase in CO_2 than for a 10% increase. This highlights the fact that the increase in LAI for a small increase in CO_2 (i.e. 35 to 38.5 Pa) is greater than the increase for a large increase in CO_2 (i.e. 35 to 70 Pa). This pattern is clearly demonstrated with NPP, which is slightly more sensitive to CO_2 than LAI, for most sites. Sites 6 and 7 (drought deciduous and rain forest) have greater sensitivities for NPP than LAI and the highest β value of 0.73 occurs at site 7 with a 10% increase in CO_2. Stomatal conductance has very little response to the 10% increase in CO_2 and the β value ranges between 0.16 at site 5 to –0.13 at site 6. Sites 2 to 5 (northern and southern boreal forest, temperate deciduous, and grass) have positive responses to an increase in CO_2 and sites 1 (tundra), and 6 to 8 (drought deciduous, rain forest and savannah) have negative responses. At sites 6 to 8, stomatal conductance decreases as CO_2 increases.

Stage 3

Test 9: Various input variables were altered to determine the effects of a climate change scenario on the sensitivity of LAI, NPP and stomatal conductance (for each of the 8 sites).

This has been set for a doubled-CO_2 climate. The following scenario has been used: an increase in atmospheric carbon dioxide of 100%, a 20% increase in temperature and a 10% increase in precipitation and relative

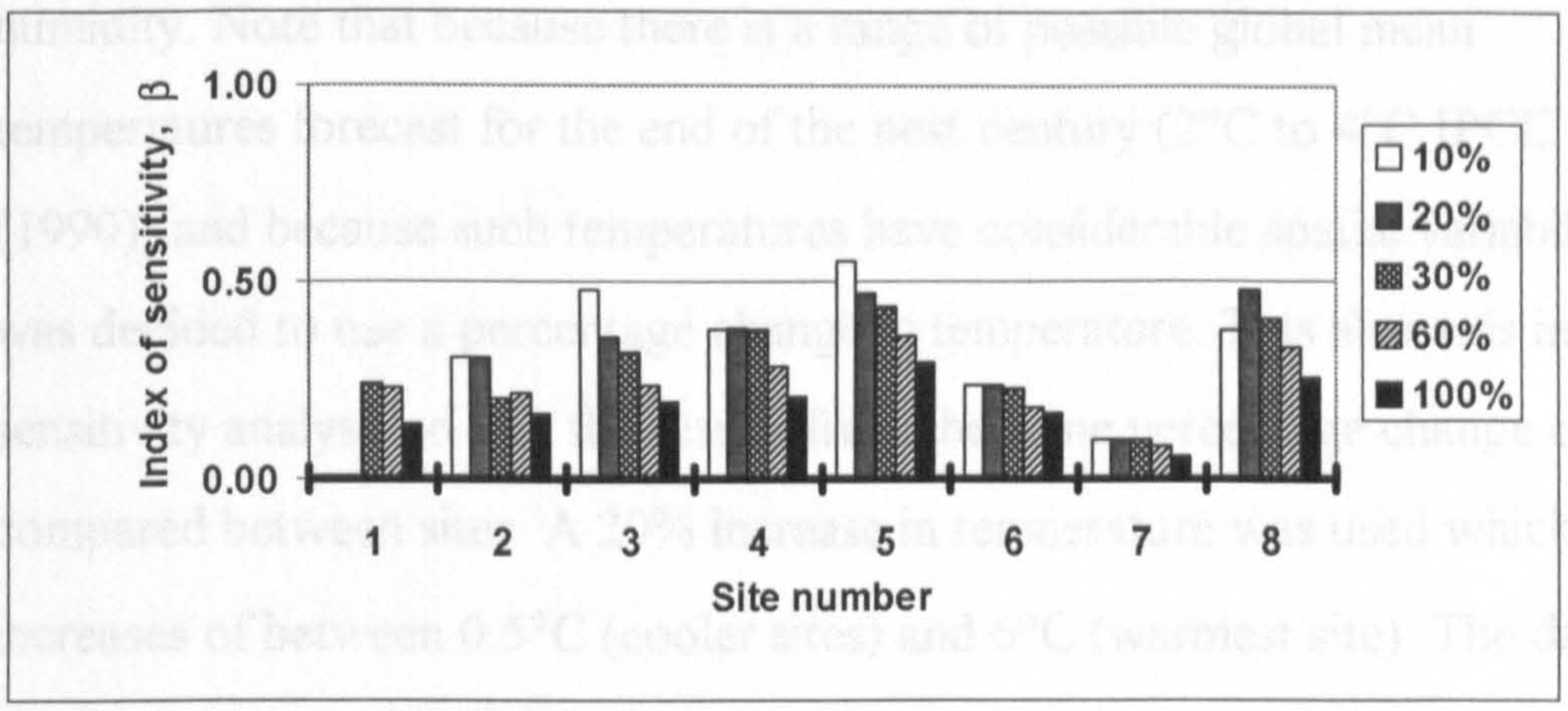

a) LAI

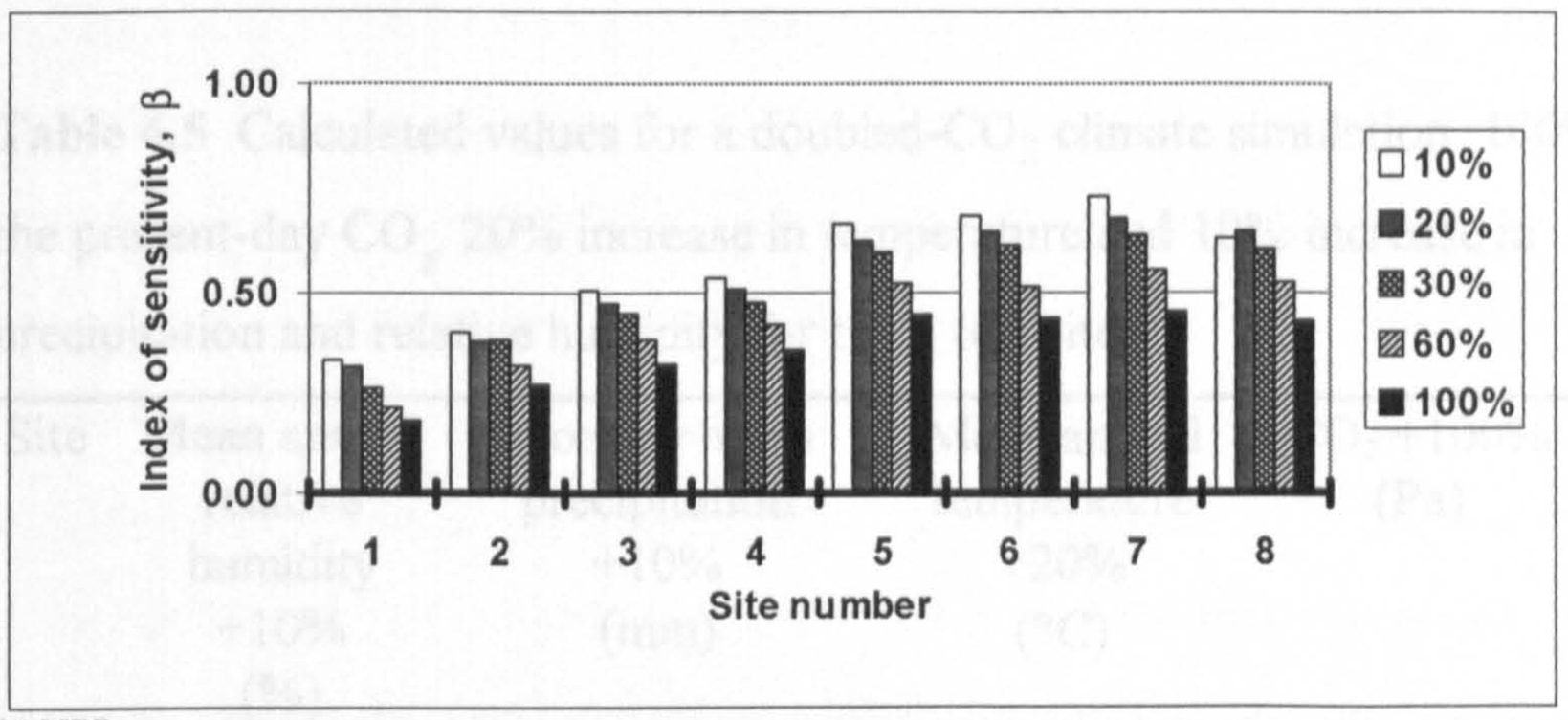

b) NPP

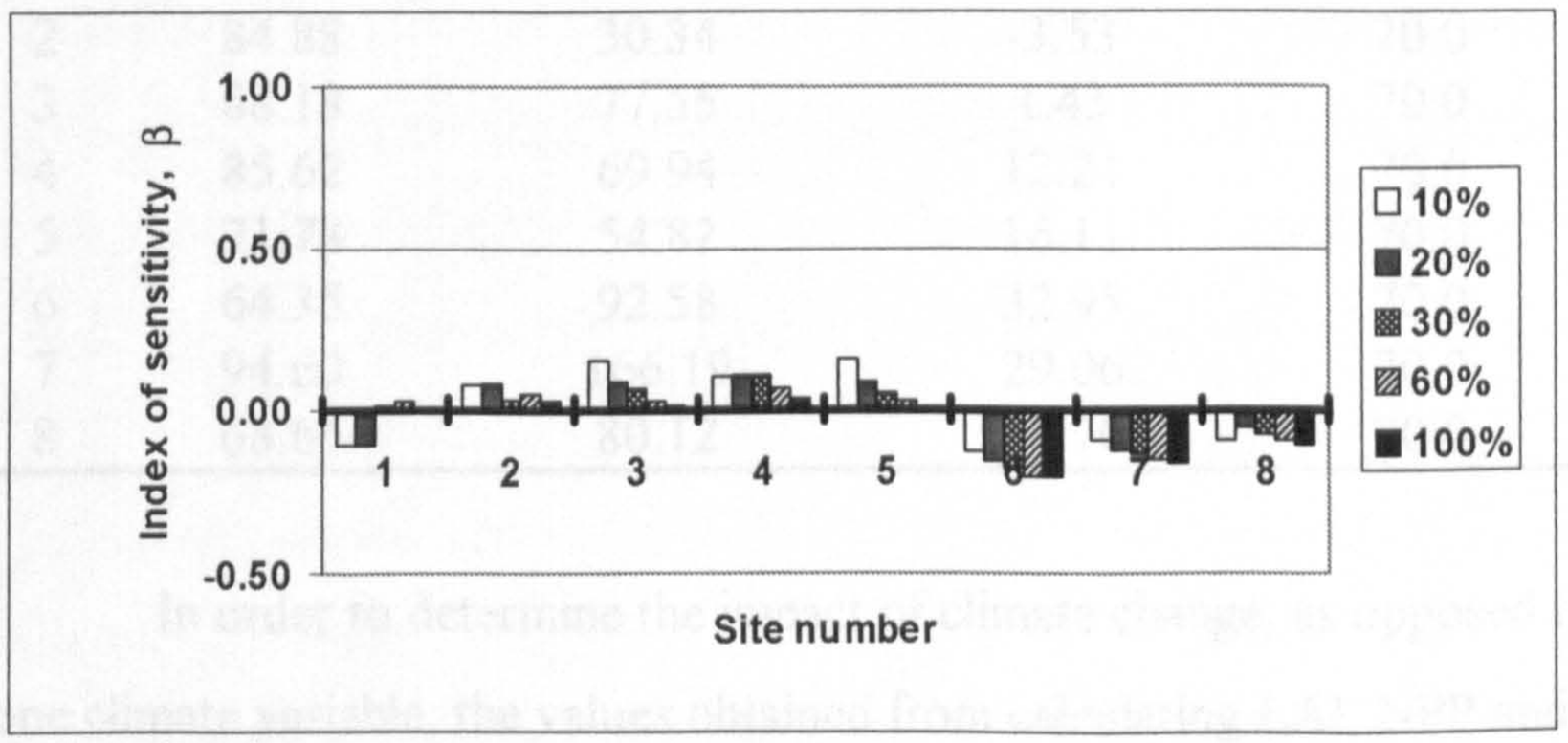

c) Stomatal conductance

Figure 4.10 a) to **c)** Index of sensitivity of LAI, NPP and stomatal conductance to 10, 20, 30, 60 and 100% increases in carbon dioxide for 8 test sites.

humidity. Note that because there is a range of possible global mean temperatures forecast for the end of the next century (2°C to 4°C IPCC (1990)) and because such temperatures have considerable spatial variability it was decided to use a percentage change in temperature. This also aids in the sensitivity analysis so that the results from the same percentage change can be compared between sites. A 20% increase in temperature was used which gives increases of between 0.5°C (cooler sites) and 6°C (warmest site). The data used are presented in Table 4.5.

Table 4.5 Calculated values for a doubled-CO_2 climate simulation. 100% of the present-day CO_2, 20% increase in temperature and 10% increase in precipitation and relative humidity for the 8 test sites.

Site	Mean annual relative humidity +10% (%)	Monthly mean precipitation +10% (mm)	Mean annual temperature +20% (°C)	CO_2 +100% (Pa)
1	87.36	17.51	-8.98	70.0
2	84.88	30.34	-3.53	70.0
3	88.18	77.55	1.43	70.0
4	85.62	69.94	12.21	70.0
5	71.78	54.82	16.11	70.0
6	64.35	92.58	32.95	70.0
7	94.60	166.19	29.06	70.0
8	68.66	80.12	24.70	70.0

In order to determine the impact of climate change, as opposed to just one climate variable, the values obtained from calculating LAI, NPP and stomatal conductance with climate change were compared to those calculated from the change in one climatic variable. The results are presented in Figure 4.11. Climatic change gives the highest LAI at all sites except for site 6 (dry deciduous) where CO_2 alone gives the highest value. At site 1 (tundra) there is very little change in LAI with all scenarios and it remains low. At site 2 (northern boreal forest) there is little difference in the LAI values with increased CO_2, relative humidity and precipitation, but there is a reduction in

LAI with the 20% increase in temperature. At site 3 (southern boreal forest), the reverse is true and the increase in temperature increases the LAI, although not by as much as with climate change. There is little change in LAI with precipitation and relative humidity increases, but a slight rise with an increase in CO_2. The LAI at site 4 (temperate deciduous forest) increases with temperature and carbon dioxide and as with site 3 there is little change with relative humidity and precipitation. Site 5 (grass) displays a similar pattern to site 4 but LAI decreases as temperature increases. At site 6 (drought deciduous) this also occurs, but there is little change in LAI with all the scenarios, although it increases slightly. Site 7 (rain forest) shows a similar pattern to site 6 although LAI is higher. Also the climate change scenario gives the greatest LAI rather than carbon dioxide alone as at site 6. Site 8 (savannah) shows very little change with temperature and only slight increases with relative humidity and precipitation. The highest LAI values occur with climate change, closely followed by the increase in CO_2. It can be seen how increasing temperature at sites 3 and 4 increases LAI. At sites 2, 5, 6, and 7 (northern boreal forest, grass, drought deciduous and rain forest), increasing temperature reduces LAI. At the other sites there is little change in LAI with increasing temperature. Rainfall and relative humidity cause slight increases in LAI at sites 4 to 8 but there is practically no change at the high latitude sites.

Similar patterns emerge with NPP with the warmer sites (sites 6,7 and 8) showing a greater sensitivity to CO_2 and the cooler sites (sites 2 and 3) to both temperature and CO_2.

In the case of stomatal conductance, humidity assumes a greater importance, particularly at sites 4 to 8. However, increasing temperature and CO_2 with the climate change scenario tempers its influence leading to reductions in stomatal conductance at sites 6, 7 and 8 with climate change.

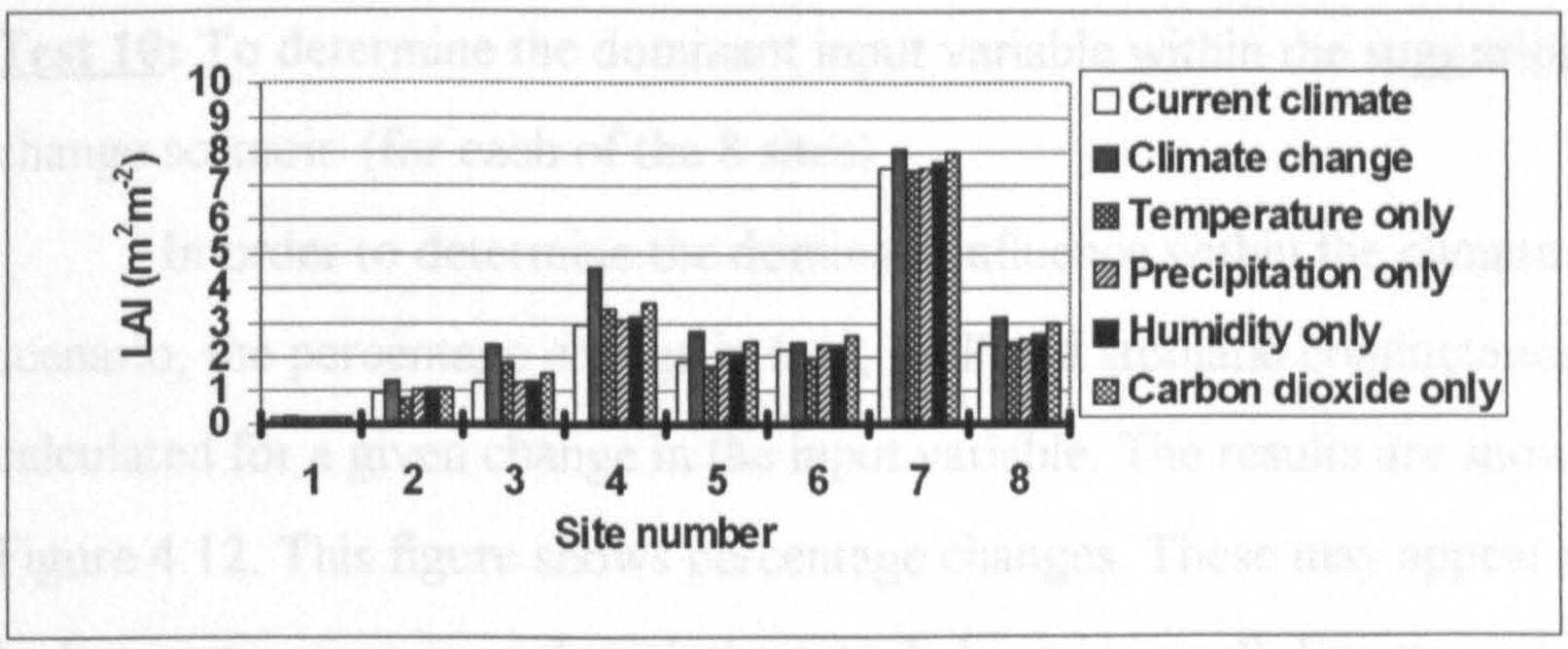

a) LAI

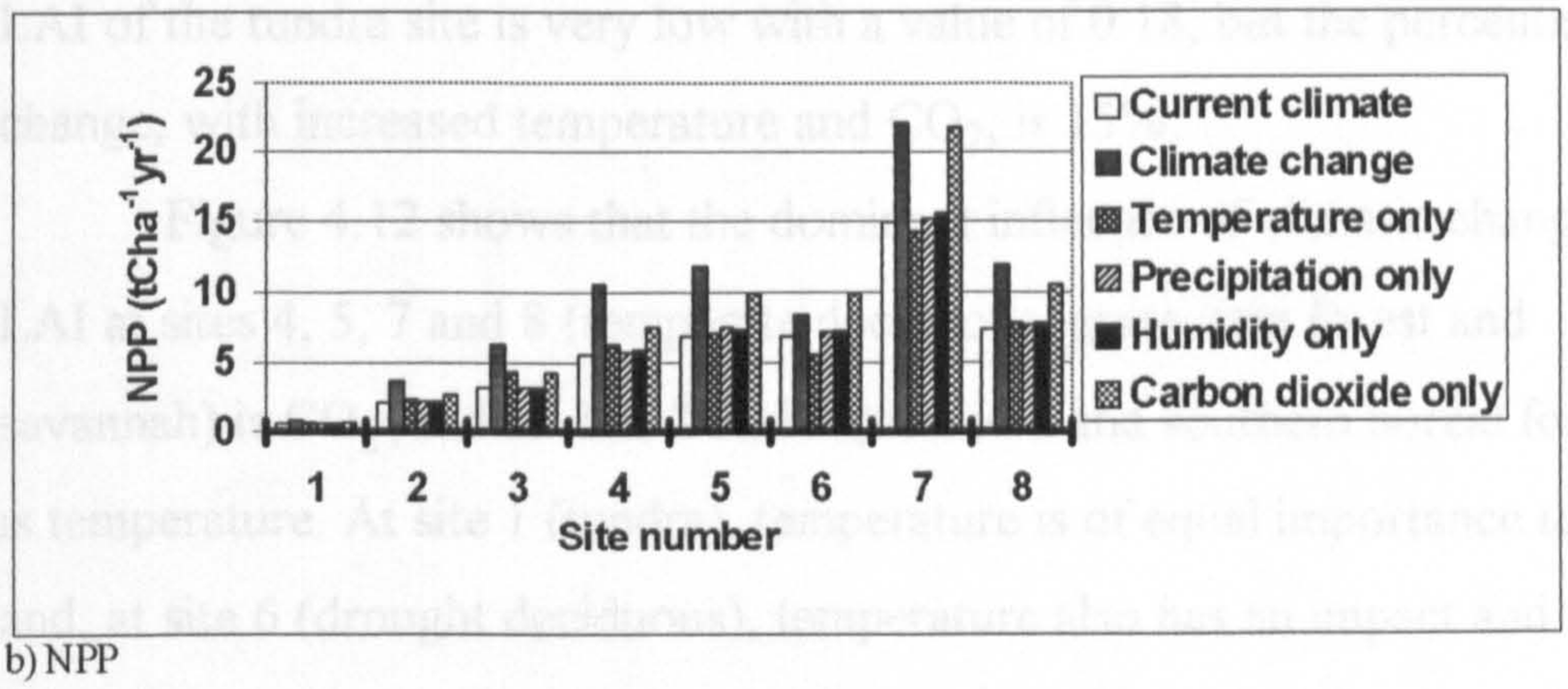

b) NPP

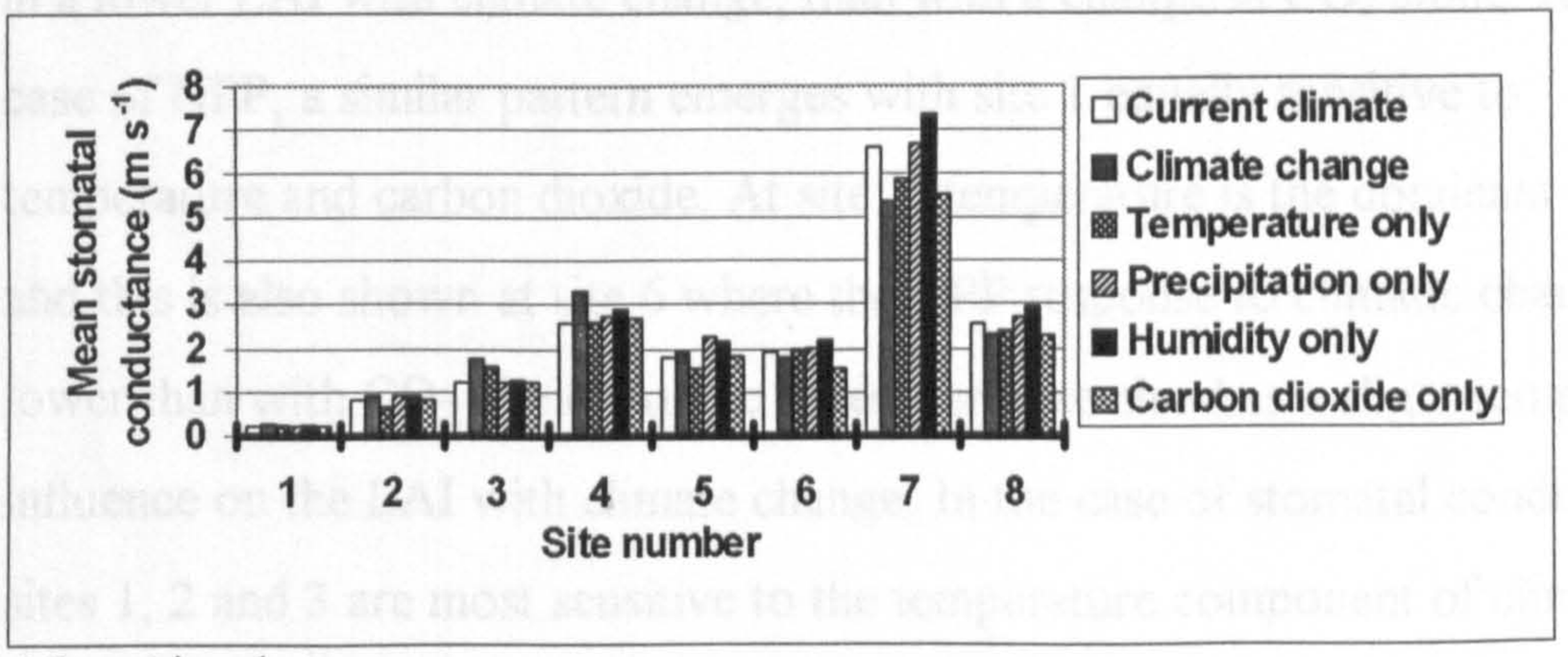

c) Stomatal conductance

Figure 4.11 a) to **c)** Values of LAI, NPP and stomatal conductance for a climate change scenario and for changes in individual climate variables for 8 test sites.

Test 10: To determine the dominant input variable within the suggested climate change scenario (for each of the 8 sites).

In order to determine the dominant influence within the climate change scenario, the percentage change in LAI, NPP and stomatal conductance was calculated for a given change in the input variable. The results are shown in Figure 4.12. This figure shows percentage changes. These may appear to be high in some cases even though the actual change is small. For example, the LAI of the tundra site is very low with a value of 0.18, but the percentage change, with increased temperature and CO_2, is 15%.

Figure 4.12 shows that the dominant influence of climatic change on LAI at sites 4, 5, 7 and 8 (temperate deciduous, grass, rain forest and savannah) is CO_2, and at sites 2 and 3 (northern and southern boreal forest) it is temperature. At site 1 (tundra), temperature is of equal importance to CO_2 and, at site 6 (drought deciduous), temperature also has an impact and results in a lower LAI with climate change, than with a change in CO_2 alone. In the case of NPP, a similar pattern emerges with site 1 equally sensitive to temperature and carbon dioxide. At site 3, temperature is the dominant variable and this is also shown at site 6 where the NPP response to climatic change is lower than with CO_2 alone. At site 7, temperature also has a slight tempering influence on the LAI with climate change. In the case of stomatal conductance, sites 1, 2 and 3 are most sensitive to the temperature component of climate change and sites 4 and 5 are most influenced by relative humidity, although a fall in temperature appears to reduce the impact of the increased relative humidity at site 5. Sites 6, 7 and 8 are mainly influenced by CO_2, which causes a decrease in stomatal conductance with climate change.

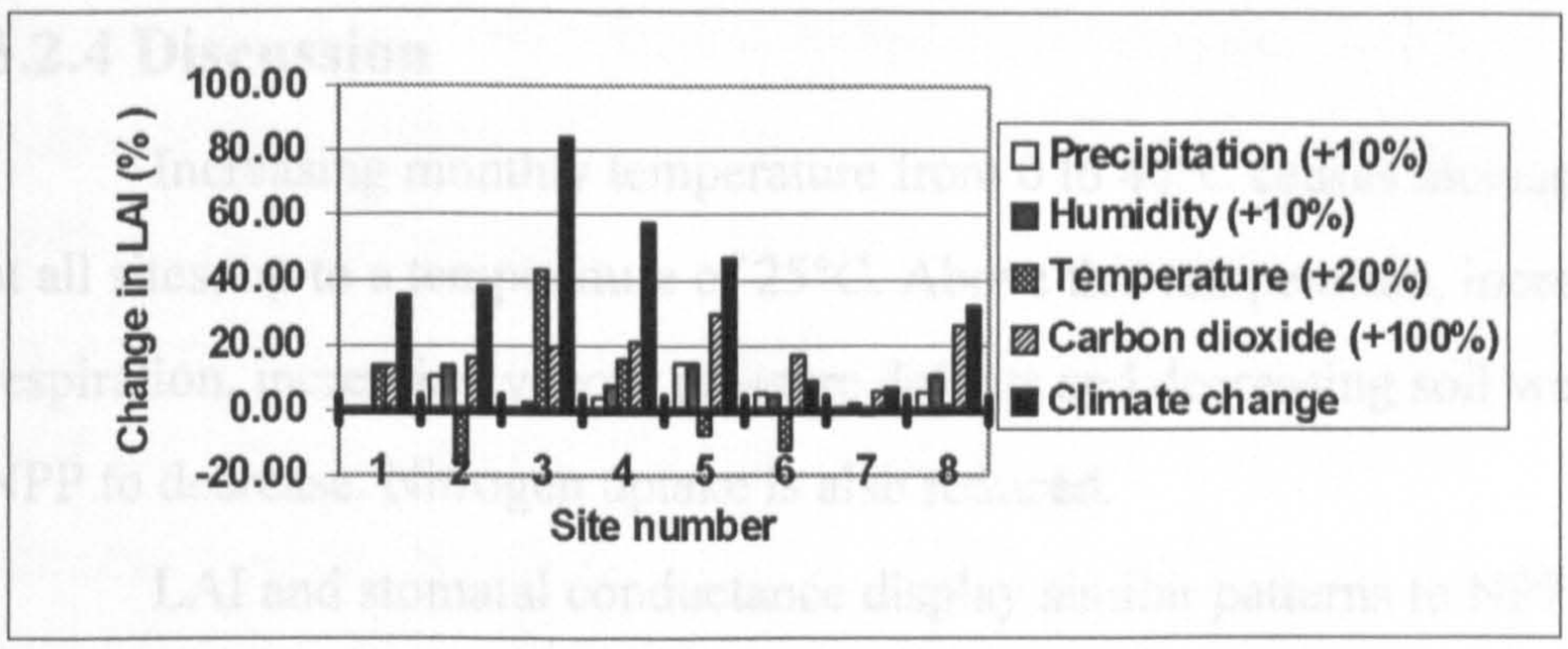

a) LAI

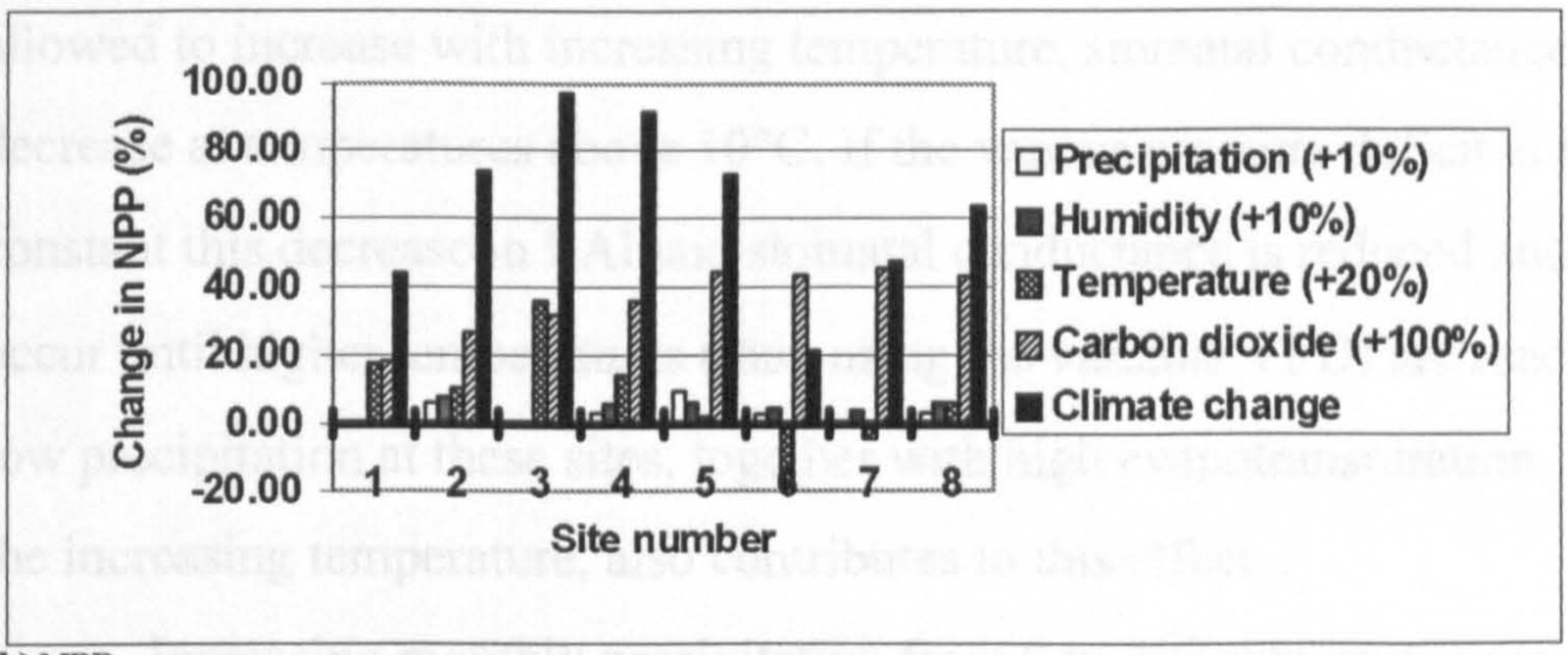

b) NPP

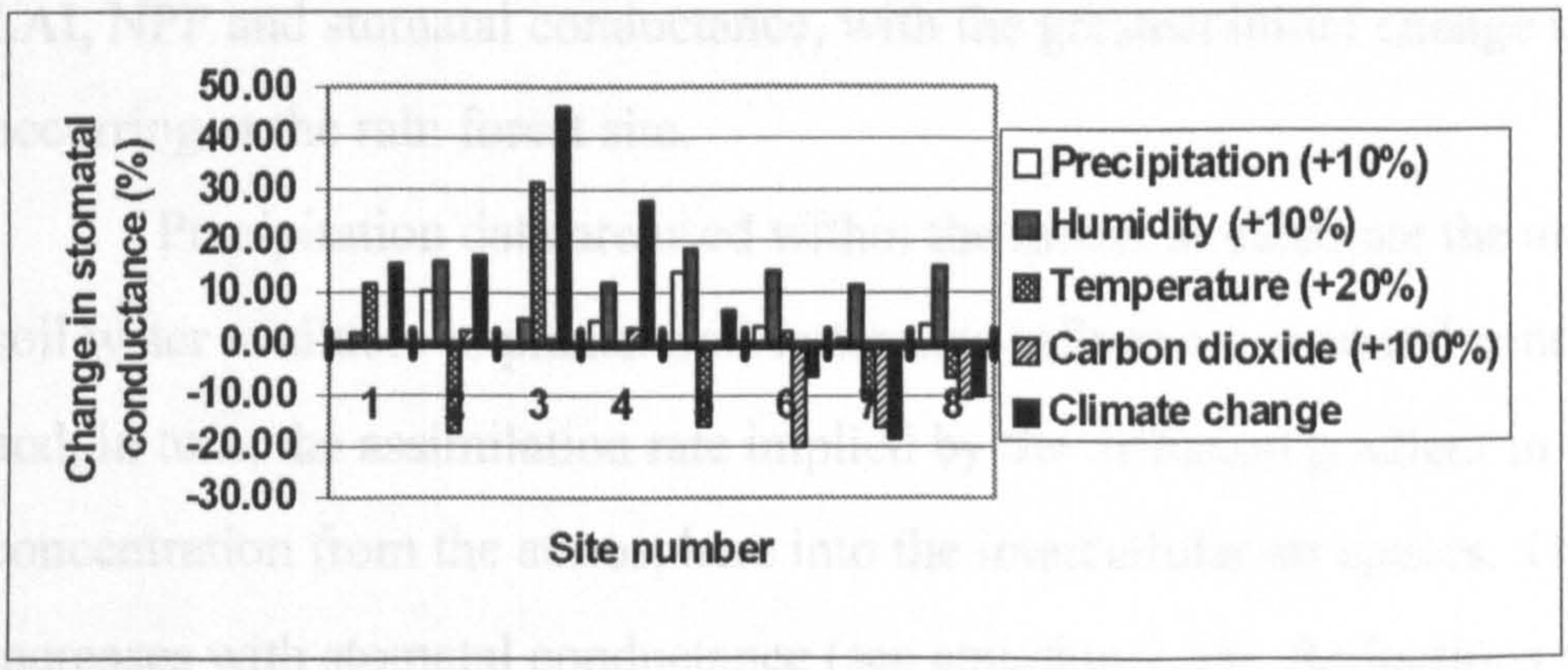

c) Stomatal conductance

Figure 4.12 Graphs showing the changes (%) in values of LAI, NPP and stomatal conductance for a given change (%) in each of the input variables: precipitation, humidity, temperature, carbon dioxide and climate change, for the 8 test sites.

3.2.4 Discussion

Increasing monthly temperature from 0 to 40°C causes increases in NPP at all sites, up to a temperature of 25°C. Above this temperature, increasing dark respiration, increasing vapour pressure deficits and decreasing soil water causes NPP to decrease. Nitrogen uptake is also reduced.

LAI and stomatal conductance display similar patterns to NPP, but, at the northern boreal site and the grassland site, if the vapour pressure deficit is allowed to increase with increasing temperature, stomatal conductance and LAI decrease at temperatures above 10°C. If the vapour pressure deficit is held constant this decrease in LAI and stomatal conductance is reduced and does not occur until higher temperatures (than using the variable VPD) are reached. The low precipitation at these sites, together with high evapotranspiration, caused by the increasing temperature, also contributes to this effect.

Increasing monthly precipitation from 0 to 200 mm causes increases in LAI, NPP and stomatal conductance, with the greatest initial change in NPP, occurring at the rain forest site.

Precipitation data are used within the model to calculate the amount of soil water available to plants. Soil water also influences stomatal conductance and, in turn, the assimilation rate implied by the diffusion gradient in CO_2 concentration from the atmosphere into the intercellular air spaces. This rate increases with stomatal conductance (see equation 2.58). Reductions in stomatal conductance occur as the soil water content declines, even though the leaf water potential remains unchanged. The hyperbolic soil water response function, k_g (w_s) (see equation 2.57), ensures conductance levels off as soil water reaches a maximum value At sites where there is no shortage of water, as in the rain forest, the LAI and NPP will be high, providing precipitation exceeds evapotranspiration and the temperatures are high enough. However further increases in precipitation do not cause any further increases in stomatal conductance, or LAI and NPP due to the asymptotic nature of the response function. The three most northern sites show no further response to

an increase in precipitation beyond a monthly precipitation value of 50 mm. Increased precipitation has a limited beneficial effect on stomatal conductance, NPP and LAI at these sites, because temperature plays a more dominant role through its effect on nitrogen uptake. Low temperatures keep assimilation, NPP and LAI low. All the other sites have an increase in LAI, NPP and stomatal conductance up to a value of 150 mm. Temperatures are greater than the other sites and the effect of additional precipitation increases assimilation. The rain forest site, the savannah site and the drought deciduous site have the greatest response to a wetting. It is interesting to note that, given a monthly rainfall amount of 200 mm, the savannah site and the drought deciduous site would have the same NPP and LAI as the rain forest, although the stomatal conductance would be slightly lower.

Increasing monthly relative humidity from 0 to 100% had little effect on LAI and NPP unless the humidity values were high.

LAI and NPP increase with increasing atmospheric CO_2 but the response is asymptotic so that in the case of LAI there was only a slight increase above 35 Pa (the present-day figure used within DOLY). NPP showed a greater response above this value, particularly for the rain forest site which had the greatest NPP value. The stomatal conductance showed a slight decrease for the rain forest site, but in general there was very little change with increasing CO_2. The values for an atmospheric partial pressure of less than 10 Pa were incorrect due to an artifact effect from the use of the Ball and Berry (1982) equation in which stomatal conductance is dependent on photosynthesis. The dry deciduous and savannah sites were also responsive to CO_2, although the stomatal conductance at these sites showed little change.

The sensitivity analysis has shown that temperature has the greatest impact on NPP and LAI particularly at the colder sites, (southern boreal forest) where there is a 35% increase in LAI for a 10% increase in temperature. Precipitation is also important and impacts on the northern boreal and the grassland sites. In the case of the northern boreal site LAI decreases by 17%

for a 10% decrease in precipitation. At the grassland site, there is a 30% increase in LAI for a 20% increase in precipitation. In the case of relative humidity, the northern boreal site and the grassland sites are again the most sensitive in relation to the other sites, though the sensitivities are low. LAI increases by 13% for a 10% increase in relative humidity at the northern boreal site, and by 22% for a 30% change at the grassland site. Atmospheric CO_2 is the variable to which there is the least sensitivity. The grassland site displays the greatest sensitivity with LAI increasing by 5% for a 10% increase in CO_2, and the rain forest site is the most sensitive with NPP. There is also some sensitivity with stomatal conductance but this is very small (around 0.25) and occurs at the dry deciduous, rain forest and savannah sites. These sites show a slight decrease in stomatal conductance at high values of atmospheric CO_2 (Figure 4.6c) which impacts on the outputs from the sensitivity analysis. At the cooler, northern sites, CO_2 has very little effect on the three variables.

The climate change simulation altered all the variables together. LAI and NPP increased at all sites with the climate change scenario, but the size of this response varied between sites. This is due to the effects of temperature, as well as the soil carbon which also varies between the sites. The four colder sites have the highest values of soil carbon (>12000 gC m^{-2}), and the warmer sites the lowest values (<12000 gC m^{-2}). All the soil nitrogen values exceed 600 gN m^{-2} at these test sites. Higher soil carbon levels reduce nitrogen uptake which in turn reduce assimilation and dark respiration. Nitrogen uptake is also influenced by soil water and temperature (see section 3.2). Increasing CO_2 by 100% means that it becomes the dominant factor in the changes in LAI and NPP caused by climate change, but it is moderated by the influence of temperature and soil water. Assimilation rises with increasing CO_2, but stomatal conductance decreases. Temperature also affects assimilation through its influence on nitrogen uptake. At temperatures below 28°C, assimilation increases as temperature increases, and then decreases above this temperature. Also, dark respiration increases with temperature and shows an initial steep

increase in rate with temperature and then a falling rate as temperature increases further. The amount of soil water and temperature also influence stomatal conductance. Providing there is sufficient water, NPP increases if assimilation increases at a faster rate than dark respiration. At the northern boreal site, and the drought deciduous site, the temperature increase reduced the effect of the increased CO_2 in the climate change scenario. In the case of the northern boreal site, precipitation is low and increasing temperatures would reduce the amount of soil water as well as increase the dark respiration rate, and these combined effects would reduce LAI and NPP. At the hotter, drought deciduous site, the increased temperatures lead to a reduction in nitrogen uptake, and greater dark respiration relative to assimilation, thereby reducing NPP. Stomatal conductance increased at the four northern sites with climate change, but it decreased at the dry deciduous, rain forest and savannah sites due to the combination of high temperatures and increased CO_2 . The climate change effect was greater than any individual effect at all sites except the dry deciduous site. At this site, the 10% increase in temperature caused a decrease in NPP, which was not offset by increased CO_2.

It is recognised that there are no comparisons between the model outputs and observations from real plants or from other models. There are a number of reasons for these omissions. The first is that a number of processes within the DOLY model (standard version) have been tested under specific conditions in Woodward *et al.* (1995) and found to compare favourably with field observations under the same conditions. It is presumed therefore that the model predictions should provide a reasonable representation of reality. Secondly, it would be extremely difficult to obtain any suitable field data to cross-check with these particular modelled data as there would be considerable variation in values between different species and experimental conditions. A number of experiments to specifically test the model output would be required for each biome. Finally, the same type of problems arise when comparing with other models in that they are often run with different input data or on different temporal or spatial scales

This chapter has shown that there is a variety of responses of the output variables to the climate input variables. This sensitivity analysis has highlighted the sites that will be most vulnerable to climate change, notably the northern boreal site, the grassland site and the dry deciduous site and has been shown to be mainly due to water limitations. CO_2 alone does not have a major effect on the output variables for the sites, compared to those effects caused by the climate inputs. However, CO_2 in conjunction with changes in these climate inputs, as part of a climate change scenario, becomes a major factor. This is due to the interactions between precipitation, temperature and assimilation, as discussed. The DOLY model has been run beyond its normal operating range, and the results have shown that it is able to model reasonably a wide range of climate scenarios.

CHAPTER 5

5.0 Global functional types derived from the DOLY model and a life-form model for use in climate change analysis

5.1 Introduction

It is well known that the world's vegetation has a major impact on the operation of the biosphere, biogeochemical fluxes and climate (Dickinson *et al.*, 1986; Melillo *et al.*, 1993). Foley and co-workers (1996) state that many general circulation models (GCMs) represent the biophysical associations between the earth's surface and the atmosphere using land surface models (e.g. BATS of Dickinson *et al.* (1986) and SiB of Sellers *et al.* (1986, 1992, 1996a, b, c)). They also state that such models operate globally with vegetation and soil characteristics geographically predefined, but by doing this potential changes in vegetation cover can be overlooked which in turn can significantly alter the climate system (e.g. Bonan *et al.*, 1992; Foley *et al.*, 1994; Henderson-Sellers and McGuffie, 1995; Randall *et al.*, 1996).

For many ecological modellers, vegetation maps are used to provide initial data rather than an end product. These data are translated into a variety of structural and physiological attributes for entry into biosphere models (Melillo *et al.*, 1993; Sellers *et al.*, 1994; Field *et al.*, 1995). This approach makes the implicit assumption that current vegetation is in equilibrium with current climate, in other words, there is no time-lag in the system between vegetation and current climate. Also, if projections of future vegetation are to be made one needs to ensure that different perhaps novel biomes (units of vegetation) are able to emerge in the future, as well as considering the dynamic

successional nature of natural ecosystems. This is not possible with many of the biosphere models mentioned earlier. Another problem that exists is that the nature, timing and extent of disturbances in vegetation is poorly understood.

Over the years there have been a number of attempts to classify global vegetation. Köppen (1936) and Holdridge (1947) used precipitation, temperature and evapotranspiration as selection criteria to predict biomes. Several classifications have been derived from a combination of historical climate and ground survey. These are well summarized by Prentice (1990).

It is not possible to look at each individual species globally as there have, in fact, been very few species studied and data on species response to environmental change are not available (Woodward, 1996). In order to avoid this problem, plant functional types may be used (Smith *et al.*, 1996). A functional type (FT) is defined as a type of plant with particular morphological, physiological and life cycle attributes, irrespective of its taxonomic classification, suitable for predicting responses to environmental change (Smith, *et al.*, 1993). In the past, functional types have been related to specific plant features for instance, their height, or LAI, with the assumption that such characteristics are coupled with their ability to survive a hostile environment. Box (1981) introduced a dominance hierarchy of plant growth forms or functional types (e.g. tree, shrub, etc.) and provided more detail on the climate variables used. More recent work has been undertaken by Woodward (1987) who builds on these ideas in order to derive leaf area index (LAI). Leaf area index provides a simple measure of plant canopy density and is widely used in land surface characterizations, as well as for estimating canopy energy and mass exchange processes. Accurate representations of LAI and climate are required in order to estimate biosphere fluxes. In addition, net primary productivity (NPP) provides useful information about vegetation biomass, and Lieth (1975) was one of the first to produce a global map of NPP from a regression equation driven by climatic data.

The ecosystems of the world can be divided into a small set of biomes

each characterized by the dominance of one or more functional types of plant. Biomes are units of vegetation or assemblages of plant functional types (Prentice *et al.*, 1992). They are based primarily on physiognomy, not floristics, and secondarily on climate (Grabherr & Kojima, 1993). Environmental conditions (both the physical environment and other competing plant types) control the geographical distribution of a dominant plant functional type (Haxeltine and Prentice, 1996).

The land cover dataset of Wilson and Henderson-Sellers (WHS, 1985) is one of a number of land-cover datasets used by both ecological and climate modellers. In this dataset the land cover classes are of actual vegetation obtained from a variety of sources and at a spatial resolution of 1° by 1°. Fifty-three possible land cover classes divide global vegetation on the basis of attributes important in climate modelling studies, such as vegetation height, seasonality and ground cover. These are further reduced by WHS to 24 classes, which are equivalent to biomes. Each land cover class contains one or more land types. The 24 land types in the WHS dataset can be further divided into 5 major groups of functional types consisting of tree, shrub, grass (or non-woody), crops and non vegetation. In this thesis, the term, life-form, has the same definition as functional type.

This chapter describes an approach to predicting dominant functional type change at the global scale, with particular reference to changes in tree distribution. Values of NPP and LAI for a given site from the DOLY model are used as input into a life-form model, a type of patch model of interacting functional types. The functional types predicted by the life-form model can be mapped globally for current vegetation. Tree physiognomy can be further sub-divided on the basis of absolute minimum temperature (Woodward, 1987). Future dominant functional types can also be predicted by using climate change scenarios. Specific areas can be studied in more detail and in this chapter the boreal forest–tundra boundary is examined as a case study.

This chapter has three main objectives:

i) to display the output from the life-form model;

ii) to show how this output can be used in climate change analysis.

iii) to develop the model

5.2 Description of the life-form model

The model described here uses the LAI and NPP from any location to predict the outcome of a simple competitive regeneration between three basic life-forms, trees, shrubs and grasses.

Bare ground, grass, shrub and tree are the four compartments of the life-form model. In GCMs, the amount of bare ground affects hydrological processes and energy fluxes. As LAI increases, the amount of bare ground decreases, which reduces irradiance at the ground surface. Transfers between most, but not all, of the compartments are possible and transfer coefficients have been derived to be appropriate for each life-form (see Appendix 3 and Table 5.1). These transfer coefficients have been based on field observations of life-forms and their growth characteristics (Woodward, 1987).

Table 5.1 Transfer coefficients for the compartment model (Figure 5.1) of life-form spread. 'Controls on coefficients'—Leaf Area Index (LAI) and Net Primary Productivity (NPP)—describes what controls are used to define the life-form specific dynamics of growth.

Coefficients	Life-form change	Controls on coefficients
A0,1	Grass to bare ground	LAI
A0,2	Shrub to bare ground	LAI
A0,3	Tree to bare ground	LAI
A1,0	Bare ground to grass	NPP
A2,0	Bare ground to shrub	NPP
A3,0	Bare ground to tree	NPP

The coefficients have been calculated for modelling the establishment and mortality of the three main life forms. The cover of each life-form can be determined at any time by using the transfer coefficients to calculate its cover relative to bare ground (see Figure 5.2). The arrangements of the compartments and the modelled transfer coefficients are shown in Figure 5.1.

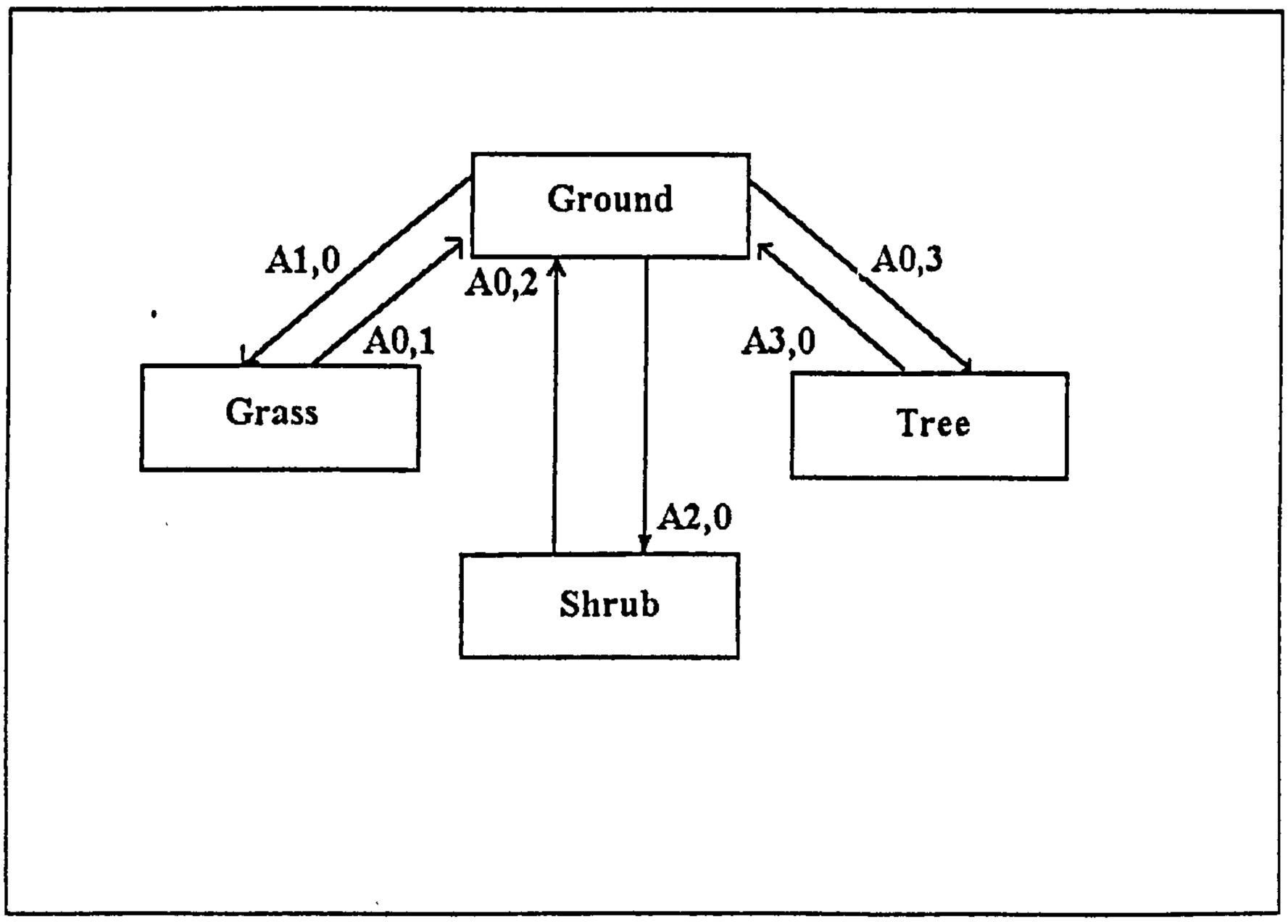

Figure 5.1 Compartment life-form mode. A*x*, *y* (where *x* and *y* range from 0 to 3), indicate transfer coefficients between the compartments which are allowed in the model.

The descriptions and basic controls of the transfer coefficients (Table 5.1) indicate that LAI and NPP are used throughout. In this model, the growth of shrubs benefits from low values of LAI and NPP. If NPP and LAI then increase in value this favours grasses initially, and then finally trees. These progressions have been devised from earlier and other work (Woodward, 1987; Melillo *et al.*, 1993).

The changes in the relative cover of trees, shrubs and grasses over a typical 50 year period are shown in Figure 5.2, for a site with a potential LAI of 5, and NPP of 5 tC ha^{-1} yr^{-1}. In this example, the greatest cover of grasses

and shrubs occurs after 5 years but then decrease as trees become the dominant life-form covering bare ground. In the Woodward and Lee (1995) paper the relative LAI and NPP 'spaces' of the three life forms are shown. These depict the dominance of shrubs in low NPP environments, the dominance of grasses in higher NPP environments and the increasing dominance of trees with increasing LAI. Increasing LAI causes the presence of trees to increase due to simulated shading effects by the tree on the grasses and shrubs (Woodward and Lee, 1995).

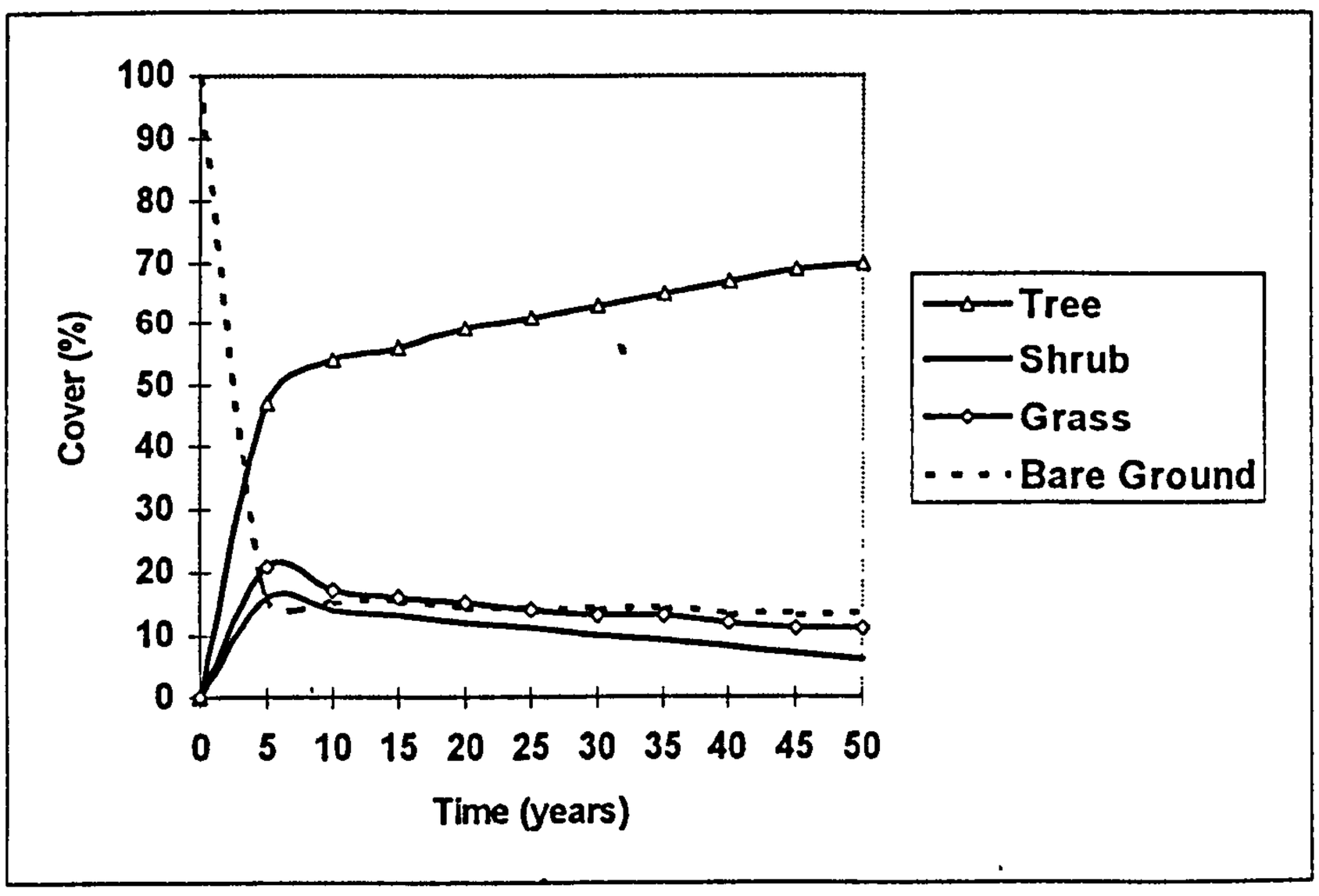

Figure 5.2 The dynamics of life form cover over a period of 50 years with a constant ceiling leaf area index (LAI) of 5 and net primary productivity (NPP) of 5 tC ha^{-1} yr^{-1} .

5.3 Methods

In order to determine the current global vegetation distribution in the form of the four main functional types of bare ground, grass, shrub and tree, the DOLY model (standard version) (see section 2.3) was driven with IIASA (International Institute for Applied Systems Analysis) data (Leemans and

Cramer, 1991) for a 0.5° by 0.5° global grid for the current climate. In addition, the model was also run with slab data from the United Kingdom Meteorological Office (UKMO) general circulation model (GCM) (for details of this dataset see Chapter 6) on a 2.5° by 3.75° global grid for the current and future climate scenarios. The predicted values of NPP and LAI were then input into the life-form model which was run over a 50 year period in order to obtain the percentage cover of the four functional types.

The tree category was sub-divided into four groups by the use of absolute minimum temperature thresholds, as shown in Table 5.2 (Woodward, 1987). An additional tree category, drought–deciduous tree, was derived from the evergreen tree category by determining the number of days in the year when the soil water content was below field capacity (0.15 g water (g soil)$^{-1}$). The model records when this occurs. If this number exceeded 100 days then the tree type was classified as drought-deciduous, instead of evergreen. This threshold was selected by observing that the actual global distribution of drought-deciduous trees (Archibold, 1995), closely matched the areas where there were more than 100 days in the year below field capacity.

Table 5.2 Absolute minimum temperature thresholds used to sub–divide the tree categories within the life-form model (Woodward, 1987). The absolute minimum temperature is calculated in the DOLY model from the mean temperature using empirical formulae supplied by Dr. Tom Smith, Department of Environmental Sciences University of Virginia.

Tree Type	Absolute Minimum Temperature Range (°C)
Evergreen	> -15
Cold deciduous	-15 to -40
Coniferous evergreen	-40 to -55
Coniferous deciduous	<-55

The functional type with the greatest coverage was extracted for eachgrid square. In some cases there was an under–representation, by a visual comparison with the global vegetation map (Archibold, 1995), of shrubs and grasses using this approach. In order to overcome this problem, additional criteria were adopted, as shown in Table 5.3a.

Table 5.3a The additional selection criteria used within the life-form model for the shrub and grass category if they are not initially selected as the dominant functional types.

Criteria	Dominant functional type
1. The bare ground coverage exceeds 50% but more than 30% of the grid square is shrub **or** there is no overall dominant functional type	Shrub
2. Grass coverage is less than the bare ground coverage but exceeds the coverage of the other categories	Grass

The resulting functional type map is shown in Figure 5.3a. The same procedure was adopted with the WHS data (WHS, 1985) which are on a 1° by 1° grid. WHS suggested 24 land types as a simplification of their original 53 land cover types. These land types from WHS (1985) were then allocated a functional type for this comparison. These are shown in Table 5.3b, and Figure 5.3b shows the map produced from these functional types.

To check the performance of the life-form model, a difference map was created between the dominant functional types from the life-form model obtained using the IIASA climate data as input (transformed to a 1° by 1° grid) and the simplified WHS land type data. The IIASA data were used to do this as they are derived from actual mean data over a 30 year period and have not been derived from a GCM. This gives an independent check to the life-form model output. In addition to this, the DOLY model was run with the GCM slab data

for current and future climate scenarios, and again functional types were extracted (Figures 5.4 to 5.7).

Table 5.3b Functional type allocation for each of the 24 land types in WHS (1985). The bare ground category covers all non-vegetated surfaces.

Type	Description	Functional type allocated
1	Water	Bare ground
2	Ice	Ice
3	Inland lake	Bare ground
4	Evergreen needleleaf tree	Tree
5	Evergreen broadleaf tree	Tree
6	Deciduous needleleaf tree	Tree
7	Deciduous broadleaf tree	Tree
8	Tropical broadleaf tree	Tree
9	Drought deciduous tree	Tree
10	Evergreen broadleaf shrub	Shrub
11	Deciduous shrub	Shrub
12	Thorn shrub	Shrub
13	Short grass and forbs	Grass
14	Long grass	Grass
15	Arable	Crop
16	Rice	Crop
17	Sugar	Crop
18	Maize	Crop
19	Cotton	Crop
20	Irrigated crop	Crop
21	Urban	Bare ground
22	Tundra	Shrub
23	Swamp	Bare ground
24	Soil	Bare ground

The tree cover was studied for the current and future climate and a more detailed analysis was carried out for the area north of 55°N to examine the boreal forest–tundra boundary and the probable shifts in this boundary with a future change in climate. The limit of 55°N was selected as the bulk of the world's boreal forest is north of this latitude (Pastor and Mladenoff, 1992; Barbour and Billings, 1988). It also aided data extraction to have a set latitude limit.

5.4 Results

5.4.1 Comparing the model results with the WHS dataset

Figure 5.3a shows the functional types derived from the life-form model. Figure 5.3b shows the functional types derived from the WHS data (Table 5.3b) which includes the additional categories of ice and crop. The difference map between the WHS land cover types and the functional types derived from the life-form model is shown in Figure 5.3c (ice is set as bare ground). This map highlights areas where the life-form model was deficient in its predictions compared to the WHS data, as well as those areas where it performed well for the present-day climate. The land cover categorised from the WHS dataset (1985) was assessed for reliability by Wilson and Henderson-Sellers (1985) themselves. They state that North America, most of Europe, the Middle East, U.S.S.R. and much of the African continent have a high reliability score. This high reliability was indicative of very recent source of data or a change of less than 2.5% at the national scale since the date of publication of the map source data. The areas with the lowest reliability were Central and South America, along the south-west coast of northern Africa, Rwanda-Burundi, Uganda, the Philippines, Thailand, Mongolia and Syria. These areas need to be considered when examining the difference map. Also, due to interpolation, and some subjective assessment of the data archives used, errors in other areas may also have arisen (Wilson and Henderson-Sellers, 1985).

The main areas of difference arise in agricultural areas where DOLY predicts mainly grass or tree. Also shown well, are areas which have been disturbed either by Man's activities or by fire. These areas, such as savannah regions would have been covered in trees but are, in fact, grass.

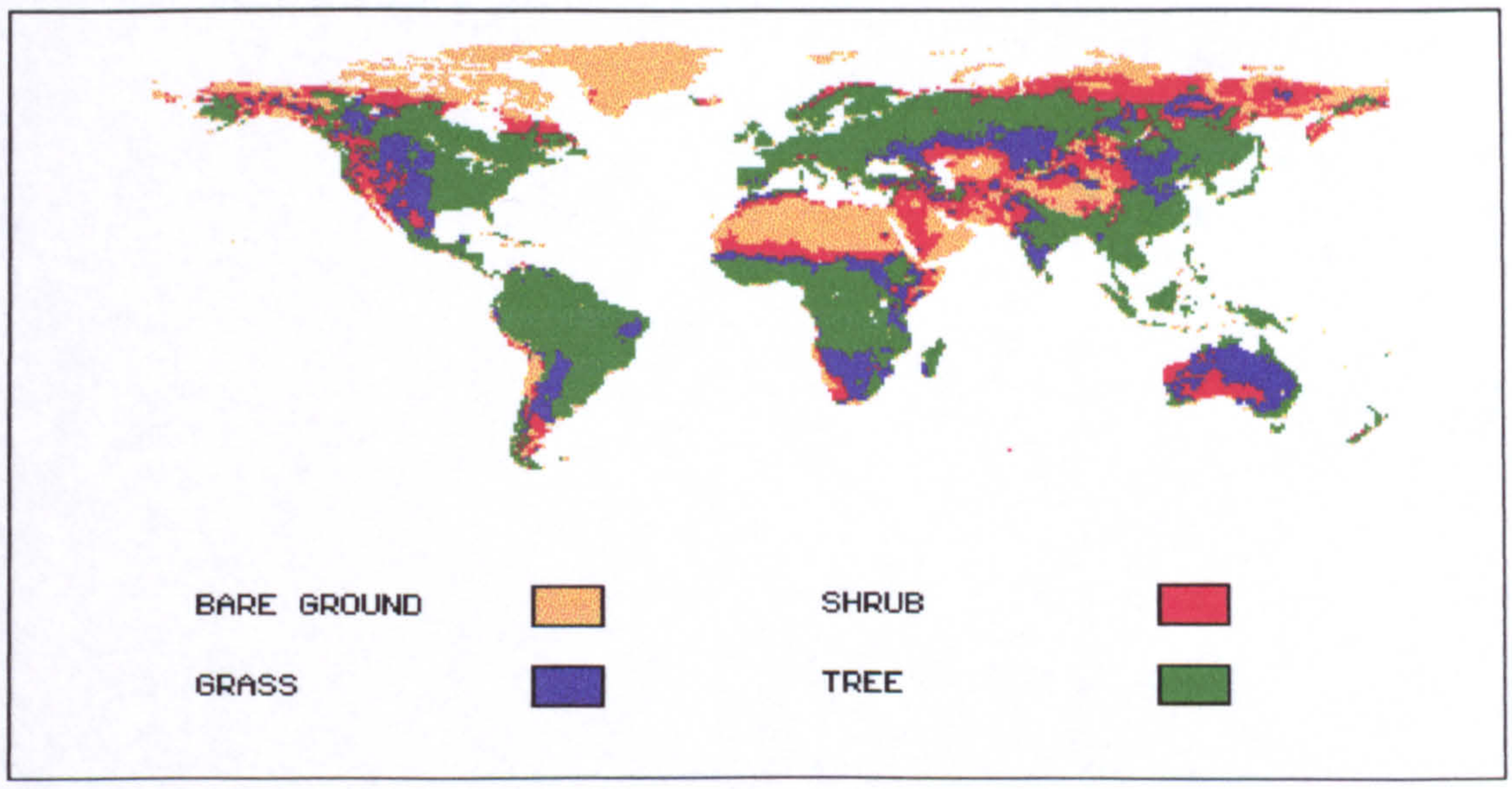

Figure 5.3a Functional types derived from DOLY (standard version) and the life-form model run with IIASA climate data transformed to a 1° × 1° grid.

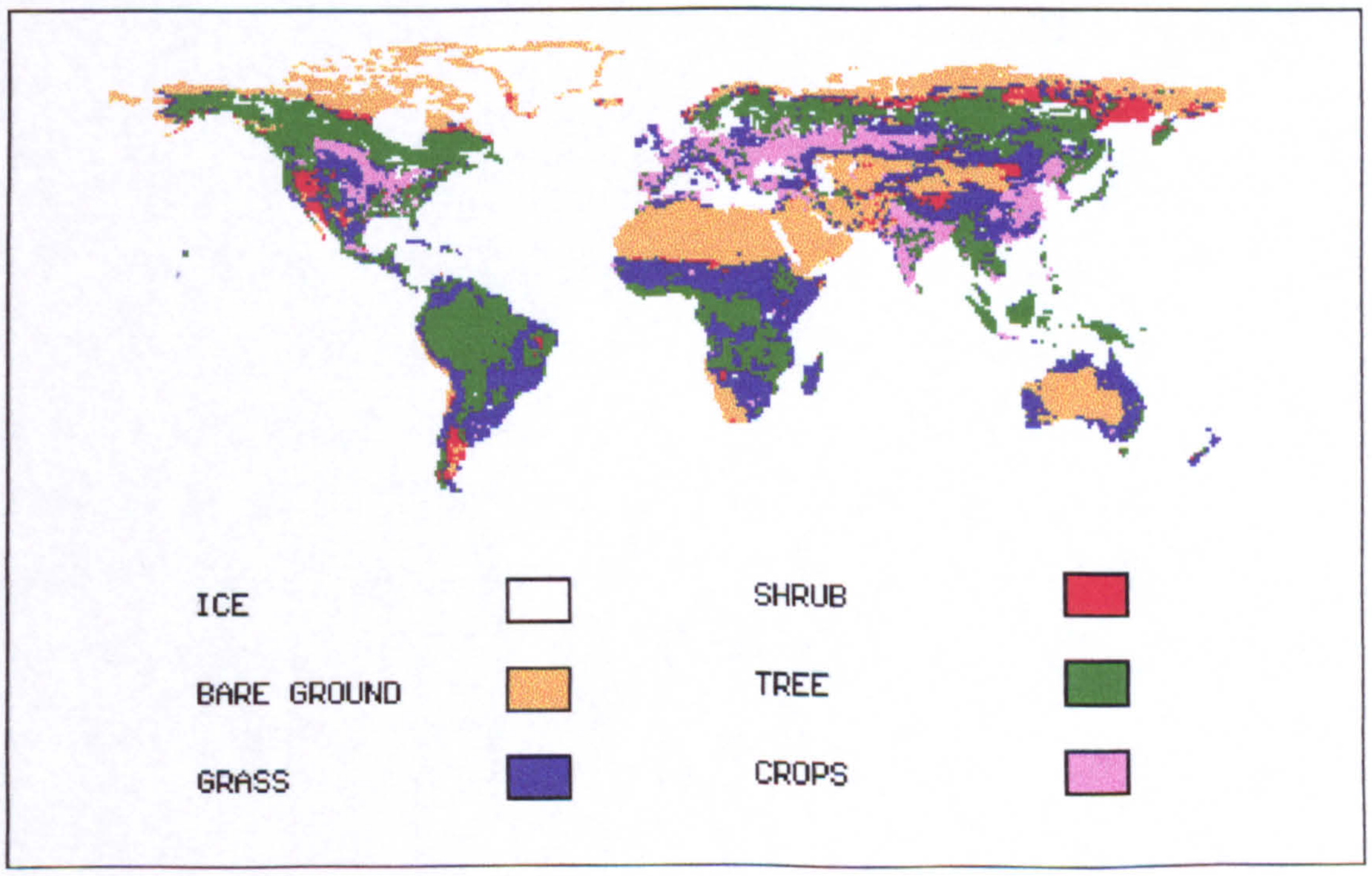

Figure 5.3b Functional types derived from the WHS land type data (see Table 5.3b)

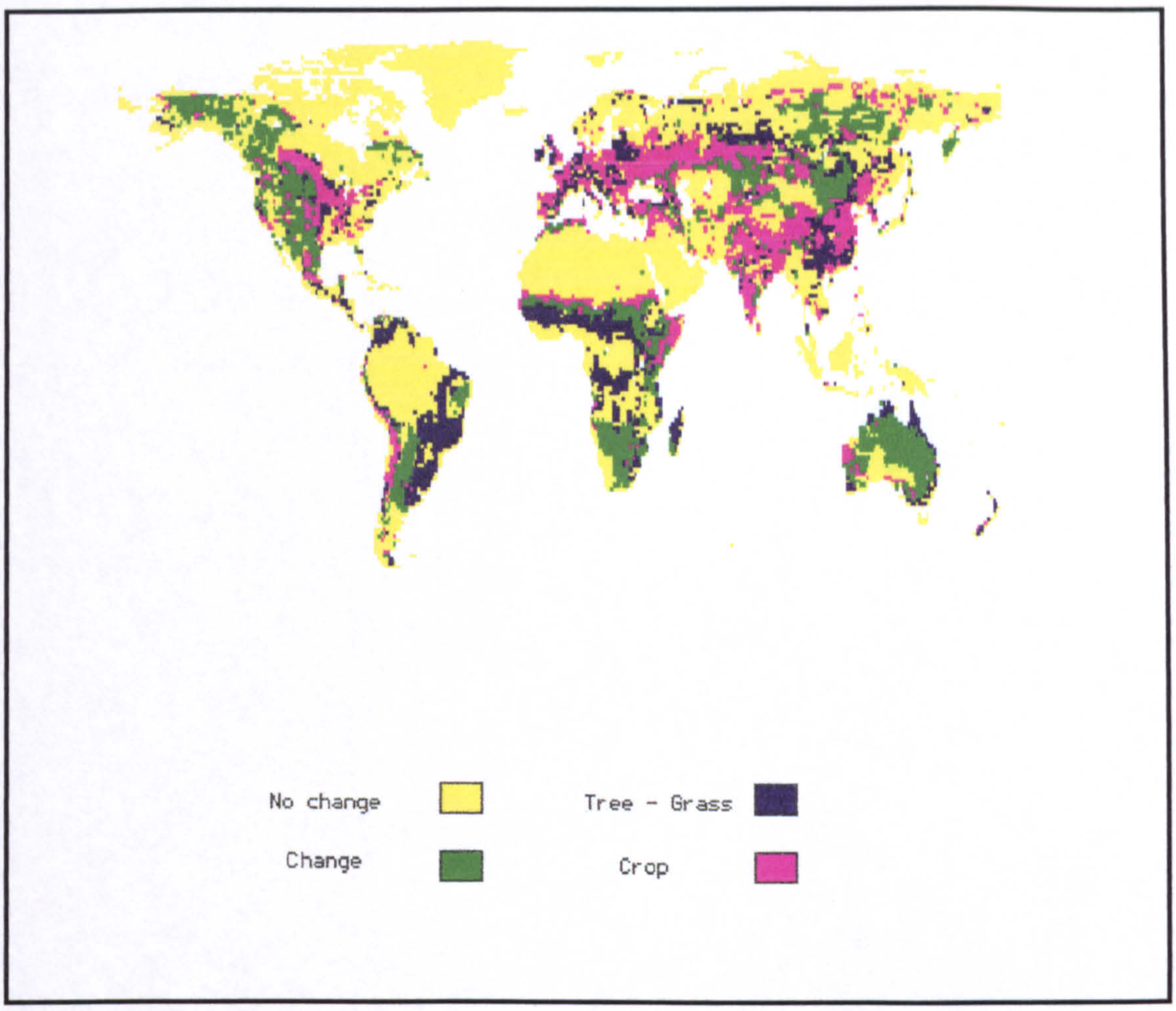

Figure 5.3c This map shows for each 1° by 1° cell, the difference between the functional types of vegetation given by the vegetation model, DOLY (standard version) and the observed primary functional type in the database of current vegetation type produced by Wilson and Henderson-Sellers (1985). Thus agricultural regions are picked out as areas where the WHS database gives crop (pink). Some of the areas categorized as tree by the DOLY model, but are in fact grass according to WHS (Tree–Grass), highlight the problems in predicting mixtures of trees and grasses in vegetation types such as savannah. Also, the effect of Man's activities mean that in some regions where DOLY predicts tree as the natural vegetation it is in reality grass due to forest clearance and grazing influences. The change category highlights those areas where the DOLY model and WHS disagree (excluding the Tree-Grass category).

The vegetated cells alone were extracted to quantify some of the differences shown in Figure 5.3. The number of sea cells and non-vegetated cells (i.e. those cells which are set as bare ground) as well as the crop cells were totalled and subtracted from the global total in order to obtain the number of vegetated cells. The number of cells in each difference category were then analysed. The results are shown in Table 5.4.

Table 5.4a The distribution and categorization of 1° × 1° cells derived from the WHS (1985) land cover map.

Category	Number of cells	
Sea and Antarctica	49190	
Land (excluding Antarctica)	15610	
Total number of land and sea cells (1° × 1° grid)	64800	
Crops		2005
Non-vegetated		3793
Natural Vegetation		9812
Total number of land cells		15610

Table 5.4b The number of naturally-vegetated cells within the functional type (FT) difference categories between the DOLY model and the WHS dataset.

DOLY FT	WHS FT	Number of cells	Percentage of all land cells
Agree (no change)	Agree (no change)	4861	50
Bare Ground	Tree	107	1
Bare Ground	Shrub	151	2
Bare Ground	Grass	339	3
Grass	Tree	378	4
Grass	Shrub	1140	12
Shrub	Tree	940	9
Shrub	Grass	0	0
Tree	Shrub	0	0
Tree	Grass	1896	19
	Total	9812	100

It is evident from Table 5.4b that only 50% of the cells agreed in this analysis. However, as was stated earlier, a number of cells have been disturbed by human activities and fire, and these in the main are represented by the Tree to Grass category. If these cells are added to those that agree, then this increases the percentage value to 69%. The main categories of disagreement (after the Tree to Grass category) include those where DOLY has predicted grass and WHS has recorded shrub (12%), and those where DOLY has predicted shrub when in fact it is tree (9%) according to WHS. These two categories account for 21% of all the land cells. Some possible reasons for these disagreements include:

i) An overestimation of grasses and shrubs.

In section 5.3 it was mentioned that the DOLY model initially under-represented shrubs and grasses and the selection procedure had to be altered to account for this. In this situation this adjustment may have been too great and

allowed too many grasses into shrubland areas (WHS) or shrubs into areas where there should be trees according to WHS. From Figure 5.3c it can be seen that many of the differences that do arise between the two datasets occur in arid areas (e.g. central Australia, northern savannah regions of Africa, southern Africa and eastern Brazil). These particular areas are difficult to classify and the vegetation may be mixtures of shrubs, grasses, or bare ground. This suggests that DOLY has overestimated the amount of grass for some of these areas, and in some cases WHS has recorded shrub instead of grass. In Alaska and north-western Canada there is another area of difference (Figure 5.3c). In this case DOLY appears to have predicted shrub instead of tree for part of the boreal forest.

ii) DOLY may be correct and WHS incorrect.

In some cases the DOLY model may have made a correct prediction and the WHS dataset is incorrect for some cells. These cells are hard to identify, but some may be along the south-west coast of North Africa or Mongolia which are areas where the WHS data were unreliable (Wilson and Henderson-Sellers, 1985).

This exercise has been a rather crude examination as to the level of accuracy of the functional types output from DOLY and the life-form model. It does show, though, that despite some errors within the WHS dataset itself, global vegetation, in terms of functional types can be represented reasonably well (almost 70% agreement if savannah regions are included).

5.4.2 Prediction of dominant functional types under future climates (slab GCM)

The DOLY and life-form models were run with GCM slab data for three different scenarios in order to obtain some indication of the possible movement of dominant functional types with climate change, and to determine whether the concentration of CO_2, or temperature and precipitation were the dominant factors driving this change. The slab GCM data for current climate

($1 \times CO_2$) and a doubled climate ($2 \times CO_2$) were used. The doubled-CO_2 climate is that for a future climate 50 years from the present. This means that the temperature is increased by about 2°C (with greater warming at high latitudes, (Sud *et al.*, 1990)) and the precipitation increased by 10%. The DOLY model was run with two partial pressures of CO_2, 35 Pa for the current climate, and 56 Pa for the future climate. The GCM operates on what is called effective CO_2. This is also referred to as CO_2 equivalent, and is calculated by adding the heating effect of the other trace gases within the atmosphere to the actual CO_2 concentration. Equivalent CO_2 concentration, therefore, has a higher value than the actual atmospheric CO_2 as used by DOLY. One particular problem that arises with the slab data is that the grid squares are so large (2.5° × 3.75°) that they miss much of the detail that would be provided by a 1° × 1° grid. However, the DOLY model is quick to run at this resolution and it does provide an indication of future global trends in vegetation. Figure 5.4 shows the functional types predicted for the current climate with a CO_2 input of 35 Pa. It can be seen how the main biomes of the world are represented by these dominant functional types. For instance, the regions with tropical forests are depicted as evergreen broadleaf tree and tundra is represented as shrub. It should be noted that at this particular stage in the model development, grasses were only been crudely defined in relation to NPP and LAI, and there is no division between C_3 and C_4 grasses. This accounts in part, for the fact that the map does not show the temperate grasslands of the world very well, with just a few grass cells representing the American prairies and the Russian steppes. It does however show some of the Pampas grasslands of South America. The savannah areas, such as the northern edges of the African rain forest, and parts of northern and central Australia, can be clearly seen and are depicted as either grass or drought–deciduous trees. The reason for the lack of grass in some of these areas, for instance, parts of South America and the Russian steppes, could be attributed to the fact that the slab precipitation data are too low in these areas (see Figure 7.3 and Table 7.3), thus permitting the shrub or bare

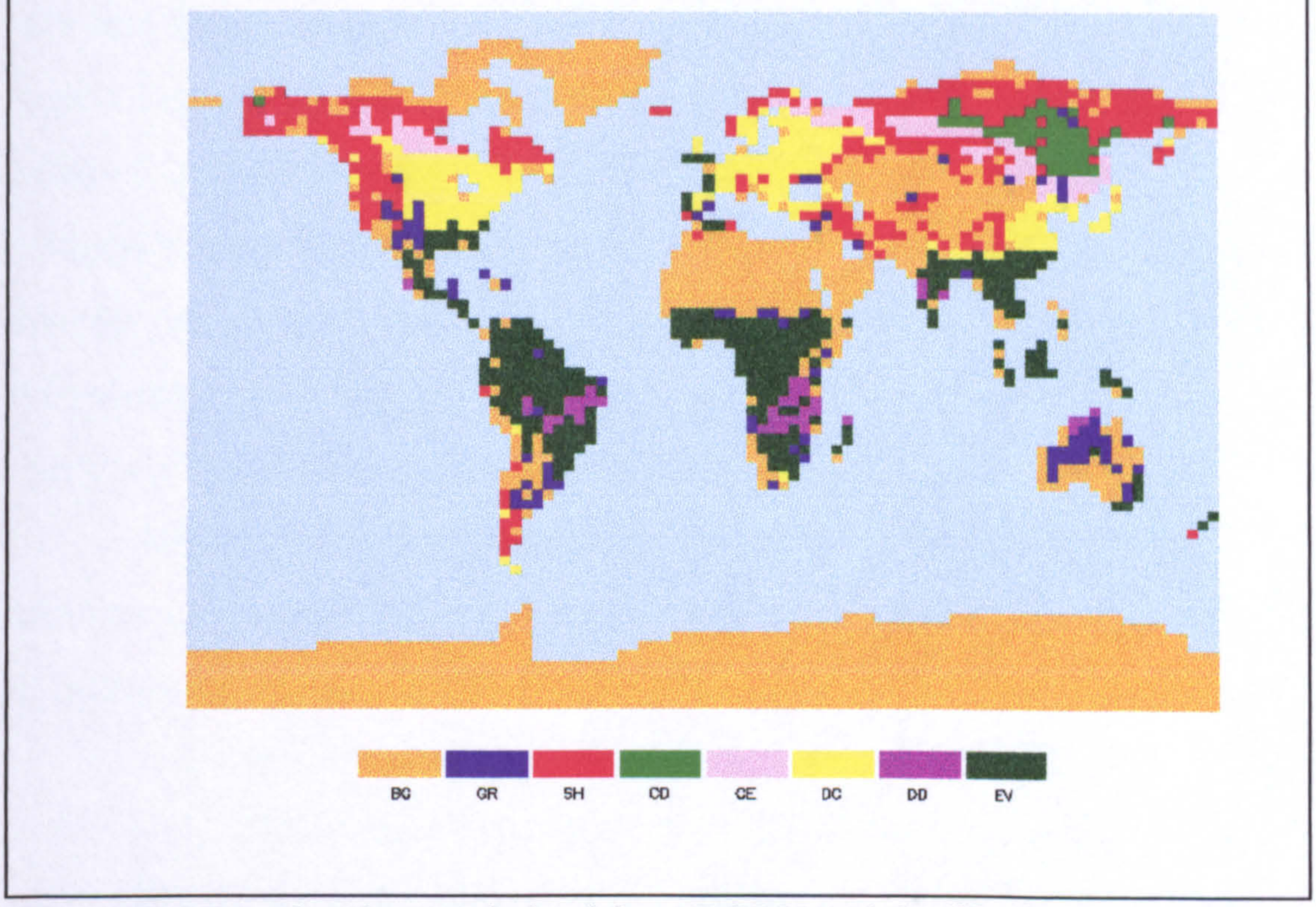

Figure 5.4 Functional types derived from DOLY and the life–form model for current climate as simulated with the UK Meteorological Office high resolution (slab) model. The abbreviations used are as follows: BG is bare ground, GR is grass, SH is shrub, CD is coniferous deciduous tree, CE is coniferous evergreen tree, DC is cold deciduous tree, DD is drought deciduous tree, and EV is evergreen tree.

ground category to cover more of the ground area and being labelled as the dominant type. Alternatively, or in addition, the classification of the dominant type may be underestimating the amount of grass and perhaps should reduce the amount of bare ground in these areas which may then increase the grass coverage. The prairies in America are depicted as cold deciduous tree instead of grass which suggests that the slab precipitation is too high in this particular region. This is supported by data from Table 7.3, that show that the slab GCM data were cooler and wetter for sites in eastern and central southern America than the data from the IIASA dataset. This would mean that trees would have an advantage over grasses in the life-form model. Also, the life-form model was

able to predict grass with the IIASA data input for the American prairies, so this also tends to suggest that the slab precipitation data are rather high in this region. Despite the limitations of the slab data, it is possible to define broadly most of the major biomes of the world such as the boreal forest, tundra, temperate deciduous forest and equatorial rain forest for the present-day and to use this knowledge, together with the future projections of climate, to ascertain the possible movement of these biomes, or at least their characteristic functional types of plants, in response to changes in climate.

Having considered the model predictions for the current vegetation we can now turn to the results for the three scenarios. The scenarios performed are as follows:

i) increase the atmospheric CO_2 partial pressure to 56 Pa in DOLY and run with the present-day slab climate data. This simulates the effect of CO_2 alone on the functional types (Figure 5.5).

ii) change the climate with no change in the atmospheric CO_2 used to run the DOLY model. This simulates a warming scenario of approximately 2°C and a 10% increase in precipitation with no difference in the atmospheric CO_2 partial pressure of 35 Pa (Figure 5.6).

These two scenarios are sensitivity tests on the model. The final scenario is a simulation with change in climate and CO_2 partial pressure.

iii) both the climate and atmospheric CO_2 value were changed so that there was warming and increased CO_2. This simulates a scenario that is likely to occur towards the middle of the 21st century when the actual atmospheric CO_2 is expected to be close to 56 Pa (IPCC, 1992) (Figure 5.7).

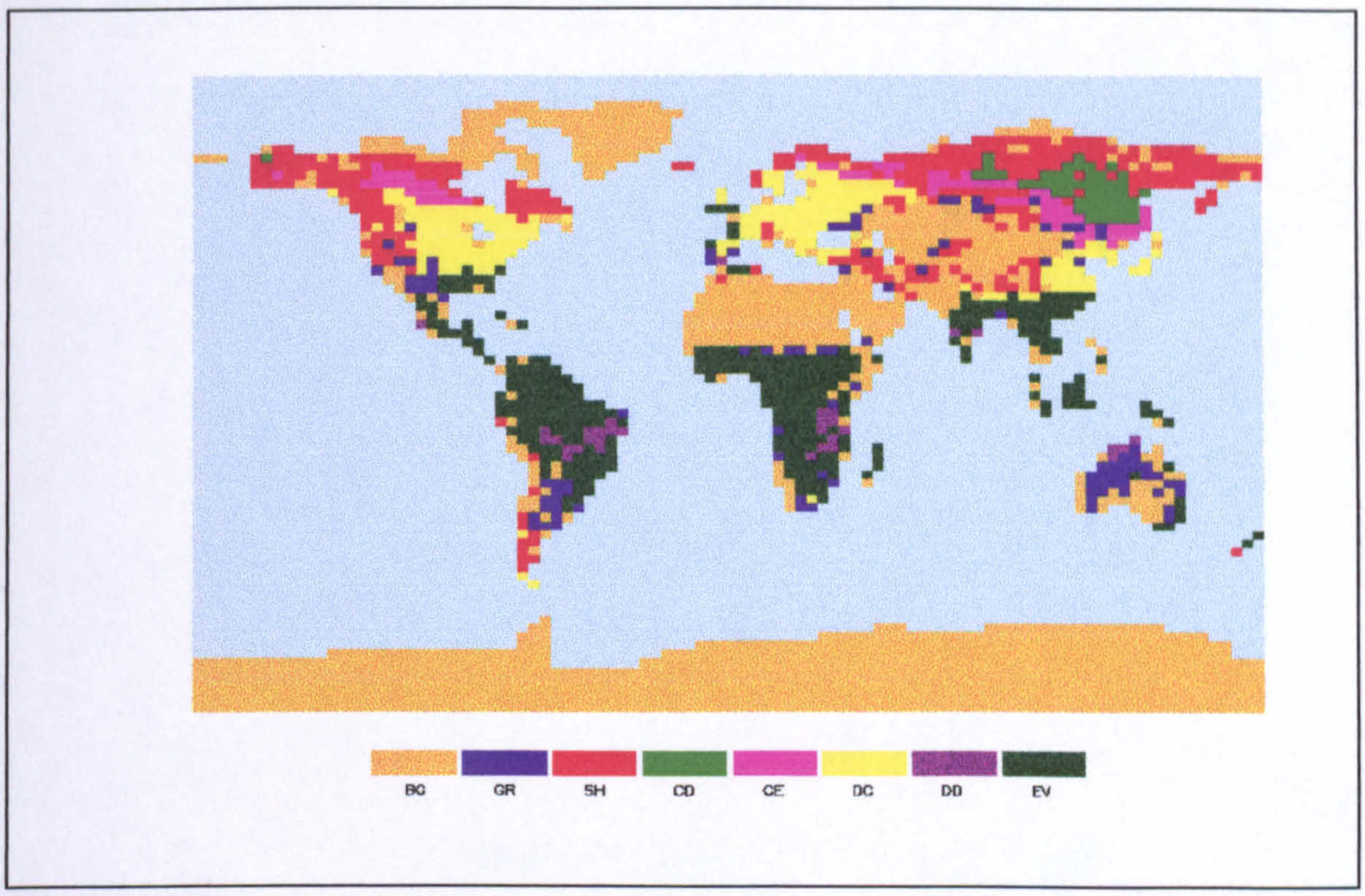

Figure 5.5 Functional types under current climate as simulated with the UK Meteorological Office high resolution (slab) model but with the CO_2 concentration increased from 35 to 56 Pa.

It should be stressed that the aim of this exercise was to ascertain the amount of influence of CO_2 on the different functional types in a climate change situation, and to show the change in the distribution of these functional types with a given climate change. In addition to warming alone, the slab data for a doubled-CO_2 climate also includes simulations from interactions between precipitation, humidity, cloud cover and other greenhouse gases due to this warming.

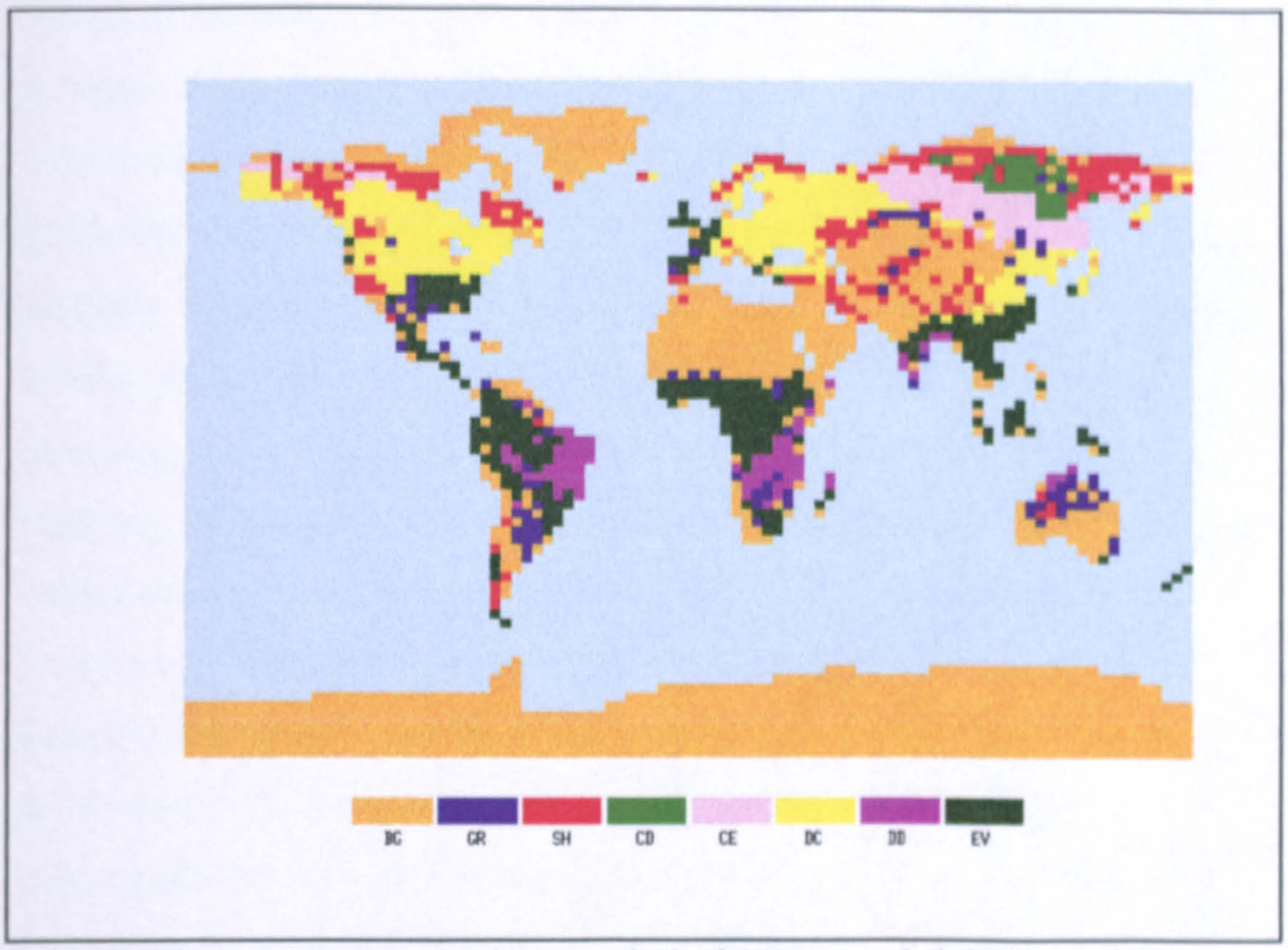

Figure 5.6 Functional types after a period of 50 years of global warming (+ 2°C, + 10% precipitation) but no increase in CO_2 partial pressure.

Figures 5.5, 5.6 and 5.7 show the new distributions of the functional types. Figure 5.5 shows that an increase in CO_2 has little impact globally on functional types, though there are interesting regional effects. For instance, in Angola, Zambia and Mozambique the functional type alters from drought deciduous tree to evergreen tree. In Argentina, the shift is from bare ground to grass, and, in a couple of cases, from grass to evergreen tree. The increases in the western U.S.A are for changes from, either grass or shrub, to cold deciduous tree, and, in northern China from bare ground to grass, or from grass to cold deciduous tree. Australia also sees a spread of grass at the expense of bare ground. A small number of cell changes occur in central Asia, and the main changes are for a change from grass to shrub, or vice versa, depending on water availability. It would appear, therefore, that increased CO_2 leads to greater water use efficiency in more arid areas and to a change from a functional type such as bare ground to grass, or from drought deciduous tree to

evergreen broadleaf tree. In the colder wetter areas, the increased CO_2 leads to a change in functional type from grass to shrub, or from shrub to tree. Figure 5.6 shows the effect of warming but with no change to CO_2. The most noticeable changes are the spread of cold deciduous trees northeastwards in northern Asia, replacing the coniferous evergreen trees and also the same shift moving northwestwards in northern Canada. In addition to these movements there is also a spread westwards of drought deciduous trees in northern Brazil replacing the evergreen broadleaf trees. Australia becomes more arid with grass being replaced by shrub or bare ground. Also there is a marked shift from evergreen broadleaf tree to bare ground along the coast from Venezuela to Brazil. This is almost certainly a feature of the slab model. These changes are to be expected in a warmer world where there is likely to be greater evapotranspiration leading to increased water loss in arid areas, and in the cooler, wetter regions such as in the high latitudes, trees are able to move into areas previously occupied by grass or shrub, due to the benefits of higher temperatures. Figure 5.7 shows the situation when both the CO_2 and climate are changed.

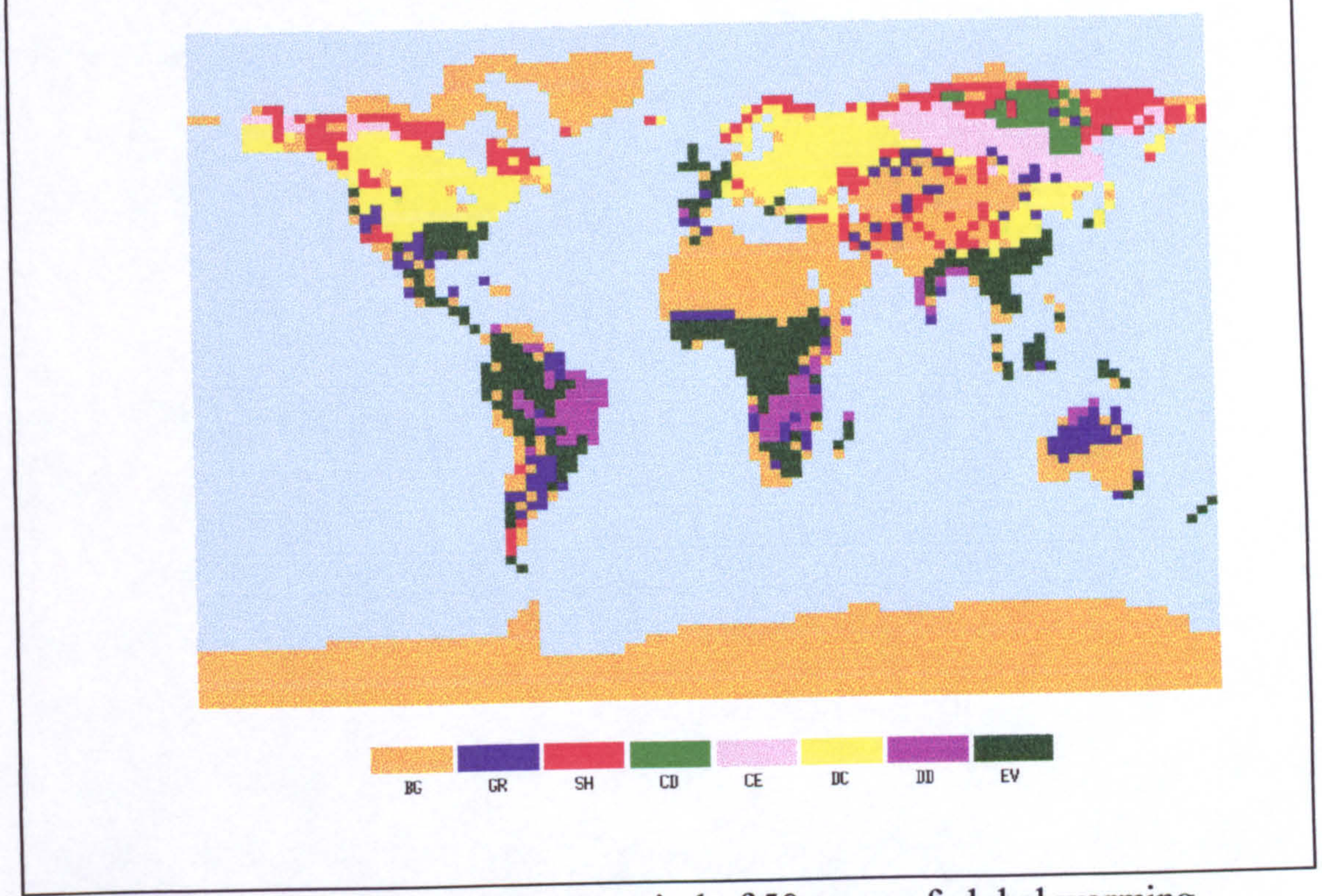

Figure 5.7 Functional types after a period of 50 years of global warming (+ 2°C, + 10% precipitation) and an increase in CO_2 concentration from 35 to 56 Pa.

At first glance, Figures 5.6 and 5.7 are very similar but on closer inspection some differences become evident. For instance, in arid areas such as central Australia and the northern savannah region of Africa (Figure 5.7), where grass was replaced by bare ground with warming, these effects have been offset slightly by increased CO_2. Also, in some cells in the western U.S.A., shrub has been replaced by grass with CO_2 and warming, but by cold deciduous trees with warming alone. The prairies are not predicted by the model partly due to the relatively high slab precipitation data for this region, but these results from the model also suggest that disturbance by fire or occassional drought is necessary to maintain grassland. To summarise, it appears temperature is the dominant component of this particular climate change scenario and that its influence far outstrips that of the CO_2 (compare figures 5.5, 5.6 and 5.7). The increased precipitation does not appear to be sufficient to counteract the increased evapotranspiration caused by the higher

temperatures. Carbon dioxide can have a moderating influence, in regions that suffer from drought by improving the water use efficiency of the vegetation.

The next section of this chapter investigates how tree cover and distribution change for the same scenarios as used in this section.

5.4.3 Climate change simulation of the cover and global distribution of trees.

The map of predicted current-day distribution of tree cover (Figure 5.8) was derived from the life-form model, which outputs the percentage cover of the four main functional types. From this output the percentage coverage for trees was extracted and plotted. The same errors arise as those with the dominant functional type, such as problems with the simulation of climate, and the assumption that the world's vegetation is completely natural, with no agricultural conversion included, as was mentioned in section 5.4.1. Woodward and Lee (1995) compared the model projections of percentage tree cover with the values derived from WHS for the same pixels. They found that 80% of the pixels were within ± 10% range of tree cover, which suggested that the major global patterns of tree cover were in good agreement. There were however marked regional differences in the projected cover. Looking at Figure 5.8 one can see how the greatest coverage of trees is in the tropics with values reaching 90%, cold deciduous forest has a coverage of around 40 to 50% and the boreal forest less than 30%. This map may be compared with Figure 5.9 which shows the actual distribution of global forests. It can be seen that the tropical rain forest in Africa is not as extensive as suggested by the model and that there is, in fact, very little forest outside the tropical rain forest areas in both Africa and South America. The forest map ignores savannah, but dense savannah could be classified as forest. The boreal forest and temperate forest regions appear to have been reasonably defined by the model but trees are shown in southern China where very few remain due to human conversions to agriculture.

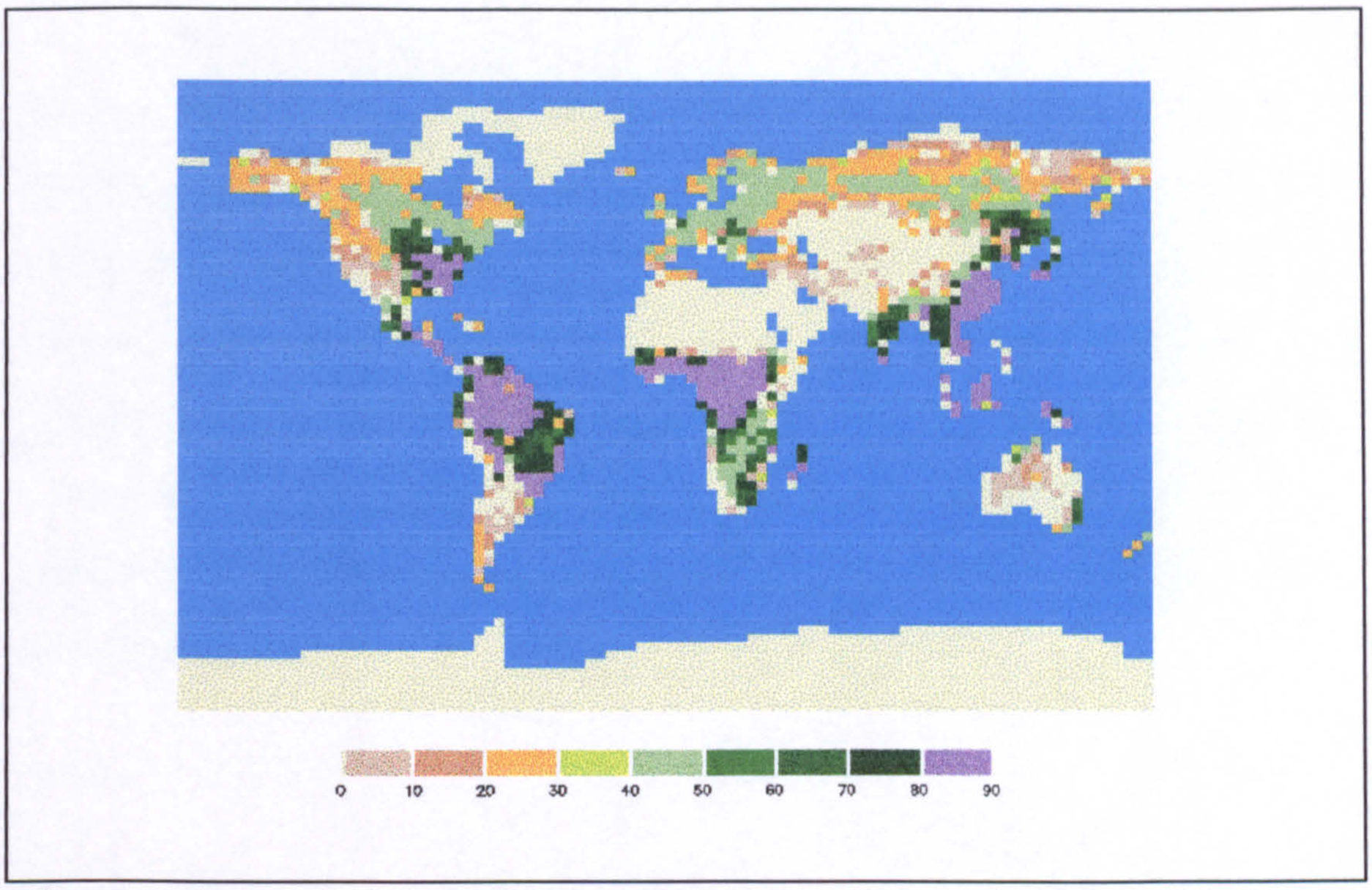

Figure 5.8 Present–day distribution of tree cover (%) as simulated with the UK Meteorological Office high resolution (slab) model.

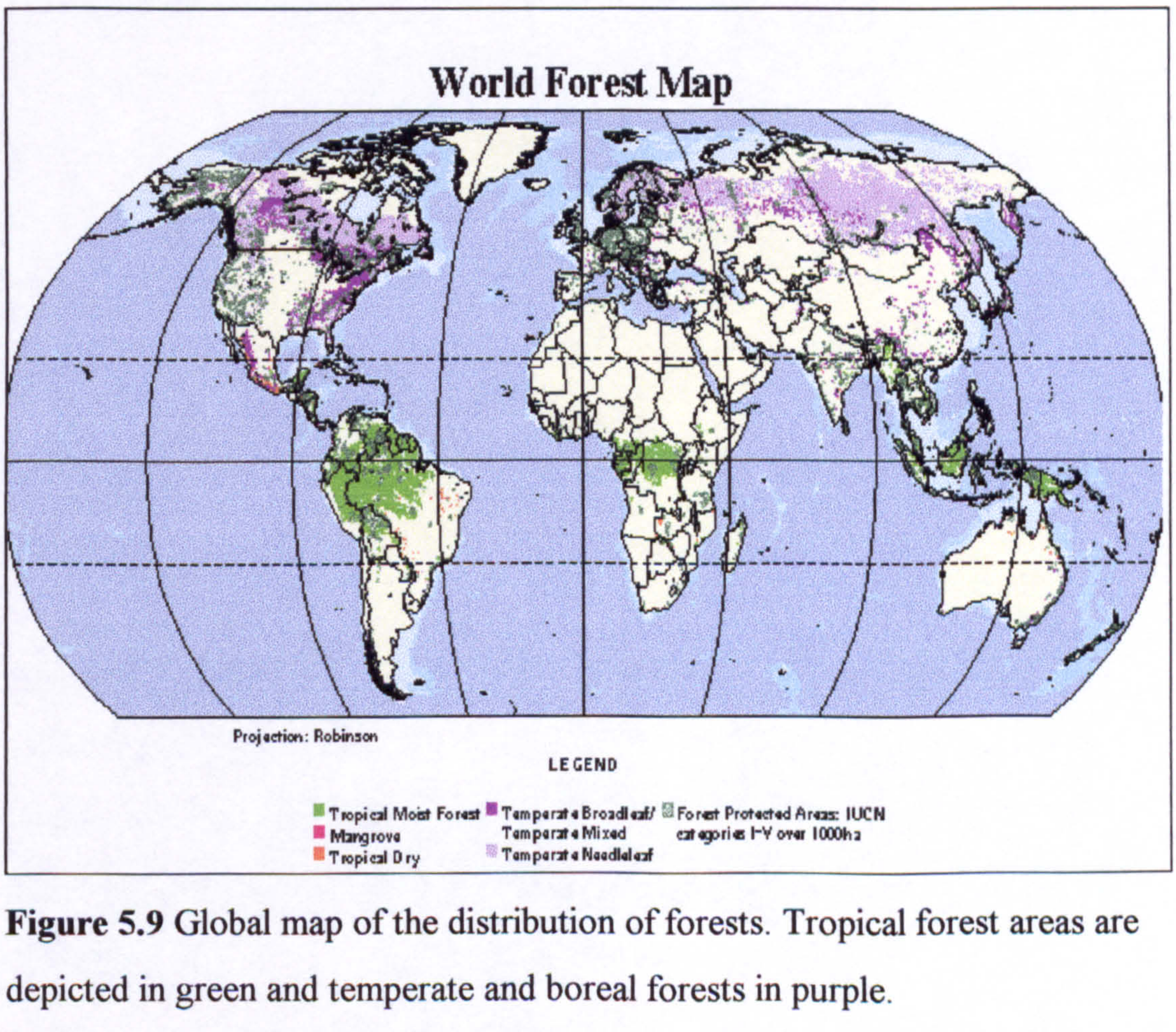

Figure 5.9 Global map of the distribution of forests. Tropical forest areas are depicted in green and temperate and boreal forests in purple.

Source: World Conservation Monitoring Centre (WCMC), Cambridge.

The same scenarios that were used for the functional type analysis were used to determine tree cover and the results are shown in Figures 5.10 to 5.12. The first scenario keeps the present-day climate but the atmospheric CO_2 within the model is increased from 35 to 56 Pa. The tree cover is calculated for 50 years of development under the current climate. With CO_2 enrichment alone (Figure 5.10), tree cover increases in southern Africa, eastern China, parts of central North and South America by around 10 to 30 percentage points, with some cells as high as 40 percentage points. In most cases the change in tree cover tends to be small (+/- 10–20 percentage points).

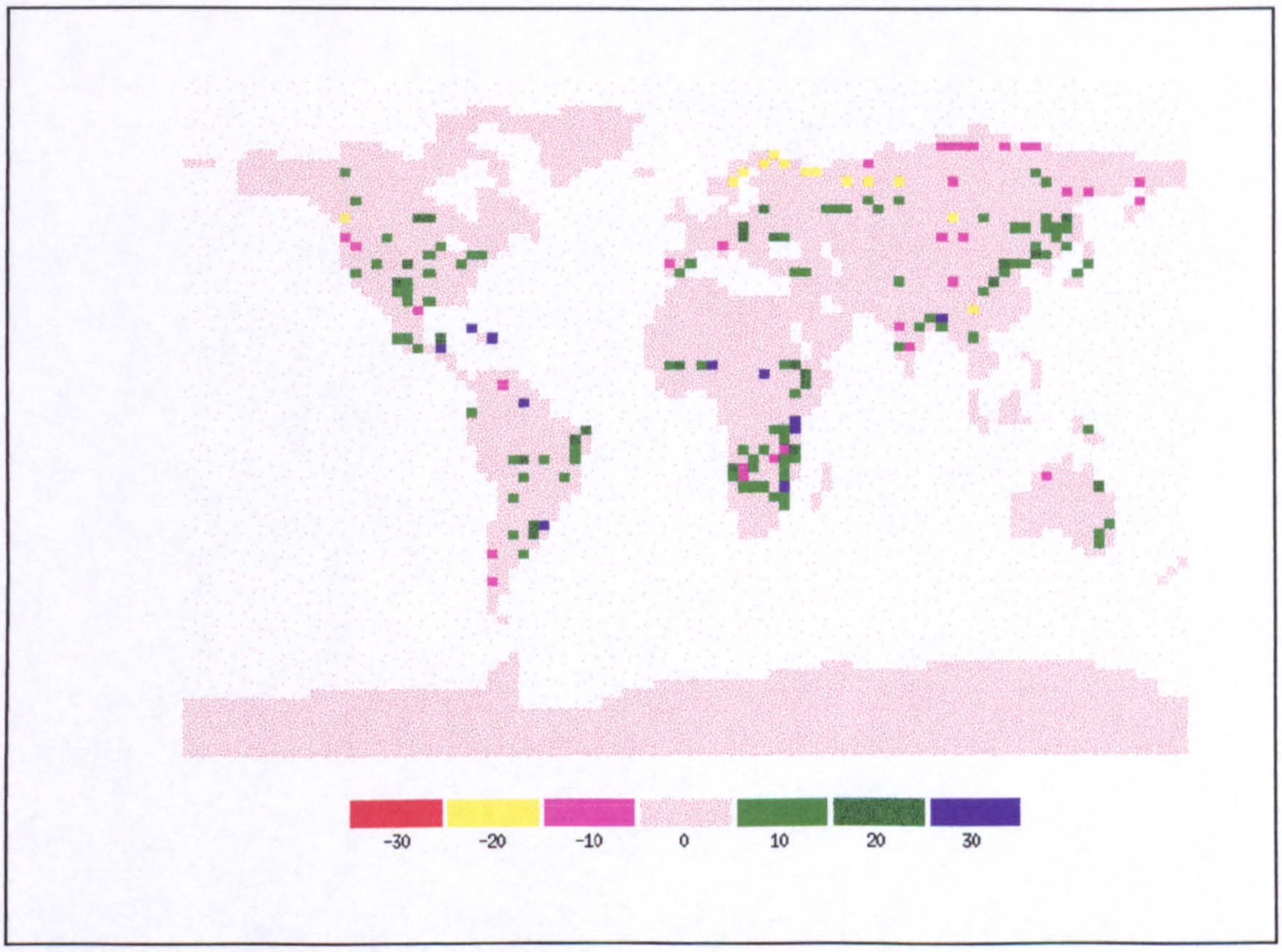

Figure 5.10 The change in global tree coverage (%) with an increase in atmospheric CO_2 from 35 Pa to 56 Pa over a period of 50 years. Positive values represent cells that have a higher percentage tree cover with elevated CO_2 than with the current climate. Negative values represent cells where the reverse is true.

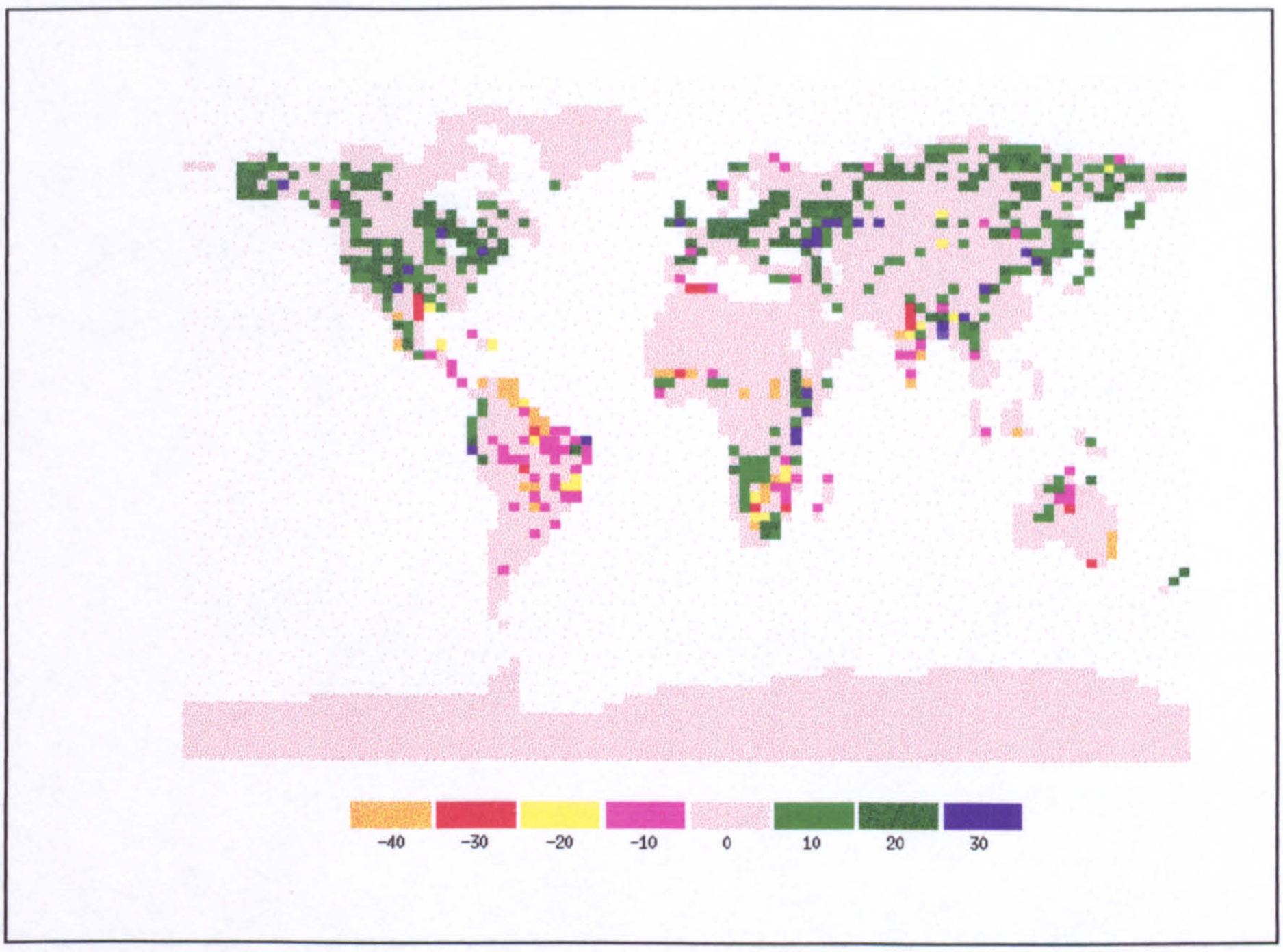

Figure 5.11 The change in global tree coverage (%) after a period of 50 years with an increase in temperature and precipitation (2°C and + 10% precipitation). Positive values represent cells that have a higher percentage tree cover with global warming than with the current climate. Negative values represent cells where the reverse is true.

Figure 5.11 shows the change in tree cover with the climate changes but with no CO_2 increase. Trees increase by the order of 10 to 30 percentage points in the boreal regions of both North America and northern Asia at the expense of shrub. This will lead to changes in the surface albedo (reflectivity) in these high latitudes as shrubs and bare ground have high winter albedos when covered by snow and trees have lower albedos even after snowfall. This means that the boreal regions are likely to experience further warming with greater absorption of solar radiation as trees spread northwards (Foley *et al.*, 1994; Bonan *et al.*, 1992; Betts *et al.*, 1997). In the warmer regions of the world, trees also increase and this is associated with the increase in precipitation in western China, Angola and Zambia. Elsewhere, there are decreases in tree

cover, because warming increases evapotranspiration, which is not offset by increases in precipitation. For instance, in Mozambique and along the coast from Venezuela to Brazil in South America there are decreases of 10 to 40 percentage points. These differences also occur in these areas when CO_2 is included as well (Figure 5.12).

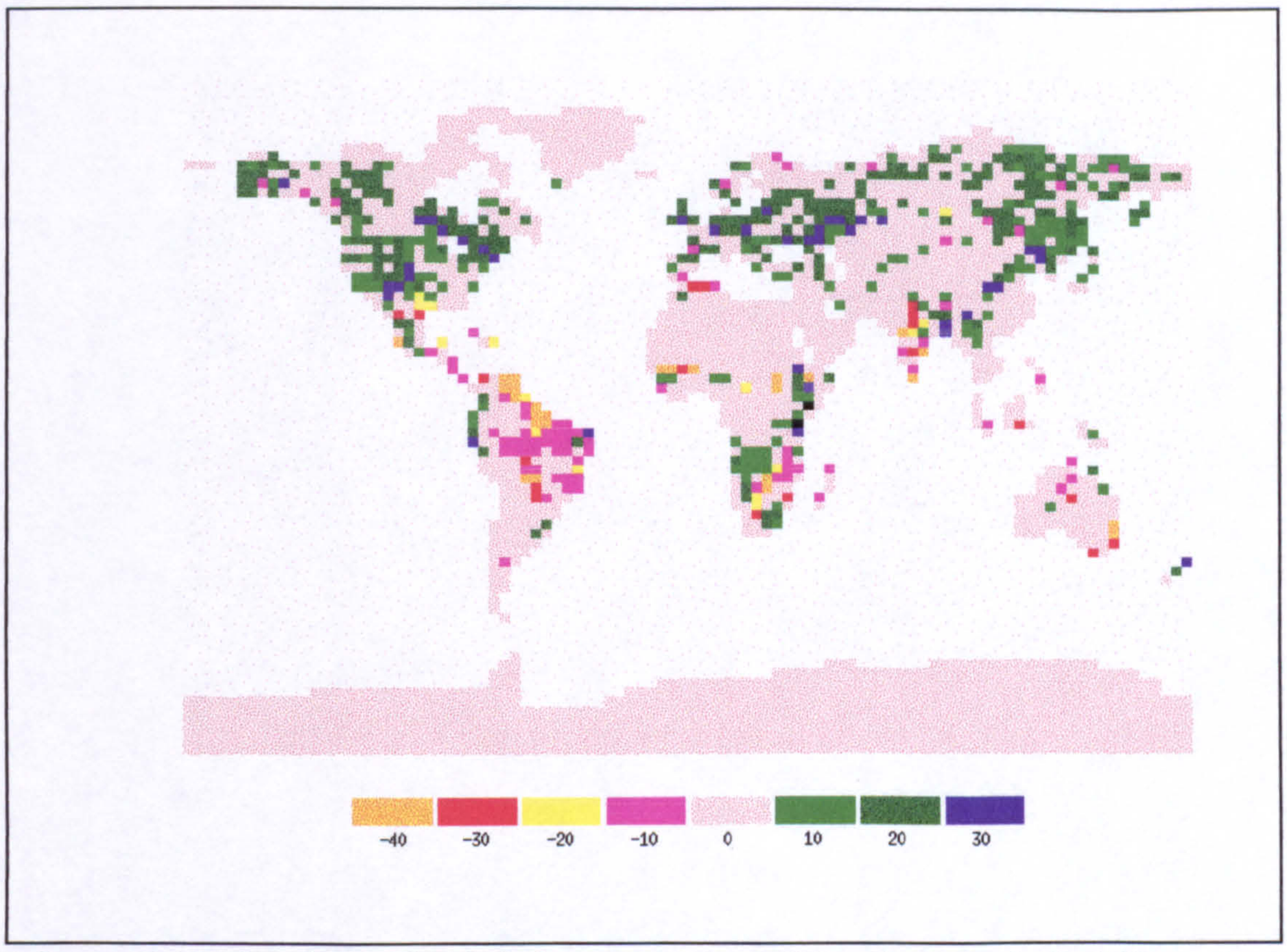

Figure 5.12 The change in global tree coverage (%) after a period of 50 years with an increase in temperature and precipitation (2°C and + 10% precipitation) and elevated CO_2 (from 35 Pa to 56 Pa). Positive values represent cells that have a higher percentage tree cover with the climate change scenario than with the current climate. Negative values represent cells where the reverse is true.

In most cases the climate effect is dominant over the CO_2 effect, but in a few cells, CO_2 moderates the effect of climate. For example, in northern Australia some cells show increased tree cover from the increased temperature and precipitation, but with increased temperature, precipitation and CO_2 there is no change in tree cover.

5.4.4 A case study—the boreal forest–tundra boundary

Many authors (Bonan *et el.*, 1990,1992; Shugart *et al.*, 1986; Solomon, 1986; Lenihan, 1993) have suggested that the area likely to be affected most by climate change is the boreal forest, and particularly in the transition zone between boreal forest and tundra. From the work carried out in the previous section and from an examination of Figure 5.12 it can be seen that there is an increase of tree cover both in Canada and the former U.S.S.R. with CO_2 enrichment and elevated temperature. From Figure 5.7, this can be linked to the spread of coniferous deciduous trees, coniferous evergreen trees and temperate deciduous trees into shrub areas. In order to quantify these changes, the area north of 55°N was examined and the number of cells with each functional type was calculated for each scenario. The area for a 2.5° × 3.75° cell between 60°N and 70°N is about 53,000 km^2, and this area decreases with latitude. The most northerly cell in the slab dataset occurs at latitude 82.5°N. Shrub was classified as the tundra biome, and coniferous evergreen added to coniferous deciduous tree, to create the boreal forest biome. Table 5.5 shows the results of the three different climate scenarios for the boreal forest and tundra alone and Table 5.6. for all the functional types

Table 5.5 shows how the tundra and boreal forest categories change with climate change. The tundra actually benefits from CO_2-enrichment but is reduced by just under a third with warming and with climate change. The boreal forest cover increases by about a fifth with climate change but is reduced

with elevated CO_2 alone, which affects the coniferous evergreen trees (see Table 5.6).

Table 5.5 The changes in the number of cells north of 55°N for the boreal forest-tundra boundary with change in climate and CO_2.

Biome	Current Climate	Elevated CO_2	Warming	Elevated CO_2 & warming
Tundra	164	170	114	116
Boreal Forest	45	40	58	58

There are fewer cells covered by boreal forest and tundra in total after climate change due to the fact that temperate deciduous trees have replaced some of the boreal forest on its southern edges, as well a few of the tundra cells.

Table 5.6 shows that coniferous evergreen trees increase from the present-day coverage with warming but decrease with CO_2-enrichment. The combined effect is the same as with warming alone and there is an increase. Coniferous deciduous tree cover decreases with both warming and climate change but there is no change in the cover with CO_2 alone. CO_2 appears to have no effect on the broadleaf deciduous trees in the region but warming and CO_2 cause almost a trebling in the cover. Shrubs increase slightly with elevated CO_2 but decrease with both warming and climate change by about the same amount.

Table 5.6 The number of cells (2.5° × 3.75°) north of 55 °N for each functional type and for each scenario of increased CO_2 alone, warming alone and climate change.

Functional Type	Current Climate	Elevated CO_2	Warming	Elevated CO_2 & warming
Bare Ground	250	250	243	243
Grass	1	0	1	0
Shrub	164	170	114	116
Trees:				
Coniferous Deciduous	19	19	15	15
Coniferous Evergreen	26	21	43	43
Broadleaf Deciduous	14	14	57	56
Broadleaf Evergreen	0	0	1	1

5.5 Discussion

This chapter has shown how it is possible to model, in two stages, the movement of dominant functional types with changes in climate and CO_2 concentration. This has been achieved using the LAI and NPP for a site and in a life-form model, to predict changes of tree, shrub and grass over a 50 year time-scale. Errors have arisen in areas where the slab GCM input data have been inaccurate but also in comparison with the present-day map of current vegetation. It has therefore been difficult to ascribe errors due to the vegetation model itself, due to the input to the model or due to errors in the current vegetation standard.

Despite these problems this approach has shown how tree cover varies with changes in climate and the atmospheric CO_2 concentration. Warming alone has the greatest effect leading to the spread of trees into tundra regions, as shown by the case study. However, although CO_2 does not have much of an impact on its own, its effect is greater in combination with climate change. This is due to interactions between CO_2 and climate which affect stomatal conductance, photosynthesis and nutrient uptake (Woodward *et al.* 1991).

Changes in the distribution of trees and their coverage are likely to affect the global climate through albedo changes, particularly winter albedo in regions with snow in the high latitudes leading to increased surface warming (Foley *et al.*, 1994). In the tropics, greater numbers of trees will lead to an increase evapotranspiration and to an increase in cloud cover. This, in turn, will lead to increased precipitation and lower surface temperatures.

The life-form model operates on the basis that it is possible for a functional type to move anywhere in the world. These movements are theoretically possible but obviously in the real world, human influence will determine the actual spread, as will the actual ability of the trees to adapt to a new niche with a different daylength and growing season. There is no disturbance in this version of the model which means that the tree functional type occurs in grassland areas which are disturbed, such as the savannahs, as

well as in some areas where crops exist. Disturbance is an important process and more recent developments of the vegetation model have an element of disturbance within them, leading to a more accurate prediction of some present-day functional types.

CHAPTER 6

6.0 Modelling the interaction between vegetation and climate through the use of a general circulation model — an application of the DOLY model.

6.1 Introduction

The sensitivity analysis performed earlier in this thesis (Chapter 4) has demonstrated how climate can influence structural variables of vegetation, such as LAI, and functional variables, such as NPP. However, vegetation also influences climate itself, through interactions with the planetary boundary layer. The vegetated surface influences fluxes of latent and sensible heat, as well as shortwave and longwave radiation. Climate variables, such as precipitation, and temperature, together with evapotranspiration are the main determinants of the distribution of current global vegetation, as demonstrated by several authors (Woodward, 1987; Holdridge, 1947; Box, 1981). However, other factors, such as soils, fire occurrence, glaciation and human influences also need consideration.

At the moment, very few general circulation models (GCMs) take account of any feedbacks that may be occurring between vegetation and climate. The work done in this field includes that by Claussen (1994, 1996) who coupled the BIOME model (Prentice *et al.*, 1992) with the ECHAM model of the Max-Planck-Institut für Meteorologie, and Sellers and co-workers (1996) who examined the effects of feedbacks on stomatal conductance for a doubled-CO_2 climate. Vegetation in most GCMs is, in effect, fixed in time.

This is an unsatisfactory situation, as a number of authors (Rowntree, 1988; Sellers *et al.*, 1996; Henderson-Sellers *et al.*, 1995) have demonstrated that climate is sensitive to the land surface cover in GCM simulations. Also, to simulate climate change effects accurately, there needs to be inclusion of an interactive global vegetation. This would also enable the prediction of future vegetation given a future climate.

This chapter has a number of objectives:

i) to demonstrate an application of the DOLY model in a GCM context;

ii) to determine whether vegetation does, in fact, affect the climate of a GCM;

iii) to determine the effect of climate change on values of LAI and NPP using the climate predictions from a GCM;

iv) to determine the effect of climate change and vegetation feedbacks on a GCM climate.

This chapter is the result of collaborative work with Dr. Peter Cox and Mr. Richard Betts of the Hadley Centre, part of the United Kingdom Meteorological Office (UKMO). They are members of the TIGER IV 3b consortium, which was funded by the Natural Environment Research Council (NERC). The division of work is shown in Table 6.1.

Table 6.1 Work undertaken by Professor Ian Woodward, Dr. Peter Mitchell, Dr. Peter Cox, Mr. Richard Betts, and myself, Susan Lee, as part of the TIGER IV 3b consortium. The results from this work are presented in this chapter.

Name	Work undertaken
Susan Lee, University of Sheffield	i) Supply of the DOLY model to the Hadley Centre. ii) Discussion with Peter and Richard concerning the DOLY model's inputs and operation.
Dr. Peter Cox, Hadley Centre.	i) Initial feedback runs with the DOLY model and the GCM. ii) Calculation of the vegetation parameters used by the GCM from the DOLY output variables. iii) Supply of vegetation feedback maps. iv) Supply of NDVI and LAI maps.
Mr. Richard Betts, Hadley Centre.	i) Later feedback runs with the DOLY model and the GCM. ii) Supply of albedo and temperature maps for March
Professor Ian Woodward and Dr. Peter Mitchell, University of Sheffield.	Additional advice concerning the interpretation of the results from the model runs.

6.2 Model description

The United Kingdom Meteorological Office (UKMO) Unified Forecast and Climate Model is a full Ocean–Atmosphere model. It has 19 vertical layers through the atmosphere; four soil layers; and 20 layers within the ocean. Additional information about this model and its response to increasing levels of greenhouse gases and sulphate aerosols is given in Mitchell *et al.*, (1995). A more simplified climate version of this is the Hadley Centre atmosphere + mixed-layer ocean model (slab model), which is quicker and easier to run. The paper by Jones *et al.* (1995) contains more details of this particular model. This model can reach equilibrium in under 15 years and represents the ocean with a 50m-deep mixed layer, with thermodynamic interaction with the atmosphere and prescribed ocean currents. There is a coupling of the atmosphere and the ocean model, which allows a reasonable representation of the seasonal cycle. For the following study, the slab model runs with a low resolution of 5.0 degree latitude by 7.5 degree longitude (1728 cells globally). However, runs of the model at a high resolution (2.5 degree latitude by 3.75 degree longitude) are also possible (6912 cells globally). There is a detailed description of the DOLY model in Chapter 2 and in Woodward *et al.* (1995). The standard DOLY version is used here. The results presented in this chapter are mainly for the low resolution data, but for additional results from the high resolution data see Betts (Ph.D. thesis in preparation) and Betts *et al.* (1997). This chapter concentrates on quantifying the feedback associated with the response of vegetation to the equilibrium climate for doubled-CO_2 concentration.

6.3 Methods

DOLY and the GCM were coupled by iterating between the two models. Both DOLY and the slab GCM perform simulations under steady–state forcing conditions, so it is possible to iterate between separate simulations by each model. This is termed asynchronous coupling. The output of one model becomes input into the other, as shown in Figure 6.1.

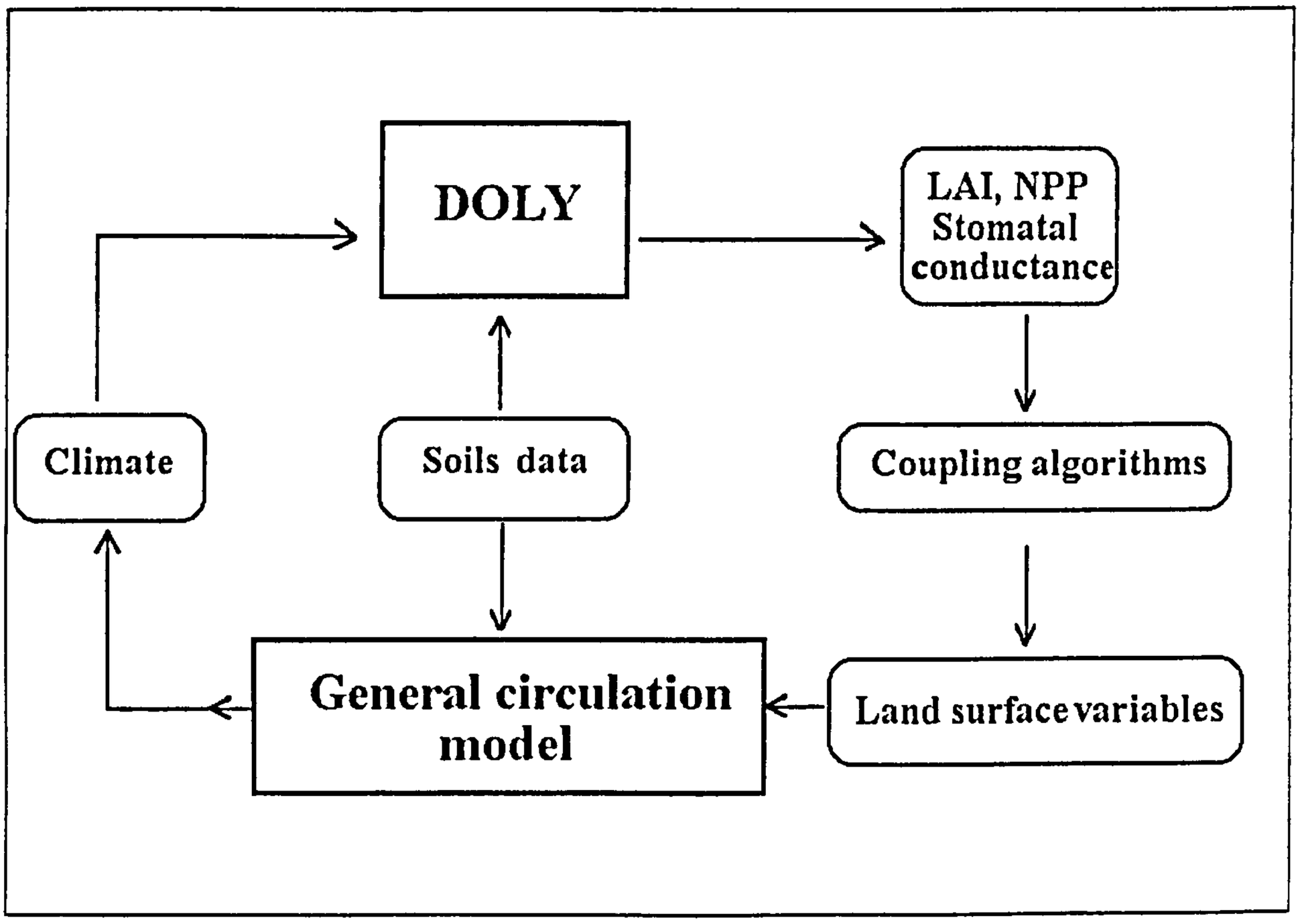

Figure 6.1 The asynchronous coupling approach. The values of the land surface variables are estimated directly from the vegetation properties predicted by DOLY using the coupling algorithms. The DOLY model uses soil carbon and nitrogen data, whereas the GCM uses data on soil colour and texture from the WHS dataset (Wilson and Henderson-Sellers, 1985), as its soils data input.

Before the coupling took place, there was a run of the DOLY model with the slab climate data to ascertain whether it was able to represent reasonably the LAI of the current vegetation. To do this, there was a visual comparison of the LAI output by the DOLY model with a map of normalized

difference vegetation index (NDVI). This visual comparison was just intended to provide a rough indicator as to whether the DOLY model predicted the correct global pattern of LAI values, rather than focusing on the actual values themselves at this stage. The calculation of NDVI uses satellite data of red and infra-red longwave radiation. The amount of red radiance is inversely proportional to the amount of chlorophyll and is sensitive to green or photosynthetically active radiation (PAR). The near infra-red (NIR) band is sensitive to green or photosynthetically active (PA) vegetation and to a lesser extent dead or non PA vegetation The red and infra-red reflectance when ratioed as a normalized difference indicates the relative vigour of vegetation in relation to its chlorophyll concentration and leafiness.

$$NDVI = (NIR–R)/(NIR+R) \quad \textbf{(6.1)}$$

where

R is 560–680 nm (visible red band), with strong absorption by chlorophyll, and NIR is 725–1100 nm (near infra-red), which is not absorbed by chlorophyll .

Figure 6.2 shows the LAI, as simulated by DOLY, and driven by slab data, on a 2.5° by 3.75° grid (high resolution) and a map of NDVI on a 1° by 1° grid (Tarpley *et al.*, 1984). The general patterns of LAI agree mostly with those of NDVI except in agricultural areas, where there is no natural vegetation. This occurs in eastern China, and in regions where there is strong rainfall seasonality such as India and south–east South America. The savannah regions of Africa have a high LAI output compared to the NDVI values. This is because DOLY is not able to account for fires that have the effect of reducing LAI.

There have been a number of studies on crops and individual plant species which have found correlations with LAI and NDVI. For instance, Daughtry *et al.*, (1984) used the NDVI in their study of crop canopies and found that there was a high correlation with LAI and absorbed photosynthetically active radiation (APAR). Rice *et al.* (1980) also used this

index with APAR and LAI and showed that NDVI closely mirrored LAI through the growing season for wheat. However, for several different species the relationship is more complex. It is not easy to make a quantitative comparison between NDVI and LAI due to the fact that the NDVI varies with vegetation type as well as LAI. For instance the shape and angle of leaves, leaf moisture and leaf age can all affect reflectance. Also, differences arise from different canopy heights and structures: arable crops have lower canopies and near random or slightly regular leaf angle distributions but forest stands have higher canopies and leaves clustered in the canopy. In addition to this, once an LAI of 5 is reached there tends to be no further increase in NDVI due to saturation effects. No distinction can be made between LAI values that are greater than 5. To overcome some of these problems, separate equations can be used for each vegetation type, for example grass, needleleaf and broadleaf canopies. This is the approach used by Nemani and Running (1995, 1996) to ascertain LAI from NDVI with a knowledge of the underlying vegetation. Also, the NDVI varies through the year, whereas DOLY predicts the maximum LAI that is able to be sustained for the year. It was therefore decided that a simple qualitative comparison would suffice at this point in order to give an indication that the DOLY model was producing reasonable results. More recent work with the SDGVM (Sheffield Dynamic Global Vegetation Model) which incorporates the DOLY model, has used the NDVI in order to attempt to validate LAI and NPP from the SDGVM. The results are presented and discussed in Chapter 9.

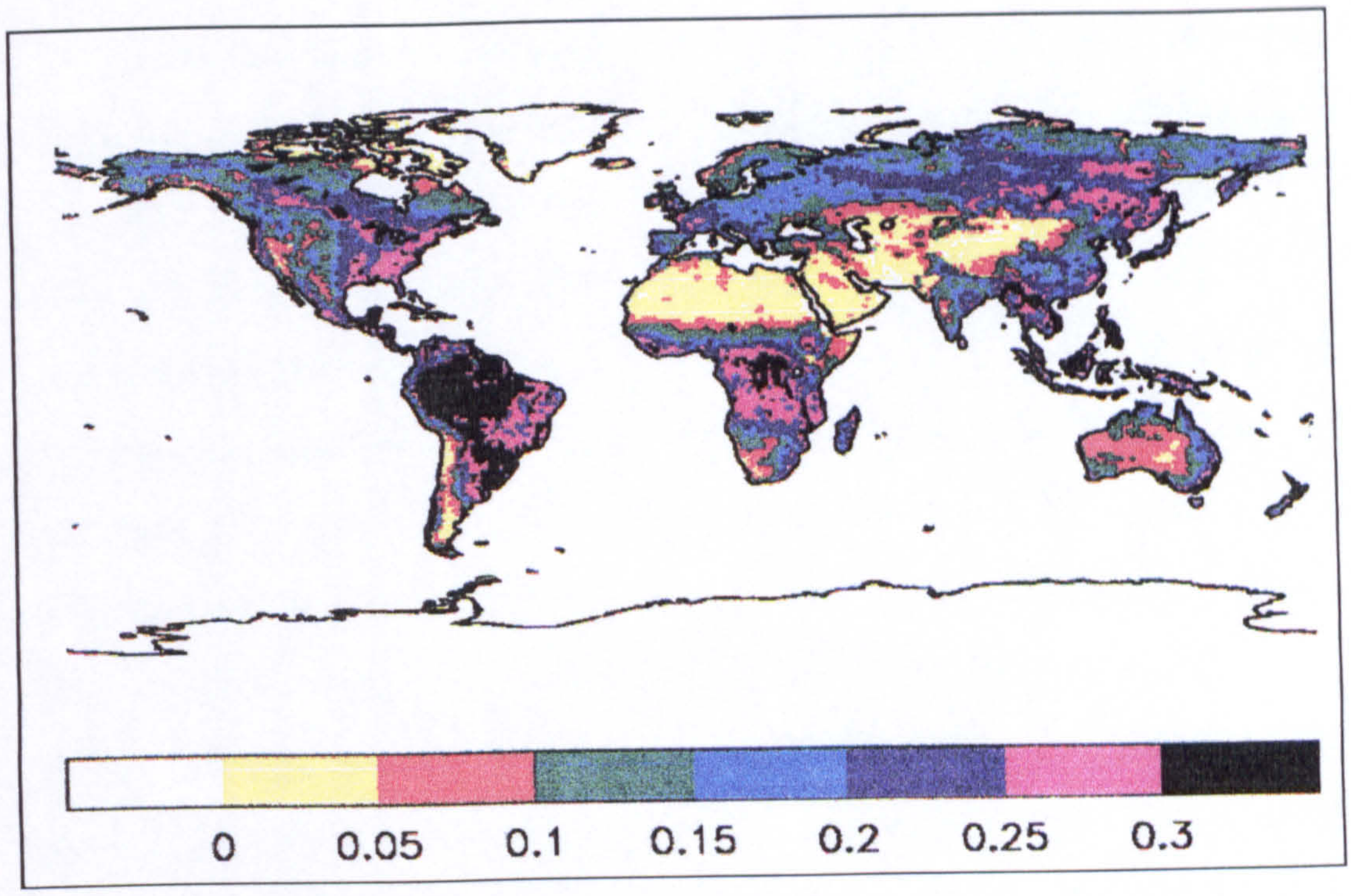

a) Normalized difference vegetation index (NDVI). NDVI values are means over the period July 1983 to June 1984 derived from radiances measured by the AVHRR sensor on the NOAA–7 satellite

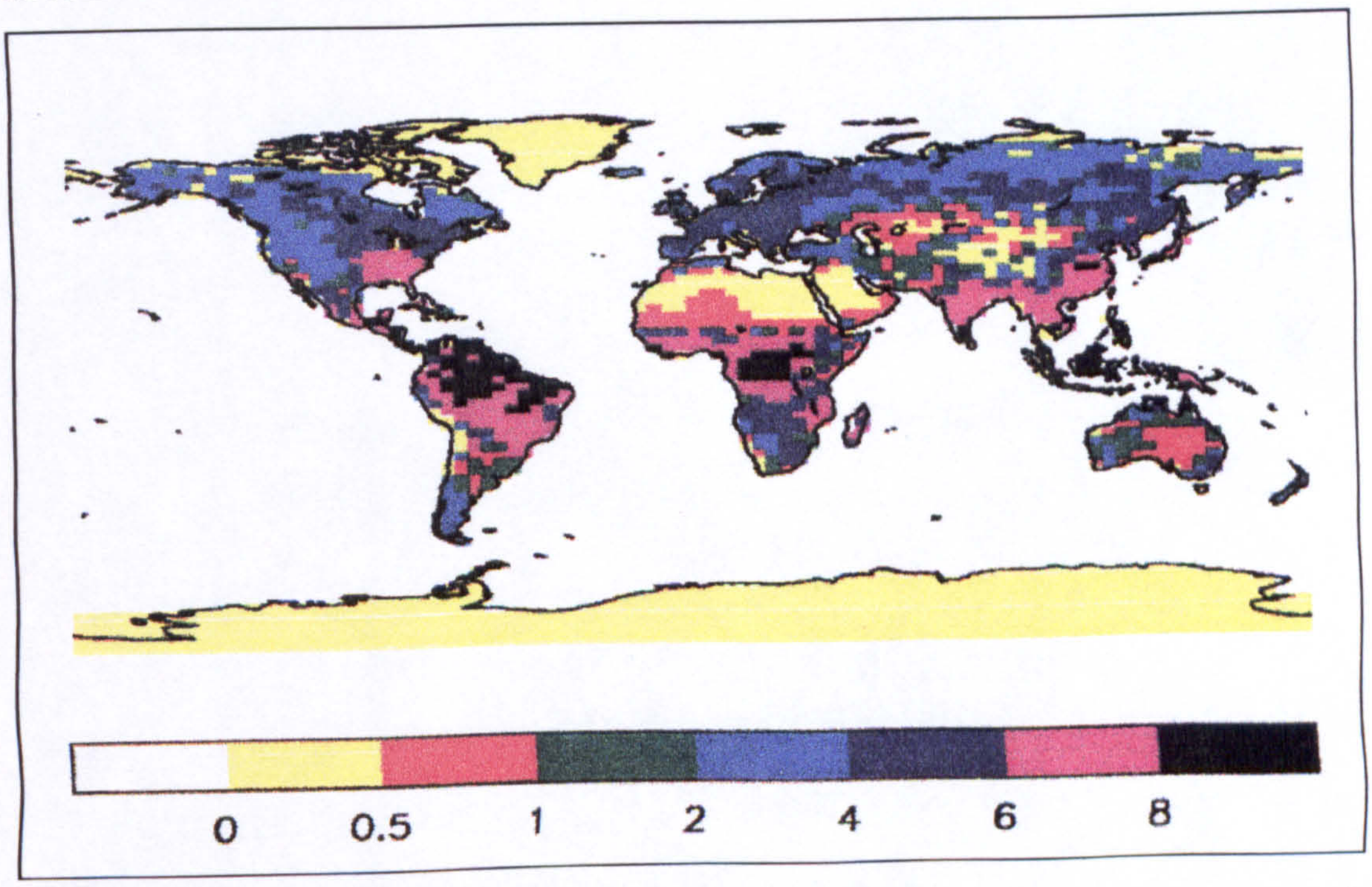

b) Leaf area index. A run of the DOLY model with data from a GCM simulation of current climate predicts these values.

Figure 6.2 Comparison of the LAI predicted by the model DOLY with the observed normalized difference vegetation index (NDVI).

The next stage was to derive the vegetation variables required by the GCM. To do this, Dr. Peter Cox from the Hadley Centre used the LAI values from DOLY to calculate a number of these variables by empirical and physically-based relationships (see Appendix 1). Note that there is the assumption that the NPP and surface resistance provided by DOLY apply to the vegetated fraction of the gridbox only. Also, the LAI from DOLY is the gridbox mean value. LAI has an impact on many GCM variables. For instance, as LAI increases, canopy storage capacity (the amount of water that remains on the vegetation canopy once it has saturated and throughfall is running) increases, but the albedo, (the amount of radiation reflected from the earth's surface) decreases. An exponential relationship is used to derive the vegetated fraction from LAI (see equation 1 in Appendix 1). Beyond an LAI of four, (where the vegetated fraction is close to 80%) the rate of increase of vegetated fraction declines. At an LAI of nine there is a 100% vegetated fraction. The derivation of mean canopy height also uses LAI. The snow-free albedo can be calculated from the effective albedo vegetated fraction using the two stream solution of Sellers (1985). This albedo is calculated for the LAI of the vegetated area with underlying soil, and the soil (or ice) albedo derived from the WHS (Wilson and Henderson-Sellers, 1985) map of soil colour classes. The deep-snow albedo calculation is similar. This calculation adds a constant value of 0.8 for the deep-snow albedo of bare soil or ice to an annual mean albedo of the vegetation fraction with underlying snow. Root depth, canopy capacity and infiltration enhancement factor are also calculated from the vegetated fraction. Shaw and Pereira (1982) demonstrated how roughness length increases with LAI but then starts to decline once the full canopy develops and the surface becomes smooth. Roughness length determines the boundary layer conductance. The calculation of surface resistance uses the mean canopy stomatal conductance output from DOLY and the vegetated fraction, and the resistance calculated for bare soil and ice.

The determination of the GCM variables then enabled the performance of the asynchronous coupling as illustrated in Figure 6.3. This involved the following steps.

i) The GCM was run with the land surface characteristics derived from the WHS dataset (Wilson and Henderson-Sellers, 1985) to simulate climate at the 1980 CO_2 concentration (323 ppmv) called $1 \times CO_2$.

ii) DOLY was then run with this simulated climate in order to obtain a simulation of 1980 vegetation.

iii) This simulated vegetation was then used in a further GCM integration with the 1980 CO_2 concentration to give a further climate simulation.

iv) Steps ii) and iii) were repeated until the iterations caused no further significant change. This was a qualitative assessment and occurred after a couple of years. This gives mutually consistent simulations of 1980 climate, C1, and vegetation, V1.

v) A GCM integration with the CO_2 concentration doubled to 646 ppmv, called $2 \times CO_2$ used the vegetation state, V1, providing a climate change simulation with no vegetation feedback. This climate is called C2.

vi) DOLY is then used to simulate a vegetation with $2 \times CO_2$.

vii) This new vegetation, V2, was then used in a further GCM simulation with $2 \times CO_2$.

viii) Stages vi) and vii) are repeated until there is no significant difference between iterations (as explained in iv). This gives mutually consistent simulations of climate, C3, and vegetation, V2 with $2 \times CO_2$ climate.

The effect of vegetation feedback on doubled-CO_2 climate is then described by the differences between climates C3 and C2.

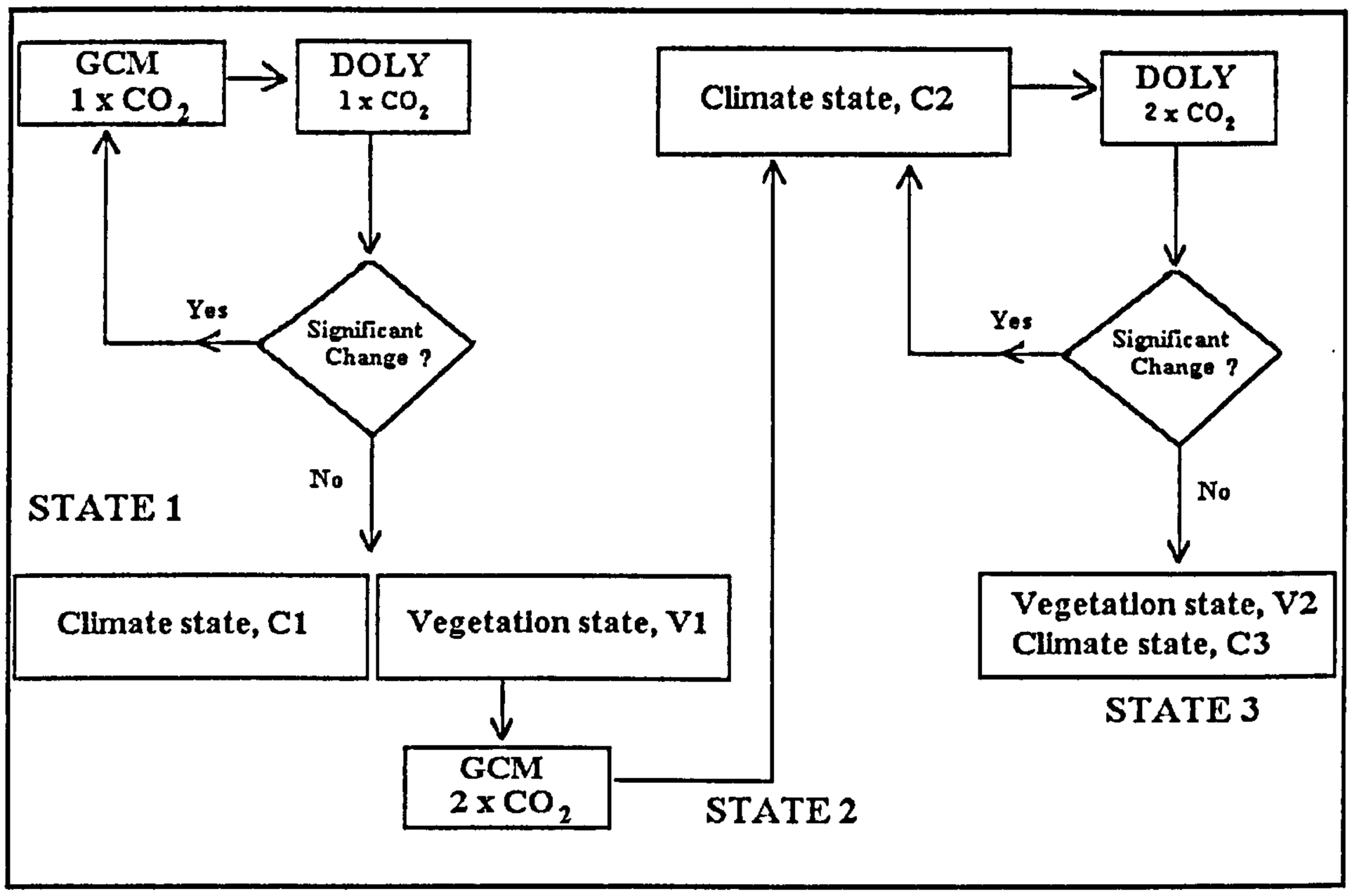

Figure 6.3 The procedure adopted to simulate climate and vegetation for differing concentration of CO_2.

State 1 occurs when the climate C1, and vegetation V1 are mutually consistent for $1 \times CO_2$.

State 2 occurs when the GCM runs with $2 \times CO_2$ and no vegetation feedbacks.

State 3 occurs when the climate C3, and vegetation V2 are mutually consistent for $2 \times CO_2$.

6.4 Results

Figures 6.4 to 6.7 present the results from the coupling processes between DOLY and the GCM. Maps supplied by Dr. Peter Cox and Richard Betts of the Hadley Centre have been used to produce these figures. These data are for the low resolution of the GCM, that is a 5° × 7.5° global grid.

Three scenarios were examined:

i) The climate change due to increased CO_2 with no vegetation feedbacks (Figure 6.3, State 2). This is the difference between C2 and C1. The results are shown in Figure 6.4. Global mean surface temperature increases by 2.5 K and the precipitation by 0.1 mm day^{-1} using this scenario. Figure 6.4a shows how a large part of the land surface experiences temperature rises of between 1 and 5 K but temperature falls of 1 to 2 K in small areas of eastern Siberia and southern Brazil. Figure 6.4b shows how the precipitation varies spatially with increases of 1 mm day^{-1} in eastern Africa and southern India, and decreases of 1 mm day^{-1} in Cameroon, Venezuela and eastern Brazil. These results differ slightly from the results from the high resolution (2.5° × 3.75° global grid) version of the slab model which are presented in Betts *et al.*, (1997). They showed that the global mean surface temperature increased by about 4 K with increased CO_2 and no vegetation feedbacks. Also, much of the land surface experienced greater temperature rises than the low resolution model, of 4 to 8 K. In the case of precipitation, much of the world experienced increases of up to 1 mm per day. The greatest increases of around 2 mm per day (equivalent to an annual increase of 730 mm) occurred in Zaire and Malaysia. There were also areas of decrease of the same magnitude in northern South America, southern Europe and south-western parts of Asia. The areas with large increases in precipitation also receive a high annual total so in percentage terms these increases would be less significant than they would be in an arid area.

The differences that occur between the two resolutions of the model are

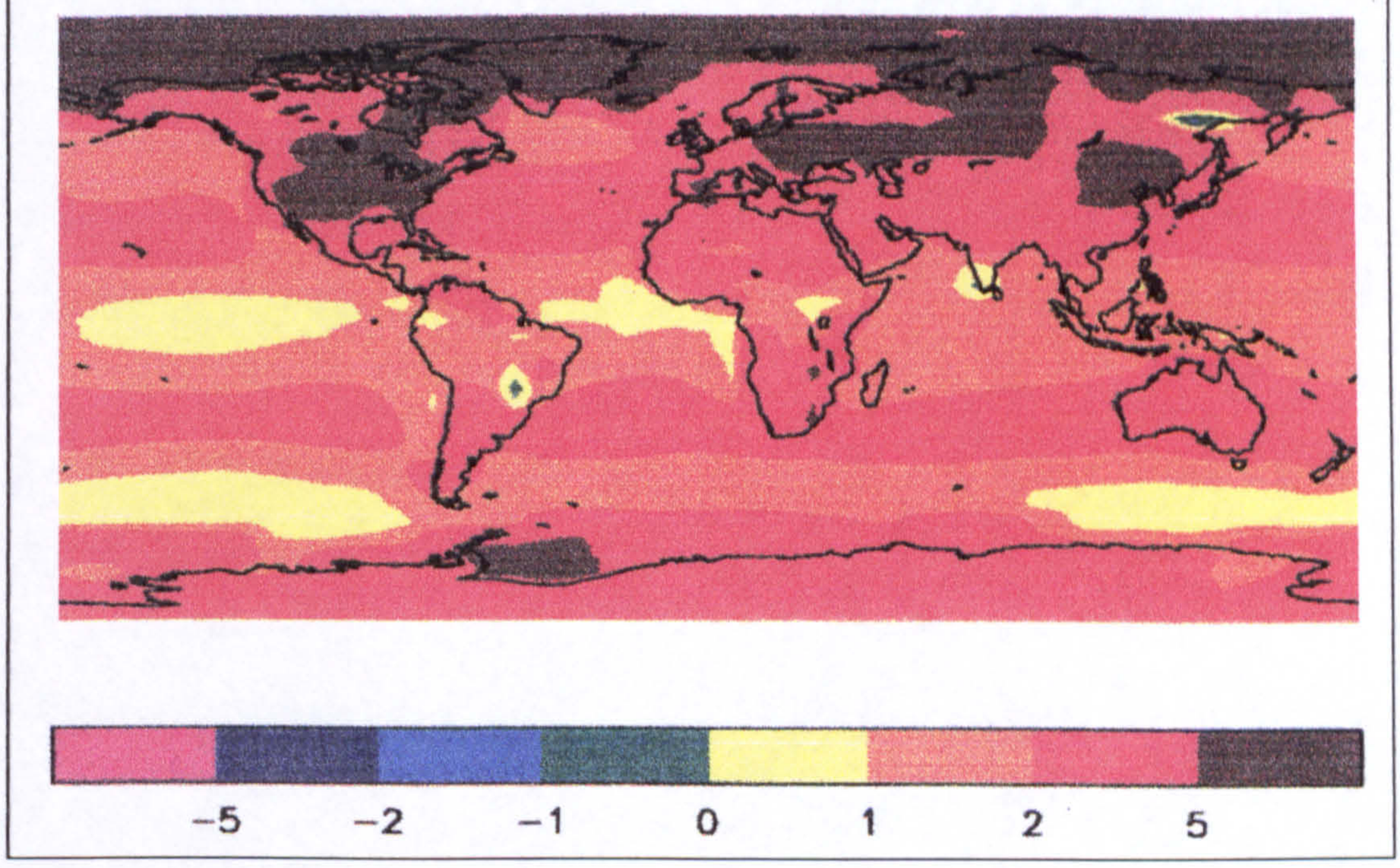

a) Change in annual mean temperature (K), diagnosed at a height of 1.5m above the surface.

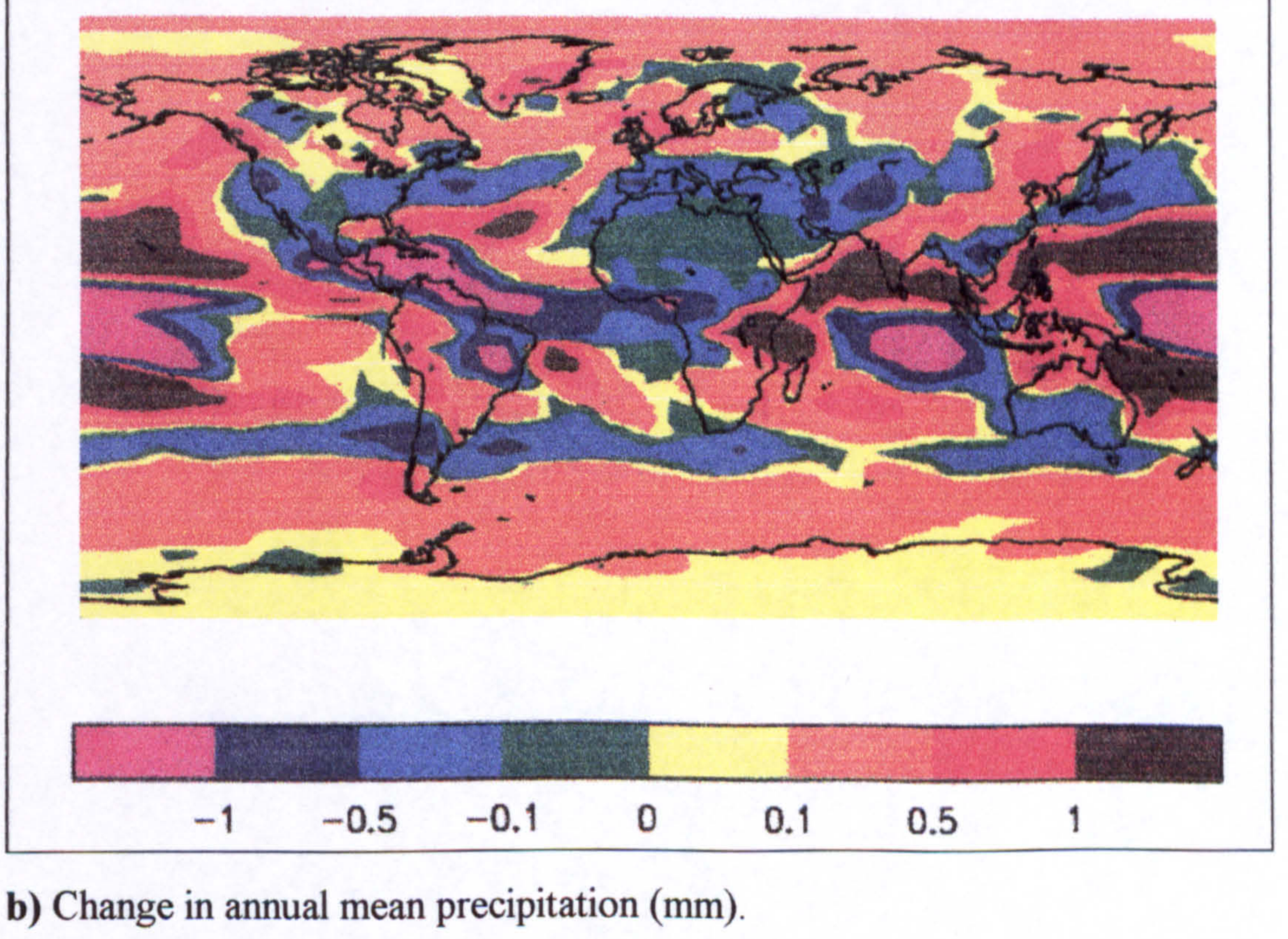

b) Change in annual mean precipitation (mm).

Figure 6.4 Climate change due to doubling CO_2, neglecting vegetation feedback, expressed as difference between climate states C2 and C1.

most likely to be attributable to the greater detail provided by the high resolution model which leads to slightly different effects, and to smoothing. However, despite the differences, both resolutions show that the land temperature increases globally with elevated CO_2 and, although the picture is more complex with the precipitation, this also shows a general global increase.

ii) The vegetation change due to increased CO_2. This is the difference between the final vegetation state, V2 and that simulated under 1 × CO_2, V1.

Figure 6.5 shows the changes in LAI and NPP due to the increase in CO_2. Much of the world experiences an increase in NPP between 0.01 and 0.3 kgC m^{-2} yr^{-1}; the greatest increases occurring in equatorial Africa, Brazil and eastern China. Areas of decrease occur in the Sahara and southern regions of Asia. LAI increases by 0.12 globally, but has decreases of the order of 0.1 to 2 in central Asia, Australia and north-eastern Africa.

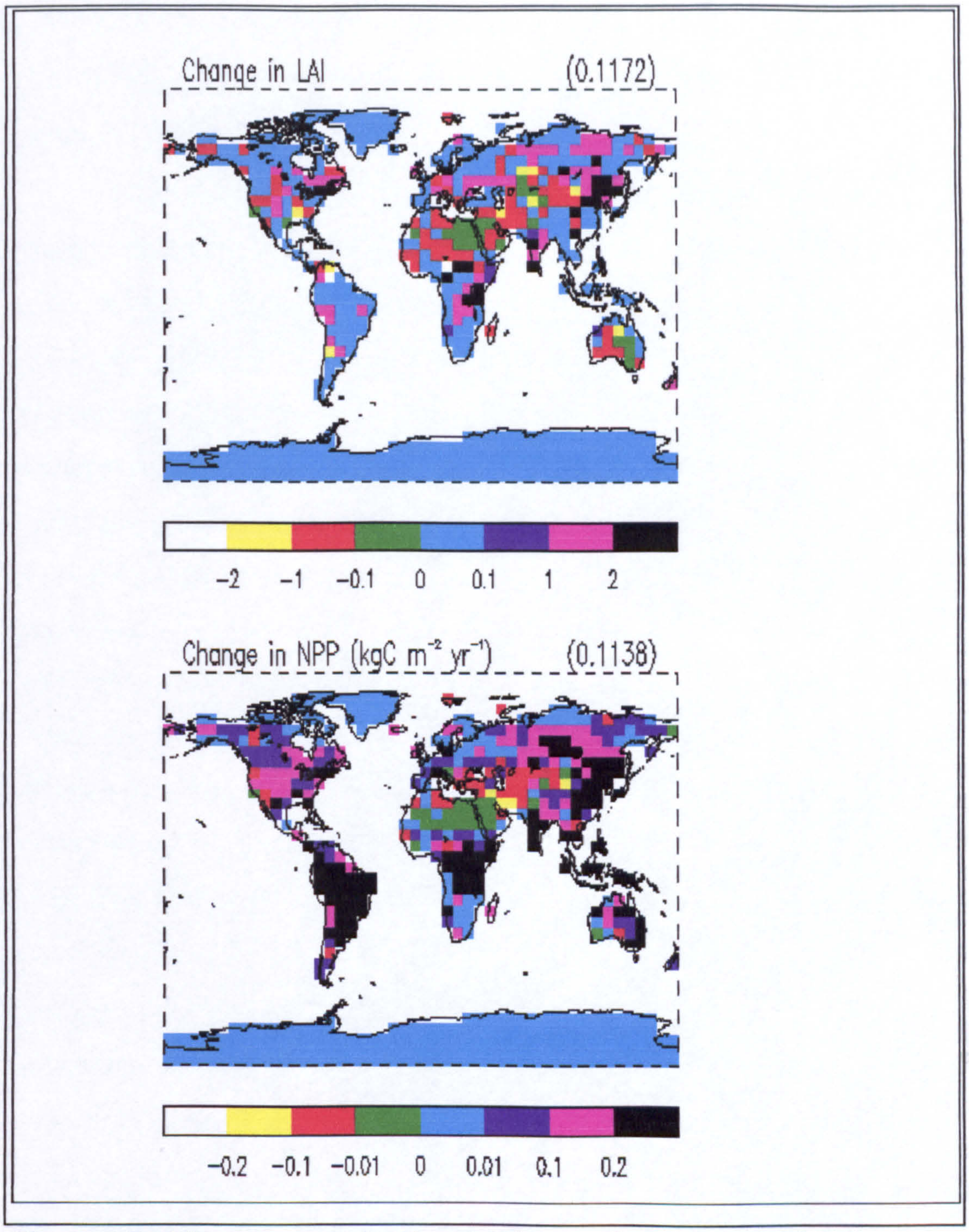

Figure 6.5 Difference maps showing the change of LAI and NPP for an increase in CO_2. LAI has an average global increase of 0.12 and NPP has an average global increase of 0.11 kgC m^{-2} yr^{-1}.

iii) The climate change due to increased CO_2 and with vegetation feedback. This is the difference between the final climate state, C3, and that simulated under $2 \times CO_2$, C2 (Figure 6.6).

Globally, there is a slight decrease in temperature of 0.09 K, but certain regions such as north-eastern parts of Asia show increases of between 1 and 2 K. Southern Sweden, the Ukraine into Russia, Turkey and Iran have increases of around 1 K. Other "hot spots" include south-east North America, the northern coast of South America, southern Chile, Senegal, and north-west Queensland and western Victoria in Australia. There are also large areas of decrease in temperature in the far north, as well as Antartica. Unusual circulation patterns set up by the GCM because of changes in the sea ice can cause these decreases. Much of the land area shows a decrease in temperature, with the greatest decreases occurring in eastern Africa, north-western Australia, eastern Argentina, northern India and the far north-east of Siberia. These areas of decreasing temperatures tend to be areas that have an increase in evapotranspiration, and therefore evaporative cooling after the inclusion of vegetation feedbacks. Also, there was an increase in root depth in the doubled-CO_2 climate in these areas, which made more soil moisture available for transpiration. The increases in surface temperature over north-eastern Asia, however, occur for different reasons. Although there was also an increase in root depth in this region, the temperature rose, rather than fell, as a result of vegetation feedback. Some other process was evidently operating to cause this. This process was most likely to have links with the surface albedo in this region. Figure 6.7 shows two global maps of changes in surface albedo (shortwave reflectivity of a surface) and surface temperature for March, with a change in climate and vegetation feedback. March was chosen because it is at the end of winter in the northern hemisphere, and is just before snow melt in the high latitudes. It would therefore show the greatest temperature and albedo differences between a vegetated and a non–vegetated surface.

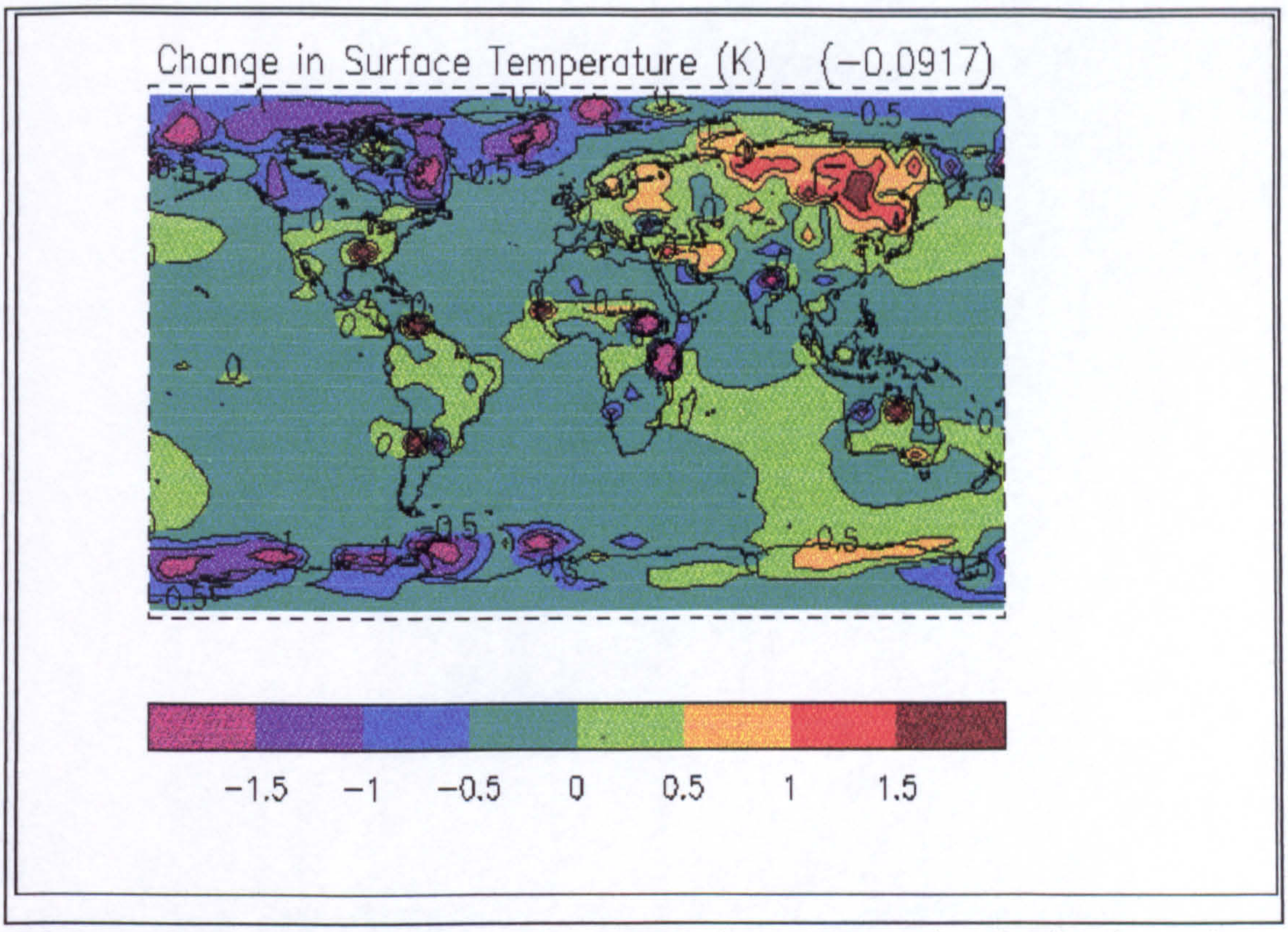

Figure 6.6 Changes in surface temperature due to vegetation feedbacks under doubled CO_2.

Links between some of the changes that occur in surface temperature for March and changes in surface albedo are evident. For instance, in north-east Asia, and north-eastern parts of Canada where there has been a decrease in albedo this has led to an increase in temperature. The increase in LAI in these regions causes deep-snow albedo to decrease by hiding the snow on the ground below taller vegetation, besides making the surface darker. The effect of this on the seasonal variation in albedo is to give a significantly lower surface albedo in winter in these regions. This results in an increase in net shortwave radiation and a rise in surface temperature. Much of Canada, however, shows a large decrease in surface temperature. From Figure 6.7 it can be seen that in north-western areas this can be attributable to an increase in albedo; but over the rest of the country, other variables, such as soil moisture and root depth have had a greater influence. There was an increase in soil moisture in the doubled-CO_2

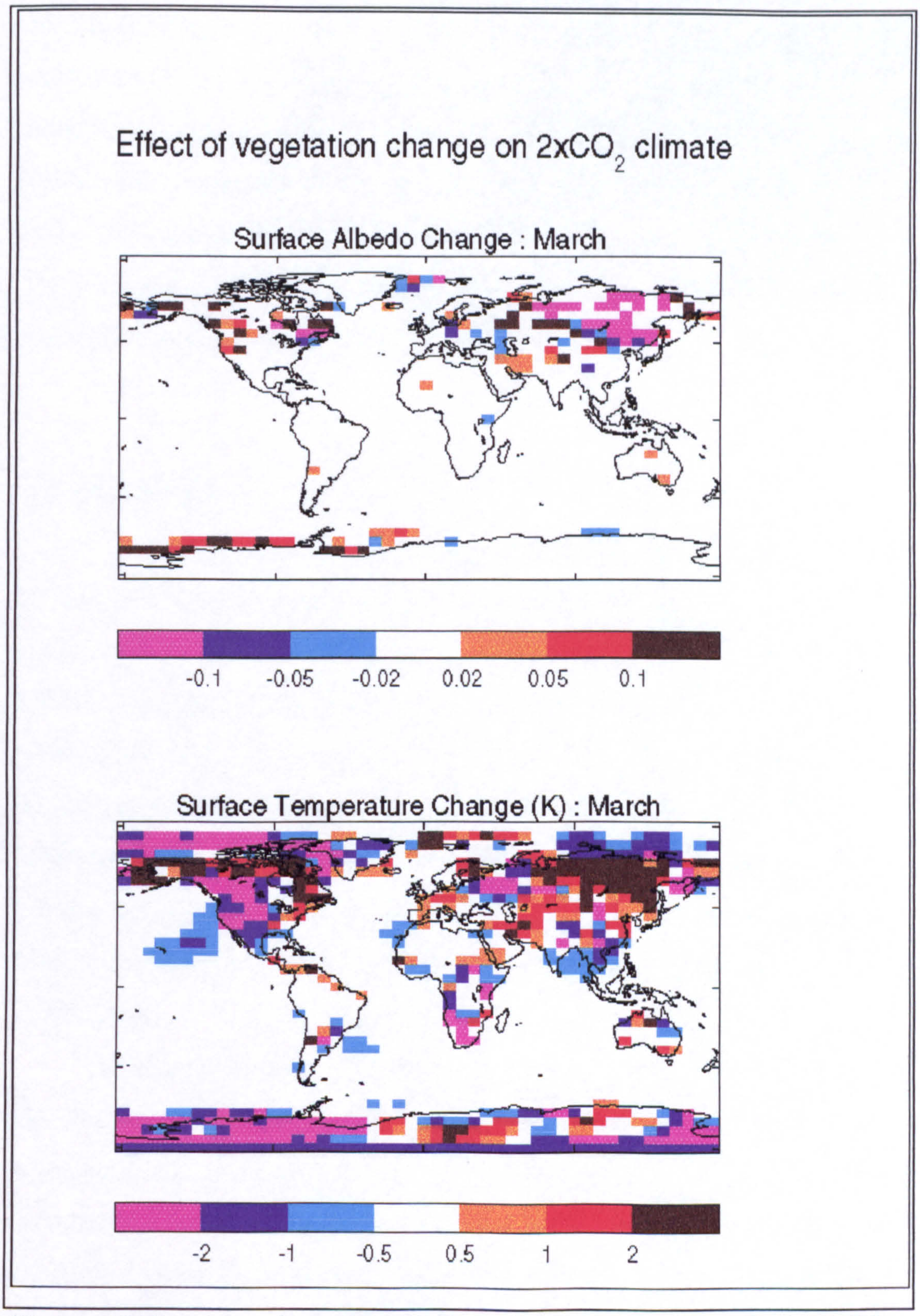

Figure 6.7 The change in surface albedo and temperature due to doubled-CO_2 and with vegetation feedback for March. This is the difference between the final climate state, C3, and that simulated under $2 \times CO_2$, C2.

climate in these areas which has provided more water for transpiration. This has led to more evapotranspiration and increased cooling. This increased evapotranspiration will not be as high as that experienced in eastern Africa, and north-western Australia, due to lower overall air temperatures, but will be sufficient to reduce the regional temperature. In addition, this region has experienced an increase in precipitation with climate change but this is smaller than the increase that occurs in eastern Asia.

6.5 Discussion

This chapter has shown how data from the vegetation model DOLY can be successful incorporated into a GCM. Vegetation is projected to affect both the present–day climate, and the future climate of a GCM through feedback effects. The effect of vegetation varies regionally and is dependent on water balance and albedo. The climate of the GCM is particularly sensitive to changes in soil moisture, evapotranspiration, root depth and albedo, caused by the addition of a variable responsive vegetation. Any changes that occur in the GCM parameters are due to changes in LAI, NPP and stomatal conductance. The overall feedback effects are small but there are important regional differences.

Further work needs to be done to examine the effect of additional iterations on the GCM, for example, the impact of incorporating the 1K temperature rise and associated changes in precipitation in north-east Asia back into the GCM. Also seasonality needs introducing so that the LAI, which is currently an annual maximum figure, will decrease in the winter months for areas with deciduous vegetation. The DOLY model is now part of the Sheffield dynamic global vegetation model (SDGVM). This model has the advantages of interactive soil carbon and nitrogen, and is able to operate with transient climate data. Additional runs with this model within the GCM would provide additional information as to the interactions between vegetation and climate.

To summarize, this chapter has shown that it is possible to couple a GCM with a mechanistic vegetation model, even with the adoption of a simple asynchronous approach. The results have shown that important climate feedbacks occur in certain regions of the world that can be directly attributable to the effect of vegetation. Future work with the SDGVM will provide more information about the links between climate and vegetation. To model the response of terrestrial ecosystems to climatic change, this model needs incorporation within an atmosphere–ocean GCM.

CHAPTER 7

7.0 An analysis of the different climate datasets used in the DOLY model

7.1 Introduction

Chapter 4 showed how the DOLY model responds to different climate variables and how this response depends very much on the global location. In addition, the modelling work in this thesis has shown that leaf area index (LAI) and net primary productivity (NPP) predicted by DOLY are very useful in highlighting deficiencies in the climate data. Other authors (Raich *et al.*, 1991, Woodward *et al.*, 1995) have stressed the requirement for accurate climate data in models. They point out that mean climate data are often imperfect for their use in exacting vegetation models. Furthermore, it is important when analysing the results from models and comparing them with others, to understand the location and magnitude of errors caused by incorrect climate data. This is particularly useful when examining general circulation model (GCM) climate data for the present-day and enables the identification of regions where possible errors may arise.

There are two aims of this chapter. The first is to compare net primary productivity (NPP) and leaf area index (LAI) from the DOLY model (water and soils version) run with three different climate datasets. Areas of disagreement are highlighted. The second is to compare the ISLSCP (International Satellite Land Surface Climatology Project) humidity data for the years 1987 and 1988 (Sellers *et al.*, 1995; Meeson *et al.*, 1995) and to show an interannual change with an El Niño event (1987 was an El Niño year. See Folland *et al.*, (1986) and Bigg, (1990) for details of regional climatic effects).

The climate datasets include the old version of the IIASA (International Institute for Applied Systems Analysis) dataset (Leemans and Cramer, 1991); the new version of the IIASA dataset called CLIMATE supplied by Wolfgang Cramer (pers. comm., 1995); the ISLSCP dataset produced by Meeson *et al.* (1995) and Sellers *et al.*, (1995); and the GCM (general circulation model) slab data (supplied by Richard Betts of the Hadley Centre). These slab data are from the GCM simulation of the 1 × CO_2 climate (Expt. CBBXCA, Dec. 1993).

Difference maps identify areas of change. These include differences in NPP and LAI arising from model runs with climate data from the old and new versions of the IIASA dataset, from the old IIASA dataset and the slab dataset and from the 1987 ISLSCP dataset and the 1988 ISLSCP dataset. Finally, differences between the humidity values for the years 1987 and 1988 from the ISLSCP dataset are examined.

7.2 Methods

Further details of each of the four datasets are given as follows.

i) Both the IIASA and CLIMATE datasets have been created from actual climate data over a 30 year period (1931 to 1960). These data have been derived from a number of sources, including Müller (1982), and entered on a 0.5° by 0.5° global grid. The temperature data were calculated for sea level and then adjusted for elevation, assuming a global moist adiabatic lapse rate of –0.6°C per 100 m altitude. However, air masses are able to hold more moisture at higher temperatures and therefore release more latent heat on condensation than those at lower temperatures. This means that moist adiabatic lapse rates increase with decreasing temperature. For high temperatures the rate can be as low as –0.4°C per 100 m altitude but increase to –0.9°C per 100 m altitude at –40°C (Barry and Chorley, 1976). Precipitation data were not adjusted for altitude due to the difficulty of defining a suitable lapse rate for precipitation and hence these data are underestimated in mountainous regions. All the data

are interpolated between actual meteorological stations using spatial averaging techniques (Leemans and Cramer, 1991), so that areas with the greatest station density are the most likely to have the most accurate data. The CLIMATE dataset is a revised form of the old IIASA dataset (Leemans and Cramer, 1991) with changes made to some of the temperature and precipitation values. In addition, the IIASA data had to be converted to the same resolution as the slab data (2.5° by 3.75°) for ease of comparison with the slab dataset. This was done by extracting the nearest IIASA cell to a slab co-ordinate.

ii) The humidity data supplied by Leemans (pers. comm., 1993) are on a 0.5° by 0.5° global grid and have been created from actual data recorded as mean monthly values over a 30 year period (1931 to 1960). Humidity is recorded at nine o'clock in the morning. A quality control procedure was implemented on these data. If the humidity for any month exceeds the value from the previous month by 50% or more, the humidity for the previous month is altered. This amended humidity is calculated from the mean of the two months before and immediately after it. This adjusted the humidity values at some sites where certain months contained values that were clearly too low compared with those of the months around them. These humidity data were totalled for the year to obtain an annual humidity figure for each grid cell. When these data were plotted on a GCM grid (2.5° by 3.75°) this adjustment affected only a small number of sites (26 GCM grid cells which are 0.6 % of the land cells). There was an increase in annual humidity of 40 percentage points in 11 grid cells, and the remaining 15 grid cells changed by ± 10 percentage points.

iii) The ISLSCP data have also been obtained from a variety of sources (Meeson *et al.*, 1995; Sellers *et al.*, 1995) for the years 1987 and 1988 on a 1° by 1° global grid. The temperature data used in this chapter have been produced by the European Centre for Medium Range Weather Forecasting (ECMWF). These were derived from data at a temporal resolution of 6 hours (i.e. four values per day). These modelled temperature data are for a height of

2 m above the ground. These data were converted to mean monthly temperatures. The mean daily temperatures were calculated from the four 6-hourly values, totalled for the month and divided by the number of days in the month. Dew point temperatures were also available, so it was possible to calculate the relative humidity (see Appendix 2). Both these datasets are on CD-ROM, Volume 3. Precipitation data were modelled by the NMC (National Meteorological Centre, Washington DC, USA) again for 6-hourly periods. These data are on CD-ROM, Volume 5.

iv) The Hadley Centre slab model (Jones *et al.*, 1995), is a simplified climate version of the United Kingdom Meteorological Office (UKMO) Unified Forecast and Climate Model, a full Ocean–Atmosphere model. The slab model consists of an atmospheric model coupled to a simple (slab) ocean model that updates sea surface temperature and sea-ice extents. This dataset is a simulation of the equilibrium state of the climate system output from the Hadley Centre slab GCM for the present-day ($1 \times CO_2$) climate. The data correspond to monthly means over a ten year period for the current concentration of atmospheric CO_2 (taken as 490 ppm by mass or about 323 ppm by volume (32.3 Pa partial pressure)). The slab model is quicker and easier to run than the full model. Section 6.2 contains additional details about the GCM. For the following study, climate output from the slab model at a resolution of 2.5° latitude by 3.75° longitude is used (6912 cells globally).

The DOLY (water and soils version) model was run with the temperature and precipitation data from the old and new versions of the IIASA dataset. The same humidity data from Leemans was used in both runs. The NPP and LAI values from the model were plotted globally. Difference maps were produced to show areas of change of both LAI and NPP. The DOLY (water and soils version) model was then run with the climate data from the old IIASA dataset and the slab data, and the same procedure, as previously described, was adopted. Both these datasets have been used in the DOLY model to predict present-day LAI and NPP values. It should be noted,

however, that the IIASA data have been derived from mean data covering the period 1931 to 1960, whereas the slab data are derived from a simulation of present-day climate. Also, the atmospheric CO_2 partial pressure for all runs of the model was set at 35 Pa but the slab climate data were simulated for a climate using 32.3 Pa (the difference in the total global NPP and the mean global LAI using the IIASA data for the two different atmospheric CO_2 partial pressures are shown in Table 7.2). Further runs were carried out using ISLSCP 1987 and 1988 data and the resulting LAI and NPP values were also compared. Finally, the ISLSCP mean annual humidity data for the years 1987 and 1988, were calculated and mapped. Specific monthly differences will not be identified as only the mean annual humidity values are compared and not the individual months. An additional difference map was then produced showing the difference in ISLSCP humidity between the two years 1987 and 1988. For each dataset the total global NPP, mean global LAI, the land area covered by the dataset and the amount of vegetated area is calculated.

For each set of difference maps of LAI and NPP, produced from the IIASA and CLIMATE data, and from the IIASA and slab data, temperature and precipitation data were extracted. These data were for specific regions of difference between the two datasets, identified from the maps. In addition, for the ISLSCP data, the vapour pressure deficit values were also calculated from the humidity and temperature data for these regions of difference. Climate data from the Müller dataset were used to compare the slab model and the IIASA climate data for some selected sites. See section 2.2.1 for more details on the Müller dataset.

7.3 Results

The LAI and NPP values predicted by the DOLY model (water and soils version) run with the CLIMATE dataset are subtracted from the values derived from the old IIASA dataset. The CLIMATE dataset is taken as being the reference dataset on the assumption that its values should be an improvement on the values in the original IIASA dataset as further validation checks have been carried out at a number of sites globally (Cramer, pers comm., 1995). The resulting difference maps are shown in Figures 7.1 and 7.2. This analysis is concerned with regions where the two datasets give noticeably different LAI and NPP values. NPP values range from 0 tC ha^{-1} yr^{-1} in desert areas to 11 tC ha^{-1} yr^{-1} in tropical rain forests (McGuire *et al.*, 1992). LAI values range from 0 in desert areas to 12 in tropical rain forests (Nemani and Running, 1996). The total global NPP and average LAI were also calculated from the old and the new IIASA datasets. Figure 7.1 shows that small negative deviations (i.e. ≤ -1) from the reference LAI occur in southern Greenland, eastern Siberia, parts of central Asia, central Australia, south Yemen and Oman, Alaska, the southwestern states of America and parts of southern America. Small positive deviations (i.e. ≤ 1) occur in the Sahara desert, southern Africa, western Australia, western Saudi Arabia and eastern Brazil. Greater changes (i.e. ≥ 2), where values from the model run with the old IIASA dataset exceed those from the CLIMATE dataset, occur in areas of high ground. These areas include south-west Arabia, the Elburz mountains south of the Caspian Sea, and the Tien Shan mountain range of western China. In addition, the south-eastern fringes of the Gobi desert and south-west USA show increases of 2 to 3. Negative deviations of 2 to 3 occur in eastern Siberia, southern Greenland, parts of Alaska, and the Andes. The same decreases also occur in the southern Sahara desert, the Somali peninsula of Africa, parts of Iran, the Himalayas, south-western Africa and central Australia.

NPP shows the same pattern of change as LAI in Figure 7.2, with the addition of areas such as eastern Brazil and parts of central Australia. These

areas show positive deviations in NPP of 2 to 3 tC ha^{-1} yr^{-1}. There are also more extensive negative deviations in eastern Siberia and central Asia and Brazil. Negative deviations of 2 to 3 tC ha^{-1} yr^{-1} also occur in Spain, northern Burma, southern China, north Vietnam, New Guinea, the northern fringes of Hudson Bay, Venezuela, southern Guyana, and around the Amazon delta.

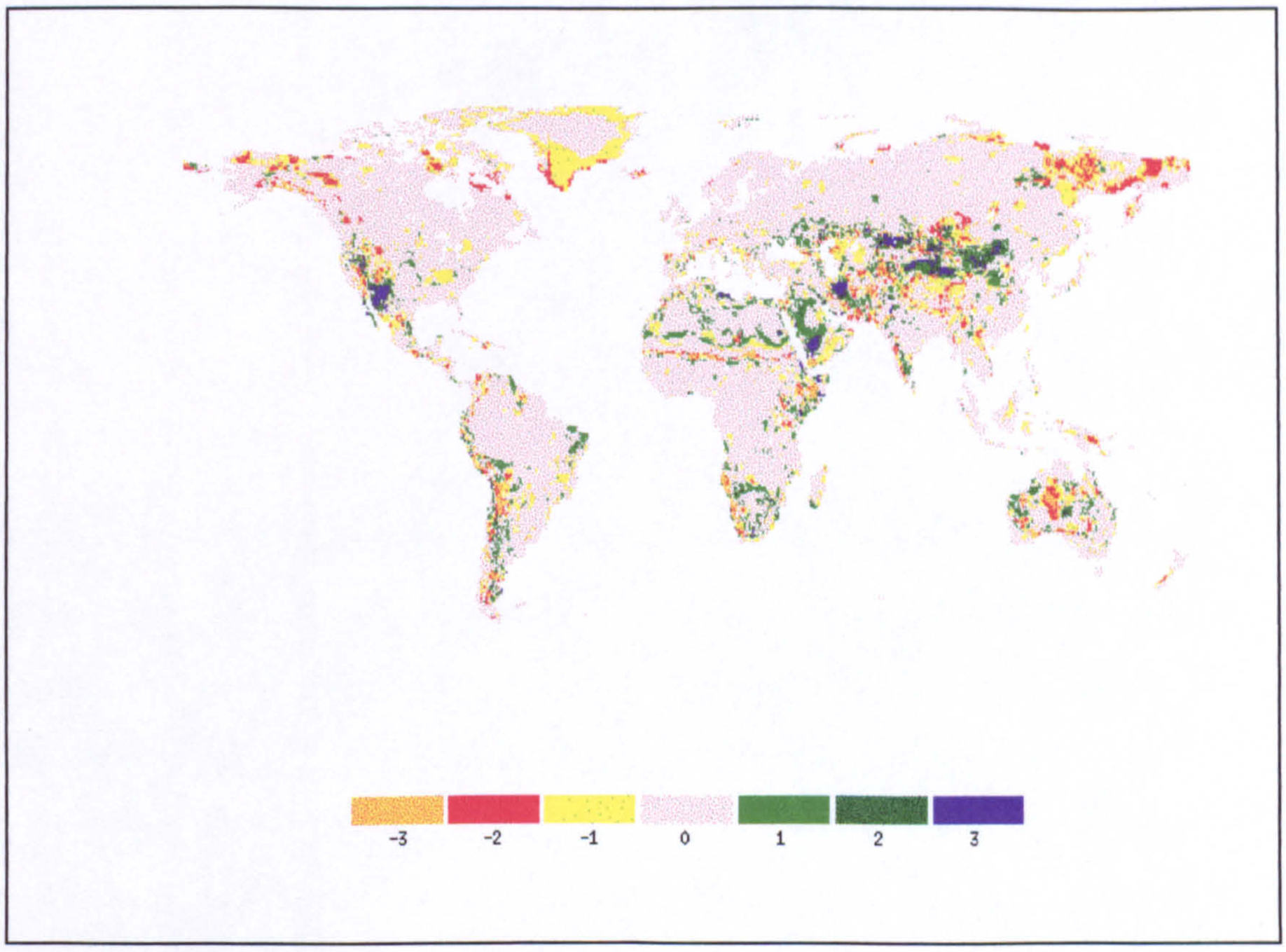

Figure 7.1 Change in LAI values derived from the DOLY model (water and soil version) using precipitation and temperature data from the IIASA dataset (Leemans and Cramer, 1991), and the CLIMATE dataset (pers. comm., Wolfgang Cramer, 1995). The absolute values of LAI range between 0 and 12. Positive deviations occur when the LAI values from the IIASA dataset exceed those of the CLIMATE dataset and negative deviations are for the reverse situation.

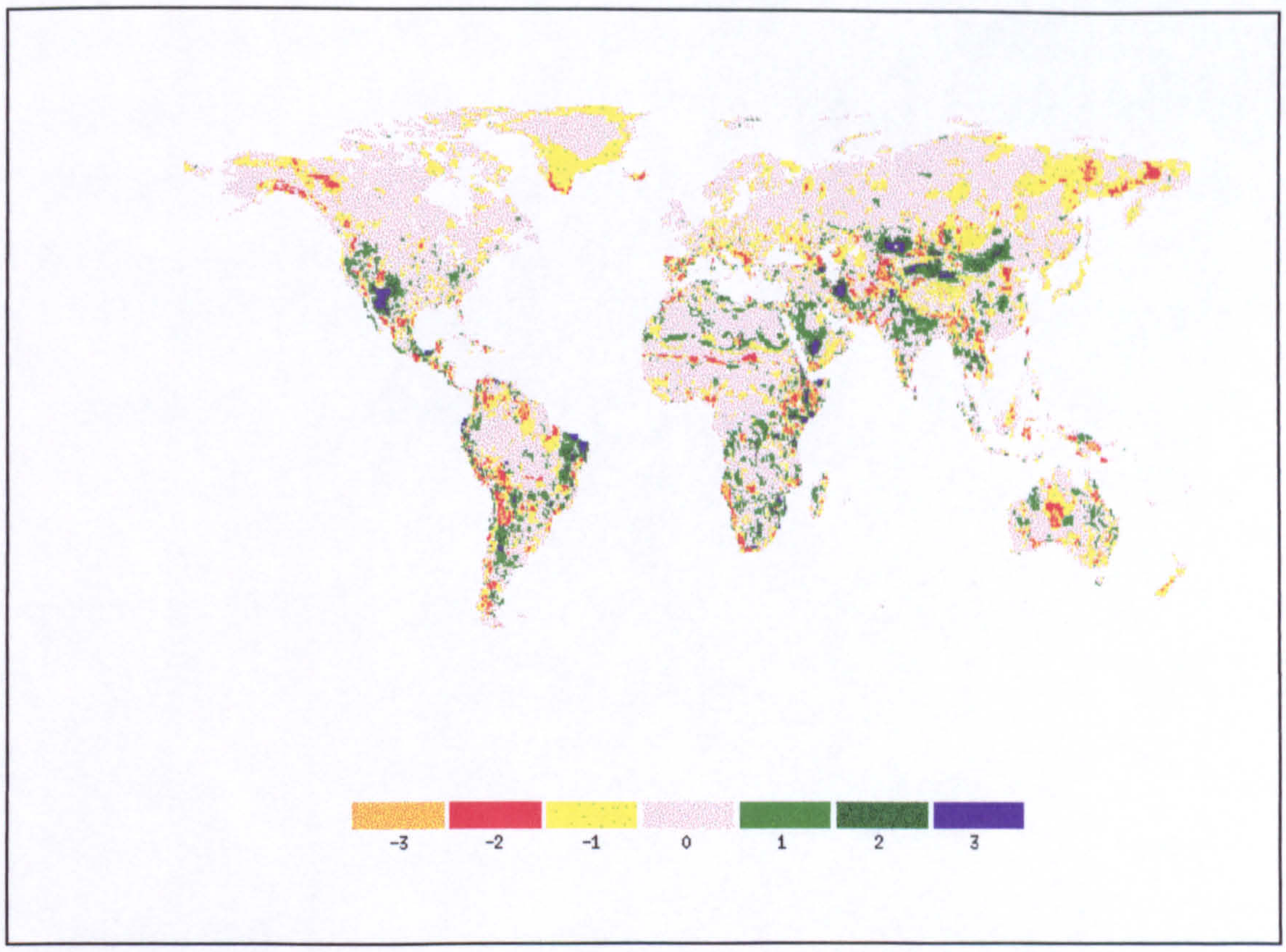

Figure 7.2 Changes in NPP values derived from the DOLY model (water and soil version) using precipitation and temperature data from the IIASA dataset (Leemans and Cramer, 1991), and the CLIMATE dataset (pers. comm., Wolfgang Cramer, 1995). Absolute values of NPP range between 0 and 11 tC ha^{-1} yr^{-1}. Positive deviations occur when the NPP values from the IIASA dataset exceed those of the CLIMATE dataset and negative deviations are for the reverse situation.

The deviations in LAI and NPP predicted by the model for different climate databases arise for a number of reasons, which are dependent on the location of the area under study. For instance, in south-west U.S.A, the rainfall is lower in the CLIMATE dataset than that in the old dataset (Table 7.1), and because this is an arid area results in lower LAI and NPP values as shown in Figures 7.1 and 7.2.

Table 7.1 Total annual rainfall (mm yr^{-1}) and mean annual temperature (°C) for 9 global locations obtained from the IIASA dataset (Leemans and Cramer, 1991) referred to as "old", and the CLIMATE dataset supplied by Wolfgang Cramer (pers. comm., 1995), referred to as "new."

Area description	Latitude & longitude	Mean temp. (old) °C	Mean temp. (new) °C	Total precip. (old) (mm yr^{-1})	Total precip. (new) (mm yr^{-1})
S.W. U.S.A.	31°N 113°W	19	18	237	168
Yemen	16°N 44°E	13	17	198	222
Tien Shan	45°N 85°E	5	4	92	193
South of the Caspian Sea	36°N 54°E	5	14	1063	153
Andes	24°S 68°W	–10.4	5	195	114
Somali peninsular	5°N 46°E	27	28	148	198
Eastern Siberia	66°N 175°E	–13	–11	163	360
Eastern Brazil	5°S 37.5°W	25	27	1572	664
Southern Sahara	20°N 0°E	29	28	74	86

Elsewhere, different effects are noted. For instance, in the Yemen (Table 7.1), both temperature and precipitation rise with the CLIMATE dataset, which causes a decrease in NPP and LAI. The deviation between the IIASA and the CLIMATE dataset is therefore positive. South of the Caspian Sea (Table 7.1), again a dry area, the precipitation has been reduced greatly in the CLIMATE dataset. The temperature increases which also cause decreases in LAI and NPP lead to a positive deviation between the two datasets. This also occurs in eastern Brazil (Table 7.1).

If we now consider the negative deviations that occur due to the NPP values from the CLIMATE dataset exceeding than those from the IIASA dataset. In the Andes, the rainfall in the new dataset is less than that of the old (Table 7.1), but the temperature is much higher, which causes increases in both NPP and LAI. Temperatures rise in the Somali peninsular and in eastern Siberia but precipitation is higher with the new dataset compared with the earlier version (Table 7.1). On the southern fringes of the Sahara, the temperature is slightly lower and the precipitation higher in the new dataset than in the earlier version. This too causes increases in LAI and NPP.

Table 7.2 shows how the two datasets compare regarding the total global NPP, mean annual LAI, land area, vegetated area and climate.The CLIMATE dataset increases the amount of global NPP which in turn increases the amount of vegetated area, although there is no difference in mean global LAI. The CLIMATE dataset also has a slightly higher global mean temperature than the IIASA dataset, which would increase the NPP providing there were no water limitations. However, the increase in mean annual rainfall does not appear to have any impact on the global mean LAI. The LAI, NPP and vegetated area are all increased with increased atmospheric CO_2 partial pressure.

Table 7.2 Total global NPP, mean global LAI, and global vegetated area predicted by the DOLY model (water and soils version). The model was run with the old IIASA dataset (at two atmospheric CO_2 partial pressures of 32 Pa and 35 Pa) and the new IIASA dataset (CLIMATE) both on a 0.5° by 0.5 ° global grid. The mean annual temperature and mean annual precipitation are also shown. The mean annual relative humidity is calculated as 72 %. The global land area is 136.2×10^6 km^2.

Dataset	Total global NPP (Gt C yr^{-1})	Mean global LAI	Global vegetated area ($\times 10^6$ km^2)	Mean annual temp. (°C)	Mean annual precipitation (mm)
IIASA (32 Pa)	52.7	4.1	106.1	10.8	672
IIASA (35 Pa)	55.9	4.2	106.5	10.8	672
CLIMATE	57.7	4.2	109.2	11.5	690

This study has shown that changes in temperature and precipitation can have important regional effects on the LAI and NPP values from the model. These effects are dependent on the current climate of a region, namely whether it is arid or cold. In Chapter 2, it was shown how vapour pressure deficit is influenced by temperature and humidity (equations 2.26 and 2.27 and Figure 2.5). This in turn affects LAI and NPP. Later in this chapter the effects of vapour pressure deficit, in addition to temperature and precipitation, will be examined in relation to the ISLSCP data.

The next comparison involved the IIASA dataset (on a 2.5° by 3.75° grid) and the GCM slab dataset from the UKMO. This comparison used the IIASA dataset instead of the CLIMATE dataset for a number of reasons. The first is a historical reason in that this comparison was made before the CLIMATE dataset become available. The second reason was that most of the

model runs in this thesis have used the IIASA dataset and, finally, the IIASA dataset has been published and the CLIMATE dataset has not to date. The aim of this comparison was to determine areas where the IIASA dataset and the slab data differed markedly. The LAI and NPP values predicted by the DOLY model (water and soils version) run with old IIASA dataset are subtracted from the slab dataset. The old IIASA dataset is taken as the reference dataset in this case on the assumption that actual climate data should be more accurate than modelled climate data. The resulting maps are shown in Figures 7.3 and 7.4. In addition, the total global NPP and average LAI were calculated from the slab data.

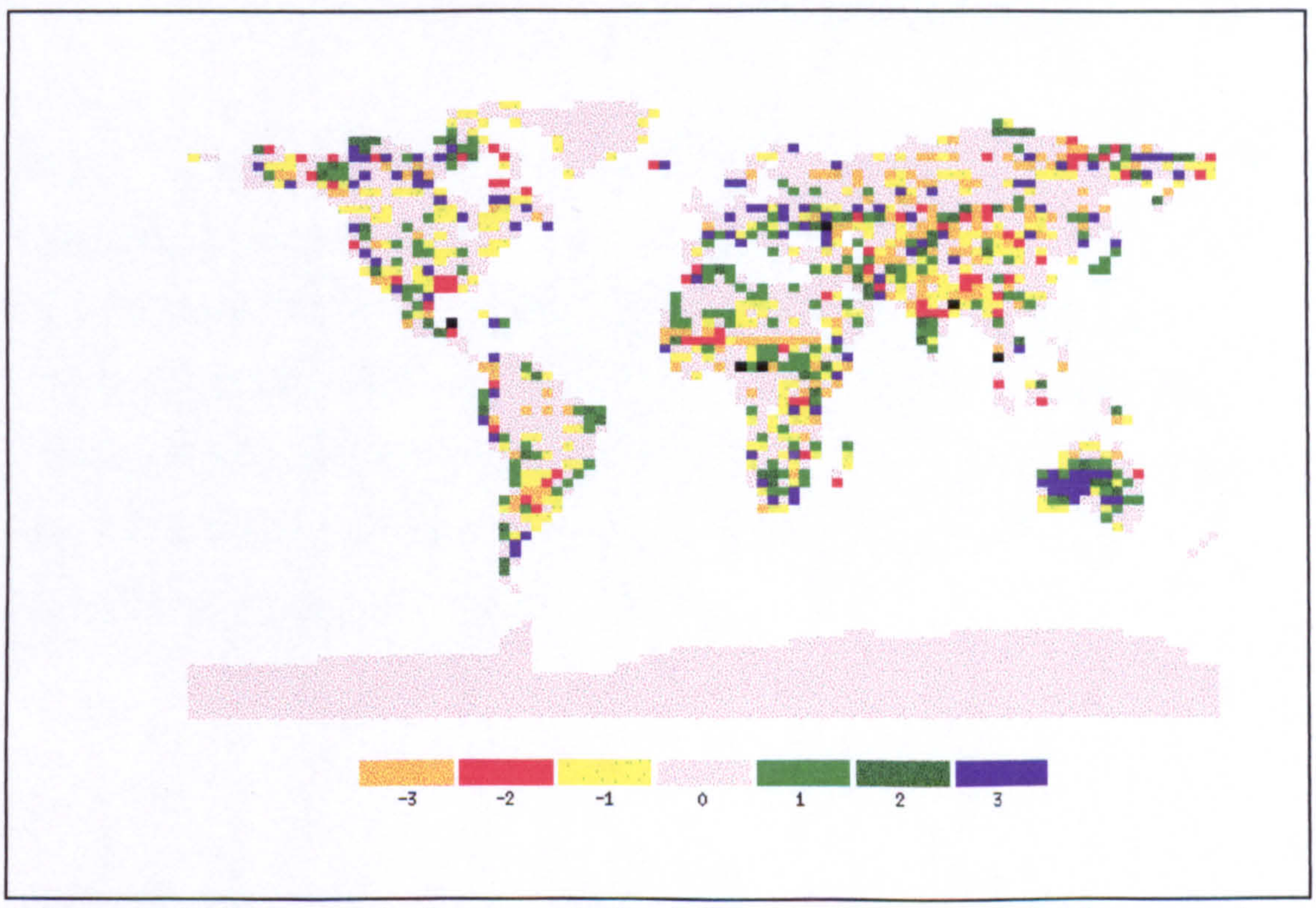

Figure 7.3 Change in LAI values derived from the DOLY model (water and soil version) using precipitation and temperature data from the IIASA dataset (Leemans and Cramer, 1991), humidity data from Leemans (pers. comm., 1993) and the slab dataset from the UKMO. The absolute values of LAI range between 0 and 12. Positive deviations occur when the LAI values from the slab dataset exceed those of the IIASA dataset and negative deviations are for the reverse situation.

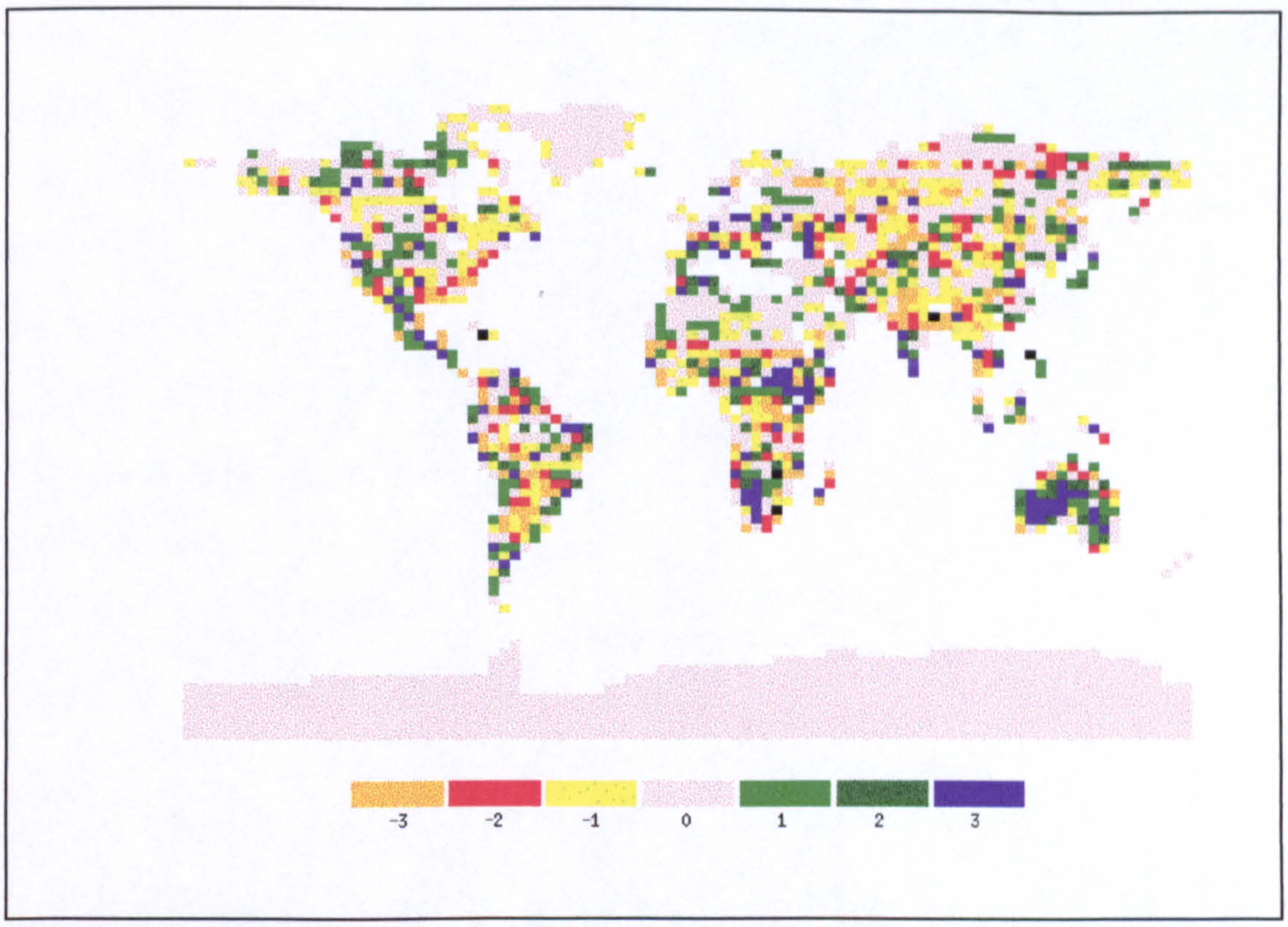

Figure 7.4 Changes in NPP values derived from the DOLY model (water and soil version) using precipitation and temperature data from the IIASA dataset (Leemans and Cramer, 1991), humidity data from Leemans (pers. comm., 1993) and the slab dataset from the UKMO. Absolute values of NPP range between 0 and 11 tC ha^{-1} yr^{-1}. Positive deviations occur when the NPP values from the slab dataset exceed those of the IIASA dataset and negative deviations are for the reverse situation.

Figure 7.3 shows the differences in LAI between the two datasets. Six main areas of negative deviations (IIASA LAI values exceed the GCM LAI values) are evident.

These are:

i) Argentina,

ii) the northern savannah regions of Africa,

iii) northern Burma and southern China,

iv) Pakistan,

v) north-eastern Siberia,

vi) northern China and western Mongolia.

Table 7.3 Total annual rainfall (mm yr^{-1}) and mean annual temperature (°C) for 16 global locations obtained from the IIASA dataset (Leemans and Cramer, 1991) referred to as "old", and the GCM slab dataset supplied by the UKMO.

Area description	Latitude & longitude	Mean temp. (old) °C	Mean temp. (slab) °C	Total precip. (old) (mm yr^{-1})	Total precip. (slab) (mm yr^{-1})
Argentina	37.5°S 60°W	13.8	15.3	804	610
Northern savannah (Africa)	15°N 30°E	26.4	26.3	206	88
Northern Burma	25°N 93.75°E	15.4	19.8	1117	2217
Pakistan	27.5°N 60°E	18.8	16.7	73	205
N.E. Siberia	72.5°N 127.5°E	–14.8	–19.2	325	186
Western Mongolia	47.5°N 93.75°E	–1.5	–1.0	166	65
Central Australia	25°S 131.25°E	20.0	19.4	196	350
Southern Africa	30°S 22.5°E	18.1	14.4	194	321
Southern South America	55°S 67.5°W	4.4	3.2	451	1601

Table 7.3 (continued)

Area description	Latitude & longitude	Mean temp. (old) °C	Mean temp. (slab) °C	Total precip. (old) (mm yr^{-1})	Total precip. (slab) (mm yr^{-1})
Northern Canada	67.5°N 131.25°W	–8.8	–7.3	151	149
Eastern coast of USA	37.5°N 78.75°W	15.4	11.7	1091	1115
South Brazil	30°S 56.25°W	15.3	20.4	1462	950
Ethiopia	5°N 33.75°E	27.8	22.9	700	1611
Uganda	2.5°N 30°E	21.4	19.9	1640	2897
SW USA	32.5°N 116.25°W	9.6	17.7	176	56
Central southern America	37.5°N 86.25°W	14.4	13.9	217	1244

Referring to Table 7.3, the LAI values in Argentina predicted from the model using slab data are lower than those using the old IIASA data. The slab model has underestimated the amount of rainfall in this region and overestimated the temperature in relation to the actual data. The total annual rainfall data from IIASA exceeds the total annual rainfall from the slab data and the IIASA temperature is also lower, the result of which leads to increases in both NPP and LAI. In the arid northern savannah regions of Africa, the slab model again underestimates the amount of rainfall (Table 7.3) giving lower LAI and NPP values than IIASA but the temperature is similar to that of the IIASA data. Elsewhere, where the climate is wetter (for instance, Burma), the higher values of LAI with the IIASA data occur due to lower rainfall values, and lower temperatures (giving lower vapour pressure deficits and leading to less evaporation) than the slab model data. In colder regions such as north-eastern Siberia, the higher LAI is due to the IIASA dataset having higher temperatures than the slab model data (Table 7.3).

Positive deviations in LAI (the values from the slab dataset exceed those from the IIASA dataset) arise in drier areas, such as central Australia, where the slab model data overestimates rainfall relative to the actual data (Table 7.3). The LAI output from the model using the slab data is therefore greater than that using the old IIASA. This also occurs in southern Africa and southern parts of South America (Table 7.3). In northern Canada, the LAI output from the model using the slab data also exceeds the values from the IIASA data. This is due to the temperatures in the slab data being slightly greater than those of the IIASA dataset for this region (Table 7.3).

Figure 7.4 shows a similar pattern to Figure 7.3. There are, however, additional negative deviations (the values from the IIASA dataset exceed those from the slab dataset) occurring along the eastern coast of the U.S.A., where the IIASA temperature data are higher and the precipitation is lower than the slab data (Table 7.3). Negative deviations also occur in eastern Zaire and southern Brazil (Table 7.3). In southern Brazil, the IIASA temperature data are lower and precipitation higher than the slab data. The higher IIASA temperature for the eastern U.S.A. has increased the NPP value, as rainfall is adequate to cover the increased evaporative demand. Positive deviations occur in Ethiopia and Uganda because the slab temperatures are lower (giving lower VPD values and reduced evaporation) than the IIASA temperatures and there is much more rainfall.

The small positive deviations in LAI and NPP that occur in the Sahara desert suggests that the slab model has predicted some precipitation in these cells where in reality there would be none (from the IIASA dataset). The small negative deviations arise where the IIASA dataset has rainfall and the slab does not. Figures 7.1 and 7.2 show that there are also some positive deviations in both LAI and NPP between the IIASA and CLIMATE dataset within some of these cells. This implies that the IIASA dataset is in error with regards to rainfall in some of these cells. If the precipitation values from the CLIMATE

dataset were used instead of the IIASA values, then the slab data would be in agreement with these values in these particular regions of the Sahara desert.

In northern Canada and north-eastern Siberia, where LAI increases with the use of slab climate data, it appears that this has been due to an overestimation of temperature relative to the IIASA dataset. However, some of these IIASA temperatures are greater than those in the CLIMATE data (Table 7.3) in north-eastern Siberia. This suggests that they may have been too high and that the slab temperature data are closer to the CLIMATE temperature data than the IIASA data. The comparison of the IIASA and CLIMATE dataset has shown that there has been an element of "correction" in the south-western states of America, and central Asia. This has also occurred in central parts of Australia, western South America and east Africa.

In order to check the accuracy of the temperature and precipitation inputs for a selection of sites where differences occurred, actual climate data were extracted from the Müller dataset (Müller, 1982) for sites that were nearest to the slab co-ordinates. The comparison of the mean annual temperature and annual precipitation are shown in Table 7.4. It can be seen that the slab model has lower rainfall values in the Sudan, southern Brazil and Argentina than the values from the Müller and IIASA datasets, which has led to lower values of NPP and LAI. In Ethiopia, Uganda and central Australia the slab rainfall values are too high giving higher values of NPP and LAI. The slab temperatures are closer to those from Müller for Sudan, South Brazil, Argentina and Ethiopia, but IIASA is closer to Müller for Uganda, central Australia and northern Siberia. Both the slab and IIASA temperatures are too warm compared with the Müller temperature for northern Canada. Spatial averaging across the grid squares is the most likely explanation for many of these discrepancies. Also, the site selected may not be representative of the climate of the grid square where it is located. Despite these limitations, Table 7.4 does highlight where major differences have occurred particularly with regards to slab precipitation. Table 7.5 shows total global NPP and mean global

LAI using the slab and the IIASA climate data. Compared to the slab climate data the amount of vegetated area is greater using the IIASA climate data, and there is a higher global NPP value. The IIASA dataset also has gives slightly higher global mean temperature than the slab dataset but the total annual rainfall is much lower. The global mean LAI does not differ much between the two datasets.

Table 7.4 Total annual rainfall (mm yr^{-1}) and mean annual temperature (°C) for 8 global locations extracted from the Müller dataset (Müller, 1982) compared with the values obtained from the IIASA and slab climate datasets.

Site and area description	Latitude & longitude	Mean Temperature (°C)			Total precipitation (mm yr^{-1})		
		Müller	IIASA	Slab	Müller	IIASA	Slab
Khartoum, Sudan.	15.6°N 32.53°E	29.2	26.4	26.3	164	206	88
Porto Alegre, South Brazil.	30.03°S 51.21°W	19.4	15.3	20.4	1297	1462	950
Buenos Aires, Argentina.	34.58°S 58.48°W	16.9	13.8	15.3	1027	804	610
Negelli, Ethiopia.	5.12° N 39.43°E	19.5	27.8	22.9	550	700	1611
Gulu, Uganda.	2.75°N 32.33°E	23.1	21.4	19.9	1470	1640	2897
Alice Springs, Australia.	23.7°S 133.88°E	20.6	20.0	19.4	252	196	350
Sachs Harbour, Canada.	71.95°N 124.73°W	-14.4	–8.8	–7.3	138	151	149
Mys Cel'uskin, Siberia.	77.72°N 104.28°E	-15.6	–14.8	–19.2	244	325	186

Table 7.5 Total global NPP, mean global LAI, and the global vegetated area predicted by the DOLY model (water and soils version). The model was run with the IIASA dataset (on a GCM resolution of 2.5° by 3.75°) and the slab climate data. The mean annual temperature and mean annual precipitation are also shown. The mean humidity for the IIASA dataset is 71% and 77% for the slab dataset. The global land area (excluding Antarctica) is 134.0×10^6 km^2. This area is slightly less than that for Table 7.2 due to the different grid resolutions used.

Dataset	Total global NPP (Gt C yr^{-1})	Mean globa l LAI	Global vegetated area ($\times 10^6$ km^2)	Mean annual temp. (°C)	Mean annual pptn. (mm)
IIASA	55.9	4.3	101.3	5.1	647
Slab (1× CO_2)	54.6	4.2	100.1	3.4	904

This comparison has shown areas where the LAI and NPP would differ were the slab climate data used instead of the IIASA dataset. The overall global difference in NPP and vegetated area is relatively small compared with the difference between the IIASA and the CLIMATE datasets (Table 7.2). This type of comparison aids in the analysis of model accuracy. Discrepancies in LAI and NPP that have arisen due to the climate inputs, rather than the model itself, can be identified and compared with other model values.

Additional runs of the DOLY model (water and soils version) used the 1987 and 1988 ISLSCP climate data. The LAI and NPP values produced from the ISLSCP 1988 data are subtracted from the ISLSCP 1987 data and the resulting maps are shown in Figure 7.5 and 7.6. The ISLSCP 1988 dataset is taken as being the reference dataset on the basis that it was not a year when an El Niño event occurred .

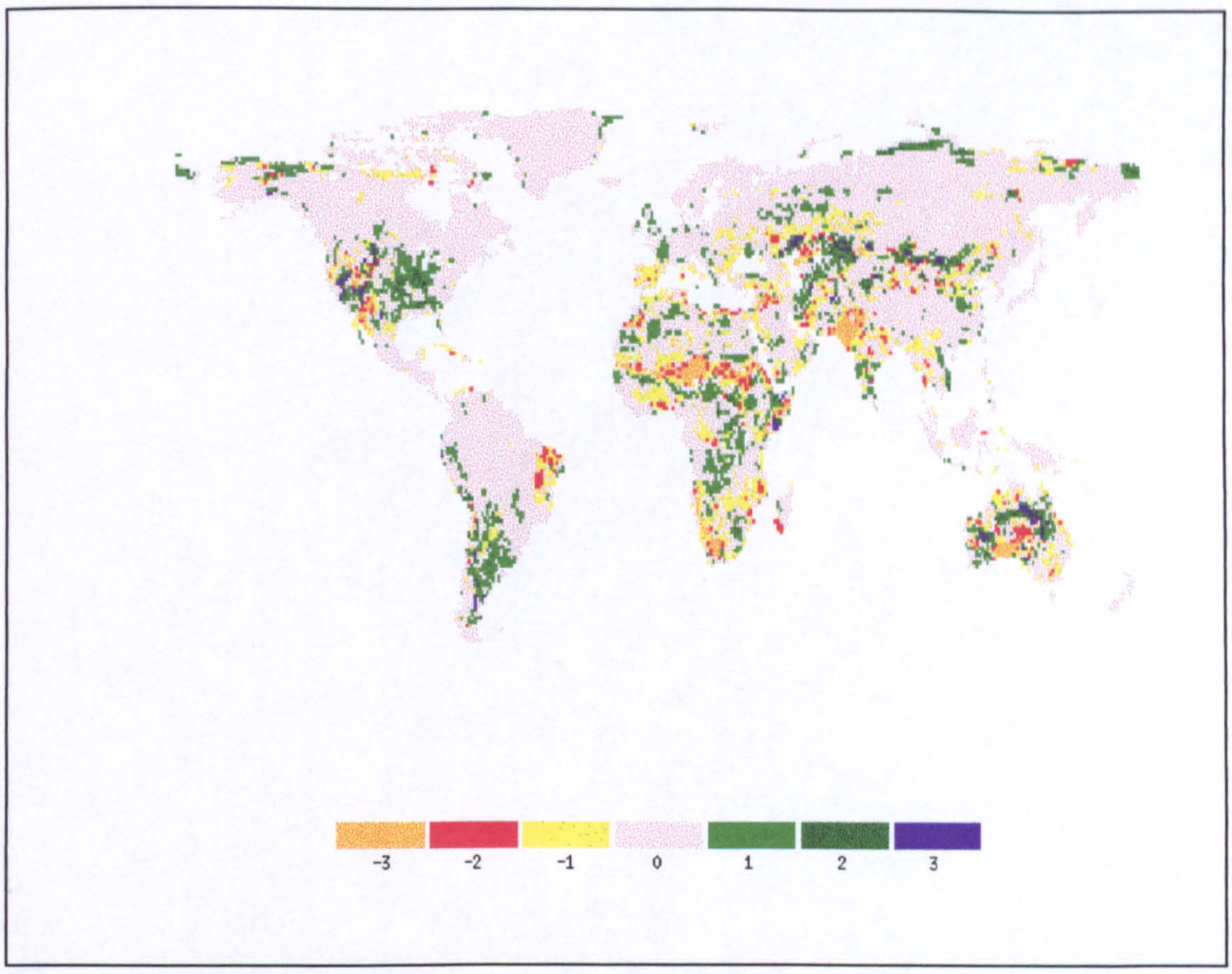

Figure 7.5 Differences between LAI values in 1987 and 1988 derived from the DOLY model (water and soil version) using the ISLSCP dataset. The absolute values of LAI range between 0 and 12. Positive deviations occur when the LAI in 1987 exceeds those of 1988 and negative deviations are for the reverse situation.

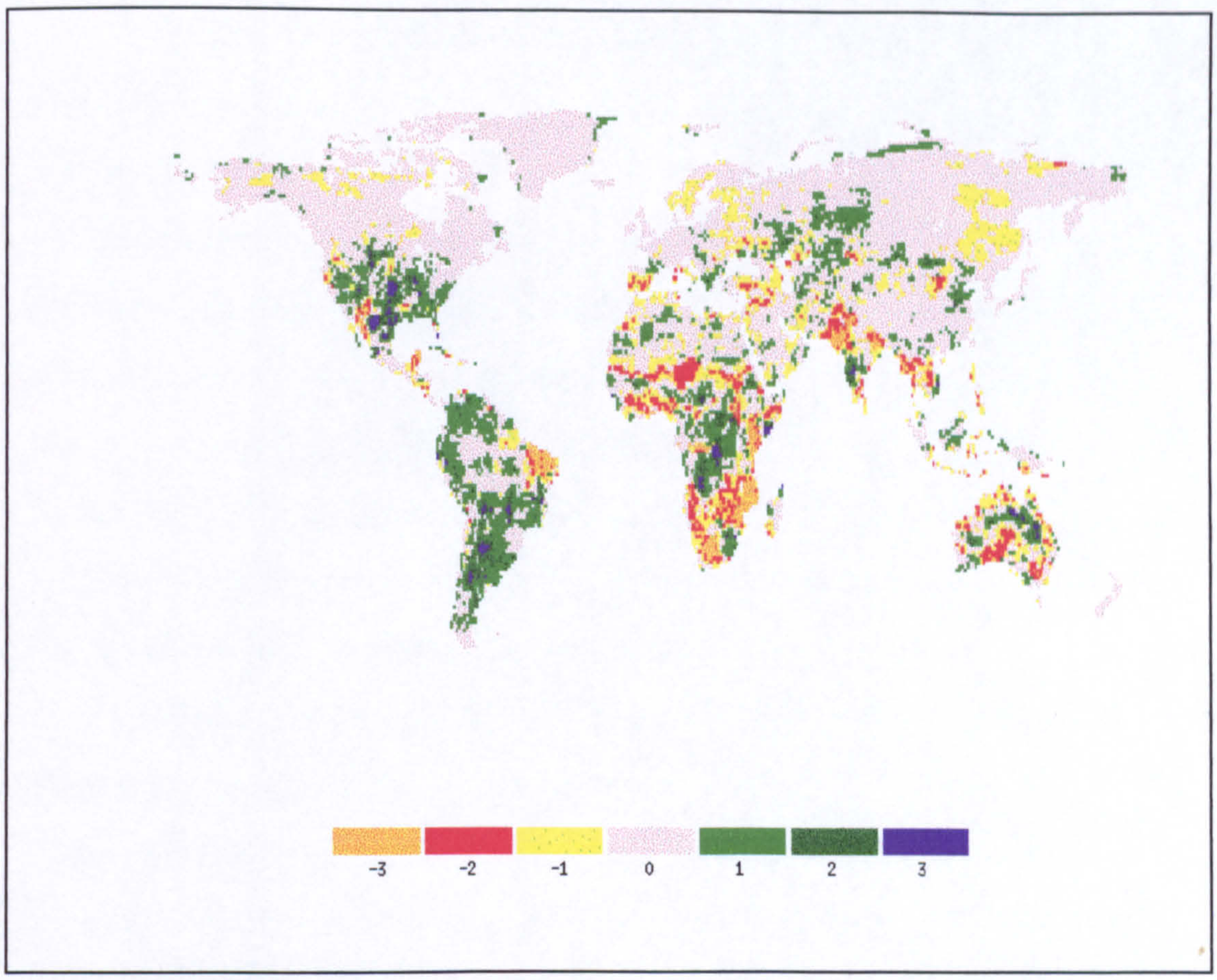

Figure 7.6 Difference between NPP values in 1987 and 1988 derived from the DOLY model (water and soil version) using the ISLSCP dataset. Absolute values of NPP range between 0 and 11 tC ha^{-1} yr^{-1}. Positive deviations occur when the NPP in 1987 exceeds those of 1988 and negative deviations are for the reverse situation.

Figure 7.5 shows that the LAI for 1987 exceeds that for 1988 in central southern America, western South America, central Asia, northern Siberia and western and northern parts of Australia. In western Australia this was due to the warmer and wetter conditions that occurred in 1987 (Table 7.6a). In northern Australia, it was also warmer and wetter in 1987 than 1988, but the VPD was lower in 1987 due to the higher humidity (Table 7.6b). In 1987, northern Siberia was slightly drier and fractionally warmer than in 1988, which caused the LAI to be higher than in 1988. In central southern America, it was warmer and much wetter in 1987 than 1988, with a lower VPD value due to the slightly higher mean humidity (Table 7.6b).

Regions where the LAI is lower in 1987 than 1988 include the northern savanna regions of Africa, southern Australia and parts of North Africa where it was drier and warmer in 1987 with higher VPD values and lower humidities (Tables 7.6a and b). In southern Australia, the VPD values were higher in 1987 than in 1988 due to a warmer temperature in 1987 and the fact that the humidity didn't change between the years (Table 7.6b). In south-western Africa, Iran and eastern Brazil, the LAI values were also lower in 1987 compared with 1988. In these regions it was warmer, though wetter in 1987 compared with 1988 (Table 7.6a), again with higher VPD values (Table 7.6b). Iran was also more humid in 1987 but the higher temperatures led to higher VPD values than 1988 (Table 7.6b).

Figure 7.6 shows the changes in NPP that occur between these two years. Southern Africa, Iran, eastern Brazil and Pakistan are areas where there has been a negative deviation (the values of 1988 exceed those of 1987) of 2 to 3 tC ha^{-1} yr^{-1}. These areas also show an LAI negative deviation of 2 to 3. Positive deviations in NPP (the values of 1987 exceed those of 1988) arise in Central Africa, southern South America, and the south and south-western states of America. In all these regions the VPD values in 1987 were lower than those of 1988 (Table 7.6b). The NPP in northern Australia in 1987 exceeded the 1988 value by 2 to 3 tC ha^{-1} yr^{-1} due to warmer and wetter conditions in

1987. The reverse effect occurred in southern Australia where it was warmer but drier with a higher VPD in 1987 (Table 7.6b) compared with 1988.

Table 7.6a Total annual rainfall (mm yr^{-1}), and mean annual temperature (°C), for 13 global locations obtained from the ISLSCP datasets (1987 and 1988).

Area description	Latitude & longitude	Mean temp. (1987) °C	Mean temp. (1988) °C	Total precip. (1987) (mm yr^{-1})	Total precip. (1988) (mm yr^{-1})
Northern Siberia	75°N 90°E	-14.8	-14.9	207	269
Western Australia	27°S 120°E	22.0	20.4	355	208
Northern Australia	17°S 135°E	27.2	26.6	776	417
East Brazil	5°S 37°W	21.1	19.6	598	573
Iran	27°N 60°E	20.1	19.0	55	18
North Africa	38°N 1°W	16.1	15.6	354	372
South Australia	30°S 130°E	19.5	18.4	163	213
Central southern America	38°N 96°W	13.5	12.3	888	563
SW USA	32°N 116°W	19.2	18.5	114	98
Northern savanna (Africa)	15°N 30°E	27.8	26.2	155	263
South-west Africa	33°S 18°E	16.5	16.1	266	223
Southern South America	55°S 67°W	5.1	4.7	518	535
Central Africa	5°N 28°E	25.3	24.2	1341	948

Table 7.6b Mean annual humidity and mean vapour pressure deficit (VPD) values for 13 global locations obtained from the ISLSCP datasets (1987 and 1988)

Area description	Latitude & longitude	Mean humidity (1987) %	Mean humidity (1988) %	Mean VPD (1987) (× 10^2 Pa)	Mean VPD (1988) (× 10^2 Pa)
Northern Siberia	75°N 90°E	91	90	0.18	0.19
Western Australia	27°S 120°E	30	30	18.45	16.78
Northern Australia	17°S 135°E	45	42	19.90	20.36
East Brazil	5°S 37°W	76	78	5.91	5.11
Iran	27°N 60°E	26	24	17.42	16.61
North Africa	38°N 1°W	70	72	5.48	5.01
South Australia	30°S 130°E	35	35	14.75	13.70
Central south America	38°N 96°W	79	74	3.23	3.77
SW USA	32°N 116°W	49	42	11.30	12.45
Northern savanna (Africa)	15°N 30°E	25	28	27.92	24.40
South-west Africa	33°S 18°E	60	59	7.60	7.53
Southern South America	55°S 67°W	82	81	1.62	1.65
Central Africa	5°N 28°E	66	56	10.82	13.41

To summarize, in dry areas such as Iran, eastern Brazil, southern and western Australia, the LAI and NPP values were reduced in 1987 due to the warmer conditions and higher VPDs that occurred in these regions. In areas where there was no water shortage such as central Africa, central southern America, and northern Australia, the warmer and much wetter conditions of 1987, compared with 1988 in these regions, led to higher humidities and lower VPDs increasing the LAI and NPP values.

Table 7.7 shows how the global NPP and LAI vary between the years, 1987 and 1988.

Table 7.7 Total global NPP, mean global LAI, and the global vegetated area predicted by the DOLY model (water and soils version). The model was run with ISLSCP climate data for 1987 (1° by 1° grid) and ISLSCP climate data for 1988. The mean annual temperature and mean annual precipitation are also shown. The mean humidity for both the ISLSCP 1987 dataset and the ISLSCP 1988 dataset is 71%. The global land area is 135.3×10^6 km^2. This area is slightly lower than that for Table 7.2 due to the different grid resolutions used.

Dataset	Total global NPP (GtC ha $^{-1}$ yr^{-1})	Mean global LAI	Global vegetated area ($\times 10^6$ km^2)	Mean annual temp. (°C)	Mean annual pptn. (mm)
ISLSCP 1987	54.5	4.0	110.7	4.3	645
ISLSCP 1988	55.4	4.0	114.1	3.7	698

It is interesting that the global NPP for 1988 is very close to the value of 55.9 GtC ha^{-1} yr^{-1}. This is the value derived from the DOLY model (water and soils version) run with the IIASA dataset and the Leeman's humidity values (see Table 7.2). However, the vegetated area of 106.5×10^6 km^2 in

Table 7.2 is slightly lower. Also the mean global temperature is lower in 1988 compared with the figures for the IIASA dataset, although the mean annual precipitation of 698 mm is slightly higher. The changes between global NPP and vegetation cover for 1987 and 1988 are a reflection of the changes in precipitation, and temperature that occur due to an El Niño event. The ISLSCP 1987 dataset has a slightly higher global mean temperature than the ISLSCP 1988 dataset but a lower NPP value due to a combination of higher VPDs and lower mean annual precipitation. There is no difference in mean annual relative humidity between the two years. The changes that occur in precipitation between the years 1987 and 1988 are shown in Figure 7.7.

Increases in precipitation contribute to the increases in NPP and LAI in the regions that have been noted previously in this section, but temperature is important too. It tends to decrease with increasing precipitation as cloud cover increases. If temperatures fall, the vapour pressure deficit decreases and humidity increases. In cold areas such as Siberia and Canada a negative deviation of 20 mm in mean annual precipitation has virtually no impact on LAI and NPP. On the other hand, the same change in a warm and dry area, such as south-west Africa causes decreases in NPP of 2 or 3 tC ha^{-1} yr^{-1} (Figure 7.6). Also, larger changes in precipitation, such as the positive deviations of 40 to 80 mm that occur in the equatorial regions of the Amazon and New Guinea have little impact on NPP and LAI. This is because there is no shortage of water in these regions. However, a negative deviation of 20 mm in the desert areas of central Australia has a noticeable effect leading to a decrease of 2 to 3 tC ha^{-1} yr^{-1} (Figure 7.6) and a LAI reduction of 2 to 3 (Figure 7.5).

Finally, an additional map has been produced which shows the difference in mean annual ISLSCP humidity between the two years 1987 and 1988 (Figure 7.8).

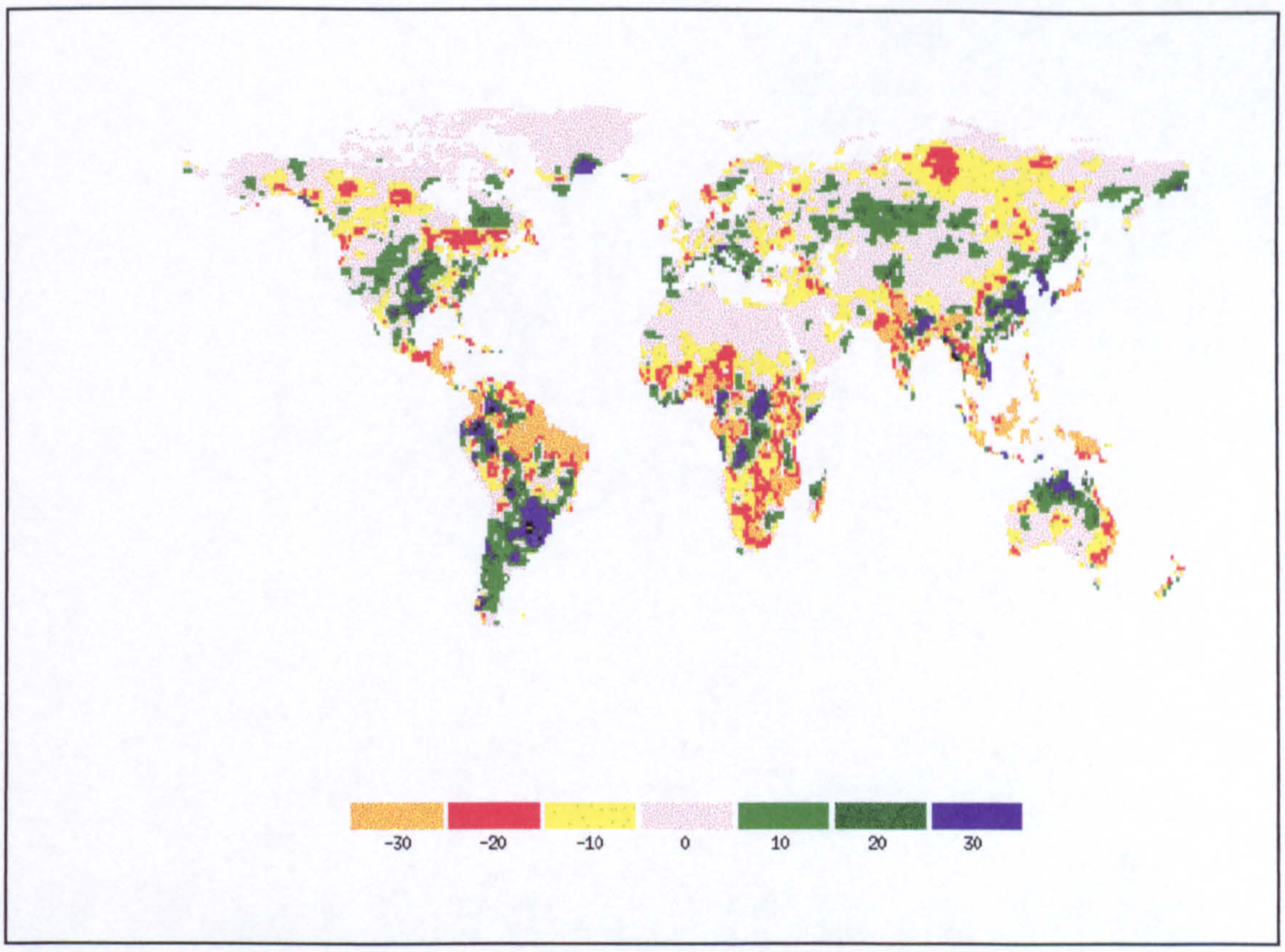

Figure 7.7 Difference in mean annual precipitation (mm) between the years, 1987 and 1988 derived from the ISLSCP dataset. Absolute values of monthly precipitation range between 0 and 500 mm (equivalent to total annual values of between 0 and 6 m) for the ISLSCP 1988 data and between 0 and 475 mm (equivalent to total annual values of between 0 and 5.7 m) for the ISLSCP 1987 data. Positive deviations occur when the precipitation in 1987 exceeds that of 1988 and negative deviations are for the reverse situation.

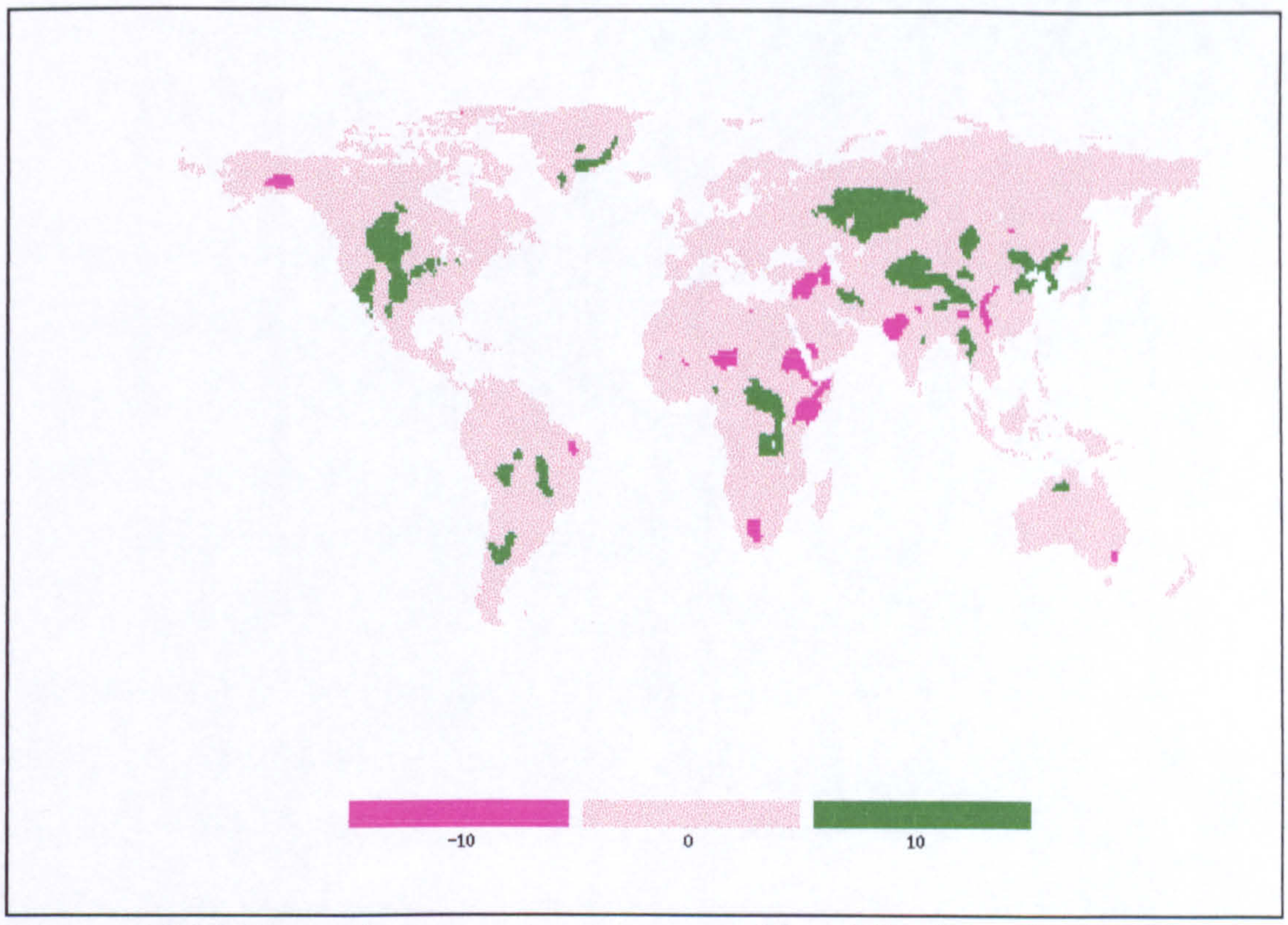

Figure 7.8 Difference between the mean annual humidity (% points) of the ISLSCP dataset for 1987 and for 1988. Absolute values of monthly humidity range between 0 and 100%. Positive deviations occur when the 1987 humidity values exceed the 1988 humidity values and negative deviations are for the reverse situation.

Figure 7.8 shows that despite the differences that arise in precipitation and temperature between the years, 1987 and 1988 (Figure 7.7), the differences in the mean humidity values between these two years are small (–10 to +10 % points). Although the mean global temperature is greater in 1987 than 1988 the mean global vapour pressure deficit for 1987 is only slightly higher than that for 1988 (2.4×10^2 Pa compared with 2.3×10^2 Pa). In western Siberia, western China, central and southern U.S.A., eastern Zaire and southern Greenland higher values of humidity occur in 1987 than 1988. This suggests that the VPD values are lower in 1987 for these areas, together with lower temperatures and increased rainfall. Areas where lower humidities occur in 1987 than in 1988 are Lebanon, Israel, Syria and southern Turkey. This also occurs in Pakistan, eastern Sudan, northern Niger, Somalia, Ethiopia and South

Africa. This suggests that the VPD values are higher in 1987 for these areas together with higher temperatures and reduced rainfall.

This map shows that, although 1987 is an El Niño year, which mainly affects global precipitation (Bigg, 1990; Folland *et al.*, 1986), the effect on humidity between these two years is minimal. This is a useful result as it suggests that mean humidity is relatively insensitive to changes in precipitation. It appears to be fairly static globally (i.e., the amount of variation is of the order of 10% points) between years, providing that there are no major vegetation changes. At the moment it is not easy to find a global dataset on humidity. This situation is likely to change though over the next few years as demand increases from the ecological modelling community for such a dataset. It is therefore difficult to obtain any reference against which to check this level of variation.

7.4 Discussion and conclusion

This chapter has shown how climate datasets influence the LAI and NPP values from the DOLY model (water and soils version). Differences in LAI and NPP that are a result of the use of these different climate datasets can be used to improve the datasets themselves. These differences highlight areas where the datasets have underestimated or overestimated precipitation and temperature.

It has been shown how increasing temperature, in a warm and arid area leads to an increased vapour pressure deficit and increased evaporative demand, reducing LAI and NPP. If there is sufficient water supply, LAI and NPP may increase. In cold regions, temperature assumes a greater importance than the water supply, and LAI and NPP increase with temperature. These effects are further modified by changes in humidity.

The Sahel, southern Brazil, the Pampas region of Argentina, eastern Africa and central Australia are the main areas where the model generates

differences in LAI and NPP values between runs using GCM slab and IIASA climate data. In the Sahel, southern Brazil and the Pampas region of Argentina, the slab model has lower precipitation amounts compared with the IIASA dataset and actual data (Table 7.4). In central and south-western Australia, and eastern Africa the slab precipitation data exceeds the IIASA data and actual data (Table 7.4). Allowing for changes to the original IIASA dataset, and comparisons with actual data, the slab model still appears to underestimate rainfall in the Sahel and overestimate it in central and south-western Australia.

Such results are useful to both GCM modellers and to ecological modellers. Areas where improvements can be made to the GCM models have been highlighted as well as areas where vegetation model output has been influenced by inaccurate climate inputs.

This work has also shown that mean global LAI varies very little with the use of different datasets and remains around 4. Global NPP and the vegetated area are more variable with a range in NPP between 54.5 GtC ha^{-1} yr^{1} (ISLSCP 1987), and 57.7 GtC ha^{-1} yr^{-1} (CLIMATE). The other datasets have NPP values of 55.4 GtC ha^{-1} yr^{-1} (ISLSCP 1988), 55.9 GtC ha^{-1} yr^{-1} (IIASA) and 54.6 GtC ha^{-1} yr^{-1} (slab, $1 \times CO_2$). All these values are remarkably similar, given the different sources and projections of the datasets.

Another result of interest is the observation that global humidity changed very little between the years 1987 and 1988. This is despite the fact that 1987 was an El Niño year. This caused increased rainfall in many parts of the world, but also droughts, for instance in central Australia, much of Africa and northeastern South America, which meant that the mean annual rainfall for 1987 was actually lower than that for 1988. The temperature differences between the years contributed to changes in vapour pressure deficit values and gave noticeable regional effects to LAI and NPP, but the mean global vapour deficit did not alter much (2.4×10^2 Pa for 1987 and 2.3×10^2 Pa for 1988).

The differences in LAI and NPP between the years 1987 and 1988 from the ISLSCP climate data have indicated the model's sensitivity to annual climatic differences.

Areas where the slab climate data are in error in relation to actual data have been identified within this chapter. This means that greater confidence can be given to the level of accuracy of outputs from the DOLY model (water and soils version) than previously. For instance, the high LAI and NPP values in central Australia, and the low values in the Sahel for the present-day can be attributed to inaccuracies in the slab precipitation data. It is important to rectify these errors in the slab climate data as the arid areas where they are incorrect are most at risk from adverse effects caused by climate change. It is also important to ensure that the present-day data is as accurate as possible to produce a realistic projection of future vegetation distribution.

CHAPTER 8

8.0 Modelling global distributions of LAI and NPP using the DOLY model run with transient climate data.

8.1 Introduction

Chapters 5 and 6 demonstrated how climate change effects may be modelled using the DOLY model. In Chapter 5 a life–form model was used to demonstrate the possible movement of vegetation in response to climate change as simulated by the UKMO (United Kingdom Meteorological Office) slab model. In Chapter 6, feedbacks between climate and vegetation were simulated by coupling the DOLY model to the slab model and there was an analysis of the effect of climate change on values of leaf area index (LAI) and net primary productivity (NPP) using the climate predictions from the slab model. The UKMO has recently made available transient climate data for the period 1831 to 2100 produced by Unified Forecast and Climate Model, a full Ocean–Atmosphere model. The data is from the version of the model known as HadCM2 (2nd Hadley Centre Coupled Model). These data provide a more accurate simulation of a possible future climate than the slab model as they account for sulphate aerosols (which reduce the rate of warming) as well as atmospheric CO_2 (scenario IS92a, see IPCC,1995). Further details on this particular version of the GCM can be obtained from Johns *et al.* (1997).

The aim of this chapter is to present global maps of LAI and NPP as predicted by the DOLY (water and soils version) model for three time periods representing the pre-industrial era, the present day and the year 2100 to show how these values vary with a simulated climate change. Values of global NPP and LAI have been calculated for each of these time periods. The values of LAI

and NPP are for natural vegetation with no allowance made for disturbance of either a human or natural type.

8.2 Methods

The DOLY (water and soils version) model was run with the transient climate data for the period 1861 to 2100 (i.e. it was integrated forward from 1861 to 2100). Three time periods: 1861–1870; 1988–1997; 2091–2100 were then selected from this run. These time periods were selected to be representative of: i) a time before atmospheric CO_2 concentrations started to increase with the pollution of the industrial revolution, ii) the present-day; and ii) a time when the concentration of atmospheric CO_2 is expected to have more than doubled. These periods are in effect "snapshots" of a complete transient run, as soil carbon and nitrogen carry through from one time period to another. These climate data consist of one file containing the latitude and longitude of each grid cell and four other files containing mean maximum temperature, mean minimum temperature, precipitation and humidity for each month of the year. The precipitation and humidity are mean monthly values. The maximum and minimum monthly temperature were totalled and divided by two to determine the mean monthly temperature for each cell. The transient data are on a 2.5° by 3.75° global grid. There are 1631 terrestrial cells in total. The temperature and precipitation data for the period 1931 to 1960 were cross-checked against the IIASA climate dataset (Leemans and Cramer, 1991) by Wolfgang Cramer. It was found that the modelled data differed noticeably from the IIASA dataset across the globe for these two variables. In order to correct for these anomalies, Cramer created correction files that adjusted the modelled data to the same values as the IIASA dataset for the 1931 to 1960 period. This correction factor was then used in conjunction with the rest of the transient data. The implicit assumption with this technique is that the modelled

data for the years outside the 1931 to 1960 period would require this same adjustment factor. It is also assumed that the increases in atmospheric CO_2 and the other greenhouse gases have been modelled correctly so that the trends in the data are correct.

The DOLY model (water and soils version) was run with the corrected transient climate data for each year within the three time periods. The atmospheric CO_2 value was altered for each year according to the IPCC IS92a scenario (the 10 year global mean values are shown in Table 8.1). The LAI values for each year were then totalled and divided by 10 to derive a mean value for each10-year period. This method was repeated with the NPP values. This technique averages the interannual variability.

8.3 Results

Global maps of the 10-year mean values of LAI and NPP were plotted for each of the three time periods, 1861–1870; 1988–1997; 2091–2100. These are shown in Figures 8.1 to 8.6 respectively. Figures 8.1 and 8.2 show the LAI and NPP values for the time peiod 1861 to 1870. It can be seen that the values of LAI range from 0 to 9 globally, with north-east Asia having values of the order of 0 to 2, the northern savanna/Sahara desert boundary in Africa has values between 0 and 3, south-western Australia has LAI values of less than 2, much of Europe ranges between 3 and 5 as does the eastern seaboard of America and southern Africa. The Gobi desert and the southern Russian steppe both have LAI values of less than 1, as does the Sahara desert and much of Saudi Arabia. The rain forest regions of South America, Zaire and Indonesia have LAI values exceeding 7.

Figure 8.2 shows a global range in NPP of between 0 and 14 tC ha^{-1} yr^{-1}. The highest values of NPP, as with LAI, occur in the equatorial rain forest regions with values exceeding 10 tC ha^{-1} yr^{-1}. Much of Europe has NPP values which range between 3 and 6 tC ha^{-1} yr^{-1} with the

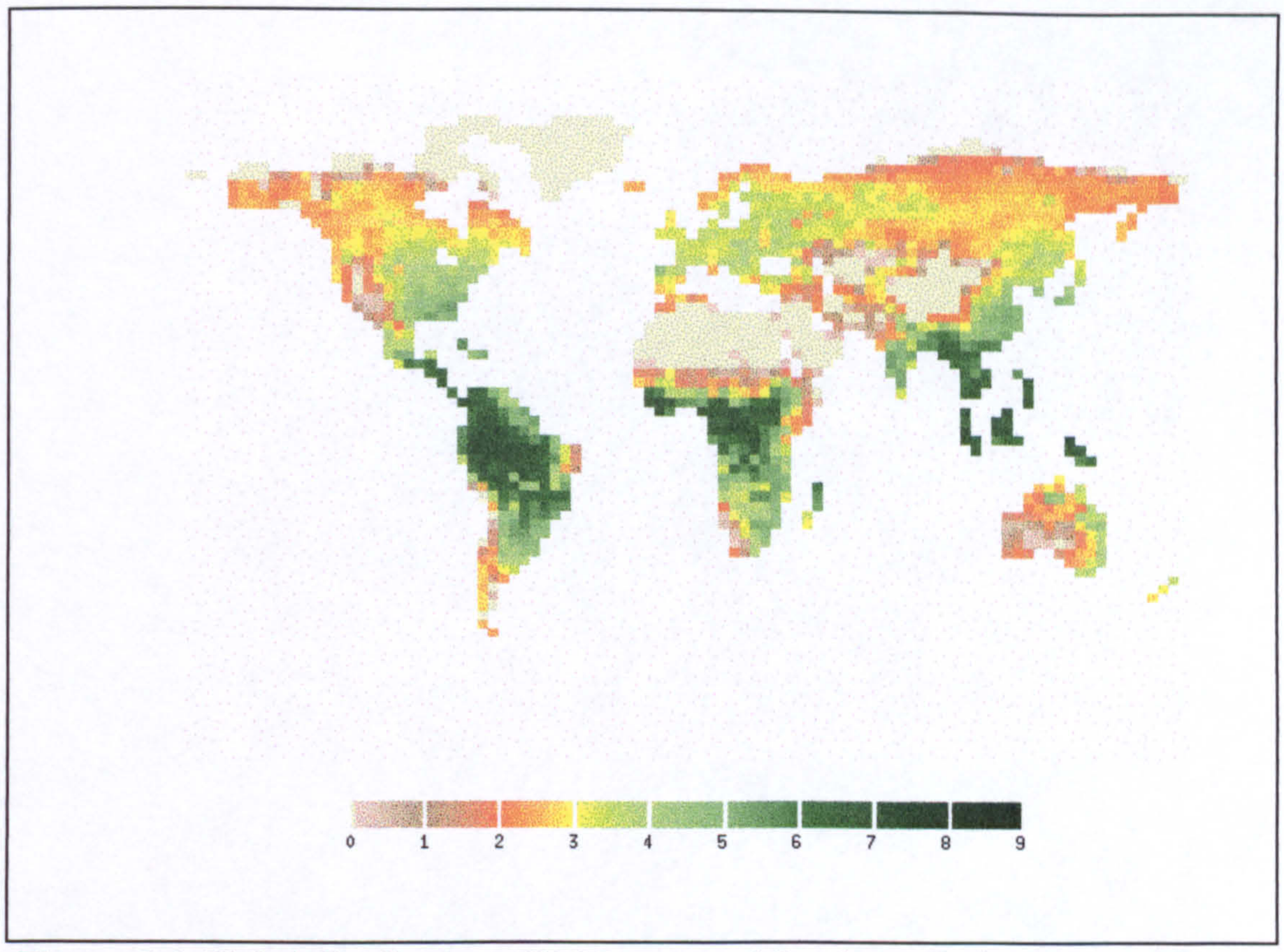

Figure 8.1 Global distribution of LAI averaged for the period 1861 to 1870.

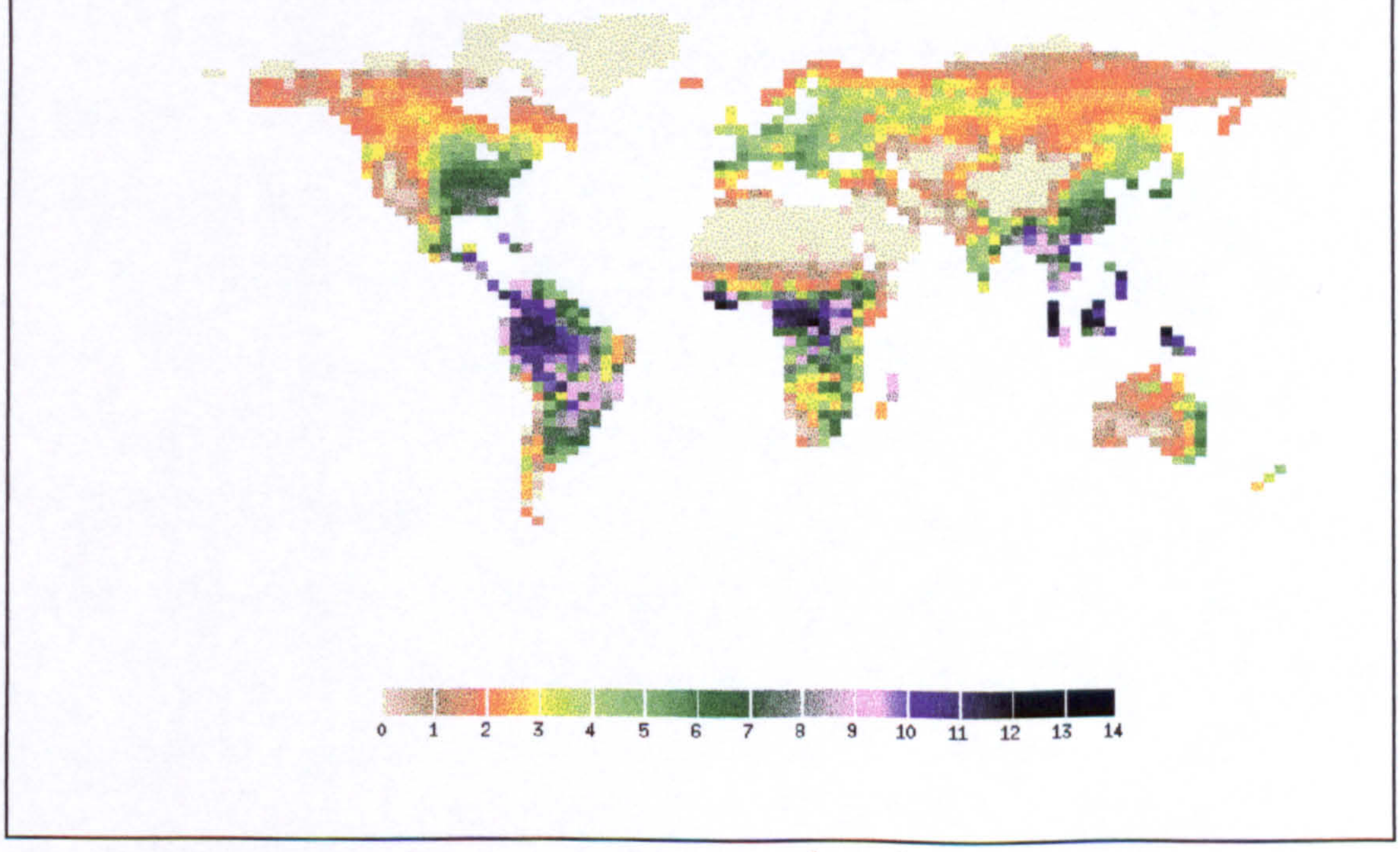

Figure 8.2 Global distribution of NPP (tC ha^{-1} yr^{-1}) averaged for the period 1861 to 1870.

eastern seaboard of America having an NPP up to 10 tC ha $^{-1}$ yr $^{-1}$. Desert areas have NPP values of less than 1 and the tundra regions range between 0 and 3 tC ha $^{-1}$ yr $^{-1}$. Figures 8.3 and 8.4 show the model predictions for the present day climate for LAI and NPP. A number of changes from the pre-industrial distribution become evident. For example, in Figure 8.3 it can be seen how there has been a slight increase in LAI of 1 on the fringes of the desert areas. LAI has also increased in north-east Asia and northwestern Canada by 1 to 2. Elsewhere, for instance in southern China, and the southern fringes of the African rain forest, the LAI has decreased by 1. In South America the LAI has increased in Brazil by 1 to 2. Slightly different patterns emerge with the NPP values (Figure 8.4). In the rain forest areas NPP has risen by 1 or 2 tC ha^{-1}yr $^{-1}$ and the higher values cover a wider area than those from the pre-industrial era. In north-east Asia, Europe, eastern America and northern Canada the NPP values have also risen by 1 or 2 tC ha^{-1}yr $^{-1}$. Such a change is more significant in the higher latitudes due to the lower initial NPP values. On the desert fringes on the Gobi, the Australian and Saharan deserts the NPP has also risen by 1 tC ha^{-1}yr $^{-1}$.

These LAI and NPP values have not been tested against other data, or compared with the results from other models as the transient data have only recently become available. However, it would be interesting to compare the LAI and NPP predicted by other models using these data with those from DOLY as well as to compare the transient data from the UKMO with similar data from, for example, the atmospheric general circulation model ECHAM. This GCM has been developed at the Max-Plank-Institut in Hamburg and the climate data used by Claussen (Claussen, 1996) to drive the BIOME model of Prentice *et al.* (1992). Validation issues concerning the DOLY model are discussed in Chapter 9.

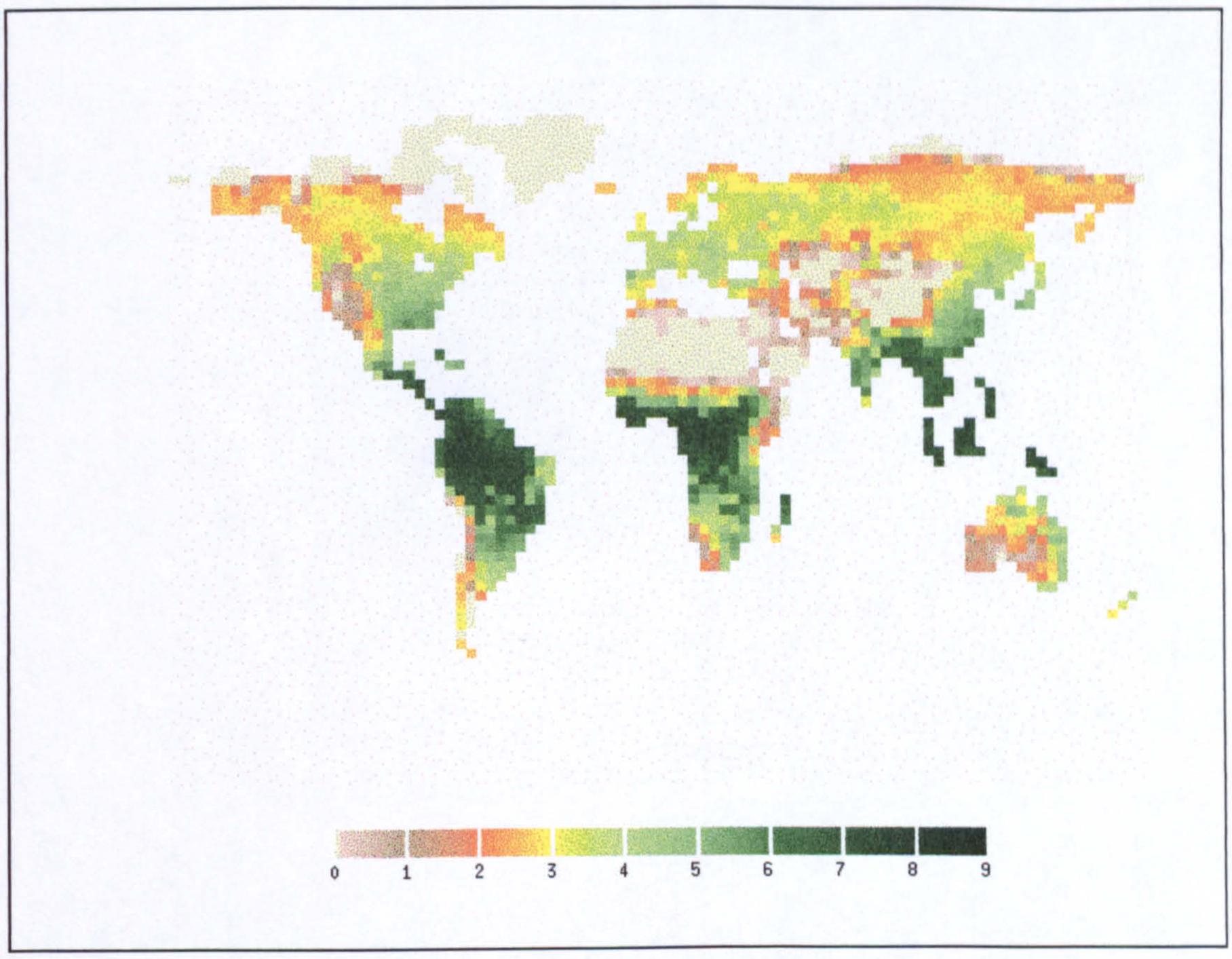

Figure 8.3 Global distribution of LAI averaged for the period 1988 to 1997.

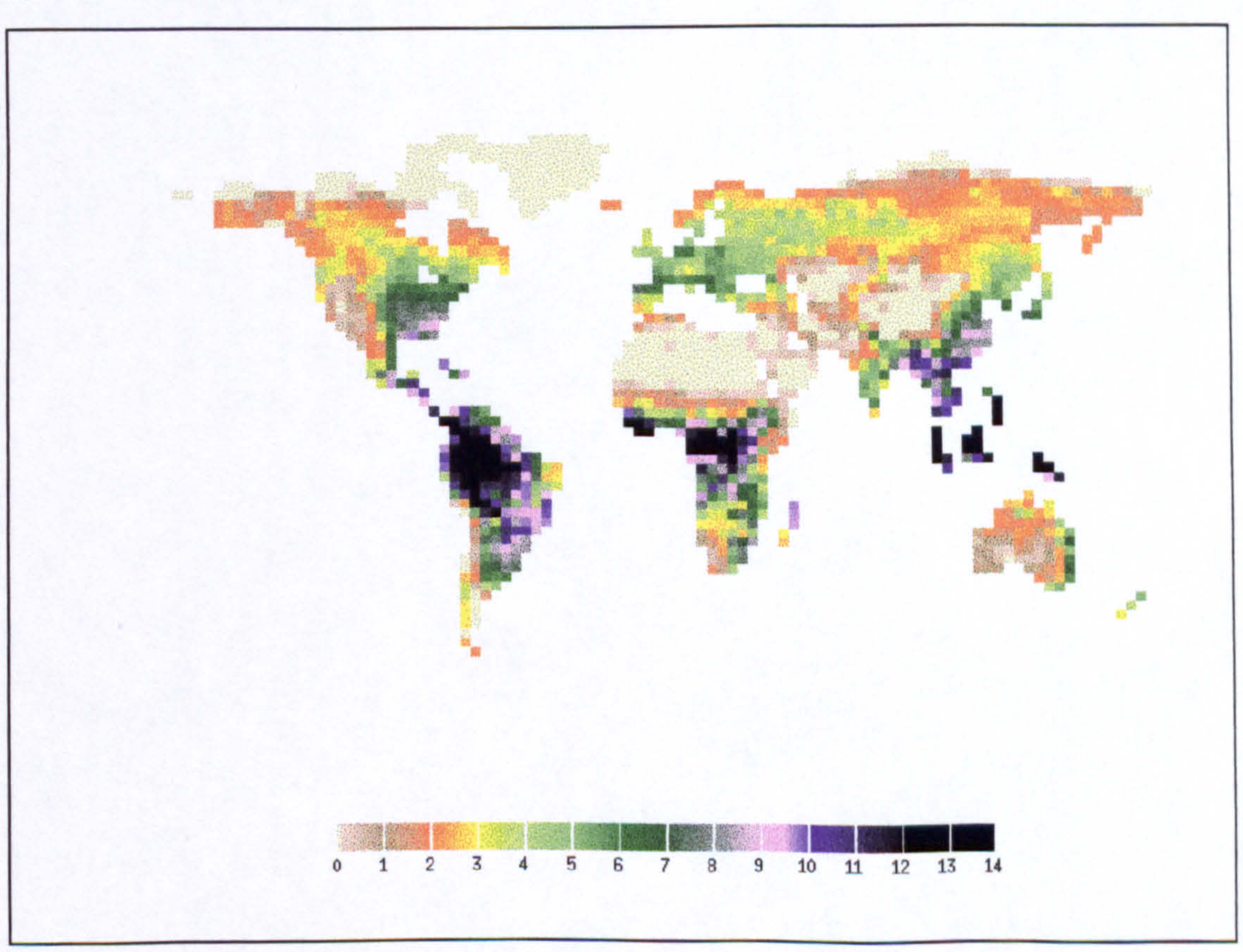

Figure 8.4 Global distribution of NPP averaged for the period 1988 to 1997.

Finally, if we now consider the future scenario for the period, 2091 to 2100 (Figures 8.5 and 8.6) it becomes immediately apparent that there have been major changes in both LAI and NPP. Looking at the LAI changes first of all (Figure 8.5), it can be seen that there has been an encroachment into many of the desert areas particularly the southern steppe of the USSR and the Gobi desert with LAI values rising by 2 and 3 in some places. Also, along the northern savannah–Sahara desert boundary, there has been a shift northwards with LAI values increasing by 1 or 2. In Australia, there has actually been a decrease of 1 on the eastern boundary of the desert but there has also been increase of around 1 on its southern fringes. Elsewhere, in the rest of the world much of Europe, North and South America, as well as central and southern Africa show increases in LAI of up to 3. The boreal forest–tundra boundary also shows marked changes where LAI values have increased from 2 or 3 for the present-day to 5 or 6 for the period 2090 to 2100. Figure 8.6 shows the effect of changing climate on NPP values (it should be noted that the scale is in steps of two to account for the greater range of values). Across much of the world the NPP has increased by around 2 or 3 tC ha $^{-1}$ yr $^{-1}$ with marked increases of up to 6 tC ha $^{-1}$ yr $^{-1}$ occurring in the rain forest regions. The encroachment on the desert boundaries is evident as is the shift northwards of the savannah–Sahara desert boundary and the shift northwards of higher NPP values in the boreal regions where boreal forest encroaches into the tundra. These effects are due to warming in the high latitudes which has been shown to be an important factor in the movement of the boreal forest northwards in Chapters 5 and 6. Also, the amount of soil moisture and evapotranspiration have an important impact on LAI and NPP in the drier regions with a changing climate and elevated CO_2. Carbon dioxide moderates the effect of warming in the more arid regions of the world by increasing the water use efficiency of the vegetation.

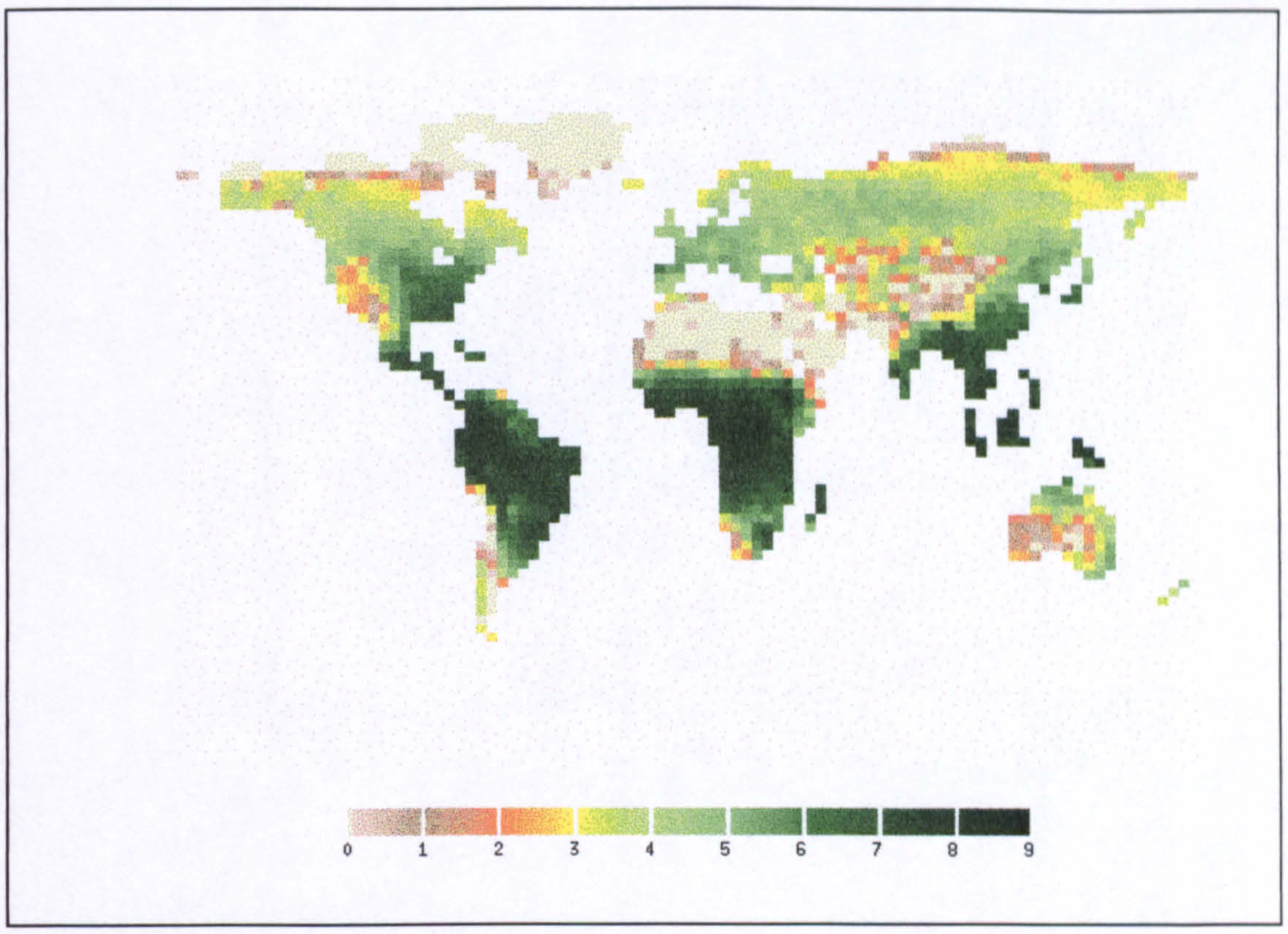

Figure 8.5 Global distribution of LAI averaged for the period 2091 to 2100.

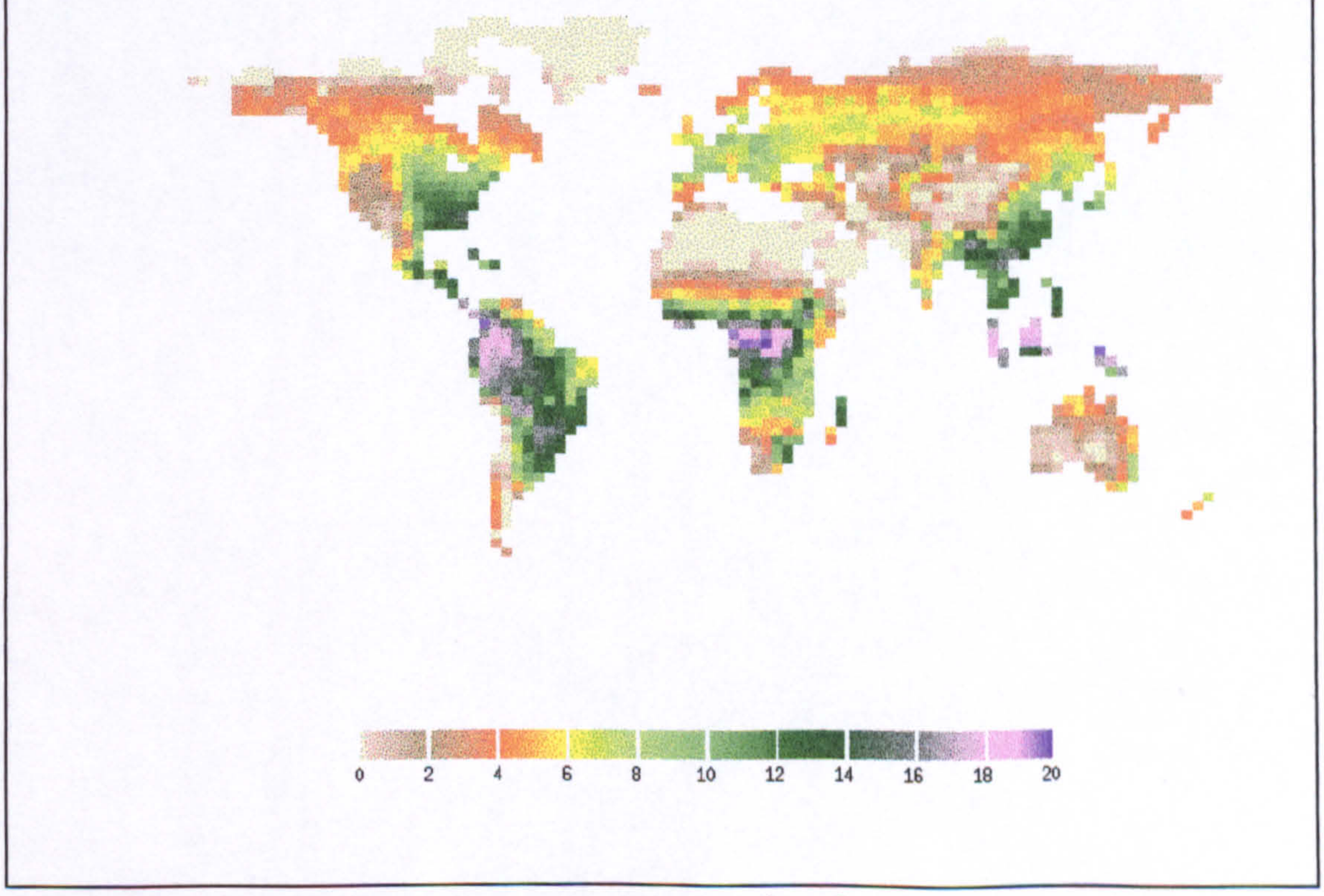

Figure 8.6 Global distribution of NPP (tC ha^{-1} yr^{-1}) averaged for the period 2091 to 2100. Note that this scale in steps of 2.

Table 8.1 shows how the global LAI and NPP change over time with the transient data. It shows that between the pre-industrial era and the year 2100, the global NPP increases by 70% and the LAI increases by one third. The global vegetated area also increases by 5%. Also the LAI and NPP values show a much greater increase between the periods 1988 to 1997 and 2091 to 2100 compared with 1861 to 1870 and 1988 to 1997 due to the greater increase in temperature and atmospheric CO_2 concentration. This is also reflected in the increase in vegetated area.

Table 8.1 Total global NPP, mean global LAI, and the global vegetated area predicted by the DOLY model (water and soils version). The model was run with the UKMO transient climate data for the periods 1861, 1997 and 2100. The global land area is 136×10^6 km^2.

Time period	Total global NPP (Gt C yr^{-1})	Mean global LAI	Global vegetated area ($\times 10^6$ km^2)	10 year mean atmospheric CO_2 (Pa)
1861 to 1870	48.5	3.6	114.2	28.9
1988 to 1997	55.0	3.8	115.5	36.0
2091 to 2100	81.6	4.8	120.3	76.8

8.4 Discussion and conclusion

This simulation has demonstrated the possible impacts of elevated CO_2 and a changing climate on LAI and NPP at both the regional and the global level. The greatest changes are likely to occur at the boreal forest–tundra boundary as has been shown by other authors (Bonan *et el.*, 1990, 1992 Shugart *et al.*, 1986; Solomon, 1986; Lenihan, 1993), as well as at the savanna–Sahara desert boundary. This assumes that the UKMO transient model is a good predictor of a future climate. It is also interesting to note the shrinking of the Gobi desert and the southern steppes, which offers promise to the possibility of agriculture in previously arid lands. Obviously there has been no element of disturbance in this simulation and it is extremely likely that the impact of forest fires will cause greater changes in the short-term. Also, it is assumed that vegetation will be able to respond to these changes in climate but this is not always possible where human activities play a major role. This simulation has been useful in that it has identified possible sensitive areas of change and shown the magnitude of changes caused by changes in CO_2 and climate as simulated by the UKMO Unified Forecast and Climate Model. These areas of change are similar to those noted by Claussen (1996) using ECHAM and the BIOME model of Prentice *et al.* (1992) although vegetation types as opposed to LAI and NPP were used in their simulation for a climate with elevated CO_2 (1145 ppm (114.5 Pa)) and a global mean surface temperature approximately 2.4°C higher than today.

CHAPTER 9

9.0 Validation issues

9.1 Introduction

This thesis has been concerned with the development of the DOLY model, its sensitivity to the soil and climate inputs, and the use of its outputs within other models. It has been stressed throughout that it is very difficult to validate the output from this model with observed data in the field or with other models.

The aim of this chapter is to discuss the issues of validation and to place the problems encountered with DOLY within this context. Other workers (Beerling and Woodward, 1998 and Beerling *et al.*, 1997) have recently attempted to validate the latest version of the vegetation model, the SDGVM (Sheffield Dynamic Global Vegetation Model). Their results are presented here as a reference against which to compare the results from the DOLY (water and soils version) model.

All models need be constantly monitored and assessed during their development to ascertain their level of accuracy in relation to the variable they are modelling. This also ensures that their output is sensible with regards to the 'real' world.

The act of validation can be defined as a conformation or corroboration, as opposed to verification that proves something to be true. However, some authors (Oreskes *et al.*, 1994), are highly critical of the whole concept of validation and discuss problems with the philosophy, as well as the terminology used in the process of validation.

Validation may be divided into two main types: structural (or

conceptual) and empirical. Structural validation is concerned with how the model represents the real world and the importance of the parameters used within the system. Such a validation is concerned with the correspondence of actual processes, system properties and measurements, to processes, parameters, and state variables in the model. Empirical validation, on the other hand, is concerned with the comparison of model predictions with observations from the actual system being modelled (Mitchell & Sheehy, 1997). The differences that arise from such a comparison need to be assessed to determine how well the model has performed.

It would be impossible in principle, to fully verify the DOLY model output, but is possible to make some attempt to validate it by comparisons with actual data, satellite data and with other models. However, none of these comparisons can be described as a truly empirical validation. Actual data are prone to errors, and, although satellite data and the output from other models, are both derived from the real world, they are, by no means, a fully accurate representation of it. It is important though, to try to obtain some indication as to a model's performance.

Most modellers use regression techniques to compare observed data with those predicted by their model (Aber and Federer, 1992; Woodward *et al.*, 1995; Parton *et al.*, 1993), or compare their results with output from other models (Raich *et al.*, 1991; Neilson and Marks; 1995; Ryan *et al.*, 1996a, b). Some, Prentice *et al.*, (1992), have used the kappa statistic to compare their model output with actual global vegetation data, but made the point that this statistic is not a perfect measure of similarity between maps. Monserud and Leemans (1992) admit that the kappa statistic has its limitations when comparing two maps with a large number of grid cells (e.g. 62,483 terrestrial land cells on a 0.5 ×0.5 degree global grid), as any two maps of such a sample size would be classified as being significantly different. Prentice *et al.* (1992), however, did develop a continuous kappa statistic that produced better results, as it was

dependent on block size and on the proportion of pixels that agreed, instead of being just a simple pixel by pixel comparison.

The DOLY model predicts the mean LAI for a given grid square over a year and its NPP is for the vegetated fraction of the grid square. Many ecological studies have recorded LAI and NPP values for a number of sites across the world, but these are at specific points for individual vegetation types (Shaver & Chapin, 1991; Sollins *et al.*, 1980; Woodmansee *et al.*, 1978). In many cases there is a good deal of uncertainty with regards to the accuracy of some of this experimental data and the error limits of field measured rates of annual NPP can be of the order of 20% (Raich *et al.*, 1991). In addition to this, it is unclear how much of the NPP occurs below-ground. In the case of LAI, there has been much work undertaken to derive an estimate of LAI from satellite data. This has met with varying degrees of success, and usually involves the introduction of correction factors. One of the more recent and promising approaches has been made by Nemani and Running (1996) who have produced a global LAI map from NDVI derived from AVHRR satellite data. Also, DeFries and Townshend (1994) have used NDVI to classify land cover at continental scales.

Woodward *et al.* (1995) tested the LAI and NPP output from DOLY (standard version) for 35 sites across the world. They stressed that because of significant errors associated with field observations, the comparison with such data is not a strong test of the model. Having said this the results presented show a good agreement between the simulated and observed NPP and the simulated and observed LAI at the sites selected.

More recently, further attempts have been made to validate output from the DOLY model. Such work has focused on the SDGVM which in effect is a combination of the DOLY model (water and soils version, see section 2.3) and a patch model which incorporates the growth, development, death and disturbance of vegetation. The results from the following two examples (sections 9.2 and 9.3) would be the same if the DOLY (water and soils version) had been used

alone. The patch model component of the SDGVM does not impact on the outputs and processes of the DOLY model.

Beerling and Woodward (1998) used the near-surface meteorological and soil texture data from the ISLSCP (International Satellite Land Surface Climatology Project) database (Sellers *et al.*, 1995; Meeson *et al.*, 1995) (see section 7.2 for further details) for 1988, to drive the SDGVM. The year, 1988, was taken as being representative of the present-day due to the availability of climate and satellite data with which to run and test the model. They compared modelled LAI and NPP with the NDVI (normalised difference vegetation index) values (see section 6.3 for further details), derived from satellite data, and also supplied as part of the ISLSCP database. NDVI is positively correlated with vegetation foliage (Goward *et al.* 1985; Justice *et al.* 1985) but this relationship is non-linear (Nemani and Running, 1996). This approach may be described as an attempt at empirical validation. In addition to this comparison, they carried out an additional model run using the UKMO (United Kingdom Meteorological Office) general circulation model (GCM) transient climate data for the present-day. These climate data, and the adjustments made to them, are described in Chapter 8. The LAI values using the GCM climate data were compared with those from the model run with the ISLSCP data for 1988.

An alternative approach using structural validation was adopted by Beerling *et al.* (1997). They carried out work in Norway as part of the EU CLIMEX (climate change experiment) project and tested various model processes from the SDGVM against actual experimental data.

The results of both these approaches to validating the DOLY model will be presented and discussed in this chapter.

9.2 Empirical validation of the DOLY model

Beerling and Woodward (1998) ran the SDGVM with the ISLSCP near-surface meteorological data for the years 1987 and 1988 on a 1° by 1° grid. The

ISLSCP soil texture data were also used. Additional model runs were carried out using GCM climate data for the years 1987 and 1988 on the lower resolution of a 2.5° by 3.75° grid. In both cases the SDGVM was spun-up to allow the soil carbon and soil nitrogen stores to reach an equilibrium state with the vegetation stores. This usually takes around 100 years. The IIASA climate dataset (Leemans and Cramer, 1991) was used for the spin-up and then the model was run with the ISLSCP data for 1988. This process was repeated with the GCM data. The model predictions of LAI were used to derive the mean growing season LAI and mean annual LAI. These were then plotted on global maps by Beerling and Woodward (1998) for both the ISLSCP and GCM data.

Beerling and Woodward (1998) found that the overall spatial pattern of mean growing season LAI was similar for both sets of predictions (ISLSCP and GCM) with high LAI values (up to 8) in the equatorial rain forests, intermediate values in the boreal forests and deciduous forests (3 to 5) and low values (<2) for deserts and grasslands. A comparison of the maps of growing season LAI and annual mean LAI, highlighted the regions of cold and drought deciduous vegetation in Africa, North and South America, Europe and Siberia. Maps of the LAI values from the GCM data and from the ISLSCP data also showed differences. For instance, there was no forest fringe along the east coast of Australia or the Pacific North West coast of the USA using the GCM data. The runs with the ISLSCP data showed too much vegetation in the southern Sahara and there was an underestimation of vegetation LAI in the high latitudes.

The resolution of the ISLSCP predictions was reduced to that of the GCM grid (2.5° by 3.75°) and the mean annual LAI values derived from the GCM data (referred to as HadCM2) were then plotted as a regression against the mean annual ISLSCP LAI values. The results are shown in Figure 9.1. If there was perfect agreement all the points would lie on a line at 45° to the x-axis with an intercept of zero on the y-axis. This does not occur although the slope of the regression line in Figure 9.1 is close to one and the intercept close to zero.

An alternative approach to validation using such data was put forward

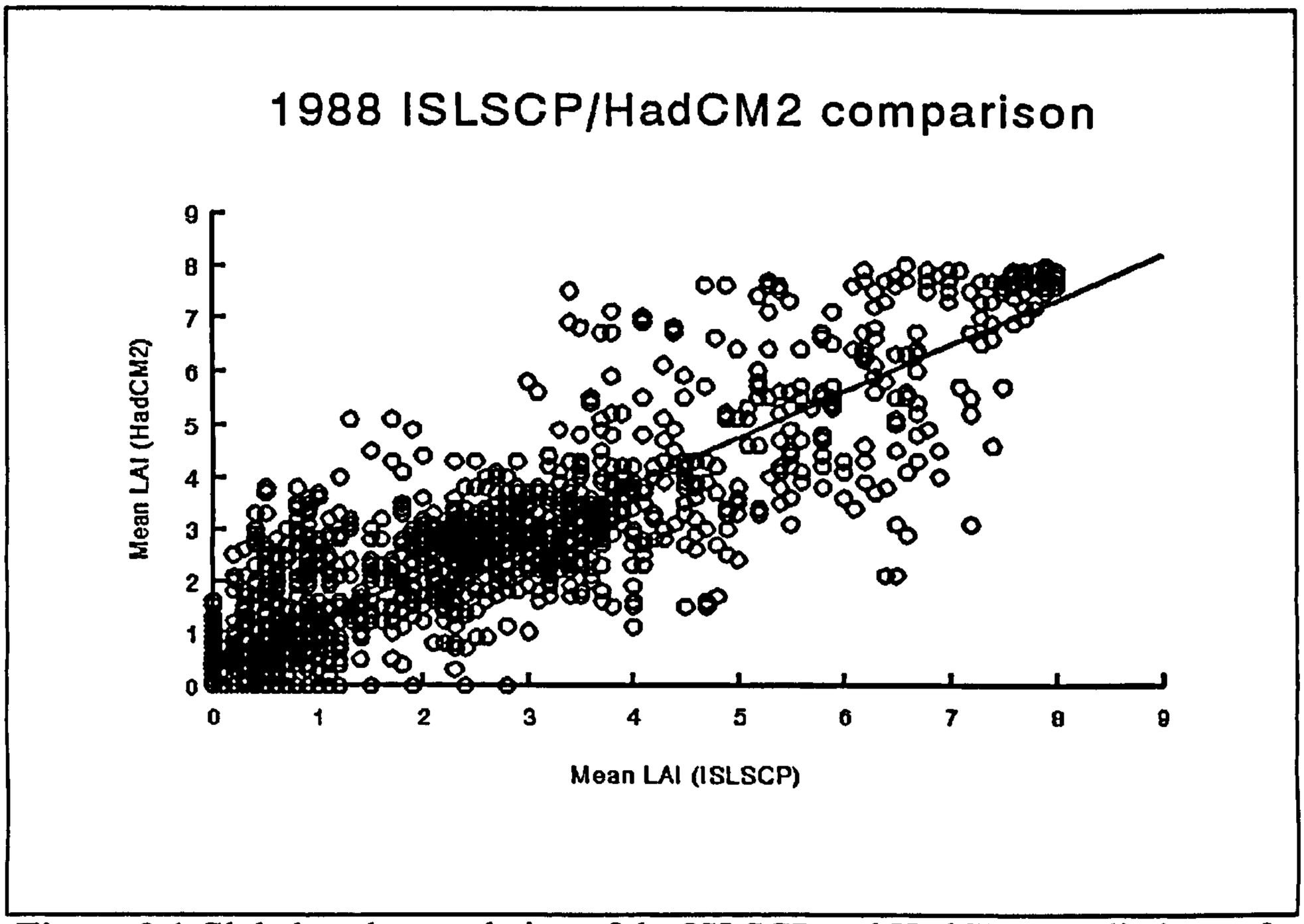

Figure 9.1 Global-scale correlation of the ISLSCP and HadCM2 predictions of mean annual LAI. The linear regression has the equation:

LAI (HadCM2) = 0.41 + 0.87×LAI (ISLSCP), $r^2 = 0.892$, n=1505

by Mitchell (1997). He rejects the use of regression analysis as a tool for empirical validation, because he states that the main purpose of regression analysis is as a tool of prediction, i.e. to predict values of y from values of x. In this particular case, it was not intended to predict GCM LAI values from the ISLSCP LAI values. It is possible to determine the difference of the slope of the regression line from a one-to-one relationship by setting a null hypothesis that the slope equals one and using a statistical test (*F*-test or *t*-test) to attempt to disprove this. If this test fails then the slope could be said not to differ significantly from unity. Mitchell (1997) points out such a test cannot be successful. This is because the more scatter in the points the greater the standard error of the slope and the smaller the computed value of the test statistic. It is therefore harder to reject the null hypothesis. The null hypothesis can either be rejected because the slope is not really different from unity or

because there is too much scatter around the line, (Mitchell, 1997). An improved approach to evaluating models is to examine the deviation between the two output datasets, in this case the ISLCP LAI minus the GCM LAI data. If the deviation is then plotted against the LAI from either model it provides some indication to any bias in the data and this can be used to estimate the range of accuracy of the prediction.

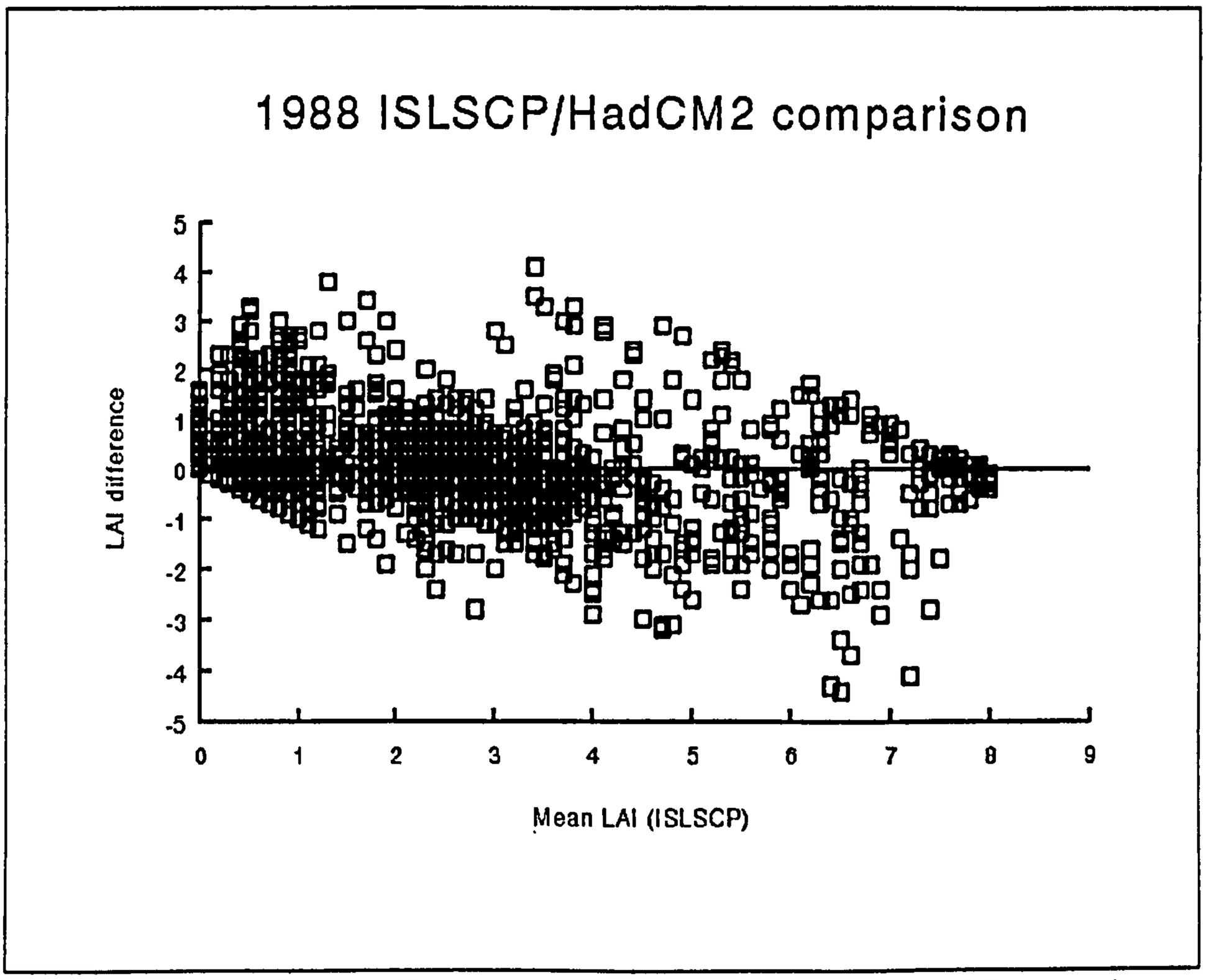

Figure 9.2 Plot of LAI differences (LAI (HadCM2) – LAI (ISLSCP)) against mean annual LAI projected from the ISLSCP CD-ROM. There is no statistically detectable trend in the differences, with LAI.

Figure 9.2 shows no observable bias in leaf area index as the plot of differences in LAI shows no trend with LAI. The slope from negative values to the zero intercept on the y-axis indicates that the LAI has a minimum value of zero. This type of plot probably emphasizes the less frequent extreme points and suffers from a degree of overlap due to having so many points (1505 in this

case). In order to obtain a quantitative picture of the distribution of differences, the LAI differences were converted to a frequency histogram (Figure 9.3).

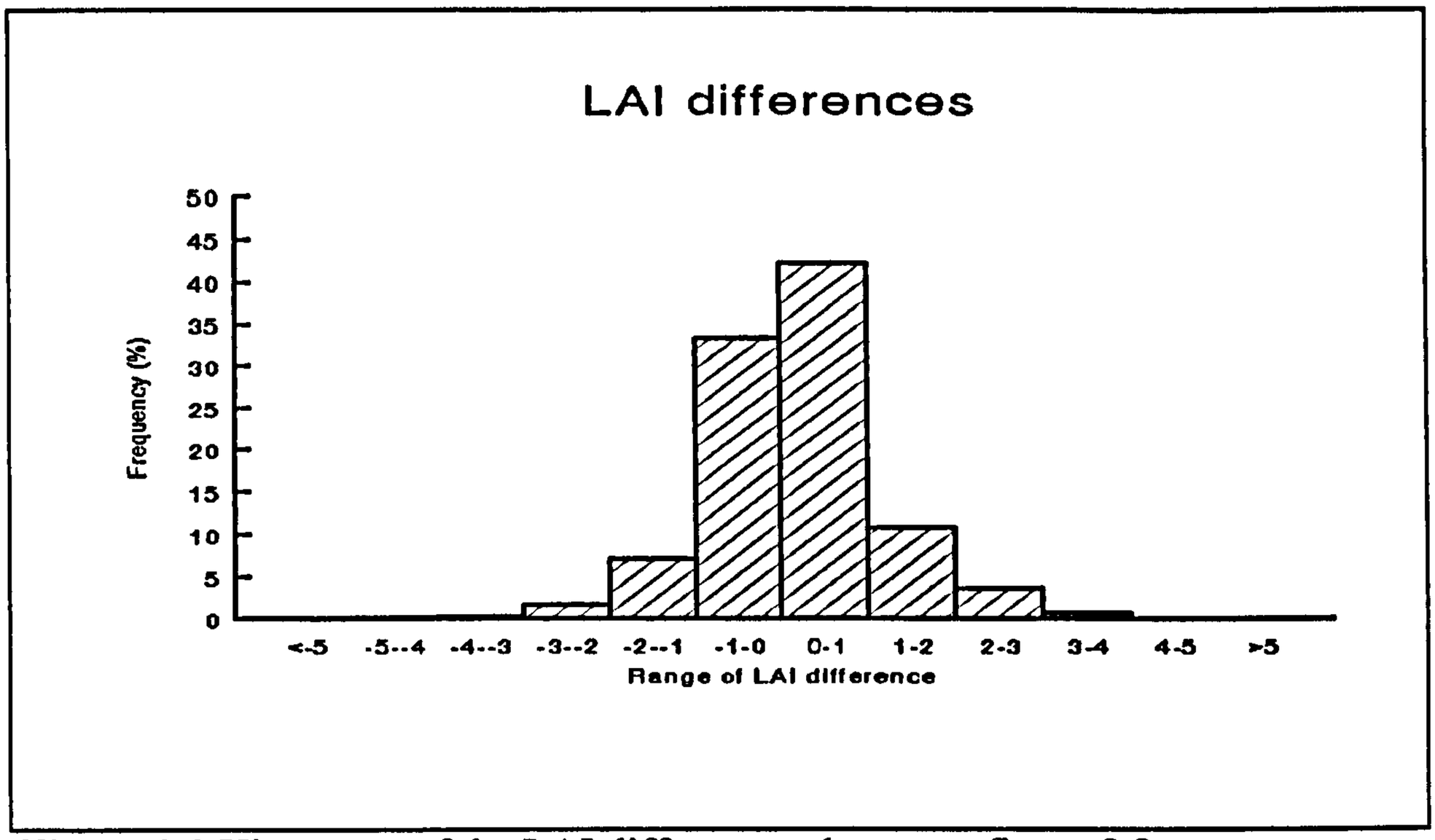

Figure 9.3 Histogram of the LAI differences shown on figure 9.2

Figure 9.3 shows close agreement between the LAI values from the ISLSCP data and those from HadCM2. Over 75% of the cells agree within a range of ± 1, and 95% are within an LAI range of ± 2. The range of actual values of LAI are between 0 and 9. The differences that do arise between the data from the two models are attributed partly to the fact that the ECMWF model is designed to address inter-annual differences, for instance during and following an El Niño event (Diaz & Markgraf, 1992).

The second test of the model predictions of LAI by Beerling and Woodward (1998) was against observations of vegetation by satellites using NDVI, which is related in a non- linear saturating manner to LAI (Nemani and Running, 1996). The NDVI is based on actual vegetation and includes areas which have been urbanized and agricultural regions, where natural vegetation has been removed. This means that a comparison between NDVI and model predictions of LAI cannot have perfect agreement. The NDVI is also sensitive to bare soil characteristics, but the effect of these characteristics on the annual

index is unknown. Ideally, the vegetation model should predict reflected fluxes of radiation and these fluxes could then be compared with those measured by the satellite. Also, it is difficult to determine the exact effect of vegetation on the reflected fluxes due to atmospheric attenuation through clouds and aerosols.

A comparison was made between the annual mean LAI values driven by both climate models and annual mean NDVI. There was a good deal of scatter between LAI from the ISLSCP 1988 climatic data and the NDVI as shown in Figure 9.4, but the asymptotic relationship between NDVI and LAI can be seen.

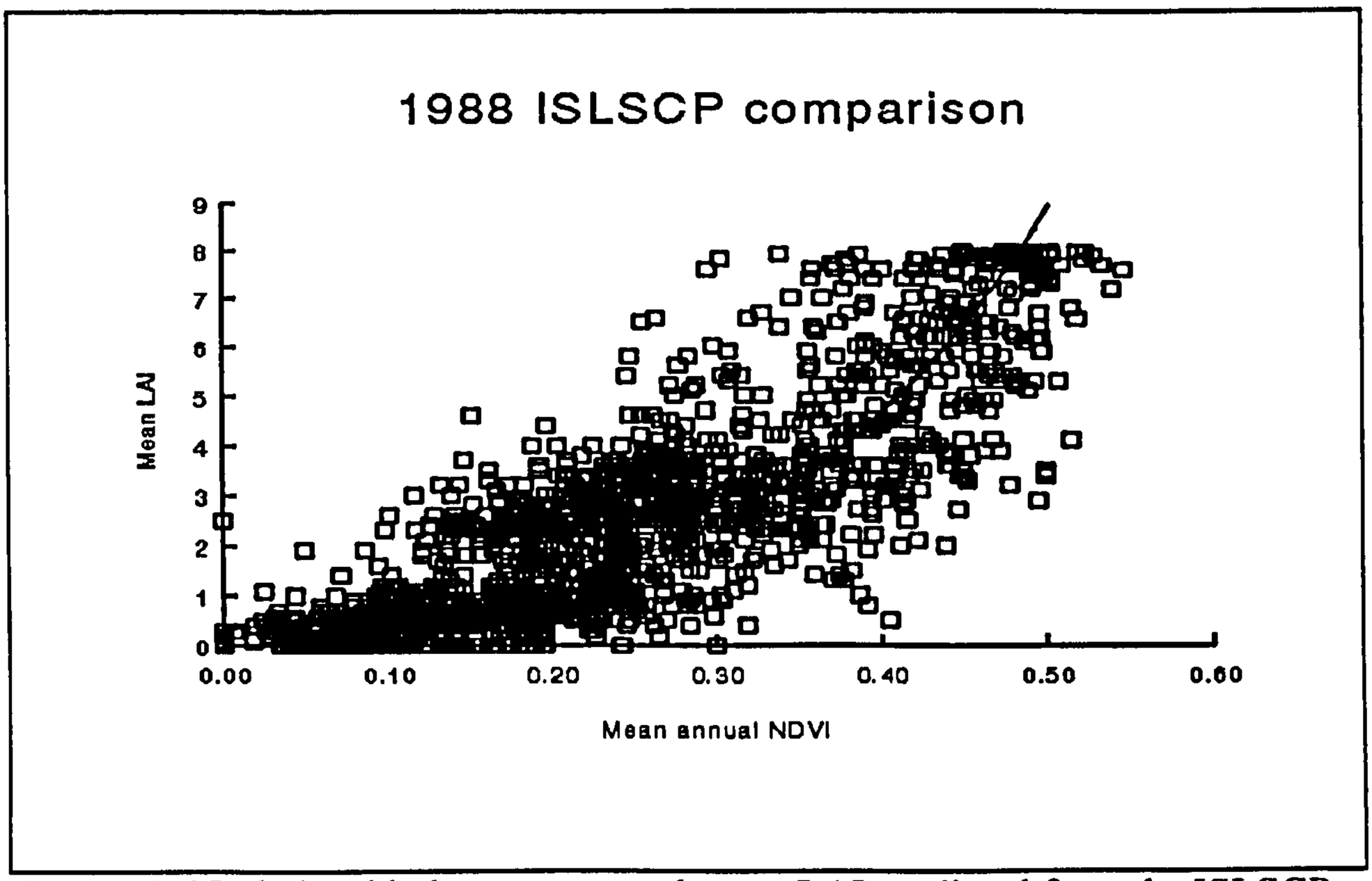

Figure 9.4 Relationship between annual mean LAI predicted from the ISLSCP 1988 climate data and the annual mean NDVI. An exponential regression line provides a general fit to the data, in which $LAI = 0.35 \times e^{6.45NDVI}$, with $r^2 = 0.79$.

The data were transformed by logarithms to the base 10 (after adding 1 to each LAI value to avoid the situation of $\log_{10}(0)$ if LAI = 0) as the relationship between LAI and NDVI is broadly exponential (Figure 9.4). For the

ISLSCP runs (1987 and 1988), LAI=1.012 × $e^{4.28NDVI}$ and $\log_{10}$ (LAI+1) =0.005 +1.859NDVI (r^2= 0.84) and for the HadCM2 runs, $\log_{10}$ (LAI+1) =0.052 + 1.733NDVI (r^2= 0.8). The estimated value of $\log_{10}$ (LAI+1) from the NDVI, is then subtracted from the vegetation model predictions of $\log_{10}$ (LAI+1) to produce an LAI difference or residual. These residuals were plotted against mean annual NDVI and a histogram produced for a quantitative assessment of the similarity between predictions and observations. This histogram is shown in Figure 9.5.

The LAI values derived from these equations for a range of NDVI values between 0 and 0.6 were compared with those from the equation used by Nemani and Running (1996) for broadleaf canopies. For NDVI values less than 0.4 there was reasonable agreement (the ISLSCP 1988 and HadCM2 LAI values were within 20% of the Nemani and Running (1996) LAI values for a given NDVI) but as the NDVI increases from 0.4 to 0.6 there is less agreement. This is due to the rapid rise in LAI beyond an NDVI of 0.4 as shown in Figure 9.4.

Figure 9.5 shows that 46% of observations fall within a LAI range of ± 1.26 and 82% fall within a LAI range of ± 1.58. 95% of observations fall within a range of ± 2. The differences that arise between the two datasets may be attributed to the fact that the ISLSCP data does not predict the high LAI values of the Pacific North West forests of the USA and the forests of southern Chile (the GCM data are also deficient in these areas). Also, there are high values of the NDVI in areas such as south-west England and Ireland which are not shown in the ISLSCP data. These areas have high rainfall and are dominated by intensive agriculture and grasslands. Such factors probably account for such high NDVI values, which are comparable to those from the equatorial rain forests (Beerling and Woodward, 1998).

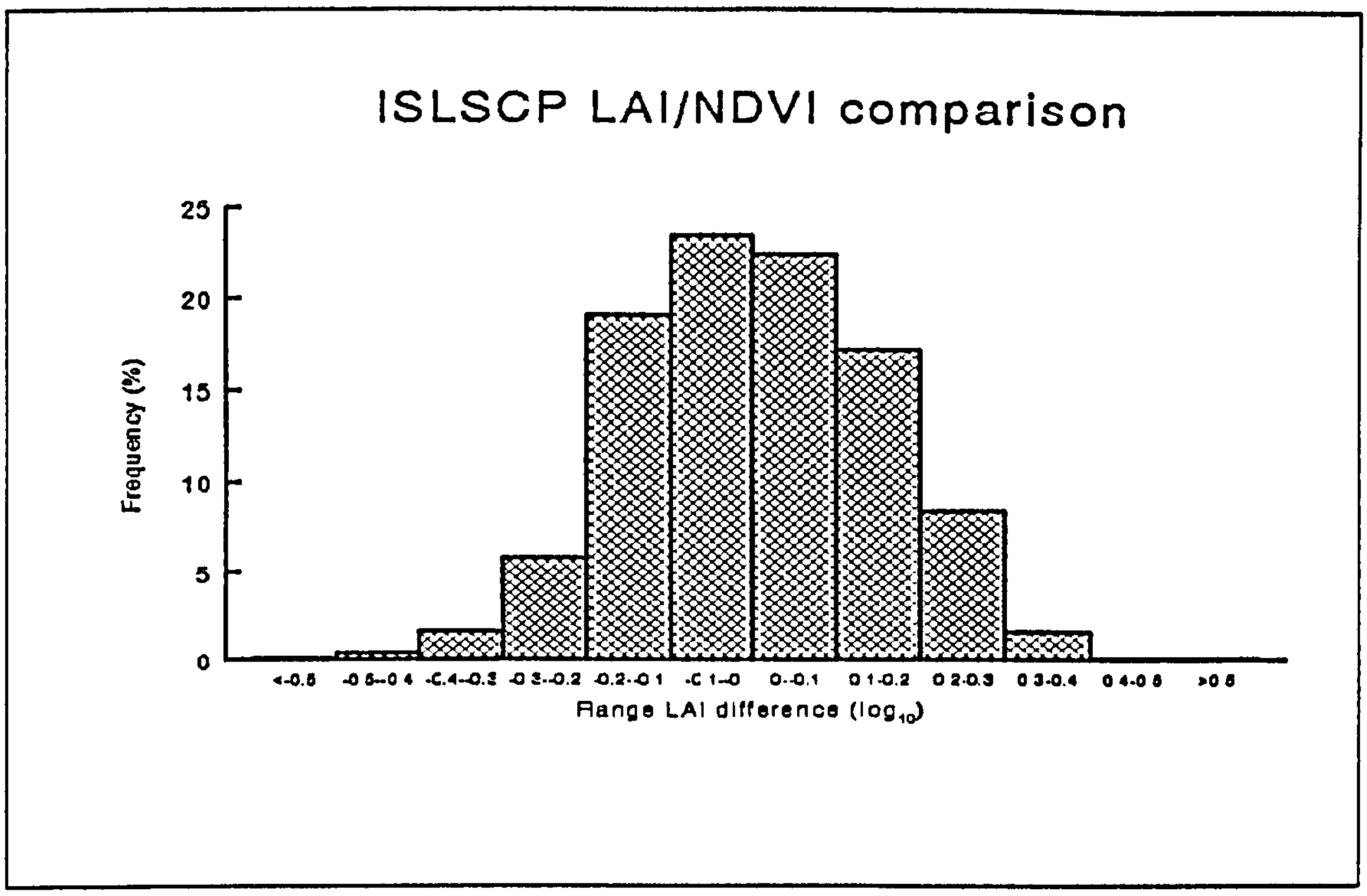

Figure 9.5 Histogram of the calculated LAI differences (see text) between ISLSCP 1988 LAI and mean annual NDVI. Note that the LAI range is in terms of $\log_{10}$. A range of $\pm$ 0.1 is equal to an LAI range of $\pm$ 1.26. A range of $\pm$ 0.2 is equal to an LAI range of $\pm$ 1.58.

The same analysis, as with the ISLSCP 1988 data, was repeated with the GCM data and the histogram of the results is shown in Figure 9.6. Figure 9.6 shows that 44% of observations fall within LAI range of $\pm$ 1.26 and 78% fall within LAI range of $\pm$ 1.58. 95% of observations fall within range of $\pm$ 2. The differences that arise between these two datasets may be attributed to the fact that in eastern and south-west Australia the GCM predictions fail to predict high LAI. There were also differences in the Pacific North West forests of America and the forests of southern Chile, as mentioned earlier.

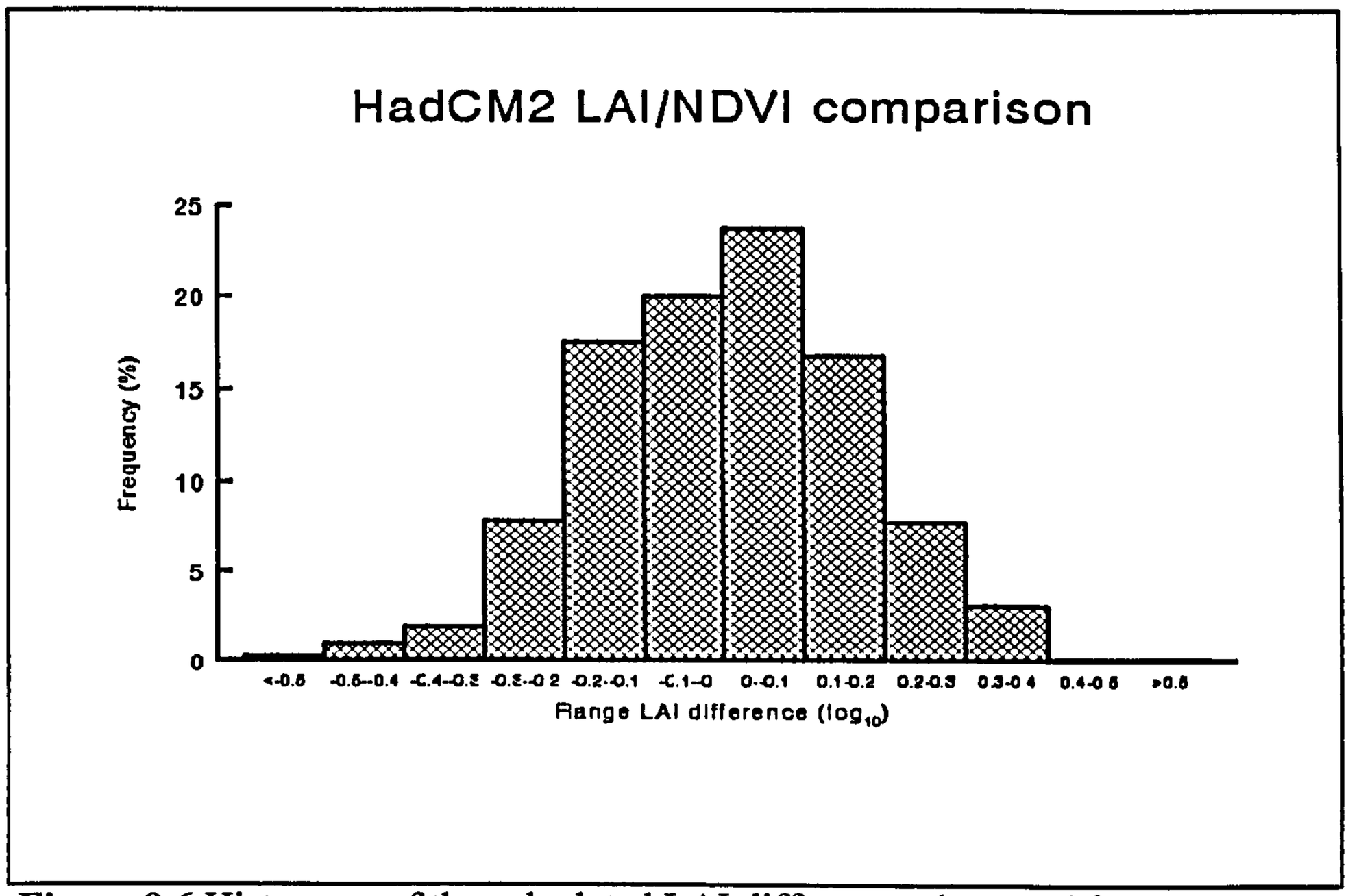

Figure 9.6 Histogram of the calculated LAI differences (see text) between HadCM2 LAI and mean annual NDVI. Note that the LAI range is in terms of $\log_{10}$. A range of ± 0.1 is equal to an LAI range of ± 1.26. A range of ± 0.2 is equal to an LAI range of ± 1.58.

Overall there is good model agreement between LAI inferred from NDVI and model predictions of LAI if the differences that have been noted between the datasets are taken into account. The global patterns of LAI show good agreement between the vegetation model runs using the two sources of modelled data. Beerling and Woodward (1998) estimate that the overall global-scale accuracy of LAI is about ± 1.5 after allowing for the various combinations in errors in the data and the model itself.

Productivity results from the photosynthetic activity of leaves, so NPP is closely correlated to vegetation LAI (Woodward *et al.* 1995). NPP is also therefore, linked to NDVI. The photosynthetic activity of the leaves is, however, also influenced by climate and edaphic factors (Beerling and Woodward, 1998).

The same procedures were carried out to test the predictions of NPP as with LAI from the model using the ISLSCP 1988 and GCM data. The NPP values from these datasets were compared with those transformed from the NDVI data. The histogram of the NPP differences for 1988 is shown in Figure 9.7 and for the GCM data in Figure 9.8.

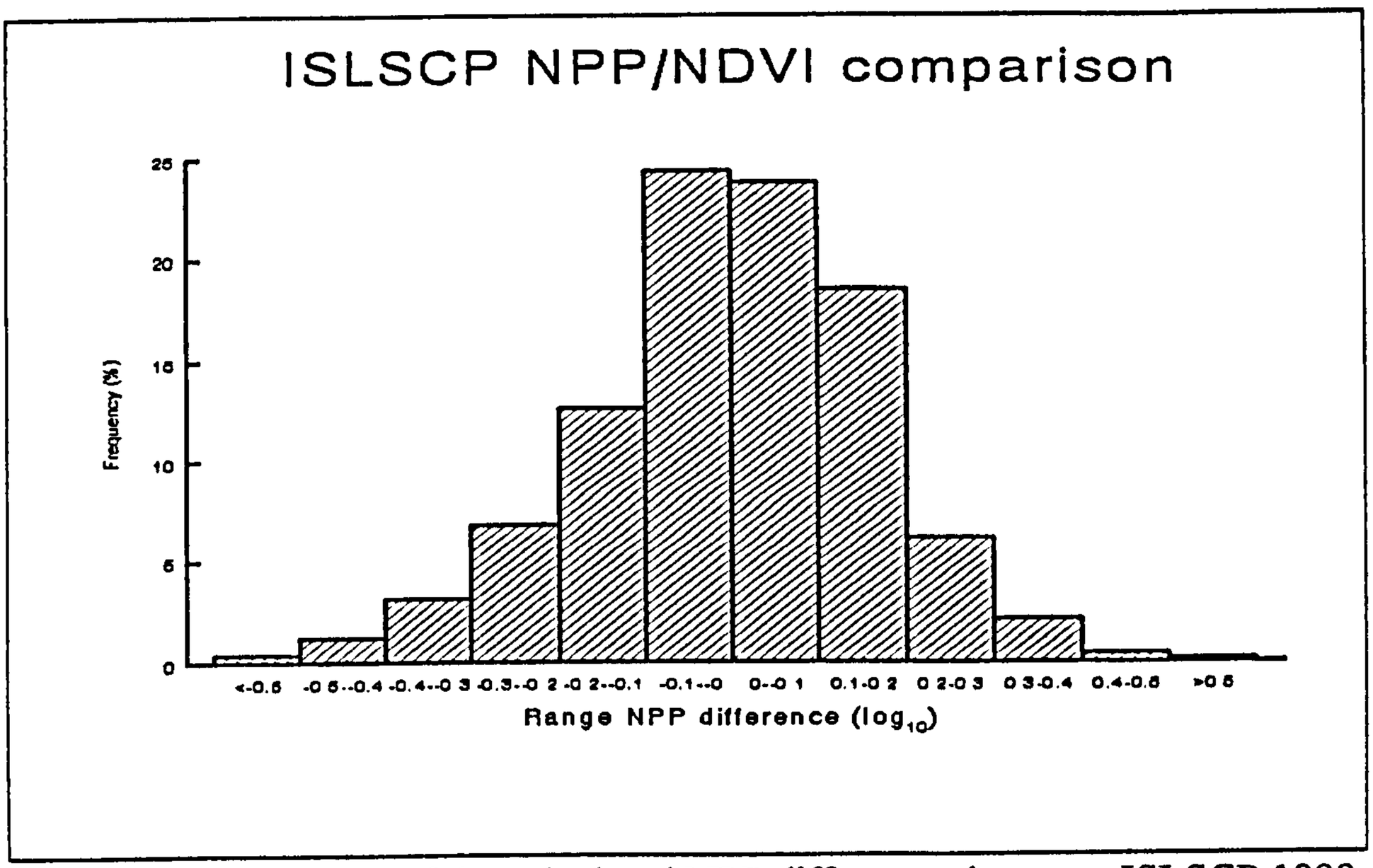

Figure 9.7 Histogram of the calculated NPP differences between ISLSCP 1988 NPP and mean annual NDVI. Note that the NPP range is in terms of $\log_{10}$. A range of $\pm$ 0.1 is equal to an NPP range of $\pm$ 1.26 tC ha^{-1} yr^{-1}. A range of $\pm$ 0.2 is equal to an NPP range of $\pm$ 1.58 tC ha^{-1} yr^{-1}.

Figure 9.7 shows that 80% of the predictions in NPP fall within a range of $\pm$ 1.58 tC ha^{-1} yr^{-1} of the predicted relationship between NDVI and NPP with 90% of observations between within about $\pm$ 2 tC ha^{-1} yr^{-1}. The range of actual NPP values are between 0 and 13 tC ha^{-1} yr^{-1}. Figure 9.8 shows a similar range of variation with the GCM data with 78% of the predictions falling within the range $\pm$ 1.58 tC ha^{-1} yr^{-1} of the predicted relationship between NDVI and NPP and 90% of observations between within about $\pm$ 2 tC ha^{-1} yr^{-1}.

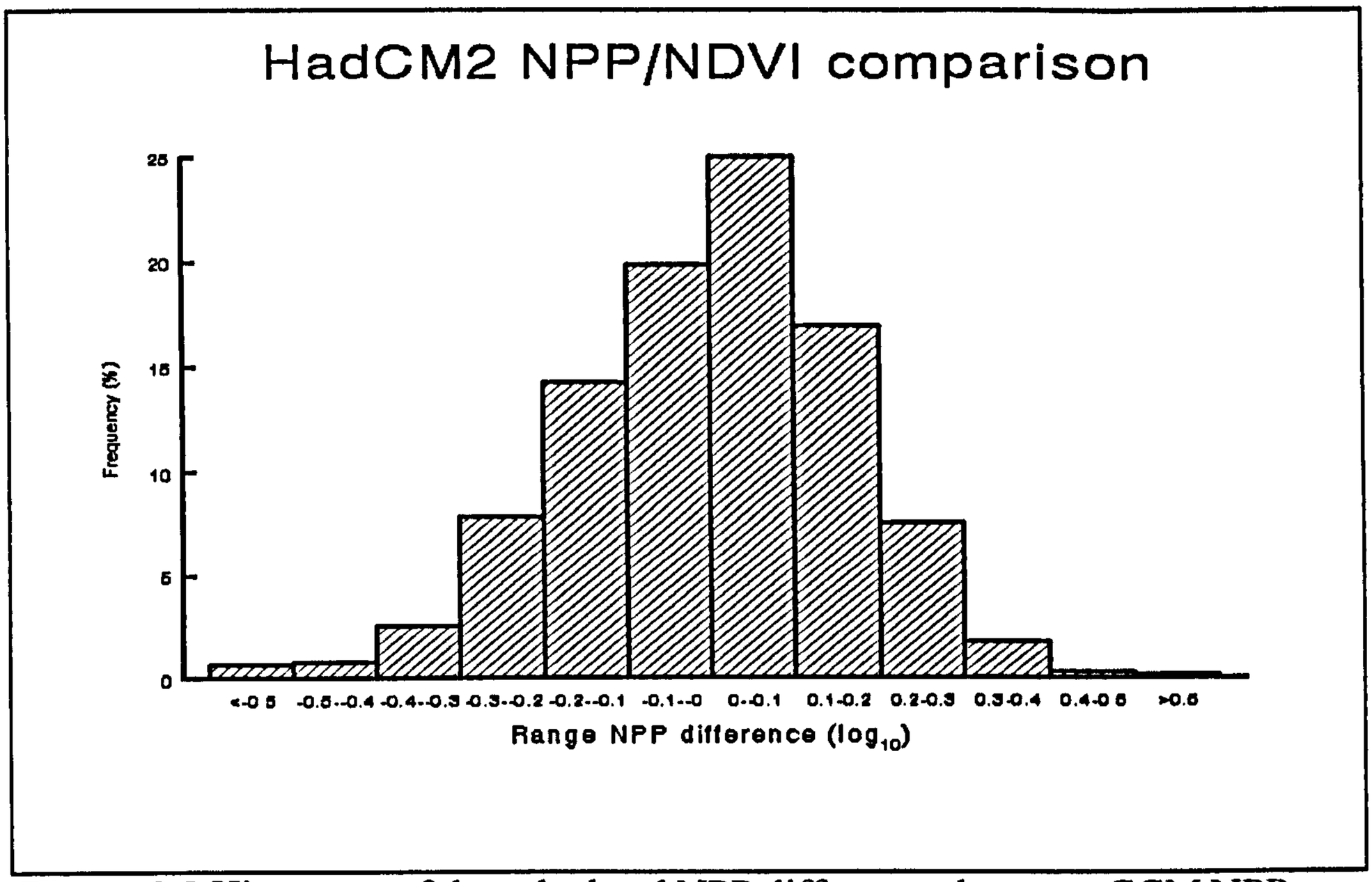

Figure 9.8 Histogram of the calculated NPP differences between GCM NPP data and mean annual NDVI. Note that the NPP range is in terms of $\log_{10}$. A range of ± 0.1 is equal to an NPP range of ± 1.26 tC ha^{-1} yr^{-1}. A range of ± 0.2 is equal to an NPP range of ± 1.58 tC ha^{-1} yr^{-1}.

Beerling and Woodward (1998) point out that a previous analysis relating observed and predicted NPP using the vegetation model (Woodward *et al.* 1995) indicated a maximum uncertainty of NPP predictions of the order of ± 1.5 tC ha^{-1} yr^{-1}, when the model was run with observed data. The uncertainty increased to ± 3 tC ha^{-1} yr^{-1} when the IIASA climate data were used to drive the vegetation model (Leemans and Cramer, 1991), due to the use of interpolation. The variable, NPP, is also difficult to measure in the field and is usually recorded as a small areal average. This in effect is a point measurement at the global scale.

9.3 Structural validation of the DOLY model

A structural approach to validating the DOLY model was adopted by Beerling *et al.* (1997) as part of the CLIMEX (climate change experiment) project. This project aimed to quantify a whole ecosystem response to climate change (CO_2 and temperature) (Dise & Jenkins, 1995), and to link specific studies of vegetation and soils with large-scale catchment measurements of nutrient fluxes and hydrology. Beerling *et al.* (1997) ran the SDGVM for a site in Norway (Risdalsheia, 58° 23' N, 8° 19' E) and compared the model results with actual data from the CLIMEX project for that site. The SDGVM was tested against several spatial scales and processes. At the leaf scale, leaf photosynthesis and water vapour fluxes of mature trees (Beerling and Woodward, 1994, 1996; Beerling *et al.*, 1996) were predicted from climate data and compared with observations. The SDGVM was also used to predict the likely responses of several ecosystem processes (photosynthesis, NPP, runoff and soil carbon concentration) and structural features (LAI) to future global environmental change. The model was run for the 1994 to 1995 period after having been spun-up with local climate data for the period 1961–1984. The comparisons were between mean monthly fluxes predicted by the model from the climate data and the instantaneous gas measurements on pine (*P. sylvestris* L.) between 0900 h and 1500 h over two days within a particular month.

The results described by Beerling *et al.* (1997) show predicted values of photosynthesis and stomatal conductance of similar orders of magnitude to the field measurements. However, photosynthetic predictions accounted for only 26% of the variance between the model predictions and observations. This was partly attributed to the very different time scales of the measurements and predictions (i.e. monthly means from the model versus instantaneous measurements made on individual days within a given month), (Beerling *et al.*, 1997). There was a better prediction of stomatal conductance with the model explaining 65% of the variance between observations and predictions. The

processes of nutrient cycling, leaf gas exchange and canopy development therefore appear to be adequately represented by the SDGVM as there is reasonable agreement between the model results and the experimental data.

Beerling *et al.* (1997) discussed the effect of down-regulation of photosynthetic proteins for plants growing under elevated CO_2, but mentioned that there had been no evidence that this had occurred to date at the CLIMEX site. They attribute the stimulation of photosynthesis with the climate change treatment to the raised intercellular CO_2 within the pine needles which can be predicted adequately by the model.

The model was also tested at the ecosystem level. Modelled values of the soil nutrient status and catchment runoff were compared with the field data. Catchment runoff may be defined as the difference between precipitation (including additional water from stemflow and leaf drip) and evapotranspiration (bare soil evaporation and vegetation transpiration) minus any water stored in the soil. Runoff was simulated from 1992 to 1995 for comparison with measurements collected as part of the RAIN (1990–1993) (Wright, 1994) and CLIMEX (1994-1995) (Jenkins, 1996) projects.

The model performed extremely well for this period with the modelled catchment runoff values very close to the observed values. A regression of the two datasets explained 92.2% of the variance. The model predictions also showed reasonable agreement (46%) with soil moisture for the period June 1994 and August 1995.

9.4 Discussion

This chapter has highlighted the issues and problems that arise when attempting to validate output from a model at a global scale.

The variables, LAI and NPP, are notoriously difficult to validate due to the scarcity of field data and also the accuracy of the field data itself. NPP is particularly inaccurate (Hall & Scurlock, 1991). In addition, point measurements do not provide estimates of mean LAI or NPP at the landscape scale, which is the finest scale of resolution of the vegetation models (Beerling and Woodward, 1998).

One of the limitations of the DOLY model is that it assumes that all vegetation is mature and that it is unaffected by human land-use activities, such as agriculture. Crops, pastures, plantations and successional vegetation need to be included. This leads to further problems when comparing LAI predicted by the model with that observed by satellite.

Satellite remote sensing has the advantage of being able to scan rapidly the whole of the earth's surface on a regular basis. There are however a number of problems with this technique such as the attenuation of the radiation fluxes by the atmosphere, instrument calibration, and different look-angles towards the vegetation. Also, the conversion of data to normalised indices tends to reduce the quality of the data particularly if it is used in correlative mode with the output of the vegetation model. Ideally, a radiative transfer model should be included in the vegetation model so that reflected solar radiation into space is predicted. This radiation can then be compared with the data from the satellites.

Models are always limited to a certain extent by their underlying climate dataset and observational data are not available at the landscape scale. Interpolation techniques are therefore necessary to give a global coverage but these appear to reduce the accuracy of the climate data (Beerling and Woodward, 1998).

Despite these problems, the empirical validation by Beerling and Woodward (1998) showed that it is possible to estimate vegetation NPP and

LAI from the SDGVM and to obtain quite accurate global-scale predictions. Such predictions have been based on a model which scales up from well-characterized plant, canopy and soil processes at the point scale to the full global scale (Beerling and Woodward, 1998).

The structural validation by Beerling *et al.* (1997) also showed that the predicted changes in leaf gas exchange, catchment hydrology and soil nutrient status compared well with observations. This implies that the processes and scaling procedures used in the SDGVM are realistic.

Overall, the DOLY model has been shown to perform well with regard to its processes as well as its outputs. With improved data analysis techniques and the development of a radiative transfer model, further improvements to the model should be possible.

10 Conclusion

The DOLY (Dynamic glObaL phytogeographY) model presented in this thesis has provided a simple way of investigating the response of global vegetation to changes in atmospheric CO_2 concentration and climatic change. In addition the model has been used to investigate the role of vegetation in climate.

Sensitivity analyses of the climate, atmospheric CO_2 concentration and the soils data used as inputs to the model have given useful insights into the behaviour of the model under a range of environmental conditions.

In addition, the influence of different climate datasets has been examined and the issues of validation, with particular reference to the DOLY model, discussed.

Leaf area index (LAI) and net primary productivity (NPP) from the DOLY model were used in a life-form model (Woodward and Lee, 1995) to predict future distributions of global vegetation with climate change, and the DOLY model itself was asynchronously coupled with a slab general circulation model (GCM) from the Hadley Centre (Jones *et al.*, 1995) to examine feedbacks between climate and vegetation (Betts *et al.*, 1997). It was also run with transient climate data to predict future values and distributions of LAI and NPP up to the year 2100. These data are from the version of the model known as HadCM2 (2nd Hadley Centre Coupled Model) (Johns *et al.*, 1997).

There are a number of limitations to the DOLY model and these need to be considered.

First of all the calculation of NPP from assimilation and maintenance respiration is dependent on whole plant allocation. Woodward *et al.* (1995)

were able to partition photosynthate between leaf and other tissue in a consistent way, by restricting LAI. The calculation used by the model assumes that all of the leaf tissue allowed by carbon and moisture constraints is synthesized in one growing season or year, which does not occur in reality. This is particularly true of evergreen vegetation. Therefore, there is likely to be a slight overestimation of NPP. This has been remedied to a certain extent by increasing the amount of maintenance respiration in the water and later versions of the DOLY model. Furthermore, it is assumed that the mass of nonleaf tissue associated with maintenance respiration is constant over the growing season or year and is equal to the amount of nonleaf tissue that is synthesized during the period. The senescence of nonleaf tissue should occur at the same rate as nonleaf tissue is synthesized for this assumption to hold true. Again this assumption is only approximated in reality and there can be significant variations (Woodward *et al.*, 1995).

The DOLY model only predicts the LAI and NPP of natural vegetation. No account is taken of disturbance factors. This means that in savannah regions the LAI and NPP predicted by the model are too high, as disturbance by burning is neglected. Also, in agricultural regions such as central North America, much of Europe, central Asia and eastern China, there is an overestimation of LAI and NPP by the model. Forest management practices would also affect the LAI and NPP values in boreal forest areas, such as northern Canada, northern Europe and Asia, as well as tropical rain forest regions. More recent work using the Sheffield Dynamic Global Vegetation Model (SDGVM) has incorporated fire disturbance, which has improved the accuracy of the model in areas such as the savannah regions of Africa.

The movement of vegetation in response to environmental change is unlikely to be instantaneous so there will be an element of lag between the change in climate and the response of the vegetation. Further work needs to be undertaken to determine the speed of response of different ecosystems to a change in climate and atmospheric CO_2 concentration. The life-form model has

shown how functional types may respond to a given climate change scenario but is not able to deal with individual species. It is not known how such species may interact with a future climate.

Soil phosphorous, which is a particularly important nutrient in the Tropics, is currently not modelled within the DOLY model. However, in the future, as more experimental data become available and modelling techniques improve, this component could be incorporated into the model.

In addition to these model limitations there is also the issue of obtaining suitable experimental data against which to validate the model. This thesis has provided data on the model responses for specific scenarios. Future work could be carried out in the field or greenhouse to simulate these scenarios and compare the results with those from the model.

Despite the limitations, one of the main strengths of the DOLY model is its ability to describe basic plant processes. This enables vegetation response mechanisms to be identified, which is particularly important in simulation and sensitivity studies, as well as understanding vegetation changes detected by satellite remote sensing. In addition, the model can be operated with a small number of climate and soil variables.

The DOLY model is not constrained by an underlying vegetation map or parameters allocated to specific biomes. The distribution of vegetation types is likely to change with environmental change and this will also alter parameters for particular biomes. If different ecosystems respond to environmental change in similar ways, the reasons can be identified using the DOLY model.

A number of conclusions may be drawn from the work carried out for this thesis.

i) The DOLY model is regionally sensitive to its soil inputs, particularly soil carbon. If soil carbon is low then nitrogen uptake is high which increases NPP, particularly in tropical regions.

ii) The DOLY model is sensitive to temperature in the high latitudes and soil water content in arid regions. The northern boreal site, the dry deciduous

site and the grassland site were the most vulnerable to climate change mainly due to water limitations.

iii) The life-form model has shown that the boreal forest–tundra boundary will move northwards with a warmer climate and elevated CO_2. This is consistent with the results from other workers (Bonan *et el.*, 1990,1992 Shugart *et al.*, 1986; Solomon, 1986; Lenihan, 1993).

iv) Vegetation has an impact on the climate of a GCM. When the DOLY model is asynchronously coupled with the UKMO slab GCM (Jones *et al.*, 1995) it leads to a number of regional changes. The most noticeable change occurs in north-east Asia where vegetation replaces snow under a climate change scenario with increased CO_2 and with vegetation feedback. This leads to an decrease in albedo and an increased temperature of between 1 and 2 K.

When the physiological and structural components of the model were generated it was found that physiological change alone (i.e. changes in NPP) had a larger effect than structural change. In the model, structural changes, e.g. LAI, seem to be homeostatic (i.e. there was very little change).

v) The use of different climate datasets affects the output of the DOLY model. The slab GCM has been shown to underestimate rainfall in the Sahel and overestimate it in central and south-western Australia

vi) Mean global LAI calculated from DOLY is 4 and mean global NPP is 55.6 GtC yr^{-1}.

vii) The use of transient GCM climate data from the Hadley Centre (HadCM2) has predicted how NPP and LAI will vary regionally by the year 2100. There is an increase in LAI and NPP in the high latitudes which is consistent with the higher temperatures in these regions and the movement of the boreal forest–tundra boundary northwards. The savanna–Sahara desert boundary also moves northwards and the Gobi desert and the southern steppes of the former Soviet Union were reduced in area by 2100.

viii) An updated version to the DOLY model (the Sheffield Dynamic Global Vegetation Model (SDGVM)) was recently validated using satellite data (Beerling and Woodward, 1998) and data from a field experiment in Norway (Beerling *et al.*, 1997). The validation against satellite data showed that it was possible to estimate vegetation NPP and LAI from the DOLY model and to obtain quite accurate global-scale predictions. Changes in leaf gas exchange, catchment hydrology and soil nutrient status compared well with observations.

Overall, the DOLY model has been shown to perform well with regard to its processes as well as its outputs.

Future work should include further coupling work with the GCM to examine the effect of additional iterations on the GCM, for example, the impact of incorporating the temperature rise and associated changes in precipitation in north-east Asia back into the GCM. Further improvements to GCMs would also help in the simulation of future climates and vegetation. In addition, a study concerned with the effects of vegetation on the atmospheric CO_2 concentration and its feedback in climate would prove useful. The DOLY model is now part of the SDGVM. This model has the advantages of including soil nitrogen and carbon cycling and is able to operate with transient climate data. Additional runs with the SDGVM within the GCM would provide additional information as to the interactions between vegetation and climate.

The DOLY model is restricted to a certain extent by the quality of the input climate and soils data. This thesis has shown how these data affect the model's output. Better climatic data are required as monthly means are often inadequate to model complex ecological processes.

Further improvements to the model could be made by using better data analysis techniques and by developing a radiative transfer model to predict reflected solar radiation into space. These data could then be directly compared with the data from the satellites.

REFERENCES

All journal abbreviations used in this thesis can be found in: Alkire, L.G. (ed.) 1989. *Periodical title abbreviation*, **1 & 2**, J.Gale Research Inc., London. Seventh edition.

Any journal title that is not abbreviated within these references has either been retained for clarity, or is not within Alkire (1989).

Aber, J.D. 1992. Terrestrial Ecosystems. In, Trenberth, K.E. (ed.), *Climate System Modeling*. Cambridge University Press, Cambridge, 173–200.

Aber, J.D. and Federer, C.A.1992. A generalised, lumped-parameter model of photosynthesis, evapotranspiration and net primary production in temperate and boreal forest ecosystems. *Oecologia*, **92**, 463–474.

Ågren, G.I., McMurtrie, R.E., Parton, W.J., Pastor, J. and Shugart, H.H. State-of-the-art of models of production-decomposition linkages in conifer and grassland ecosystems. 1991. *Ecol. Appl.*, **1**, 118–138.

Aphalo, P.J. and Jarvis, P.G. 1991. Do stomata respond to relative humidity? *Plant, Cell, and Environ.*, **14**, 127–132.

Aphalo, P.J. and Jarvis, P.G. 1993. An analysis of Ball's empirical model of stomatal conductance. *Ann Bot.*, **72**, 321–327.

Archibold, O.W. 1995. *Ecology of World Vegetation*. Chapman and Hall.

Bagyaraj, D.J. 1989. Mycorrhizas, In, H. Lieth and M.J.A.Werger (eds.). *Ecosystems of the World Vol. 14B. Tropical Rain Forest Ecosystems: Structure and Function*, Elsevier, Amsterdam, 537–546.

Ball, J.T., Woodrow, I.E. and Berry, J.A. 1987. A model predicting stomatal conductance and its contribution to the control of photosynthesis under different environmental conditions. In, I. Biggins (ed.). *Progress in Photosynthesis Research*, Vol. *IV, Proceedings of the VIIth International Congress on Photosynthesis,* Nijhoff, Dordrecht, Netherlands, 221–224.

Barbour, M.G. and Billings, W.D. 1988. *North American Terrestrial Vegetation*. Cambridge University Press.

Barnola, J.M., Raynaud, D., Korotkevich, Y.S. & Lorius, C. 1987. Vostok ice core provides 160,000-year record of atmospheric CO_2. *Nature*, **329**, 408–413.

Barry, R.G. and Chorley R.J. 1976. *Atmosphere, weather and climate*. Methuen & Co. Ltd. London. 3rd edition. Reprint. 432 pp.

Beerling, D.J. and Woodward, F.I. 1994. The climate change experiment (CLIMEX): phenology and gas exchange responses of boreal vegetation to global change. *Global Ecol. Biogr. Letts*, **4**, 17–26.

Beerling, D.J. and Woodward, F.I. 1996. *In situ* responses of boreal vegetation to elevated CO_2 and temperature: first season results. *Global Ecol. Biogr. Letts*, **5**, 117–127.

Beerling, D.J. and Woodward, F.I. (1998, in preparation). 400 million years of biogeography.

Beerling, D.J., Heath, J., Woodward, F.I., & Mansfield, T.A. 1996. Drought-CO_2 interactions in trees: observations and mechanisms. *New Phytol.*, **134**, 235–242.

Beerling, D.J., Woodward, F.I., Lomas, M.& Jenkins, A.J. (1997, in press).Testing the responses of a dynamic global vegetation model to environmental change: a comparison of observations and predictions. *Global Ecol. Biogr. Letts*, **7.**

Beniston, M. and Fox, D.G. 1996. Impacts of Climate Change on Mountain Regions. In ,Watson, R.T., Zinyowera, M.C., & Moss, R.H. (eds.). *Climate Change 1995. Impacts, Adaptations and Mitigation of Climate Change: Scientific -Technical Analyses*. Contribution of Working Group II to the Second Assessment Report of the Intergovernmental Panel on Climate Change. Cambridge University Press, Cambridge, 191–213.

Betts, R.A. 1998. Ph.D. thesis, University of Reading, in preparation.

Betts, R.A., Cox, P.M., Lee, S.E. & Woodward, F.I. 1997. Contrasting physiological and structural vegetation feedbacks in climate change simulations. *Nature*, **387**, 796–799.

Bigg, G.R. 1990. EL Niño and the Southern Oscillation. *Weather*, **45**, 2-8.

Bonan, G.B. 1992. Soil temperature as an ecological factor in boreal forests, In, H. Shugart, R. Leemans, and G.B. Bonan (eds.). *A Systems Analysis of the Global Boreal Forest*, Cambridge University Press, New York, 126–143.

Bonan, G.B. Shugart, H.H., D.L. Urban. 1990. The sensitivity of some high-latitude boreal forests to climatic parameters. *Clim. Change*, **16**, 9–29.

Bonan, G.B., Pollard, D. & Thompson, S.L. 1992. Effects of boreal forest vegetation on global climate. *Nature* **359**, 716–718.

Botkin, D.B., Janak, J.F, and Wallis, J.R. 1972. Some ecological consequences of a computer model of forest growth. *J. Ecol.*, **60**, 849–872.

Box, E.O. 1981. *Macroclimate and Plant Forms: An Introduction to Predictive Modeling in Phytogeography*. Junk. The Hague.

Bravo, F.P. and Uribe, E.G. 1981. Temperature dependence on concentration kinetics of absorption of phosphate and potassium in corn roots. *Plant Physiol.*, **67**, 815–819.

Briffa, K.R., Bartholin, T.S., Eckstein, D., Jones, P.D., Karlén, W., Schweingruber, F.H. & Zetterberg, P. 1990. A 1400-year tree-ring record of summer temperatures in Fennoscandia. *Nature*, **346**, 434–439.

Brinkmann, W.L.F. 1989. Hydrology, In, H. Lieth and M.J.A. Werger (eds.). *Ecosystems of the World Vol. 14B. Tropical Rain Forest Ecosystems: Biogeographical and Ecological Studies*, Elsevier, Amsterdam, 89–98.

Cannell, M.G.R.1982. *World Forest Biomes and Primary Production Data.* Academic Press. New York.

Chabot, B.F. 1979. Metabolic and enzymatic adaptations to low temperature, In, L.S. Underwood, L.L. Tieszen, A.B. Callahan and G.E. Folk (eds.).

Comparative Mechanisms of Cold Adaptation, Academic Press, New York, 283–301.

Chapin, F.S. III, Vitousek, P.M., and Van Cleve, K.1986. The nature of nutrient limitation in plant communities. *Am. Nat.,* **127,** 48–58.

Chapin, F.S. III, Bret-Harte, M.S., Hobbie, S.E. & Zhong, H. 1996. Plant functional types as predictors of transient responses of arctic vegetation to global change. *J. of Veg. Sci.*, **7**, 347–358.

Clark, F.E., Cole, C.V. and Bowman, R.A. 1980. Nutrient cycling. In, A.I. Breymeyer and G.M. van Dyne (eds.). *Grasslands, System Analysis and Man,* Cambridge University Press, Cambridge, 659–712.

Clarkson, D.T. 1985. Factors affecting mineral acquisition by higher plants. *Ann. Rev. Plant Physiol.*, **36**, 77–115.

Clarkson, D.T. and Warner, A. 1979. Relationship between root temperature and the transport of ammonium and nitrate ions by Italian and perennial rye grass (*Lolium multiflorum* and *Lolium perenne*). *Plant Physiol.*, **64**, 557–561.

Claussen, M. 1994. On coupling global biome models with climate models. *Clim. Res.*, **4**, 203–221.

Claussen, M. 1996. Variability of global biome patterns as a function of initial and boundary conditions in a climate model. *Clim. Dyn.*, **12**, 371–379.

CLIMAP Project Members. 1981. Seasonal reconstructions of the earth's surface at the last glacial maximum. *Geol. Soc. Am. Map Chart Ser.*, MC-36.

COHMAP Members. 1988. Major Climatic Changes of the Last 18,000 years: Observations and Model Simulations. *Science*, **24**, 1043–1052.

Collatz, G.J., Ribas-Carbo, M. and Berry, J.A. 1992. Coupled photosynthesis-stomatal conductance model for leaves of C4 plants *Aust. J. of Plant Physiol.,* **19**, 519–538.

Colman, E.A.1947.A laboratory procedure for determining the field capacity of soils. *Soil Sci.*, **63**, 277-283.

Cotrufo, M.F. and Ineson, P. 1994. Elevated CO_2 reduces field decomposition rates of Betula pendula (Roth.) leaf litter. *Oecologia*, **106**, 525–530.

Cosby, B.J. Hornberger,G.M., Clapp, R.B. and Ginn, T.R. 1984. A statistical exploration of the relationship of soil moisture characteristics to the physical properties of soils. *Water Resour. Res.*, **21**, 51–63.

Dai, A. and Fung, I.Y. 1993. Can climate variability contribute to the missing CO2 sink? *Global Biogeochem. Cycles*, **7**, 599–609.

Dansgaard, W., Johnsen, S.J., Clausen, H.B., Dahl-Jensen, D., Gundestrup, N.S., Hamme, C.U., Hvidberg, C.S., Steffensen, J.P., Sveinbjornsdottir, A.E., Jouzel, J., Bond, G. 1993. Evidence for general instability of past climate from a 250-kyr ice-core record. *Nature*, **364**, 218–220.

Daughtry, C.S.T., Gallo, K.P., Biehl, L.L., Kanemasu, E.E., Asrar, G., Blad, B.L., Norman, J.M. & Gardner, B.R. 1984. Spectral estimates of the agronomic characteristics of crop canopies. *Proceedings of 1984 Machine Processing of Remotely Sensed Data Symposium*. Purdue University, 348–356.

Davis, M.B. 1981. Quaternary history and the stability of forest communities. In, D.C. West, H.H. Shugart, and D.B. Botkin (eds.). *Forest Succession*, Springer-Verlag. 132–153.

Davis, M.B., Woods, K.D., Webb, S.L. and Futyama, D. 1986. Dispersal versus climate: expansion of Fagus and Tsuga into the Upper Great Lakes Region. *Vegetatio*, **67**, 93–103.

De Candolle A.I., 1855. *Geographique Botanique Raisonee.* Paris: Masson. [Not seen, cited in Woodward, 1987].

DeFries, R.S. and Townshend, J.R.G. 1994. NDVI-derived land cover classifications at a global scale. *Int. J. Remote Sens.*, **15**, 3567–3586.

Diaz, H.F. & Markgraf, V.(eds.). 1992. *El Niño Historical and Paleoclimatic Aspects of the Southern Oscillation*. Cambridge University Press.

Dickinson R.E., 1984. Modeling evapotranspiration for three-dimensional global climate models. In, J.E.Hanson and T.Takahashi (eds.). Climate Processes and Climate Sensitivity. *Geophys. Monogr.*, **29**, Maurice Ewing Volume 5 , Amer. Geophys. Union, 58–72.

Dickinson, R.E., Henderson-Sellers, A., Kennedy, P.J. and Wilson, M.F. 1986. Biosphere-Atmosphere Transfer Scheme (BATS) for the NCAR Community Climate Model. *National Center for Atmospheric Research (NCAR) Technical Note*. NCAR/TN-275+STR Boulder, Colorado.

Dise, N.B. & Jenkins, A.J. 1995. *The CLIMEX Project: whole catchment manipulation of CO_2 and temperature*. CEC. Brussels.

Edmisten, J. 1970. Preliminary studies of the nitrogen budget of a tropical rain forest. In, H.T. Odum and R.F. Pigeon (eds.). *A Tropical Rain Forest: A Study of Irradiation and Ecology at El Verde, Puerto Rico,* U.S. Atomic Energy Commission, Washington, H211-5.

Elliott-Fisk, D.L. 1988. The Boreal Forest. In, M.G. Barbour and W.D. Billings (eds.). *North American Terrestrial Vegetation*. Cambridge University Press. 33–62.

Emanuel, W.R., Shugart, H.H. and Stevenson, M.P. 1985a. Climatic change and the broad-scale distribution of terrestrial ecosystem complexes. *Clim.Change* **7**, 29–43.

Emanuel, W.R., Shugart, H.H. and Stevenson, M.P. 1985b. Response to comment: Climatic change and the broad-scale distribution of terrestrial ecosystem complexes. *Clim. Change* **7**, 457–460.

Farquhar, G.D., von Caemmerer, S., and Berry, J.A. 1980. A biochemical model of photosynthetic CO_2 assimilation in leaves of C_3 species. *Planta*, **149**, 78–90.

Farquhar, G.D. and Von Caemmerer, S. 1982. Modelling of photosynthetic response to environment. In, O.L. Lange, P.S. Nobel, C.B. Osmond, and H.Ziegler (eds.). *Encyclopedia of Plant Physiology, New Series, vol. 12B, Physiol. Plant Ecol. II*, Springer-Verlag, New York, 549–587.

Farquhar, G.D., O'Leary, M.H., Berry, J.A. 1982. On the relationship between carbon isotope discrimination and the intercellular carbon dioxide concentration in leaves. *Aust. J. of Plant Physiol.*, **9**, 121–137.

Field, C.B., Randerson, J.T., & Malmstrom, C. 1995. Global net primary production: combining ecology and remote sensing. *Remote Sens. Environ.*, **51**, 74–88.

Flanagan, P.W. and Van Cleve, K. 1983. Nutrient cycling in relation to decomposition and organic matter quality in taiga ecosystems. *Can. J. Forest Res.*, **13**, 795–817.

Foley, J.A., Kutzbach, J.E., Coe, M.T. & Levis, S. 1994. Feedbacks between climate and boreal forests during the Holocene epoch. *Nature* **371**, 52–54.

Foley, J.A., Prentice, I.C., Ramankutty, N., Levis, S., Pollard, D. Sitch, S. and Haxeltine, A. 1996. An integrated biosphere model of land surface processes, terrestrial carbon balance, and vegetation dynamics. *Global Biogeochem. Cycles*, **10**, 603–628.

Folland, C.K., Palmer, T.N. and Parker, D.E. 1986.Sahel rainfall and worldwide sea temperatures. *Nature*, **320**, 602–607.

Friend, A.D. 1991. Use of a model of photosynthesis and leaf micro-environment to predict optimum stomatal conductance and leaf nitrogen partitioning. *Plant, Cell, Environ.*, **14**, 895–905.

Friend, A.D., & Woodward, F.I. 1990. Evolutionary and ecophysiological responses of mountain plants to the growing season environment. *Adv. Ecol. Res.* **20**, 59–124.

Friend, A.D., Shugart, H.H., & Running, S.W. 1993. A physiology-based gap model of forest dynamics. *Ecology*, **74**, 792–797.

Gallimore, R.G. & Kutzbach, J.E 1989 Effects of soil-moisture on the sensitivity of a climate model to earth orbital forcing at 9000-yr-BP. *Clim. Change*, **14**, 175–205.

Gates, D.M. 1980. *Biophysical Ecology*. New York: Springer-Verlag.

Gates, D.M. 1985. Global biospheric response to increasing atmospheric carbon dioxide concentration. In, *Direct effects of increasing carbon dioxide on vegetation*. B.R. Strain and J.D. Cure (eds.). United States Department of Energy, Office of Energy Research, Carbon Dioxide Research Division, Washington, D.C. 171–184.

Genthon, C., Barnola, J.M., Raynaud, D., Lorius, C., Jouzel, J., Barkov, N.I., Korotkevich, Y.S., & Kotlyakov, V.M. 1987. Vostok ice core: climatic response to CO_2 and orbital forcing changes over the last climatic cycle. *Nature*, **329**, 414–418.

Gollan, T., Passioura, J.B. & Munns, R. 1986. Soil water status affects the stomatal conductance of fully turgid wheat and sunflower leaves. *Aust. J. Plant Physiol.*, **13**, 459–464.

Gollan, T., Schurr, U., & Schulze, E.C. 1992. Stomatal responses to drying soil in relation to changes in the xylem sap composition of *Helianthus annus*, I. The concentration of cations, anions, amino acids in, and pH of the xylem sap. *Plant, Cell, Environ.*, **15**, 551–559.

Gordon, A.G. 1983. Nutrient cycling dynamics in differing spruce and mixed wood ecosystems in Ontario and the effects of nutrient removals through harvesting. In, R.W. Wein, R.R. Riewe & I.R.(eds.). *Resources and Dynamics of the Boreal Zone*, Methuen, Association of Canadian Universities for Northern Studies, Ottawa, 97–118.

Gordon, A.G. and Van Cleve, K. 1983. Seasonal patterns of nitrogen mineralization following harvesting in the white spruce forests of interior Alaska. In, R.W. Wein, R.R. Riewe & I.R.(eds.). *Resources and Dynamics of the Boreal Zone*, Methuen, Association of Canadian Universities for Northern Studies, Ottawa, 119–130.

Goward, S.N., Tucker, C.J., & Dye, D.J. 1985. North American vegetation patterns evaluated with the NOAA-7 Advanced Very High Resolution Radiometer. *Vegetatio*, **64**, 3–14.

Grabherr, G. & Kojima, S.1993. Vegetation diversity and classification systems. In, Solomon, A.M. & Shugart, H.H. (eds.). *Vegetation Dynamics and Global Change*, London (Chapman & Hall), 218–232.

Grace, J., Fasehun, F.E. & Dixon, M.A. 1980. Boundary layer conductance of the leaves of some tropical timber trees. *Plant, Cell and Environ.*, **3**, 443–450.

Grace, J., Okalai, D.U.U., & Fasehun, F.E. 1982. Stomatal conductance of two tropical trees during the wet season in Nigeria. *J. Appl. Ecol.*, **19**, 659–670.

Greco, S., Moss, R.H., Viner, D. and Jenne, R. 1994. *Climate Scenarios and Socioeconomic Projections for IPCC WGII Assessment*. IPCC, Washington DC.

Guetter, P.J. and Kutzbach, J.E. 1990. A modified Köppen classification applied to model simulations of glacial and interglacial climates. *Clim. Change* **16**, 193–215.

Gupta, S.C. and Larson, W.E. 1979. Estimating soil water retention characteristics from particle size distribution, organic matter percent and bulk density. *Water Resour. Res.*, **15**, 1633–1635.

Hack, J.J. 1992. Climate system simulation: basic numerical and computational concepts. In, Trenberth, K.E. (ed.). *Climate System Modeling*. Cambridge University Press, Cambridge, 283–318.

Hall, D.O. & Scurlock, J.M.O. 1991. Climate change and the productivity of natural grasslands. *Ann. Bot.*, **67** (Supplement 1), 49–55.

Harley, P.C., Thomas, R.B., Reynolds, J.F. & Strain, B.R. 1992. Modelling photosynthesis of cotton grown in elevated CO_2. *Plant, Cell and Environ.*, **15**, 271–282.

Haxeltine, A. & Prentice, I.C. 1996. BIOME3: An equilibrium terrestrial biosphere model based on ecophysical constraints, resource availability, and competition among plant functional types. *Global Biogeochem. Cycles*, **10**, 693–709.

Haxeltine, A., Prentice, I.C., and Cresswell, I.D. 1996. A coupled carbon and water flux model to predict vegetation structure. *J. Veg. Sci.*, **7**, 651–666.

Hay, R.K.M. and Walker, A.J. 1989. *An Introduction to the Physiology of Crop Yield.* Longman, White Plains, N.Y.

Hayes, A.J. 1965. Studies in the decomposition of coniferous leaf litter. I. Physical and chemical changes. *J. Soil Sci.*, **16**, 121–140.

Henderson-Sellers, A., Pitman, A.J., Love, P.K., Irannejad, P., & Chen, T.H. 1995. The Project for Intercomparison of Land Surface Parameterization Schemes (PILPS): Phases 2 & 3. *Bull. Amer. Meteorol. Soc.*, **76**, 489–503.

Henderson-Sellers, A.,& McGuffie, K.1995. Global climate models and 'dynamic' vegetation changes. *Global Change Biology*, **1**, 63–75.

Henderson-Sellers, A., McGuffie, K., Gross, C. 1995. Sensitivity of global climate model simulations to increased stomatal–resistance and CO_2 increases. *J. Clim.*, **8**, 1738–1756.

Holding, A.J. 1981. The microflora of tundra. In, L.C. Bliss, O.W. Heal, and J.J. Moore (eds.). *Tundra Ecosystems: A Comparative Analysis*, Cambridge University Press, Cambridge, 561–585.

Holdridge, L.R. 1947. Determination of world plant formations from simple climatic data. *Science*, **105**, 367–368.

Holdridge, L.R., Grenke, W.C., Hatheway, W.H., Liang, T. and Tosi, J.A. 1971. *Forest Environments in Tropical Life Zones,* Pergammon Press, Oxford.

Houghton, J.T., Jenkins, G.J., Ephraums, J.J.(eds.) 1990. *Climate Change. The Intergovernmental Panel on Climate Change (IPCC) Scientific Assessment.* World Meteorological Organisation (WMO).Cambridge University Press, Cambridge.

Houghton, J.T., Callander, B.A. and Varney, S.K. 1992. *Climatic Change. The Supplementary Report to the Intergovernmental Panel on Climate*

Change (IPCC) Scientific Assessment. Cambridge University Press, Cambridge.

Howell, T.A., Meek, D.W. & Hatfield, J.L. Relationship of photosynthetically active radiation to shortwave radiation in the San Joaquin Valley. *Agric. Meteor.*, **28**, 157–175. [Not seen, cited in Monteith and Unsworth, 1990].

Humboldt, A. von & Bonpland, A. 1805. *Essai sur la Geographie des Plantes: Accompagne d'un Tableau Physique des Regions Equinoxiales.* Paris. [Not seen, cited in Woodward, 1987].

Hunt, H.W., Trlica, M.J., Redente, E.F., Moore, J.C., Detling, J.K., Kittel, T.G.F, Walter, D.E., Fowler, M.C., Klein, D.A., Elliott, E.T. 1991. Simulation model for the effects of climate change on temperate grassland ecosystems. *Ecol. Model..*, **53**, 205–246.

Intergovernmental Panel on Climate Change (IPCC). 1990. *Climate Change: The IPCC Scientific Assessment.* Houghton, J.T., Jenkins, G.J. and Ephraums, J.J.(eds.). Cambridge University Press, Cambridge.

Intergovernmental Panel on Climate Change (IPCC). 1992. *Climatic Change. The Supplementary Report to the IPCC Scientific Assessment.* Houghton, J.T., Callander, B.A. and Varney, S.K. (eds.). Cambridge University Press, Cambridge.

Intergovernmental Panel on Climate Change (IPCC).1995. *Climate Change 1994. Radiative Forcing of Climate Change and An Evaluation of the IPCC IS92 Emission Scenarios*. Houghton, J.T., Meira Filho, L.G., Bruce, J., Lee Hoesung, Callander, B.A., Haites, E., Harris, N., and Maskell, K. (eds.). Reports of Working Groups I and III of the Intergovernmental Panel on Climate Change, forming part of the IPCC Special Report to the first session of the Conference of the Parties to the UN Framework Convention on Climate Change. Cambridge University Press, Cambridge.

Intergovernmental Panel on Climate Change (IPCC). 1996. *Climate Change 1995. Impacts, Adaptations and Mitigation of Climate Change: Scientific-Technical Analyses. Contribution of Working Group II to the Second Assessment Report of the Intergovernmental Panel on Climate Change*. Watson, R.T., Zinyowera, M.C., & Moss, R.H.(eds.). Cambridge University Press, Cambridge.

Jenkins, A.J. (ed.). 1996. *CLIMEX Project: results from the second year of treatment*. Climate Change Research Report 6/96. Norwegian Institute for Water Research, Oslo.

Johns, T.C., Carnell, R.E., Crossley, J.F., Gregory, J.M., Mitchell, J. F. B., Senior, C.A., Tett, S.F.B. and Wood, R.A. 1997. The second Hadley Centre coupled ocean-atmosphere GCM: Model description, spinup and validation. *Clim. Dyn.*, **13**, 103–134.

Johnsen, S.J. Clausen, H.B., Dansgaard, W., Fuhrer, K., Gundestrup, N., Hammer, C.U., Iversen, P., Jouzel, J., Stauffer, B., Steffensen, J.P. 1992. Irregular glacial interstadials recorded in a new Greenland ice core. *Nature*, **359**, 311–313.

Johnson, D.A. and Calcwell, M.M. 1975. Gas exchange of four arctic and alpine tundra plant species in relation to atmospheric and soil moisture stress. *Oecologia,* **24**, 159–73.

Jordan, C.F. 1985. *Nutrient Cycling in Tropical Forest Ecosystems,* Wiley, Chichester.

Jones, H.G. 1983. *Plants and Microclimate–A quantitative approach to environmental plant physiology*. Cambridge University Press. 1st edition.

Jones, H.G. 1992. *Plants and Microclimate–A quantitative approach to environmental plant physiology*. Cambridge University Press. 2nd edition.

Jones, R.G. Murphy, J.M., & Noguer, M. 1995. Simulation of climate change over Europe using a nested regional climate model. Part I. Assessment

of control climate including sensitivity to location of lateral boundaries. *Quart. J. of Royal Meteorol. Soc.*, **121**, Pt.B, 1413–1449.

Jordan, D.B. and Ogren, W.L..The CO_2 /O_2 specificity of ribulose 1,5-bisphosphate carboxylase/oxygenase: Dependence on ribulose-bisphosphate concentration, pH and temperature, *Planta*, **161**, 308–313.

Jouzel, J., Lorius, C., Petit, J.R.,Genthon, C., Barkov, N.I., Kotlyakov, V.M., Petrov,V.M. 1987. Vostok ice core: a continuous isotope temperature record over the last climatic cycle (160,00 years). *Nature*, **329**, 403–408.

Jouzel, J., Barkov, N.I., Barnola, J.M.,Bender, M., Chappellaz, J.,Genthon,C, Kotlyakov, V.M., Lipenkov,V., Lorius,C., Petit, J.R., Raynaud, D., Raisbeck,G., Ritz,C., Sowers, T., Stievenard, M.,Yiou, F.,Yiou, P. 1993. Extending the Vostok ice-core record of paleoclimate to the penultimate glacial period. *Nature*, **364**, 407–412.

Justice, C.O., Townshend, J.R.G., Holben, B.N., and Tucker, C. J. 1985. Analysis of the phenology of global vegetation using meteorological satellite data. *Int. J. Remote Sens.*, **6**, 1271–1318.

Kauppi, P. & Posch, M.1985. Sensitivity of boreal forests to possible climatic warming. *Clim. Change*, **7**, 45–54.

Köppen, W. 1936. Das Geographisches System der Klimate. In, W. Köppen and R. Geiger (eds.). *Handbuch der Klimatologie* I(C). Gebruder, Borntraeger, Berlin.

Körner, Ch., Scheel, J.A., & Bauer, H. 1979. Maximum leaf diffusive conductance in vascular plants. *Photosynthetica,* **13**, 45–82.

Körner, Ch. 1994. Leaf diffusive conductances in the major vegetation types of the globe. In, Schulze, E.-D. & Caldwell, M. (eds.). *Ecophysiology of photosynthesis*. Ecol. Stud., **100**, 463–489.

Kutzbach, J.E. 1992. Modelling large climatic changes of the past. In, Trenberth, K.E (ed.). *Climate System Modeling*. Cambridge University Press, Cambridge, 669–688.

Landsberg, J.J. and James, G.B. 1971. Wind profiles in plant canopies: studies on an analytical model. *J. Appl. Ecol.*, **8**, 729–742.

Larsen, J.A. 1980. *The boreal ecosystem.* Academic. New York.

Leemans, R. and Cramer, W.P. 1991. *The IIASA database for mean monthly values of temperature, precipitation, and cloudiness on a global terrestrial grid.* Laxenburg, Austria (International Institute for Applied Systems Analysis). RR-91-18, 1–62.

Lenihan, J.M.1993. Ecological response surfaces for North American boreal tree species and their use in forest classification. *J. Veg. Sci.*, **4**, 667–680.

Lieth, H. 1975. Modeling the primary production of the world. In, Lieth, H. & Whittaker, R.H. (eds.). *Primary productivity of the world.* Springer-Verlag, New York, NY, 237–263.

Lockwood, J.G. 1979. *Causes of Climate*. E. Arnold, London.

McClaugherty, C.A., Pastor, J., Aber, J.D. & Melillo, J.M. 1985. Forest litter decomposition in relation to soil nitrogen dynamics and litter quality. *Ecology,* **66**, 266–75.

McCown, B.H. 1978. The interactions of organic nutrients, soil nitrogen and soil temperature and plant growth and survival in the arctic environment. In, L.L.Tieszen (ed.). *Vegetation and Production Ecology of an Alaskan Arctic Tundra*. Springer, New York, 435–456.

McGuire, A.D., Melillo, J.M., Joyce, L.A., Kicklighter, D.W., Grace, A.L., Moore III, B. and Vorosmarty, C.J. 1992. Interactions Between Carbon and Nitrogen Dynamics in Estimating Net Primary Productivity for Potential Vegetation in North America. *Global Biogeochem. Cycles*, **6**, 101–124.

McMurtrie, R.E., Rook, D.A. and Kelliher, F.M.1990b. Modelling the yield of Pinus radiata on a site limited by water and nitrogen. *For. Ecol. & Mgt.*, **30**, 381–413.

McMurtrie, R.E. and Landsberg, J.J. 1992. Using a simulation model to evaluate the effect of water and nutrients on the growth and carbon partitioning of Pinus radiata. *For. Ecol. & Mgt.*, **52**, 243–260.

McMurtrie, R.E., Leuning, R.,Thompson, W.A.& Wheeler, A.M. 1992. A model of canopy photosynthesis and water use incorporating a mechanistic formulation of leaf CO_2 exchange. *For. Ecol. & Mgt.*, **52**, 261–278.

McMurtrie, R.E. and Wang, Y.P. 1993. Mathematical models of the photosynthetic response of tree stands to rising CO_2 concentrations and temperatures. *Plant, Cell, Environ.*, **16**,1–13.

McNaughton, K.G. and Jarvis, P.G. 1983. Predicting effects of vegetation changes on transpiration and evaporation. In, T.T. Kozlowski (ed.). *Water Deficits and Plant Growth, VII.* Academic Press, New York. 1 –47.

Mearns, L.0., Schneider, S.H., Thompson, S.L. and McDaniel, L.R. 1990. Analysis of climate variability in general circulation models: Comparison with observations and changes in variability in 2 × CO_2 experiments. *J. Geophys. Res.*, **95**, 20469–20490.

Meehl, G.A. 1992. Global coupled models: atmosphere, ocean, sea ice. In, Trenberth, K.E. (ed.). *Climate System Modeling*. Cambridge University Press, Cambridge, 555–582.

Meeson, B.W., Corprew, F.E., McManus, J.M.P., Myers, D.M., Closs, J.W., Sun, K.-J., Sunday, D.J., Sellers, P.J. 1995. *ISLSCP Initiative I-Global Data Sets for Land-Atmosphere Models, 1987–1988.* Volumes 1–5. Published on CD by NASA (USA_NASA_GDAAC_ISLSCP_001-USA_NASA_GDAAC_ISLSCP_005).

Melillo, J.M., Aber, J.D. and Muratore, J.F. 1982. Nitrogen and lignin control of hardwood leaf litter decomposition dynamics. *Ecology*, **63**, 621–626.

Melillo, J.M., McGuire, A.D., Kicklighter, D.W., B. Moore III, Vörösmarty, C.J. and Schloss, A.L. 1993. Global climate change and terrestrial net primary production, *Nature*, **363**, 234–240.

Milankovitch, M. 1920. *Théorie Mathématique des Phenomènes Thermiques Produits par la Radiation Solaire.* Gauthier-Villars: Académie Yougoslave des Sciences et des Arts de Zagreb. [Not seen, cited in Woodward, 1987].

Milankovitch, M. 1930. Mathematische Klimalehre und astronomische theorie der Klimschwankungen. In, Köppen, W. & Geiger, R. (eds.). *Handbuch der Klimatologie. 1. Teil A*. Berlin: Borntraeger. [Not seen, cited in Woodward, 1987].

Milankovitch, M. 1941. *Canon of Insolation and the Ice Age Problem*. Beograd, Köninglich Serbische Akademie. 484 pp. (English translation by Israel program for Scientific Translation and published for the U.S. Department of Commerce and the National Science Foundation). [Not seen, cited in Woodward, 1987].

Mitchell, J.F.B. Johns, T.C., Gregory, J.M., Tett, S.F.B. 1995. Climate response to increasing levels of greenhouse gases and sulphate aerosols. *Nature* **376**, 501–504.

Mitchell, P.L. 1997. Misuse of Regression for Empirical Validation of Models. *Agric. Syst.*, **54**, 313–326. Pub. by Elsevier Science Ltd.

Mitchell, P.L. and Sheehy, J.E. 1997. Comparison of predictions and observations to assess model performance: a method of empirical observation. In, M.J. Kopf, .S. Teng, P.K. Aggarwal, J. Bouma, B.A.M. Bouman, J.W. Jones & H.H. van Laar (eds.). *Applications of System Approaches at the Field Level*. Kluwer, Dordrecht, The Netherlands, 437–451.

Mladenoff, D.J. 1987. Dynamics of nitrogen mineralization and nitrification in hemlock and hardwood treefall gaps. *Ecology*, **68**, 1171–1180.

Monserud, R.A. and Leemans, R. 1992. Comparing global vegetation maps with the Kappa statistic. *Ecological Model.*, **62**, 275–293.

Monteith, J.L. 1965. Evaporation and environment. In, C.E. Fogg (ed.). *The State and Movement of Water on Living Organisms*, Cambridge University Press.

Monteith, J.L. 1973. *Principles of Environmental Physics.* Arnold (London).

Monteith, J.L. 1976. (Ed.) *Vegetation and the Atmosphere*, II, Case Studies. Academic Press, London.

Monteith, J.L.and Unsworth, M.H. 1990. *Principles of Environmental Physics*, 2nd edition, Edward Arnold, London.

Mooney, H.A. and Gulmon, S.L. 1982. Constraints on leaf structure and function in reference to herbivory. *BioSci.*, **32**, 198–206.

Moore, T.R. 1984. Litter decomposition in a subarctic spruce-lichen woodland, eastern Canada. *Ecology*, **65**, 299–308.

Müller, M.J. 1982. *Selected Climatic Data for a Global Set of Standard Stations for Vegetation Science*. Junk, The Hague.

Nadelhoffer, K.J. Aber, J.D. and Melillo, J.M. 1983. Leaf-litter production and soil organic matter dynamics along a nitrogen-availability gradient in southern Wisconsin (U.S.A). *Can. J. Forest Res.*, **13**, 12–21.

Neilson, R.P. 1995. A model for predicting continental scale vegetation distribution and water balance. *Ecol. Appl.* **5**, 362–385.

Neilson, R.P. & Marks, D. 1995. A global perspective of regional vegetation and hydrologic sensitivities from climatic change. *J. Veg. Sci.*, **5**, 715–730.

Nemani, R.R. & Running, S.W. 1995. Global land cover changes and their impact on climate. *Clim. Change*, **31**, 395–413.

Nemani, R.R. & Running, S.W. 1996. Implementation of a hierarchical global vegetation classification in ecosystem function models. *J. Veg. Sci.*, **7**, 337–346.

Nye, P.H. and Greenland, D.J. 1960. *The Soil Under Shifting Cultivation.* Technical Communication No. 51, Commonwealth Agriculture Bureaux, Farnham Royal.

Oke, T.R. 1978. *Boundary Layer Climates.* Methuen & Co. Ltd.

Oreskes, N., Shrader-Frechette, K. & Belitz, K. 1994. Verification, validation and confirmation of numerical models in the earth sciences. *Science*, **263**, 641–646.

Parton, W.J., Schimel, D.S., Cole, C.V. and Ojima, D.S. 1987. Analysis of factors controlling soil organic matter levels in Great Plains grasslands. *Soil Sci. Soc. Am. J.*, **51**, 1173–1179.

Parton, W.J., Scurlock, J.M.O., Ojima, D.S., Gilmanov, T.G., Scholes, R.J., Schimel, D.S., Kirchner, T., Menaut, J.-C., Seastedt, T., Moyia, E. Garcia, Kamnalrut, A. and Kinyamario, J.I. 1993. Observations and modelling of biomass and soil organic matter dynamics for the grassland biome worldwide. *Global Biogeochem. Cycles*, **7**, 785–809.

Pastor, J. and Bockheim, J.G. 1984. Distribution and cycling of nutrients in an aspen-mixed hardwood-spodsol ecosystem in northern Wisconsin. *Ecology*, **65**, 339–353.

Pastor, J., Aber, J.D., McClaugherty, C.A. and Melillo, J.M. 1984. Above-ground production and N and P cycling along a nitrogen mineralization gradient on Blackhawk Island, Wisconsin. *Ecology*, **65**, 25–28.

Pastor, J. and Post, W.M. 1986. Influence of Climate, Soil-Moisture, and Succession on Forest Carbon and Nitrogen Cycles. *Biogeochemi.*, **2**, 3–27.

Pastor, J., Gardner, R.H., Dale, V.H., and Post, W.M. 1987. Successional changes in nitrogen availability as a potential factor contributing to spruce declines in boreal North America. *Can. J. Forest Res.*, **17**, 1394–1400.

Pastor , J. and Mladenoff, D.J. 1992. The southern boreal - northern hardwood forest border. In, Shugart, H.H. Leemans, R. and Bonan, G.B. (eds.). *A*

Systems Analysis of the Global Boreal Forest, Cambridge University Press, Cambridge, U.K.

Penman, H.L. 1948. Natural evaporation from open water, bare soil and grass. *Proc. R. Soc. London, Series A*, **193**, 120–145.

Post, W.M., Emanuel, W.R, Zinke, P.J., & Stangenberger. 1982. Soil carbon pools and world life zones. *Nature*, **298**, 156–159.

Post, W.M., Pastor, J., Zinke, P.J. & Stangenberger, A.G. 1985. Global patterns of soil nitrogen storage. *Nature,* **317**, 613–616.

Prentice, I.C. 1986. Vegetation responses to past climatic variation. *Vegetatio*, **67**, 131–141.

Prentice, I.C. 1990. Bioclimatic distribution of vegetation for General Circulation Model studies. *J. Geophys. Res.*, **95**, 11811–11830.

Prentice, I.C., Cramer, W.P., Harrison, S.P., Leemans, R., Monserud, R.A. and Solomon, A.M. 1992. A global biome model based on plant physiology and dominance, soil properties and climate. *J. Biogeogr.*, **19**, 117–134.

Priestley, C.H.B. and Taylor, R.J. 1972. On the assessment of surface heat flux and evaporation using large-scale parameters. *Mon. Wea. Rev.*, **100**, 81–92.

Raich, J.W., Rastetter, E.B, Melillo, J.M., Kicklighter, D.W., Steudler, P.A., Peterson, B.J., Grace, A.L., Moore III, B. and Vorosmarty, C.J.1991. Potential Net Primary Productivity in South America: Application of a global model. *Ecol. Appl.*, **1**, 399–429.

Randall, D.A., Dazlich, D.A., Zhang, C., Denning, A.S., Sellers, P.J., Tucker, C.J., Bounoua, L., Los, S.O., Justice, C.O., Fung, I. 1996. A revised land-surface parameterization (SiB2) for GCMs .3. The greening of the Colorado state-university general-circulation model. *J. Clim.*, **9**, 738–763.

Rastetter, E.B., Ryan, M.G., Shaver, G.R., Melillo, J.M., Nadelhoffer, K.J., Hobbie, J.E., & Aber, J.D. 1991.A general biogeochemical model

describing the responses of the C and N cycles in terrestrial ecosystems to changes in CO_2, climate and N deposition. *Tree Physiol.* **9**, 101–126.

Raynaud, D. and Siegenthaler, U. 1993. Role of trace gases : the problem of lead and lag. In, *Global Changes in the Perspective of the Past.* Eddy, J.A. and Oeschger, H. (eds.). John Wiley & Sons, Chichester, 173–188.

Read, D.J. 1990. Mycorrhizas in ecosystems. *Exper.*, **47**, 376–391.

Reid, C.P.P., Kidd, F.A., and Ekwebelam, S.A.1983. Nitrogen nutrition, photosynthesis and carbon allocation in ectomycorrhizal pine. *Plant & Soil,* **71**, 415–432.

Reynolds, J.F., Hilbert, D.W.,Chen, J.L.,Harley, P.C.,Kemp, P.R.,& Leadley, P.W. 1992. *Modeling the Response of Plants and Ecosystems to Elevated CO_2 and Climate Change.* Rep. DOE/ER-60490T-H1, Carbon Dioxide Res. Div., U.S. Dep. Energy, Washington, D.C.

Rice, D.P., Crist, E.P. and Malila, W.A. 1980. *Applicability of selected wheat R.S. technology to corn and soybeans.* Env. Res. Inst. of Mich. Final Report No. 124000–9–F.

Risser, P.G. 1988. Abiotic controls on primary productivity and nutrient cycles in North American grasslands. In, L.R. Pomeroy and J.J. Alberts (eds.). *Concepts of Ecosystem Ecology,* Springer, New York.

Rosenberg, N.J. 1974. *Microclimate: the Biological Environment.* Wiley, New York.

Rowntree, P.R. 1988. Review of general circulation models as a basis for predicting the effects of vegetation change on climate. *Proceedings of the UN University Workshop on Forest, Climate and Hydrology-Regional Impacts, Tokyo (UN University).*

Running, S.W. and Hunt, E.R. Jr. 1993. Generalization of a forest ecosystem process model for other biomes, BIOME-BGC, and an application for global-scale models. In, J.R. Ehleringer, and C. Field (eds.). *Scaling Processes Between Leaf and Landscape Levels.* Academic Press, San Diego, Calif., 141–158.

Russell, E.W. 1988. *Russell's soil conditions and plant growth.* Alan Wild (ed.).11th ed. Longman Scientific and Technical. Longman Group U.K. Limited. Co. Pub. in U.S. with John Wiley.

Rutter, A.J., Morton, A.J., and Robins, P.C. 1975 A predictive model of rainfall interception in forests. II. Generalisation of the model and comparison with observations in some coniferous and hardwood stands. *J. Appl. Ecol.*, **12**, 367–380.

Ryan, M.G., Hunt, E.R., Jr, McMurtrie, R.E., Ågren G.I., Aber, J.D., Friend, A.D., Rastetter, E.B., Pullman, W.M., Raison, R.J. & Linder, S. 1996. Comparing Models of Ecosystem Function for Temperate Conifer Forests. I. Model Description and Validation. In, *Global Change: Effects on Coniferous Forests and Grasslands*. Breymeyer, A.I., Hall, D.O., Melillo, J.M. & Ågren, G.I.(eds.). 1996 SCOPE, John Wiley & Sons Ltd, 313–362.

Ryan, M.G., McMurtrie, R.E., Ågren G.I., Hunt, E.R., Jr, Aber, J.D., Friend, A.D., Rastetter, E.B.& Pullman, W.M. 1996. Comparing Models of Ecosystem Function for Temperate Conifer Forests. II. Simulations of the Effect of Climate Change. In, Global Change: Effects on Coniferous Forests and Grasslands. Breymeyer, A.I., Hall, D.O., Melillo, J.M. & Ågren, G.I.(eds.). 1996 SCOPE, John Wiley & Sons Ltd, 363–387.

Sarmiento, G. 1984. *The Ecology of Neotropical Savannas.* Harvard University Press, Cambridge.

Schneider, S.H. 1986. Can Modeling of the Ancient Past Verify Prediction of Future Climates? (editorial), *Clim. Change*, **8**, 117–119.

Schneider, S.H. 1992. Introduction to climate modeling. In, Trenberth, K.E. (ed.) *Climate System Modeling*. Cambridge University Press, Cambridge, 3–26.

Schneider, S.H. 1996. *Laboratory Earth. The Planetary Gamble We Can't Afford To Lose*. Weidenfeld and Nicolson, London.

Schimel, D., Enting, I.G., Heimann, M., Wigley, T.M.L, Raynaud, D., Alves, D., Siegenthaler, U. 1995. CO_2 and the Carbon Cycle. In, Houghton, J.T., Meira Filho, L.G., Bruce, J., Lee Hoesung, Callander, B.A., Haites, E., Harris, N., and Maskell, K. (eds.). Intergovernmental Panel on Climate Change (IPCC) 1995. *Climate Change 1994. Radiative Forcing of Climate Change and An Evaluation of the IPCC IS92 Emission Scenarios.* Cambridge University Press, Cambridge, 35–71.

Sellers, P.J. 1985. Canopy reflectance, photosynthesis and transpiration. *International Journal of Remote Sensing,* **6**, 1335–1372.

Sellers, P.J. 1992. Biophysical models of land surface processes. In, Trenberth, K.E. (ed.) *Climate System Modeling*, Cambridge University Press, 451–490.

Sellers, P.J., Mintz, Y., Sud, Y.C. & Dalcher, A. 1986.A simple biosphere model (SiB) for use within general circulation models. *J. Atmos. Sci.,* **43**, 505–531.

Sellers, P.J., Berry, J.A., Collatz, G.J., Field, C.B., and Hall, F.G. 1992. Canopy reflectance, photosynthesis and transpiration, III. A reanalysis using improved leaf models and a new canopy integration scheme. *Remote Sens. Environ.*, **42**, 187–216.

Sellers, P.J. Los, S., Tucker, C., Justice, C., Dazlich, D., Collatz, G., & Randall, D. 1994. A revised land surface parameterisation (SiB2) for atmospheric GCMs. Part 2: The generation of global fields of terrestrial biophysical parameters from satellite data. *Int. J. Remote Sens.*, **15**, 3519–3546.

Sellers, P.J., Meeson, B.W., Closs, J.W., Collatz, J., Corprew, F.E., Dazlich, D., Hall, F.G., Kerr, Y.,Koster, R., Los, S., Mitchell, K. McManus, J.M.P., Myers, D.M., Sun, K.-J., Try, P. 1995. An Overview of the ISLSCP Initiative I Global Data Sets. On: *ISLSCP Initiative I-Global Data Sets for Land-Atmosphere Models, 1987–1988.* Volumes 1–5. Published on CD by NASA. Volume 1: USA_NASA_GDAAC_ISLSCP_001.

Sellers, P.J., Bounoua, L., Collatz, G.J., Randall, D.A., Dazlich, D.A., Los, S.O., Berry, J.A., Fung, I., Tucker, C.J., Field, C.B., Jensen, T.G. 1996a. Comparison of radiative and physiological effects of doubled atmospheric CO_2 on climate. *Science*, **271**, 1402–1406.

Sellers, P.J., Randall, D.A., Collatz, G.J., Berry, J.A., Field, C.B. Dazlich, D.A., Zhang, C., Collelo, G.D., Bounoua, L. 1996b. A revised land-surface parameterization (SiB2) for atmospheric GCMS .1. Model formulation. *J. Clim.*, **9**, 676–705.

Sellers, P.J., Los, S.O., Tucker, C.J., Justice, C.O., Dazlich, D.A., Collatz, G.J., Randall, D.A. 1996c. A revised land-surface parameterization (SiB2) for atmospheric GCMS .2. The generation of global fields of terrestrial biophysical parameters from satellite data.. *J. Clim.*, **9**, 706–737.

Sharkey, T.D. 1985. Photosynthesis in intact leaves of C_3 plants: physics, physiology and rate limitations. *Bot.Rev.*, **51**, 53–105.

Shaw, R.H. and Pereira, A.R. 1982. Aerodynamic roughness of a plant canopy: A numerical experiment. *Agric. Meteor.*, **26**, 51–65.

Shaver, G.R. & Chapin III, F.S. 1991. Production: biomass relationships and element cycling in contrasting arctic vegetation types, *Ecol. Monogr.*, **61**, 1–31.

Shugart, H.H. 1984. *A Theory of Forest Dynamics*. Springer-Verlag, New York, 278 pp.

Shugart, H.H. Antonovsky, M. Ya., Jarvis, P.G., & Sandford, A.P. 1986. CO_2, climatic change and forest ecosystems. In, B. Bolin, B.R. Doos, J. Jager, and R.A. Warrick (eds.). *The Greenhouse Effect, Climatic Change, and Ecosystems, SCOPE 29*, John Wiley and Sons, Chichester, 475–521.

Shugart, H.H., Leemans, R., and Bonan, G.B. 1992. *A Systems Analysis of the Global Boreal Forest*. Cambridge University Press.

Shukla, J. & Mintz, Y. 1982. Influence of land-surface evapotranspiration on the earth's climate. *Science*, **215**, 1498–1501.

Smith, T.M., Leemans, R, Shugart, H.H. 1992. Sensitivity of terrestrial carbon storage to CO_2-induced climate change: Comparison of four scenarios based on general circulation models. *Clim. Change*, **21**, 367–384.

Smith, T.M., Shugart, H.H., Woodward, F.I. & Burton, P.J. 1993. Plant functional types. In, Solomon, A.M. & Shugart, H.H. (eds.). *Vegetation Dynamics and Global Change*. London (Chapman & Hall), 272–292.

Smith, T.M., Shugart, H.H.,& Woodward, F.I. 1996. *Plant Functional Types*, Cambridge University Press, Cambridge.

Sollins, P. Grier, C.C., McCorison, F.M., Cromack, Jr., K., Fogel, R.,& Fredriksen, R.L. 1980. The internal element cycles of an old-growth Douglas-fir ecosystem in western Oregon. *Ecol. Monogr.*, **50**, 261–285.

Solomon, A.M. 1986. Transient responses of forests to CO_2-induced climate change: Simulation modeling experiments in Eastern North America. *Oecologia (Berlin)*, **68**, 567–579.

Sprugel, D.G. 1989. The relationship of evergreeness, crown architecture, and leaf size. *Am. Nat.*, **133**, 465–479.

Stark, N.M. and Jordan, C.F. 1978. The nutrient content of plants and soils from Brazil and Surinam. *Biotropica,* **2**, 51–60.

Stoner, W.A. and Miller, P.C. 1975. Water relations of plant species in the wet coastal tundra at Barrow, Alaska. *Arct. Alp. Res.*, **7**, 109–124.

Sud, Y.C., Sellers, P.J., Mintz, Y, Chou, M.D., Walker, G.K., & Smith, W.E. Influence of the biosphere on the global circulation and hydrological cycle–a simulation experiment. *Agric. For. Meteor..*, **52**, 133–180.

Sutton, R.T. and Allen, M.R. 1997. Decadal predictability of North Atlantic sea surface temperature and climate. *Nature*, **388**, 563–567.

Tarpley, J.D., Schneider, S.R. & Money, R.L. 1984. Global vegetation indices from the NOAA–7 meteorological satellite. *J. Clim. and App. Meteorol.*, **23**, 491–494.

Tedrow, J.C.F. 1970. Soils of the subarctic regions. In, Ecology of the subarctic regime. *Proceedings of the Helsinki Symposium.* UNESCO, New York, 189–206

Tedrow, J.C.F. 1977. *Soils of the polar landscapes*. Rutgers University Press, New Brunswick, N.J., U.S.A.

Tennent, R.M. 1976. *Science data book.* Oliver and Boyd, Edinburgh. 104 pp.

Tieszen, L.L. 1978. Photosynthesis in the principal Barrow Alaska species: a summary of field and laboratory responses. In, L.L. Tieszen (ed.). *Vegetation and Production Ecology of an Alaskan Arctic Tundra*, Springer, New York, 241–268.

Tieszen, L.L. Senyimba, M.M., Imbamba, S.K. and Troughton, J.H. 1979. The distribution of C_3 and C_4 grasses and carbon isotope discrimination along an altitudinal and moisture gradient in Kenya. *Oecologia*, **37**, 337–350.

Turco, R.P. 1992. Atmospheric chemistry. In, Trenberth, K.E. (ed.). *Climate System Modeling,* Cambridge University Press, Cambridge, 201–240.

Urban, D.L. and Shugart, H.H. 1992. Individual based models of forest succession. In, D.C. Glenn-Lewin, R.K. Peet and T.V. Veblen (eds.). *Plant succession -theory and prediction. Population and community biology series 11*, Chapman and Hall, 249–292.

Van Cleve, K. and Oliver, L.K. 1982. Growth response of postfire quaking aspen (*Populus tremuloides* Michx.) to N, P, and K fertilisation. *Canadian Journal of Forest Research*, **12**, 160–165.

Van Cleve, K., Oliver, L., Schlentner, R. Viereck, L.A. & Dryness, C.T. 1983b. Productivity and nutrient cycling in taiga forest ecosystems. *Can. J. Forest Res.*, **13**, 747–766.

Viro, P. 1967. Forest manuring on mineral soils. *Medd. Nor. Skogforsoksves,* **23**, 113–136.

Webb, T. III. 1986. Is vegetation in equilibrium with climate? How to interpret late Quaternary pollen data. *Vegetatio*, **67**, 75–91.

Webb, T. III., Bartlein, P.J. & Kutzbach, J.E. 1987. Climatic Change in Eastern North America During the Past 18,000 years: Comparison of Pollen Data with Model Results. In, Ruddiman, W.F. & Wright, H.E. Jr. (eds.). *North America and Adjacent Oceans during the last Deglaciations, Geology of North America.* Vol. K-3, Geological Society of America, Boulder, CO, 447–462.

Webb, T. III and Bartlein, P.J. 1992. Global changes during the last 3 million years: climatic controls and biotic responses. *Ann Rev. Ecol.*, **23**, 141–173.

Whittaker, R.H. 1975. *Communities and Ecosystems*. 2nd ed. Macmillan Publishing Co., Inc., New York, U.S.A. 387 pp.

Wilson, M.F. & Henderson-Sellers, A.1985. A global archive of land cover and soils data for use in General Circulation Models. *Journal of Climatol.*, **5**, 119–143.

Wigley, T.M.L. and Rapier, S.C.B. 1990. Natural variability of the climate system and detection of the greenhouse effect. *Nature*, **344**, 324–327.

Woodmansee, R.G. 1978. Additions and losses of nitrogen in grassland ecosystems. *BioSci.*, **28**, 448–453.

Woodmansee, R.G., Dodd, J.L., Bowman, R.A., Clark, F.E., & Dickinson, C.E. 1978. Nitrogen budget of a shortgrass prairie ecosystem. *Oecologia*, **34**, 363–376.

Woodward, F.I. 1987. *Climate and Plant Distribution*, Cambridge University Press, Cambridge, U.K.

Woodward, F.I. 1993. Leaf responses to the environment and extrapolation to larger scales. In, Solomon, A.M. & Shugart, H.H.(eds.). *Vegetation Dynamics and Global Change*, Chapman & Hall, London, 71–100.

Woodward, F.I. 1996. Developing the potential for describing the terrestrial biosphere's response to a changing climate. In, Walker, B. & Steffen, W. (Eds.). *Global Change and Terrestrial Ecosystems*. IGBP Book Series 2. Cambridge University Press, 511-528.

Woodward, F.I. and Sheehy, J.E. 1983. *Principles and Measurements in Environmental Biology*. Butterworths. London.

Woodward, F.I., Thompson, G.B. & McKee, I.F. 1991. The effects of elevated concentrations of carbon dioxide on individual plants, populations, communities and ecosystems. *Ann. Bot.*, **67** (Supplement 1), 23–38.

Woodward, F.I. & Lee, S.E. 1994. Modelling terrestrial vegetation. *The Globe* **21**, 5–6.

Woodward, F.I. and Smith, T.M.. 1994a. Prediction and measurements of the maximum photosynthetic rate, Amax, at the global scale. In, E.D. Schulze and M.M. Caldwell (eds.). Ecophysiology of Photosynthesis, *Ecol. Stud.*, **100**, Springer-Verlag, New York, 491–509.

Woodward, F.I. and Smith, T.M. 1994b. Global photosynthesis and stomatal conductance: Modelling the controls by soils and climate. *Adv. Bot. Res.*, **20**, 1–41.

Woodward, F.I. and Lee, S.E. 1995. Global scale forest function and distribution. *Forestry,* **68**, 317–325.

Woodward, F.I., Smith, T.M. and Emanuel, W.R. 1995. A global land primary productivity and phytogeography model. *Global Biogeochem. Cycles*, **9**, 471–490.

Wright, R.F. 1994. *RAIN Project. Risdalsheia data report for June 1990–May 1994*. Acid Rain Research Report 36/94. Norwegian Institute for Water Research, Oslo.

Wullschleger, S.D.1993. Biochemical limitations to carbon assimilation in C_3 plants–A retrospective analysis of the A/C_i curves from 109 species. *J. Exp. Bot.*, **44**, 907–920.

Zachos, J.C., Flower, B.P., Paul, H. 1997. Orbitally paced climate oscillations across the Oligocene/Miocene boundary. *Nature*, **388**, 567–570.

Zinke, P.J., Stangenberger, A.G., Post, W.M., Emanuel, W.R., and Olson, J.S. 1984. *Worldwide Organic Soil Carbon and Nitrogen Data*, ORNL/TM-8857, Oak Ridge National Laboratory, Oak Ridge, Tennessee.

APPENDIX 1

Derivation of GCM vegetation parameters

GCM vegetation parameters

Vegetated fraction	ν
Snow-free albedo	α_o
Deep-snow albedo	α_s
Roughness length	z_o
Root depth (m)	z_d
Canopy capacity (mm)	c_m
Surface resistance (s m^{-1})	r_s
Infiltration enhancement factor	F_v

LAI of vegetated area (m^2 leaf m^2 covered ground)	$L_v = L/\nu$
Mean canopy height (m)	$h = 0.807\, L_a^{2.137}$

Calculation of GCM parameters

1) Vegetated fraction

$$\nu = 1 - \exp(-L/L^*) \quad (1)$$

where $L^* = 2.0$

2) Snow-free albedo

$$\alpha_o = \alpha_{ov}\nu + \alpha_{os}(1-\nu) \quad (2)$$

where α_{os} is the snow (or ice) albedo derived from the WHS map of soil colour classes and α_{ov} is the effective albedo of the vegetated fraction derived from the two stream solution of Sellers (1985) for L_v with underlying soil (assuming leaf reflection and transmission coefficients of $\alpha_{vis} = 0.11$, $\alpha_{nir} = 0.48$, $\tau_{vis} =$

0.06, τ_{nir} = 0.20). The effective albedo is the annual mean of the albedo dependent on zenith angle, $\alpha_{ov}(t)$, weighted with the solar radiation at the top of the atmosphere, $R_{toa}(t)$, thus:

$$\alpha_{ov} = \frac{1}{\langle R_{toa} \rangle \tau} \int_0^\tau R_{toa}(t) \alpha_{0v}(t) dt \qquad (3)$$

where τ is 1 year.

3) Deep-snow albedo

$$\alpha_s = \alpha_{sv} v + \alpha_{ss}(1-v) \qquad (4)$$

where α_{ss} = 0.80 is the deep-snow albedo of bare soil or ice, and α_{sv} is the annual mean albedo of the vegetated fraction derived from the two stream solution of Sellers (1985) for L_v with underlying snow (see snow-free albedo).

4) Roughness length:

$$\frac{1}{(\log l_b / z_0)^2} = \frac{v}{(\log l_b / z_{0v})^2} + \frac{1-v}{(\log l_b / z_{os})^2} \qquad (5)$$

where l_b = 550m is the "blending height", z_{0s} is the roughness length of the bare soil (0.0003m) or ice (0.0001m), and z_{0v} = f(h, L_v) is the roughness length of the vegetation derived from the fit to the results of Shaw and Pereira (1982).

5) Root depth:

$$z_d = z_{dv} v + z_{ds}(1-v) \qquad (6)$$

where z_{ds} is the root depth of bare soil (0.1 m) or ice (0 m), and z_{dv} is the root depth of the vegetated fraction, given by

$$z_{dv} = z_{ds} + 1.4\,(1-\exp\{-h/20\}). \qquad (7)$$

6) Canopy capacity:

$$c_m = c_{mv} + c_{ms}(1-v) \qquad (8)$$

where c_{ms} is the canopy capacity of bare soil (0.5 mm) or ice (0 mm), and c_{mv} is the canopy capacity of the vegetated fraction given by

$$c_{mv} = 0.5 + 0.05L_v \,. \tag{9}$$

7) Surface resistance

$$\frac{1}{r_s} = \frac{v}{r_{sv}} + \frac{1-v}{r_{ss}} \tag{10}$$

where r_{ss} is the surface resistance of the bare soil (100 s m^{-1}) or ice (0 s m^{-1}), and r_{sv} is the surface resistance of the vegetation provided by DOLY (from mean canopy conductance).

8) Infiltration enhancement factor:

$$F_v = F_{vv}v + F_{vs}(1-v) \tag{11}$$

where F_{vs} is the infiltration enhancement factor of bare soil (0.5) or ice (0) and F_{vv} is the infiltration enhancement factor of the vegetated fraction, given by

$$F_{vv} = 4\, z_{dv}. \tag{12}$$

This appendix was produced from equations supplied by Dr Peter Cox of the Hadley Centre.

APPENDIX 2

Derivation of relative humidity from the ISLSCP dataset

The relative humidity values were calculated from the ISLSCP data as follows. The 0600 and 1200 hours dew point temperature and air temperature were extracted for each day, for the years 1987 and 1988. The 0900 hours value was calculated by taking the mean of the 0600 hours and 1200 hours values. The average 0900 hours value was then calculated for each month of the year by totalling the daily values for that month and dividing by the number of days in the month.

Relative humidity expresses the actual moisture content of a sample of air as a percentage of that contained in the same volume of saturated air at the same temperature. The dew point temperature is the temperature at which saturation occurs if the air is cooled at constant pressure without the addition or removal of vapour. When the air temperature and dew-point temperature are equal the relative humidity is 100%. In general the relative humidity varies inversely with temperature during the day, tending to be lower in the early afternoon and higher at night.(Barry and Chorley, 1977).

Relative humidity can be determined from:

$$\frac{e_{sd}}{e_{sa}} \times 100 \qquad (1)$$

where e_{sd} is the saturated vapour pressure at the dew point temperature, and, e_{sa} is the saturated vapour pressure at the air temperature.

Saturated vapour pressure can be calculated for both the air temperature and the dewpoint temperature using the following equations:

$$e_{sd} = 6.108\exp\left((17.269t_d)/(237.3+t_d)\right)\times 100 \qquad (2)$$

where t_d is the mean monthly dew point temperature

$$e_{sa} = 6.108\exp\left((17.269t_a)/(237.3+t_a)\right)\times 100 \qquad (3)$$

where t_a is the mean monthly air temperature

APPENDIX 3

Derivation of transition matrix elements for the life-form model

LAI and NPP predicted by the DOLY (water and soils version) model are both used to determine the proportion of the three main life forms of grass, shrub and tree, and the area of bare ground in each grid square. No distinction is made between C_3 and C_4 grasses. In addition, no account is taken of carbon conservation, and the turnover of plant parts. Also, there are no disturbance calculations, although the life-form model is able to model disturbance. Such calculations could easily be incorporated at a later date. The proportion of bare ground at vegetation equilibrium is calculated as the fraction of irradiance not intercepted by the predicted LAI (Woodward, 1996).

Variables

The functional types were allocated the following numbers:

Bare ground = 0, grass = 1, shrub = 2, tree = 3.

Ground cover (%) of a functional type, i, is defined as S(i).

Initial ground cover (%) of :

bare ground, S(0) = 100

grass, S(1) = 0

shrub, S(2) = 0

tree, S(3) = 0

yr is the number of years for vegetation to reach a new equilibrium starting from 100% bare ground. This is assumed to occur at 50 years in this thesis.

L is LAI

N is NPP (tC ha^{-1} yr^{-1})

T is total vegetated cover (%)

A (j,k) is a transfer coefficient where j and k are functional type numbers (0 to 3). A(0,1) means that the transfer coefficient is the coefficient that is used to calculate the rate of change in the fraction of grass relative to bare ground. These coefficients vary between life-forms. These empirical coefficients have been derived by Professor Ian Woodward based on field observations of life-forms and their growth characteristics (Woodward, 1987, 1996) and from work done by Melillo *et al.* (1993). LAI and NPP are used to calculate life-form specific rates of establishment and mortality. The rate of change in the fraction of the three life-forms is modelled using transfer coefficients.

Modelling Procedure

i) Input LAI and NPP derived from the DOLY (standard version). These are taken to be the LAI and NPP of the vegetation at equilibrium.

ii) If LAI and NPP are zero the bare ground cover is set to 1 (i.e. 100%).

iii) Calculate the fractional bare ground cover, B, as follows:

$$B = \exp(-0.5L) \quad (1)$$

iv) Calculate vegetation cover of the three life-forms using the transfer coefficients (see below).

Transfer coefficients

Grass to bare ground, A(0,1)

$$A(0,1) = 0.03/(\exp(-0.4L)) \quad (2)$$

Shrub to bare ground, A(0,2)

$$A(0,2) = 0.02/(\exp(-0.4L)) \quad (3)$$

Tree to bare ground, A(0,3)

$$A(0,3) = 0.28/L \quad (4)$$

Bare ground to grass, A(1,0)

$$A(1,0) = (0.4N)/(3.0+N) \quad (5)$$

Bare ground to shrub, A(2,0)

$$A(2,0) = 0.67((0.2N)/(0.3+N)) \quad (6)$$

Bare ground to tree, A(3,0)

$$A(3,0) = 0.4/(2.5+N) \quad (7)$$

All other possible coefficients are set to zero.

v) For each year, yr, the fractional amount of total vegetation coverage, $svar_{yr}$, for a given life-form (in this case grass = 1) is calculated as follows:

$$svar_{yr} = svar_{yr-1}+(A(1,0) \times S(0))+ (A(1,1) \times S(1))+(A(1,2) \times S(2))+ (A(1,3) \times S(3)) \quad (8)$$

vi) At the end of 50 years, S(i) is set to $svar_{50}$ for life-form, i. The fractional cover of bare ground, F_{bg} is then calculated as follows:

$$F_{bg}=S(0)/(B\times100) \quad (9)$$

and the fractional cover ($F_{S(i)}$) for each life-form, i, relative to fractional bare ground cover:

$$F_{S(i)} = S(i)/F_{bg} \quad (10)$$

vii) The total vegetated cover of all vegetated life-forms, T, at the end of this 50 year period is:

$$T = F_{S(1)}+F_{S(2)}+F_{S(3)} \quad (11)$$

viii) Finally, the coverage of vegetation, S(i), of a given life-form, i, for the 50 year period is:

$$S(i) = F_{S(i)}\times((100.0-S(0))/T) \quad (12)$$

Global scale forest function and distribution

F. I. WOODWARD AND S. E. LEE

Department of Animal and Plant Sciences, University of Sheffield, P.O. Box 601, Sheffield, S10 2UQ, England

Summary

A model is described for predicting the dynamic changes in the proportion of tree, shrub and grass life forms at the global scale. This model is driven by the impacts of climate, soils and CO_2 on global vegetation leaf area index and net primary productivity. The life-form model has been used to explore the influences of global warming and continued CO_2 increase on tree cover. This reflects a realization from other modelling work that forested vegetation, at the global scale, exerts significant influences on climate, and so it is important to assess the potential for this feedback under climatic change.

An increase in CO_2 from 350 to 560 p.p.m. is modelled to have only a small impact on tree cover, under current climate. A regionally-consistent and global increase in temperature of *c.*2°C and a 10 per cent increase in precipitation, but with no increase in CO_2, indicates a significant potential for trees to spread into current shrub tundra, over a period of 50 years This could lead to regional warming, through changes in winter albedo. The effect of the CO_2 increase is most noticeable in interaction with increases in temperature (2°C) and precipitation (10 per cent). In this case the life-form model projects further increases in tree cover, particularly in areas with seasonally low periods of precipitation.

Introduction

The CO_2 concentration of the atmosphere has been steadily increasing since the eighteenth century, due to human activities of burning fossil fuels and significant areas of global forests (Keeling *et al.*, 1989; Watson *et al.*, 1990). These human activities are generally at the expense of the World's natural vegetation, which is being continually changed to either urban sprawl or agriculture. In addition to the inevitable losses in species diversity there are less well known and quantified effects on global climate. Model experiments with general circulation models (GCMs) have shown, even with simple simulations of vegetation function, that terrestrial vegetation tempers the global climate, enhancing precipitation and reducing temperature extremes (Shukla and Mintz, 1982; Sud *et al.*, 1990).

More detailed regional simulations of vegetation–climate interactions have clearly demonstrated the important part played by vegetation in maintaining regional climates. Circulation model experiments in which the whole of the Brazilian rainforest is replaced by grassland (Lean and Warrilow, 1989; Shukla *et al.*, 1990) indicate the establishment of a new semi-arid and stable climate, into which the rain forest

could not readily establish. Such predictions follow from calculations which show that 50 per cent of the rainfall of the Amazon basin is derived from local evaporation (Salati *et al.*, 1979). Global forests may also be exerting further dampening effects on global climate, through the fertilizing effects of increasing atmospheric concentrations of CO_2 and oxides of nitrogen on growth and carbon sequestration, which in turn reduces the rate of CO_2 increase in the atmosphere (D'Arrigo *et al.*, 1987; Hudson *et al.*, 1994). A range of different approaches appear to indicate that significant amounts of anthropogenic CO_2 are being sequestered by terrestrial vegetation and that these sinks for CO_2 are in forests, either or both northern temperate forests and tropical forests (Tans *et al.*, 1990; Dai and Fung, 1993).

A serious problem remains in assessing these temporal trends in global effects, particularly from a modelling approach and from flux measurements at a very small number of sites, and this is ignorance of the timing, nature and extent of all types of disturbances in vegetation, particularly forests. In addition, model experiments to date have not considered the dynamic, successional nature of natural ecosystems. This paper describes an approach to predicting the dynamics of vegetation change at the global scale, with particular reference to changes in tree and forest distribution.

Model description

A basic plant process model underlies the model, described here, of life-form dynamics. Briefly the underlying model (Woodward *et al.*, 1995) models the effects of climate, $CO_2$and soil nutrients in defining the leaf area index (LAI) and net primary productivity (NPP) of vegetation. The model has no underlying map of vegetation but models LAI and NPP by scaling up from basic plant processes of photosynthesis, respiration, nutrient and water uptake and evapotranspiration to global-scale distributions. An underlying map of soil carbon and nitrogen is required to parameterize the variables in the photosynthesis model and is described by Woodward and Smith (1994). The model described here uses the LAI and NPP modelled for any location, to predict the outcome of a simple competitive succession between three basic life forms, trees, shrubs and grasses.

The life-form model is devised as a compartment model, with bare ground, grass, shrub and tree as the four compartments. Some, but not all possible transfers between the compartments are possible, and these transfer coefficients have been derived to be appropriate for each life-form, based on field observations of the growth characteristics of the life-forms (Woodward, 1987). The arrangements of the compartments and the modelled transfer coefficients are shown in Figure 1. The descriptions and basic controls of the transfer coefficients (Table 1) indicate that LAI and NPP and used throughout. In the model, low LAI and NPP will maximize the growth of shrubs, increasing the NPP and LAI will first favour grasses and then finally trees. These progressions have been devised from earlier work (Woodward, 1987; Melillo *et al.*, 1993).

A typical 50-year dynamic of changes in the

Table 1: Transfer coefficients for the compartment model (Figure 1) of life form spread. 'Controls on coefficients'—Leaf Area Index (LAI) and Net Primary Productivity (NPP)—describes which controls are used to define the life-form specific dynamics of growth

Coefficients	Life form change	Controls on coefficients
A0,1	Grass to bare ground	LAI
A0,2	Shrub to bare ground	LAI
A0,3	Tree to bare ground	LAI
A1,0	Bare ground to grass	NPP
A2,0	Bare ground to shrub	NPP and LAI
A3,0	Bare ground to tree	NPP

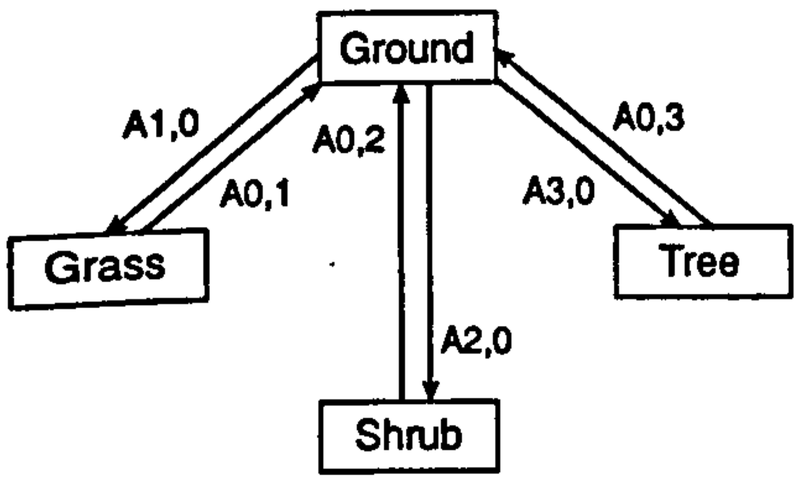

Figure 1. Compartment life form mode. *Ax,y*, (where *x* and *y* range from 0 to 3) indicate transfer coefficients between the compartments which are allowed in the model.

relative cover of trees, shrubs and grasses is shown (Figure 2) for a site with a potential LAI of 5 and NPP of 5 tC ha^{-1} a^{-1}. The relative LAI and NPP 'spaces' of the three life-forms indicate the dominance of shrubs in low NPP environments (Figure 3), the dominance of grasses in higher NPP environments (Figure 4) and the increasing dominance of trees with increasing LAI (Figure 5). The strong dominance of LAI in defining the presence of trees can be amplified through a simulated effect of shading by trees on the shorter life-forms.

Testing the model

The model has been applied globally, using an underlying soil carbon and nitrogen database (Woodward *et al.*, 1995) and driven by a current-day simulation climate database derived from the UK Meteorological Office GCM (coarse resolution slab model), and obtained from the Meteorological Office. The map of predicted current-day distribution of tree cover (Figure 6) has some errors which are not directly due to the model itself. The first source of errors is from the simulation of climate, the second source arises from assuming that the World's vegetation is completely natural, with no agricultural conversion included. With these two sources of error in mind, it is interesting to consider the test of the model output. The test has been achieved against a global set of projected, actual vegetation (Wilson and Henderson-Sellers, 1985). It should also be pointed out that this map also has significant errors, through various sources such as spatial averaging and uncertain physiognomic classification.

In order to carry out the test, model projections of percentage tree cover (Figure 6), for 4313 pixels of the World's terrestrial surface, are subtracted from the tree cover estimates

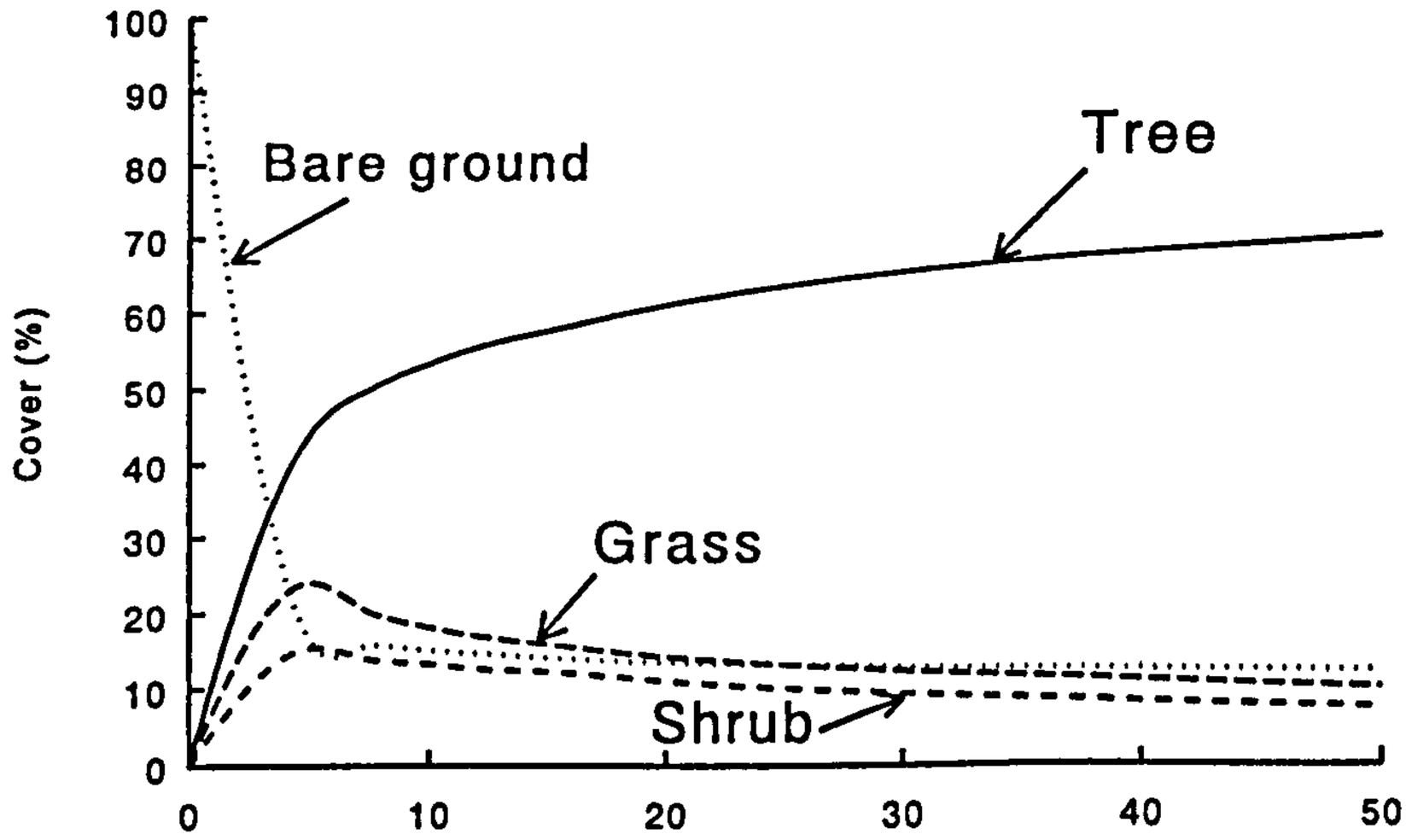

Figure 2. Example of the dynamics of life form cover over a period of 50 years, with a constant ceiling leaf area index (LAI) of 5 and net primary productivity (NPP) of 5 tC ha^{-1} a^{-1}.

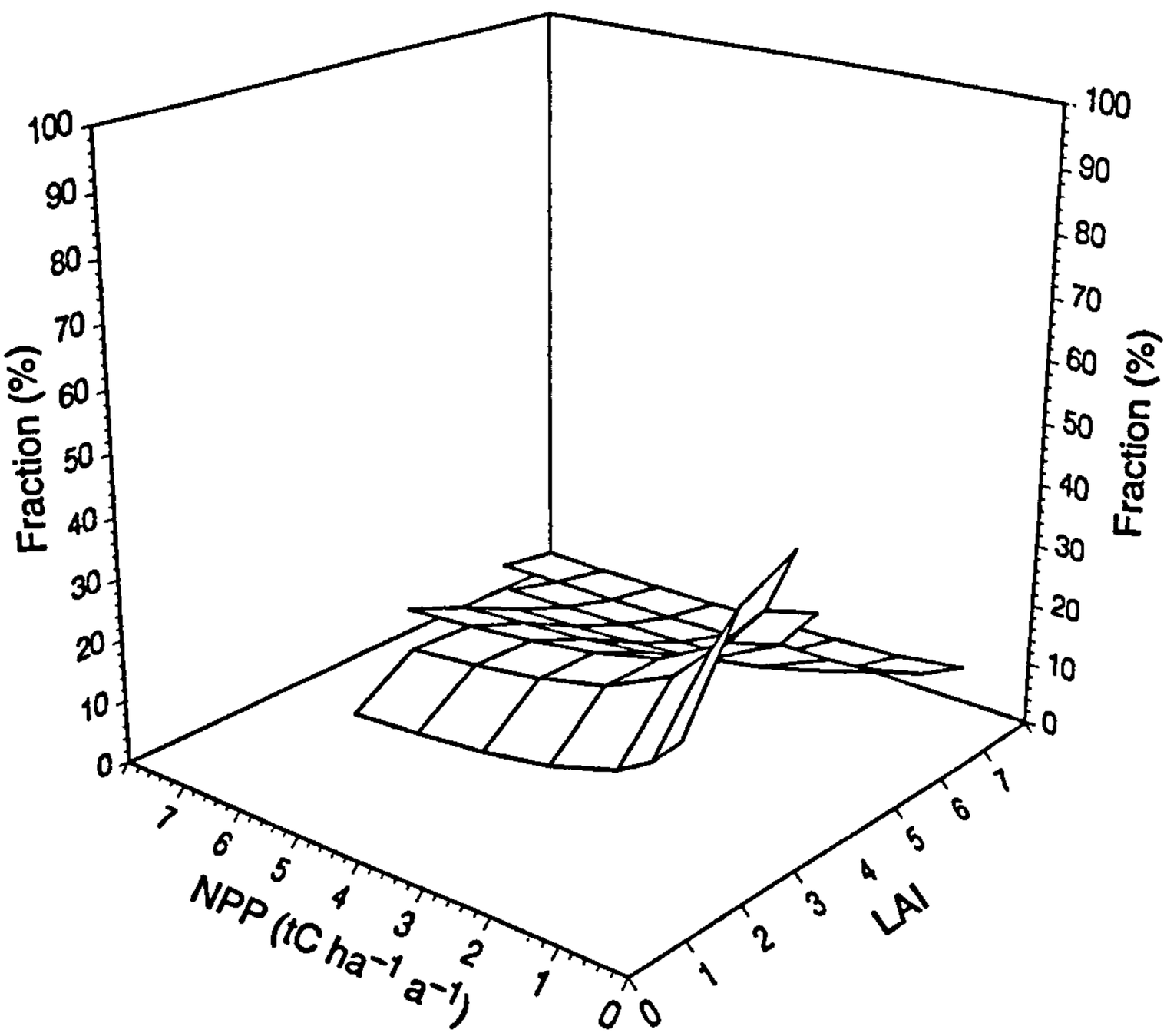

Figure 3. Modelled fraction of shrub cover with changes in LAI and NPP.

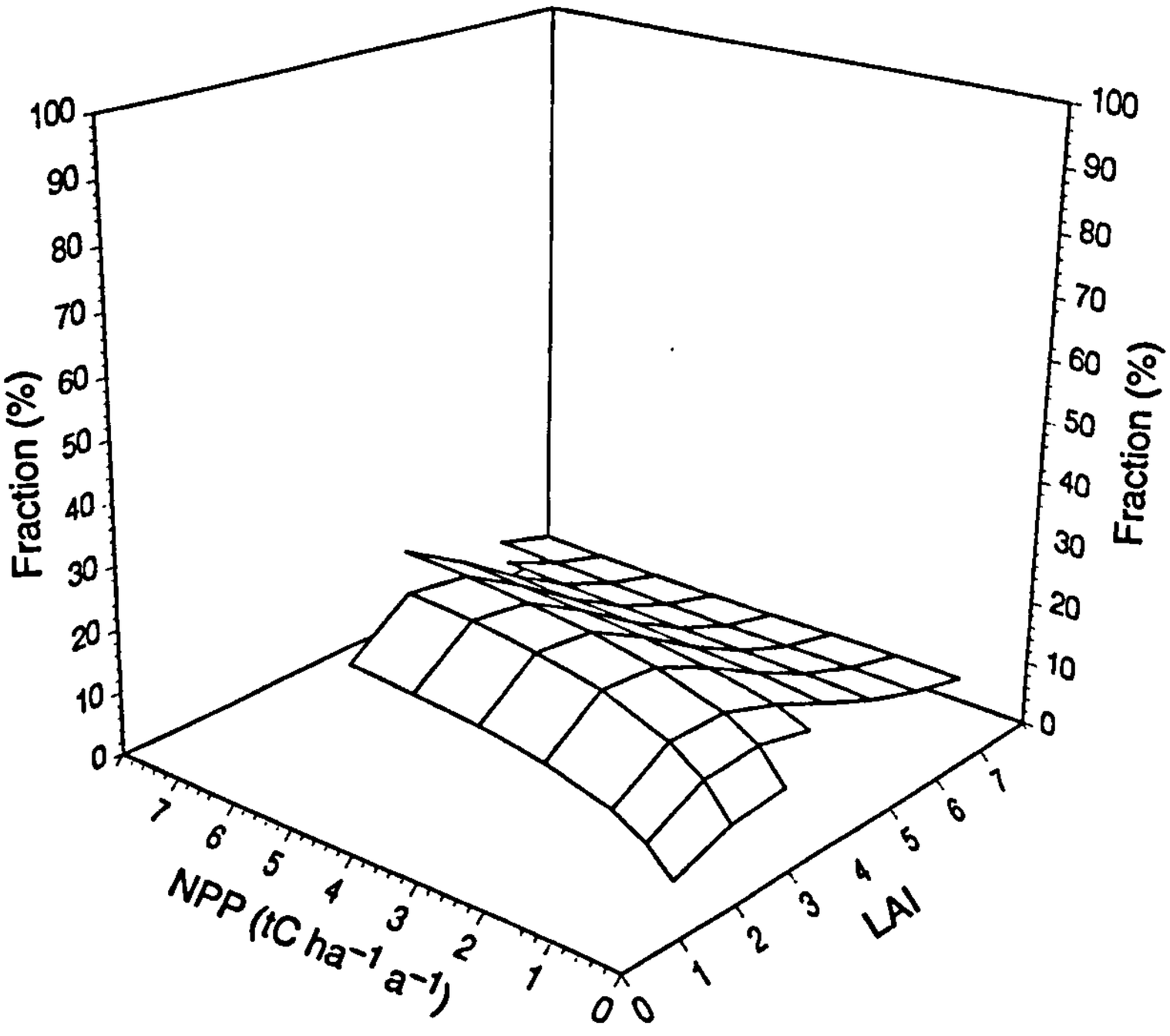

Figure 4. Modelled fraction of grass cover with changes in LAI and NPP.

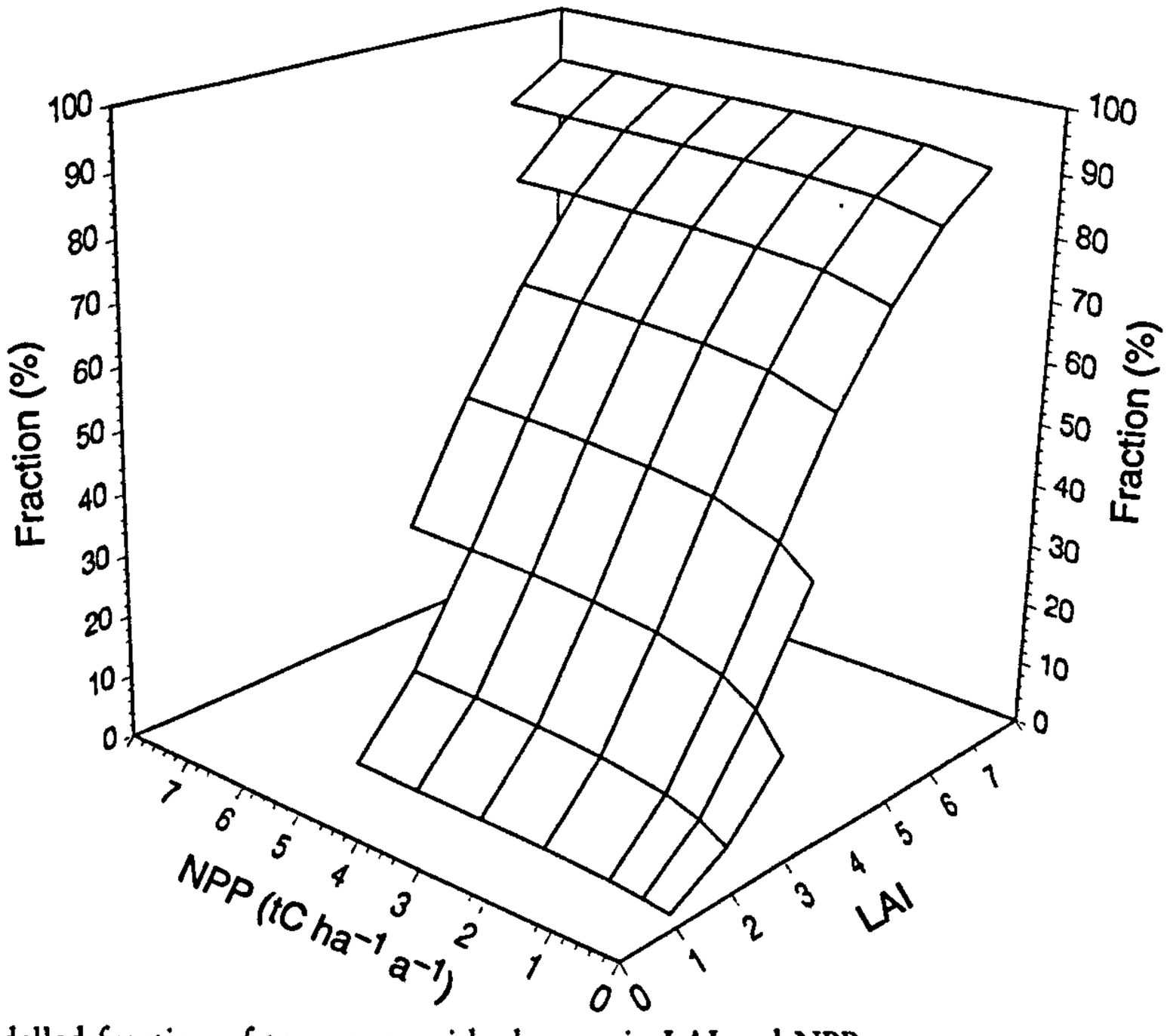

Figure 5. Modelled fraction of tree cover with changes in LAI and NPP.

over the same pixels from the map of Wilson and Henderson-Sellers. It was found that 80 per cent of these pixels were within ±10 per cent range of tree cover. This indicates that the major global patterns of tree cover are in good agreement. If the limits of agreement in terms of cover are relaxed to ±30 per cent, then there is only a 9 per cent increase in the number of pixels. This suggests that the two maps have quite marked regional differences in projected cover. However this does not detract from the good global-scale similarities between the maps of tree cover.

Model runs for future climates

The simplest scenario test has been achieved by retaining the same underlying climate as the base case (Figure 6) but with a CO_2 enrichment from 350 to 560 p.p.m. In this case the tree cover after 50 years of development under the current climate (Figure 6) is run for a further 50 years of gradual increase in CO_2 to the target of 560 p.p.m., but with the same climate. This increase has a rather small influence on tree cover (Figure 7). The effects, where they occur, are seen at the more arid extremes of tree occurrence, for example in south-east Asia and Africa.

Changing the global climate over a period of 50 years (Houghton *et al.*, 1992) by a *c.*2°C warming and a +10 per cent increase in precipitation (with greater warming at increasing latitude, as e.g. Sud *et al.*, 1990) exerts much larger effects (Figure 8). The model was run in the same manner as with CO_2 increase, allowing simple transient increases in temperature and precipitation to occur over 50 years. The resultant change in tree cover (Figure 8) does not include any CO_2 increase. Unlike the CO_2-alone case (Figure 7), marked changes in tree cover are predicted to occur over 50 years.

Particularly marked changes occur at the northern high latitudes, with tree cover spreading into the former shrub tundra. These changes will feedback on climate by changing the winter albedo of these regions from high (very reflective) when snow-covered and shrub-dominated to low when tree-dominated, even with snow accumulation. At lower latitudes, the model projects increasing tree cover in areas towards

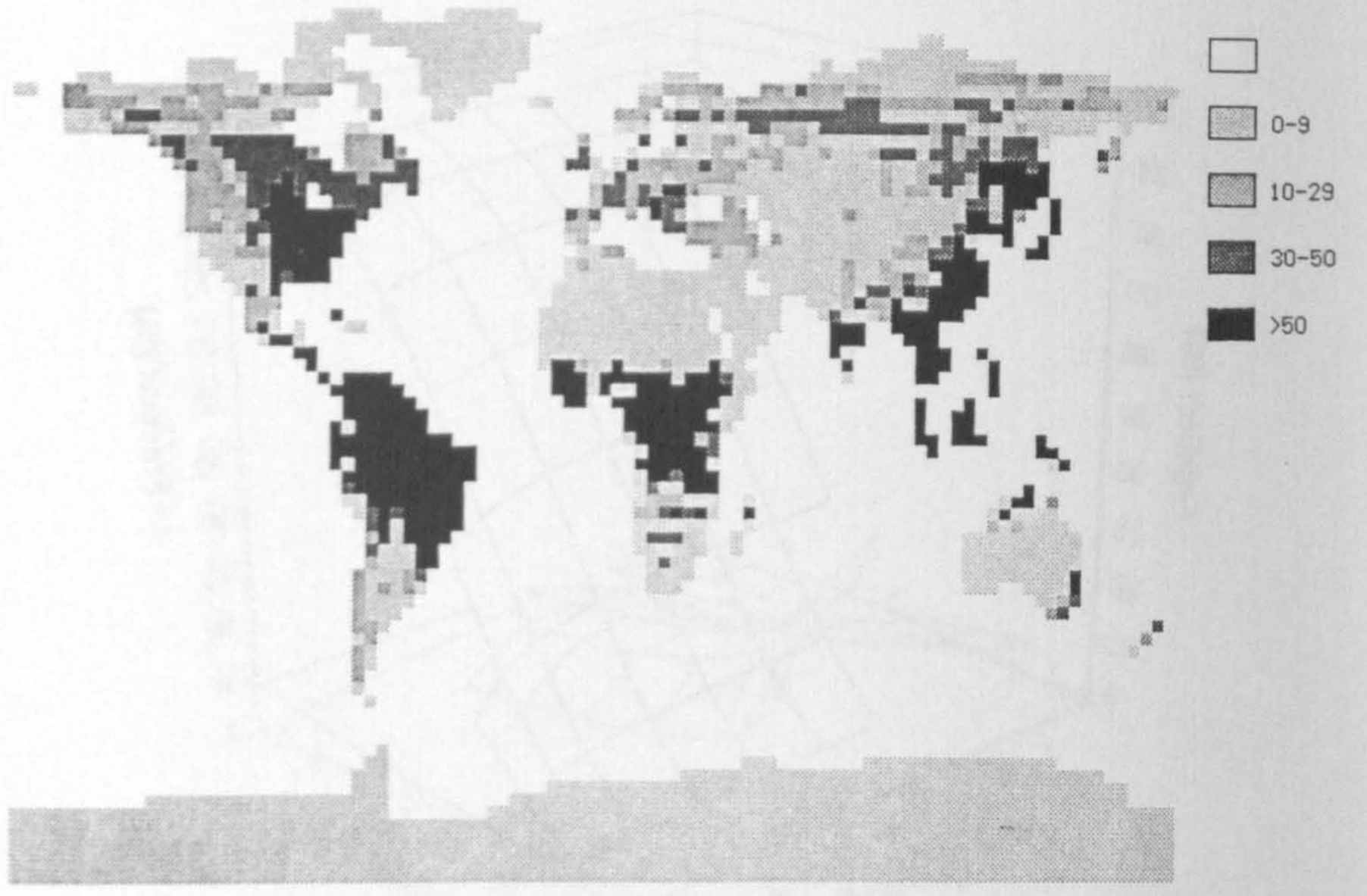

Figure 6. Tree cover (%) under current climate as simulated with the UK Meteorological Office coarse resolution (slab) model.

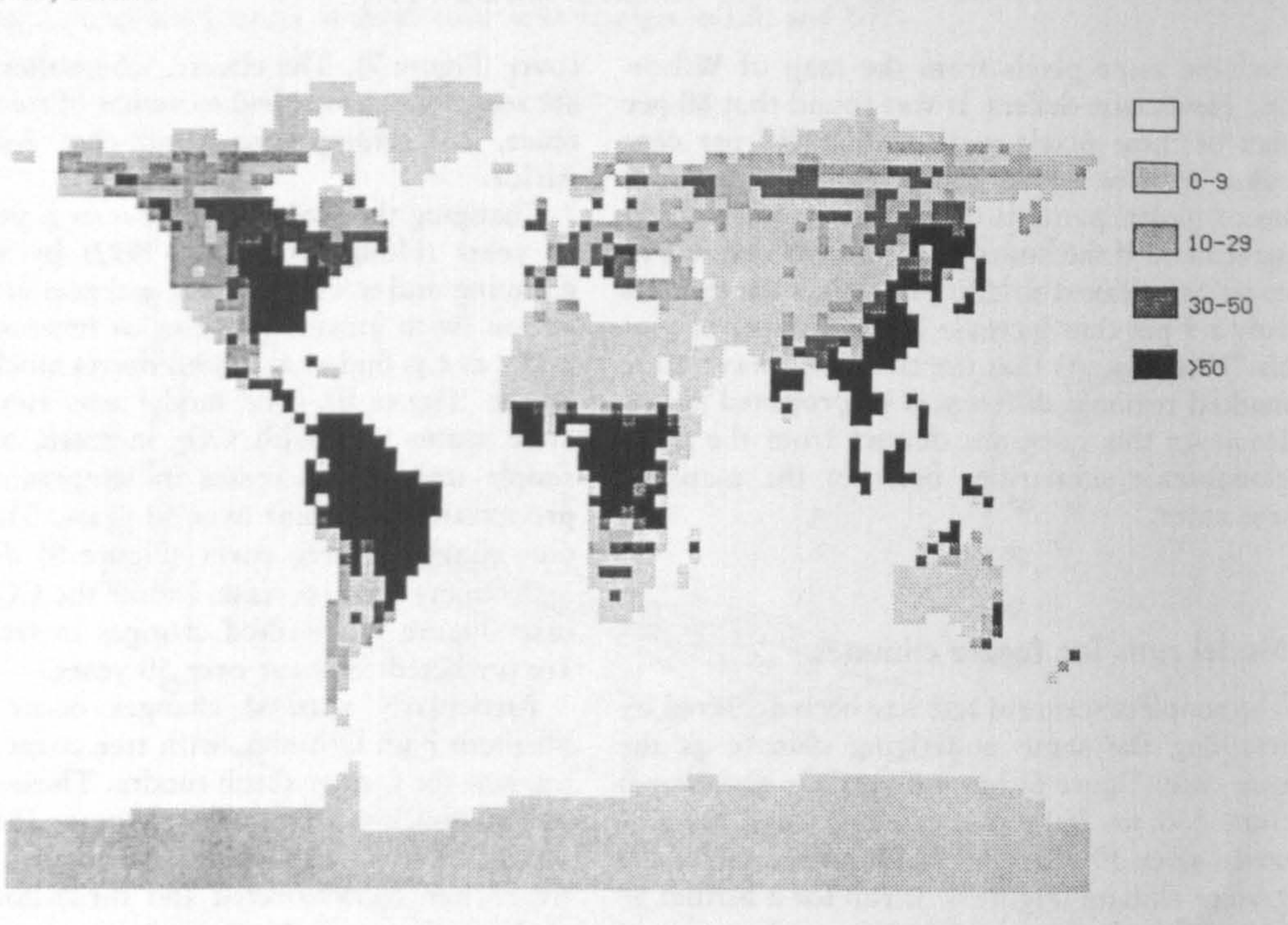

Figure 7. Tree cover (%) under current climate but with the CO_2 concentration increased from 350 to 560 p.p.m. over a period of 50 years.

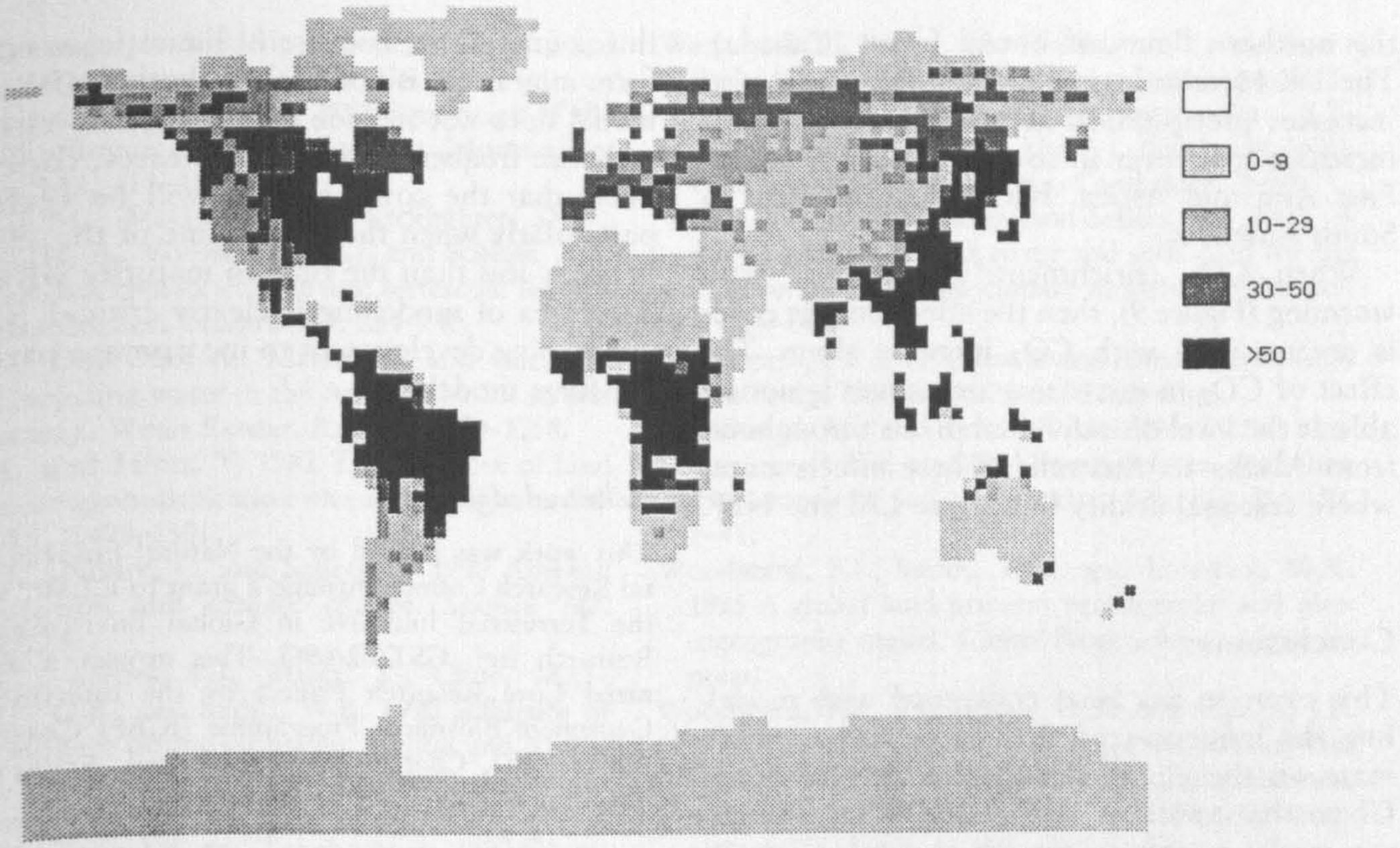

Figure 8. Tree cover (%) after a period of 50 years of global warming (+2°C, +10% precipitation) but no increase in CO_2 concentration.

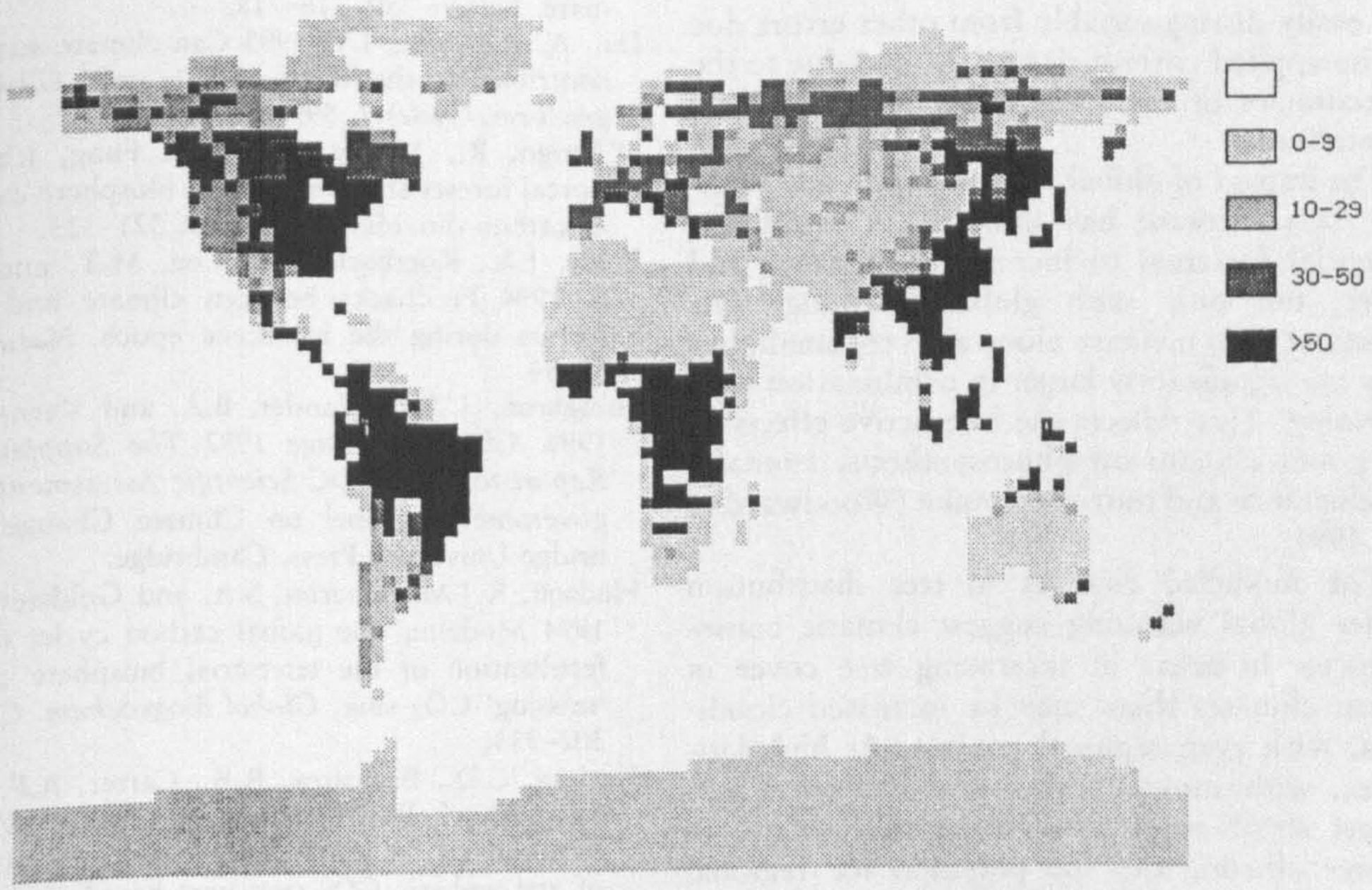

Figure 9. Tree cover (%) after a period of 50 years of global warming (+2°C, +10% precipitation) and an increase in CO_2 concentration from 350 to 560 p.p.m.

the northern limits of boreal forest (Canada). The UK Meteorological Office slab model also increases precipitation at lower latitudes. This increases tree cover in southern Europe, South-East Asia and Africa, but with little effect in South America.

When CO_2 enrichment is modelled with warming (Figure 9), then the effect on tree cover is greater than with CO_2 increase alone. The effect of CO_2 in increasing tree cover is noticeable at the level of individual pixels throughout, from Alaska to Australia. These effects occur where seasonal aridity limits tree LAI and NPP.

Conclusions

This exercise has been concerned with modelling the influences of changes in CO_2 and climate on the global distribution of tree cover. Given the inputs of LAI and NPP for any site the model is able to predict the dynamic relationships between the proportion of trees, shrubs and grasses. The approach is effective in predicting the present-day proportions of these life-forms, although the errors in prediction are not easily distinguishable from other errors due to the applied current-day GCM and due to the inaccuracies of the present-day map of actual vegetation.

The impact of global warming with and without CO_2 increase has indicated a significant potential for trees to increase their range and cover, but only with global warming. The effects of CO_2 increase alone are very small, but they are significantly larger in combination with warming. This reflects the interactive effects of CO_2 and climate on photosynthesis, stomatal conductance and nutrient uptake (Woodward *et al.*, 1991).

The modelled changes in tree distribution under global warming suggest climatic consequences. In areas of increasing tree cover in warm climates there may be increased cloudiness, with even regional cooling. At high latitudes, with snowfall, the spread of trees into dwarf shrub tundra will cause a decrease in winter albedo, and the potential for regional warming (Bonan *et al.*, 1992; Foley *et al.*, 1994).

The life-form model assumes that all life-forms can reach all sites. The degree to which this is unrealistic, because of limitations to life-form migration, is not known. As described, the model does not include disturbance. If the disturbance frequency of a site increases, then it is likely that the cover of trees will be reduced, particularly when the return time of the disturbance is less than the time to maturity of trees. This area of modelling is clearly critical and is an ongoing development to incorporate into the life-form model.

Acknowledgements

This work was funded by the Natural Environmental Research Council through a grant to F.I.W. under the Terrestrial Initiative in Global Environmental Research (ref. GST/02/696). This project a recognized Core Research Project by the International Geosphere Biosphere Programme (IGBP) Core Project Global Change and Terrestrial Ecosystems (GCTE).

References

Bonan, G.B., Pollard, D. and Thompson, S.L. 1992 Effects of boreal forest vegetation on global climate. *Nature* 359, 716–718.

Dai, A. and Fung, I.Y. 1993 Can climate variability contribute to the 'missing' CO_2 sink? *Global Biogeochem. Cycles* 7, 599–609.

D'Arrigo, R., Jacoby, G.C. and Fung, I.Y. 1987 Boreal forests and atmosphere–biosphere exchange of carbon dioxide. *Nature* 329, 321–323.

Foley, J.A., Kutzbach, J.E., Coe, M.T. and Levis, S. 1994 Feedbacks between climate and boreal forests during the Holocene epoch. *Nature* 371, 52–54.

Houghton, J.T., Callander, B.A. and Varney, S.K. 1992 *Climate Change 1992 The Supplementary Report to the IPCDC Scientific Assessment*. Intergovernmental Panel on Climate Change. Cambridge University Press, Cambridge.

Hudson, R.J.M., Gherini, S.A. and Goldstein, R.A. 1994 Modeling the global carbon cycle: nitrogen fertilization of the terrestrial biosphere and the 'missing' CO_2 sink. *Global Biogeochem. Cycles* 8, 307–333.

Keeling, C.D., Bacastow, R.B., Carter, A.F., Piper, S.C., Whorf, T.P., Heimann, M., Mook, W.G. and Roeoloffzen, H. 1989 A three-dimensional model of atmospheric CO_2 transport based on observed winds. 1. Analysis of observational data. In *Aspects of Climate Variability in the Pacific and the Western Americas*. D.H. Peterson (ed.). Geophysi-

cal Monograph Vol. 55, American Geophysical Union, Washington, D.C., 165–236.
Lean, J. and Warrilow, D.A. 1989 Simulation of the regional climatic impact of Amazon deforestation. *Nature* 342, 411–413.
Melillo, J.M., McGuire, A.D., Kicklighter, D.W., Moore III, B., Vorosmarty, C.J. and Schloss, A.L. 1993 Global climate change and terrestrial net primary production. *Nature* 363, 234–240.
Salati, E., Dall'Olio, A., Matsui, E. and Gat, J.R. 1979 Recycling water in the Amazon basin: an isotopic study. *Water Resour. Res.* 15, 1250–1258.
Shukla, J. and Mintz, Y. 1982 The influence of land surface evapotranspiration on earth``s climate. *Science* 215, 1498–1501.
Shukla, J., Nobre, C. and Sellers, P. 1990 Amazon deforestation and climate change. *Science* 247, 1322–1325.
Sud, Y.C., Sellers, P.J., Mintz, Y., Chou, M.D., Walker, G.K. and Smith, W.E. 1990 Influence of the biosphere on the global circulation and hydrological cycle—a simulation experiment. *Agric. For. Meteorol.* 52, 133–180.
Tans, P.P., Fung, I.Y. and Takahashi, T. 1990 Observational constraints on the global atmospheric CO_2 budget. *Science* 247, 1431–1438.
Watson, R.T., Rodhe, H., Oeschger, H. and Siegenthaler, U. 1990 Greenhouse gases and aerosols. In *Climate Change, the IPCC Assessment.* J.T. Houghton, G.J. Jenkins and J.J. Ephraums (eds). Cambridge University Press, Cambridge, 7–40.
Wilson, M.F. and Henderson-Sellers, A. 1985 A global archive of land cover and soils data for use in general circulation climate models. *J. Climatol.* 5, 119–143.
Woodward, F.I. 1987 *Climate and Plant Distribution.* Cambridge University Press, Cambridge.
Woodward, F.I. and Smith, T.M. 1994 Global photosynthesis and stomatal conductance: modelling the controls by soil and climate. *Adv. Bot. Res.* 20, 1–41.
Woodward, F.I., Smith, T.M. and Emanuel, W.R. 1995 A global land primary productivity and phytogeography model. *Global Biogeochem. Cycles* (in press).
Woodward, F.I., Thompson, G.B. and McKee, I.F. 1991 The effects of elevated concentrations of carbon dioxide on individual plants, populations, communities and ecosystems. *Ann. Bot.* 67 (Supplement 1), 23–38.

Received 12 December 1994

Contrasting physiological and structural vegetation feedbacks in climate change simulations

Richard A. Betts*, Peter M. Cox*, Susan E. Lee† & F. Ian Woodward†

** Hadley Centre, Meteorological Office, Bracknell RG12 2SY, UK*
† Department of Animal and Plant Sciences, University of Sheffield, Sheffield S10 2TN, UK

Anthropogenic increases in the atmospheric concentration of carbon dioxide and other greenhouse gases are predicted to cause a warming of the global climate by modifying radiative forcing[1]. Carbon dioxide concentration increases may make a further contribution to warming by inducing a physiological response of the global vegetation—a reduced stomatal conductance, which suppresses transpiration[2]. Moreover, a CO_2-enriched atmosphere and the corresponding change in climate may also alter the density of vegetation cover, thus modifying the physical characteristics of the land surface to provide yet another climate feedback[3–6]. But such feedbacks from changes in vegetation structure have not yet been incorporated into general circulation model predictions of future climate change. Here we use a general circulation model iteratively coupled to an equilibrium vegetation model to quantify the effects of both physiological and structural vegetation feedbacks on a doubled-CO_2 climate. On a global scale, changes in vegetation structure are found to partially offset physiological vegetation–climate feedbacks in the long term, but overall vegetation feedbacks provide significant regional-scale effects.

The Sheffield University vegetation model simulates global vegetation under steady-state conditions of climate and atmospheric CO_2 (ref. 7). It models the physiological processes of nutrient uptake, photosynthesis, respiration and stomatal limitation of transpiration, and uses these to determine the vegetation structural character in terms of foliage density. The outputs of this model are: (1) leaf area index (LAI), the area of leaf surface per unit area of ground; and (2) daytime mean canopy conductance (g_c), the net transpirational conductance of all stomata integrated (numerically) over the canopy depth. LAI is purely a structural variable, whereas g_c contains both structural and physiological contributions. The

contemporary vegetation simulation has been validated against point measurements[7].

The Hadley Centre general circulation model (GCM) used here is a simplified version of that used for climate change prediction[8,9], consisting of an explicit representation of the global atmospheric circulation and a thermodynamic 'mixed-layer' ocean model with prescribed heat transports to represent ocean currents[10]. The simulations presented here neglect the relative cooling effect of increased sulphate aerosol concentrations[8]; this omission and that of explicit ocean current modelling means that the results cannot be regarded as a state-of-the-art prediction. Instead, they demonstrate the effect of vegetation feedback on climate sensitivity to atmospheric CO_2 concentrations.

The GCM land surface scheme is of moderate complexity[11], with the land surface state defined by seven prognostic variables: root-zone soil moisture, lying snow, intercepted canopy water, and the temperatures of four soil layers in the vertical. The surface energy partitioning, evapotranspiration, runoff and snowmelt are parametrized using driving variables from the atmosphere model and seven vegetation-specific land surface parameters[3]. The main parameters are: root depth, determining the depth of soil from which water can be extracted for transpiration; snow-free and deep-snow albedos, determining the fraction of incident solar radiation reflected from the surface; roughness length, determining the aerodynamic resistance for turbulent transfers; and surface conductance, determining the additional resistance for water vapour transfers in drought-free conditions. Over vegetated surfaces, the latter accounts for the control of transpiration by stomata, but is a prescribed vegetation-specific constant in this version of the scheme.

The GCM and vegetation model were coupled by iterating between the two models, each providing boundary conditions for the other. The GCM supplied climatological monthly means to the vegetation model, which returned the global distributions of LAI and g_c. The latter were used to redefine the GCM land surface parameters for the next iteration, with surface conductance incorporating g_c directly, and the remaining structural parameters being derived semi-empirically from LAI (Fig. 1).

The physiological and structural vegetation feedbacks on CO_2-induced climate change were isolated and quantified using the following four coupled simulations. (1) Both climate and vegetation consistent with an atmospheric CO_2 concentration of 323 parts per million by volume, p.p.m.v. ($1 \times CO_2$; simulation C). (2) The climate at equilibrium under $2 \times CO_2$ (646 p.p.m.v.) radiative forcing, but with the physiological and structural characteristics of the vegetation held at the $1 \times CO_2$ state (simulation R). (3) $2 \times CO_2$ radiative forcing and $1 \times CO_2$ vegetation structure, but with surface conductance including direct effects of $2 \times CO_2$ and the associated climate change on plant physiology (simulation RP). (4) $2 \times CO_2$ radiative forcing with both the physiology and structure allowed to reach a new equilibrium state under $2 \times CO_2$ and the associated climate (simulation RPS).

The difference between simulations R and C represents the standard GCM sensitivity to CO_2 excluding vegetation feedbacks, and the difference between RP and R defines the additional climate change resulting from the direct physiological effects (a comparable experiment to that in ref. 2). Finally, the difference between RPS and R demonstrates the combined effect of physiological and structural vegetation change on the climate sensitivity; this is the main new result of this work.

The radiation-only $2 \times CO_2$ sensitivity (R − C) of this version of the GCM was 4.3 K, which is at the high end of the IPCC range[1]. The modelled climate change showed relatively large changes in temperature and precipitation in the tropics (Fig. 2), associated with strong cloud-mediated feedbacks. The physiological response in

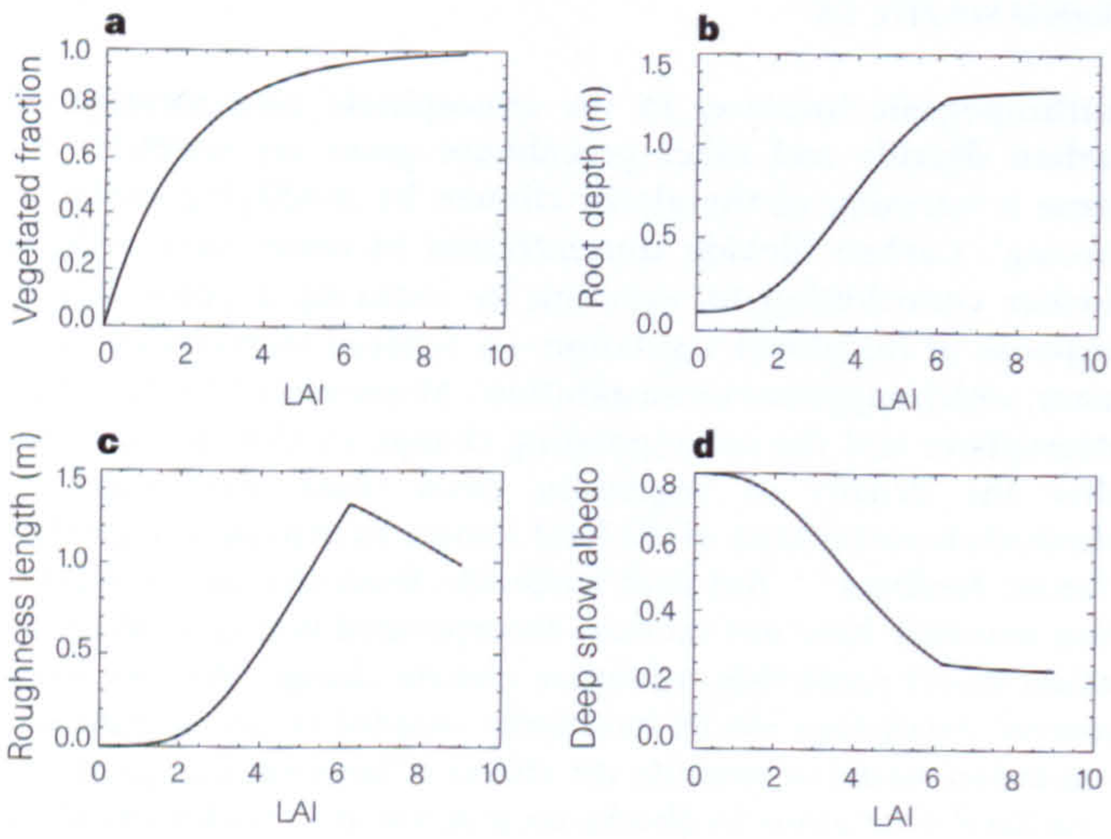

Figure 1 Derivation of GCM land surface parameters from leaf area index (LAI). **a**, Vegetated fraction is the fractional ground area covered by vegetation; this determines the relative weighting of values appropriate to vegetation and soil for the other variables. An empirical fit with the literature data[16–18] shows that vegetated fraction increases with LAI, saturating at higher values. **b**, The mean root depth is found empirically[16–20] to increase with LAI in the grid-box mean, and is also assumed to be linearly correlated with the maximum infiltration rate at the soil surface. **c**, Roughness length increases with LAI at low leaf areas, but decreases with LAI at higher values as the canopy becomes closed[21]. **d**, Deep-snow albedo[17] is the upper limit of surface reflectance in deep-snow conditions, and this decreases with LAI as more of the snow is masked by the darker vegetation. Snow-free albedo shows a similar but less pronounced relationship.

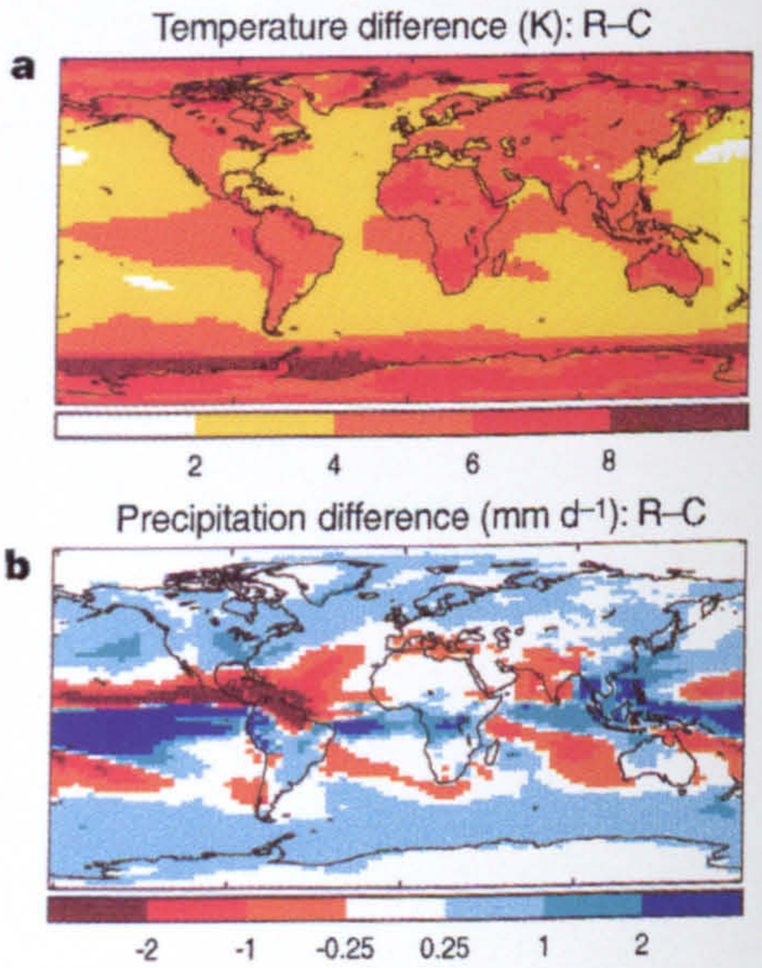

Figure 2 Climate change due to doubling the atmospheric concentration of CO_2, neglecting vegetation feedback, expressed as differences between simulations R and C (see text). **a**, Change in annual mean temperature, diagnosed at a height of 1.5 m above the surface. **b**, Change in annual mean precipitation.

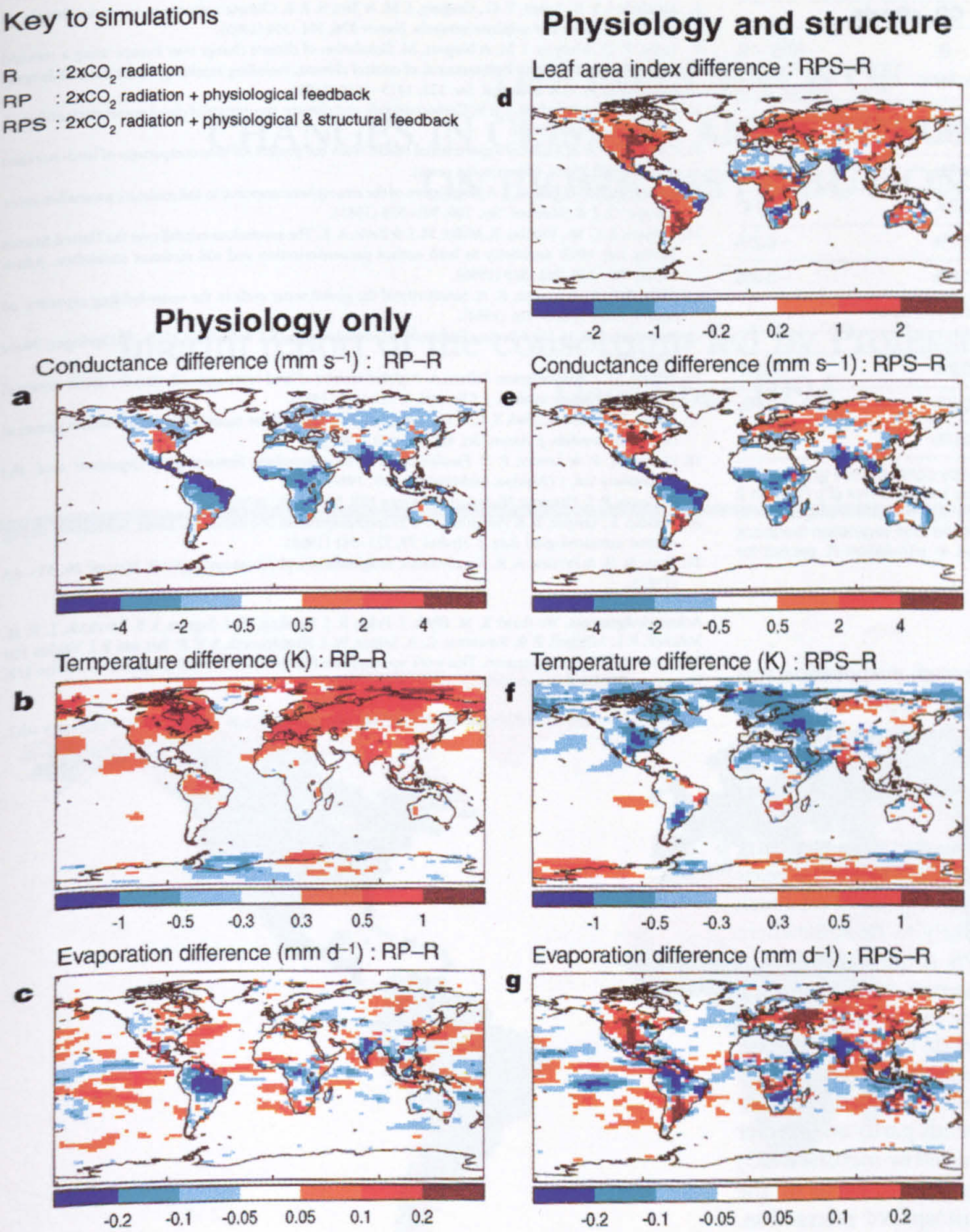

Figure 3 Physiological and structural vegetation change under doubled atmospheric CO_2 concentration ($2 \times CO_2$), and feedback of each on $2 \times CO_2$ climate. **a**, Change in canopy conductance due to physiological response to $2 \times CO_2$ and the associated climate change. **b**, Effect of physiological feedback on $2 \times CO_2$ temperature. **c**, Effect of physiological feedback on $2 \times CO_2$ evaporation. **d**, Change in leaf area index due to structural response to $2 \times CO_2$ and the associated climate change. **e**, Change in canopy conductance due to both physiological and structural response. **f**, Combined effect of both physiological and structural feedback on $2 \times CO_2$ temperature. **g**, Combined effect of both physiological and structural feedback on $2 \times CO_2$ evaporation. 40% of the land surface experienced vegetation feedbacks on temperature (RPS – R) of at least 5% of the magnitude of the changes due to radiative forcing alone (R – C). 13% of the land showed relative temperature feedbacks of 10% or more. The relative evaporation feedbacks were larger and more widespread, with 74% of the land surface having a relative feedback of 10% or more, and 30% showing a feedback of over 50%. Vegetation-induced evaporation changes were larger than the greenhouse-gas-only changes for 18% of the land surface. Calculation of *t*-statistics for grid-point annual means showed that most temperature changes of 0.5 K or more were significant at the 1% confidence level or better. The exceptions to this were in the polar and sub-polar regions, where significance was reduced by higher interannual variability. In Siberia, temperature changes of 0.5 K were significant at 5% or better, while in Antarctica and the Arctic Ocean, little of the temperature change was significant at better than 20%. Almost all land evaporation changes of 0.1 mm d^{-1} were significant at 1%.

simulation RP was a general reduction in g_c relative to simulation R (Fig. 3a), consistent with increased water-use efficiency under $2 \times CO_2$. Some areas with modified hydrological regimes experienced g_c increases caused by increased humidity, but the global mean change was a reduction of ~20% (Table 1). These caused significant feedbacks on climate (RP – R), with temperature increasing by up to 1 K over Northern Hemisphere land (Fig. 3b). The large conductance decreases in the tropical forests produced small temperature changes but appreciable reductions in evapotranspiration (Fig. 3c). The modelled effects of physiology on mean land temperature, evapotranspiration and conductance are all in close agreement with those from a previous study[2].

The structural response in simulation RPS was a widespread increase in LAI relative to simulation R (Fig. 3d), due to increased productivity and water-use efficiency under the new CO_2 concentration and climate. The greatest LAI increases were in regions of increased rainfall. These changes acted to offset the physiological reductions in conductance, and at high latitudes the result was an overall increase in g_c (Fig. 3e); this is contrary to the result obtained when allowing physiological change alone (Fig. 3a). Elsewhere, the reduced g_c seen in simulation RP also occurred in simulation RPS; the reductions were smaller than in RP, except in regions where significantly reduced rainfall (Fig. 2b) had caused conspicuous reductions in LAI (Fig. 3d). The combined effect of physiology and structure was a reduction of ~12% in g_c in the global mean (Table 1), which is considerably less than the reduction due to physiology alone.

The combined physiological and structural vegetation feedbacks had significant effects on the climate sensitivity (RPS – R; Fig. 3f,g). Structural changes acted via two competing effects; increased LAI tended to warm the land surface by lowering its albedo[4–6] and to cool the land surface by enhancing evaporation (and consequently cloud cover[12,13]) via increases in root depth[14], roughness length[15] and surface conductance. Similarly, decreased LAI tended to cool the surface via increased albedo, and warm the surface via reduced evaporation. The albedo effect dominated in regions where the vegetation was sparse, or where the underlying surface was much more reflective than the vegetation such as in snow-covered regions[4–6]; however, the evaporation effect dominated elsewhere. Temperature changes (Fig. 3f) were therefore negatively correlated with LAI changes (Fig. 3d), except in sparsely vegetated regions and also northern Siberia, where greater LAI caused a warming via

Table 1 Global mean vegetation feedbacks on 2 × CO_2 climate

Variable	R	RP − R	RPS − R
	Mean over land		
LAI	3.38	0.0%	7.2%
g_c	6.09 mms^{-1}	− 19.6%	− 12.1%
T_s	284.4 K	0.2 K	− 0.1 K
P	2.50 mm d^{-1}	− 0.7%	− 0.2%
E	1.54 mm d^{-1}	− 1.8%	− 0.3%
	Mean over land and ocean		
T_s	290.2 K	0.2 K	− 0.1 K
P	3.41 mm d^{-1}	0.0%	− 0.1%
E	3.41 mm d^{-1}	0.0%	− 0.1%

Mean values and perturbations to leaf area index (LAI), canopy conductance (g_c), screen-level temperature (T_s), total precipitation (P) and total surface moisture flux (E). Column 2 shows absolute values for simulation R (radiation only), column 3 shows the changes due to the physiological response only (RP − R), and column 4 gives the total vegetation feedback (RPS − R). Changes are given as percentages of the value in simulation R, except for temperature changes which are given in K.

increased masking of snow. The feedback through evaporation was significantly modified by structural changes, especially in the middle- and high-latitude regions (compare Fig. 3c and g). However, transpiration from the tropical rainforests, which experienced negligible changes in LAI, was still significantly reduced compared to simulation R.

It is important to recognize that changes in vegetation structure may lag the physiological response to increased CO_2 by several years or even decades. Therefore, the actual effect of vegetation feedback on climate at the time of CO_2 doubling is likely to lie somewhere between the results of simulations RP and RPS. A full assessment of this will require a model of vegetation dynamics fully integrated within a GCM. Nevertheless, our results show that changes in land surface properties due to vegetation can provide climatic feedback mechanisms that are both positive and negative in relation to climate change due to radiative forcing alone; furthermore, they demonstrate that the sign of the feedback depends partly on whether local vegetation growth is enhanced or suppressed by increased CO_2 concentration and the associated climate change, and partly on the nature of the locally dominant surface–atmosphere interaction. Both physiological and structural characteristics of the vegetation have been shown to be important, with changes in one property often counteracting changes in another. In the global mean, the competing effects of increased water use efficiency and increased LAI cause a small surface evaporation change relative to the climate change simulation with fixed vegetation properties. We conclude that a short-term enhancement of regional climate warming by vegetation physiology may eventually be mitigated by a longer term modification of surface characteristics due to vegetation morphology. As this work does not account for the timescales involved in the full suite of vegetation feedbacks, the next stage should be to include dynamical changes in both vegetation physiology and structure in GCM predictions of future climate change. □

Received 28 October 1996; accepted 28 April 1997.

1. Houghton, J. T. *et al.* (eds) *Climate Change 1995* (Cambridge Univ. Press, 1995).
2. Sellers, P. J. *et al.* Comparison of radiative and physiological effects of doubled atmospheric CO_2 on climate. *Science* **271**, 1402–1406 (1996).
3. Lean, J. & Rowntree, P. R. A GCM simulation of the impact of Amazonian deforestation on climate using an improved canopy representation. *Q. J. R. Meteorol. Soc.* **119**, 509–530 (1993).
4. Bonan, G. B., Pollard, D. & Thompson, S. L. Effects of boreal forest vegetation on global climate. *Nature* **359**, 716–718 (1992).
5. Foley, J. A., Kutzbach, J. E., Coe, M. T. & Levis, S. Feedbacks between climate and boreal forests during the Holocene epoch. *Nature* **371**, 52–54 (1994).
6. Gallimore, R. G. & Kutzbach, J. E. Role of orbitally induced changes in tundra area in the onset of glaciation. *Nature* **381**, 503–505 (1996).
7. Woodward, F., Smith, T. M. & Emanuel, W. R. A global land primary productivity and phytogeography model. *Glob. Biogeochem. Cycles* **9**, 471–490 (1995).
8. Mitchell, J. F. B., Johns, T. C., Gregory, J. M. & Tett, S. F. B. Climate response to increasing levels of greenhouse gases and sulphate aerosols. *Nature* **376**, 501–504 (1995).
9. Jones, R. G., Murphy, J. M. & Noguer, M. Simulation of climate change over Europe using a nested regional-climate model. I: Assessment of control climate, including sensitivity to location of lateral boundaries. *Q. J. R. Meteorol. Soc.* **121**, 1413–1449 (1995).
10. Senior, C. A. & Mitchell, J. F. B. Carbon dioxide and climate: the impact of cloud parameterization. *J. Clim.* **6**, 393–418 (1993).
11. Chen, T. H. *et al.* Cabauw experimental results from the project for intercomparison of land-surface schemes (PILPS). *J. Clim.* (in the press).
12. Rowntree, P. R. & Bolton, J. A. Simulation of the atmospheric response to soil moisture anomalies over Europe. *Q. J. R. Meteorol. Soc.* **109**, 501–526 (1983).
13. Beljaars, A. C. M., Viterbo, P., Miller, M. J. & Betts, A. K. The anomolous rainfall over the United States during July 1993: sensitivity to land surface parameterization and soil moisture anomalies. *Mon. Weath. Rev.* **124**, 362–383 (1996).
14. Milly, P. C. D. & Dunne, K. A. Sensitivity of the global water cycle to the water-holding capacity of land. *J. Clim.* **7**, 506–526 (1994).
15. Rowntree, P. R. in *Land Surface Evaporation* (eds Schmugge, T. J. & Andre, J. C.) 5–30 (Springer, New York, 1991).
16. Wilson, M. F. & Henderson-Sellers, A. A global archive of land cover and soils data for use in general circulation climate models. *J. Climatol.* **5**, 119–143 (1985).
17. Sellers, P. J., Mitz, Y., Sud, Y. C. & Dalcher, A. A simple biosphere model (SiB) for use within general circulation models. *J. Atmos. Sci.* **43**, 505–531 (1986).
18. Lowry, W. P. & Lowry, P. P. *Fundamentals of Biometeorology. Interactions of Organisms and the Atmosphere* Vol. 1 (Peavine, McMinnville, OR, 1989).
19. Eagleson, P. S. *Dynamic Hydrology* (McGraw Hill, New York, 1970).
20. Halldin, S., Saugier, B. & Pontailler, F. Y. Evapotranspiration of a deciduous forest. Simulation using routine meteorological data. *J. Hydrol.* **75**, 323–341 (1984).
21. Shaw, R. H. & Pereira, A. R. Aerodynamic roughness of a plant canopy. *Agricult. Meterol.* **26**, 51–65 (1982).

Acknowledgements. We thank E. M. Blyth, J. Foley, R. J. Harding, W. J. Ingram, J. E. Lovelock, J. F. B. Mitchell, P. L. Mitchell, P. R. Rowntree, C. A. Senior, W. J. Shuttleworth, S. F. B. Tett and P. J. Valdes for comments, advice and discussion. This work was supported by the NERC TIGER programme and the UK Department of the Environment.

Correspondence and requests for materials should be addressed to R.A.B. (e-mail: rabetts@meto.gov.uk).

CLIMATE AND VEGETATION CHANGE

THE INFLUENCE OF CHANGES IN CLIMATE AND CARBON DIOXIDE ON BIOME DISTRIBUTION

Interim report of the consortium led by Professor F.I. Woodward
December 1994

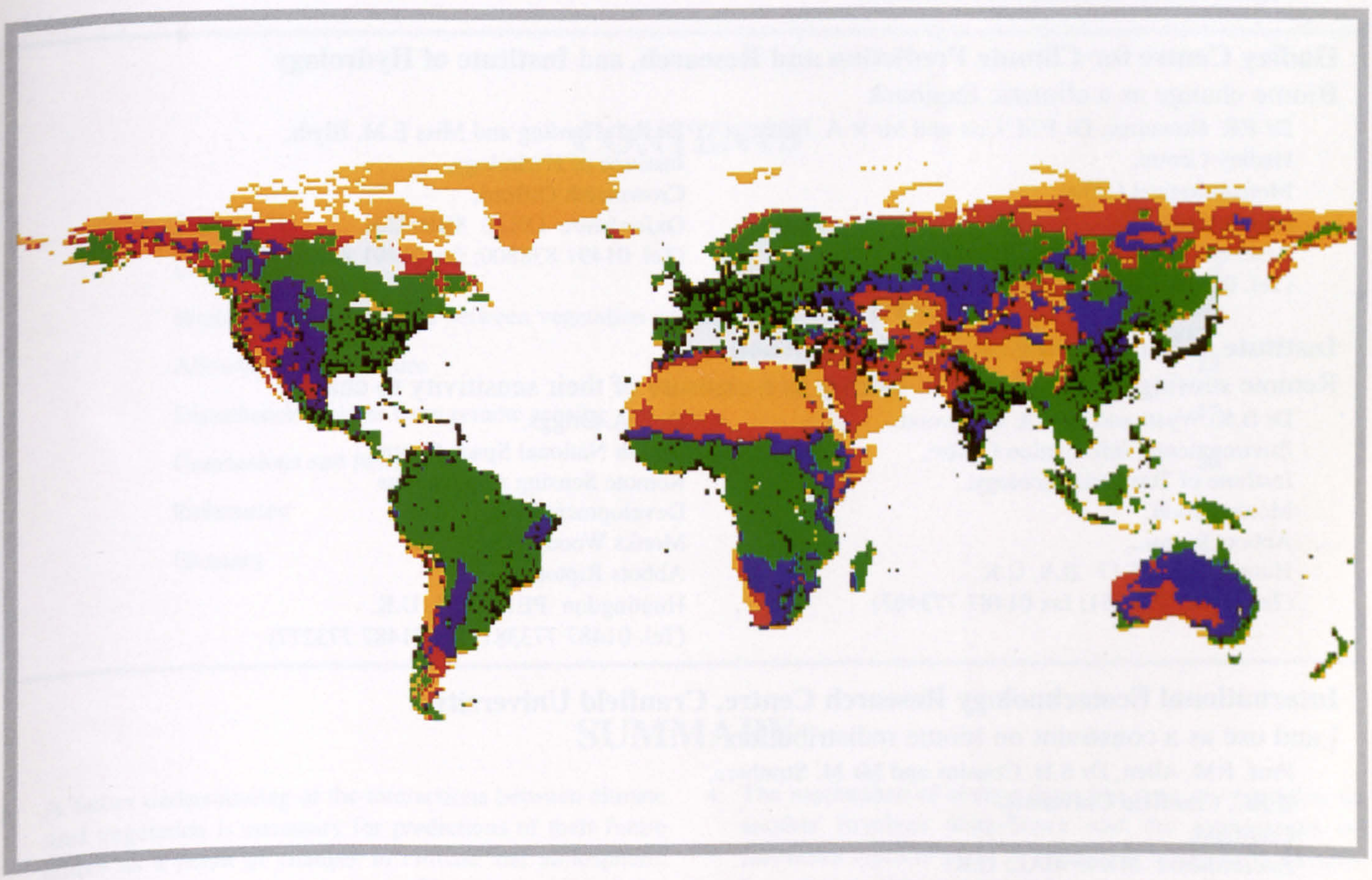

Project 3b of Tiger IV: a NERC community research programme
A core Research Project of IGBP Global Change and Terrestrial Ecosystems

CLIMATE AND VEGETATION CHANGE
THE INFLUENCE OF CHANGES IN CLIMATE AND CARBON DIOXIDE ON BIOME DISTRIBUTION

TIGER IV Project 3b Consortium leader: Professor F.I. Woodward
A Core Research Project (2303) of the Global Change in Terrestrial Ecosystems component of the International Geosphere–Biosphere Programme

Members of the Consortium

University of Sheffield

Modelling vegetation at biome and patch scales

Prof. F.I. Woodward, Dr P.L. Mitchell, Miss S.E. Lee and Dr J.E. Sheehy,
Department of Animal and Plant Sciences,
Sheffield S10 2UQ, U.K.
(Tel. 0114 282 4649; fax 0114 276 0159)

Hadley Centre for Climate Prediction and Research, and Institute of Hydrology

Biome change as a climatic feedback

Dr P.R. Rowntree, Dr P.M. Cox and Mr R.A. Betts,
Hadley Centre,
Meteorological Office,
London Road,
Bracknell RG12 2SY, U.K.
(Tel. 01344 420242; fax 01344 ~~854998~~ 854898)

Dr R.J. Harding and Miss E.M. Blyth,
Institute of Hydrology,
Crowmarsh Gifford,
Oxfordshire OX10 8BB, U.K.
(Tel. 01491 838800; fax 01491 ~~832256~~ 692424)

Institute of Terrestrial Ecology, Monks Wood

Remote sensing of disturbance in biomes as a measure of their sensitivity to change

Dr B.K. Wyatt and Dr J.A. Eastwood,
Environmental Information Centre,
Institute of Terrestrial Ecology,
Monks Wood,
Abbots Ripton,
Huntingdon PE17 2LS, U.K.
(Tel. 01487 773381; fax 01487 773467)

Dr S.A. Briggs,
British National Space Centre,
Remote Sensing Applications
Development Unit,
Monks Wood,
Abbots Ripton,
Huntingdon PE17 2LS, U.K.
(Tel. 01487 773381; fax 01487 773277)

International Ecotechnology Research Centre, Cranfield University

Land use as a constraint on biome redistribution

Prof. P.M. Allen, Dr S.H. Cousins and Mr M. Strathern,
IERC, Cranfield University,
Cranfield,
Bedfordshire MK43 0AL, U.K.
(Tel. 01234 754097; fax 01234 750163)

Terrestrial Initiative in Global Environmental Research

The TIGER programme of research into climate change and its consequences is funded by the Natural Environment Research Council

Programme Manager: Mr M.A. Beran,
Institute of Hydrology,
Crowmarsh Gifford,
Oxfordshire OX10 8BB, U.K.
(Tel. 01491 838800; fax 01491 ~~838097~~ 692430)

FOREWORD

by Dr Brian Walker, Chairman of GCTE

The research described in this document forms part of the U.K.'s Terrestrial Initiative in Global Environmental Research. It deals specifically with the problem of how changes in climate and carbon dioxide will affect the distribution of the major biomes, and as such it is of particular relevance to the international effort aimed at understanding the role the terrestrial biosphere plays in our global earth system. The impetus given by this TIGER initiative has already resulted in rapid and exciting advances. The past year has seen the first ever coupled run of a dynamic vegetation model and a general circulation model (GCM) with the results indicating that there are marked regional impacts of vegetation on climate but little global effect.

There have been significant developments in the efforts to include the effects of human land use at the global scale, which means that the vegetation cover used in GCMs is getting closer to the actual cover (and therefore the actual land surface processes) rather than the potential cover as used at present. The development of a generic, global scale patch model is leading to the realization of predicting dynamic changes in vegetation structure.

These developments highlight why this project is of particular importance to the objectives of the Global Change and Terrestrial Ecosystem Core Project of the International Geosphere–Biosphere Programme. I am pleased to have the opportunity to express my strong support for the work and commend the U.K. Natural Environment Research Council for taking this initiative.

CONTENTS

SUMMARY

1. A better understanding of the interactions between climate and vegetation is necessary for predictions of their future states as a result of changes in climate and atmospheric carbon dioxide concentration. This is achieved by constructing mechanistic models of climate and of vegetation that are validated by their ability to predict correctly the current patterns over the globe.

2. A coupled run of vegetation and climate models shows that there is a significant feed back of vegetation to climate at the regional scale for temperature and soil moisture. The effect averaged over the whole globe is small.

3. Since a large fraction of the terrestrial surface has been converted from natural vegetation to agriculture, a further model predicts the location, area and yield of crops from the distribution of human population, and how these will alter as climate and population change.

4. The mechanism of change from one type of vegetation to another involves disturbance and the interactions of functional types of plant as vegetation regenerates. Images from remote sensing satellites are being used to detect and quantify rates of disturbance, starting in forests. These figures for gap dynamics will feed into a patch model of vegetation change that is being developed.

5. This co-ordinated modelling work, originating in and funded by the TIGER programme, and approved by GCTE, has the ultimate aim of producing an integrated dynamic global vegetation model coupled with a general circulation model to provide better predictions of future changes.

6. A glossary is provided at the back of this report since multi-disciplinary research such as this has to use specialized terms from each field of research.

INTRODUCTION

The interdependence of vegetation and climate

Mankind depends on vegetation for food, fuel, building materials, drugs and less tangible benefits such as recreation and as a source of genetic diversity. There is, naturally, interest in how the vegetation of the earth will change if the climate changes, as seems likely if the concentration of carbon dioxide in the atmosphere continues to increase (Houghton *et al.* 1990). This interest extends not only to managed land—agriculture and intensive forestry—but also to natural vegetation. Just as general circulation models (GCMs) enable us to predict how the climate may change as the concentration of carbon dioxide increases so there is a need for models to predict the response of vegetation to climate. There is an increasing realization that vegetation affects climate at the global scale because the presence and types of vegetation determine certain properties of the earth's surface, such as albedo and surface roughness, that are important in GCMs (Baskin 1993). Any increased fixation of carbon dioxide in photosynthesis will affect the concentration in the atmosphere, and changes in transpiration greatly affect the amounts and circulation of water in the atmosphere. At present, GCMs take a simplified view of current vegetation and assume that it does not change. However, as climate changes so also will the functioning and distribution of vegetation. Feedbacks between climate and vegetation can be achieved by coupling a vegetation model to a GCM and running them together. Comparing a GCM run with static vegetation and a run with changing vegetation will demonstrate how large is the effect of vegetation on climate.

The simplest model of vegetation in relation to climate predicts the equilibrium condition. Put simply this means: new climate, new matching vegetation, instantly. But many types of vegetation change slowly because the component plants are long-lived and rather tolerant of incremental change. The lags can be hundreds of years for forests. To model the mechanism of change at the appropriate time-scale a dynamic vegetation model is required.

The opportunity for change occurs when existing vegetation is disturbed, leading to the creation of gaps in which new plants can grow. This disturbance may be at the scale of single plants, such as when individuals die (endogenous community dynamics) or at much larger scales following incidents such as fire or windthrow (Pickett & White 1985). The spatial and temporal scales of disturbance critically determine the rate at which vegetation can change. Remote sensing of the earth's surface, especially by satellites, offers a means of detecting and measuring the scales of disturbance at work in different kinds of vegetation (see, for example, Nelson *et al.* 1994). This allows the gap dynamics to be predicted and used in a patch model where individual types of plants grow and interact. The outcome may be regeneration of the same set of plant types so that the vegetation is the same as before, or a different set producing a different kind of vegetation. Only a mechanistic patch model such as this can allow the possible appearance of novel forms of vegetation. This is important because we know from the pollen record that vegetation types unlike any existing nowadays occurred in the recent past, composed of the species we recognize today but in different combinations (Webb 1987).

The present state of the earth's surface includes a large fraction dominated by agriculture. Here the mechanisms operating between climate and natural vegetation have been disrupted by man. A different model is needed to understand and predict the occurrence and type of agriculture at any point on the earth, based on the location of populations and their economic status. In general, populations obtain food locally but their economic status determines their technical expertise, reflected in intensification of farming, and their ability to import food from elsewhere. This model of agriculture operates within constraints of climate and soil that limit the range of crops that can be grown at one place.

Modelling vegetation and climate

The earth's climate and vegetation as a whole are not amenable to experimentation so that modelling is the only method of study. It integrates observations on components of the system, increases our understanding and allows us to make predictions. How can we believe models? First, models can be validated by demonstrating that they can predict the present climate and vegetation. The GCM run with current vegetation must reproduce the current climate. The vegetation model must reproduce the vegetation observed today when run with today's climate. Secondly, the models must be mechanistic, that is, based on our understanding of how climate and vegetation operate. The GCM mechanistically simulates the transfer of energy and water between three-dimensional cells representing layers of the atmosphere above an area of the earth's surface. Vegetation models can be mechanistic if they simulate the responses of vegetation to climate and soils in a way that reflects an understanding of plant physiology (Woodward 1987). The alternative to a mechanistic model is a correlative one, in which observations of existing climate and vegetation are used to correlate putative cause and response.

But correlations do not promote understanding and do not allow extrapolation beyond the range of conditions from which the data were gathered. Much of the effort in the work reported here has necessarily gone into making the models mechanistic and validating them by predicting correctly the observed present state.

It is important to understand the scale of work and prediction. In space, the GCM has cells on the earth's surface measuring several hundreds of kilometres on each side. In terms of vegetation, the models operate at the scale of biomes, the units of vegetation in a classification based on physiognomy which can include the structure, height and seasonality of vegetation (Grabherr & Kojima 1993). In the patch models it is not individual species that compete but functional types (FTs). These are kinds of plants that have similar growth forms, life histories, and physiological responses to environmental factors (Smith *et al.* 1993). Prentice *et al.* (1992) used biomes and functional types in a similar sort of model. The work of the consortium is not designed to predict the effects of climate change on a particular species such as the northern limit at which maize can be grown in the U.K. Rather, it aims to achieve a broader view of the earth's vegetation, including agriculture, at a spatial scale of thousands of square kilometres, and changes in decades to centuries rather than year by year.

The members of the consortium bring specialized knowledge and software to this multi-disciplinary project. The modelling of vegetation continues work begun in the 1980s at Cambridge (Woodward 1987). The GCM is that developed by the Hadley Centre for Climate Prediction and Research (part of the Meteorological Office) and the role of vegetation in the GCM extends work being undertaken by the Institute of Hydrology. The expertise in remote sensing at the Institute of Terrestrial Ecology at Monks Wood is used for estimation of disturbance regimes, and for refinement of databases of current vegetation which are used to validate the models. Modelling agriculture in relation to population is carried out by the International Ecotechnology Research Centre of Cranfield University. Details of individual projects and personnel are given on p.2.

Objectives of the consortium

1. To couple vegetation models with a GCM so that vegetation and climate interact fully.
2. To model the effect of man's agricultural activity, driven by population density and demands, to overlay actual vegetation on the potential, natural vegetation.
3. To construct patch-scale models of the interaction of different functional types of plant so that different biomes can emerge mechanistically with changes in climate and after whatever disturbance occurs that initiates regeneration.

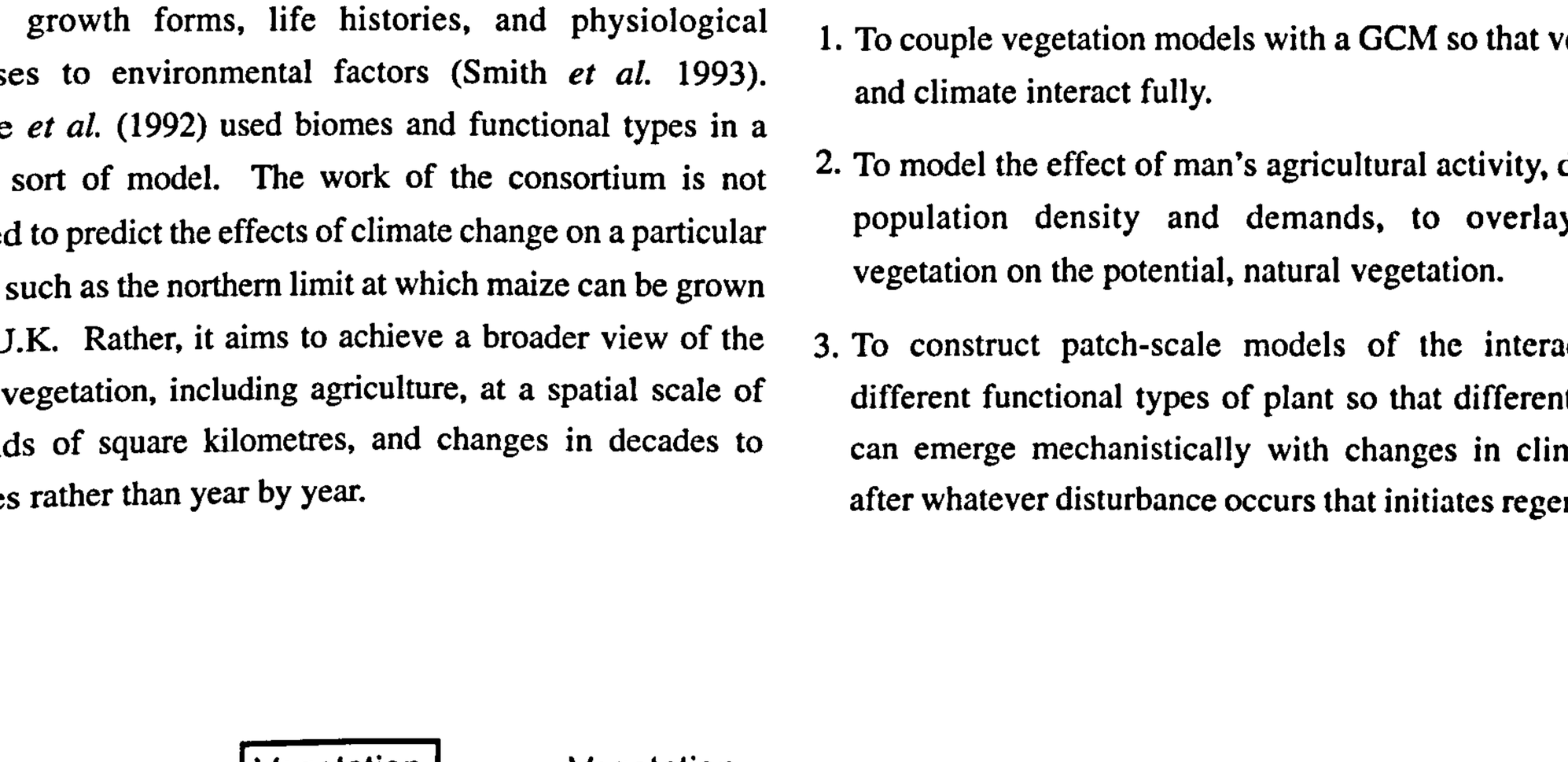

Figure 1. Outline of the modelling process to couple climate and vegetation models, and to model the emergence of biomes from functional types. The values of the vegetation parameters are estimated direct from the vegetation properties predicted by the vegetation models. An alternative route through functional types (pecked line) can also be used when FTs are inferred from the vegetation properties. The values of the vegetation parameters associated with each FT are then taken from a table prepared before the computer run.

6 Outline of the project

Figure 1 illustrates how the coupling of climate and vegetation models is achieved. Brief explanations are given here of each element in the process and further details can be found in later sections of this report.

1. Climate.

The outputs of the GCM and the driving climatic variables of the vegetation models include air temperature, rainfall, wind speed, humidity and solar radiation. The GCM operates with time steps of 30–60 minutes and accumulates and averages the values month by month. The vegetation models can operate at similar time steps or may use monthly averages.

2. Soil properties.

For the GCM the physical characteristics of the soil are summarized by seven parameters. The concentrations of soil carbon and nitrogen in the rootable depth are required for the vegetation model.

3. Vegetation models.

The vegetation models World and DOLY (Dynamic Global Phytogeography Model) are driven by variables for climate and soil and require certain site parameters such as latitude. The balance between rainfall and evapotranspiration determines the maximum leaf area index (LAI) that can be supported. The LAI, the amount of solar radiation, and nutrient uptake from the soil together control the fixing of carbon dioxide in photosynthesis which provides predictions of net primary production (NPP) after losses by respiration are accounted for. The height of the vegetation is related to LAI.

4. Vegetation properties.

The properties of vegetation predicted by the vegetation models include LAI, height, canopy conductance for water, and net primary production. These are available month by month and as a total or average for the year.

5. Functional types.

The three basic FTs used here are tree, shrub, and perennial non-woody (effectively grasses). The FTs present at any point are inferred from the vegetation properties and limiting values of climate, especially the absolute minimum temperature.

6. Vegetation parameters.

These properties of vegetation required for the GCM are the following:

surface resistance to evaporation;
snow-free albedo;
cold deep-snow albedo;
surface roughness;
rooting depth;
canopy water capacity; and
infiltration enhancement factor.
The value of each of these is estimated from the appropriate vegetation properties.

7. General circulation model.

The Hadley Centre GCM is a mechanistic model of the working of the earth's atmosphere, divided into 19 layers and either 6912 cells of $2^1/2°$ latitude by $3^3/4°$ longitude (high resolution) or 1728 cells of 5° latitude by $7^1/2°$ longitude (low resolution). The properties of the surface in each cell needed for the model are the proportion covered by vegetation, the seven vegetation parameters and the seven soil parameters.

8. Patch model with gap dynamics.

For the coupling of climate and vegetation it is sufficient to go direct from predicted vegetation properties to vegetation parameters, or to infer the FTs and then look up the appropriate value for the parameters in a table. However, the biomes themselves are of interest and these must emerge from a mechanistic model and an overview of the interactions between FTs. The opportunity for interaction comes when a disturbance disrupts the vegetation and allows regeneration to occur. The major natural disturbances are fire, windthrow and severe drought. If the outcome of the interaction of the FTs available is the same as previously then no change in biome takes place; if the outcome is different because of the changed climate then a different biome emerges.

9. Biomes.

At the global scale, it is the effect of climate change on biomes that is relevant because biomes are sources of biodiversity and potential sources of food, fuel, building materials and drugs. Initially the land cover classes of Wilson & Henderson-Sellers (1985) are treated as biomes. Each contains several land types or vegetation components, equivalent to FTs. Over much of the earth's surface natural vegetation has been replaced by that where man controls the FTs present and the regime of disturbance. This is modelled through the demand of the world's population for agricultural products.

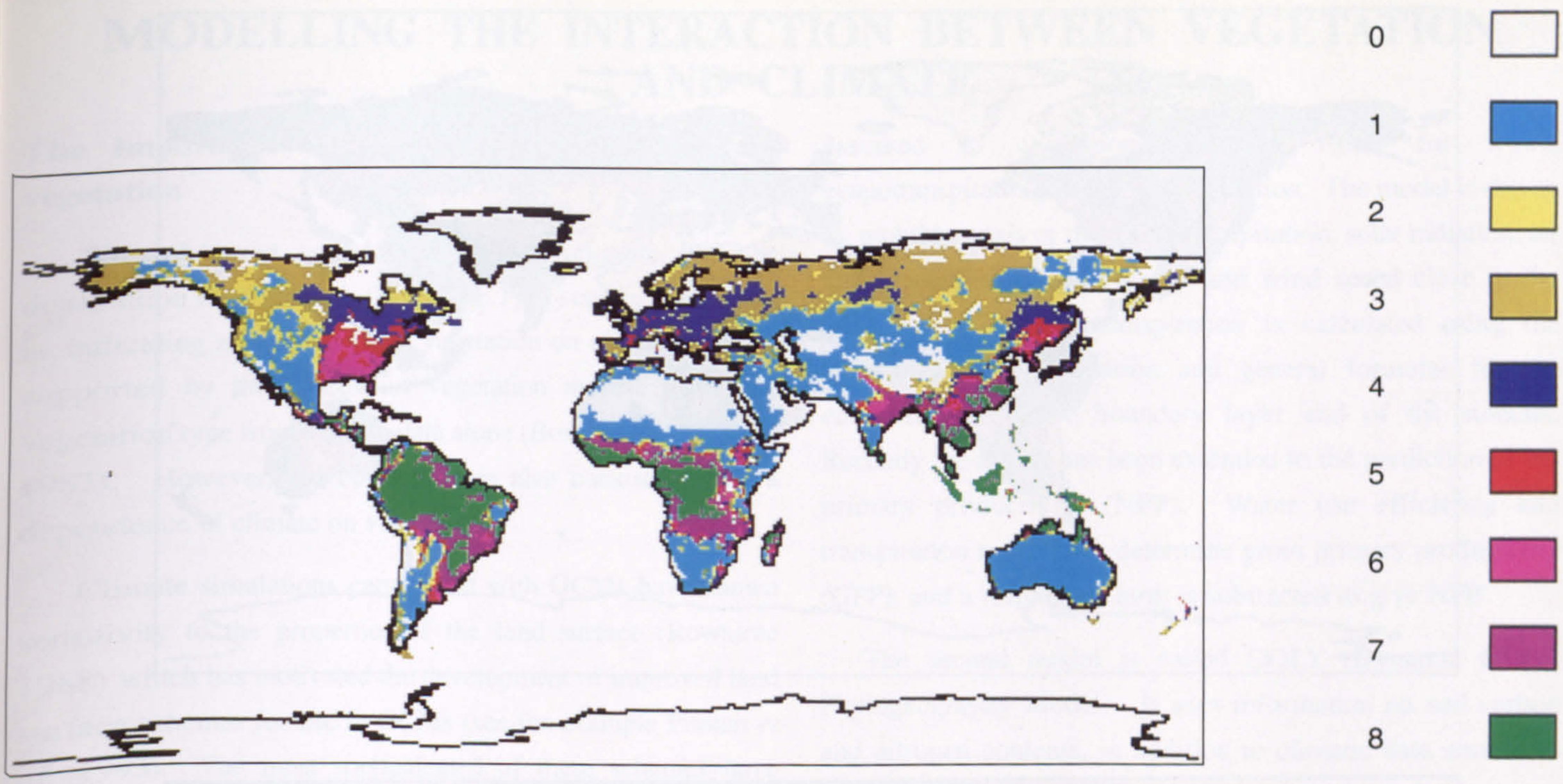

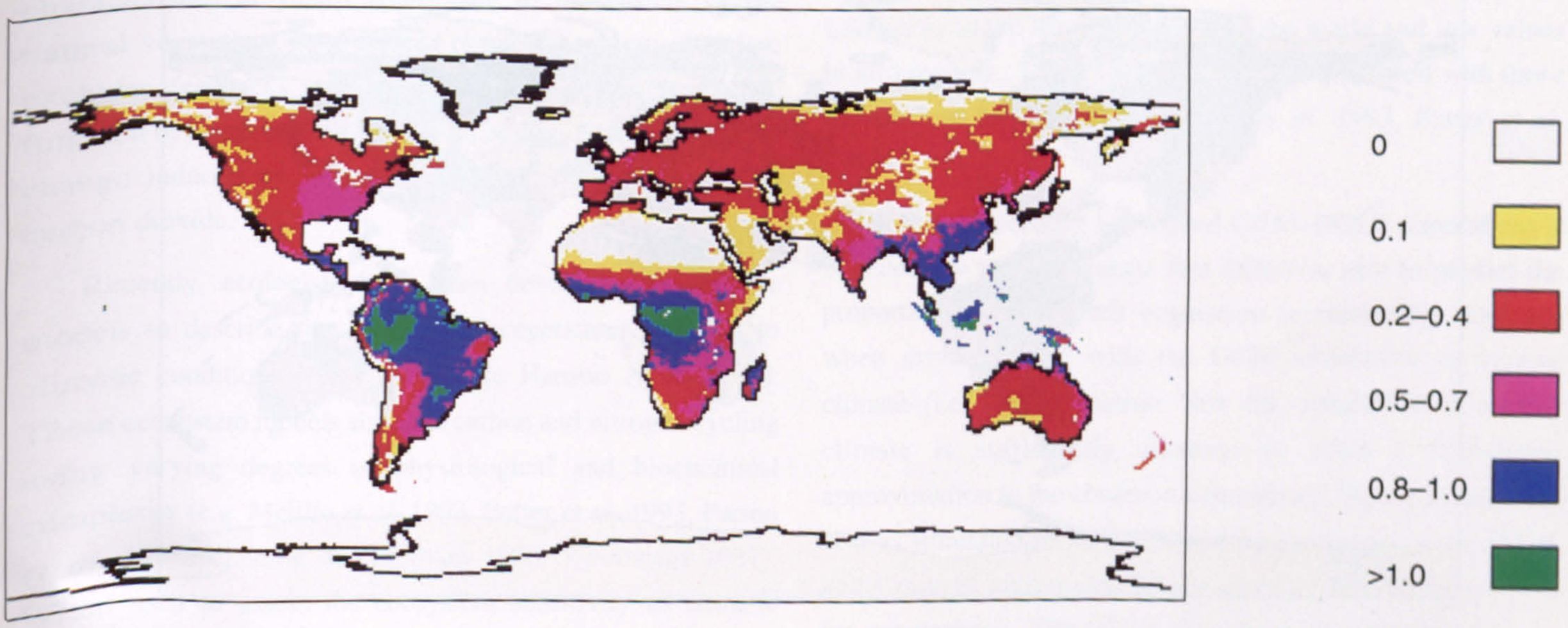

Figure 2. Vegetation properties predicted by the model DOLY run under the current observed climate. Records from meteorological stations were interpolated and smoothed to create a database of climatic variables for the world on a $^1/_2°$ by $^1/_2°$ grid (Leemans & Cramer 1991).

Upper map: leaf area index. High LAI occurs in regions with sufficient rainfall, for at least a large part of the year, to support evapotranspiration. Evapotranspiration is driven primarily by the vapour pressure deficit of the atmosphere and by the energy in solar radiation received by the vegetation canopy that must be dissipated by the evaporation of water. Where potential evapotranspiration exceeds rainfall only sparse vegetation, LAI 1–2, or none at all can exist.

Lower map: net primary production, in kilograms of carbon per square metre per year. The amount of primary production depends first of all on the leafiness of the canopy, measured as LAI, receiving solar radiation for photosynthesis. The carbon dioxide lost in respiration of the leaf canopy and of other parts of the plants is subtracted to leave the NPP. The NPP is highest where high LAI coincides with climates suitable for growth all year. Temperate climates with winter or drought seasons restrict NPP relative to what might be possible with the LAI predicted.

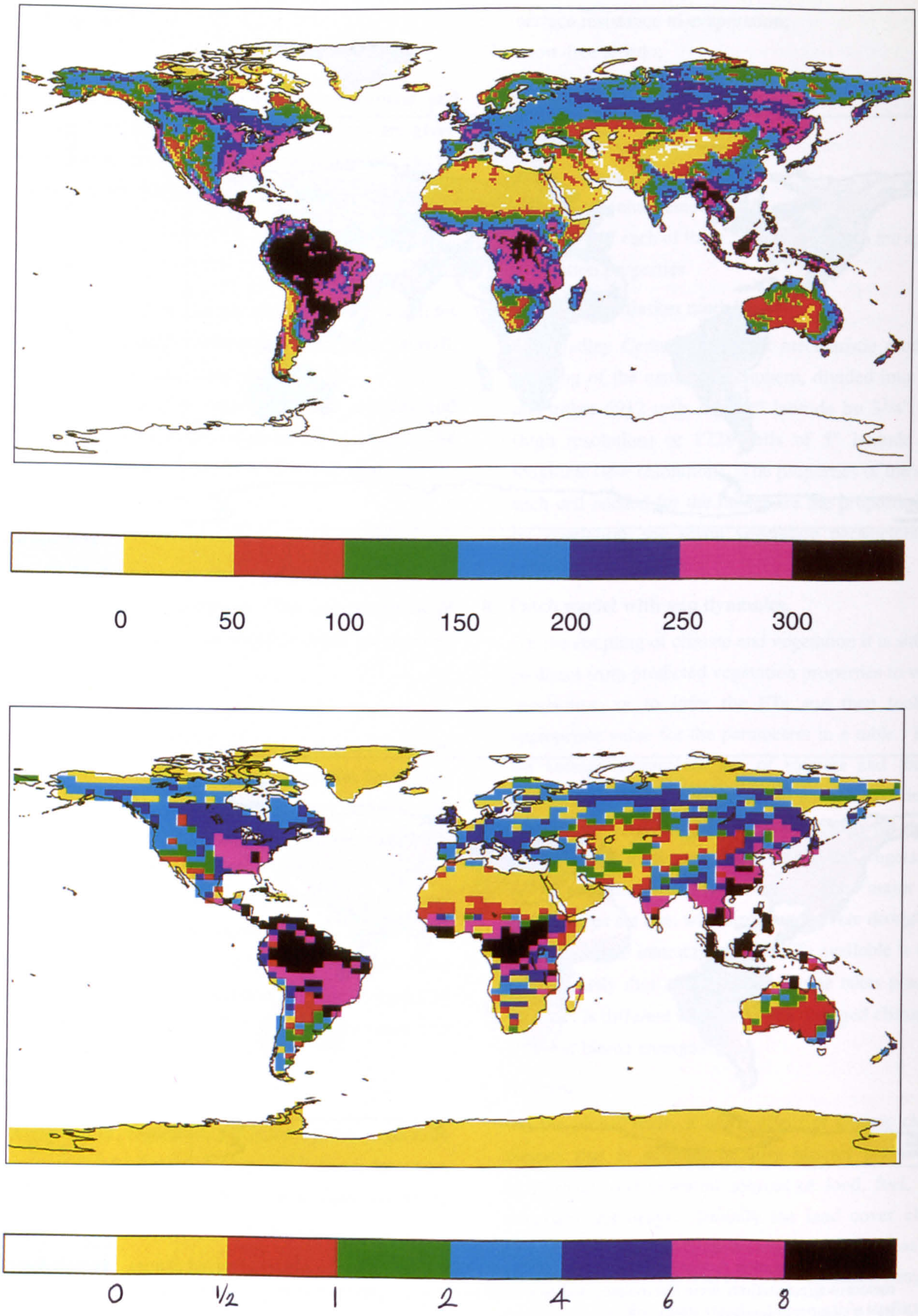

Figure 3. Comparison of the LAI predicted by the model DOLY with the observed normalized difference vegetation index (NDVI). Note that the colour scale for NDVI is linear but that for LAI is almost logarithmic.

Upper map: normalized difference vegetation index. The NDVI values are means over the period July 1983 to June 1984 derived from radiances measured by the AVHRR sensor on the NOAA–7 satellite. The data are plotted on a grid of 1° by 1° (Tarpley *et al.* 1984).

Lower map: leaf area index. These values are predictions from DOLY when driven by climatic means derived from a GCM simulation of the current climate.

MODELLING THE INTERACTION BETWEEN VEGETATION AND CLIMATE

The importance of feedbacks between climate and vegetation

The observed correlation between climate and the distribution of vegetation (Holdridge 1947) can be interpreted as indicating a dependence of vegetation on climate. This is supported by the success of vegetation models to predict vegetation type from climate data alone (Box 1981, Woodward 1987). However, the correlation is also consistent with a dependence of climate on vegetation.

Climate simulations carried out with GCMs have shown sensitivity to the properties of the land surface (Rowntree 1988) which has motivated the development of improved land surface schemes for use in GCMs (see for example Pitman *et al.* 1993). The most sophisticated of these schemes have detailed treatments of the surface fluxes of heat, moisture and momentum, and model the dependence of these fluxes on both vegetation and soil (e.g. Sellers *et al.* 1986, Warrilow & Buckley 1988, Verseghy 1991). The soil and vegetation type are required inputs. The application of such schemes to GCM climate simulation involves fixing the land surface characteristics at values appropriate to the current or the natural vegetation. Any derived climate sensitivity therefore excludes feedbacks associated with changes in vegetation function or distribution, which could be significant for climatic change induced by increased concentration of atmospheric carbon dioxide.

Recently, ecologists have been developing large-scale models to describe the response of vegetation and soils to climatic conditions (see for example Hanson *et al.* 1985). These ecosystem models simulate carbon and nitrogen cycling using varying degrees of physiological and biochemical complexity (e.g. Melillo *et al.* 1993, Potter *et al.* 1993, Parton *et al.* 1988, Running & Coughlan 1988, Woodward 1987). When used to assess the ecosystem sensitivity to climatic change, they are invariably used in an offline mode, with the climatic change prescribed (normally from GCM output) and independent of any subsequent ecosystem changes. Once again vegetation–climate feedbacks are neglected.

Vegetation models and their validation

The first model used in this project, called World, is an updated version of a model described in detail by Woodward (1987) and Woodward (1993). It relies on a water balance approach to predict leaf area index (LAI). The local LAI is assumed to correspond to the value for which evapotranspiration matches precipitation. The model is driven by monthly totals or means of precipitation, solar radiation, air temperature, relative humidity and wind speed close to the land surface. Evapotranspiration is calculated using the Penman–Monteith equation and general formulae for the conductances of the boundary layer and of the stomata. Recently the model has been extended to the prediction of net primary productivity (NPP). Water use efficiency and transpiration are used to determine gross primary productivity (GPP), and a respiration term is subtracted to give NPP.

The second model is called DOLY (Dynamic Global Phytogeography Model). It uses information on soil carbon and nitrogen contents, in addition to climatic data similar to those used by World. Photosynthesis and nitrogen uptake are calculated explicitly. Like World the primary outputs are LAI, which is determined by long-term hydrological and carbon budgets, and NPP, which is calculated as net photosynthesis minus respiration. Figure 2 shows maps of LAI and NPP as produced by DOLY when driven by observed climate (Leemans & Cramer 1991). The areas of high NPP and high LAI occur in the tropical regions of the world and low values in arid regions. These values of NPP compare well with those recorded in the literature (Melillo *et al.* 1993, Potter *et al.* 1993).

Before proceeding to coupled GCM–DOLY simulations it is necessary to demonstrate that DOLY is able to predict the properties of the current vegetation to reasonable accuracy when driven offline with the GCM simulation of current climate (i.e. to demonstrate that the simulation of current climate is sufficiently accurate to yield a reasonable approximation to the observed vegetation). Figure 3 shows the LAI as simulated by DOLY driven by the output of the GCM, and a map of normalized difference vegetation index (NDVI) for comparison. The NDVI is derived from observations by satellite of radiation reflected by the surface of the earth in the red and infra-red wavebands and is a general measure of leafiness. Qualitative agreement is good except in areas which do not have natural vegetation (e.g. agricultural areas) or which have strong seasonality in rainfall (e.g. India). The problem of including the influence of man is to be met by imposing a mask of agricultural land over the predicted natural vegetation, currently under development at Cranfield University (see below). The effects of rainfall seasonality may be more effectively incorporated by driving DOLY with GCM predictions of the difference between rainfall and runoff, i.e.

10 with the water that stays in the soil initially and is available to vegetation, rather than rainfall alone. In addition, the database of soil properties is imperfect and this inevitably feeds through to the predictions from DOLY. However, aside from these inadequacies, the overall comparison is encouraging.

Figure 4 shows the predicted changes in vegetation structure and function resulting from a doubling of the atmospheric carbon dioxide concentration. The model DOLY was run using climatic means from the low resolution version of the Hadley Centre GCM which has cells of 5° latitude by $7^1/2°$ longitude. The changes represent the difference in the vegetation states predicted by DOLY for the present (323 ppm) and doubled (646 ppm) carbon dioxide concentration climates of the GCM. Although doubling atmospheric carbon dioxide concentration is predicted to increase the global mean values of LAI and NPP, the spatial pattern of changes is complex with some regions suffering decreases in vegetation cover and productivity, because the climate becomes less favourable. The reduction of canopy conductance in the doubled carbon dioxide world is more consistent but the map of changes still shows significant spatial variability.

Procedure for demonstrating feedback

A major aim of this project is to model the effect of these climate–vegetation feedbacks on climate sensitivity and the response of ecosystems to climatic change. Ultimately this will require the inclusion of a fully dynamic vegetation model within an atmosphere–ocean GCM but as a preliminary step we have concentrated on quantifying the feedback associated with the response of vegetation to the equilibrium climate for doubled carbon dioxide concentration. The methodology involves an iterative coupling between the vegetation models developed at the University of Sheffield and the GCM of the Hadley Centre.

(i) The GCM is used to simulate the climate with doubled carbon dioxide concentration, given the current vegetation (state A).
(ii) The vegetation model predicts the vegetation properties of the land surface under this new climate.
(iii) New GCM land surface parameters are derived from the outputs of the vegetation model.
(iv) The GCM is used to simulate the climate with doubled carbon dioxide concentration, given the new vegetation.
(v) Steps (ii) to (iv) are repeated until consistent climate and vegetation equilibria are reached (state B).

The feedback associated with vegetation change is described by the difference between states B and A.

Coupling DOLY to the GCM

The coupling procedure entails the derivation of the GCM land surface parameters from the outputs of DOLY (step (iii) above). The land surface within the Hadley Centre GCM is described by the fraction of vegetation cover, seven vegetation parameters (which include albedo, roughness length and stomatal resistance) and seven soil parameters. Stomatal resistance of the canopy can be taken direct from DOLY which models it explicitly. An initial attempt has been made to derive the remaining parameters directly from the predicted values of LAI and NPP, although later versions of the coupling may involve an intermediate inference of plant functional types.

Climate from vegetation—closing the loop

Figure 5 displays the climatic feedback associated with vegetation change for the doubled carbon dioxide climate (646 ppm). These simulations were carried out using the low resolution version of the Hadley Centre GCM which has cells of 5° latitude by $7^1/2°$ longitude. The difference maps are annual means derived from a single sweep through steps (i) to (iv) above. Although changes in the global mean surface temperature are minimal, the vegetation feedback leads to significant regional changes. Similarly there are some large local changes in soil moisture availability, which result directly from the changes in land surface parameters (e.g. changes in rooting depth) and also from subsequent changes in the atmospheric circulation. Although these results are preliminary, they do give some indication of the importance of vegetation change and demonstrate the feasibility of this coupling procedure.

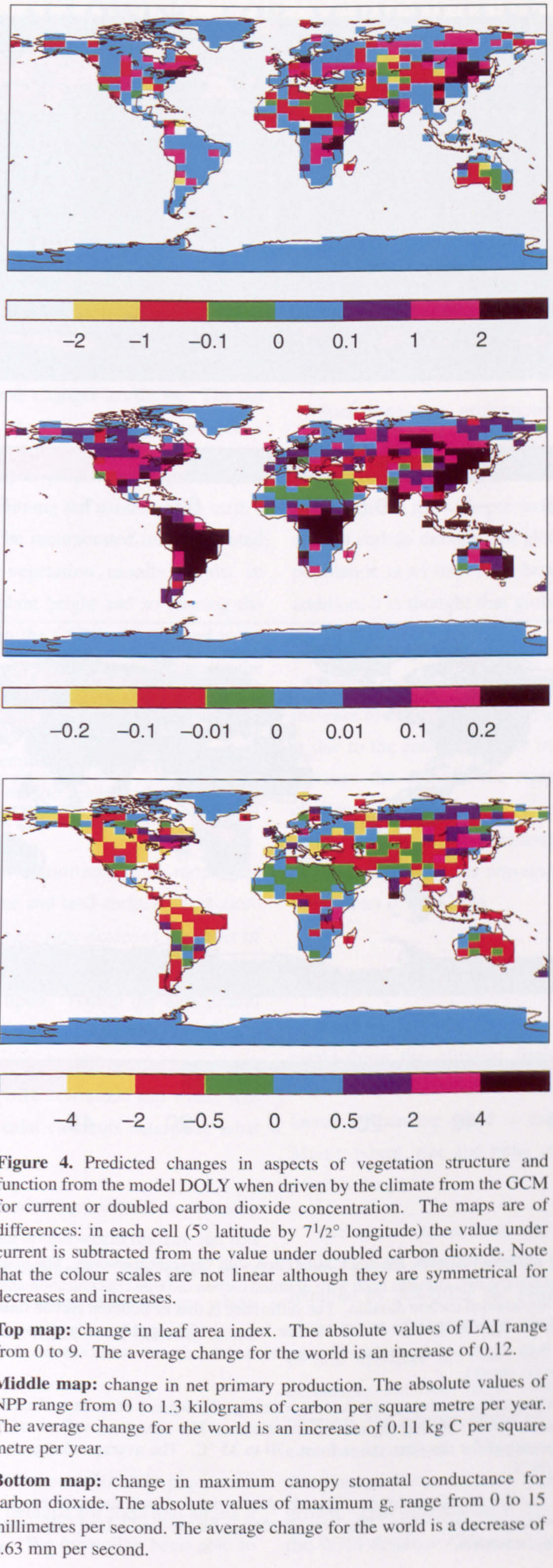

Figure 4. Predicted changes in aspects of vegetation structure and function from the model DOLY when driven by the climate from the GCM for current or doubled carbon dioxide concentration. The maps are of differences: in each cell (5° latitude by $7\frac{1}{2}$° longitude) the value under current is subtracted from the value under doubled carbon dioxide. Note that the colour scales are not linear although they are symmetrical for decreases and increases.

Top map: change in leaf area index. The absolute values of LAI range from 0 to 9. The average change for the world is an increase of 0.12.

Middle map: change in net primary production. The absolute values of NPP range from 0 to 1.3 kilograms of carbon per square metre per year. The average change for the world is an increase of 0.11 kg C per square metre per year.

Bottom map: change in maximum canopy stomatal conductance for carbon dioxide. The absolute values of maximum g_c range from 0 to 15 millimetres per second. The average change for the world is a decrease of 0.63 mm per second.

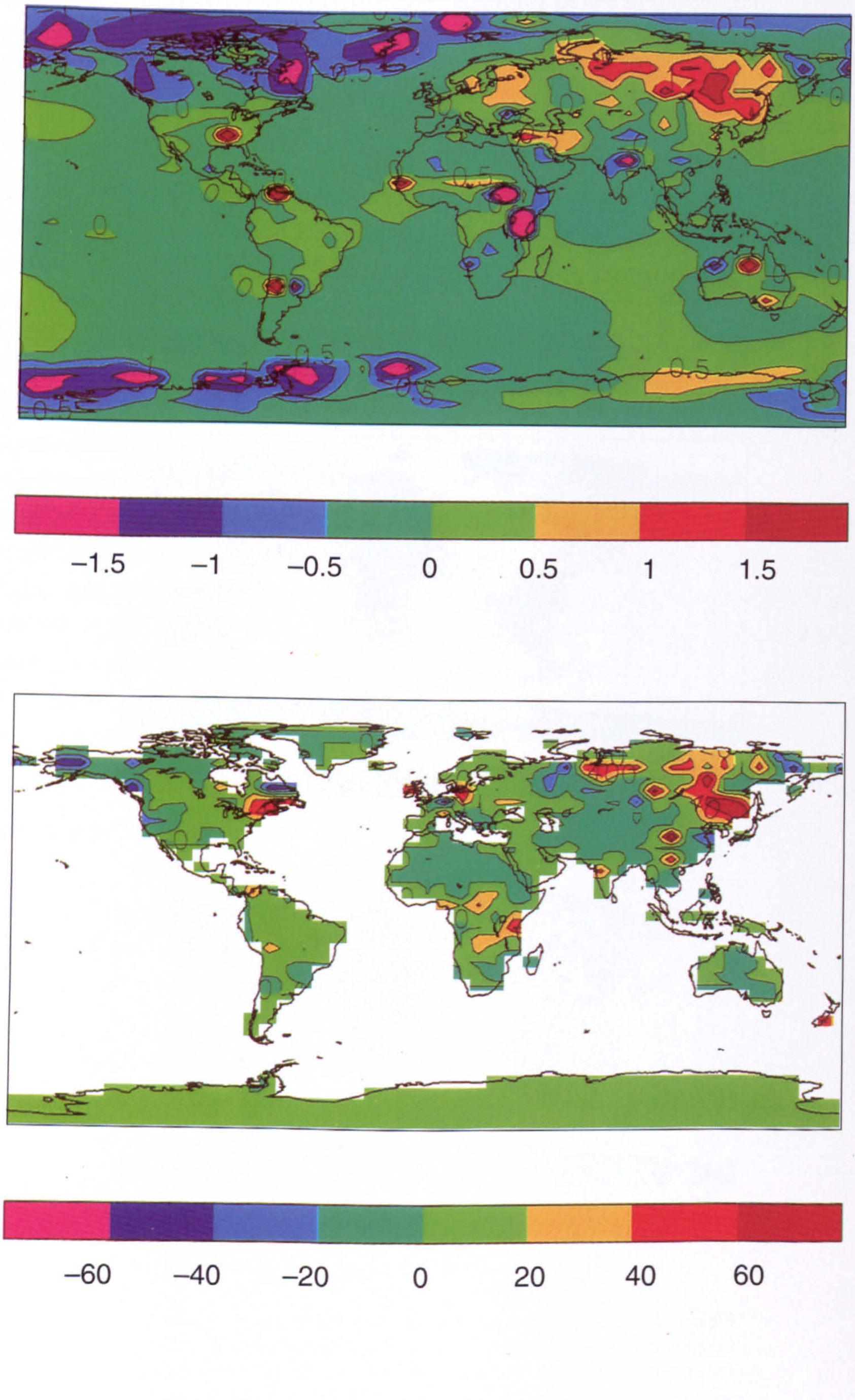

Figure 5. The modelled climatic feedback associated with vegetation change. The maps represent the difference between the two climates each with doubled carbon dioxide concentration and the vegetation for current or for doubled carbon dioxide. The difference is that of doubled carbon dioxide vegetation minus the current vegetation, thus the difference between the equilibrium vegetation coupled with climate (state B in step (v) of the explanation above), and the climate with constant, current vegetation (state A in step (i) above).

Upper map: change in air temperature (kelvin = centigrade degree) near the surface of the earth, i.e. comparable with usual meteorological observations. The absolute values of global surface temperature, averaged for the year, range from –70 to 35 °C. The average change for the world is a decrease of 0.09 °C.

Lower map: change in soil moisture. The absolute values of soil moisture range from 0 to 330 kilograms of water per square metre. The average change for the world, land only, is an increase of 4.2 kg water per square metre.

Crops as vegetation

Much of the earth that is suitable for agriculture has already seen the replacement of natural vegetation by agriculture. The distribution of natural vegetation will increasingly be influenced by the demands for food from a global population both increasing and becoming more wealthy. Where climate change allows for greater productivity there is a potential for agriculture to extend into naturally vegetated lands which were previously considered marginal. Conversely, semi-natural vegetation will establish itself where agricultural lands go out of production because of adverse changes in climate. The net result is likely to reduce areas of existing natural vegetation.

Clearly, agriculture is going to play an even greater part than it currently does in determining the nature of the earth's surface and this will have to be incorporated into integrated GCMs. Removing natural vegetation usually results in reducing the annual average plant height and so altering the surface roughness parameter in the GCM. Crops tend to be annuals with periods of bare soil which show as changes in the albedo of the region; the amount of water evaporated from the crop will also differ from the natural vegetation. All of these factors need to be taken into account in setting parameters for the earth's surface dependent on the realistic distribution of vegetation.

The approach taken by the consortium is to model the *processes* involved in the climate and land-surface interaction. This is particularly important where time-scales of the order of decades and centuries are involved for which correlative relationships cannot be relied upon. Within the agricultural sector we have sought to capture the major features of demand and supply of food: how many people will require how much food and where, i.e. where will it be consumed and where will it be supplied from? These spatial elements determine what vegetation occurs where.

Even for the most widely traded agricultural commodity today, cereals, only 23% is traded on the world market, the rest remaining in local or regional markets. This gives us a substantial reason for relating agriculture to the regions where people live; more specifically we relate food demand to the location of cities.

Human population

Using a database of world cities over 200,000 population we have been able to locate the demand for food and adjust it for income level of the country. We have also been able to apportion the food demand of the non-urban population for each country to the markets of the cities. The result of this allocation of demand is shown in Figure 6.

We can also use the distribution of population as the means to locate the future demand for food. Cities are stable sites on time-scales of one or two centuries, evidenced by Roman and Mediaeval cities in Britain for example. We therefore believe that we are justified in allocating future national populations to the year 2150, as predicted by United Nations statistics, to existing cities to generate the location of future food demand.

Such long-term projections must be treated as one of a number of possible scenarios. In order for global modelling outputs to be comparable certain benchmark scenarios are familiar, such as twice pre-industrial carbon dioxide, or twice current carbon dioxide. In global change terms twice current population is an important benchmark for impact studies. In addition, it is thought that global population could stabilize at 11–12 thousand million.

Double human population is likely to mean a four-fold increase in the demand for agricultural yield from plants. This is due to the anticipated rise in incomes which is expected to increase the demand for meat and non-staple foods. The challenge to the supply side of agriculture is therefore considerable and it will undoubtedly affect the characteristics of the land surface, as represented by the soil and vegetation parameters in the GCM.

The distribution of crops

Each of the world's major crops can be modelled by establishing the climatic limits to its distribution and the relationship between climate and yield. The other important factor influencing yield is the income level of the farmer. Maize, wheat, rice and other arable land are modelled as the primary crops.

The approach we have used here is illustrated by maize (Figures 7–9). We established the current growing conditions required by searching the literature. Thus maize requires a given range of degree days above 10 °C and a certain amount of soil moisture on those days. By mapping where these conditions are met, either currently or for computed future climates, the regions which have the potential to grow maize can be identified. We have also examined the global distribution of the soils on which each of the major crops is grown. This information is available at a 1° by 1° scale from the WHS database (Wilson & Henderson-Sellers 1985) in the

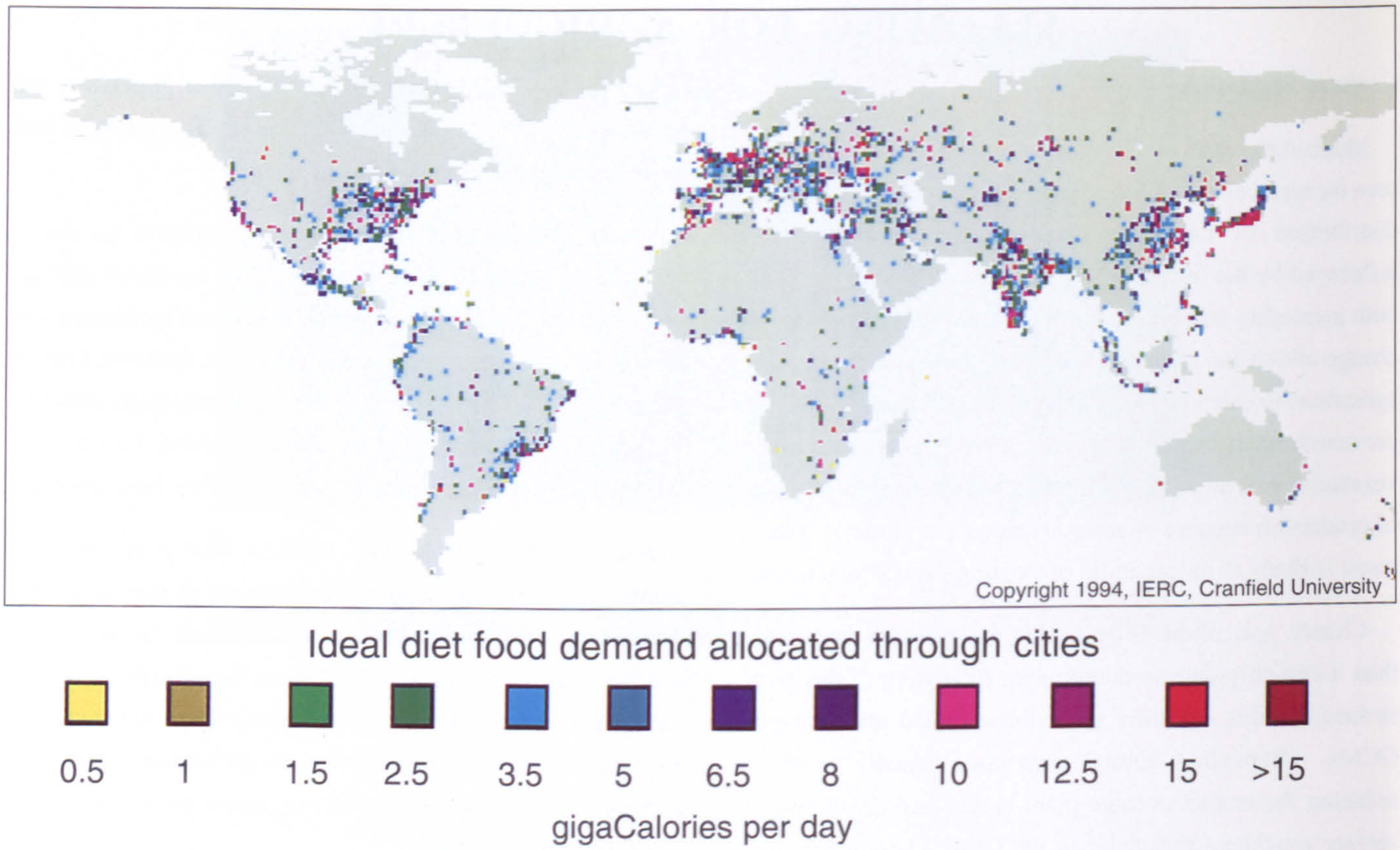

Figure 6. Daily food demand of the world, based on standardized food requirements, allocated to cities. The energy in food is measured in Calories (= 1000 calories = 4184 J) and 1 gigaCalorie is 4.2×10^{12} J. These are absolute amounts allocated to a point location; for example, Perth, Western Australia has a food demand in the range of 12.5–15 GCal per day (52×10^{12} to 63×10^{12} J per day).

GCM and enables a finer resolution of the probable distribution of the crop.

Allocating agricultural land

Where land is suitable climatically for more than one type of crop we make the assumption that the one which provides the greater calorific yield is the one grown. In the case of C3 crops such as wheat this will take over from C4 maize under conditions of high carbon dioxide where there is an overlap in suitable growing conditions.

The major validation exercise of the agricultural model is to simulate current agricultural distribution from the split of local and world trade for each city. This division will be based on the relationship between food imports and relative incomes. We assume that local needs are met first and the remaining traded food is supplied from the most productive areas and so leads to a conservative estimate of the minimum agricultural area. Case studies of particular countries are used to generate other conditions of trade. It must also be borne in mind that global cereal harvests have trebled over the 40 years 1948–1988.

On the above basis of trade and local supply of agricultural goods, the conditions of double carbon dioxide and double human population can be simulated and the land surface allocated appropriately to agriculture or natural vegetation.

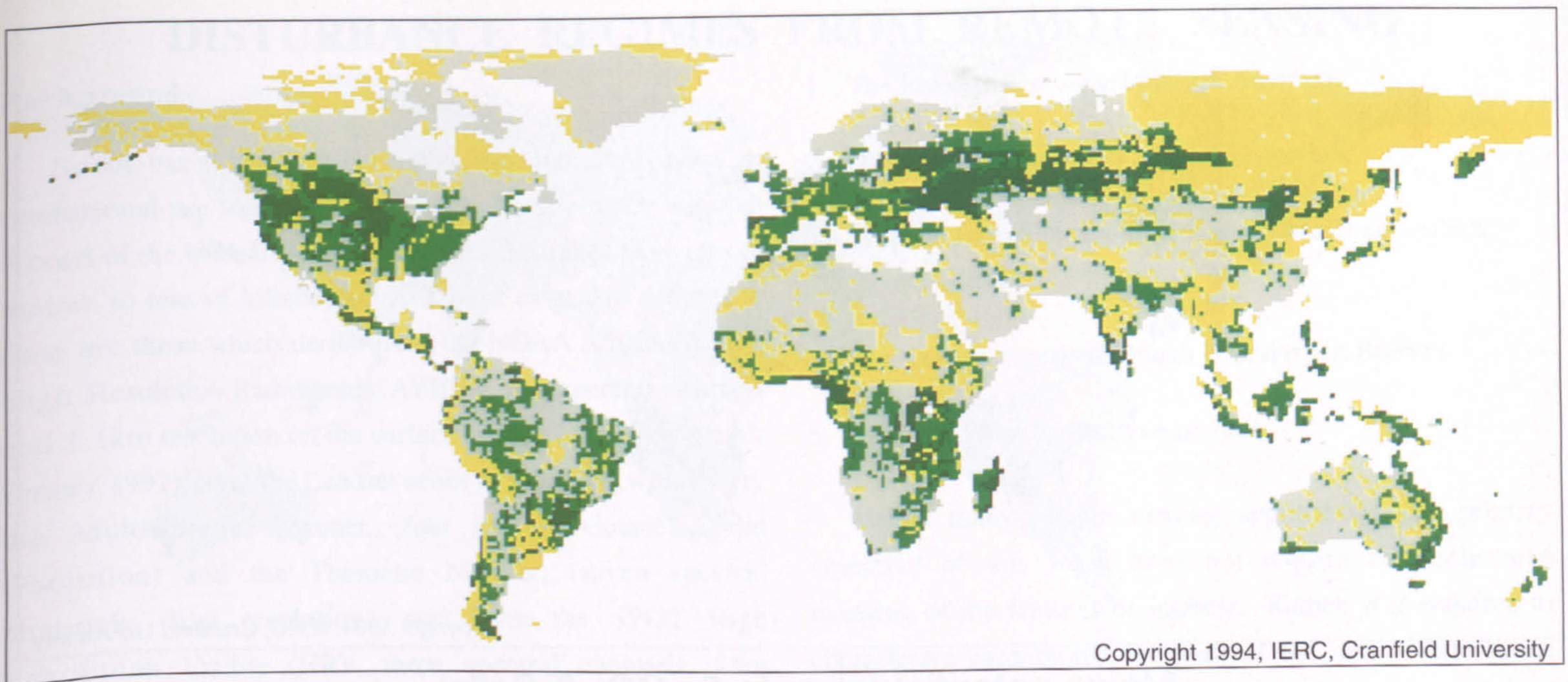

Figure 7. Classification of the earth's surface by its potential for growing maize as a crop.

Map above: suitability of the soil.

Map below: suitability of the climate with doubled carbon dioxide concentration, in terms of temperature and rainfall.

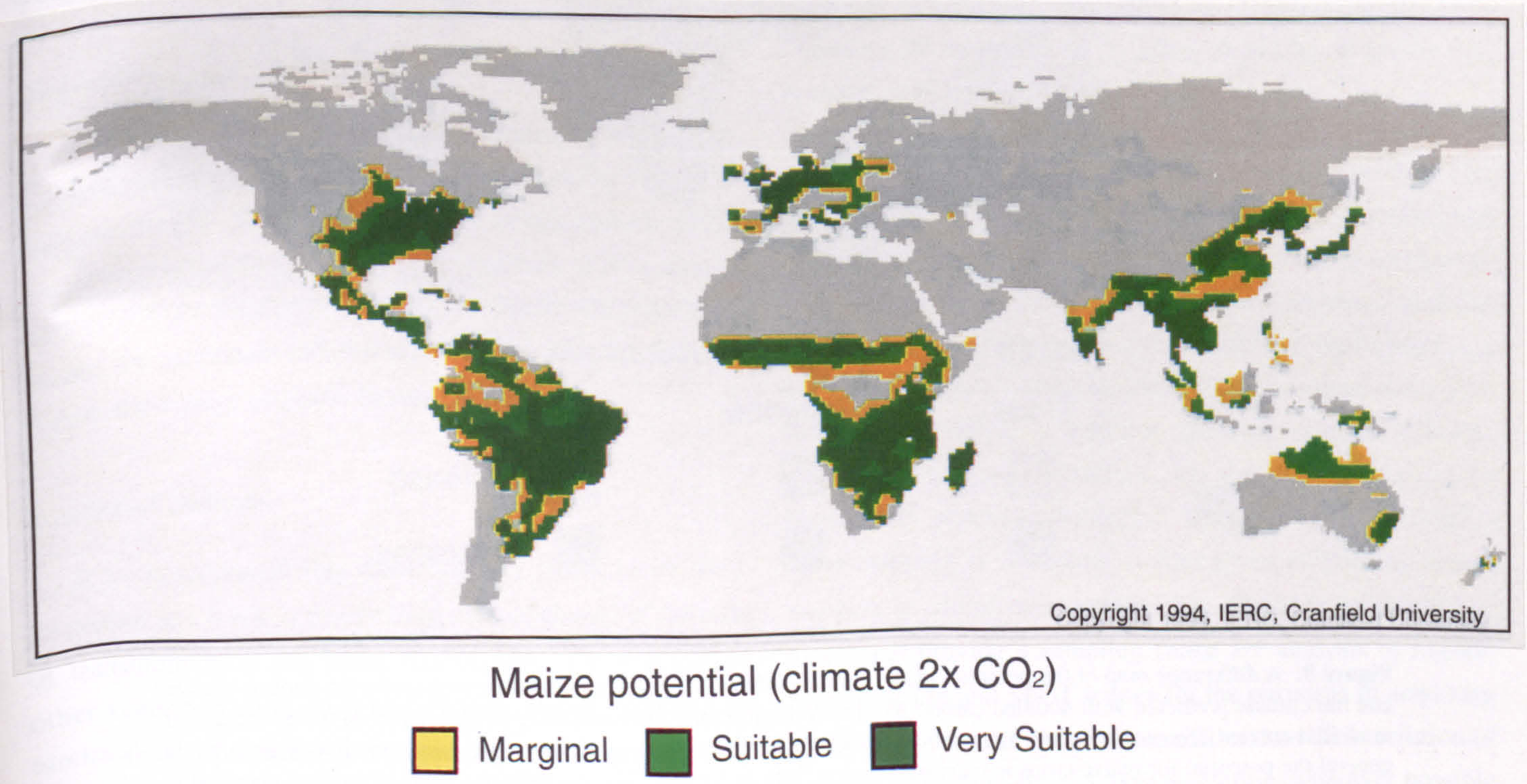

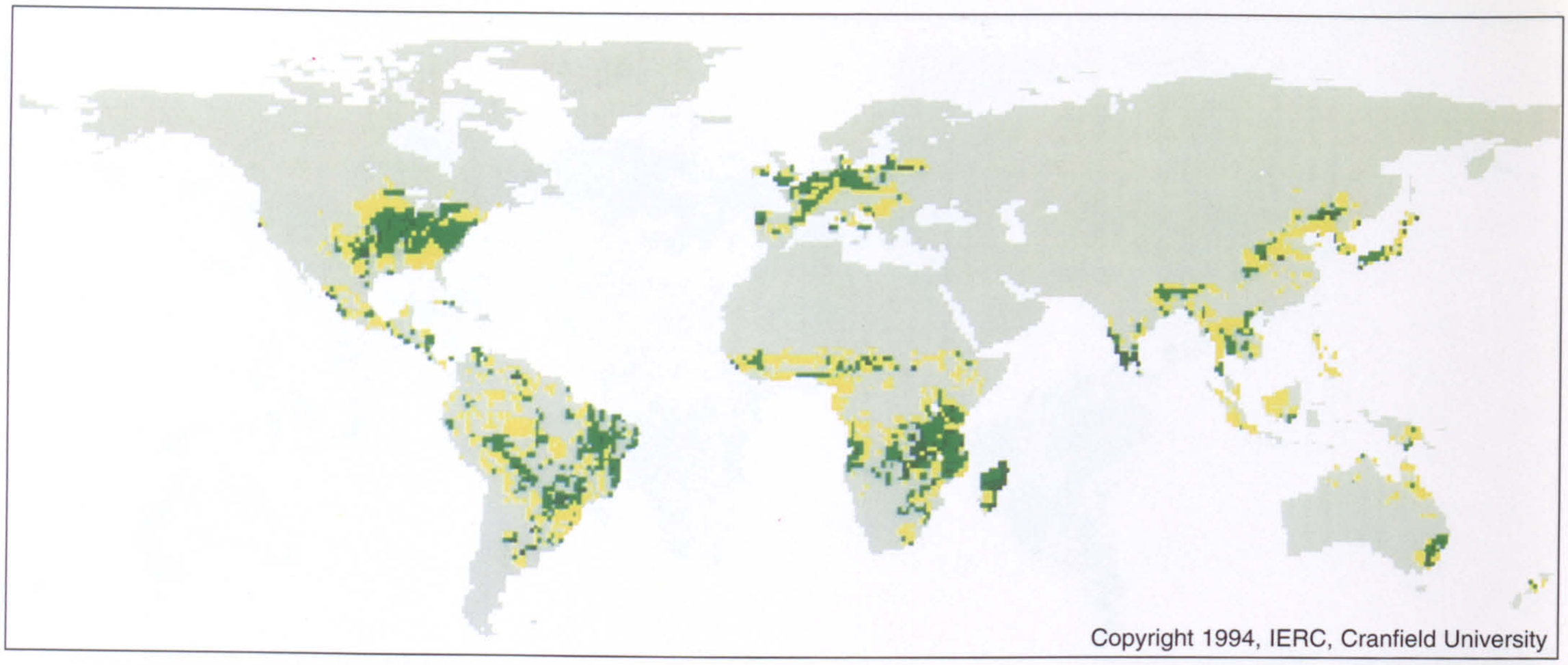

Figure 8. Classification of the earth's surface by its potential for growing maize as a crop under a climate with doubled carbon dioxide concentration. This is a combination of the suitabilities based on soil and on temperature and rainfall (Figure 7) followed by reclassification into three grades. The more detailed pattern of soil suitability modifies the large-scale pattern of suitability based on climate to produce a more realistic prediction of where maize could be grown under a doubled carbon dioxide climate.

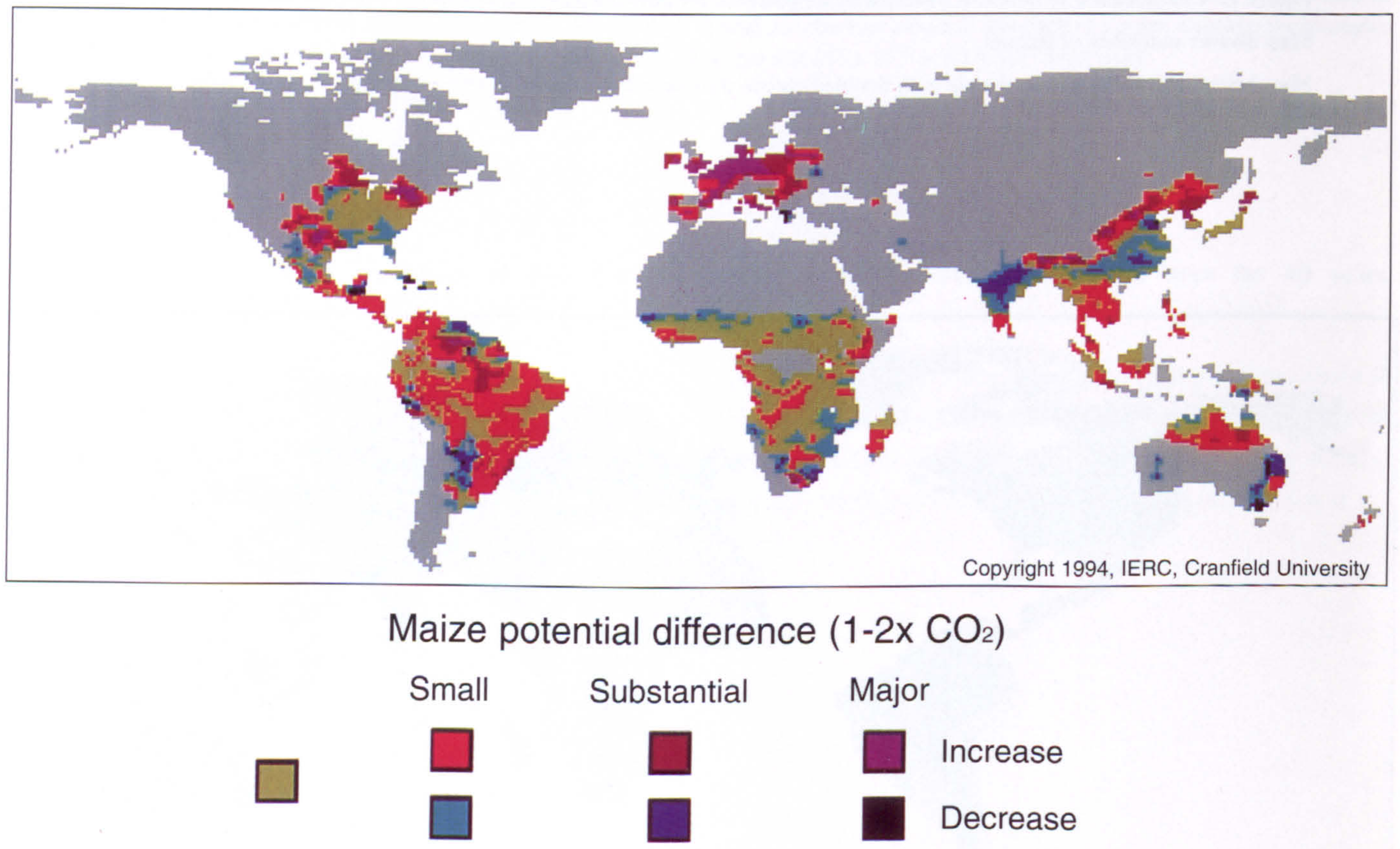

Figure 9. A difference map of the potential of the earth's surface for growing maize as a crop under the current climate and the climate predicted with doubled carbon dioxide concentration. The suitability of each point on a map drawn for modelled current climate (not shown) is subtracted from the corresponding point on the map shown as Figure 8. In general the potential for maize crops is increased, particularly in Europe. The conspicuous areas of reduced potential in India and south-east China have little practical importance since maize is not grown there, for reasons of dietary preference.

Background

Space-based earth observation systems have been in operational use for more than 15 years and provide a global record of the land surface at resolutions that range from tens of metres to tens of kilometres. The most extensive datasets in time are those which derive from the NOAA Advanced Very High Resolution Radiometer (AVHRR, five spectral channels and 1.1km resolution on the surface of the earth—Hastings & Emery 1992), from the Landsat series of satellites, which carry the Multi-spectral Scanner, (four spectral channels, 80m resolution) and the Thematic Mapper, (seven spectral channels, 30m resolution), and from the SPOT High Resolution Visible (HRV, three spectral channels, 25m resolution) (National Remote Sensing Centre 1987). There is a rich literature describing the use of these image sets for vegetation mapping at various scales and extents. Multi-spectral classification (Richards & Kelly 1984) and seasonal patterns in vegetation indices, computed as ratios or differences in the radiometric responses at different wavelengths (Lambin & Strahler 1994), are the commonest means used to differentiate vegetated and non-vegetated surfaces or to distinguish individual vegetation types. There is ample evidence of the feasibility of using remote sensing to detect, in areas of otherwise continuous vegetation, signs of disturbance from fire, windthrow and human activity (e.g. Chuvieco & Martin 1994, Albers *et al.* 1990, Malingreau & Tucker 1988). Figure 10 shows an example from our current work.

Objectives

Here, these techniques are being exploited to assist in modelling the dynamics of the responses of global biomes to climate change. The specific objective of this element of the research programme is to use remotely-sensed data to acquire statistics of the frequency (in time), the density (in space), the extent, the magnitude and, if possible, the origin of disturbance events for a range of global biomes.

Outline of methods

It is hypothesized that disturbance is likely to be most important as a factor in determining rates of change in the case of transitions involving forest biomes, since the structure of other vegetation units, such as savannah, steppe grassland or tundra already presents opportunities for colonization by new species. The work has therefore focused on the following globally significant forest biomes.

1. The boreal forest zone of North America.
2. Other evergreen forests in North America.
3. Tropical forests in South America (Brazil) and Africa (Cameroons).
4. The tropical forest–savannah boundary in Bolivia.
5. Seasonal forests in south-east Asia.

Unlike many remote sensing applications, the primary objective of this work does not require comprehensive mapping of the features of interest. Rather, it is required to characterize each biome in terms of the above disturbance statistics. These statistics then form an input to the models of gap dynamics described below. An important initial step in the development of the method was therefore to design a sampling strategy that is capable of delivering the disturbance statistics at acceptable cost.

The resolution of remotely-sensed imagery is a critical factor in determining the spatial extent of features which can be detected by this means (Townshend 1981). Forest gaps which can be colonized by new plants may range in size from the order of metres (in endogenous processes) to many kilometres (in the case of fires, windthrow and deforestation). It was therefore necessary to take into consideration the need for extensive spatial coverage (to achieve good representation of variability on the ground), high spatial resolution (to allow detection of relatively small areas of disturbance), and high frequency of repeat cover (to allow detection of cyclic, e.g. seasonal, events).

Only SPOT and TM can reliably detect gaps less than 1 ha or so. However, the coverage of single SPOT (65 x 65km) and TM (185 x 185km) scenes is so limited in global terms that the provision of globally representative disturbance statistics would be prohibitively expensive. In addition, the repeat cycle (about 10–18 days, depending on latitude), compounded by the incidence of cloud, in practice seriously constrains multi-temporal coverage. Therefore, the approach adopted is a hierarchical sampling strategy. Images from the AVHRR allow mapping of the extent of the biomes of interest, permit mapping of disturbances greater than 10 square kilometres in extent and provide a sampling frame for analysis of higher-resolution TM and SPOT scenes for the purposes of acquiring statistics on areas of disturbance smaller than the resolution of AVHRR. The images are 1.1km resolution, wherever possible using cloud-free composites of daily images on a 10-day cycle.

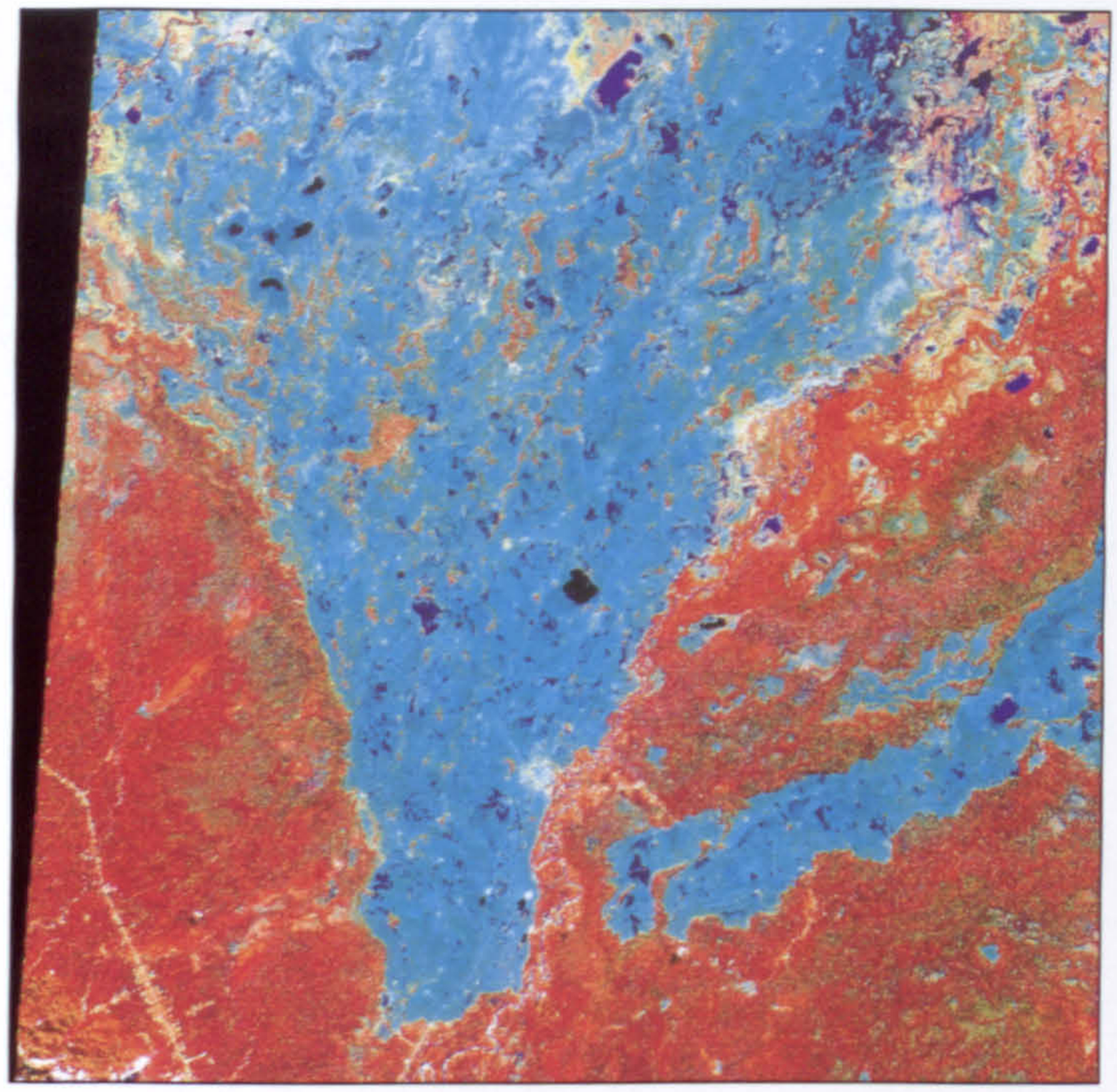

Figure 10. A satellite image processed to reveal disturbance in tropical forest. This false colour image from the Landsat TM is 100 x 100km (north at the top) and shows part of the department of Beni, northern Bolivia. Forest is displayed as reddish, savannah as light blue, and water as dark blue or black. Disturbance shows up as orange tones: the darker the orange, the more severe the disturbance or the greater the recovery. The larger disturbances in the forest are probably caused by fire. Disturbance along the river running from bottom centre to top right arises from flooding. Human disturbance along the road in the south-west corner is also visible.

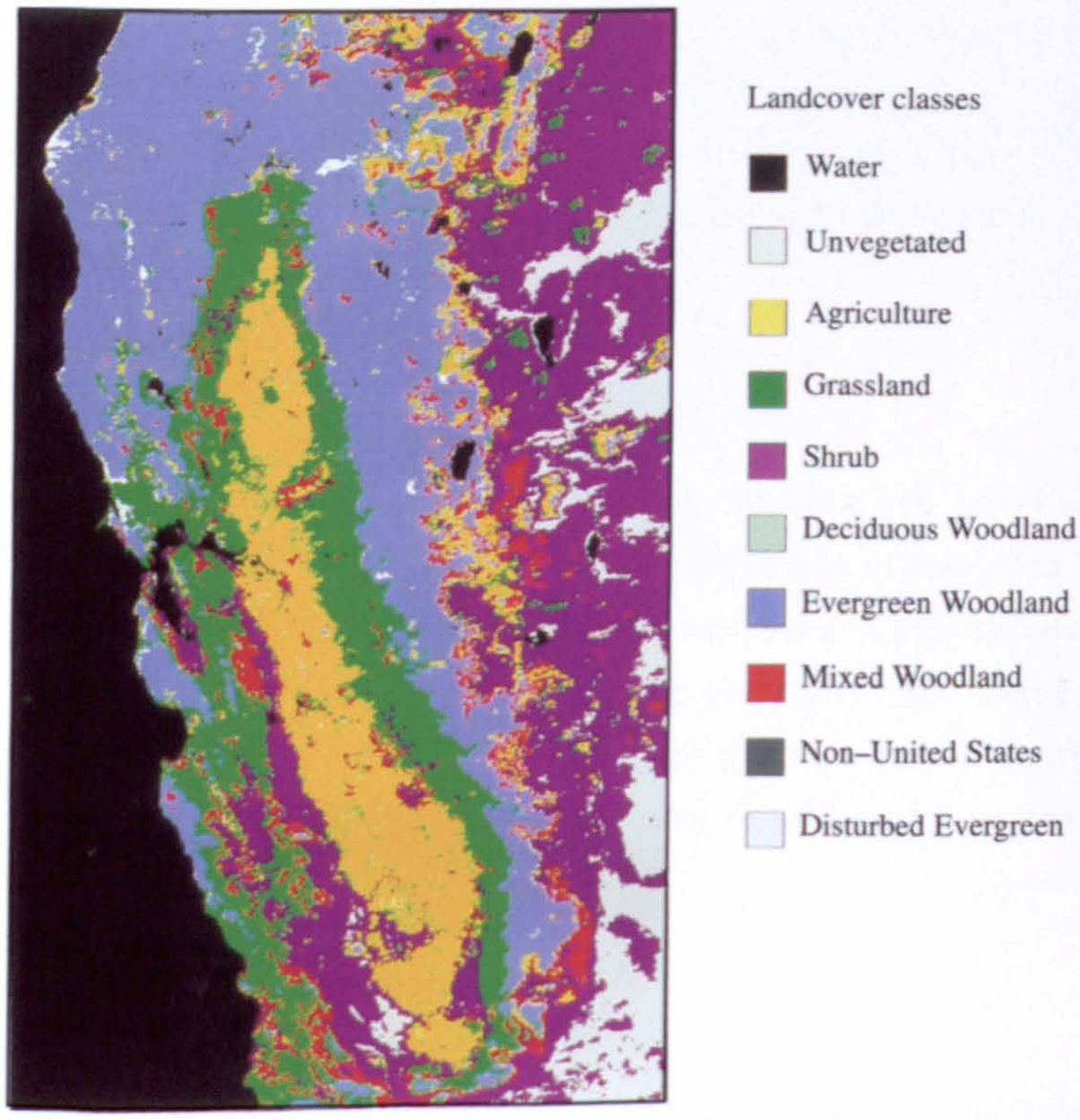

Figure 11. Vegetation types in California classified from the normalized difference vegetation index derived from images of the AVHRR. This image is approximately 850 km from top to bottom; north is at the top. The evergreen forests are on the Coast Ranges (to the west) and the edges of the Sierra Nevada (to the east of the central valley of agricultural land). Note that the disturbed areas are a very small fraction of the evergreen forest area, as expected: disturbance from windthrow or fire in many forests accounts for about 1% of the area each year (Runkle 1985, Johnson 1992).

Results

United States of America

Composite images of the normalized difference vegetation index (NDVI) from the AVHRR at fortnightly intervals at 1km resolution for 1990–1992 and a 1990 prototype dataset recording land cover characteristics were obtained from the EROS Data Centre (Loveland *et al.* 1991).

The combined database was used to investigate the size, frequency and spatial distribution of disturbances in evergreen forests in the conterminous USA. The initial stage was to simplify the 159 class land cover map into a map of eight classes. Four of these are vegetation clearly dominated by one of the functional types (FTs) that can be inferred from the outputs of the vegetation models. The final vegetation map, which broadly follows the approach advocated in Running, Loveland & Pierce (1994), contained the following classes.

Land cover class	Dominant functional type
1. Grassland	Perennial non-woody (grass)
2. Shrubland	Shrub
3. Deciduous woodland	Deciduous tree
4. Evergreen woodland	Evergreen tree
5. Mixed woodland	Deciduous tree, evergreen tree
6. Agriculture	Various; not specified
7. Unvegetated	None
8. Water	None

The six vegetation classes in the simplified land cover map were formed in such a way that any of the original classes containing a mixture of trees and other vegetation types were classified into the appropriate non-tree class in the simplified scheme. The split into deciduous and evergreen classes reflects the functional difference between trees which have a seasonal variability in LAI, constrained by temperature or water availability, from those which do not. Encroachment of agriculture into natural ecosystems is an important source of disturbance; for this reason, the classification distinguishes between natural and agricultural systems, although this necessitates the inclusion within the agriculture class of plants with a wide range of structural characteristics.

The phenology of deciduous and mixed forests mean that foliage increases from spring until late summer and decreases throughout autumn to a winter minimum. The NDVI profile follows this pattern too. In contrast, in evergreen forests the amount of foliage and the NDVI are fairly stable throughout the year. Large-scale disturbances in temperate and boreal forests are usually caused by fire or windthrow. Forest fires lead to a loss of foliage and hence a decrease in NDVI. The effects of windthrow are more subtle but also lead to a decrease in NDVI. The work of Kasischke *et al.* (1993) showed that the effects of forest fires could be detected in boreal forests because they cause a temporary decrease in an otherwise stable or increasing NDVI profile. There is very little true boreal forest in the conterminous USA but a similar procedure allowed areas of disturbance within evergreen coniferous forests to be clearly identified from anomalies in their seasonal NDVI profile (Figure 11).

Bolivia

Until completion of the IGBP Global Land Cover project (Townshend 1992), the AVHRR dataset for South America is less complete than in the USA and no land cover dataset is available. Imagery covering the savannah–forest boundary in Bolivia was therefore processed differently from the North American data, using unsupervised classification procedures to mask out areas of cloud and to reduce the data to simple maps of forest and non-forest classes. The big problem is the post-classification labelling of the data into meaningful forest or non-forest classes. This relies on good quality Landsat TM data within the imagery or other reliable vegetation maps of the region or both. Two regions along the savannah–forest boundary were chosen, for which suitable TM data were available. Images for both sites were acquired during 1991 and processed in the same way as the AVHRR data. Extensive unforested areas were removed from subsequent analysis of forest gaps because they do not represent disturbances. Single pixel gaps have also been excluded from the analysis because we cannot be sure that they represent true disturbances rather than image noise. The resultant images were used to generate statistics on the size of forest and non-forest parcels within each scene (see Figure 12). Acquisition of comparable data from the mid-1980s is in hand to allow us to explore rates of change in forest disturbance over this period.

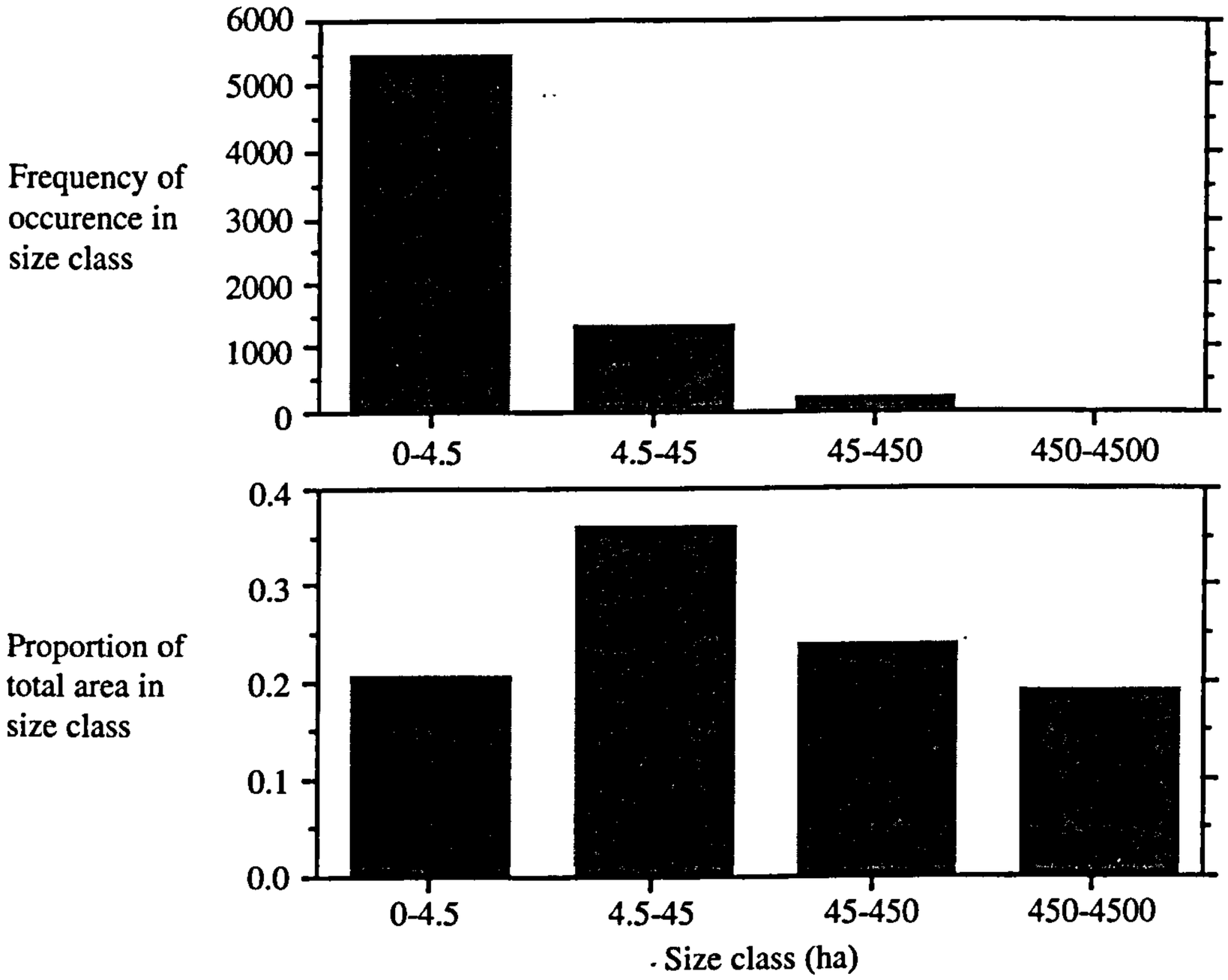

Figure 12. The size distribution of patches of disturbance on forest land detected on the remotely sensed image of part of Bolivia (Figure 10). The upper histogram is the distribution of numbers of disturbed patches; the lower one is the distribution of area. Note that the area classes increase logarithmically to cover the enormous range of size. In this forest there are very many small disturbances but only two in the 450–4500 ha size class. There is a more uniform distribution of area in each class. The total disturbed area was 49,822 ha. In South America many small fires (or other disturbances) contribute significantly to the area disturbed. This contrasts with boreal forest in Alaska where 96% of the total area burnt in 1990 was in fires of 2000 ha or above (Kasischke *et al.* 1993).

CONCLUSIONS AND FUTURE WORK

The consortium has achieved its objectives in obtaining data and constructing models to predict the influence of climate and carbon dioxide on the earth's vegetation. In particular,

(1) the model DOLY predicts the properties of vegetation successfully, and has been coupled with the GCM to quantify the effects of vegetation on climate;
(2) the effect of climate change on the potential distribution of maize as a crop has been demonstrated; and
(3) disturbance regimes for forest have been obtained from remote sensing.

With the addition of the map of agricultural land, predicted from current human population, it will be possible to repeat the model runs to see the effects of vegetation on climate with global vegetation much closer to the actual current vegetation. Further work will concentrate on a more dynamic modelling of climate–vegetation interactions. Key areas are the inclusion of seasonality (currently LAI is fixed throughout the year in the GCM although DOLY can predict LAI and NPP month by month), and the modelling of soil carbon and nitrogen cycling (at the moment the concentrations of carbon and nitrogen in the soil are fixed values for each point on the earth). The next stage will include an improved representation of semi-arid regions based on work carried out at the Institute of Hydrology. Tests of DOLY against a variety of hydrological datasets have shown the model to be sensitive to the formulation of soil/vegetation/atmosphere transfer processes in semi-arid regions and in particular the treatment of surfaces with significant areas of bare soil. Work is planned to improve the representation of sparse vegetation in general.

Special emphasis is being placed on extending DOLY to simulate the dynamics of vegetation change. A promising approach is to use the predicted values of NPP and LAI to define a probability of vegetation change from one functional type to another (e.g. tree to shrub or shrub to grass). The fractional coverage of each functional type can be updated using the resulting transition matrix. Figure 13 compares the map of functional types simulated in this manner with the actual distribution derived from the database of Wilson & Henderson-Sellers (1985). There is generally good agreement except in regions which are dominated by agriculture, such as areas of Europe, central Asia and the central parts of the USA.

The work at Cranfield University will be extended to other crops so that the model for predicting agricultural demands from population distribution can be completed. This model can be driven by the projected population for dates in the future so that the effects of changes in population can be added to those of climate.

The remote sensing component of the consortium will continue to provide disturbance regimes for different regions and biomes. Work is in hand to process 1km resolution AVHRR data for peninsular south-east Asia, supplied as part of a collaboration with the Remote Sensing Institute of the European Union's Joint Research Centre. Completion of this work and extraction of gap statistics awaits the receipt of high-resolution Landsat-TM data.

The ultimate aim of the consortium is to integrate all this modelling activity into a dynamic global vegetation model (DGVM) that will require only climatic, soils and population data to drive it. The DGVM will include the effects of man, the mechanism of natural vegetation change through disturbance, and the indirect effects of changing climate on both these aspects. This will provide a flexible and reliable means of predicting changes in climate and land cover. The effects of different scenarios of climatic and population change can be explored and the results will contribute to the formulation of appropriate policies for such issues as carbon dioxide emissions, population growth, agricultural development and world trade.

REFERENCES

Albers, B.J., Strahler, A.H., Li, X., Liang, S. & Clarke, K.C. 1990. Radiometric measurements of gap probability in conifer tree canopies. Remote Sensing of Environment 34: 179–192.

Baskin, Y. 1993. Ecologists put some life into models of a changing world. Science 259: 1694–1696.

Box, E.O. 1981. Macroclimate and Plant Forms: An Introduction to Predictive Modeling in Phytogeography. The Hague (Dr W. Junk).

Chuvieco, E., & Martin, M.P. 1994. Global fire mapping and fire danger estimation using AVHRR images. Photogrammetric Engineering and Remote Sensing 60: 563–570.

Grabherr, G. & Kojima, S. 1993. Vegetation diversity and classification systems. In: Solomon, A.M. & Shugart, H.H. (editors) Vegetation Dynamics and Global Change, pp.218–232. London (Chapman & Hall).

Hanson, J.D., Parton, W.J. & Innis, G.S. 1985. Plant growth and production of grassland ecosystems: a comparison of models. Ecological Modelling 29: 131–144.

Hastings, D.A., & Emery, W.J. 1992. The Advanced Very High Resolution Radiometer (AVHRR): a brief reference guide. Photogrammetric Engineering and Remote Sensing 58: 1183–1188.

Holdridge, L.R. 1947. Determination of world plant formulations from simple climatic data. Science 105: 367–368.

Houghton, J.T., Jenkins, G.J. & Ephraums, J.J. (editors). 1990. Climate Change: the IPCC Scientific Assessment. Cambridge (Cambridge University Press).

Johnson, E.A. 1992. Fire and Vegetation Dynamics: Studies from the North American Boreal Forest. Cambridge (Cambridge University Press).

Kasischke, E.S., French, N.H.F., Harrell, P., Christensen, N.L., Ustin, S.L. & Barry, D. 1993. Monitoring of wildfires in boreal forests using large area AVHRR NDVI composite image data. Remote Sensing of Environment 45: 61–71.

Lambin, E.F. & Strahler, A.H. 1994. Change-vector analysis in multi-temporal space: a tool to detect and categorize land-cover change processes using high temporal-resolution satellite data. Remote Sensing of Environment 48: 231–244.

Leemans, R. & Cramer, W.P. 1991. The IIASA database for mean monthly values of temperature, precipitation, and cloudiness on a global terrestrial grid. Laxenburg, Austria (International Institute for Applied Systems Analysis).

Loveland, T.R., Merchant, J.W., Ohlen, D.O. & Brown, J.F. 1991. Development of a land-cover characteristics database for the conterminous U.S. Photogrammetric Engineering and Remote Sensing 57: 1453–1463.

Malingreau, J.P. & Tucker, C.J. 1988. Large-scale deforestation in the Southeastern Amazon basin of Brazil. Ambio 17: 49–55.

Melillo, J.M., McGuire, A.D, Kicklighter, D.W., Moore, B., Vorosmarty, C.J. & Schloss, A.L. 1993. Global climate change and terrestrial net primary production. Nature 363: 234–239.

National Remote Sensing Centre. 1987. Data Users' Guide. Issue 3. Farnborough, UK (NRSC).

Nelson, B.W., Kapos, V., Adams, J.B., Oliveira, W.J., Braun, O.S.P. & do Amaral, I.L. 1994. Forest disturbance by large blowdowns in the Brazilian Amazon. Ecology 75: 853–858.

Parton, W.J., Stewart, J.W.B. & Cole, C.V. 1988. Dynamics of C, N, P and S in grassland soils: a model. Biogeochemistry 5: 109–131.

Pickett, S.T.A. & White, P.S. (editors). 1985. The Ecology of Natural Disturbance and Patch Dynamics. London (Academic Press).

Pitman, A.J. et al. 1993. Project for Intercomparison of Land-Surface Parameterization Schemes (PILPS). Results from Off-Line Control Simulations (Phase 1a). International GEWEX Project Office, Publication No.7.

Potter, C.S., Randerson, J.T., Field, C.B., Matson, P.A., Vitousek, P.M., Mooney, H.A. & Klooster, S.A. 1993. Terrestrial ecosystem production: a process model based on global satellite and surface data. Global Biogeochemical Cycles 7: 811–841.

Prentice, I.C., Cramer, W., Harrison, S.P., Leeman, R., Monserud, R.A. & Solomon, A.M. 1992. A global biome model based on plant physiology and dominance, soil properties and climate. Journal of Biogeography 19: 117–134.

Richards, J.A. & Kelly, D.J. 1984. On the concept of spectral class. International Journal of Remote Sensing 5: 987–991.

Rowntree, P.R. 1988. Review of general circulation models as a basis for predicting the effects of vegetation change on climate. Proceedings of the UN University Workshop on Forest, Climate and Hydrology—Regional Impacts. Tokyo (UN University).

Runkle, J.R. 1985. Disturbance regimes in temperate forests. In: Pickett, S.T.A. & White, P.S. (editors) The Ecology of Natural

22 Disturbance and Patch Dynamics, pp.17–33. London (Academic Press).

Running, S.W. & Coughlan, J.C. 1988. A general model of forest ecosystem processes for regional applications. I. Hydrologic balance, canopy gas exchange and primary production processes. Ecological Modelling 42: 125–154.

Running, S.W., Loveland, T.R. & Pierce, L.L. 1994. A vegetation classification logic based on remote sensing for use in global biogeochemical models. Ambio 23: 77–81.

Sellers, P.J., Mintz, Y., Sud, Y.C. & Dalcher, A. 1986. A simple biosphere model (SiB) for use within general circulation models. Journal of Atmospheric Science 43: 505–531.

Smith, T.M., Shugart, H.H., Woodward, F.I. & Burton, P.J. 1993. Plant functional types. In: Solomon, A.M. & Shugart, H.H. (editors) Vegetation Dynamics and Global Change, pp.272–292. London (Chapman & Hall).

Tarpley, J.D., Schneider, S.R. & Money, R.L. 1984. Global vegetation indices from the NOAA–7 meteorological satellite. Journal of Climatology and Applied Meteorology 23: 491–494.

Townshend, J.R.G. 1981. Effects of spatial resolution on the classification of land cover type. In: Fuller, R.M. (editor) Proceedings of the Symposium on Ecological Mapping, pp.101–112. Huntingdon, U.K. (Institute of Terrestrial Ecology).

Townshend, J.R.G. (editor). 1992. Improved data for land applications: a proposal for a new high resolution data set. Stockholm (International Geosphere–Biosphere Programme).

Verseghy, D.L. 1991. CLASS—a Canadian Land Surface Scheme for GCMs. I. Soil model. International Journal of Climatology 2: 111–133.

Warrilow, D.A. & Buckley, E. 1989. The impact of land surface processes on the moisture budget of a climate model. Annales Geophysicae 7: 439–449.

Webb, T. 1987. The appearance and disappearance of major vegetation assemblages: long-term vegetational dynamics in eastern North America. Vegetatio 69: 177–187.

Wilson, M.F. & Henderson-Sellers, A. 1985. A global archive of land cover and soils data for use in General Circulation Models. Journal of Climatology 5: 119–143.

Woodward, F.I. 1987. Climate and Plant Distribution. Cambridge (Cambridge University Press).

Woodward, F.I. 1993. Leaf responses to the environment and extrapolation to larger scales. In: Solomon, A.M. & Shugart, H.H. (editors) Vegetation Dynamics and Global Change, pp.71–100. London (Chapman & Hall).

Publications connected with this TIGER project

Beerling, D.J. & Woodward, F.I. 1994. The climate change experiment (CLIMEX): phenology and gas exchange responses of boreal vegetation to global change. Global Ecology and Biogeography Letters 4: 17–26.

Woodward, F.I. & Lee, S.E. 1994. Modelling terrestrial vegetation. The Globe (newsletter of the U.K. Global Change Office, Swindon), issue no. 21, pp.5–6.

Woodward, F.I., Smith, T.M. & Emanuel, W.R. Submitted. A global land primary productivity and phytogeography model. Global Biogeochemical Cycles (submitted August 1994).

Woodward, F.I. & Lee, S.E. Submitted. Global scale forest function and distribution. Forestry (submitted December 1994).

GLOSSARY

Albedo The reflectivity of the surface of the earth to solar radiation.

AVHRR Advanced Very High Resolution Radiometer: an instrument on board the NOAA series of satellites measuring the radiance of the earth's surface in five wavebands at 1.1km spatial resolution.

Biome A large-scale unit of classification of vegetation as tropical forest, savannah, tundra, etc. Biomes are recognized primarily by the physiognomy of the vegetation—what it looks like in terms of structure—rather than by the species it contains. They can be mapped at scales of around 1:15 million.

Boundary layer The layer of still or slowly moving air next to a surface, through which molecules or heat move by diffusion between the surface and the bulk air which is well mixed by turbulence. The boundary layer can be next to an individual leaf, a leaf canopy, or the earth as a whole (the planetary boundary layer).

C3 The basic biochemical pathway of photosynthesis adds the one-carbon molecule, carbon dioxide, to a five-carbon molecule which is immediately split into two three-carbon molecules, the first products of carbon fixation, hence C3. This pathway is inhibited by oxygen concentrations currently found in the atmosphere and, partly for that reason, responds to increases in carbon dioxide concentration.

C4 A number of plant species, mostly grasses of hot, dry regions, fix carbon dioxide initially on to a three-carbon compound to make a four-carbon molecule, hence C4. This pathway then feeds the fixed carbon to the C3 process out of reach of oxygen. Consequently C4 plants scavenge carbon dioxide from air efficiently even at the current low concentrations and their rates of photosynthesis respond much less to increases in atmospheric carbon dioxide concentration.

Canopy water capacity The amount of water, usually in the range 1–3mm of rainfall, that can be held on a leaf canopy before it drains down the stems or drips from the leaves.

Conductance The term which relates a flux of a substance to the driving force under which it moves. Here the flux is of water vapour in evapotranspiration or of carbon dioxide in photosynthesis and the conductance of a leaf depends on how widely open are the stomata (stomatal conductance) and the thickness of the boundary layer. Conductance is the reciprocal of resistance; they can be interchanged but sometimes one concept is more convenient than the other.

Correlative model A type of empirical model—see model types.

Deforestation The change in land use from forest to something else, thus a man-made process with intent or neglect. The loss of forest cover by fire or windthrow is not deforestation but a natural disturbance.

Disturbance The removal of vegetation cover by an identifiable event such as fire, windthrow, landslip, insect outbreak, and so on. By extension, endogenous community dynamics, where individual plants die of old age and create gaps in which new individuals can grow, is also classed as a disturbance.

DOLY Dynamic GlObaL PhytogeographY Model. A vegetation model driven by climate and soil properties that predicts the maximum rate of photosynthesis, the maximum stomatal conductance, leaf area index, and net primary productivity.

Empirical model See model types.

Evapotranspiration Water lost by evaporation from the soil and by transpiration from vegetation taken together.

Functional type (FT) A type of plant with particular morphological, physiological and life cycle attributes, irrespective of its taxonomic classification. Here functional types are arrived at by successive splitting of vegetation as an entity. The initial divisions are based on woodiness, perennial or annual and deciduous or evergreen habit. Functional *groups* can be formed by collecting together species having similar attributes, working from the bottom upwards.

GCM General circulation model: a mechanistic model of the working of the atmosphere which simulates the transfers of water, heat and momentum between compartments made up by dividing the atmosphere into layers above cells in a grid on the surface of the earth. The oceans are similarly divided into layers beneath the cells although a simplified version of the GCM operates with the oceans as a single layer.

GCTE Global Change and Terrestrial Ecosystems: part of the IGBP. The GCTE encourages co-ordinated research into the effects of changes in climate, atmospheric composition, and land use on terrestrial ecosystems. It is organized into three foci: ecosystem physiology, change in ecosystem structure, and impacts on agriculture and forestry. For further information contact GCTE Core Project Office, CSIRO Division of Wildlife and Ecology, P.O. Box 84, Lyneham ACT 2602, Australia (telephone +61 6 242 1742; fax +61 6 241 2362; telex 62284).

GPP Gross primary productivity: the amount of carbon fixed initially by photosynthesis before any is lost in respiration.

IGBP International Geosphere–Biosphere Programme: an organization set up by the International Council of Scientific Unions to promote research in global environmental change through a number of core projects including GCTE.

Infiltration enhancement factor A factor allowing for the fact that rainfall enters the soil faster (up to six times faster) beneath vegetation than on bare soil because of the leaf litter and better soil porosity.

LAI Leaf area index: the leaf area of a canopy divided by the ground area that it covers, thus the average number of leaves arranged horizontally above the ground. It is a concept at the field scale not that of individual plants. Discontinuous canopies can have a value for LAI, and LAI can be less than one.

Mechanistic model See model types.

Model types Empirical models are usually a tidier, more convenient way of expressing relationships of data. Any predictive capability is limited to the range of examples used in the model. Mechanistic models, in contrast, attempt to reflect the underlying relationships of components of a system so that they increase understanding and allow prediction in a wider range of cases. Since the natural world is organized hierarchically even a mechanistic model is empirical at some level of organization but it is empirical at one or two levels below the level at which understanding and prediction are required.

NDVI Normalized difference vegetation index: the ratio of reflectance in red and near infra-red wavebands as a normalized difference index—(IR – R)/(IR + R)—which can take values from –1 to +1 and is zero when IR = R. In practice vegetation reflects more infra-red than red so the NDVI runs from 0 to +1. Since leaves absorb most incident red radiation, as part of the radiation used in photosynthesis, and reflect or transmit most of the infra-red, the NDVI is related to the leafiness of the vegetation, almost linearly with LAI but tending to saturate at LAI over about 4.

NPP Net primary productivity: the carbon fixed by photosynthesis less the losses through respiration of all parts of the plant.

Parameter In modelling, parameters are variable factors held constant in a particular case, often representing something in the system being modelled. They should not be confused with driving, state or output variables, each of which may take many values or change continuously, or with constants that convert from one unit to another or with universal constants such as π. Here we distinguish between the vegetation properties (output variables) predicted by the vegetation models and the vegetation parameters needed by the GCM.

Pixel The smallest element in an image captured by a digital sensor and manipulated on a computer.

Resistance The reciprocal of conductance, q.v.

Roughness Aerodynamic roughness of vegetation measures the tendency of a vegetation canopy not to be smooth, which would allow laminar flow of air in the boundary layer, but rough which causes turbulence in the air flow.

SPOT Système Probatoire pour l'Observation de la Terre: a French remote sensing satellite.

TIGER Terrestrial Initiative in Global Environmental Research: a community research programme of the Natural Environment Research Council into climate change and its consequences. Contact address for further information on p.2.

TM Thematic Mapper: an instrument on board the Landsat series of remote sensing satellites.

Unsupervised classification The procedure in image analysis where an objective clustering algorithm groups together pixels in the image having similar properties. The task is then to relate these classes to land use or vegetation types on the ground. Supervised classification uses training areas on the image for which ground data are available to relate ground classes to image classes which can then be applied to the rest of the image or to other images.

Vapour pressure deficit The difference between the vapour pressure of the air, a measure of humidity, and the amount of water it could hold when saturated at that temperature. The VPD effectively measures the drying power of the air.

Water use efficiency The amount of water lost in transpiration while fixing one unit of carbon in photosynthesis. It is usually measured as the ratio of transpiration to photosynthesis either as instantaneous rates or as totals accumulated over a stated period such as the growing season.

World The model World is driven by climate variables and soil properties and predicts leaf area index and net primary productivity, for any point on the earth, based on a hydrological balance between precipitation and potential evapotranspiration.

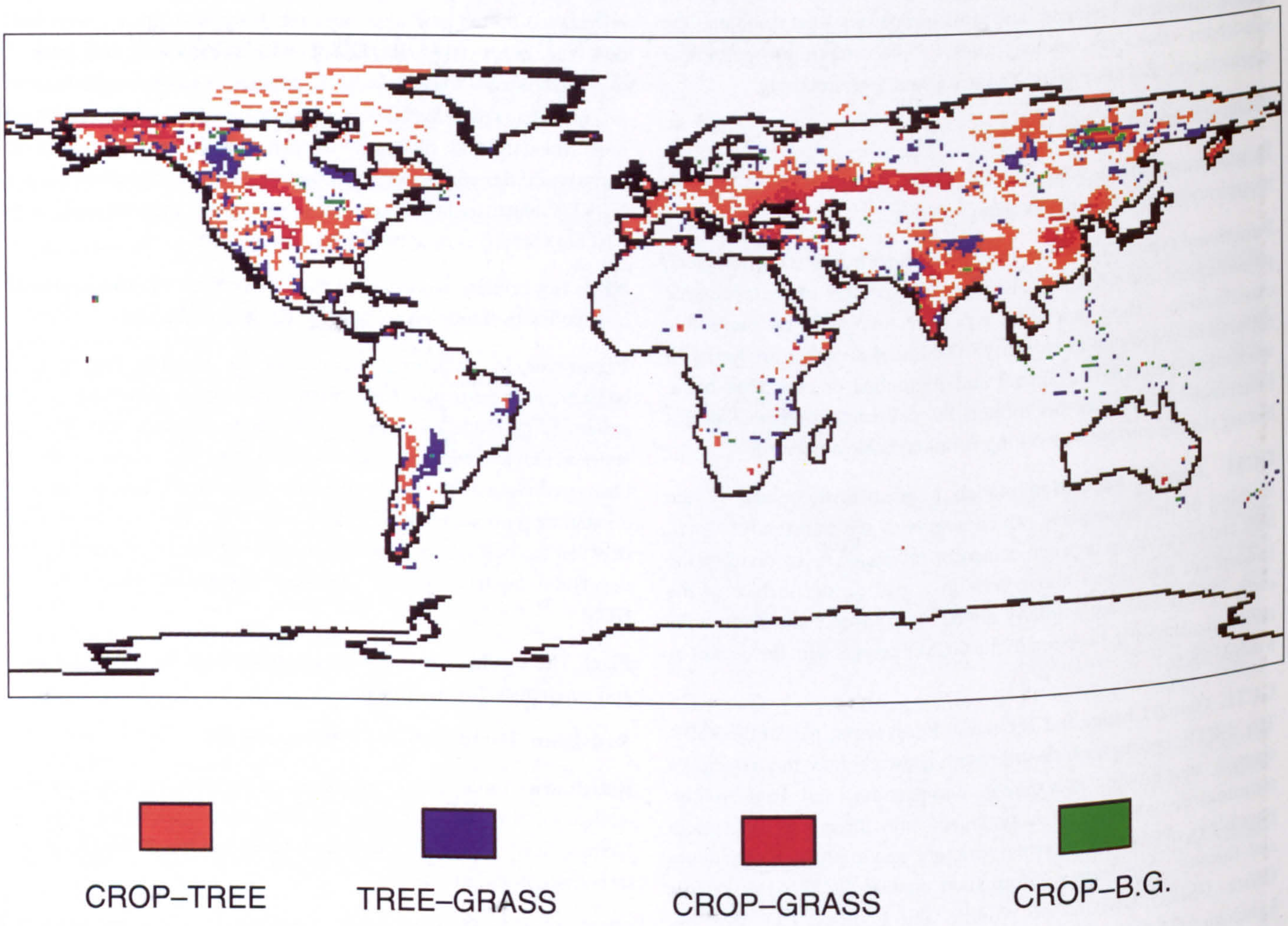

Figure 13. This map shows, for each 1° by 1° cell, the difference between the observed primary functional type in the database of current vegetation produced by Wilson & Henderson-Sellers (1985) and the functional types of plant given by the vegetation model DOLY. The WHS database is of land cover classes each of which contains land or vegetation types which are equivalent to FTs. The model DOLY predicts vegetation properties and from these the main FT is inferred (B.G. is base ground). Thus agricultural regions are picked out as areas where the WHS database gives crop but the model predicts tree or grass (crop–tree and crop–grass in the map key). Some of the areas categorized as tree–grass highlight problems in predicting mixtures of trees and grass in vegetation types such as savannah and along the diffuse border of the boreal forest and tundra.

Map on front cover. This shows the main functional type for each 1° by 1° cell, inferred from the vegetation properties predicted by the model DOLY, overlain by a map of cities of over 200,000 population. The tree functional type is shown as green, shrubs as red, grass as blue, bare ground as yellow and cities as black.

Edited by P.L. Mitchell
Figure 1 drawn by S.M. Diamond
Layout of front cover designed by G. Woods
Printed by ArcherPrint, Sheffield S8 0JZ (tel. (0114) 258 4557)